

# AGARD

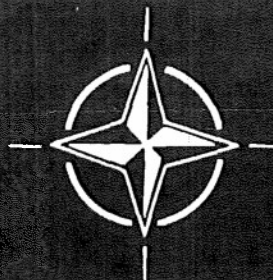
ADVISORY GROUP FOR AEROSPACE RESEARCH & DEVELOPMENT

7 RUE ANGELLE 92200 NEUILLY SUR SEINE FRANCE

AGARD ADVISORY REPORT No.224

## Boundary Layer Simulation and Control in Wind Tunnels

NORTH ATLANTIC TREATY ORGANIZATION



DISTRIBUTION AND AVAILABILITY  
ON BACK COVER

PROPERTY OF U.S. AIR FORCE  
AEDC TECHNICAL LIBRARY  
ARNOLD AFB, TN 37389

NORTH ATLANTIC TREATY ORGANIZATION  
ADVISORY GROUP FOR AEROSPACE RESEARCH AND DEVELOPMENT  
(ORGANISATION DU TRAITE DE L'ATLANTIQUE NORD)

AGARD Advisory Report No.224  
**BOUNDARY LAYER SIMULATION AND CONTROL IN WIND TUNNELS**  
**Report of the Fluid Dynamics Panel Working Group 09**



## THE MISSION OF AGARD

According to its Charter, the mission of AGARD is to bring together the leading personalities of the NATO nations in the fields of science and technology relating to aerospace for the following purposes:

- Recommending effective ways for the member nations to use their research and development capabilities for the common benefit of the NATO community;
- Providing scientific and technical advice and assistance to the Military Committee in the field of aerospace research and development (with particular regard to its military application);
- Continuously stimulating advances in the aerospace sciences relevant to strengthening the common defence posture;
- Improving the co-operation among member nations in aerospace research and development;
- Exchange of scientific and technical information;
- Providing assistance to member nations for the purpose of increasing their scientific and technical potential;
- Rendering scientific and technical assistance, as requested, to other NATO bodies and to member nations in connection with research and development problems in the aerospace field.

The highest authority within AGARD is the National Delegates Board consisting of officially appointed senior representatives from each member nation. The mission of AGARD is carried out through the Panels which are composed of experts appointed by the National Delegates, the Consultant and Exchange Programme and the Aerospace Applications Studies Programme. The results of AGARD work are reported to the member nations and the NATO Authorities through the AGARD series of publications of which this is one.

Participation in AGARD activities is by invitation only and is normally limited to citizens of the NATO nations.

The content of this publication has been reproduced  
directly from material supplied by AGARD or the authors.

Published April 1988

Copyright © AGARD 1988  
All Rights Reserved

ISBN 92-835-0457-7



*Printed by Specialised Printing Services Limited  
40 Chigwell Lane, Loughton, Essex IG10 3TZ*

## PREFACE

This report contains the results of a study performed by AGARD Working Group 09 on boundary layer simulation in wind tunnels with emphasis on the transonic speed regime. The working group was active under the auspices of the AGARD Fluid Dynamics Panel. The participants in the study represented Canada, France, Germany, Italy, Netherlands, United Kingdom, United States, and Turkey.

This report is intended to display the current state-of-the-art in boundary layer simulation where Reynolds number is or cannot be simulated and give attention to wind tunnel effects as well as to document the physical aspects of boundary layer simulation and the research needed. Finally, a simulation methodology is proposed which can serve wind tunnel user and operator as an ordered thinking process for the design of wind tunnel tests where viscous effects are important.

M.L.LASTER  
Chairman  
Working Group 09

\* \* \*

Ce rapport présente les résultats d'une étude réalisée par le Groupe de travail AGARD 09 sur la simulation de la couche limite en soufflerie, en mettant l'accent sur le régime transsonique. Le Groupe de travail s'est réuni sous l'égide du Panel AGARD de la Dynamique des Fluides. Les membres du groupe ont représenté les Nations suivantes: le Canada, la France, l'Allemagne, l'Italie, les Pays Bas, le Royaume Uni, les Etats Unis et la Turquie.

Le présent rapport donne un aperçu de l'état de l'art dans le domaine de la simulation de la couche limite, où le nombre de Reynolds n'est pas ou ne peut pas être simulé, examine les effets créés en soufflerie, documente les aspects physiques de la simulation de la couche limite et précise les besoins en matière de recherche.

Enfin, il est proposé une méthodologie de simulation de la couche limite qui peut servir aux utilisateurs et aux opérateurs des souffleries comme ligne de pensée pour la définition de certains essais en soufflerie où les effets visqueux sont d'une importance particulière.

# CONTENTS

	Page
<b>PREFACE</b>	<b>iii</b>
<b>1. INTRODUCTION</b>	<b>1</b>
<b>2. REVIEW OF BOUNDARY LAYER SIMULATION PROCEDURES</b>	<b>3</b>
2.1 INTRODUCTION	3
2.2 CONFIGURATION ASPECTS	5
2.2.1 MISSILES, FUSELAGES AND SIMILAR BODIES by J.L.Potter	5
2.2.2 HIGH-ASPECT-RATIO WINGS by J.B.Peterson, Jr	21
2.2.3 DELTA WING CONFIGURATIONS by J.Szodruch	30
2.2.4 COMPLEX CONFIGURATIONS by A.G.T.Cross	50
2.3 WIND TUNNEL ASPECTS	68
2.3.1 REYNOLDS NUMBER EFFECTS AND THE WIND TUNNEL ENVIRONMENT by A.Elsenaar	68
2.3.2 TECHNIQUES FOR BOUNDARY LAYER TRIPPING AND CONTROL by G.P.Russo	80
2.4 SUMMARY AND RECOMMENDATIONS	91
<b>3. SIMULATION/EXTRAPOLATION METHODOLOGY</b>	<b>93</b>
3.1 INTRODUCTION by E.Reshotko	94
3.2 GENERAL FRAMEWORK	96
3.2.1 AN OUTLINE OF THE METHODOLOGY by A.B.Haines and A.Elsenaar	96
3.2.2 EXPERIMENTAL TOOLS: THE TUNNEL AND THE MODEL by A.B.Haines and A.Elsenaar	111
3.2.3 COMPUTATIONAL TOOLS FOR SIMULATION METHODOLOGIES by Y.Y.Chan	115
3.2.4 EMPIRICAL TOOLS FOR SIMULATION METHODOLOGIES by A.Elsenaar and A.B.Haines	132
3.3 APPLICATIONS	139
3.3.1 TRANSPORT-TYPE CONFIGURATIONS by A.B.Haines and A.Elsenaar	139
3.3.2 COMBAT AIRCRAFT by A.B.Haines	164
3.3.3 MISSILES, FUSELAGES AND SIMILAR BODIES by J.L.Potter	191
3.4 CONCLUSIONS by E.Reshotko	209
<b>4. PHYSICAL ASPECTS OF BOUNDARY LAYER SIMULATION AND ASSOCIATED RESEARCH REQUIREMENTS</b>	<b>210</b>
4.1 INTRODUCTION by E.Stanewsky	211
4.2 CRITICAL FLOW PHENOMENA by E.Stanewsky	211
4.3 BOUNDARY LAYER DEVELOPMENT AND TRANSITION by R.Michel	217
4.4 DEVELOPMENT AND ANALYSIS OF TURBULENT NON-EQUILIBRIUM BOUNDARY LAYERS by A.G.T.Cross	250
4.5 SHOCK BOUNDARY LAYER INTERACTION by E.Stanewsky	271
4.6 CLASSICAL SEPARATION, TRAILING-EDGE FLOWS AND BUFFETING by J.L.van Ingen	306
4.7 VORTEX FLOWS by E.M.Kraft	338
4.8 ENVIRONMENTAL EFFECTS ON TRANSITION AND BOUNDARY LAYER CHARACTERISTICS by C.Ciray	356

4.9 BOUNDARY LAYER MANIPULATION  
by E.M.Kraft 409

4.10 SUMMARY OF FUTURE RESEARCH AND CONCLUSION  
by E.Stanewsky 447



## Boundary Layer Simulation and Control Report of the AGARD Fluid Dynamics Panel Working Group 09

### 1.0 Introduction

The problem of boundary layer simulation in wind tunnels is well known. The chief fluid dynamic parameter for scaling viscous flows, the Reynolds number, often cannot be matched when larger aircraft and missiles are tested in present-day transonic wind tunnels. Furthermore, it is important to note that matching Reynolds numbers based on some dimension parameter such as wing chord or body diameter may not result in duplication of all the relevant viscous-fluid-related phenomena. For example, wind tunnel noise is widely recognized to influence transition Reynolds number. Evidence of this was obtained in transition test of the AEDC 100 cone tested in several North American and European wind tunnels.

In attempting to duplicate flight conditions the experimentalists have required to artificially simulate boundary layer transition at a matching relative location with 'tripping' devices or try to trip the boundary layer at some location to match some other parameter such as trailing edge boundary layer thickness in hopes of duplicating viscous/inviscid flow interactions. Not only transition location and boundary layer thickness but velocity profile and detailed character of the turbulence most likely will cause one tripped boundary layer to be unlike the full scale naturally turbulent counterpart.

A deficiency in simulation of boundary layer properties is believed to affect shock wave and boundary layer separation locations, with marked effects on aerodynamic forces. These problems are particularly severe in transonic flows because shock wave-boundary layer interaction often has a strong influence on overall aerodynamic performance. Observation of experimentalists at various wind tunnel facilities reveal that boundary layer simulation is approached without detailed knowledge of the physics of the process, with techniques varying from one facility to another. The wind tunnel users generally apply "tripping" procedures without regard to unique tunnel environments. This is brought about in part because in-depth information of the tunnel environment and its effect on boundary layer simulation is usually not available.

Therefore, it is necessary to critically examine simulation requirements related to boundary layer characteristics and to try to formulate criteria for guidance of experiments using transonic wind tunnels.

Boundary Layer simulation in wind tunnels is not a well defined science in the absence of Reynolds number simulation but largely dependent upon varied techniques employed by individual experimentalists. The purpose of Working Group 09 is to assess the state-of-the-art in wind tunnels at high subsonic and transonic speeds and recommend research which will aid in improving understanding and prediction of aerodynamic forces on aircraft and missiles.

The mission of Working Group 09 was scoped as follows:

1. Critically review what conditions must be achieved to yield adequate simulation for typical transonic aircraft and missiles tested in wind tunnels at Reynolds numbers less than those corresponding to the full-scale counterparts in free flight. The focus will be upon high subsonic and transonic speeds.
2. Conduct a review of current boundary layer simulation criteria, their ranges of applicability, and the techniques used to satisfy these criteria. Identify areas of conflicting criteria and recommend investigations to resolve the conflicts.
3. Define needed research to improve understanding of the flow physics necessary for proper boundary layer simulation and research needed to identify and compare wind tunnel environmental effects on boundary layer simulation.
4. Propose a simulation methodology based on results of the above.
5. Define a confirmation program to test recommended simulation methodology.

The Working Group had six meetings beginning in May 1984 and the final meeting was held October 1986.

The Working Group was divided into three committees; review (state-of-the-art), simulation methodology, and research. Sections 2.0, 3.0, and 4.0 of this report reflect the work of these respective committees. The scope of each committee's activity was:

#### Review (State-of-the-art)

- Current boundary layer simulation practices
- Conditions to achieve adequate simulation
- Identify Conflicting Criteria
- Conflict Resolution - Recommendations

#### Simulation Methodology

- Propose methods
- Assess potential adequacies and inadequacies
- Propose AGARD methodology
- Propose confirmation program

#### Research

- Review research of flow physics
- Propose needed theoretical and experimental research

The participants in AGARD FDP Working Group 09 were:

Y. Y. Chan	NAE, CANADA
R. Michel	ONERA-CERT, FRANCE
C. Armand	ONERA-MODANE, FRANCE
E. Stanewsky	DFVLR, GERMANY
J. Szodruch	MBB-BREMEN, GERMANY
G. P. Russo	U OF NAPLES, ITALY
J. L. Van Ingen	Delft U, NETHERLANDS
A. Elsenaar	NLR, NETHERLANDS
A. B. Haines	ARA, UNITED KINGDOM
A. G. T. Cross	BRITISH AEROSPACE, UNITED KINGDOM
E. Kraft	CALSPAN-AEDC, U. S.
J. L. Potter	VANDERBILT U, U. S.
J. Peterson	NASA LANGLEY, U. S.
Eli Reshotko	CASE WESTERN RESERVE U, U. S.
M. L. Laster	USAF/AEDC, U. S.-Chairman
C. Ciray	Metu, Turkey

The participants in the committees were:

State of Art-Review

C. Armand  
J. Szodruch  
A. Elsenaar-Chairman  
A. G. T. Cross  
J. L. Potter  
J. Peterson

Methodology

Y. Y. Chan  
C. Armand  
G. P. Russo  
A. Elsenaar  
A. B. Haines  
E. Reshotko-Chairman  
J. L. Potter

Research

R. Michel  
E. Stanewsky-Chairman  
J. Szodruch  
J. L Van Ingen  
A. G. T. Cross  
E. Kraft  
J. Peterson  
C. Ciray



## SECTION 2.0

### REVIEW OF BOUNDARY LAYER SIMULATION PROCEDURES

BY

REVIEW COMMITTEE

#### 2.1 INTRODUCTION

The scope of the working group is well described in Section 1. Its basic aim is to propose a simulation methodology that can be defined as "a scheme in which a wind tunnel testing procedure is defined together with the means for extrapolating the wind tunnel results to flight conditions" (E. Roshotko). In order to achieve this goal the activities of the group have been split into three committees: Review, Simulation Methodology and Research.

At the first working group meeting (Brussels, May 1984) nearly all participants presented a review largely based on their own observations. The larger part of these reviews was of particular relevance to the Review Committee. Also, a publication by J. L. Potter "Review of Requirements and Status of Simulation and Scaling of Transonic Flows" was distributed shortly after the meeting. As its title implies, this report more or less covers the assignment of the Review Committee. It was nevertheless decided at the first meeting of the committee to have a review by each committee member of the national situation. This resulted in a number of reviews, presented at the second meeting in Toronto, October 1984. These reviews range from a few pages to a very detailed report (attachment 1). This large variation in scope is mainly caused by some overlap with the "Brussel" presentations on the other hand.

In order to reach a state of convergence the committee divided their work subsequently along phenomenological lines (see table of contents) and the outcome of this survey is reflected in this report.

A few remarks have to be made at the end of this introduction. Firstly, simulation methodologies (either existing, or still to be developed) are closely coupled with the existing evidence on Reynolds number effects. It is not intended in this review to present a detailed account of observed Reynolds number effects\* but, as one will see, a part of this review is devoted to observations regarding Reynolds number effects.

Also, one should be well aware of the fact that it is intended in this section to review rather than to recommend particular simulation techniques. For that reason, the review is not a collection of recipes that can be applied faithfully in the wind tunnel. Instead, the reasoning behind a particular technique is described. Only a better understanding opens the way to improve upon existing practice.

Finally, there is a chance of overlap with the work of the other two committees. This overlap can be reduced by a rapid dispersal of the outcome of the committee among the other working group members. For this reason the work presented here had to be done under some pressure of time.

\*AGARD-FDP also assigned T.W. Binion, E. Stanewsky and A. Elsenaar to write an AGARDograph on Reynolds number effects.

## ATTACHMENT 1

## LIST OF NATIONAL REVIEWS

## U.S.A./Canada

reviewed by J.L. Potter  
"A summary of a 1984 survey of aerodynamicists  
regarding boundary layer tripping for  
simulating high Reynolds numbers"  
(WG09/RC/CR-01; 19 pages, 18 figures)

## United Kingdom

reviewed by A.G.T. Cross  
"High Reynolds Number Simulation"  
U.K. Industry Approach"  
(WG09/RC/CR-01; 19 pages, 18 figures)

## France

reviewed by C. Armand  
"Techniques Transition"  
(WG09/RC-AR-01; 2 pages with figures + list of references)

## Germany

reviewed by J. Szodruch  
referred is to the presentation in Brussels, May 1984, by the same author.  
"Transition fixing methods used by MBB,  
civil aircraft division"  
(WG09/RC/SZ-01; 17 pages with figures)

## Italy

reviewed by G.P. Russo  
"High Reynolds number simulation in Italy"  
(WG09/RC/RU-02; 1 1/2 page)

## The Netherlands

reviewed by A. Elsenaar  
"Some examples of current practice with respect to  
Reynolds number extrapolation; a NLR contribution"  
(WG09/RC/EL-07; 4 pages)

## SECTION 2.2 CONFIGURATIONAL ASPECTS

### SECTION 2.2.1 MISSILES, FUSELAGE AND SIMILAR BODIES

by

J. Leith Potter  
Consulting Engineer  
200 Sheffield Place  
Nashville, TN 37215, USA

#### 2.2.1.1 INTRODUCTION

The problem of simulating higher Reynolds numbers during wind tunnel testing of missiles and fuselages has not received as much attention as it has in regard to aircraft wings, particularly transport wings. That is because the configurations and sizes of typical missiles frequently allow testing at full-scale Reynolds numbers, and also, flows over missiles and fuselages are not usually as critically tailored to specific operating conditions as wing flows are. However, there are some important results arising from Reynolds number dependent flow phenomena that affect forces and moments on these bodies. (It has proved difficult to coin a descriptive term for the "not-wings" bodies discussed in this section. They will be rather loosely termed "fuselages" or "bodies" hereafter, and it should be noted that wings are discussed separately.)

The flows over these bodies may be of the type where only localized areas of boundary layer separation exist, such as may occur on boattails. There are also situations wherein large areas of separation are encountered, but the separation lines are not affected by Reynolds number, being essentially fixed by salient edges. Abrupt changes in body contour can produce this case; many base flows are examples. Thirdly, they may be of the type associated with a relatively slender body at high incidence with flow separation and strong vortical effects. The first two cases need little elaboration in regard to Reynolds number effects, but the latter is more complex; the leeside flow may be divided into several subcategories. The situations usually encountered by a slender, pointed body of revolution are:

- (1) Vortex-free flow --- this occurs at angles of attack,  $\alpha$ , less than roughly 5 to 20 degrees for most cases. Boundary layer transition usually moves forward on lee surfaces for increasing angles of attack. At the same time, it may move aft on windward surfaces when angles of attack are small, then forward as angles increase.
- (2) Symmetric vortex flow --- this occurs in lee flows for angles of attack in the range of perhaps 10 to 40 degrees.
- (3) Steady asymmetric vortex flow --- the range may be approximately 10 to 70 degrees; this is a subsonic or transonic phenomenon.
- (4) Unsteady wake-like flow --- arises when the body is above roughly 60-70 degrees.

The overlap in these angles of attack is much reduced when a particular shape is specified. Mach number affects the angle of attack ranges indicated above, as does nose apex angle, ratio of nose length to after body length, body fineness ratio and cross section. Examples may be found in the extensive review by Peake and Tobak (Ref. 1). When crossflow Mach number,  $M_c = M_{\infty} \sin \alpha$ , reaches the transonic level, say  $M_c < 0.8$ , shock waves form in the supercritical crossflow, tending to enforce flow symmetry and suppressing asymmetric loadings. A very thorough investigation of one ogive-cylinder configuration in subsonic flow has been reported by Lamont in Ref. 2 where marked Reynolds number influence is displayed.

The emphasis on vortical phenomena associated with high incidence should not be interpreted as disregard of scaling problems under other conditions. Boattails are one feature of afterbodies that may pose a Reynolds number simulation problem for experimenters. An exhaust plume or plumes may also be involved. Trips comprised of typical roughness elements and, sometimes, vortex generators may be relied on for establishing a turbulent boundary layer. It is important to bear in mind that increased Reynolds number,  $Re_{\infty}$ , actual or simulated, does not necessarily reduce overall drag coefficient,  $C_D$ . The net effect depends upon the losses and gains in expanding and recompressing regions of the flow, and  $C_D$  may increase or decrease with  $Re$  in different ranges of the latter parameter.

Upswept rear fuselages, such as one sees on C-130, C-141, Caribou, Buffalo, Breguet 941, and C5A aircraft, experience flow separation and present questions regarding high  $Re$  simulation. Practical design solutions that have been devised to stabilize the often unsteady vortical flows in such cases are use of strakes or sharp fuselage afterbody corners. Vortex generators may be used on either full-scale or wind tunnel models to improve flow conditions. The presence of wakes from wings, nacelles, undercarriage fairings, propellers, etc. may complicate these flows and perhaps override Reynolds number effects.

This section presents a review of current practices for coping with the simulation deficiency when tests of elongated bodies are conducted at Reynolds numbers appreciably lower than full-scale values. High subsonic, transonic, and low-supersonic ranges of Mach number are covered; hypersonic conditions are excluded although much of the discussion is also relevant to high Mach number flows. Because the flows considered here may or may not have supersonic regions and shock

waves, it is important to remain alert to the differences that shock-boundary layer interaction may impose upon any conclusions that are based upon shock-free flows. Drag and side force variations generated by changes in Reynolds number receive the principal attention. The working premise is that the higher Reynolds number simulation goal implies also that a turbulent boundary layer is desired and that it has to be established by artificial means.

#### 2.2.1.2 BODIES AT LOW INCIDENCE

A slender body at low angle of attack presents a simulation problem very similar in many respects to an airfoil. Boundary layer tripping to achieve a turbulent layer upstream of any afterbody shocks or flow separation normally will be done by conventional forward-tripping means, i.e., a band of grit or other roughness elements is placed near the nose. The trip typically is located 3-10 percent of body length from the stagnation point. A local Reynolds number ( $Re$ ) of  $10^5$  based on wetted length is consistent with Braslow's criteria (Ref. 3), which most often are the basis for sizing trip heights for subsonic-to-low supersonic Mach numbers. For higher Mach numbers, the methods proposed by Refs. 4-5 often are used. Obtaining an accurate estimate of full-scale drag coefficient and establishing turbulent flow ahead of a boattail, inlet, or fins may be the objectives. Experimental verification of tripping and persistence of a turbulent boundary layer downstream should not be neglected because of the possibility of relaminarization.

Aft tripping, i.e., tripping 10-to 15-percent of body length ahead of the station where a turbulent boundary layer of the least feasible thickness is wanted, is an alternative to forward tripping. A more extended discussion of this, with mention of advantages and disadvantages, is given in various reports, e.g., Ref. 6. While forward tripping and a consequent nearly all-turbulent boundary layer may be preferred for drag studies involving extrapolation of  $C_D$  to higher  $Re$ , aft tripping may be preferred for studies of inlet or afterbody flows where relative boundary layer thickness as well as the laminar or turbulent state can be a significant simulation parameter, cf. Ref. 7. In particularly sensitive cases, not only boundary layer state and relative thickness but also shape factor should be matched for complete simulation. However, it is important to always remember that variations in tunnel freestream conditions (calibration), interference from other model or support structures, and jet influence can be at least as critical as refinements in boundary layer simulation.

Local edge-of-boundary layer flow conditions should be used in calculating boundary layer thickness and the trip Reynolds number. These calculations also must be appropriate for the axisymmetric or 3-D flow of interest. Fortunately, the improvements in computational capabilities now make such calculations more accurate and less troublesome than they once were. In the context of this report, which is confined to current practice, there is little more to be said regarding bodies at low incidence to the freestream flow. The abundance of material on airfoils and wings adequately covers the general subject. (See Section 2.2.2 of this report and references given there.) Therefore, the remainder of this section mainly concerns special features of fuselage afterbody flows and vortical flows of the type generated by elongated bodies at larger angles of incidence.

#### 2.2.1.3 AFTERBODY TESTING

A general factor in afterbody testing that often accounts for the observed Reynolds number effect is the interaction between viscous and inviscid phenomena, i.e., the change in pressure distribution caused by thickened or thinned, separated or unseparated boundary layers. This is illustrated by Fig. 1, taken from Ref. 7. The drag coefficient in Fig. 1 is the pressure drag coefficient for the afterbody, based on body maximum cross section area.

Pozniak (Ref. 7), after reviewing a large number of reports, calls attention to the need to account for effects of unit Reynolds number on tunnel calibration and the significance of different Mach number regimes and boattail steepness combinations. He then states that -

At subsonic Mach numbers and in the absence of flow separations, significant but compensating pressure changes (on afterbodies) often are found, resulting in little effect on the afterbody pressure drag of complete afterbodies.

In the presence of flow separations, the effects of Reynolds number tend to be small when the location of the flow separation is fixed as a result of a sudden change in the boattail contour, but on afterbodies with smooth boattailing, changes in afterbody drag depend on the effects of Reynolds number on the location of the point of separation; conflicting factors are involved and the afterbody drag can increase, decrease, or remain unaffected by Reynolds number changes.

Figure 1 illustrates the danger of simply extrapolating a trend of drag coefficients in a limited range of Reynolds number. In general terms, it shows low afterbody drag coefficient at very high, flight  $Re$  where the thin boundary layer would have been attached over much or all of the boattail. This would allow recompression on the rear of the body, thereby lowering drag. At low  $Re$ , as may exist in wind tunnels, the thick boundary layer cannot penetrate the region of rising pressure and it separates. However, drag coefficients may be affected in opposing ways. When the separation occurs very early on the boattail, the overexpansion near the shoulder is eliminated and drag is relatively low. At intermediate  $Re$ , when the separation occurs downstream of the overexpansion but upstream of the recompression, there is higher drag. Often the opposing effects on drag arising from movement of separation or change in effective body contour brought about by changed displacement boundary layer thickness nearly cancel over a range of  $Re$ . When that occurs, afterbody drag coefficient is almost constant, cf. Ref. 8. (It will be noted that in this discussion a turbulent boundary layer is assumed.)

For Mach number ( $M_\infty$ ) below the critical, and boattails on which separation does not occur, effects of  $Re$  may be predicted on the basis of corresponding changes in displacement thickness, i.e., changes in effective body contour. In the same low Mach number regime, a smooth but steep boattail contour on which separation occurs can show the trends illustrated in Fig. 1. As already noted, effectively cancelled effects and nearly constant drag are possible in this case. Simulating higher  $Re$  by boundary layer modification may be misleading if it does not match the changes in state and relative thickness that would occur naturally.

With higher subsonic Mach number, when shocks occur on the boattail, the observed effect of increased  $Re$  has often been a decrease in drag-rise  $M_\infty$ . This can be due to increased expansion made possible by the thinner boundary layer on the upstream part of the boattail followed by a shock and separation downstream preventing or minimizing pressure recovery there. Factors to consider when planning a test are the probable effect of trips on shock location and the ability of the boundary layer to withstand the pressure gradients. The same interaction exists for boattails at supersonic speeds, and it is usual for the boattail drag to increase with  $Re$ . However, an opposite trend may be found for the same configuration at subsonic Mach numbers. This is illustrated in Fig. 2, from Ref. 7, where an effect of propulsive jets is also shown. Afterbody drag coefficient is here based on wing area.

#### 2.2.1.4 BODIES AT HIGH INCIDENCE

Present practice for simulating higher Reynolds numbers in wind tunnel testing is usually aimed at reproducing or clarifying the sequence of events so nicely illustrated in Ref. 2. Figures 3-4 are taken directly from that source and presented here for the convenience of the reader. The nomenclature,  $CNO$  and  $CYO$ , represent overall normal and side-force coefficients, respectively, and  $Re_D$  is based on body diameter and freestream flow. Reference 2 should be consulted for a full discussion, and it should be borne in mind that higher Mach numbers or differences in body shape can affect the results depicted in Figs. 3-4.

The underlying cause of the type of Reynolds number effects shown in Figs. 3-4 is explained by the character of the flow separation and lee-side vortices. Figures 5-6, also from Ref. 2, help to make this clear. Depending on the laminar, transitional, or fully turbulent nature of the boundary layer, Fig. 5 shows that the magnitude of influence of the vortical flow varies. In this example, laminar or turbulent separations produce roughly equal side force and normal force coefficients for angles of attack in the range of 50-60 degrees, and transitional boundary layer separations cause the least effect. One may speculate that the consistent asymmetry that causes the side force is not maintained under the more intense fluctuation of local velocities and transition locations typical of transitional regions. It should be noted that Lamont's pressure distributions suggest the presence of laminar separation bubbles just ahead of transition under the conditions he labels transitional. Such bubbles are, of course, familiar features of laminar flows in adverse pressure gradients on 2-D and 3-D shapes. The critical influence of minute model nose irregularities or flow asymmetries in determining direction of the forces generated by vortical separation is reflected in Fig. 7, from Ref. 2, which shows how side force direction depended on roll angle of the nominally axisymmetric body in a low-turbulence wind tunnel.

Thus, although there is no great difference between basic techniques for tripping boundary layers on wings or elongated bodies, the latter often will require that trips be positioned all downstream along the body ahead of the separation line to assure turbulent flow at higher angles of attack (if that is the predicted full-scale situation). It is obviously important that the boundary layer trips fulfill their function of creating a turbulent boundary layer without also artificially fixing the separation lines. If the latter occurs, the forces in the plane of symmetry as well as the side force may not accurately represent high Reynolds number conditions. Circumferential locations of separation, denoted by the angle  $O_s$ , have been shown to vary with body shape, longitudinal station, angle of attack, Mach and Reynolds number. Figures 8-10 from Refs. 1 and 12, illustrate this point. Subscript 1 denotes primary separation.

The simpler geometries of axisymmetric bodies represented in the figures illustrating the types of lee-side flows encountered in tests of bodies at higher incidences have not included typical aircraft fuselages. However, the latter produce essentially the same flow fields and their greater full-scale Reynolds numbers may be more troublesome insofar as simulation is concerned. An interesting collection of papers dealing with fuselage forebodies, strakes, and other airplane and missile flows is contained in Ref. 13. References 14-18 also include much of value in regard to vortical flows, but boundary layer tripping practices are not covered. In general, the techniques are somewhat standardized in basic approach and empirical in regard to trip sizing and placement. Therefore, details of particular testing applications are seldom described.

#### 2.2.1.5 MODES OF TRANSITION WITH SEPARATION

When the Reynolds number is low enough for the boundary layer to be laminar at the separation angle,  $O_s$ , the relatively unstable laminar free shear layer may undergo transition to turbulence, and the turbulent layer may reattach to the body surface. This condition is identified as "free shear layer reattachment." A short separation bubble is a feature of such a case, and the locus of points of reattachment forms a reattachment line of transitional flow. An elongated body at intermediate angles of attack will have 3-dimensional flow, so that a component of flow along attachment lines usually exists. This secondary flow, when unstable, provides the contamination that is referred to in discussions of transition in this type of boundary layer. Hence, "attachment line contamination" is a mode of transition that may be encountered. Another form of secondary flow is created by the 3-D boundary layer profile that typifies crossflow, regardless of

whether separation exists, and this provides a third destabilizing influence or "crossflow transition." Finally, there is the type of boundary layer transition that would be expected if the flow were axisymmetric and unseparated, i.e., "streamwise flow transition." There are critical Reynolds numbers corresponding to all of these modes of transition.

Poll (Refs. 19-21) has analyzed transition associated with cylindrical bodies at high incidence in subsonic flow. Other relevant references are given therein. Figures 11 a-b, from Ref. 20, show the regimes of  $\alpha$  and  $Re$  where the various modes of transition may be expected when testing a long, pointed body of circular cross section at angle of attack in a low-turbulence subsonic tunnel. In Fig. 11,  $Re$  is the freestream Reynolds number based on cylinder diameter. The letters L, B, and T indicate regimes of laminar, short-bubble separation with transition, and turbulent boundary layer flow, respectively, as determined by Lamont in his experiments (Ref. 2). Quantitative parameters defining the regions for these boundary layer states are discussed in Refs. 19-20, where Poll suggests that use of appropriate trips may lower the boundaries by factors of  $1/3$ . In Ref. 20 he has reviewed in depth the subject of transition on a cylindrical afterbody at incidence in subsonic flow, and includes an analysis of the effect on crossflow drag and normal force. Reference 21 concerns a detailed experimental study of the transition process on the windward surface of a yawed cylinder.

#### 2.2.1.6 BOUNDARY LAYER TRIPPING

The development of the boundary layer and its separation on typical pointed bodies at incidence has caused several investigators to place boundary layer trips along helical paths, as shown in Fig. 12 a-b, which is taken from Rao (Ref. 22). One can see in Fig. 8 that the angle  $\theta_g$ , measured circumferentially from the windward attachment line, is considerably greater near the noses of pointed bodies, so that if one wanted to trip just upstream of separation, a helical placement that approximately parallels the separation line would be appropriate. A question could be raised regarding the correct name of the trips in such cases. They are not tripping the boundary layer in the traditional sense; their primary role is to cause symmetrical separation. For that purpose, 2-D (e.g., wire) trips probably are more effective than 3-D (e.g., grit) trips. In some cases experimenters may want symmetrical separation, but, for example, Lamont's data show that asymmetrical separation and large side forces may also be associated with fully turbulent, high Reynolds number boundary layers. Therefore, suppressing asymmetric separation by locating trips so as to provide symmetrical salient edges is not truly simulating high Reynolds numbers.

The distinction between a boundary layer trip and a "separation holder" or "mini strake" is possibly illustrated in Fig. 13 a-b, from Ref. 23. There it will be noted that the "nose wire trips" had a diameter of 0.159 cm or 0.0626 in., whereas the "nose grit strip" was number 46 carborundum. The average grain diameter of the latter material is given as 0.014 in. by the Carborundum Company. Thus, the wire trip was 4.5 times higher than the grit. It seems likely that the 3-D grit strip was sufficient to cause boundary layer transition, (local flow conditions are not given) but it apparently had far less influence on the rolling moment variation with sideslip. Presumably this resulted because the wire "trip" acted more like a "separation fixer" or "mini strake."

When crossflow Mach number is roughly 0.5-0.8, asymmetrical separation usually will be prevented by symmetrically located crossflow shock waves and shock-induced separation. This is illustrated in Fig. 14. When it is necessary to trip the boundary layer for simulating higher Reynolds numbers in transonic and supersonic testing, tripping should be accomplished sufficiently upstream of the crossflow shock location to avoid interaction between trips and shocks. Current practice for wings or airfoils is to make this distance at least 10-15 percent of chord. For bodies of revolution this would correspond to about 40 percent of body radius.

#### 2.2.1.7 CONCLUDING REMARKS

Emphasis has been placed on a review of flow conditions that are important to scaling and simulation for fuselage and missile bodies. It is pointed out that care must be taken to plan boundary layer tripping so as to accomplish the desired objective of simulating higher Reynolds numbers without also altering the flow field external to the boundary layer in ways that do not follow from boundary layer transition. This latter pitfall is encountered when tripping so thickens the boundary layer that relative thickness at the critical station on the body is much greater than the full-scale value. For example, this may happen at inlets, boattails, or bases of bodies. Another manifestation of this error is found when trips also serve to locate and stabilize separation and associated vortices. This is a danger when testing bodies at higher angles of incidence.

Boundary layer tripping with the aim to simulate higher Reynolds numbers in testing fuselages and missiles normally has been done with a narrow band of sparsely distributed grit at a station 3-10 percent of body length downstream of the nose. The trip band typically is on the order of 0.05 inches or 0.13 cm wide and only 3-10 percent of its area is occupied by particles of grit, microspheres, or other roughness elements. Sometimes the axial location is determined by the  $Re = 10^5$  criterion recommended in Ref. 3 for placing trips. Some experimenters use a roughness height of 80 percent of that given by Ref. 3 for 2-D bodies, considering that their 3-D or axisymmetric models have thinner boundary layers than 2-D bodies under the same flow conditions.

In view of the features of flows over bodies at high angles of attack, as reviewed here, it appears that a simple circumferential trip near the nose of a body often will not suffice. When high angles of attack are involved, a longitudinal trip along the windward attachment line or a pair of trips along the body will be needed if a turbulent boundary layer is to be obtained ahead of separation and/or shock interaction.

It will no doubt be noted that free flight may involve more varied vehicle motion than the static wind tunnel cases represented in this discussion. Thus, the spatial asymmetries in separation, transition and vortex shedding may change with time at varying rates in flight. This will not eliminate the phenomena illustrated by the wind tunnel data, and simulation of higher Reynolds numbers would be approached in the same way.

The complexity of this problem justifies careful planning and extra time in the wind tunnel to better understand the simulation requirements of a particular test.

#### 2.2.1.8 REFERENCES

1. Peake, David J. and Tobak, Murray. "Three-dimensional interactions and vortical flows with emphasis on high speeds." NASA TM-81169, March 1980, (also Agardograph 252, July 1980).
2. Lamont, P. J., "Pressures around an inclined ogive cylinder with laminar, transitional, or turbulent separation." AIAA Journal, 20, Nov. 1982, pp. 1492-1499.
3. Braslow, Albert L., "Effect of distributed granular-type roughness on boundary-layer transition at supersonic speeds with and without surface cooling." NACA RML 58A17, Mar. 1958. (Also see AGARD Rept. 254, April 1960, and NASA TN D-3579, Sept. 1966.)
4. Potter, J. Leith and Whitfield, Jack D. "Effects of slight nose bluntness and roughness on boundary layer transition in supersonic flows." Journal of Fluid Mechanics, 12, Pt. 4, April 1962, pp. 501-535. (Also see AEDC TR-60-5, March 1960.)
5. Van Driest, E. R. and Blumer, C. B. "Boundary layer transition at supersonic speeds: roughness effects with heat transfer." AIAA Journal, 6, April 1968, pp. 603-607. (Also see Journal of the Aerospace Sciences, 29, August 1962, pp. 909-916.
6. Potter, J. Leith. "Review of requirements and status of simulation and scaling of transonic, viscous flows." AEDC-TR-84-23, Sept. 1984.
7. Pozniak, O. M. "A Review of the effect of Reynolds number on afterbody drag." Aircraft Research Assoc., Ltd. Report 56, May 1980.
8. Reubush, David E. "The effect of Reynolds number on boattail drag." AIAA Journal of Aircraft, 13, May 1976, pp. 334-337.
9. Wilcox, F. A. and Chamberlin, R. "Reynolds number effects on boattail drag of exhaust nozzles from wind tunnel and flight tests." AGARD CP-150, March 1975 or NASA TM X-71548, Sept. 1974.
10. Price, E. A. "Afterbody drag investigation of a twin-nozzle fighter-type model at Mach numbers from 0.6 to 1.5." AEDC-TR-72-87, Aug. 1972.
11. Price, E. A. "Afterbody aerodynamic characteristics and support system interference on a twin-jet fighter-type aircraft model at Mach numbers from 0.6 to 1.5. AEDC-TR-74-13, April 1974.
12. Nielsen, Jack N. "Nonlinear flow phenomena at high angles of attack and recent advances in their prediction." In AGARD-CP-336, Sept. 1982.
13. "High Angle of Attack Aerodynamics." AGARD-CP-247, Jan. 1979.
14. "Three dimensional and unsteady separation at high Reynolds numbers." AGARD-LS-94, Feb. 1978.
15. "Flow Separation." AGARD-CP-168, Nov. 1975.
16. "Aerodynamics of vortical type flows in three dimensions." AGARD-CP-342, July 1983.
17. "Missile Aerodynamics." AGARD-LS-98, Feb. 1979.
18. "Missile Aerodynamics." AGARD-CP-336, Sept. 1982.
19. Poll, D. I. A. "Some effects of boundary layer transition on slender axisymmetric bodies at incidence in incompressible flow." In AGARD-CP-336, Sept. 1982.
20. Poll, D. I. A. "On the effects of boundary layer transition on a cylindrical afterbody at incidence in low-speed flow." To be published in The Aeronautical Journal of the Royal Aeronautical Society, 1985.
21. Poll, D. I. A. "Some observations of the transition process on the windward face of a long yawed cylinder." Journal of Fluid Mechanics, 150, 1985, pp. 329-356.
22. Rao, D. M. "Vortical flow management for improved configuration aerodynamics - recent experiences." In AGARD-CP-342, July 1983.
23. Erickson, Gary E. and Gilbert, William P. "Experimental investigation of forebody and wing leading-edge vortex interactions at high angles of attack." In AGARD-CP-342, July 1983.



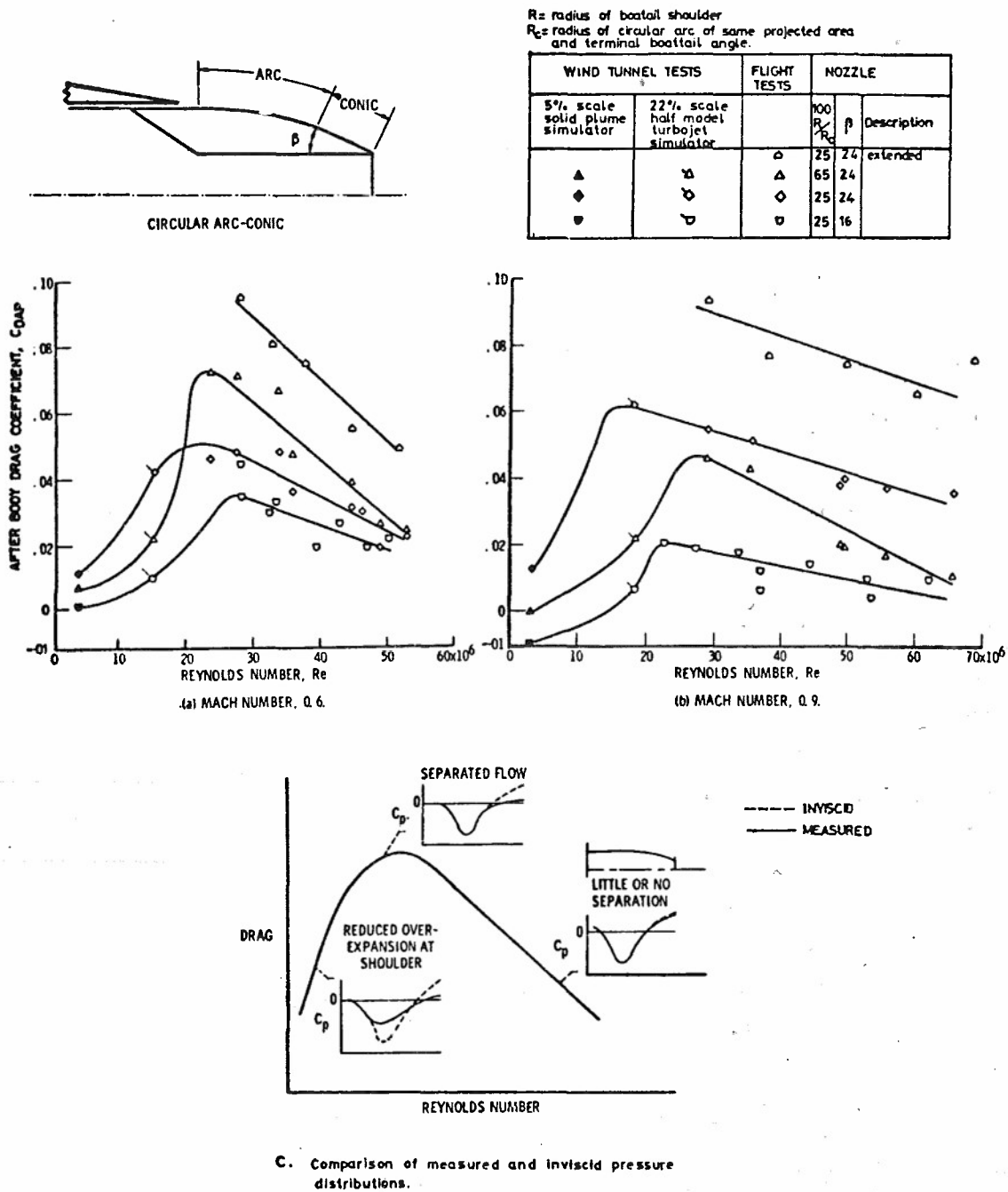


Fig. 1 Example of effects of Reynolds number on boattail drag.  
(From Ref. 7 where data are credited to Ref. 9 of this paper.)

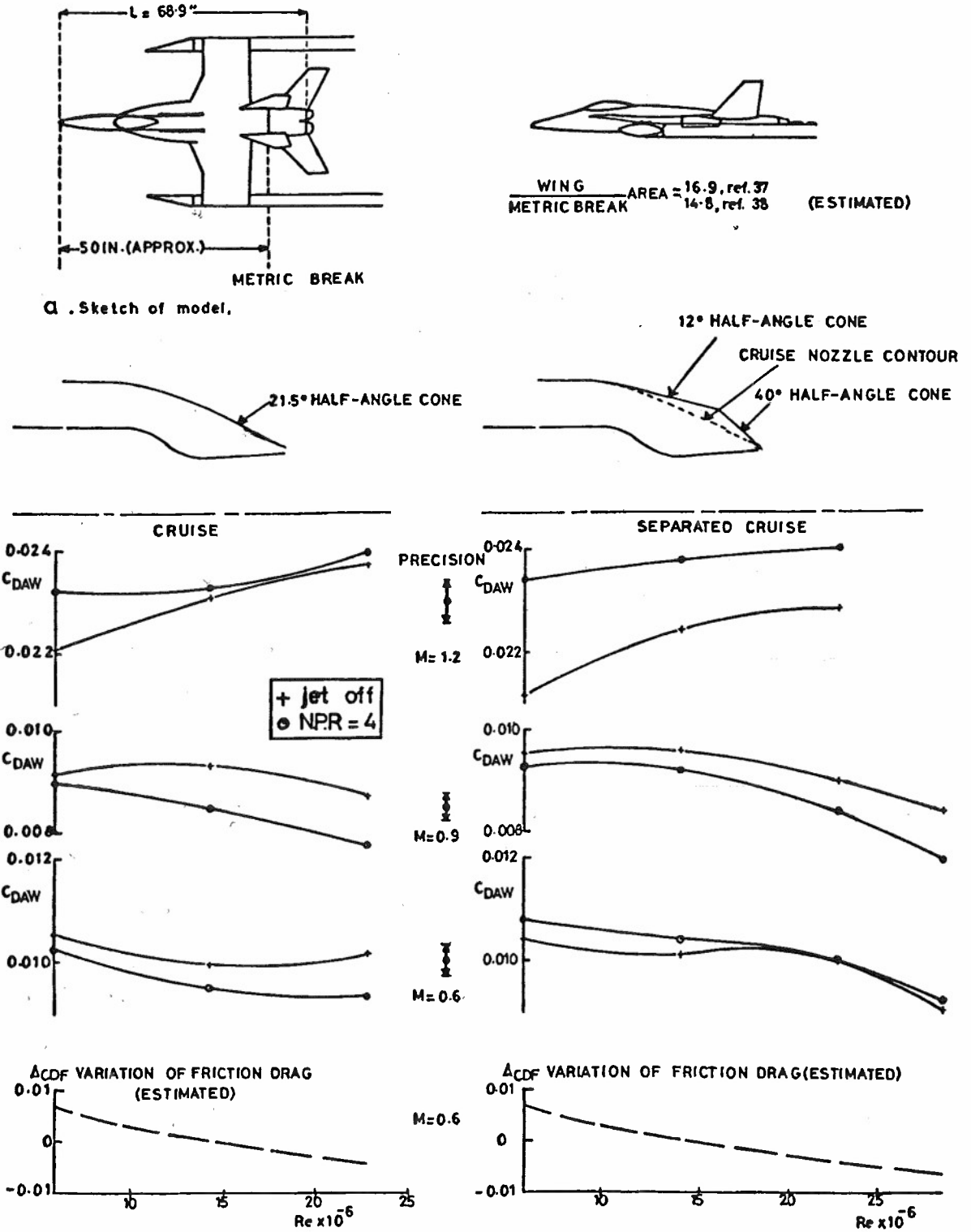


Fig. 2 A comparison of Mach and Reynolds number effects on afterbody drag, with and without propulsion jets.

(From Ref. 7 where data are credited to Refs. 10-11 of this paper.)

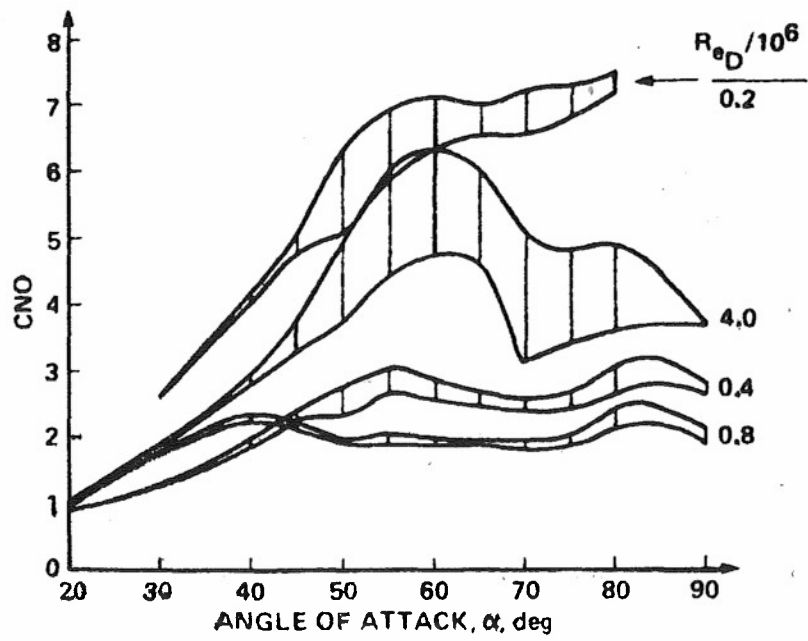


Fig. 3 Example of variation of normal force with Reynolds number and angle of attack.  
(From Ref. 2.)

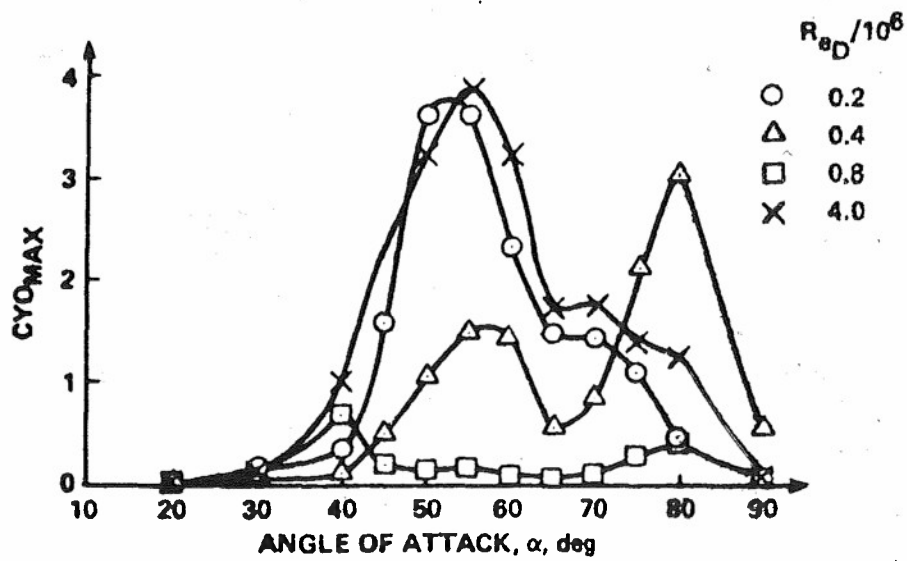


Fig. 4 Example of variation of maximum side force with Reynolds number and angle of attack.  
(From Ref. 2.)

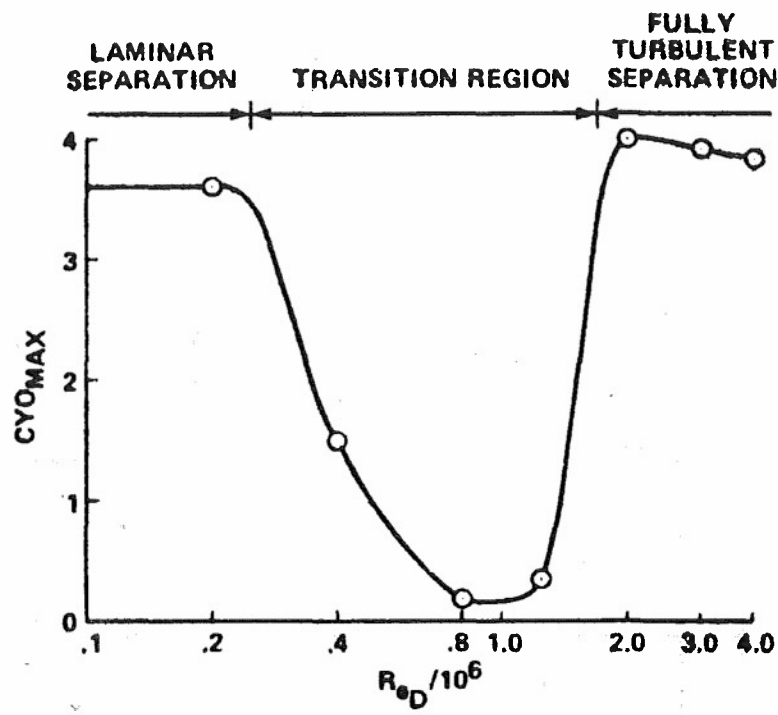


Fig. 5 Example of Reynolds number effect on variation of maximum side force on an ogive cylinder at constant angle of attack. (From Ref. 2.)

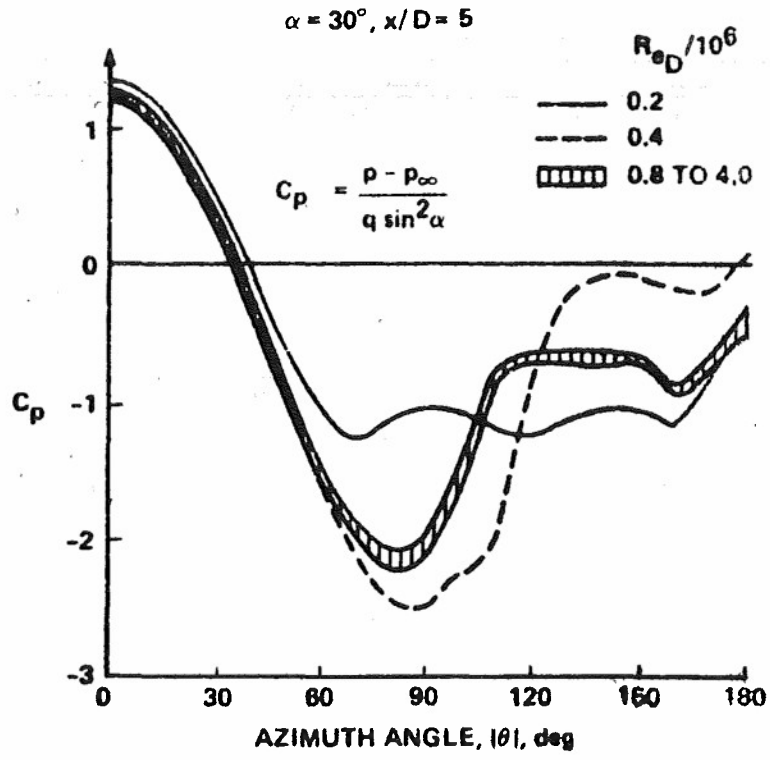


Fig. 6 Example of pressure distributions around an inclined cylinder. (From Ref. 2.)

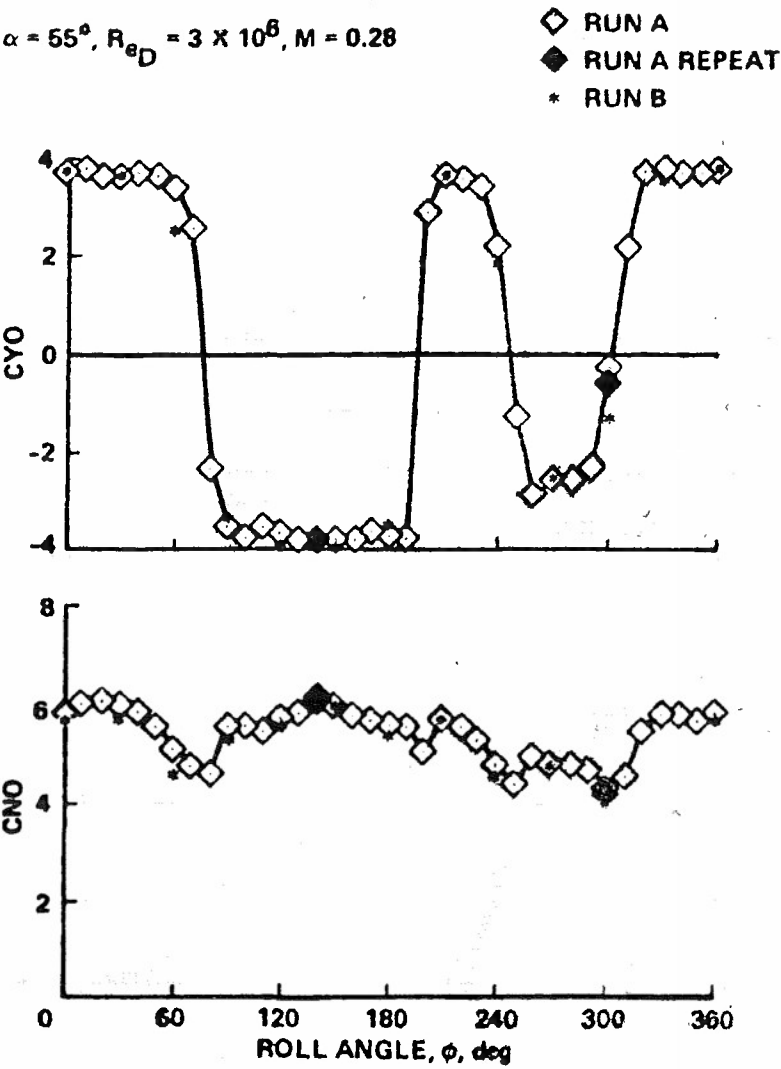


Fig. 7 Illustration of sensitivity of asymmetrical loads to roll angle.  
(From Ref. 2.)

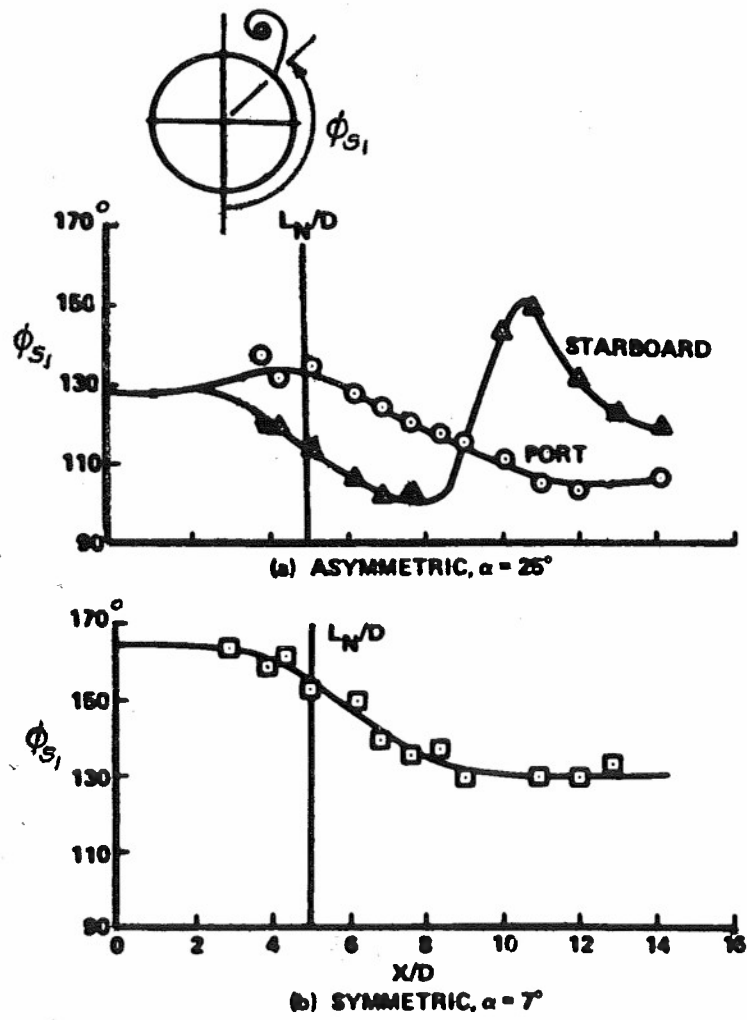


Fig. 8 Example of separation locations along a cone-cylinder.  
(Adapted from Ref. 1.)

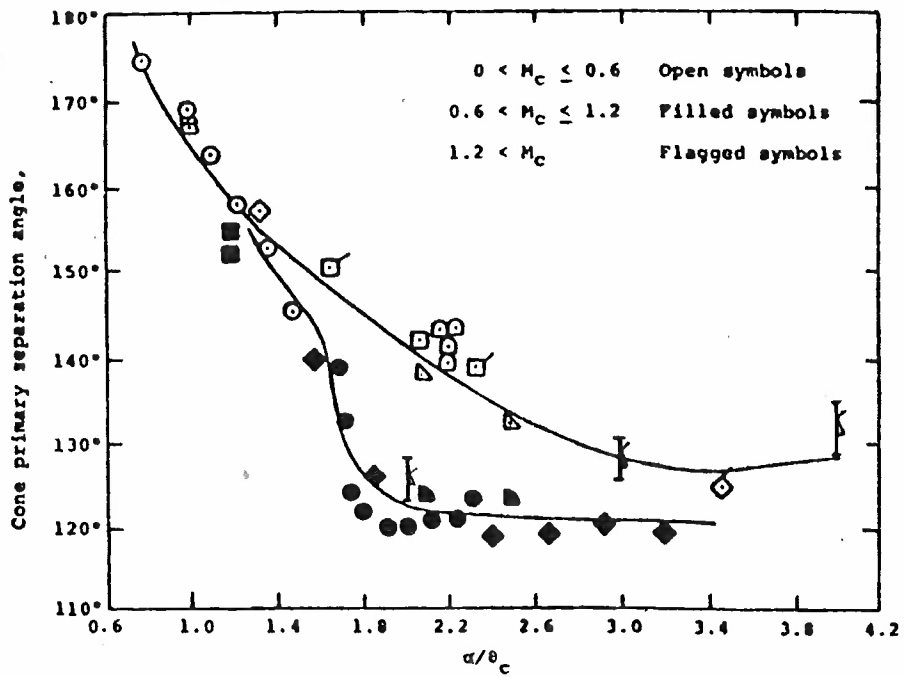


Fig. 9 Correlation of primary separation locations on a cone as a function of relative angle of attack.  
(From Ref. 12.)

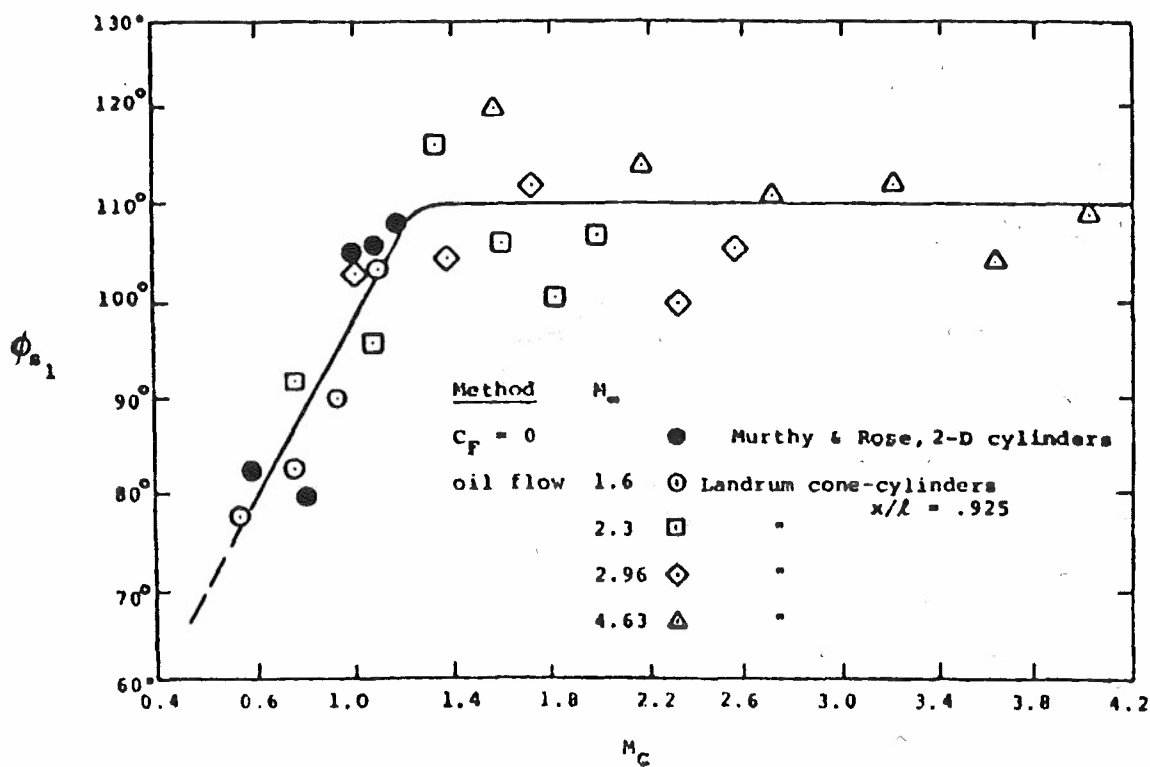
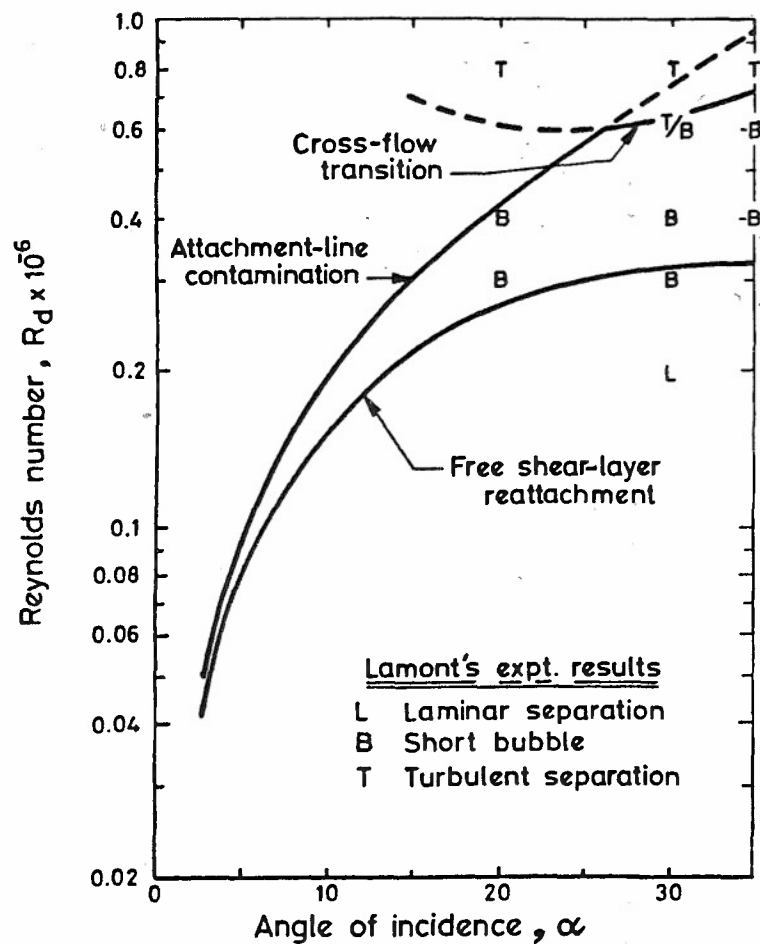
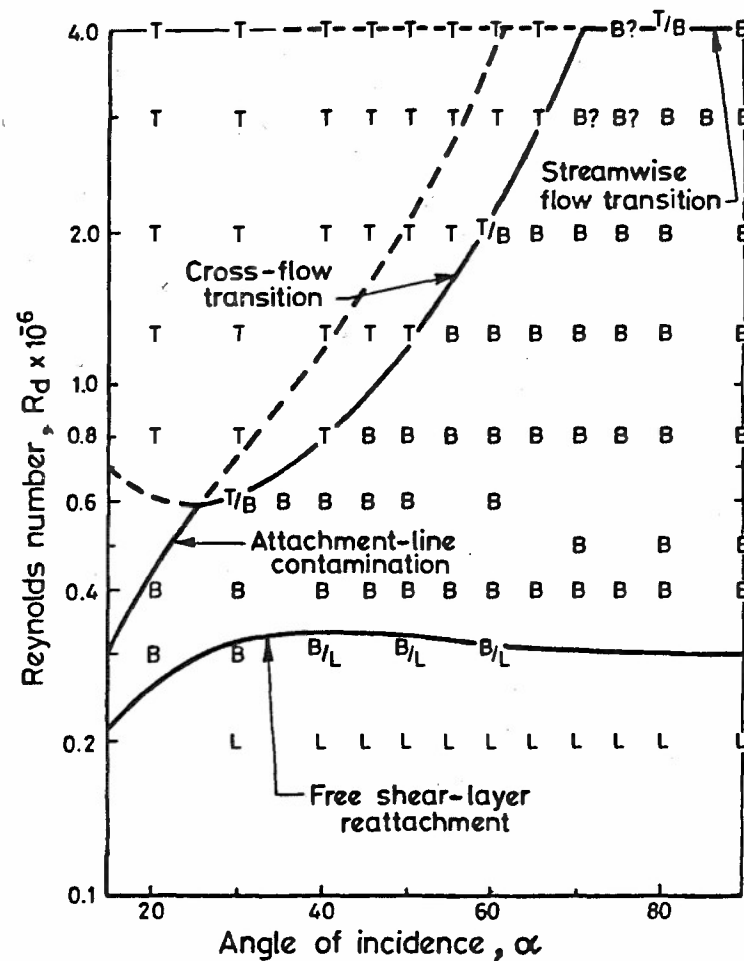


Fig. 10 Correlation of primary separation locations on 2-D cylinders and cylindrical afterbodies of cone-cylinders.  
(From Ref. 12.)





(a) Incidences up to  $35^\circ$



(b) Incidences from  $20^\circ$  to  $90^\circ$

Fig. 11 Illustration of the types of transition on cylindrical afterbodies and a comparison of predicted and measured results.  
(From Ref. 19.)

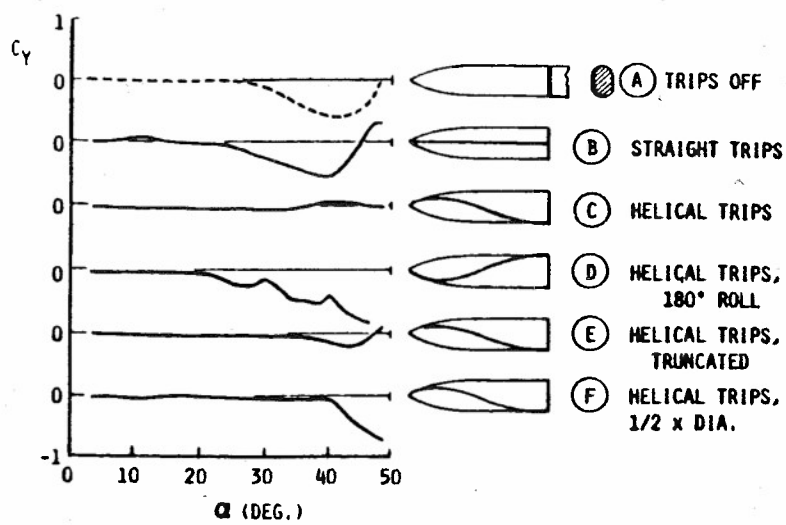
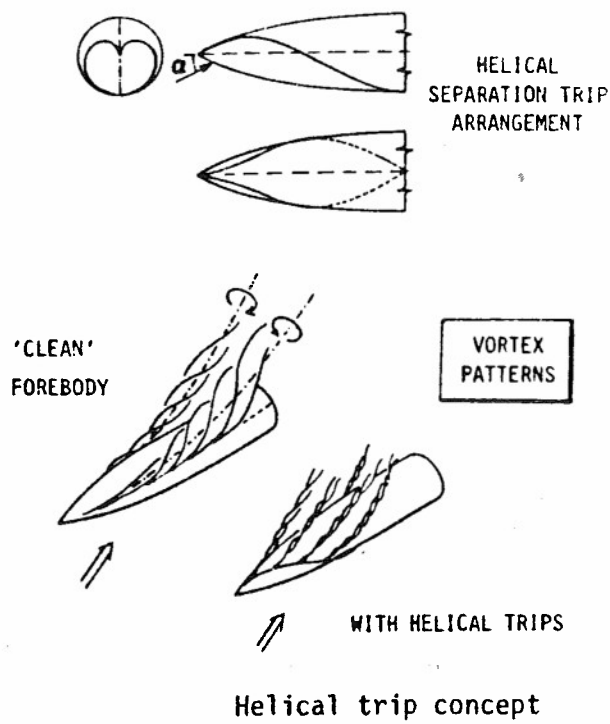
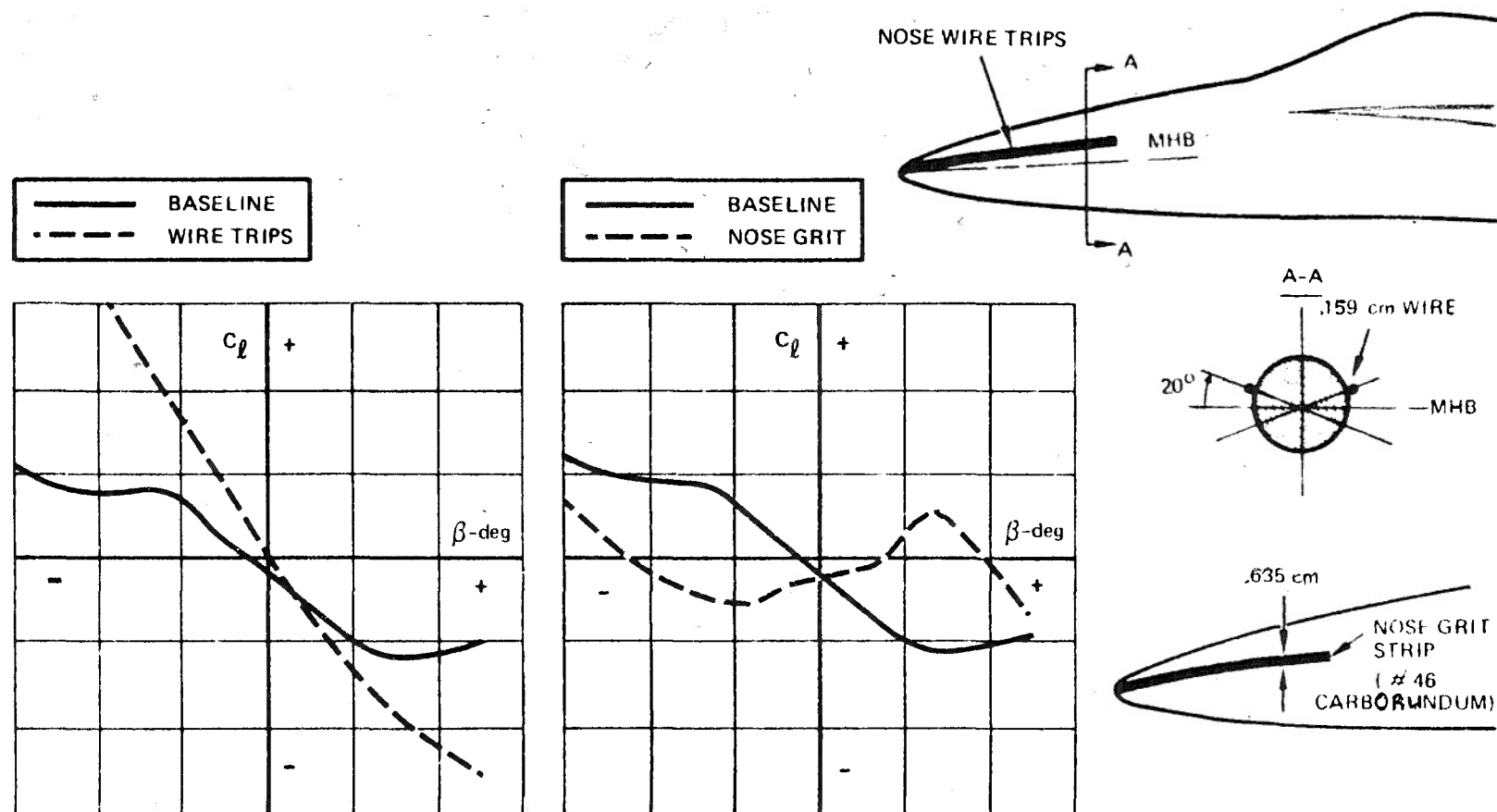


Fig. 12 Example of the use of helical trips.  
(From Ref. 22.)



EFFECTS OF NOSE GRIT AND NOSE WIRE TRIPS ON ROLLING MOMENT VARIATION  
WITH SIDESLIP;  $\delta_n = 25$  DEGREES ;  $Re_{\bar{c}} = 1.6 (10^6)$ ;  $\alpha = 35$  DEGREES.

Fig. 13 Comparison of results obtained with a band of grit and a much thicker wire.  
(From Ref. 23.)

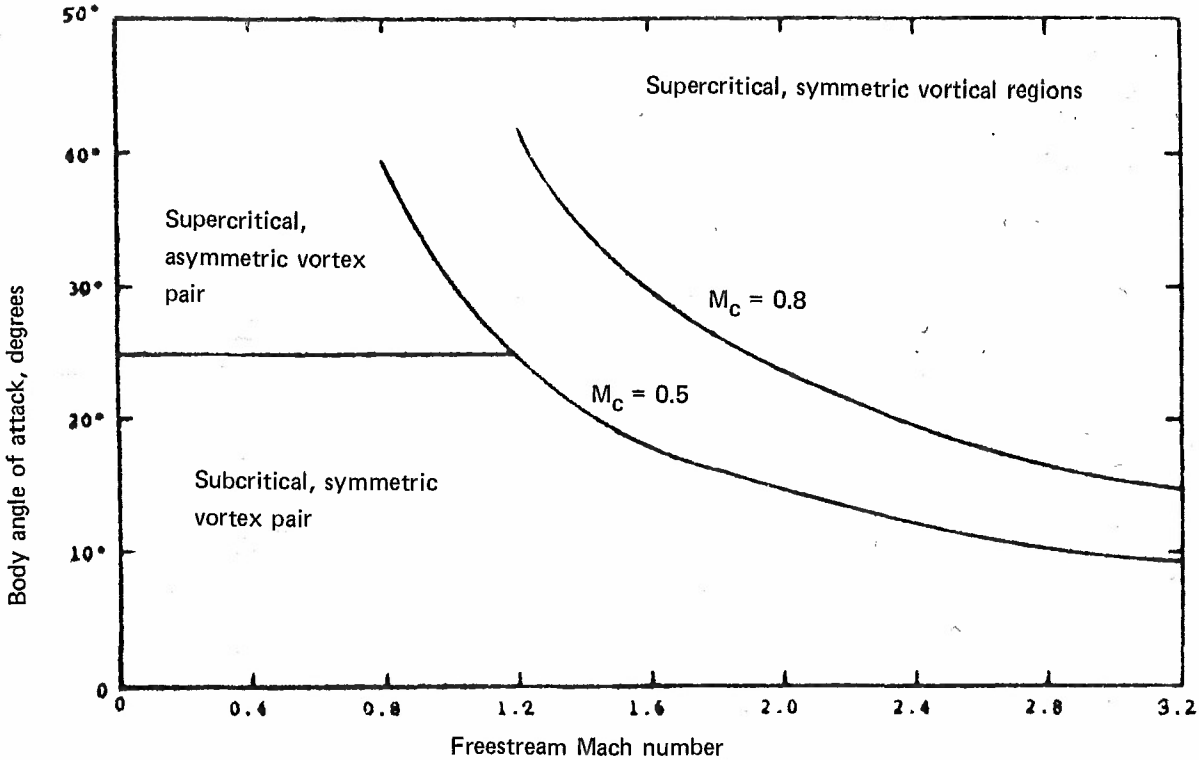


Fig. 14 Approximate boundaries for various types of vortices.  
(From Ref. 12.)

## SECTION 2.2.2 HIGH-ASPECT-RATIO WINGS

by

John B. Peterson, Jr  
NASA Langley Research Center  
MS 294  
Hampton, VA 23665, USA

### 2.2.2.1- INTRODUCTION

High-aspect-ratio aircraft include most transport aircraft such as commercial and military transports, business aircraft, and cargo aircraft. Generally, these types of aircraft are designed to cruise over a narrow range of lift coefficients and Mach numbers in the performance of their mission. Emphasis is therefore placed on the cruise performance of transport aircraft and every effort is made to obtain accurate wind-tunnel data to use as a basis for prediction of full-scale cruise performance. However, off-cruise performance is also important and methods have been developed for extrapolating wind-tunnel data on buffet and flutter at transonic speeds.

Transport-type aircraft have been tested extensively in various wind tunnels around the world and many different test techniques have been developed to simulate higher Reynolds numbers. Methods developed for one tunnel may not be applicable to another tunnel because of differences in size, Reynolds number capability, running time, test objectives, etc. Many of the methods of boundary-layer control developed in two-dimensional airfoil testing can be applied in tests of transport configurations, but sometimes the three-dimensional flow fields that develop on transport aircraft can make application of the two-dimensional methods difficult or impossible.

The following discussion is intended to be a representative, but not exhaustive, survey of the various methods of high Reynolds number simulation in the testing of high-aspect-ratio aircraft.

### 2.2.2.2- SUBSONIC MINIMUM DRAG

In wind-tunnel tests of transport-type models, transition is generally fixed near the leading edge in subsonic tests. This insures that the boundary layer is turbulent on the model in areas where it would be turbulent on the full-scale aircraft. In some cases, tests are made with free transition, though this is not the generally accepted procedure. In such cases, instabilities, such as crossflow in the boundary layer or adverse pressure gradients on the model, are depended on to trip the boundary layer.

In any case, it is important to know where transition occurs on the model so that skin-friction drag on the wind-tunnel model can be calculated. The transition position can be determined by a flow visualization method such as the oil-flow or chemical-sublimation methods described in section 2.3.2 of this report. Often, flow visualization is used when boundary-layer trips are used to make sure that the trips are effective. Sometimes, the trips are sized and applied to the model using standard procedures which have been shown to satisfactorily fix transition in previous tests and, therefore, flow visualization is not used.

Once the transition position is known, the drag measured in the wind tunnel can be extrapolated to full scale by calculating the difference in skin friction on the model and the skin friction in flight. Usually, the difference in skin friction is determined from the theoretical skin-friction laws and shape factors, determined empirically, or determined from the velocity distribution over the model.

Generally, it is assumed that the boundary layer on the full-scale aircraft is turbulent at the leading edge. This is a conservative assumption, since the extrapolated drag is highest under this assumption. There are several ways that the boundary layer might be tripped at the leading edge of the full-scale airplane. The roughness of practical construction and/or dirt and insects accumulated on the leading edges of the wing can be large enough to cause transition (refs. 1 and 2). Also, at high Reynolds numbers, the boundary layer on a swept wing can be tripped by crossflow instabilities in the boundary layer, or the attachment line boundary layer can have a high enough Reynolds number to support turbulent contamination along the span of the wing, which causes the entire wing boundary layer to be turbulent. At full-scale Reynolds number, the fuselage Reynolds number is usually high enough so that the natural transition position is a small percentage of the fuselage length and, therefore, the fuselage boundary layer can be assumed to be fully turbulent.

### 2.2.2.3- COMPRESSIBILITY DRAG

At transonic speeds, the shock boundary-layer interaction and position of the shock on the upper surface of the airfoil can be Reynolds-number sensitive. Therefore, considerable attention has been paid to this problem.

It is important that the boundary layer at the shock location on the model be turbulent, if that is the case at high Reynolds numbers, because the interaction between the shock wave and the boundary layer differs considerably for a laminar boundary layer as compared to a turbulent boundary layer. Therefore, at low Reynolds numbers, transition is usually fixed with a boundary-layer trip.

Some researchers fix transition near the leading edge for transonic tests. The data then must be corrected for the effect of Reynolds number by theory. For cases where separation does not occur at low Reynolds numbers, this method seems to work quite well (ref. 3).

Another method of obtaining data at low Reynolds numbers, on airfoils that tend to separate over the aft part of the airfoil, is to thicken the trailing edge of the airfoil so that the pressure gradients are reduced (see ref. 4). The data are then corrected with the help of theory for the difference in geometry and corrected to full-scale Reynolds numbers.

In 1968, Blackwell (ref. 5) suggested that transition should be fixed further aft than the normal position near the leading edge of the airfoil so that the relative thickness of the boundary layer at or near the trailing edge of the airfoil would match that expected in flight. His data showed that when the transition is fixed just ahead of the shock wave so that the boundary-layer thickness is matched at the trailing edge of the wing, the shock wave will then be located at the same  $x/c$  on the wind-tunnel model as it is in full scale. This procedure is used by many researchers today with some other researchers matching the relative boundary-layer thickness at the shock. It is important that the trip be placed ahead of both the position of natural transition and the position of the shock on the airfoil. These positions are determined by sublimation visualization and/or by oil-flow visualization tests in the wind tunnel (see Section 2.3.2). The trip is then generally located about 0.1 chord ahead of the shock position on the wing (ref. 6). If the trip is located too close to the shock position, laminar boundary-layer separation could occur ahead of the trip. If the Reynolds number of the test is not too small, matching the relative thickness of the boundary layer at the trailing edge of the airfoil is possible with a trip that is 0.1 chord, or more, ahead of the shock position. However, if the shock is far forward, which can occur near the fuselage and tips of the wing, or if the test Reynolds number is quite small in comparison to the flight Reynolds number, it may not be possible to fix the transition far enough aft to match the relative boundary-layer thickness at the trailing edge.

Haines (ref. 6) has extended Blackwell's procedure of aft tripping to cover a large range of Mach numbers and lift coefficients. He has shown that the boundary-layer trip should be located in different positions on the airfoil depending on the  $C_L$  and Mach number of the test. In general, in tests with an advanced wing design, at least two and possibly three trip locations should be used. Figure 1 shows, in a qualitative way, the regions where a forward-, middle-, and aft-located trip should be used. The exact locations of the regions are dependent upon the airfoil characteristics and have to be developed from examination of the measured pressures on the airfoil or information from oil-flow visualization backed by an interpretation of drag data. The forward trip is located about 7 or 8 percent of the chord so as not to interfere with the leading-edge flow, which can be quite sensitive to small surface deviations. The forward trip should be downstream of the suction peak at the leading edge and downstream of the immediate adverse pressure gradient behind this peak. The middle and aft trips are located ahead of the shock by about 10 to 15 percent of the chord. Haines has found that, as the angle of attack is increased at high Mach numbers, the forward movement of the shock tends to be delayed by a "hesitation" when the shock is about 0.1 to 0.15 chord aft of the trip. This anomalous behavior is an indication that a trip should not be located too close to the shock wave.

A description of the various regions of application of the forward, middle, and aft trips is given at the bottom of figure 1. A very complete and thorough description of this method of simulating high Reynolds numbers is given by Haines in reference 6.

#### 2.2.2.4- DRAG DUE TO LIFT

If the test Reynolds number is relatively low, the drag due to lift obtained in the wind tunnel may have to be corrected to full-scale Reynolds numbers. Some researchers use the measured or theoretical span-load distribution and calculate the drag due to lift theoretically. The measured data for the drag due to lift is then corrected to the theoretical value.

In another method proposed by Henderson (ref. 7), the leading-edge suction is related to the Reynolds number based on the leading-edge radius (see figure 2). The leading-edge suction,  $s$ , shown in figure 2, is the percentage of the theoretical suction force developed by the leading edge of the wing. An illustration of how the suction parameter,  $s$ , is obtained from experimental data is shown in figure 3. The curve of zero-percent suction is obtained from  $\Delta C_D = C_L \tan \alpha$ , and the curve of 100-percent suction is obtained from the spanwise lift distribution on the wing, assuming fully attached flow at the leading edge.

From figure 2, the suction parameter,  $s$ , can be determined for the wind-tunnel model and for the full-scale airplane. Then, by calculating the differences in the drag due to lift for the wind-tunnel model and for the full-scale airplane from the suction parameter and the theoretical drag due to lift, the wind-tunnel results for drag due to lift can be corrected for the effect of Reynolds number.

Other similar methods for correcting the drag due to lift measured in the wind tunnel are given in references 8, 9, and 10. All methods for correcting the drag due to lift for the effect of changes in Reynolds number must be used with caution; however, since they generally predict increases in performance for the full-scale airplane compared to the wind-tunnel results, these methods have been known to give overly optimistic results.

#### 2.2.2.5- FLUTTER AND BUFFET TESTS

Flutter tests are generally conducted at low lift coefficients where adverse pressure gradients are small and, therefore, the boundary layer will generally remain attached. Since Reynolds number effects are small on these types of flow, the Reynolds number effects on flutter boundaries are expected to be small (see ref. 11). No special procedures are used to simulate full-scale Reynolds numbers in the wind tunnel other than tripping the boundary layer near the leading edge to insure that the boundary layer is turbulent over the surfaces. If there are shocks in the flow, aft tripping could be used to make the relative thickness of the boundary layer at the trailing edge the same as in full-scale flow, similar to the procedure for wings near the drag-rise Mach number.

Buffet tests, on the other hand, are conducted at high angles of attack. There are significant areas of adverse pressure gradient and the boundary layer generally separates. In general, the effect of Reynolds number on the buffet boundary depends on the configuration of the wing. For configurations with sharp, highly-swept leading edges, the Reynolds number effects are small, since the separation is forced at the leading edge at all Reynolds numbers. For rounded leading edge, unswept wings, Reynolds number can have a considerable effect on the angle of attack for buffet onset, as shown in figure 4 from reference 12. In this figure, there is no uniform trend with Reynolds number and, therefore, extrapolation of low Reynolds number data to full scale is difficult. However, transition was not fixed for these tests and, therefore, the variations shown in figure 4 may be a result of changes in transition position with changes in Reynolds number.

There are other cases where wind-tunnel and full-scale buffet boundaries agreed well on configurations with rounded leading edges. One such case is shown in figure 5 from reference 13. The model was tested at a Reynolds number of  $0.9$  to  $1.3 \times 10^6$  and the airplane was flown at Reynolds numbers of  $20$  to  $28 \times 10^6$ . In this case, the model was constructed as a flutter model and the surfaces were very rough. Transition was probably caused near the leading edge by this roughness. Another case is shown in figure 6 from reference 14, which shows the buffet boundary for the L-1011 transport obtained from wind-tunnel data compared to flight values. Transition was fixed near the leading edge for these tests, but the author states that other tests with the transition trip located further aft showed essentially the same results indicating that this particular configuration would probably be relatively insensitive to Reynolds number.

Elsenaar, in reference 3, shows the effect of Reynolds number on the maximum lift coefficient of a transport configuration at transonic speeds. The data in figure 7 are shown at various spanwise stations for transition free and transition fixed at 5-percent chord. This figure shows that the fixed transition data are consistent at all of the spanwise stations over the Reynolds number range tested, increasing the confidence that the data can be extrapolated to larger Reynolds numbers.

Many aircraft manufacturers use a combination of theory and empirical methods to predict buffet boundaries on transport aircraft. Unfortunately, these methods are usually proprietary to the manufacturer. The procedure used at the Douglas Aircraft company is outlined in reference 15. It uses the calculated shock upstream Mach number and the shock position as a fraction of the chord to determine if the airfoil is in a buffet condition. The regions of buffet are proprietary, however, and are not given.

#### 2.2.2.6- LOADS

Extrapolation of the pressures and loads measured on the wing of a transport aircraft to full-scale Reynolds numbers is important in the design of the structure of transport aircraft. One method was developed by Cahill and Conner (ref. 16) and Khan and Cahill (ref. 17) to predict the pressure distribution on a wing at full-scale Reynolds number using low Reynolds number wind-tunnel data.

They plot a curve of  $C_{p,te}$  against the parameter  $K$  where

$$K = \frac{(M_e^2 - 1)}{(\gamma + 1) \sqrt{\frac{C_f}{2}} M_e^2}$$

and  $M_e$  is the normal Mach number and  $C_f$  is the skin friction just upstream of the shock. The curve which resembles that shown in figure 8 is developed at a constant Reynolds number using data from the wind tunnel. Khan and Cahill have found that the shape of this curve is constant and only shifts by certain increments of  $\Delta K$  and  $\Delta C_{p,te}$  with changes in Reynolds number. They have also found that the shifts in  $K$  and  $C_{p,te}$  are a universal function of Reynolds number so that the curve can be constructed for full-scale Reynolds number from the data obtained in the wind tunnel.



Also, a curve of shock position against trailing-edge pressure at a constant Mach number and angle of attack is developed using data from the wind tunnel with transition fixed at various locations, various Reynolds numbers, and even vortex generator data, if it is available. Then, with this curve and the curve of  $K$  versus  $C_{p,te}$  at full-scale Reynolds number, the location of the shocks on the airfoil and the  $C_p$  at the trailing edge can be determined. This information together with the shape of the pressure rise through the shock (given in ref. 17) and the stipulation that the normal Mach number behind the shock is one, allows development of the entire pressure distribution over the airfoil at full-scale Reynolds number. The procedure does not apply to cases where the separation occurs at the shock and is restricted to moderate angles of attack. In cases where separation occurs at the shock, scale effects are expected to be small, if there is a turbulent boundary layer at the shock location.

#### 2.2.2.7- CONCLUDING REMARKS

This review of the methods of simulating high Reynolds numbers on high-aspect-ratio wings leads to the following comments.

Many different test techniques have been developed in various wind tunnels around the world to simulate higher Reynolds numbers on high-aspect-ratio wings, but methods developed for one tunnel may not be applicable to another tunnel because of differences in wind tunnels such as size, Reynolds number capability, run time, test objectives, etc.

For subsonic tests, transition is usually fixed with a boundary layer trip near the leading edge. If transition is not fixed, then a boundary layer visualization method, such as sublimation, is used to determine the location of transition. Even if transition is fixed, visualization is often used to determine the effectiveness of the trip.

For transonic tests, it is important that the boundary layer be turbulent at the shock location, if that is the case at high Reynolds numbers, because the interaction between the shock wave and the boundary layer differs considerably for a laminar boundary layer as compared to a turbulent boundary layer. The position of the boundary-layer trip used in various tunnels varies from near the leading edge (ref. 3) to just in front of the shock wave, but not less than 10 to 15 percent of the chord in front of the shock wave, if possible. This may require two or three trip locations to be used at the various lift coefficients tested, as explained by Haines (ref. 6). Another way of simulating higher Reynolds numbers on airfoils, which tend to separate over the aft part of the airfoil, is to thicken the trailing edge (ref. 4).

If the wind-tunnel test is conducted at very low Reynolds number, the drag due to lift measured in the tunnel may be corrected for the effects of Reynolds number by one of the methods discussed in this section.

Flutter and buffet tests were discussed and it is apparent that there is much room for improvement in methods used for the prediction of buffet boundaries at high speed, but most wind-tunnel experiments seem to indicate that fixing transition gives more uniform changes with changes in Reynolds number.

A method developed by Cahill, Conner, and Khan (refs. 16 and 17) for correcting load and pressure data on a wing to higher Reynolds numbers was also outlined.

It is apparent that there remains much work to be done in the area of high Reynolds number simulation on high-aspect-ratio wings except in the simplest cases.

#### REFERENCES

1. Peterson, John B., Jr.; and Fisher, David F.: Flight Investigation of Insect Contamination and Its Alleviation. CTOL Transport Technology - 1978, NASA TP-2036, 1978.
2. Holmes, Bruce J.; and Obara, C. J.: Observations and Implications of Natural Laminar Flow on Practical Airplane Surfaces. Journal of Aircraft, Vol. 20, December 1983.
3. Elsenaar, A.: Experiences with Transition Fixation in the High-Speed Regime at NLR. Grenzschichtsteuerung durch Transitionsfixierung (Boundary Layer Control by Transition Fixing), DFVLR Mitteilung 84-17.
4. Haines, A. B.: Review of Post-1974 Evidence on Scale Effects at High Subsonic Speeds. ARA Memo 218.
5. Blackwell, J. A., Jr.: Preliminary Study of the Effects of Reynolds Number and Boundary-Layer Transition Location on Shock-Induced Separation. NASA TN D-5003, January 1969.
6. Haines, A. B.: Notes on Transition Fixing and the Interpretation of Drag Data with Different Transition Fixes. ARA Memo 243, November 1982.
7. Henderson, William F.: Studies of Various Factors Affecting Drag Due to Lift at Subsonic Speeds. NASA TN D-3584, October 1966.

8. Engineering Sciences Data Unit: Introductory Sheet on Subcritical Lift-Dependent Drag of Wings; ESDU 66031. ESDU International Ltd., Nov. 1974.
9. Gardner, D.; and Weir, J.: The Drag Due to Lift of Plane Wings at Subsonic Speeds. *Journal of the Royal Aeronautical Society*, Vol. 70, May 1966, pp. 595-599.
10. Frost, Richard C.; and Rutherford, Robbie: Subsonic Wing Span Efficiency. *AIAA Journal*, Vol. 1, No. 4, April 1963, pp. 931-933.
11. Maybe, Dennis G.: Some Remarks on Dynamic Aeroelastic Model Tests in Cryogenic Wind Tunnels. NASA CR-145029, September 1975.
12. Boyden, Richmond P.; and Johnson, William G.: Results of Buffet Tests in a Cryogenic Wind Tunnel. NASA TM 84520, September 1982.
13. Reed, Wilmer H., III: Comparisons of Flight Measurements with Predictions from Aeroelastic Models in the NASA Langley Transonic Dynamics Tunnel. AGARD Conference Proceedings No. 187. Flight/Ground Testing Facilities Correlation. April 1976.
14. Hopps, R. H.; and Danforth, E. C. B.: Correlation of Wind-Tunnel and Flight-Test Data for the Lockheed L-1011 Tristar Airplane. AGARD Conference Proceedings No. 242. Performance Prediction Methods, May 1978.
15. Henne, P. A.; Dahlin, J. A.; and Peavey, C. C.: Applied Computational Transonics - Capabilities and Limitations. David Nixon, editor, *Transonic Aerodynamics*, Vol. 81 of Progress in Astronautics and Aeronautics, 1982.
16. Cahill, J. F.; and Connor, P. C.: Correlation of Data Relating to Shock-Induced Trailing Edge Separation and Extrapolation to Flight Reynolds Number. NASA CR-3178, September 1979.
17. Khan, Mohammad M. S.; and Cahill, Jones F.: New Considerations on Scale Extrapolation of Wing Pressure Distributions Affected by Transonic Shock-Induced Separation. Lockheed-Georgia Company, LG 83ER0055, March 1983.

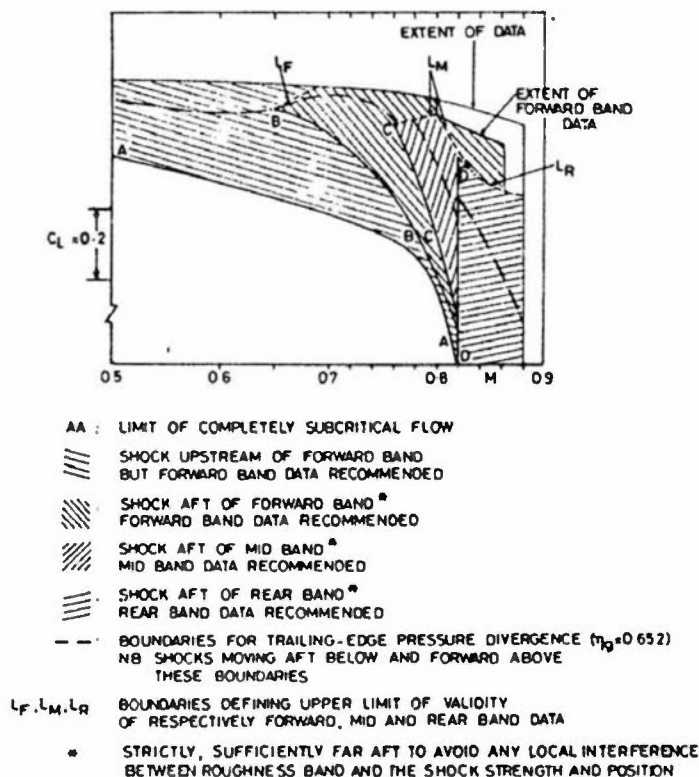


Figure 1.- Regions of validity of data with different roughness bands on a wing upper surface. (From Haines, reference 6.)

CHOICE OF PARAMETERS  
 $s$  = MEASURED  $C_s$  IN % OF THEORETICAL  $C_s$ ;  $M < 0.30$

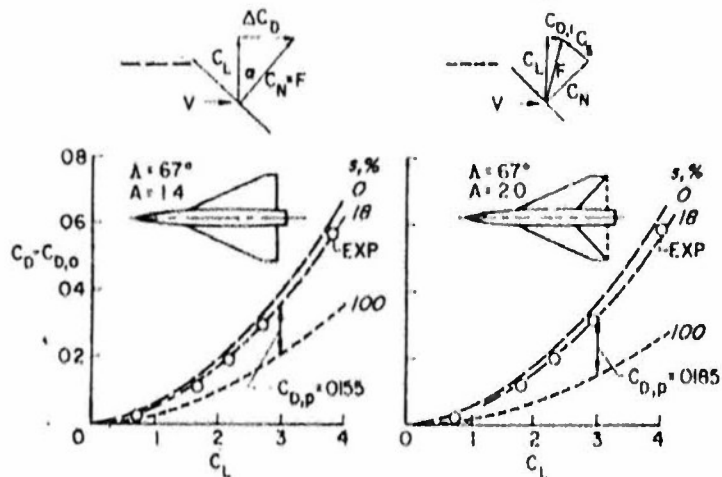


Figure 3.- Definition of the suction parameter,  $s$ , as obtained from experimental data.

CORRELATION OF  $s$   
 SYMMETRICAL WINGS;  $\Lambda = 49^\circ$  TO  $73^\circ$ ;  $C_{L,op}$ ;  $M < 0.30$

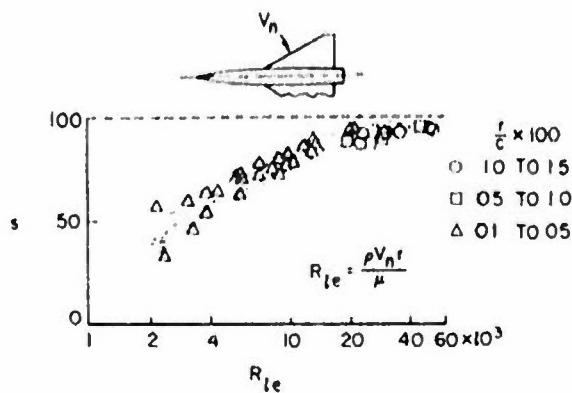


Figure 2.- Suction parameter,  $s$ , as a function of the leading-edge Reynolds number,  $R_{le}$ .

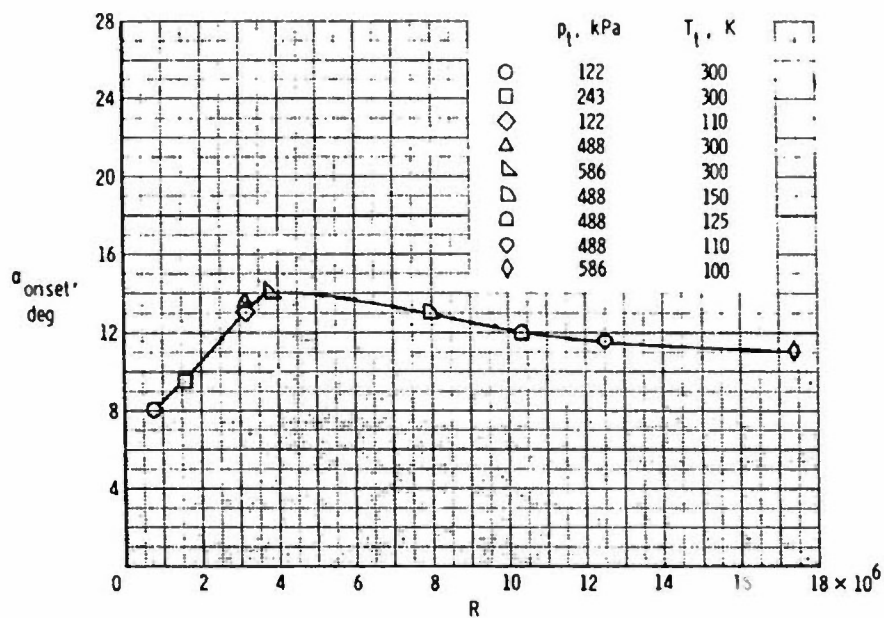


Figure 4.- Effect of Reynolds number on buffet-onset angle of attack for the NPL 9510 wing model.  $M = 0.3$ .

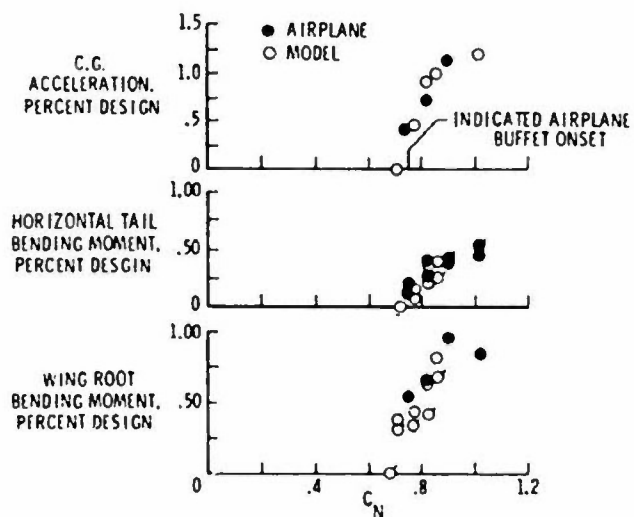


Figure 5.- Comparison of buffet response from airplane and model tests.  $M = 0.76$ , wing sweep =  $26^\circ$ .

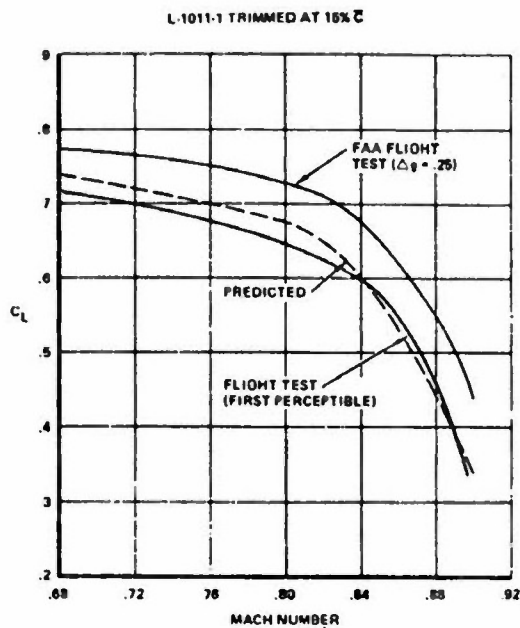


Figure 6.- Comparison of the buffet onset boundary from wind-tunnel tests with flight measurements for the L-1011. (From Hopps and Danforth, reference 14.)

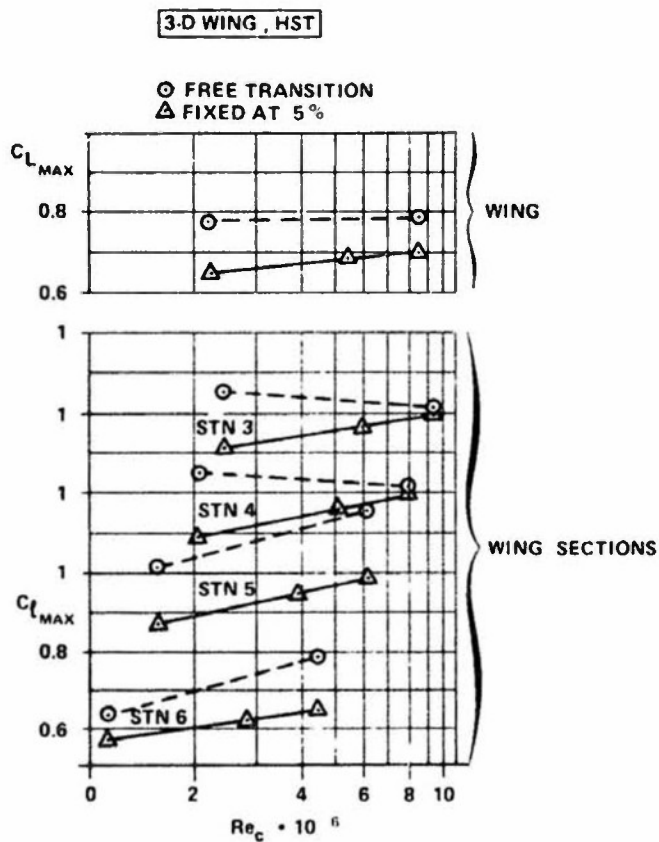


Figure 7.- Effect of Reynolds number on the maximum lift coefficient on a 3-D wing at various spanwise stations with and without fixed transition. (From Elsenaar, reference 3.)

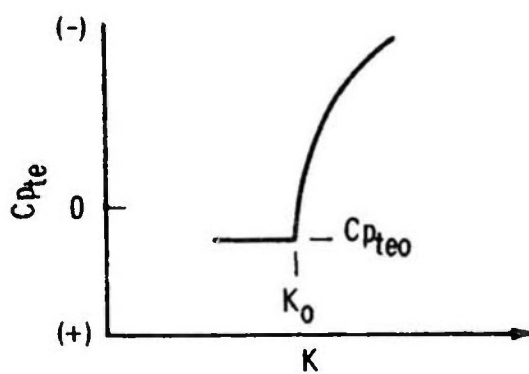


Figure 8.- Trailing-edge pressure coefficient as a function of the correlation parameter  $K$ . (From Khan and Cahill, reference 17.)

## SECTION 2.2.3 DELTA WING CONFIGURATIONS

by J. Szodrich  
Messerschmitt-Bölkow-Blohm GmbH  
Civil Transport Aircraft Division  
TE 2101 Huncfeldstrasse 1-5  
2800 Bremen 1  
Federal Republic of Germany

### 2.2.3.1 INTRODUCTION

The flow field over a slender delta wing at angle of attack immersed in a supersonic stream can be divided into two characteristic regions. The windward or pressure side faces the oncoming flow and is strongly influenced by the bow shock wave; the leeward or suction side is dominated by the effects of inviscid/viscous interaction. It is mainly the leeward flow which is then affected by Reynolds number changes and especially these effects are discussed in more detail in the present paper.

In the past, for subsonic, transonic and supersonic free stream Mach numbers the essential issue of design with slender wings, where vortices occur over the wing at virtually every flight condition, is to fix the location of the separation lines so that the vehicle is always controllable. This is why Reynolds number effects in these flow regimes have been considered of secondary importance. On the other hand at hypersonic speeds the influence of Reynolds number on peak heating as well as on the development and size of characteristic patterns in the flow field are more important. Here hypersonic viscous interaction (characterized by a parameter depending on Mach- and Reynolds number) is dominating, especially near the wing apex, and the vortices induce high rates of heat transfer along attachment lines.

In the following, the discussion shall be confined to free stream Mach numbers from high subsonic to supersonic. With respect to Reynolds number effects it is of major importance to define the different types of vortical flow in that velocity range and to consider the influence of wing geometry.

The given reference list in the appendix is by no means complete, however, the cited reports contain the majority of available literature on that subject.

### 2.2.3.2 FLOW FIELDS AND BOUNDARIES

The main variables for the leeside flow over delta wings are Mach number, angle of attack, wing geometry (leading edges, cross-sectional shape) and Reynolds number. For the purpose of systematizing the flow, a delta wing is considered having straight leading edges and essentially conical flow (i. e. conditions on the surface and in the flow field are constant along a ray from the wing apex), either fully laminar or fully turbulent.

It then appears sufficient to describe the flow in a plane normal to the leading edge, using the parameters of Mach number and angle of attack. These components,  $M_N$  and  $\alpha_N$ , are:

$$M_N = M_\infty \sqrt{1 - \sin^2 \Lambda \cdot \cos^2 (\alpha + \beta)}$$

$$\alpha_N = \tan^{-1} \frac{\tan (\alpha + \beta)}{\cos \Lambda} - \tan^{-1} \frac{\tan \beta}{\cos \Lambda}$$

where  $\Lambda$  is the leading-edge sweep angle and  $\beta$  is the upper surface wedge angle in the plane of symmetry [1]. The angle of attack  $\alpha$  is measured in the meridian plane between the wind vector and the ridge line (the leeward generator) on the upper surface. The parameter  $M_N$  and  $\alpha_N$ , which are taken to characterize the flow field, are illustrated in Figure 1. For a flat-topped delta wing with  $\beta = 0^\circ$ , the equations reduce to those given by Stanbrook and Squire [2]. It should be noted that in incompressible flow the parameters of relative incidence  $\alpha / \lambda$ , and cross-flow velocity  $U_\infty \sin \alpha$  have been used to correlate delta wing results ( $\lambda$  is the semi-angle at the wing apex).

The parameter  $M_N$  then describes the position of the sonic line, i. e. whether the leading edge is inside or outside the Mach cone. Using this criterion together with angle of attack as a first approximation to define types of flow, mainly four leeside characteristics can be recognized [2]. These flow fields and associated skin-friction line patterns are sketched in Figure 2. Apart from the simple solution with attached flow over the entire leeside, two types of symmetrical, separated flow are shown. Depending on the normal Mach number, the first is the well known "leading-edge-separation" and the second type is the "shock-induced separation". A more detailed description on the formation of these types of flow is also given in [1].

#### 2.2.3.2.1 The $\alpha_N$ - $M_N$ Diagram

On the basis of the above considerations Stanbrook and Squire evaluated the available experimental results in an  $\alpha_N$  vs  $M_N$  diagram, defining regions of attached and separated flow at the leading edge [2]. The boundary between these two regions has since been called the "StanbrookSquire Boundary". We shall abbreviate this term to SSB in the ensuing text. Notice that we are assuming that the sweep

angle  $\Lambda$  can be effectively removed as a governing parameter by utilizing the formulation for  $\alpha_N$  and  $M_N$ , and only one explicit experiment has been conducted with models of varying sweep angle and in streams of varying  $M_\infty$  to verify that identical flow fields are produced at particular coordinates  $\alpha_N$ ,  $M_N$  [3].

Figure 3 shows experimental results for sharp leading edges together with other results for wing-body combinations. The zone between separated and attached leading-edge flow representing the limits for the change over from one flow type to the other, is a narrow band and coincides only at higher  $\alpha_N$  with  $M_N = 1$ , the limit between subsonic and supersonic leading-edges. The experimental investigations carried out thus far allow a detailed description of the flow structure about the leeward flow as sketched in Figure 4a and 4b [1].

However, since most experiments are conducted with relatively small models, a careful interpretation of the results is usually required. Figure 4a shows the skin-friction line pattern and form of the external flow for the case of leading-edge separation at moderate angle of attack. The conical lines of separation and attachment are denoted on the leeward surface by angles  $\theta_S$  and  $\theta_A$ , respectively. Figure 4b shows the details of the flow field when the flow is attached at the leading edge but separates inboard (the "shock-induced" type). The difference between attached and separated flow at the leading edge is evident from the skin-friction line pattern on Figure 1. When the flow is attached, the local direction of the skin-friction lines is away from the leading edge; when it is detached, the converse is true.

Further detailed studies with flat-topped thick delta wings (thickness-to-chord ratio = 0.25) lead to an extended  $\alpha_N$ - $M_N$ -diagram with additional types of flow [4], as seen in Figure 5. A description and discussion of the new types of flow is found in [1] with additional information in [5].

Having established the basic leeward flow fields, the boundary layer development and transition effects as well as the influence of Reynolds number on the flow field boundaries and effects of wing geometries shall be reviewed.

#### 2.2.3.2.2 The Influence of Reynolds Number

So far in the above discussion in a first approximation only fully laminar or fully turbulent flows have been considered. Studies on boundary layer transition and the associated longitudinal vortices developing from amplifying instabilities in the laminar zone imply that these may be exerting an important influence on the development of the leeward flow. In [6-9] the existence and behaviour of longitudinal vortices with respect to Reynolds number were investigated.

The boundary layer development indicates an influence of Reynolds number on the types of flow in the  $\alpha_N$ - $M_N$ -diagram [Fig. 5]. For leading-edge flow conditions from subsonic to supersonic when flow separation is fixed at the leading edge (regions 6, 3, 2 and 1 in Fig. 5) the vortex position and intensity, and thus the suction pressure, vary while the type of flow remains nearly unchanged [10]. In contrast, since the secondary separation lines are not fixed, the disposition of the secondary vortices may be influenced by Reynolds number to a larger extent. The effect of transition on the secondary separation lines is shown in Figure 6, together with the chordwise transition position [11]. For further illustration, the locations of the secondary separation lines vs Reynolds number are plotted for supersonic as well as subsonic free-stream Mach numbers on Figures 7a and 7b, respectively [1]. There is a noticeable movement of the secondary separation line position towards the leading edge as Reynolds number  $R_{L\infty}$  increases from  $10^4$  to  $10^7$ .

As angle of attack increases to higher values, the transition zone moves closer to the wing apex, so that any effect of transition becomes less at the measurement station shown on Figures 7a and 7b. The consequence is a slowdown in the rate of movement of the secondary separation line position in the turbulent flow. We should note that the form of the static pressure distribution across the wing semi-span attributed to the primary vortex evidences an increase of the peak suction pressure level as we proceed from laminar to turbulent flow. Correspondingly, the effect of the secondary vortices on broadening the width of the suction pressure zones is greater in laminar than in turbulent flow, as is evident in Figure 8 [12].

These pressure distributions imply increasing lift with higher Reynolds number as seen in Figure 9a [13]. These results are confirmed in other investigations as well [14]. Opposite results for the same type of flow but for wings with rounded leading edges have been found in [15]. For these geometries in [16] various examples are shown where high Reynolds number leads to a loss of lift due to decreased suction peaks.

The flow development is illustrated in Figure 9b [16]. Both cases in Figure 9 are well to the left of the SSB, at  $M_N = 0.33$  and  $0.13$ , respectively. While for the rounded leading edge there might be attached flow at higher Reynolds numbers, it is argued in [16] that lift loss also occurs for the sharp edged delta wing due to vortex breakdown at higher Reynolds number.

Therefore, at least for sharp edged delta wings, the boundaries in the  $\alpha_N$ - $M_N$  diagram for leading-edge separation seem not to be influenced considerably by Reynolds number variations. On the contrary, the types of flow on the right hand side of the SSB [regions 4 and 5 in Figure 5] are found to be Reynolds number dependent [10]. Figure 10 shows that as Reynolds number increases, the effects of transition in region 4 diminish until at sufficiently high Reynolds number ( $R_{L\infty} = 10^7$ ), region 4 can no longer be ascertained [1]. The flow field develops directly from one with leading-edge separation for  $M_N < 1$  (region 2) to one with shock-induced separation for  $M_N > 1$  (region 5).

Furthermore the position of the boundary between region 5 and region 6 in figure 5 is dependent on Reynolds number as well, Figure 11. Therefore Figure 5 is strictly valid only for one Reynolds number as was pointed out in [10].



### 2.2.3.2.3 The Influence of Wing Geometry

The discussion so far centered around delta wings with sharp and straight leading edges and flat upper surfaces. However, changing the collection of parameters that describe the body geometry might lead to different boundary positions between the types of flow and might change as well the Reynolds number sensitivity.

In the following only the geometry of the leading edge shall be discussed further due to the relatively large importance compared to other cross-sectional geometry parameters. A first example is given by the disposition of the SSB due to rounded leading edges, as the evaluation of experimental results in Figure 12 suggest [2]. In comparison with the SSB for sharp edges, a broad region results where both separated and attached flows may be found in the  $\alpha_N$  vs  $M_N$  diagram. From what has been described earlier it may also be deduced that the rather broad region results from evaluating different Reynolds number cases and different radii. The tendency, however, is evident from Figure 12, showing that a round leading edge tends to suppress leading-edge separation to larger incidences. This is also confirmed in Figure 13 where the lift for sharp and round leading edges is plotted and compared to the linear lift. Finally it seems reasonable that the larger the leading edge radius the greater the dependency on Reynolds number [17].

The leeside flow of wings with non-straight leading edges has found considerable interest in the past, mainly in connection with strake or leading edge extension (LEX) vortex flows. Basic investigations with increasing or decreasing sweep angles downstream the apex have been performed at subsonic [18] and supersonic [19] free-stream Mach numbers. It was found that the interference effects between the leading-edge vortices from different chordwise stations are higher in the case of a wing with decreasing leading-edge sweep while the flow field over a wing with increasing sweep is more similar to a wing with straight leading edges.

Wings with curved leading edges (i. e. "gothic" or "ogee" plan form) have shown attached flow along part of the leading edge and separated flow along the remainder, the extent of each type of flow varying with both Mach number and incidence [2]. Reynolds number is believed to have an effect similar to what has been shown earlier with respect to disposition of secondary separation lines and vortex intensities (suction peaks). The  $\alpha_N$ - $M_N$  systematic, especially the SSB is no longer valid.

### 2.2.3.3 VORTEX BREAKDOWN

At certain angles of attack and leading-edge sweep angles the vortex flow over delta wings with leading-edge separation has been observed to breakdown. This phenomenon is regarded as an expansion of the spiral vortices by transition from laminar to turbulent flow. Thus vortex breakdown is sometimes considered as a second dynamic flow condition, while other investigators call it an unstable condition. Vortex breakdown starts downstream the trailing edge and moves upstream with increasing incidence. The movement of vortex burst location, the hysteresis unstable region with vortex oscillations are shown in Figure 14 [20], for incompressible flow. There seems to be a final position of the breakdown location which ties for delta wing with sweep angles between 70° and 85° at about 30 % to 40 % of the wing chord.

As summarized in [21], vortex breakdown has been observed only in highly swirling flows. An apparently necessary condition for breakdown is a positive or adverse pressure gradient appearing near the vortex core (and not necessarily in the outer vortex regions). Then the approaching flow is decelerated and a zero velocity point is formed on the vortex axis with reversed flow near the axis. A large increase of turbulent intensity occurs and downstream a new vortex structure with an expanded vortex core is established.

Since vortex breakdown depends also on the position of the leading edge with respect to the free-stream direction, the yaw angle becomes an important parameter. In Figure 15 the roll stability versus angle of attack for a fixed yaw angle  $\beta$  is plotted. There is a loss of lateral stability due to the asymmetric breakdown [20].

The results presented here are from observations at subsonic freestream velocities, however, there are investigations at transonic and supersonic Mach numbers showing similar flow developments and characteristics.

It has been stated that Reynolds number effects on vortex breakdown position, vortex core location are negligible [22]. A large number of references have been evaluated for onset of vortex breakdown at the trailing edge, as observed in water tunnels, wind tunnel and flight. Figure 16 seems to suggest that only angle of attack and leading-edge sweep angle are the major parameters. Although there is a rather large scatter ( $\Delta\alpha \sim \pm 5^\circ$ ) there seems to be no systematic Reynolds number effect detectable, bearing in mind that really high Reynolds number do not exist for evaluation.

On the other hand the angle of attack for vortex breakdown at the trailing edge agrees, in general, reasonably well with a reduction in the rate increase of axial velocity with angle of attack. Water tunnel and windtunnel data show a Reynolds number effect on axial velocity, as seen in Figure 17 [22], and then it might be concluded that vortex breakdown is dependent on Reynolds number. Unfortunately only few investigations on Reynolds number influence are known in order to be able to develop a more detailed description of the vortex breakdown at higher Reynolds number.

#### 2.2.3.4 TRANSITION FIXING

It has been pointed out earlier that the goal in designing delta wings is not to suppress separation but rather to control it, for instance by fixing separation to the leading edges. But even then, the above discussion has shown a considerable influence of Reynolds number on the lift of delta wings due to the different development of vortices with laminar or turbulent separation (see Figure 8 and 9). The simulation of high Reynolds number conditions can be achieved by transition fixing.

The problem with transition fixing is that it has to be employed according to the type of flow encountered and, associated with that, according to the wing geometry. This is further aggravated by the fact that the type of flow might depend on Reynolds number as well. Thus a test at low Reynolds number, even with transition fixed, might not give the correct answer since the type of flow at high Reynolds number is different.

If on a sharp edged delta wing leading-edge separation is assumed then only the secondary separation line needs to be fixed. The example in Figure 18 [23] shows transition fixing along a conical line from the apex of the wing using a Carborundum band. The pressure distribution documents the at least partial success of fixing. According to Figure 10 one would expect a rather flat suction peak for laminar separation while in the turbulent case a narrow and even higher suction peak develops. Figure 18 depicts all these characteristics when employing a transition trip, however, the turbulent suction peaks are not as high as expected [23].

The second example in Figure 19 [13] shows that here transition fixing at low Reynolds number can lead to suction peaks of similar magnitude as observed with free transition at higher Reynolds numbers. Unfortunately, it is not known how and where the transition trip was applied. The pressure distributions seem to indicate that in this special case for  $Re = 2.5 \times 10^6$  there is already turbulent separation. The transition fixed case only differs with respect to the suction peak location, i. e. the vortex center position.

For shock-induced separation transition fixing should be applied ahead of the shock, i. e. a fixing trip on a conical ray through the apex would be applied, similar to the one for fixing secondary separation. No explicit examples with transition fixing are known for this type of flow. An indication of Reynolds number effects on the pressure distribution is given in [9].

Changing the wing geometry might lead to higher Reynolds number sensitivity. As an example serves the delta wing with round leading edges. Transition trips can be applied again on a conical ray in the vicinity of the leading edge. However, also streamwise trips wrapped around the leading edge are possible, inducing leading edge contamination. Finally modifications of the leading edge radius could be considered to simulated high Reynolds number flows, provided the simulation goal is actually known. The disadvantage of altering the leading-edge shape is at least for supersonic flow the influence on the bow shock and the associated changes on the lower side flow field and the impact on the upper surface.

There is a strong coupling between separation and wing motion (e. g. pitching) and also transition is sensitive to wing motion. The problem then arises with dynamic testing, since no tripping device (as it is known so far) can be used [20].

#### 2.2.3.5 CONCLUSIONS

These notes present the current status of delta wing research with respect to Reynolds number effects. Prediction of flight characteristics from wind tunnel tests requires detailed knowledge of the different leeside types of flow and how they vary with Reynolds number. Besides the flow conditions, the wing geometry, notably leading-edge radius, wing thickness, and cross-sectional shape, is of importance. Due to windtunnel wall effects and support interferences, which might lead to vortex breakdown or similar effects as induced by Reynolds number variation, a careful designed test set-up is recommended.

#### 2.2.3.6 REFERENCES

- |     |                               |  |
|-----|-------------------------------|--|
| [1] | Szodruch, J.<br>Peake, O.J.   | Leeward Flow over delta wings at supersonic speeds.<br>NASA TM 81 187, 1980  |
| [2] | Stanbrook, A.<br>Squire, L.C. | Possible Types of Flow at Swept Leading Edges.<br>Aeronaut. Quart., vol. XV, 1964, pp. 72-82.  |
| [3] | Miller, D.S.<br>Wood, R.M.    | Leeside flows over delta wings at supersonic speeds.<br>J. Aircraft, vol. 21, no. 9, pp. 680-686, 1984.  |
| [4] | Szodruch, J.                  | Leeseiten-Strömung bei schlanken Deltaflügeln endlicher Dicke<br>(Lee Side Flow over Slender Delta Wings with Large Thickness-to-Chord Ratio).<br>ILR Bericht 23, Techn. Univ. Berlin, 1977. |

- [ 5 ] Szodruch, J.      Messung und Sichtbarmachung der leeseitigen Wandschubspannungen  
Monson, D.J.      bei Deltaflügeln im Überschall. (Measurement and visualization of  
leeward skin-friction on delta wings at supersonic speeds)  
Z. Flugwiss. Weltraumforsch. 6 (1982), Heft 4.
- [ 6 ] Ginoux, J.J.      Recent developments in boundary layer  
research.  
AGARDograph 97, 1965.
- [ 7 ] Maltby, R.L.      Flow Visualization in Wind Tunnels Using Indicators.  
AGARDograph 70, April 1962.
- [ 8 ] Ginoux, J.J.      Instabilité de la Couche Limite sur Ailes en Flèche  
(Instability of the Boundary Layer on Swept Wings).  
Zeitschr. f. Flugwissenschaften, 16. Jrg., Heft 8/9, 1967,  
pp. 302 - 305.
- [ 9 ] Szodruch, J.      Experimental study of supersonic viscous leeside flow over a slender  
delta wing.  
NASA TM 81 248, 1980.
- [ 10 ] Szodruch, J.      Reynold number influence on leeside flowfields.  
AIAA Journ., vol. 16, no. 12, pp. 1306-1309, Dec. 1978.
- [ 11 ] Schlichting, H.      A survey of some recent research investigations on boundary layers  
and heat transfer.  
J. Appl. Mech., vol. 38, pp. 289 - 300, 1971.
- [ 12 ] Peake, D.J.      Three Dimensional Interactions and Vortical Flows  
Tobak, M.      with Emphasis on High Speeds.  
AGARDograph, Febr. 1980; also NASA TM 81169, March 1980.
- [ 13 ]      High Reynolds number research.  
NASA CP 2009, 1976
- [ 14 ] Wardlaw, A.B.      High angle-of-attack missile aerodynamics.  
AGARD-LS-98, Febr. 1979.
- [ 15 ] Wentz, W.H.      Vortex breakdown on slender sharp edged wings.  
Kohlman, O.L.      J. Aircraft, vol. 8, no. 3, pp. 156 - 161, March 1971.
- [ 16 ] Potter, J.L.      Review of requirements and status of simulation and scaling of  
transonic viscous flows.  
C-TR-84-23, 1984.
- [ 17 ] Poll, D.I.A.      On the generation and subsequent development of spiral vortex flow  
over a swept back wing.  
AGARD CP 342, July 1983.
- [ 18 ] Hoeijmakers, H.W.M.      Vortex flow over delta and double-delta wings.  
Vaatstra, W.      J. Aircraft, vol. 20, no. 9,  
Verhaagen, N.G.      pp. 825 - 832, Sept. 1983.
- [ 19 ] Henke, R.      Windtunnel tests of delta wings at  $M = 2.5$ .  
Cranfield Institute of Technology, CoA Memo 8216, 1982
- [ 20 ] Ericsson, L.E.      Vortex-induced asymmetric loads in 2-d  
Reding, J.P.      and 3-d flows.  
AIAA-80-D181, 1980.
- [ 21 ] Kraft, E.M.      A survey of vortical flow phenomena in aerodynamics.  
Report for AGARD WG 09, 1984.
- [ 22 ] Erickson, G.E.      Flow studies of slender wing vortices Northrop Corporation, Aircraft -  
Division, unpublished paper, 1980 (partly published in "Water tunnel  
studies of leading edge vortices".  
AIAA 80-1423, 1980).
- [ 23 ] Stahl, W.H.      Aerodynamics of low aspect ratio wings.  
AGARD-LS-98, Febr. 1979.
- [ 24 ] Karon, A.      Separated vortex flow over slender wings between side walls.  
Delft University of Technology,  
Report LR-300, Aug. 1980.

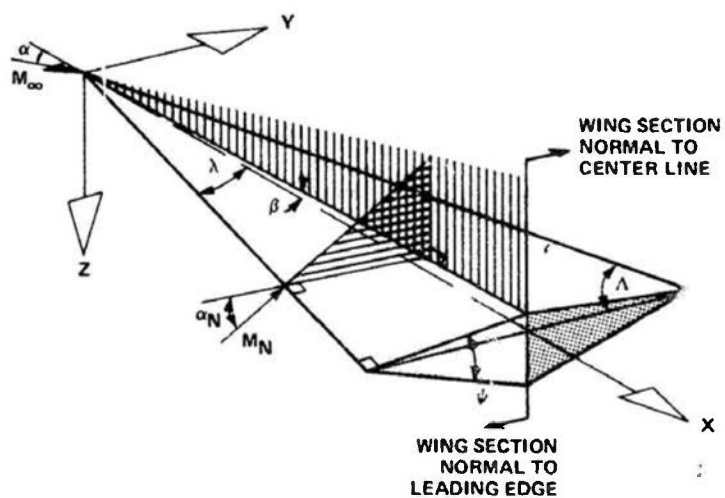


Figure 1: Delta wing geometry and flow components [1]

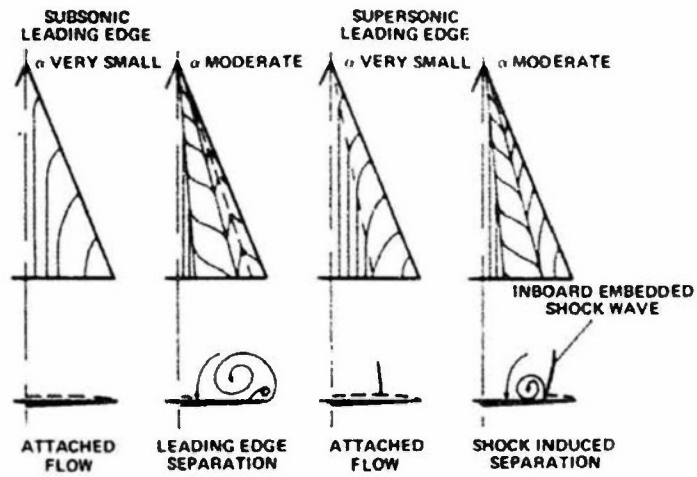


Figure 2: Flow structure and skin friction line pattern on leeward side of slender delta wings [2]

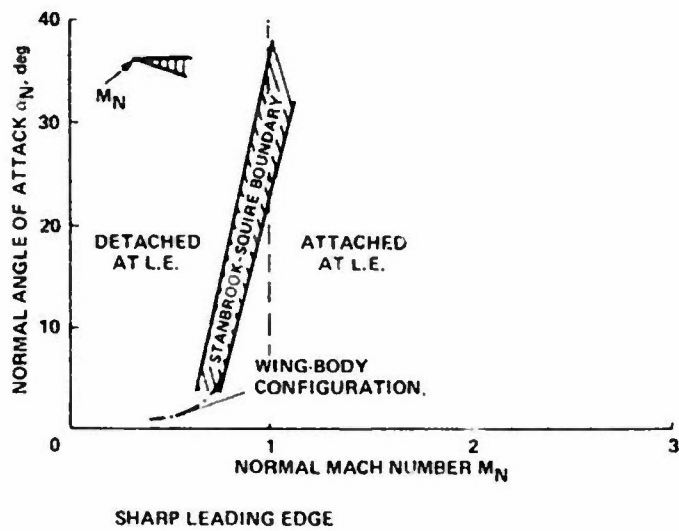


Figure 3: Detached and attached leading edge flow [1]

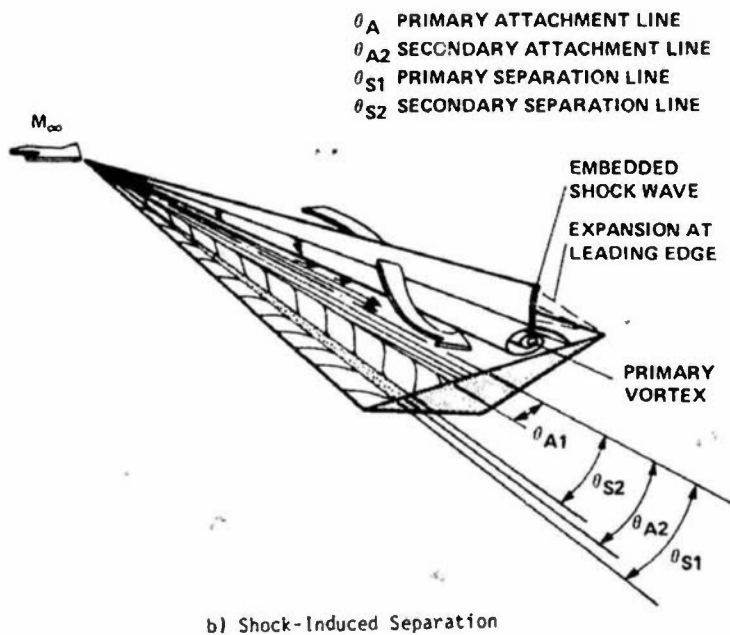
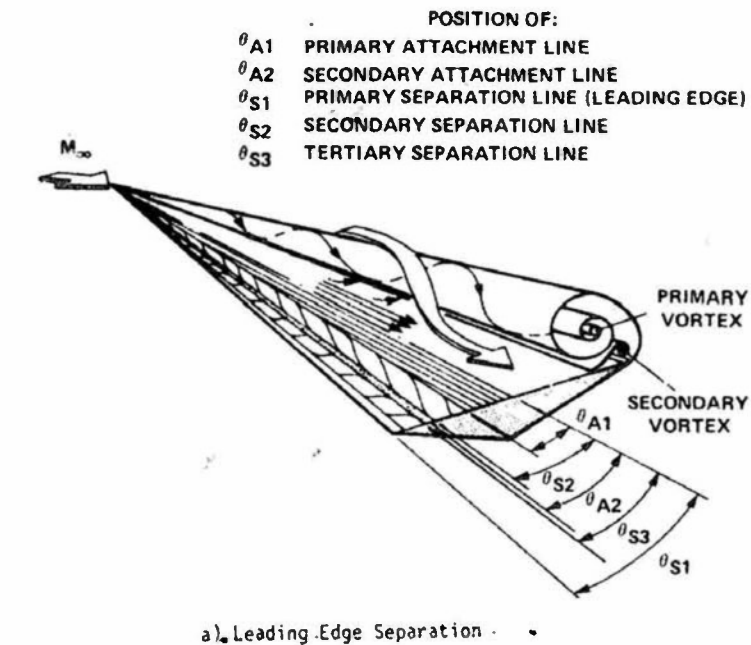


Figure 4: Skin-friction line pattern and external flow structure about flat-topped delta wing [1]

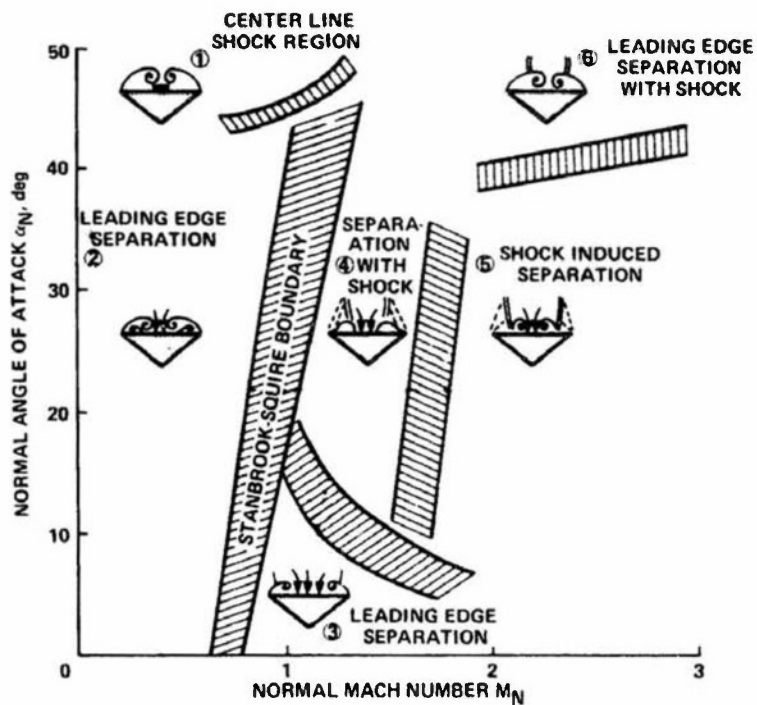


Figure 5: Lee side flow regimes over thick delta wings at supersonic speeds -  $\alpha_N$  vs  $M_N$  diagram [4]

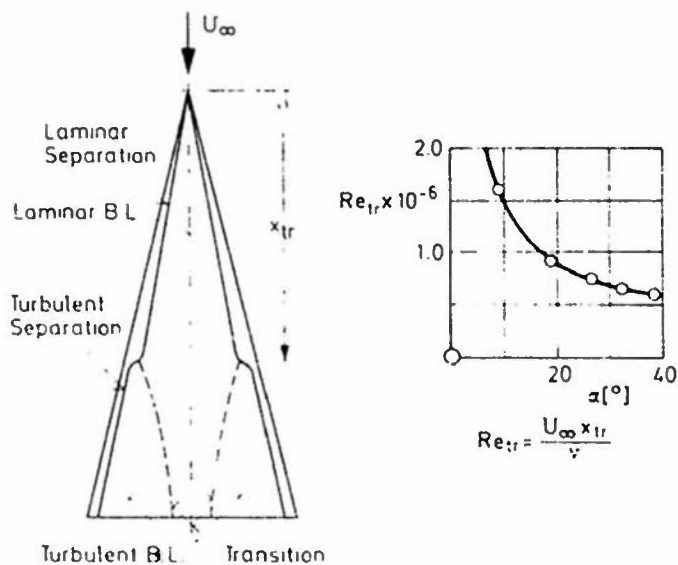


Figure 6: Boundary layer flow on suction side of slender delta wing [11]

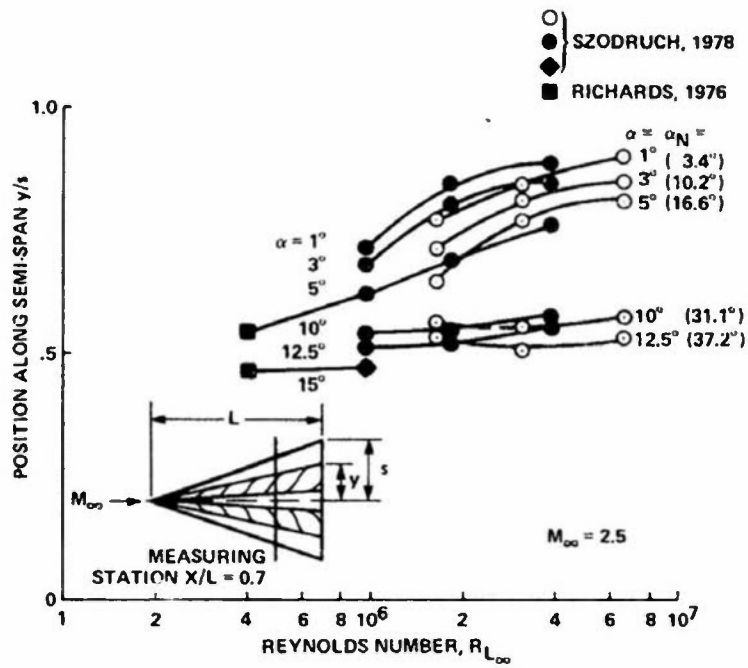


Figure 7a: Influence of Reynolds number on skin-friction line pattern (secondary separation line).  
Supersonic Mach numbers [1]



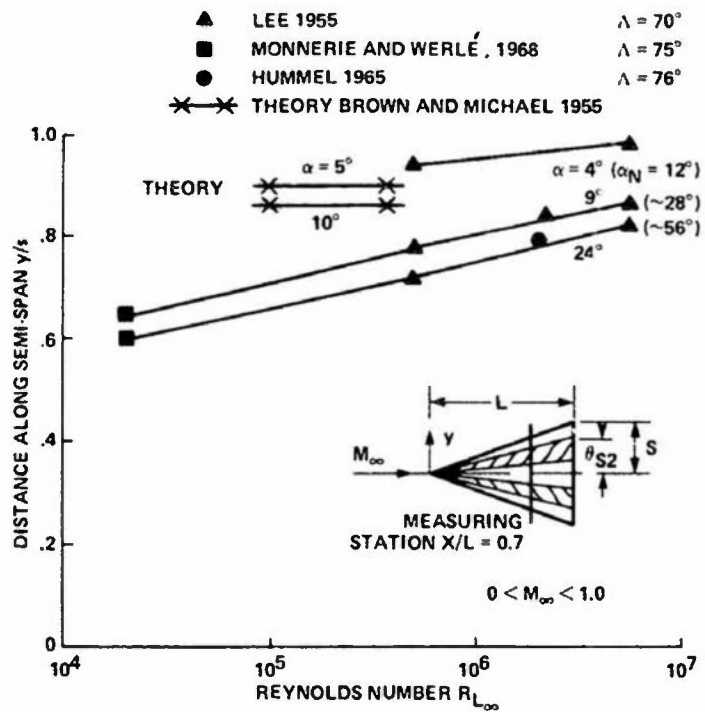


Figure 7b: Influence of Reynolds number  
 on skin-friction line pattern  
 (secondary separation line).

Subsonic Mach numbers [1]

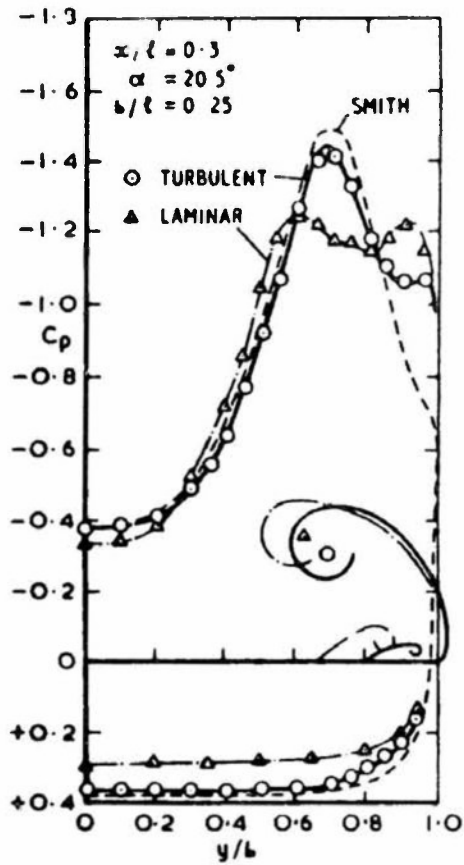


Figure 8: Pressure distributions over a thin delta wing at low speeds with laminar and with turbulent flow [12]

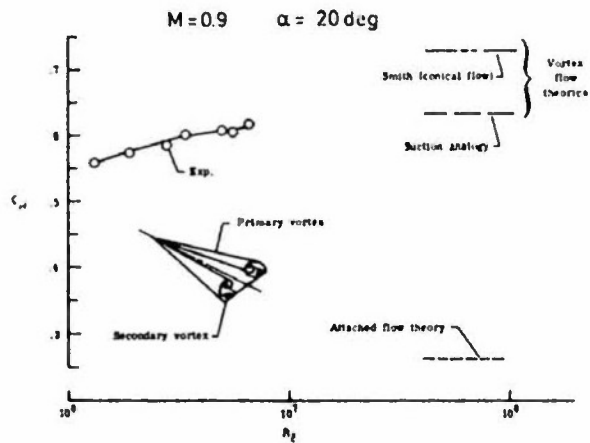


Figure 9a: Effect of Reynolds number on leading-edge vortex flow  
 $A = 0.52 \delta$ ; [13]

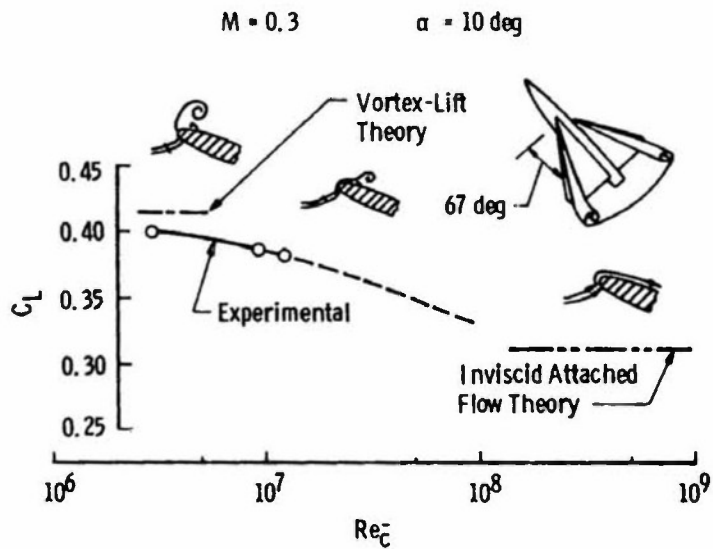


Figure 9b: Variation of lift coefficient with Reynolds number  
 where leading-edge separation and vortical flow  
 exist. [16]

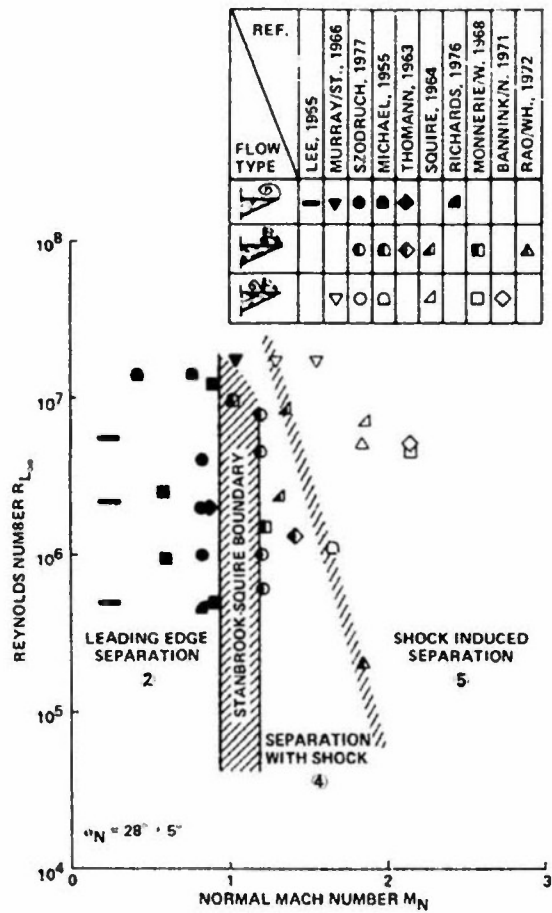


Figure 10: Influence of Reynolds number on flow types and boundaries at constant  $\alpha_N$  [1]

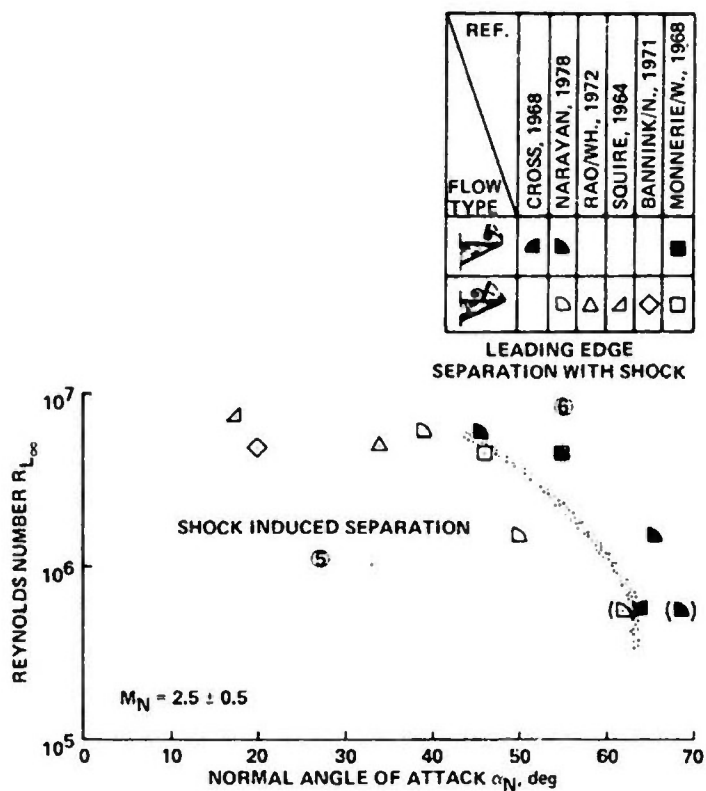


Figure 11: Influence of Reynolds number on flow types and boundaries at constant  $M_N$  [1]

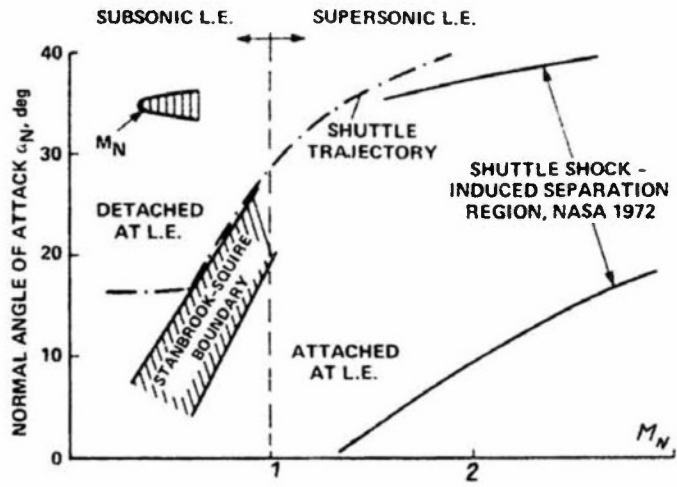


Figure 12: Boundary between detached and attached leading-edge flow for rounded edges [1,2]

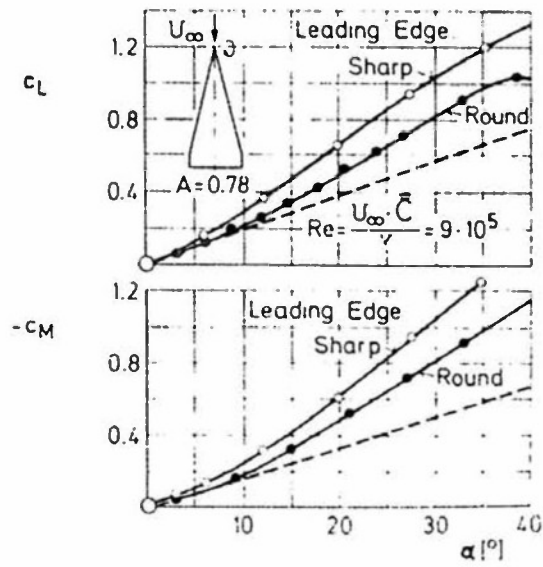


Figure 13: Influence of leading-edge shape on lift and moment coefficients for slender delta wing [23]

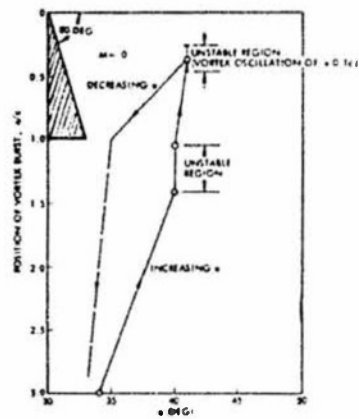


Figure 14: Hysteresis and unstable vortex burst locations [20]

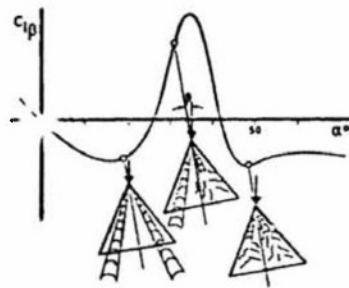


Figure 15: Roll stability versus angle of attack for a pure delta wing [20]

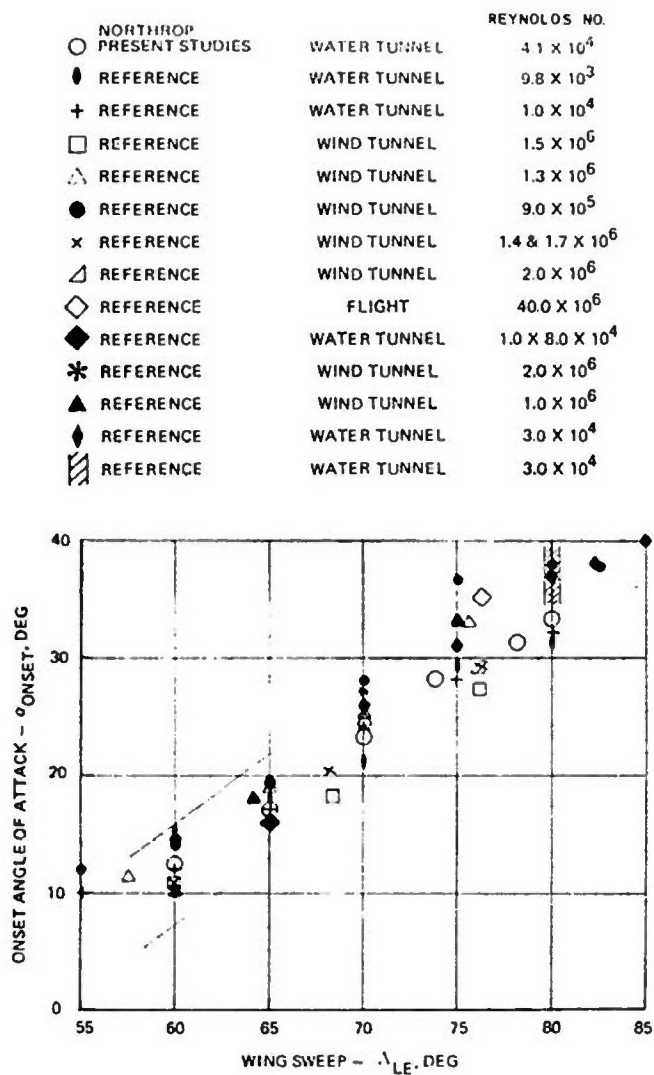


Figure 16: Onset of vortex breakdown at the trailing edge of delta wings [22]



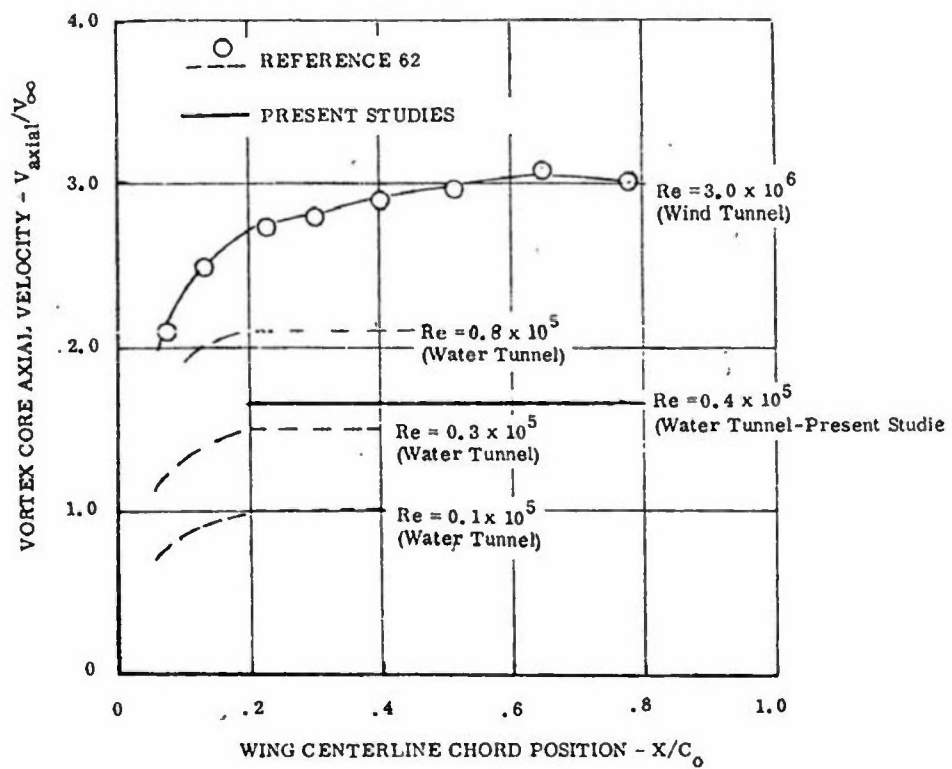


Figure 17: Vortex core axial velocity - 65° Delta Wing  
 $\alpha = 15^\circ$  [22]

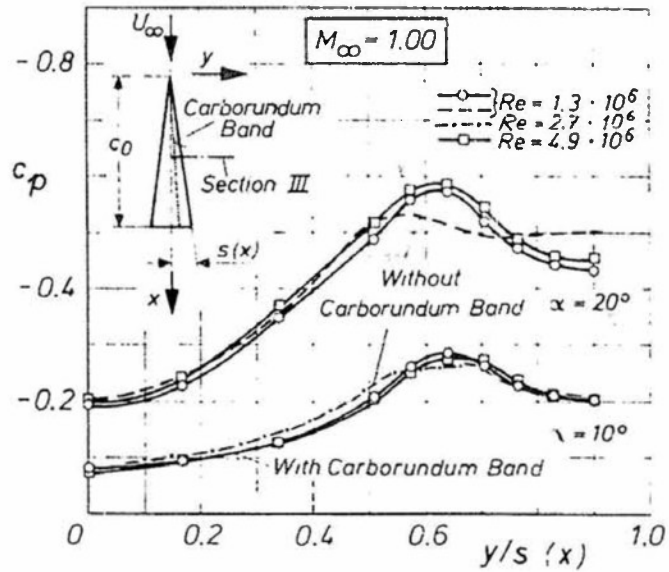


Figure 18: Spanwise pressure distributions on suction side with transition strip [23]

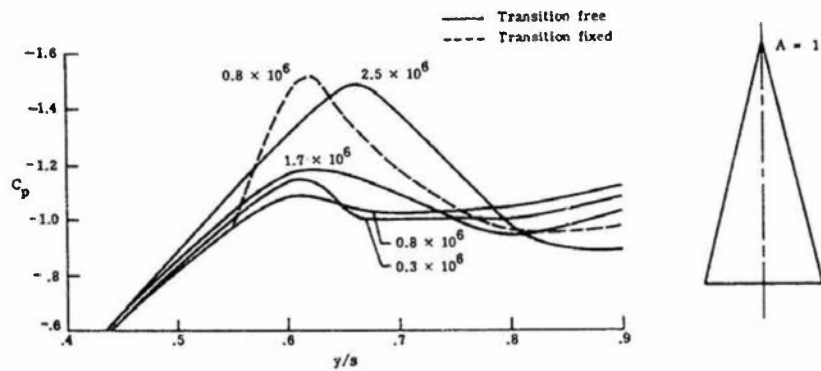


Figure 19: Suction peaks for various Reynolds numbers [13]

## SECTION 2.2.4 COMPLEX CONFIGURATIONS

by A.G.T. Cross  
British Aerospace plc  
Aircraft Group - Weybridge Division  
Brough, N. Humberside, HU15 1EQ, UK

### 2.2.4.1 Introduction

The practice of simulating high flight Reynolds number behaviour in a low Reynolds number facility is well known. However the problems now encountered at transonic speeds are considerable and vary for different model designs such that it is difficult to predict with real confidence the actual flight conditions. In two dimensions these scale effects become more apparent as the degree of supercritical flow is increased and in particular with rearward movement of shocks. In three dimensions the problems are more severe particularly when wing sweep is high due to vortex and turbulent attachment line flows, both of which are Reynolds number dependent and when complex configurations are considered the potential for scale sensitive effects is considerable owing to the many regions where flow separation can occur. The designer will often seek to avoid scale sensitive flow separations in model tests and this amounts to designing for low Reynolds number with a reduction in the potential gains to be had for design for full scale. By furthering the understanding of scale effects more reliable use can be made of Reynolds number simulation techniques, so enabling design for conditions closer to full scale with significant gains in flight performance.

These notes review the current practice with regards to high Reynolds number simulation in transonic wind tunnels for industrial standards of testing relating to complex aircraft configurations.

### 2.2.4.2 Background

The modern combat aircraft is a highly complex geometric shape as can be seen in Figure 1. Not only are the geometries complex, but there is a great diversity of forms of which just a few are reproduced here and so it should not be surprising that difficulties are encountered when testing models of such aircraft in the wind tunnel.

Each model test has to be considered on its own particular merits, unless the experience gained from previous similar designs can be drawn upon. For this reason there tends to be a general awareness of the simulation problems with remedies for specific cases, but with few hard and fast rules that can be called a general methodology. Indeed it is interesting to note that the main conclusion of Haines in Reference 1 is that the present position is unsatisfactory and that the case for a high Reynolds number testing facility is now stronger than ever. However in the absence of the full scale condition being achieved any increase in Reynolds number may only make a small difference unless some minimum and generally uncertain critical value is achieved.

Owing to the importance of effects such as free stream turbulence and tunnel wall interference, to name but two, simulation methodologies are not necessarily transportable from one tunnel to another. Unfortunately industry cannot support the necessary research work required to develop procedures for its own facilities and the tendency is to adopt the more general experience of the research establishments. For aircraft the wing remains the main scale sensitive component owing to the separations that occur at high lift, though for combat aircraft in particular, the interaction with the fuselage, pylons, external stores and other lifting surfaces becomes very important. High incidence non-attached flows are now very much part of the fighter aircraft's operational flight regime and this poses particular simulation difficulties.

For transport aircraft, manufacturers can generally make use of a large data base resulting from tunnel tests and flight test data originating from previous designs. This is particularly true for designs involving an evolving family of aircraft and such data bases, correctly used, can enable a fair degree of precision at full scale with reductions in operating cost, or other benefits. The emphasis is then on the accurate prediction of performance and providing the customer with guarantees.

For military aircraft it is difficult to see such an approach being successful as the tendency now is for more complex configurations with each case having to be considered on its own merits. Even so some form of simulation methodology is necessary, though this may in practice be little more than an awareness of the problems involved and without any real remedy.

The ability to develop adequate simulation techniques for the military aircraft is further frustrated by the high costs associated with model manufacture, model testing and flight testing; the latter of which at typically \$9000 per flight is particularly expensive, while often being the sole source of high Reynolds number data. For this reason the basic requirement of industry is a minimum of testing and this generally results in a shortage of good quality data for confirming the soundness of either existing or new simulation techniques.

While speaking of flight data, it should be appreciated that this is in the form of forces and moments as determined from flight performance and estimated engine performance. On the other hand, tunnel tests do not generally include engine effects and intake and jet orifices are usually extended by simple fore and aft bodies. Thus the scope for uncertainties between tunnel tests and flight is very large and differences cannot be merely considered as a Reynolds number effect. Where scale sensitive separations are suspected and some improvement in flight performance is required this will generally result in further tunnel tests involving simple remedial modifications such as vortex generators, or fences. The "state of the art" is that for any new design corrective measures of this sort would generally be necessary though any major redesign would be considered a failure.

For projects involving radically new concepts the uncertainties between tunnel tests and actual flight performance may be very large. For such cases and well before the design is finalised a special aircraft may be built and flown to demonstrate the design at full, or near full scale. Obviously any improvement in simulation methodology that reduces the need for such expensive tests is clearly welcome though it is ironic that this can only really materialise if more, and of improved quality, flight data becomes available to assist in the development of simulation methodology.

#### 2.2.4.3 Separation

When complex configurations are considered, such as that of a complete fighter aircraft, the potential for scale sensitivity is great owing to the many regions where separation can occur. The most common areas where separation can be present and their effect on design are listed as follows:

Forebody	High incidence flow where asymmetric vortices and sideforce may result in lateral stability problems including nose slicing.
Canopy	Separations and low frequency turbulence giving rise to cockpit internal noise problems at high speed low level flight conditions.
Diverter	Drag penalties.
Intakes	Intake pressure recovery degradation resulting in reduced engine efficiency.
Strakes	High incidence vortex flow effecting maximum lift and longitudinal and lateral stability.
Wing	Leading and trailing edge separations and shock induced separations effecting high speed and low speed buffet boundaries, maximum useable lift and longitudinal and lateral stability. Forebody vortex bursting.
Stores	Drag producing separations and vortex flows effecting maximum speed, range, and sustained and instantaneous rates of turn.
Spoilers	Intentional separation for high drag, lift dumping and or lateral control.
Flaps	Separations at high lift and during transonic manoeuvre.
Junctions	Wing/body junction vortex influencing flow breakdown on inner wing region. Wing/pylon junction vortex producing drag.
Airbrakes	Intentional steady, symmetric, separation to produce high drag.
Afterbody	Base drag.

It is not practical to cope with so many problem areas and so it is usual to restrict attention to the more dominant scale sensitive regions. Thus at low incidence there is a tendency to concentrate on the wing and its interaction with other components in its close proximity, while at high incidence the flow over the forebody becomes important as this can generate asymmetric forces that effect lateral stability.

Base drag originating from the fuselage, or external stores, is sensitive to Reynolds number when separation occurs on a smooth boattail contour and this type of flow can, as discussed in Reference 2, require the allowance for Reynolds number during the wind tunnel calibration. The temptation in design is then to introduce a salient edge to fix the separation and reduce sensitivity to Reynolds number and this approach is often used more generally for controlling unavoidable smooth body separations.

A further problem associated with the complexity of the configuration is that of the low Reynolds number based on the characteristic length of the components, as in order to make a complete model the various components are inevitably much smaller than those that can be tested in isolation. For such complete models, testing at Reynolds numbers as low as 3 million is not uncommon.

#### 2.2.4.4 Low Sweep Wings

The wing is still the most important feature of a complex aircraft configuration and the main aim during testing is to ensure a turbulent boundary layer at the shock and to

reduce the boundary layer thickness to minimise scale error at the shock and trailing edge. The former requirement is based on the full scale flow being turbulent close to the leading edge resulting in a turbulent shock boundary layer interaction. Transition fixing is used to ensure that the flow is turbulent and the downstream position of the fix controls the scale of the boundary layer at the shock and trailing edge.

This approach is developed from two dimensional considerations and can only be used when wing sweeps are low and three dimensional effects not too severe. Reducing the scale of the boundary layer requires transition bands to be moved rearward, but the final position must not be so close to the shock that forward shock movement at separation is inhibited by a favourable interaction with the transition band.

The use of such transition fixing places importance on reproducing the relevant full scale flow phenomenon and so often it is considered without any correlation of tunnel and flight test data and there is generally limited direct experimental evidence from previous designs to substantiate the approach or suggest an alternative.

The approach to transition fixing in the ARA 2.74m x 2.44m tunnel is described by Haines in Reference 3. Forward, mid and aft transition band fixing is considered and Haines produces a chart, reproduced here as Figure 2, showing qualitatively the range of applicability of all the various types of band. The main point to be noticed from this chart is that no single fixing band satisfies the full range of conditions and so ideally a very costly test programme should be carried out involving progressively more forward fixing bands as the shock moves forward. In practice, as exemplified by Figure 2, it is most usual to consider two or three band positions, though an additional band or two might be used if it is considered necessary.

From Figure 2 it will be noticed that at moderate Mach numbers, where high lift is associated with forward shocks, forward transition fixing is used even when the shock moves forwards of the band. Thus although free transition tests would be more appropriate in some forward shock cases this would not be generally considered worth the cost of additional special tests.

At the high Mach numbers and while the flow is attached forward, mid and rear fixing bands are used depending on lift level and Mach number. However, as the lift is further increased and separated flow becomes involved, forward shock movement requires a progressive and eventual return to the forward fixing position. The general guideline for such tests is that a particular transition band remains valid until the shock creeps forward to within a 10 to 15% model chord distance of the band.

The need to use different transition band positions is further complicated by aeroelastic effects which are different at model and full scale and which imply different geometries at different loadings for a given unloaded wing shape. For a model corresponding to a high performance aircraft, each design point requires a different model wing to be tested with its own fix, or range of fix positions, and certain standard fix positions common to all wings may be necessary to provide reference data. Often this reference data will be obtained as transition free results during preliminary testing of each model wing.

Scale effects have been studied on three dimensional wing-body models in the RAE transonic tunnel and are reported in References 4 and 5. The tests constitute one of the few comprehensive investigations of scale effects for transport and combat type models and so they are well worth further discussion here. Figures 3 and 4 are taken from this source and show the effect of Reynolds number for a wing swept at 25 degrees and for a Mach number of .825. The results are typical of low Reynolds number tunnel tests and show an interaction of the trailing edge flow with the shock. At high Reynolds number (see Figure 4) the expected rearward movement of the shock with increasing incidence ceases at a value of 1.3 degrees. Above this value separation, as revealed by the falling trailing edge pressure, halts the advancement and then causes the shock to move forward rapidly.

At low Reynolds number (see Figure 3) the trailing edge separation occurs earlier and forward shock movement starts at around 0.2 degrees of incidence.

Though the results just shown are typical, a completely reversed effect is found for tests on the same model at the lower Mach number of 0.68 for which the nominal shock position is well forward. These results are reproduced here as Figures 5 and 6. At the low Reynolds number, as revealed by Figure 5, forward movement of the shock now starts at around an incidence of 8.3 degrees while at high Reynolds number, Figure 6, shows this forward movement at around 7.3 degrees. The nominal shock position was not so far forward as to interact with the transition fixing band and so the tests apparently indicate an adverse scale effect for shocks that are well forward. Clearly this effect needs further investigation though this is beyond the scope of these present notes.

#### 2.2.4.5 High Sweep Wings

As far as high Reynolds number simulation methodology is concerned a complex configuration can be considered as any configuration for which three dimensional effects become important. Thus for combat aircraft relatively simple aircraft geometries can be considered complex if the wing sweep is high and a different approach to that previously described is then required.

Where configurations are designed for attached flow, three dimensional effects are less important and the tendency is to concentrate on the shock boundary layer interaction and



trailing edge flow and the approach is similar to that for low sweep high aspect ratio wings. In these cases the improved state of computational methods enables a good understanding of the flows involved and much can be done to avoid scale sensitive problems.

However as Moss, Reference 6 points out the tendency is now to design complex configurations involving leading edge cranks, leading edge wing root extensions and integrated pylons and stores. The configuration has to operate well beyond the attached flow regime and high sensitivity to scale effects is to be expected. Often, as Moss points out, the flow will be naturally turbulent from the leading edge at tunnel Reynolds number due to high sweep and turbulent contamination from the fuselage. In these cases little can be done and transition free tests have to be carried out.

The problem of turbulent attachment line flow is essentially a three dimensional problem and the possibility of its existence increases as the wing sweep or strictly speaking the attachment line sweep increases. Thus in addition to considering two dimensional Tollmien-Schlichting type instability of the laminar boundary layer consideration is also given to leading edge contamination and, that other three dimensional effect, instability of the crossflow velocity profile. Hall and Treadgold, Reference 7, summarise the current calculation methods now in common use for assessing laminar flow instability and outline the main problems to be contended with. Figure 7 is taken from Reference 7 and shows how transition varies with Reynolds number for a swept wing. Figure 8 also taken from this work shows the actual results for wings swept at 60 and 30 degrees.

When forward fixing is used to produce fully turbulent flow from the leading edge the possibility of relaminarisation further downstream must be considered. Such relaminarisation may occur further outboard on the attachment line due to reduced sweep in that region of the wing, or may occur in a strong favourable pressure gradient as the flow moves away from the attachment line. In these cases more rearward fixing may be necessary to produce turbulent flow over the majority of the wing as a best compromise to fully turbulent flow. The commonly used criteria for assessing relaminarisation are considered by Hall and Treadgold and so further repetition is not warranted in these present notes.

#### 2.2.4.6 Drag Prediction

At cruise conditions a high lift to drag ratio is required for maximum aerodynamic efficiency of an aircraft and this parameter is sensitive to small changes in drag around the design point. The flow over the majority of the configuration is attached at cruise and the main aim of any simulation is to get the drag right. Now a far field analysis such as that of Squire and Young, Reference 8, shows that viscous drag can be related to the boundary layer condition at trailing edges in terms of the displacement and momentum thicknesses. Thus one approach to testing could be to make some attempt to scale the boundary layers correctly at the trailing edges with only some very minimal extrapolation of results to full scale. However the difficulty of using different transition fixing positions for different Reynolds numbers, to enable extrapolation, creates more problems than it solves. The more usual approach is then simply to fix transition well forward, on the basis that this is so at full scale, and then correct for Reynolds number using traditional skin friction and form factor methods.

When the cruise speed is high, the situation is potentially more complex than this as it then becomes necessary to consider simulating correctly the shock boundary layer interactions. In these cases there is a need to scale the boundary layer just ahead of the shock and rearward fixing may be used if the shock is sufficiently far aft. For Reynolds number correction, use is again made of skin friction and form factor methods, but, as the transition positions at model and full scale can vary widely, the calculations are more involved and are sensitive to the assumed full scale natural transition position.

The forward fixing procedure relies on naturally forward transition at full scale and so in principle, for lower flight Reynolds numbers a more rearward fixing position may be necessary though this is not generally used in practice. However the designer will attempt to establish the model and full scale natural transition locations to decide whether at the model scale it is necessary to bring the fixing band right up to a wing leading edge in order to simulate turbulent attachment line flow as previously discussed for highly swept wings.

Green, Reference 9, describes how the boundary layer on a wind tunnel model can be scaled to simulate full scale behaviour both at the shock and at the trailing edge by use of forward transition and distributed surface suction downstream of transition. Indeed Green shows that by using an ideal distribution of suction, based on simulating full scale skin friction on the model, that the boundary layer can be simulated everywhere. However the technique is costly and requires interactive use of computational fluid dynamics methods to calculate the boundary layers and suction levels. For this reason the technique is not currently suitable for industrial testing. However in the future the reduced costs of computational fluid dynamics and the increasing demands of precision, when testing in the wind tunnel, may make this simulation method much more practical.

#### 2.2.4.7 Buffet Onset

In three dimensions, wings at high subsonic speed experience a strong outboard normal shock and this interacts with the trailing edge flow in much the same way as with the

comparable two dimensional aerofoil problem. If the available test Reynolds numbers are low the main problem is that of premature trailing edge separation.

The three dimensional problem can be illustrated using the results of Reference 4. With this experiment measurements were made on a variable sweep wing over a range of Mach number and for two nominal Reynolds numbers differing by almost one order of magnitude. From the measured pressure distributions the type of separation was determined at buffet onset for a wing sweep of 25 degrees and the class of separation is presented here, in Figure 9, to show the qualitative variation with Reynolds number and Mach number. Though transition free results would be expected to show a much greater variation, it should be understood that these particular results were obtained with a forward transition fix location in order to highlight the problems at transonic speeds with the traditional simulation technique. All the observations were of class B1 separation except for a single class B2 separation and some evidence that Class A separation might occur at full scale at the higher Mach numbers but not at the lower ones.

The main points to notice are that the class of separation changes with Reynolds number and that the potential variation increases as the Mach number is increased. This latter effect comes of course from the rearward movement and strengthening of the shock with increased Mach number. Figure 9 also shows that test Reynolds numbers greater than 3 or 4 million will be required if a full scale class B1 type separation is to be correctly modelled, while test Reynolds numbers greater than 12-20 million are required, depending on the Mach number, if a full scale class A type separation is present. This minimum Reynolds number requirement would be necessary for a simulation methodology based on Reynolds number extrapolation and so the actual methodology used must reflect the range of tunnel Reynolds number available and the intended flight Reynolds number range.

There are two basic schools of thought concerning low Reynolds number testing. One considers the modelling of the class of separation as being of prime importance and the other considers this desirable though not essential. Both approaches are based largely on experience of successful designs, but the former more cautious approach is more desirable for designs for which there is little past experience.

When test Reynolds numbers are below the critical limit for the full scale class of separation it is necessary to reduce the tendency for trailing edge separation as can be inferred from Figure 9. One means of achieving this aim is to add small amounts of thickness to the upper surface trailing edge region of the wind tunnel model to alleviate the local adverse pressure gradients.

Such base thickness is usually determined from design calculations that give similar values of boundary layer shape parameter, or other indicator of separation, at the trailing edge for both wind tunnel model and full scale design. This technique can be used with aft fixing, with the aft fix used to scale the boundary layer at the shock and the base thickness used to control the premature trailing edge separation, so providing the two degrees of freedom necessary to simulate flow breakdown. However the technique requires different model geometries at different design conditions and different test Reynolds numbers and so like most advanced simulation techniques gives rise to an expensive test program that tends to limit, if not prohibit, its use. In addition the technique is either dependent on an implicit faith in computational fluid dynamics, or like more traditional methods, must be supported by a wealth of previous design experience.

For these reasons it is more usual to use aft fixing alone when test Reynolds numbers are below the critical limit for the full scale class of separation. The current practice is to choose a fixing position that correctly scales the boundary layer just upstream of the shock such that the shock boundary layer interaction is controlled and the growth of the boundary layer at the trailing edge is minimised. By way of example, Figure 10 shows forward and aft transition band positions as used during tests on a small combat aircraft model and Figure 11 shows the isobars measured near buffet onset during the tests. The position of the aft transition band was chosen following the determination of the shock system from flow visualization studies and the spanwise variation of this band involves a crank as part of an attempt to follow the rationalised position of the leading shock contour. Figure 11 shows a dramatic difference between the isobar patterns for the two transition band positions and shows that the premature forward movement of the shock system resulting from premature trailing edge separation can be controlled using aft fixing.

#### 2.2.4.8 Post Buffet Performance

A notable requirement of fighter aircraft is the need to conduct manoeuvres at high incidence and under conditions of high longitudinal and normal acceleration. All this is well beyond buffet onset with the flow over the majority of the wing and over parts of the fuselage separated. In addition the high loading on the structure gives rise to significant aeroelastic distortion.

On the other hand, model tests aim for a steady level flow condition which is clearly not appropriate to agile combat performance while high incidence in the tunnel can give rise to very large blockage and tunnel wall interference. As the standard corrections are only first order accurate they are of uncertain benefit for these conditions and results are often left uncorrected.

It is against this basic level of uncertainty that we must consider the high Reynolds number simulation problem.

The main requirement of model tests at these high lift conditions will be to demonstrate reasonably smooth force and moment characteristics and adequate stability in this non linear region. Lateral stability is particularly important for its effect on spin recovery and in this respect asymmetric vortex formation on the forebody and leading edge separations on the wing are important. Reynolds number dependence on lateral forces is particularly important for smooth forebody shapes, as is confirmed by References 10 and 11, where primary separation positions are dependent on the boundary layer flow. Vortices originating from the forebody may burst in the strong adverse pressure gradients over the wing and, as the vortex core is a form of shear layer, dependence on Reynolds number may result.

#### 2.2.4.9 Secondary Influences

For very complex configurations the approach is to start with a more simple configuration and this will generally involve a clean wing free of strakes, pylons and stores. For this relatively simple case forward, rearward or free transition will be used depending largely on the wing sweep and the final decision for the appropriate position will follow tunnel testing. This basic fixing will then be used for the more complex case, but with each additional component of the configuration having its own appropriate fix. Naturally the various components of the configuration interact with each other and so whilst this building block approach provides a logical means of tackling complex geometries it has its limitations. The strake is one example where the wing flow can be drastically changed by the addition of a further component and in these cases it may be necessary to reappraise the transition fix as used on the wing. Bearing this in mind consideration will now be given to the various components.

Strakes are tested transition free, as these are thin and can be considered sharp edged, though this ignores the effect of Reynolds number on the secondary vortices. As drag is important forward fixing is used on fuselages, fins, tailplanes and all external equipment such as stores and pylons. At high incidence many of these forward fixes become inappropriate, but may be retained to simplify the test programme. If forebody problems are suspected additional tests may be carried out with lateral transition tripping devices on the forebody.

Where the choice of appropriate fix remains ambiguous results, will be obtained for more than one fix to reveal the problem areas and to give an indication of the degree of uncertainty.

#### 2.2.4.10 Conclusions

The approach to high Reynolds number simulation when conducting transonic wind tunnel tests on models regarded as complex configurations has been briefly discussed. The costs of testing, the needs of industry and the complexity of the simulation problem result in an approach that is practical though relying more on experience than hard scientific evidence. The main conclusions, or observations, can be summarised as follows:

1. Simulation methodology is based largely on two dimensional flow experience and can be used with confidence only for high aspect ratio low sweep wings.
2. Tunnel testing becomes more expensive as the degree of precision of simulation methodology is increased. This tends to have a conservative effect on testing, but once any advanced technique has been shown to provide genuine improvement it is quickly brought into use.
3. The costs of implementing simulation techniques tends to result in a range of methods in use at any one time with the simpler methods used whenever they are applicable.
4. Design calculations using proven computational fluid dynamic codes are often used to establish differences in important parameters at model and flight scale. Such information may then be used in the simulation methodology with no further course for redress.
5. Differences in parameters such as free stream turbulence require caution when comparing the results of tunnel tests carried out in different facilities.
6. Often the range of tunnel Reynolds numbers is too small to permit accurate extrapolation of results to full scale.
7. For combat aircraft at high incidence the uncertainty of scale effect is such that correction of wind tunnel results to full scale is often not attempted.



## 2.2.4.11 References

1. Haines, A. B. Review of post - 1974 evidence on scale effects at high subsonic speeds.  
ARA memo 218.
2. Pozniak, O. M. A review of the effect of Reynolds number on afterbody drag.  
ARA report 56, May 1980.
3. Haines, A. B. Notes on transition fixing and the interpretation of drag data with different transition fixes.  
ARA memo 243, November 1982.
4. Weeks, D. J. An investigation of scale effects on the transonic flow over swept wings. Part 1: Measurements on a model of a transport-aircraft configuration.  
ARC RM 3842 PART 1, November 1976.
5. Weeks, D. J.  
Hodges, J. An investigation of scale effects on the transonic flow over swept wings. Part 2: Measurements on a model of a variable - sweep strike - fighter configuration.  
ARC RM 3842 PART 2, November 1976.
6. Moss, G. F. Review committee of AGARD/FDP WG/09 - Boundary layer simulation in wind tunnels. Contribution from RAE Farnborough transonic wind tunnels.  
Private correspondence, July 1984.
7. Hall, M. G.  
Treadgold, D. A. Difficulties in predicting boundary-layer transition on swept wings.  
RAE TM 1465, December 1972.
8. Squire, H. B.  
Young, A. D. The calculation of profile drag of aerofoils.  
ARC RM 1838, November 1937.
9. Green, J. E. Some aspects of viscous-inviscid interactions at transonic speeds and their dependence on Reynolds number.  
AGARD CP 83-71, April 1971.
10. Skow, A. M.  
Erickson, G. E. Modern fighter aircraft design for high angle of attack manoeuvring.  
AGARD LS 121-82, March 1982.
11. Gregoriou, G. Modern missile design for high angle of attack.  
AGARD LS 121-82, March 1982.

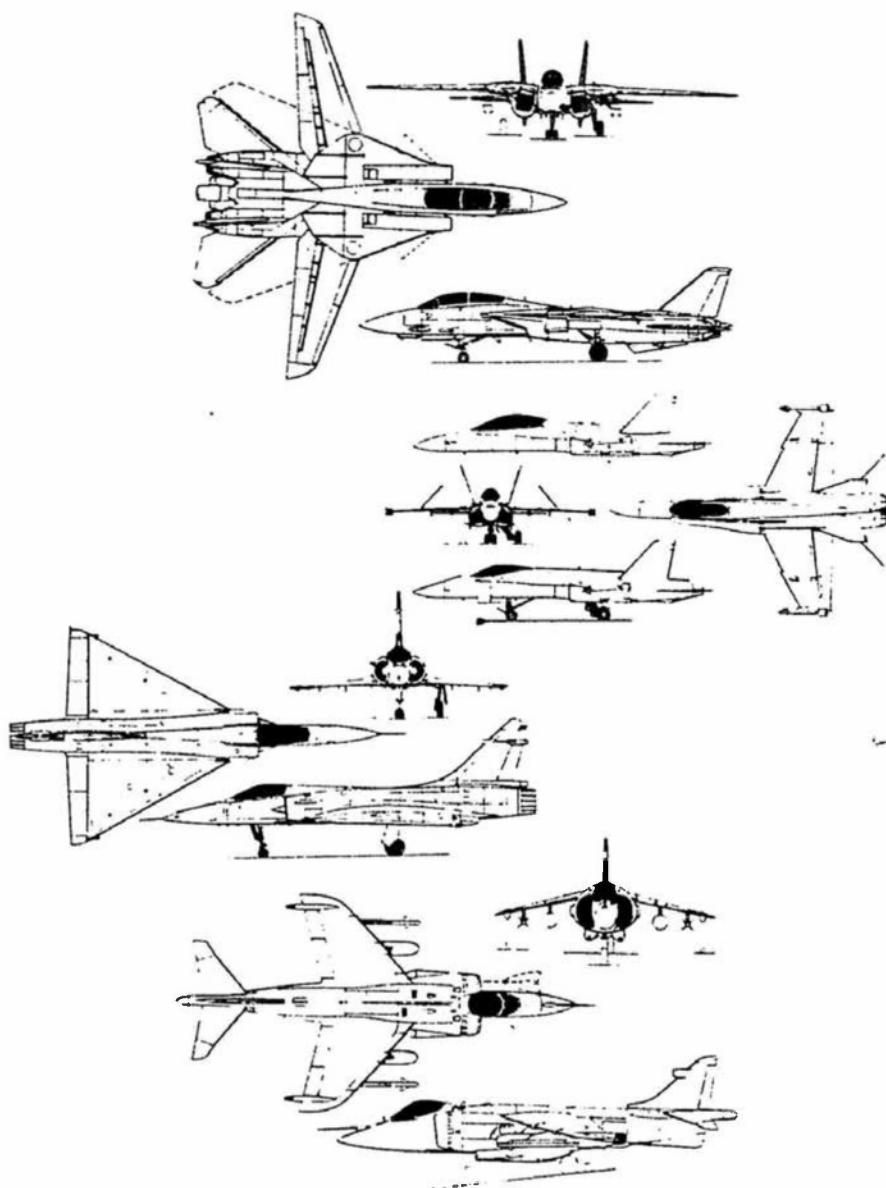
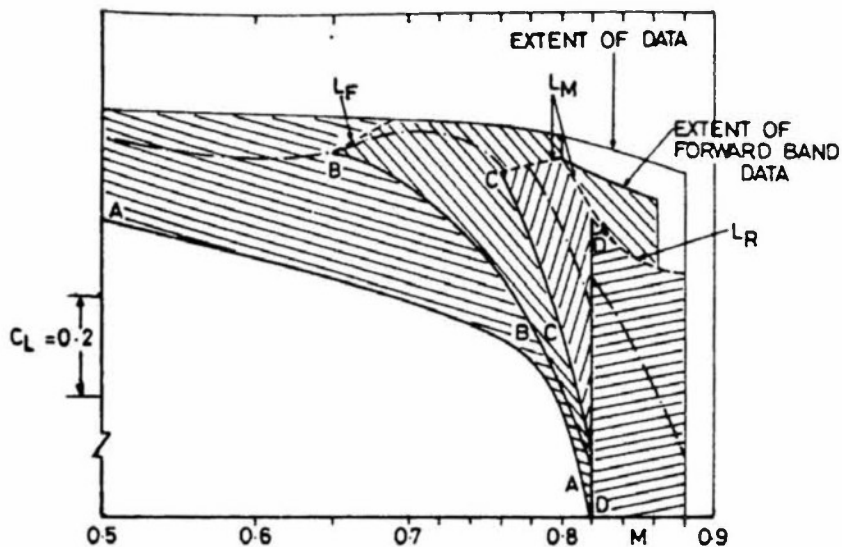


Figure 1  
Section 2.2.4

Combat aircraft shapes



AA : LIMIT OF COMPLETELY SUBCRITICAL FLOW

/// : SHOCK UPSTREAM OF FORWARD BAND  
BUT FORWARD BAND DATA RECOMMENDED

/// : SHOCK AFT OF FORWARD BAND \*  
FORWARD BAND DATA RECOMMENDED

/// : SHOCK AFT OF MID BAND \*  
MID BAND DATA RECOMMENDED

/// : SHOCK AFT OF REAR BAND \*  
REAR BAND DATA RECOMMENDED

--- : BOUNDARIES FOR TRAILING-EDGE PRESSURE DIVERGENCE ( $\eta_g = 0.652$ )  
N.B. SHOCKS MOVING AFT BELOW AND FORWARD ABOVE  
THESE BOUNDARIES

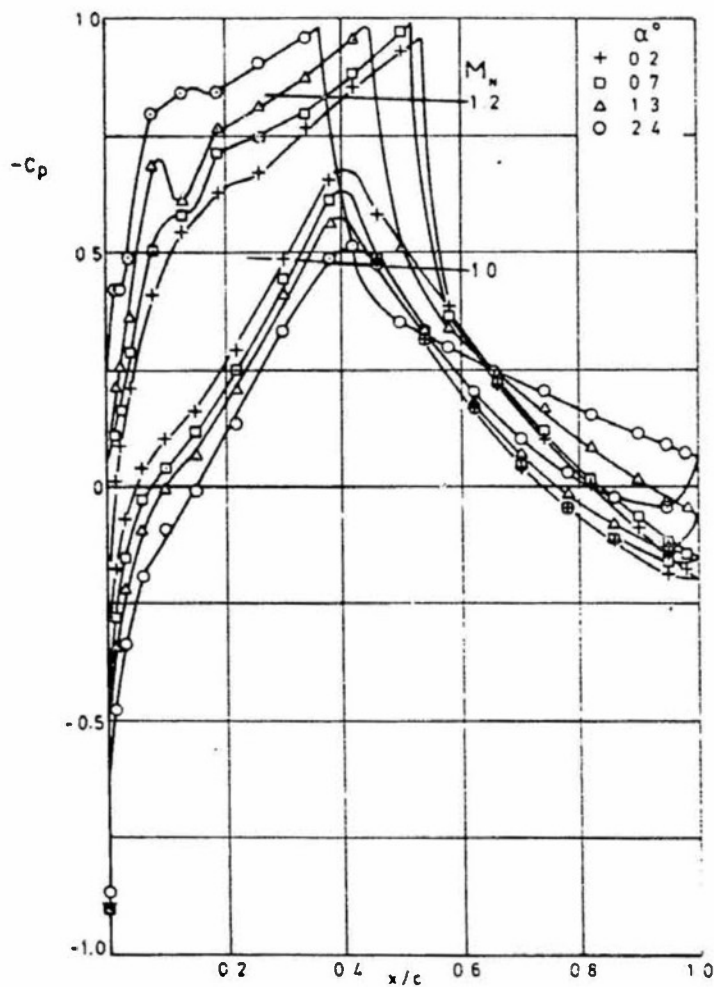
$L_F, L_M, L_R$  : BOUNDARIES DEFINING UPPER LIMIT OF VALIDITY  
OF RESPECTIVELY FORWARD, MID AND REAR BAND DATA

\* : STRICTLY, SUFFICIENTLY FAR AFT TO AVOID ANY LOCAL INTERFERENCE  
BETWEEN ROUGHNESS BAND AND THE SHOCK STRENGTH AND POSITION

Figure 2  
Section 2.2.4

The validity of wind tunnel data for different  
transition fix positions on aircraft model wings

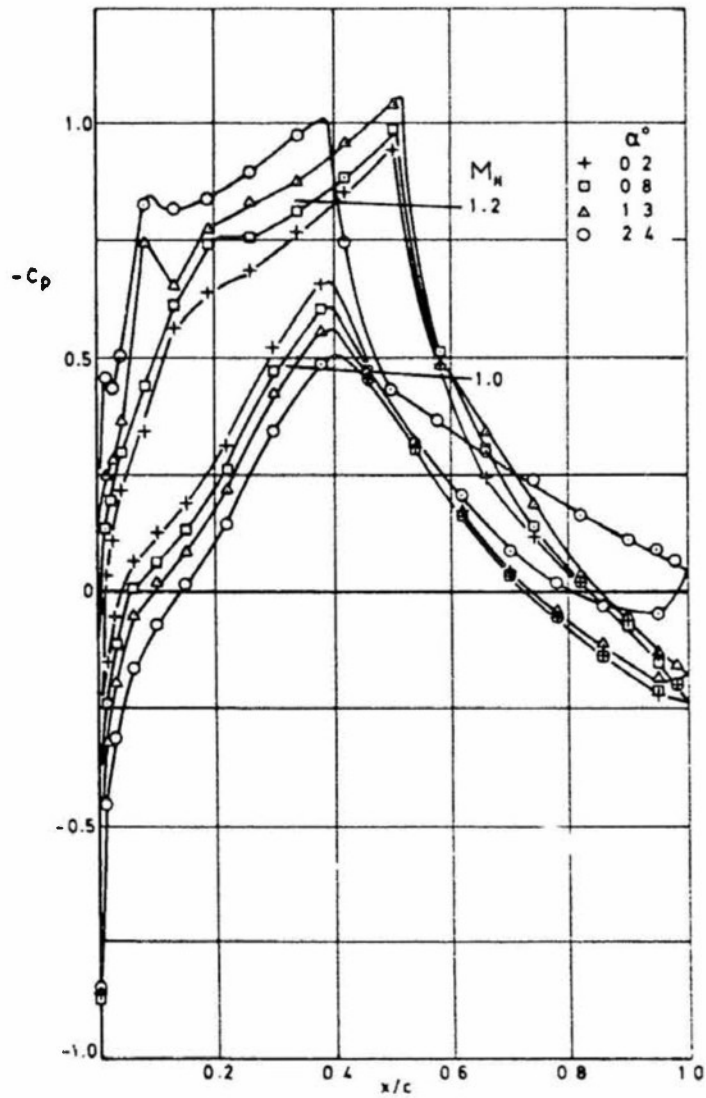
From A.B. Haines: AEA memo 147, November 1961



Measured pressure distributions.  $M = 0.825$ ,  $\lambda = 25^\circ$ ,  $\tau = 0.75$ ,  
 $R_L = 2.3 \times 10^6$ . Fixed transition

Figure 3  
 Section 1.1.4

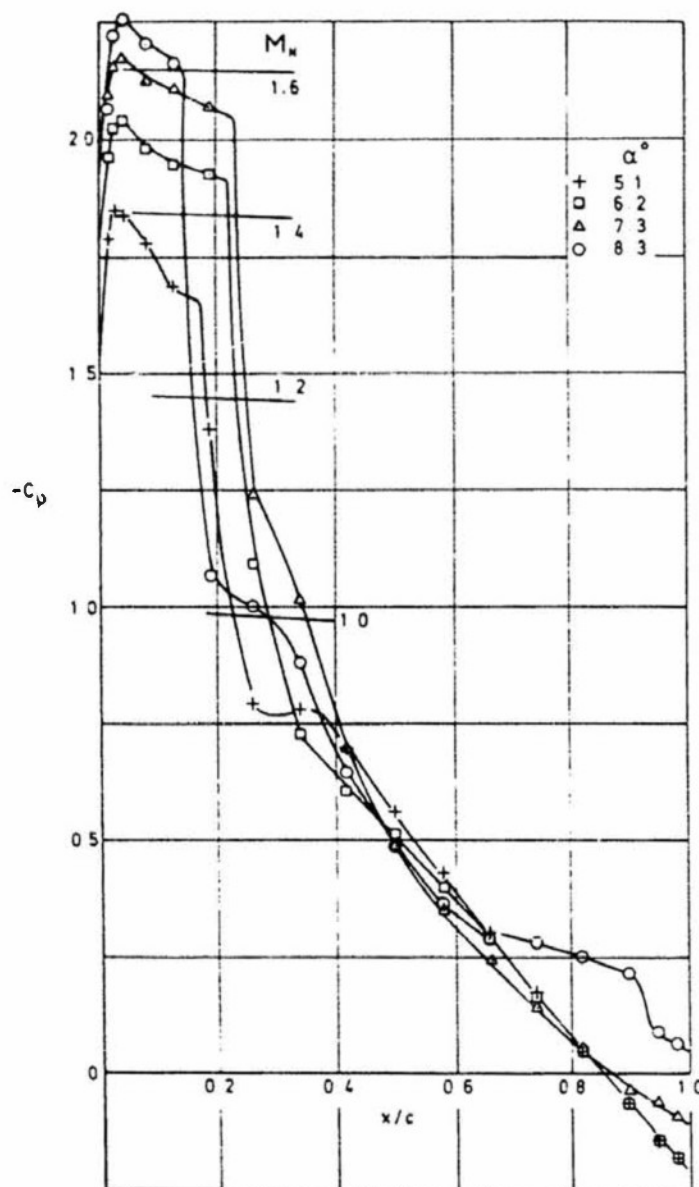
From D.J. Weeks and J. Hodges: APT RM 3342 PART I, November 1976



Measured pressure distributions.  $M = 0.825$ ,  $\Lambda = 25^\circ$ ,  $\eta = 0.75$ ,  
 $R_\xi = 12.3 \times 10^6$ . Fixed transition

Figure 4  
 Section 2.2.4

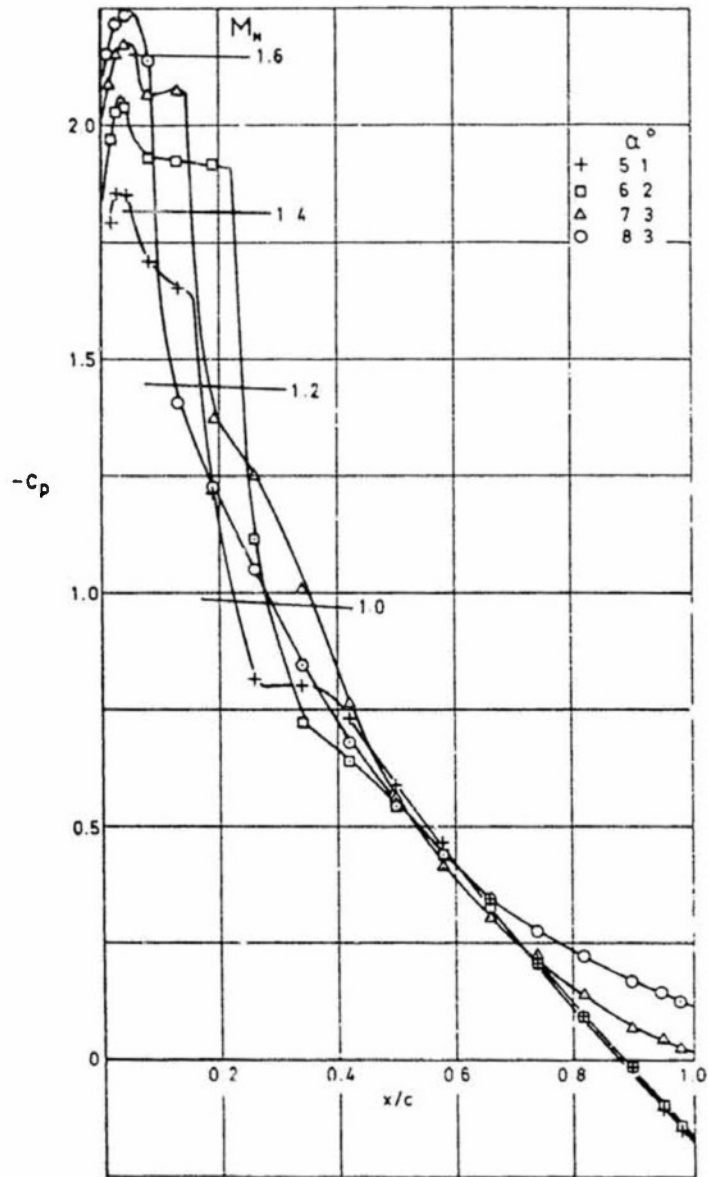
From D.J. Weeks and J. Hodges: ARC RM 3342 PART 2, November 1976



Measured upper-surface pressure distributions.  $M = 0.68$ ,  $\alpha = 25^\circ$ ,  
 $\eta = 0.75$ ,  $R_c = 4.6 \times 10^6$ . Fixed transition

Figure 5  
 Section 2.2.4

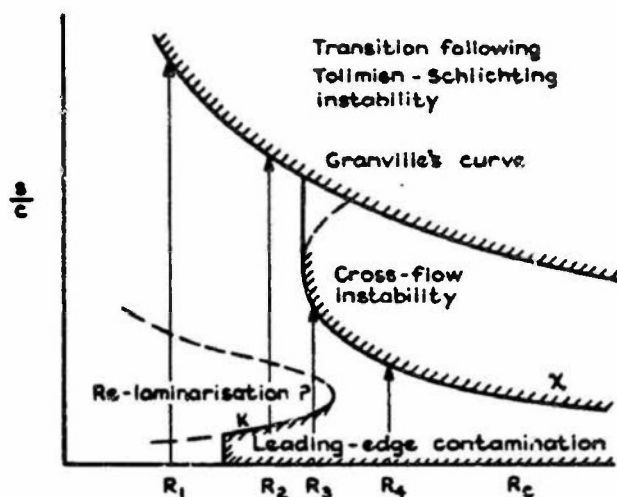
From D.J. Weeks and C. Hedges: ARO RM 3842 PART I, November 1976



Measured upper-surface pressure distributions.  $M = 0.68$ ,  $\lambda = 25^\circ$ ,  
 $\eta = 0.75$ ,  $R_{\bar{c}} = 14.8 \times 10^6$ . Fixed transition

Figure 5  
 Section 2.2.4

From D.J. Weeks and J. Hodges: ARC FM 3842 PART 2, November 1976



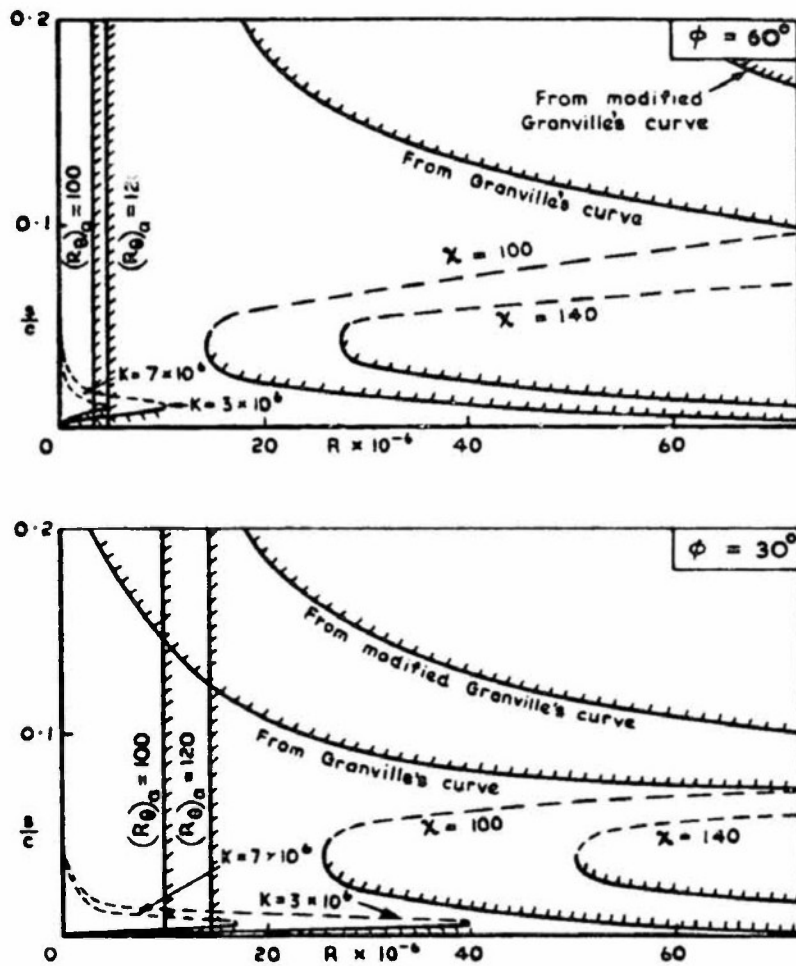
- At  $R_1$  Transition follows from Tollmien-Schlichting instability
- At  $R_2$  Leading-edge contamination, followed possibly by re-laminarisation and then transition through Tollmien-Schlichting instability
- At  $R_3$  Leading-edge contamination, followed possibly by re-laminarisation and then transition through cross-flow instability
- At  $R_4$  Transition follows from cross-flow instability if leading-edge contamination were absent

Schematic sketch of the movement with Reynolds number of the predicted point of transition or of instability

Figure 7  
Section 2.2.4

From M.G. Hall and D.A. Treadgold: RAE TM 1465, December 1972





The movement with Reynolds number of the  
predicted point of transition or of instability

Figure 8  
Section 2.1.4

From M.G. Hall and D.A. Treadwell: RAE TM 1468, December 1971

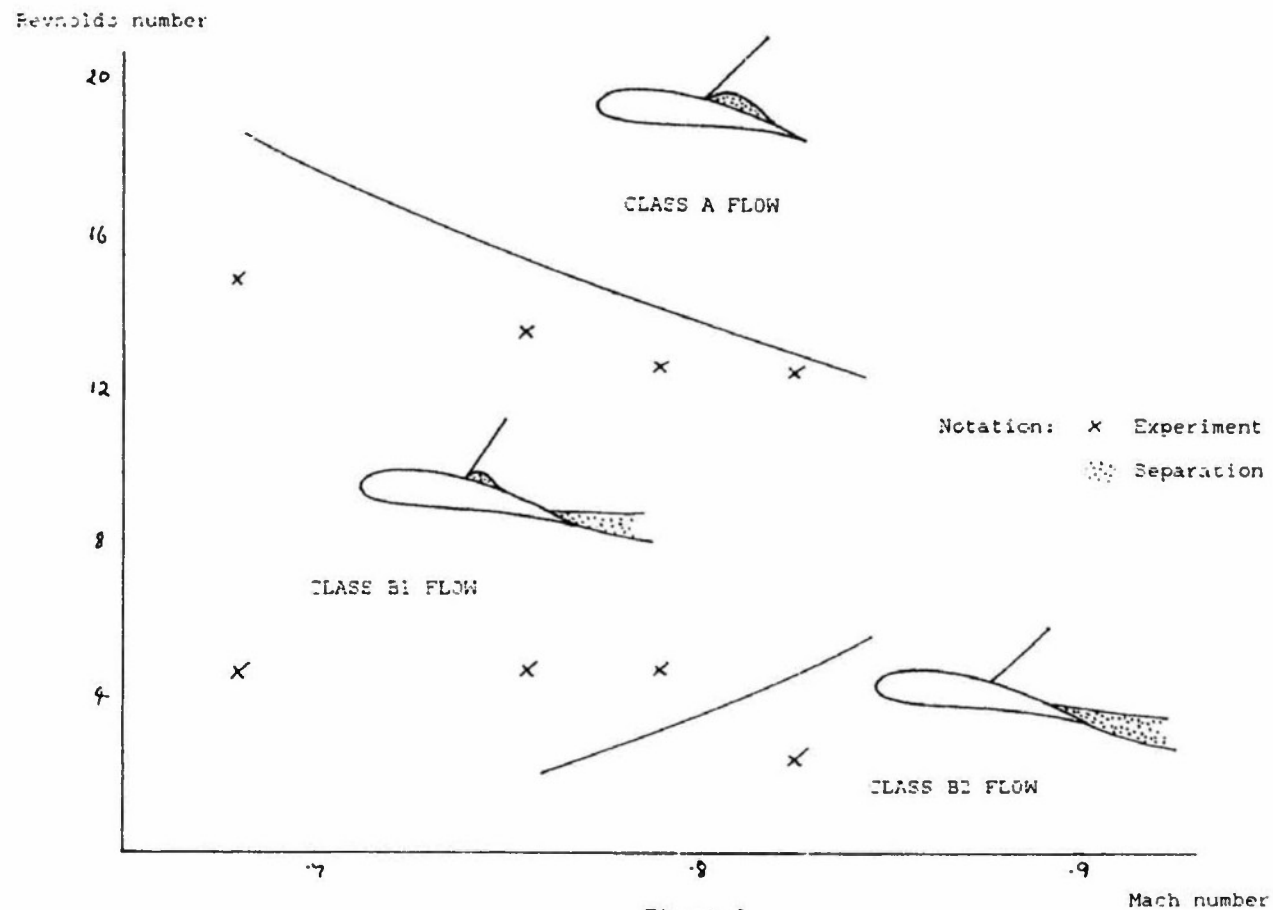


Figure 9  
Section 2.2.4

Qualitative assessment of flow type  
at buffet onset for a low sweep wing

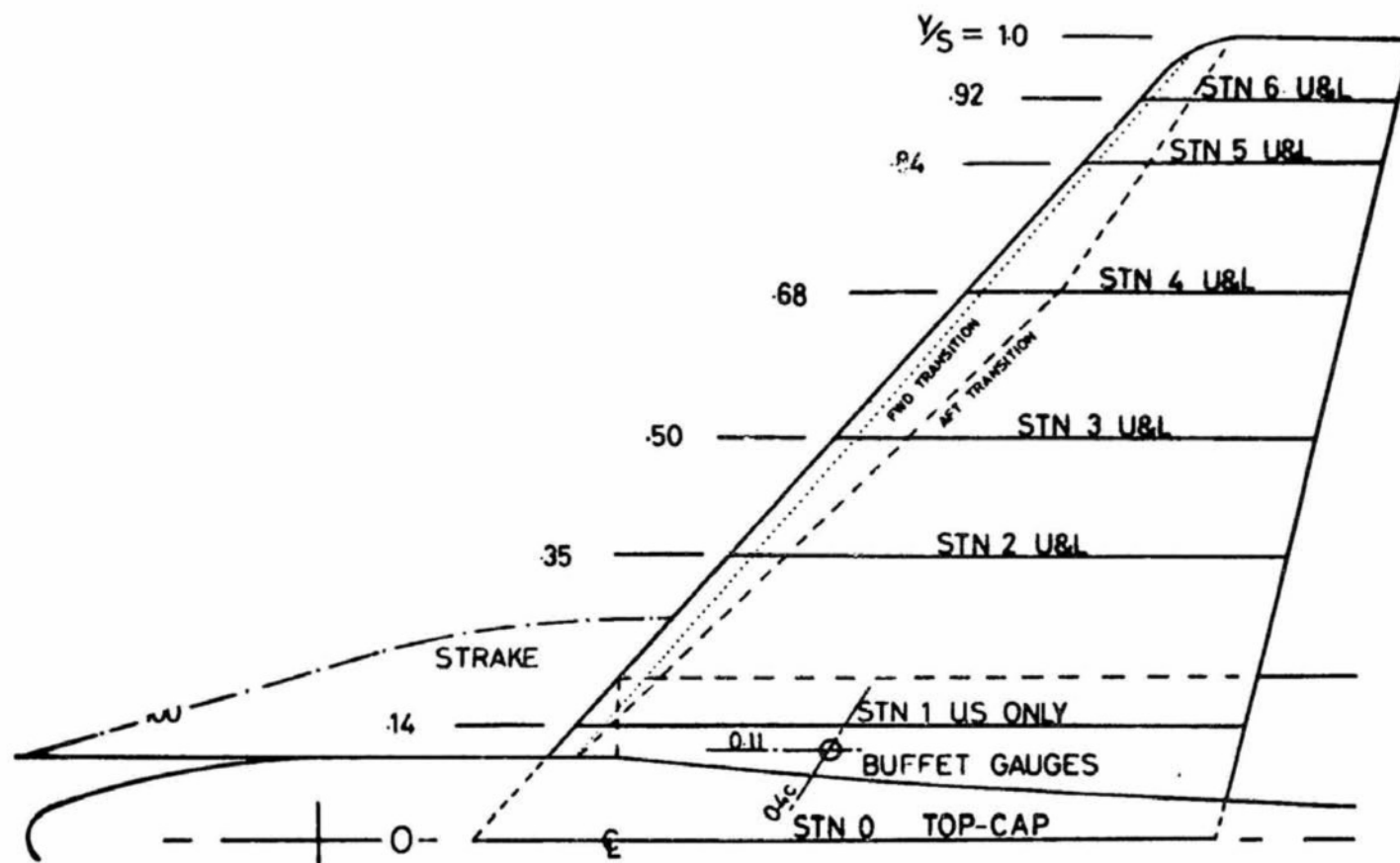


Figure 10  
Section 2.2.4

Forward and aft transition fix positions on  
a small combat aircraft wind tunnel model

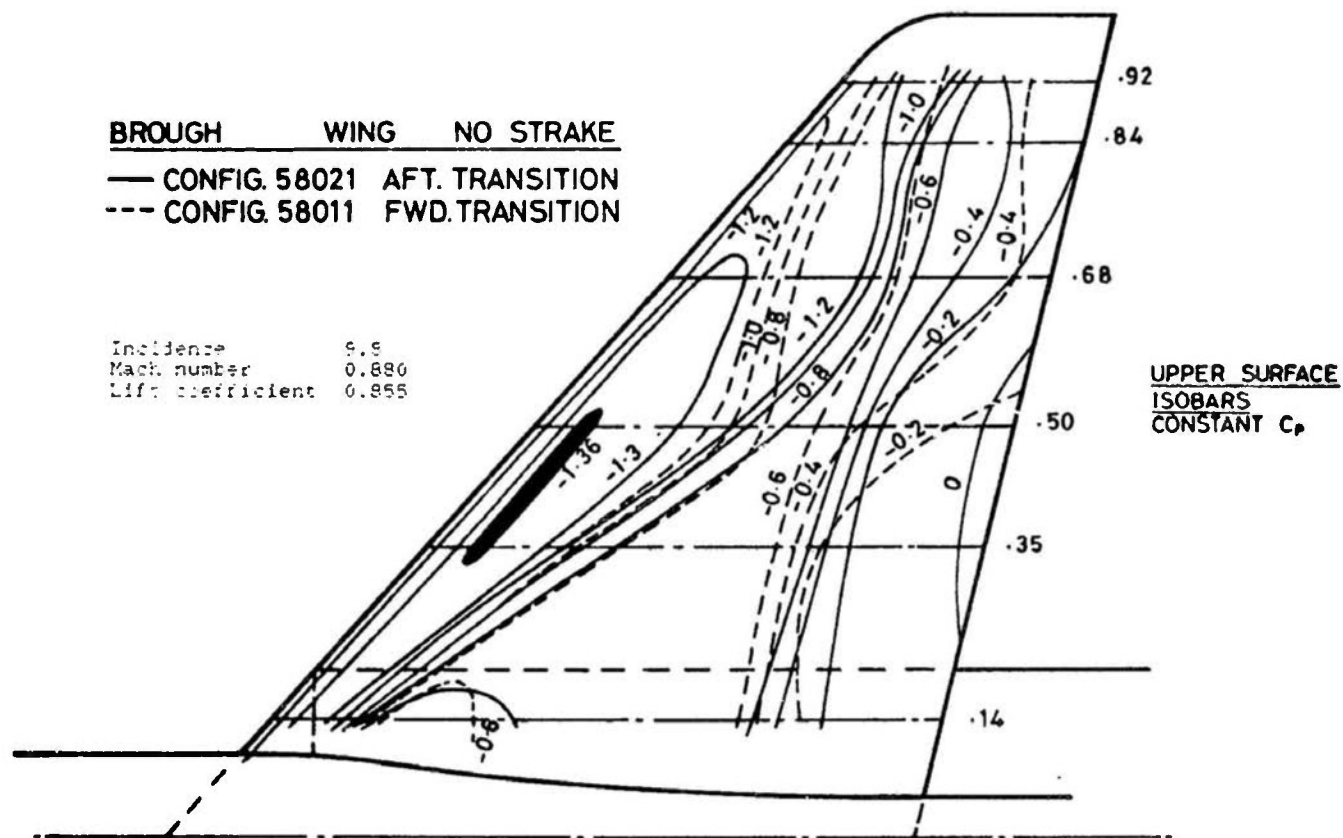


Figure 11  
 Section 2.2.4

Effect of transition on shock position near buffet onset

## SECTION 2.3 WIND TUNNEL ASPECTS

### SECTION 2.3.1

#### REYNOLDS NUMBER EFFECTS AND THE WIND TUNNEL ENVIRONMENT

by

A. Elsenaar  
National Aerospace Laboratory (NLR)  
Anthony Fokkerweg 2  
1059 CM Amsterdam  
THE NETHERLANDS

#### 2.3.1.1 INTRODUCTION

A particular set of experimental results is liable to experimental error and/or unwanted of even unknown influences of the windtunnel environment. These effects may very well change in magnitude with the tunnel Reynolds number. This point has been raised many times (see, e.g. McCroskey at the round table discussion of the 1983 AGARD Specialist Meeting on Wall Interference, ref. 1; fig. 1). From the point of view of the development of a simulation methodology for high Reynolds number prediction, the observation is of utmost importance: it confuses the existing evidence on Reynolds number effects and it may effect in a direct way a particular simulation methodology.

For that reason a short review will be presented of the available evidence with respect to the problem of "pseudo" Reynolds number effects due to the tunnel itself. The review is not complete. Instead it is attempted to highlight the most important physical phenomena. Where possible use is made of the most recent publications, in particular the AGARD Conferences on Wall Interference and Wind Tunnel Test Techniques (ref. 1 and 2).

#### 2.3.1.2 TUNNEL CALIBRATION

The calibration of the empty test section of a windtunnel may be considered as the basis of all subsequent testing and data reduction in that particular windtunnel. The calibration itself can be Reynolds Number dependent. A nice illustration of this effect is the so called "Reynolds number paradox" on afterbody drag (fig. 2a). O.M. Pozniak (ref. 3) has written a comprehensive review on this effect in relation with "true" Reynolds number effects. Part of the paradox could be explained from a Reynolds Number dependence of the tunnel calibration (fig. 2b). The apparent afterbody drag (either from force measurement or from pressure integration) is extremely sensitive to a variation in the reference static pressure: a variation in pressure coefficient of 0.01 roughly corresponds to 100 drag counts for the afterbody drag (based on frontal area).

This shows that it is essential to calibrate the windtunnel as a function of Reynolds number. Incidentally, similar effects are introduced by static pressure gradients originating from wall interference (section 3) or model support systems (not discussed here).

#### 2.3.1.3 WALL INTERFERENCE

Wall interference is a classical problem in experimental aerodynamics. In the last decennium a significant progress has been made in this field as a recent review by Mokry, Cahn and Jones (ref. 4) reveals together with the outcome of the AGARD specialist meeting in London, 1982 (ref. 1). In the present context we are mainly interested in its relation with Reynolds Number effects.

The figures 3 and 4 then illustrate how wall interference effects can affect measured Reynolds Number trends. The evidence is somewhat conflicting. In figure 3, taken from reference 4, a comparison is presented of drag-rise and maximum lift as measured on one airfoil (CAST-10) tested in three wind tunnels, including two high Reynolds number facilities (the cryogenic 0.3m tunnel of NASA Langley and the Compressible Flow Wind Tunnel of Lockheed-Georgia). The figures 3a and 3b reveal large variations in maximum lift and drag-rise.

However, when the maximum lift development with Reynolds Number is plotted for the actual measured drag-rise Mach Number, a rather consistent trend is found (fig. 3c). A tentative explanation is that part of the measurements are corrupted by a wall interference effect (either from top and bottom wall or from the side walls (section 4)) that introduces an uncertainty in the actual Mach Number.

Figure 4, on the other hand, shows the result of a similar comparison, this time the CAST-7 airfoil tested in various windtunnels (ref. 5). A fair agreement is observed in Reynolds Number trends for drag, maximum lift and angle of incidence at constant lift. The absolute levels, however, show a rather large variation, a variation that is reduced considerably when only wall interference corrected data (measured boundary condition methods for the ONERA S3Ma and the NLR Pilot Tunnel, flexible walls for the ONERA T-2 and a classical homogeneous boundary condition method for the ARA 2-D tunnel) are considered. It is, however, interesting to note that the wall interference corrections in this case hardly influence the Reynolds Number trends.

One can conclude from these two-dimensional results that some suspicion with respect to Reynolds Number effects on wall interference is justified but not necessarily true in all cases. This can also be explained to some extent. Chan (ref. 6) has actually measured the boundary condition with respect to the flow through porous walls. His results indicate a dependence of the outflow velocity on the displacement thickness of the tunnel wall boundary layer provided that the holes are large compared with

the displacement thickness,  $\delta^*$ . Since  $\delta^*$  is a function of the tunnel unit Reynolds Number, some variation of the wall characteristics with Reynolds Number is not unlikely. Binion (ref. 7) has used a similar relation to calculate the Reynolds Number effect on the angle of incidence correction using classical theory for a typical 3-dimensional configuration. The effect can not be neglected in that case (fig. 6).

More direct evidence is obtained by Smith of NLR (see ref. 8) who actually determined from a measured boundary condition technique (ref. 9) the wall interference corrections for a two-dimensional airfoil as tested in the NLR slotted high speed tunnel HST. In this particular case the Reynolds number effect on the corrections is rather small, although a variation in Mach number of the order of .002 is not insignificant for the assessment of Reynolds Number effects on the drag-rise boundary. It is sometimes suggested that porous walls are more susceptible to Reynolds Number changes than slotted walls. The flow along sharp edges, like the slots in ventilated walls, is known to be Reynolds Number independent and Chan's work reveals that this is not always the case for porous walls. Finally it should be noted that Mach Number and incidence corrections represent only a part of the wall interference effects. Static pressure gradients as discussed in section 2 may effect drag, upwash variations may effect the pressure distribution and the pitching moment for configuration with tail surfaces. For two-dimensional testing the side wall boundary layer adds to the uncertainty as will be discussed now.

#### 2.3.1.4 SIDE WALL EFFECTS

Side-wall boundary layer effects represent a serious problem in two-dimensional testing as figure 8 illustrates (ref. 11). The observed correlation of airfoil lift with the side-wall boundary layer displacement thickness suggests that the tunnel unit Reynolds Number will have an effect as well. Some indication of this effect may be obtained from Barnwell's theory (ref. 12) that provides a Mach Number correction as a function of free stream Mach Number, airfoil chord/width ratio and side-wall boundary layer displacement thickness. An estimate of this effect is presented in figure 8, using Barnwell's theory (but modified by P.R. Ashill to allow for three-dimensional effects; ref. 13) and assuming a  $Re^{1/5}$  dependence of the side wall boundary layer displacement thickness  $\delta^*$ . The figure indicates that this is a potential problem area, particular for low aspect ratios. In general, however, it is recommended to use aspect ratios larger than 2 for two-dimensional testing (ref. 12) and the problem is then less severe.

#### 2.3.1.5 FLOW QUALITY

It has been recognized for a long time that a certain standard of flow quality is required in wind-tunnel testing. This problem has been studied thoroughly as part of the specification for high Reynolds Number facilities in the 1970's (ref. 14, 15). More recent information can be obtained from the references 16 and 17.

Is there a relation between flow quality and Reynolds Number effects? Figure 10a, taken from reference 29, shows how the transition Reynolds Number appears to be a function of the unit Reynolds Number. The problem was for that reason known at the end of the sixties as the "unit Reynolds Number effect". It was also observed that for a constant unit Reynolds Number the transition length increased with the tunnel dimensions (fig. 10b). The physical explanation must be found in the tunnel noise, radiated from the tunnel wall boundary layers as it is well known that noise, like free-stream turbulence has a large effect on transition. In 1982 Dougherty (ref. 10) was able to correlate for a large number of windtunnels and some flight tests, the transition Reynolds Number with the pressure fluctuation level as measured on the surface of a 10 degree cone (fig. 11). The scatter in the results, however, is still considerable. This is not surprising. Other aspects of flow quality, like the energy distribution over the wave lengths are of importance as well. Also a correction for temperature non-equilibrium (see section 6) and Mach Number effects has been applied to the data of figure 11.

The forementioned examples are related to (almost) zero pressure gradient flows on flat plate or cone configurations. It shows that the transition length may change when a Reynolds Number variation is introduced by changing the unit Reynolds Number. How will this effect experimental results in the more general case of realistic airfoils or wings? Its effect will depend on the particular pressure distribution as figure 12 (taken from ref. 30) indicates. Free stream turbulence reduces the sensitivity of transition to pressure gradient. Reynolds Number trends with free transition will be particular sensitive to turbulence intensity as the theoretical exercise presented in figure 13 (reference 14a) demonstrates. The resulting transition point variations will have a large effect on the measured drag values. For transonic flows the effect on the pressure distribution may be large as well since it is well known that the shock-wave boundary layer interaction is critically dependent on the state of the boundary layer, either laminar or turbulent (see figure 14 taken from reference 20 and dating from 1955.). This is even more true for modern supercritical airfoils where the interaction with trailing edge separation acts like an amplifier of these effects. It is precisely this uncertainty that necessitates transition fixing in drag studies, as is generally done.

Apart from the observed effect on transition variation, a direct effect of turbulent intensity on the development of a turbulent boundary layer should also be noted. This has been studied extensively by Green (ref. 21) who was able to transform turbulence intensity into an effective Reynolds number. More recent studies (e.g. ref. 31 and 32) have indicated that the turbulence length scale is of importance as well. A purely empirical correlation is presented in figure 15 taken from ref. 31. In most existing windtunnels, the turbulence intensity is much less than 1 percent and the effects can then almost be neglected. In reference 22 some variation is observed in separation development due to free-

stream turbulence but these tests have been made at very low Reynolds Numbers. A similar example is taken from reference 23 and presented in figure 16. One should be careful in drawing conclusions however. Flow with weak shocks near the "design condition" are known to be sensitive to all kinds of small changes in flow conditions.

#### 2.3.1.6 TEMPERATURE NON-EQUILIBRIUM

Ross (ref. 24) and Dougherty and Fisher (ref. 18) have shown that the transition Reynolds Number strongly depends on the ratio of the actual to the adiabatic wall temperature (see fig. 17b). These transition point changes will effect the drag and lift characteristics as has been studied in more detail by Lynch et al (fig. 17a; ref. 25) in connection with a cryogenic blow-down facility. Similar work by ONERA (ref. 26) has indicated also that deviations from the adiabatic wall temperature should be less than 1 percent. This introduces an important requirement in cryogenic testing from the point of view of temperature control of model and free-stream conditions. The problem can be solved, however by pre-cooling the model unless heated elements are present in the model itself (like instrumentation compartments) that introduce a heat-flow in critical areas of the model.

#### 2.3.1.7 SURFACE ROUGHNESS

Both transition and turbulent boundary layer development are influenced by surface roughness. To determine if the surface is hydraulically smooth, a number of criteria are known. Most criteria are based on a Reynolds Number based on roughness height and the local velocity or local skin-friction velocity. For a good review is referred to references 27 and 28.

The effect of surface roughness on transition is by far the most important. There are two different aspects. On the one hand, when laminar boundary layer development is required, the roughness should not introduce unwanted or premature transition (see e.g. fig. 18a from ref. 19a). On the other hand, when a turbulent boundary layer is simulated by a tripping device, the device should be effective for a range of flow conditions, including Reynolds number (see e.g. fig. 18b). Since the criteria for a strip to be effective are reasonably well established (see e.g. ref. 27), only the Reynolds number dependence of the critical roughness height will be noted here. This is governed by the relation:

$$k/c \propto Re_c^{-1/2}$$

where  $k/c$  is the roughness height relative to the airfoil chord. The rather strong dependence on Reynolds Number makes it desirable or even necessary to change transition strips when the Reynolds Number is varied in a particular test. This is not always done and significant errors in the measurement may result from a not effective or oversized transition strip (see below). The same relation indicates the very high degree of surface finish that is required for high Reynolds Number cryogenic testing. This clearly indicates that surface roughness or transition strips may introduce unwanted "pseudo" Reynolds Number effects.

Once the boundary layer is turbulent, surface roughness causes a stronger growth in boundary layer thickness and hence a larger drag. One can distinguish between the effects of distributed surface roughness (see ref. 28) and the effects of a discrete roughness, like an oversized transition strip (fig. 19a) or a transition strip that is still present in the turbulent boundary layer (fig. 19b). These effects can also be Reynolds Number dependent.

#### 2.3.1.8 MODEL DEFORMATION

When the Reynolds Number is changed by variation of stagnation pressure, the wing-load will alter accordingly. Wing twist as a result of torsion and (swept) wing bending is a typical example (fig. 20 taken from ref. 7).

Other examples are deflections of control surfaces and variations in slat and flap positions. The effects, proportional to the loads and hence to unit Reynolds Number of a particular tunnel, may corrupt the measured Reynolds Number trends. It should be noted, however, that deformation effects can be equally important at flight conditions, depending on the particular configuration and/or load factor.

For that reason it is quite common to perform the aerodynamic calculations and windtunnel tests for the deformed ("jig") shape. With respect to wing deformation three effects, with an increasing severity, can be distinguished. Wing twist variation will cause a change in induced drag due to a small variation in wing loading. This effect can in general be calculated confidently. Secondly, the local wing section characteristics will be affected and this can be important when the shock-wave development depends critically on flow conditions. Strip-theory can be applied to derive corrections. Thirdly, the wing deformation might result in important variations in the three-dimensional flow pattern, separation being a typical example. In that case corrections are hardly possible and the basic shape of the windtunnel model must be adjusted. In the other two cases, corrections are possible on the basis of the measured or calculated differences in deformation between windtunnel and flight.

## 2.3.1.9 CONCLUDING REMARKS

If one adds all the uncertainties introduced by tunnel environmental effects, one may wonder if Reynolda Number trends as measured in windtunnels should be believed at all. The situation is, fortunately, not that bad. A large part of the discussed phenomena can be avoided with proper measures. For some other effects like wall-interference or wing deformation, corrections are possible although more refinement is required. They are just part of "sound aerodynamic testing". Unfortunately, this was not always evident in the past and for this reason the available Reynolds Number data should always be scrutinized with respect to this kind of "pseudo" Reynolds Number effects.

However, one particular problem area is of very much concern and will remain so in the future. The natural transition position appears to be critically dependent on a large number of variables: pressure distribution, tunnel noise and turbulence, temperature non-equilibrium, surface roughness ... and Reynolds Number. For that reason differences in transition location between windtunnel and flight are likely to occur for other reasons than Reynolds Number differences. This point is very well illustrated with figure 11. The scatter band shows a variation in transition Reynolds Number of 30 percent. Such an uncertainty in transition location is not acceptable in windtunnel testing: some characteristics (like drag and shock-induced separation) are known to be very sensitive for the state of the boundary layer. Since reliable theoretical predictions of transition are not yet available, it will remain good practice to either artificially fix the boundary layer or to measure the transition location.

## 2.3.1.10 REFERENCES

- 1 Wall Interference in Wind Tunnels, Fluid Dynamics Panel Specialist Meeting, London, May 1982. ACARD CP No. 335.
- 2 Wind Tunnels and Testing Techniques, Fluid Dynamics Panel Symposium, Çesme, Turkey, September 1983. AGARD CP No. 348.
- 3 Pozniak, O.M.. A Review of the effect of Reynolds Number on afterbody drag. ARA Report 56 (1980).
- 4 Stanewsky, E. et al. High Reynolds Number tests on the CAST 10-2/DOA 2 transonic airfoil at ambient and cryogenic temperature conditions. AGARD CP No. 348, paper 10 (1983).
- 5 Elsenaar, A., Stanewsky, E.. A Report of a CARTEur Action Group on "Two-Dimensional Transonic Testing Methods". ACARD CP No. 335, paper 5 (1982).
- 6 Chan, Y.Y.. Wall boundary-layer effects in transonic wind tunnels. AGARD CP No. 335, paper 7 (1982).
- 7 Binion, T.W.. Private communication.
- 8 Boersen, S.J., Elsenaar, A.. Half-model testing in the NLR High Speed Wind Tunnel HST; its technique and application. ACARD CP No. 348, paper 23 (1983).
- 9 Smith, J.. A Method for determining 2D Wall interference on an aerofoil from measured pressure distributions near the walls and on the model. NLR TR 81016 U (1981).
- 10 Mokry, M., Chan, Y.Y., Jones, D.J.. Two-dimensional wind tunnel wall interference. AGARDograph No. 281 (1983).
- 11 Michel, R.. Presentation on first meeting of ACARD WG09, Brussels, May 1984.
- 12 Barnwell, R.W.. Similarity rule for sidewall boundary-layer effect in two-dimensional wind tunnels. AIAA Journal, Sept. 1980.
- 13 Ashill, P.R.. G.RTEur AE (AC-02) activities.
- 14 Pankhurst, R.C.. Large Windtunnels: Required Characteristics and the Performance of Various Types of Transonic Facility. AGARD Report No. 615 (1973) with particular reference to:
- 14a Michel, R.. Effects of flow turbulence and noise on aerodynamic phenomena and windtunnel results. AGARD-R-615 (1973).
- 15 Hartzuiker, J.P. et al. On the flow quality necessary for the large European high Reynolds Number transonic Windtunnel LEIIRT. October 1975.
- 16 Steinle, F., Stanewsky, E.. Wind tunnel flow quality and data accuracy requirements. ACARD-AR-184 (1982).
- 17 Owen, F.K. et al. An evaluation of factors affecting the flow quality in wind tunnels. ACARD-CP-348, paper 12 (1983).
- 18 Dougherty, N.S., Fisher, D.F.. Boundary layer transition on a 10-degree cone: Wind Tunnel/Flight data correlation. AIAA-8D-0154 (1980).
- 19 Nenni, J.P., Gluyas, C.L.. Aerodynamics design and analysis of LFC surface. Astronautics and Aeronautics, July 1966.
- 19a Lachman, G.V. (ed.) Boundary Layer and Flow Control Volume 2, pp. 637-681 (1961)
- 20 Holder, D.W., Percy, H.H., Gadd, G.E.. The interaction between shock waves and boundary layers. ARC, CP No. 180 (1955).
- 21 Green, J.E.. On the influence of free-stream turbulence on a turbulent boundary layer, as it relates to windtunnel testing at subsonic speeds. RAE TR 72201 (1972)
- 22 Raghunathan, S., McAdam, R.J.W.. The effect of free-stream turbulence on pressure fluctuations in transonic flow. AIAA-84-1581.
- 23 Chan, Y.Y.. Presentation on first meeting of ACARD WG 09, Brussels, May 1984.
- 24 Ross, R., Rohne, P.B.. Kullite conc boundary-layer transition tests in the 0.55 x 0.42 m2 NLR transonic pilot tunnel. NLR Memorandum AC-78-038 (1978)
- 25 Lynch, F.T. et al. Nonadiabatic model wall effects on transonic airfoil performance in a cryogenic windtunnel. AGARD-CP-348, paper 14 (1983).
- 26 Mignosi, A., Dor, J.E.. La soufflerie cryogenique a parois adaptables T2 de l'ONERA/CERT. AGARD-CP-348, paper 3 (1983).
- 27 Grenzschichtsteuerung durch transitionsfixierung. DFVLR-Mitt.84-17.
- 28 Schlichting, H.. Boundary Layer Theory. 5.xth Edition, Mc Graw Hill, 1968.
- 29 Pate, S.R., Schueler, C.J.. Radiated Aerodynamic Noise Effects on Boundary-Layer Transition In Supersonic and Hypersonic Wind Tunnels. AIAA Journal, Vol. 7, no 3 (1969).



- 30 Michel, R., Coustols, E., Arnal, D.. Transition Calculations in Three-Dimensional Flows. ONERA TP no. 1985-7.
- 31 Hancock, P.E., Bradshaw, P.. The Effect of Free-Stream Turbulence on Turbulent Boundary Layers Transactions of the ASME, Vol. 105, Sept. 1983.
- 32 Meier, H.U., Kreplin, H.P.. Influence of Freestream Turbulence on Boundary Layer Development. AIAA Journal, Vol. 18, 1980.

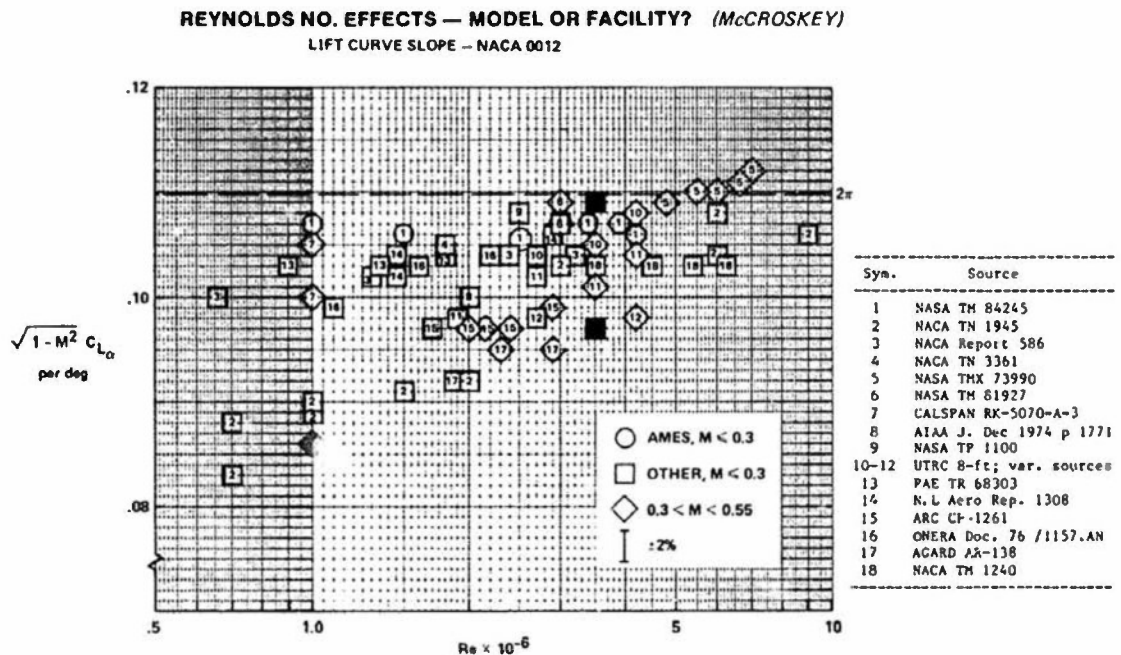


Fig. 1 Reynolds Number Effects on lift curve slope of NACA 0012 : Model or Facility ?  
(from ref. 1)

SYM	SPONSOR	Re VARIED BY	EFFECT ON
A	LEWIS	SCALE	NOZZLE
B		DENSITY	
C	AFFDL	DENSITY	AIRFRAME
D			NOZZLE
E	LANGLEY	DENSITY TEMP SCALE	NOZZLE

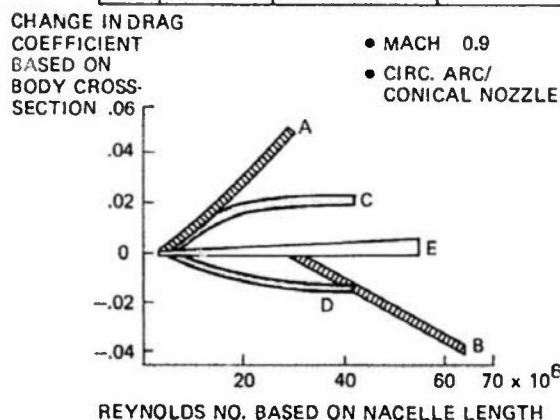
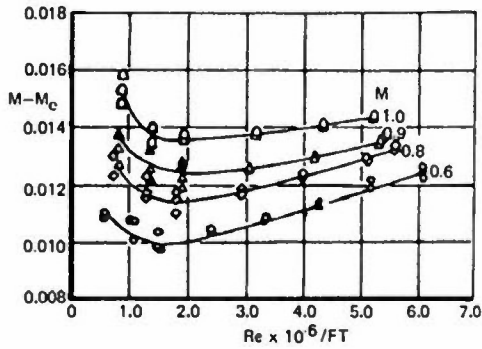
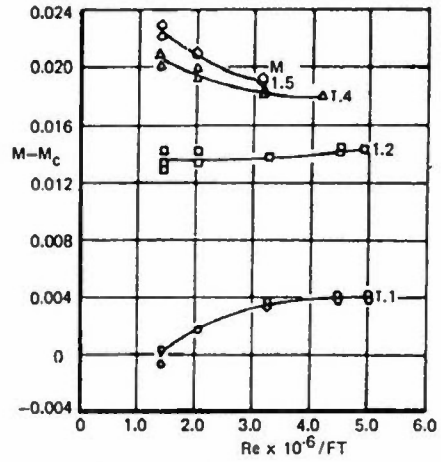


Fig. 2a The Reynolds Number paradox  
(from ref. 3)

$M$  = Average Centre Line Mach Number (From STN.8.2 to 28.2)  
 $M_c$  = Equivalent Plenum Chamber Mach Number



Wall angle,  $\theta_W = 0^\circ$



$\theta_W$  = Optimum angle Schedule

Fig. 2b An example of a Reynolds number dependent tunnel calibration (from ref. 3)

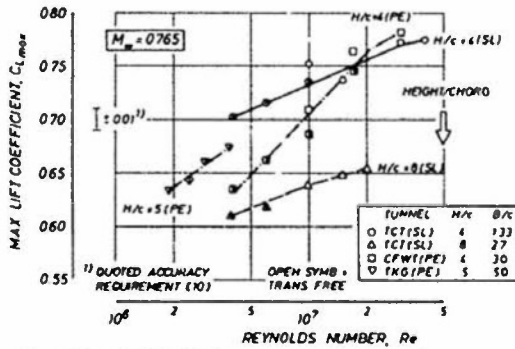


Fig. 3a CAST-10 in various windtunnels : variation of maximum lift with Reynolds number

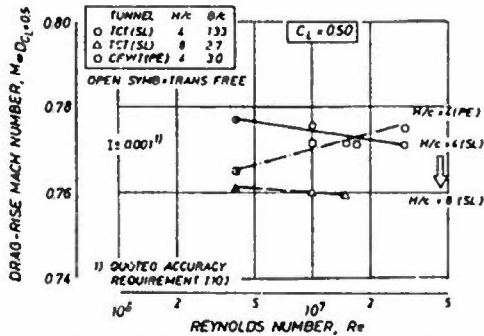


Fig. 3b CAST-10 in various windtunnels : variation of drag rise boundary

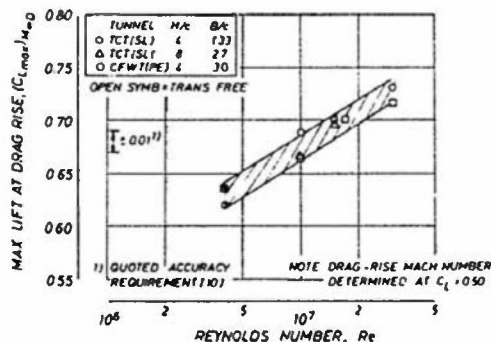


Fig. 3c CAST-10 in various windtunnels : maximum lift at drag rise (from ref. 4)

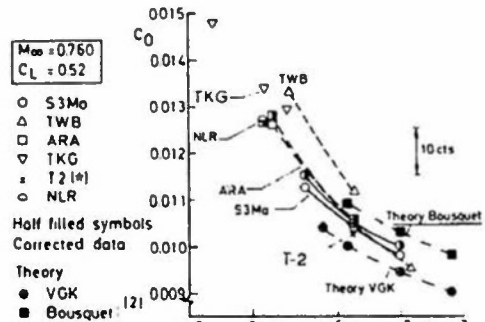


Fig. 4a CAST-7 in various windtunnels : drag comparison

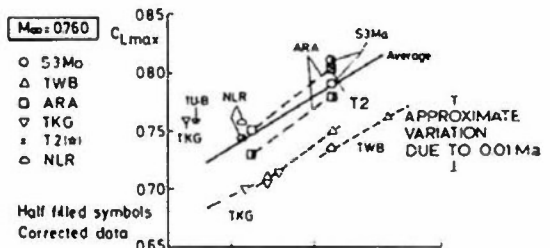


Fig. 4b CAST-7 in various windtunnels : maximum lift

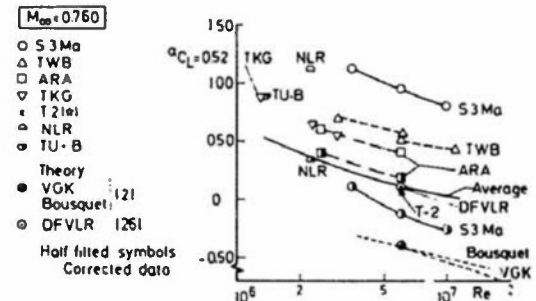


Fig. 4c CAST-7 in various windtunnels : angle of incidence at constant lift (from ref. 5)

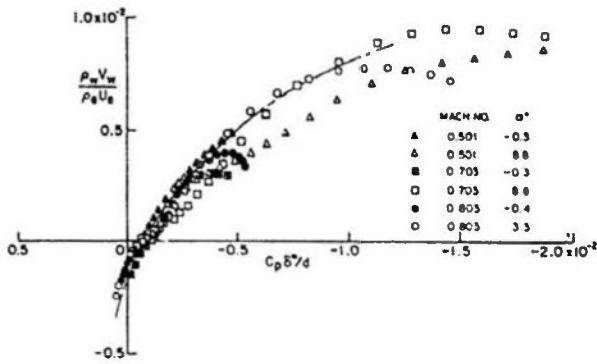


Fig. 5a Wall characteristics of a ventilated (porous) wall ( $\delta^*/d \leq 0.25$ ) (from ref. 6)

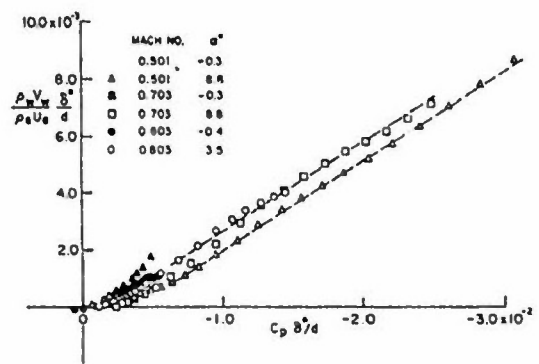
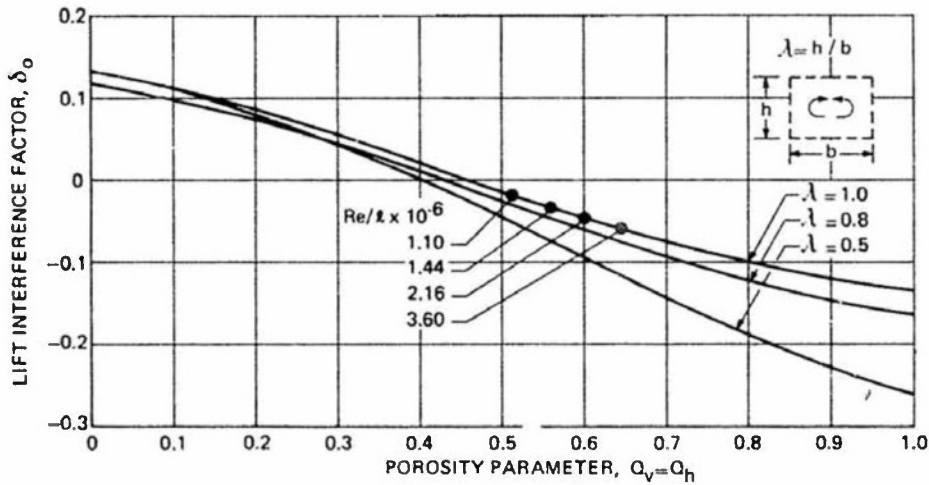


Fig. 5b Wall characteristics of a ventilated (porous) wall ( $\delta^*/d \geq 0.25$ ) (from ref. 6)



A = 10, M = 0.3, T = 5%

$Re/\lambda \times 10^{-6}$	$dC_p/d\theta$	$Q$	$\delta_o$	$\Delta\alpha = 57.3 \text{ (S/C)} \delta_o C_L$
1.10	1.9	0.51	-0.020	-0.09 $C_L$
1.44	1.59	0.56	-0.035	-0.159 $C_L$
2.16	1.35	0.60	-0.050	-0.227 $C_L$
3.60	1.10	0.64	-0.065	-0.295 $C_L$

Fig. 6 Variation of wall interference (upwash) with unit Reynolds number (from ref. 7)

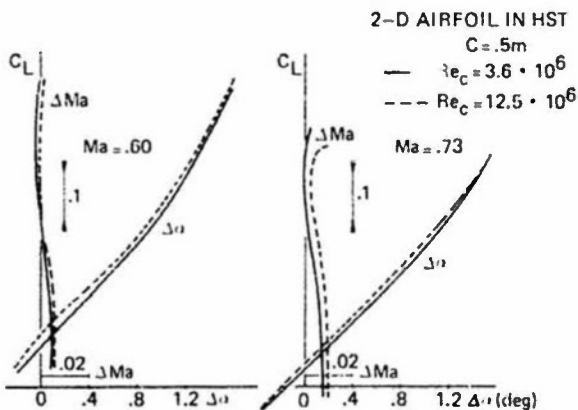


Fig. 7 Blockage ( $\Delta \text{Mach}$ ) and incidence ( $\Delta \alpha$ ) corrections calculated from measured top and bottom wall pressure distributions (from ref. 8)

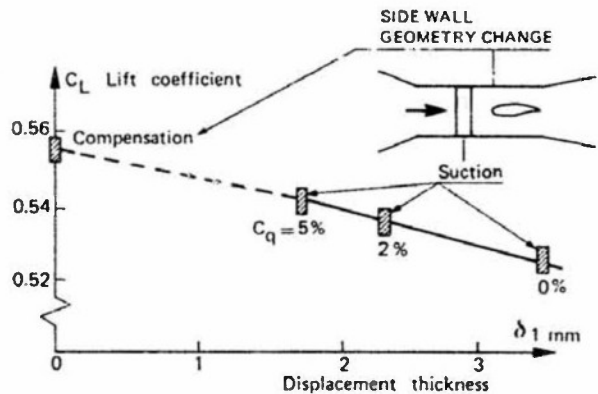


Fig. 8 Variation of lift-coefficient with side wall boundary layer thickness (from ref. 11)

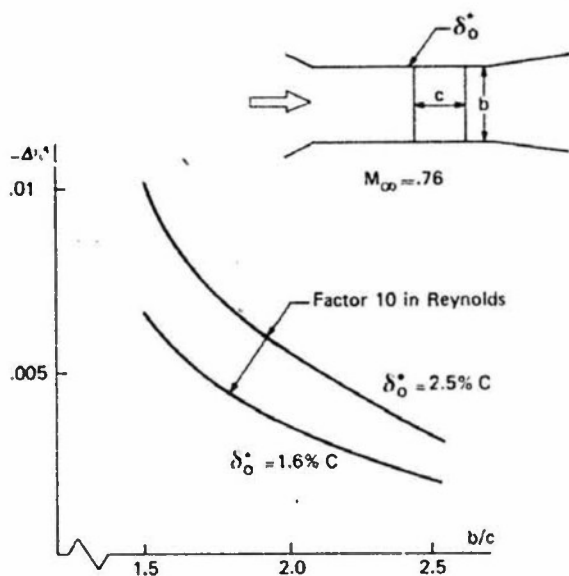


Fig. 9 Estimated Reynolds number effect on blockage due to tunnel side walls (by the author)

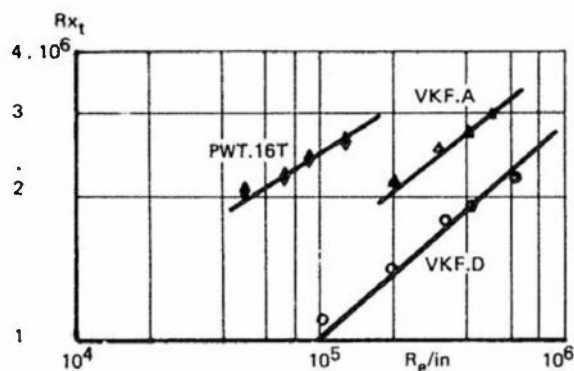


Fig. 10a Unit Reynolds number effect on transition ( $M_\infty = 3$ ; zero pressure gradient)

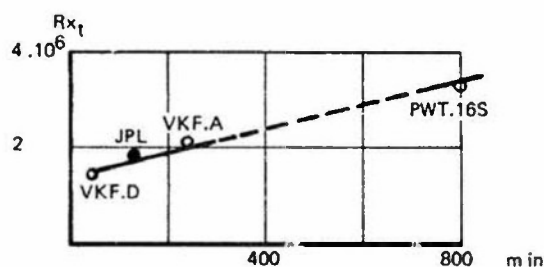


Fig. 10b Effect of tunnel size on transition (constant unit Reynolds number of  $2 \times 10^5$  per inch) (from ref. 29)

Sym	Tunnel	Sym	Tunnel
○	AEDC Tunnel 16T	□	NASA/Ames 12 PT
●	AEDC Tunnel 16T (Walls Taped)	▽	RAE Bedford 8 x 8 SWT
△	AEDC Tunnel 4T	■	NASA/Langley 16 TT
▲	AEDC Tunnel 4T (Walls with Tape or Screen)	▲	NASA/Langley 16 TDT
◇	ONERA 6 x 6 S-2 Modane	◆	NASA/Langley 8 TPT
▽	NASA/Ames 11 TWT	●	NSR&DC 7 x 10 T
▽	NASA/Ames 11 TWT (Walls Taped)	△	NASA/Langley 4 SPT
▹	NASA/Ames 14 TWT	◇	RAE Bedford 3 x 4 HST
✕	NASA/Ames 14 TWT (Walls Taped)	□	NASA/Ames 9 x 7 SWT
○	Calspan 8 TWT	△	NASA/Langley 4 SUPWT (TS No. 1)
○	ARA, Ltd. Bedford 9 x 8	●	Flight Data, Fig. 18

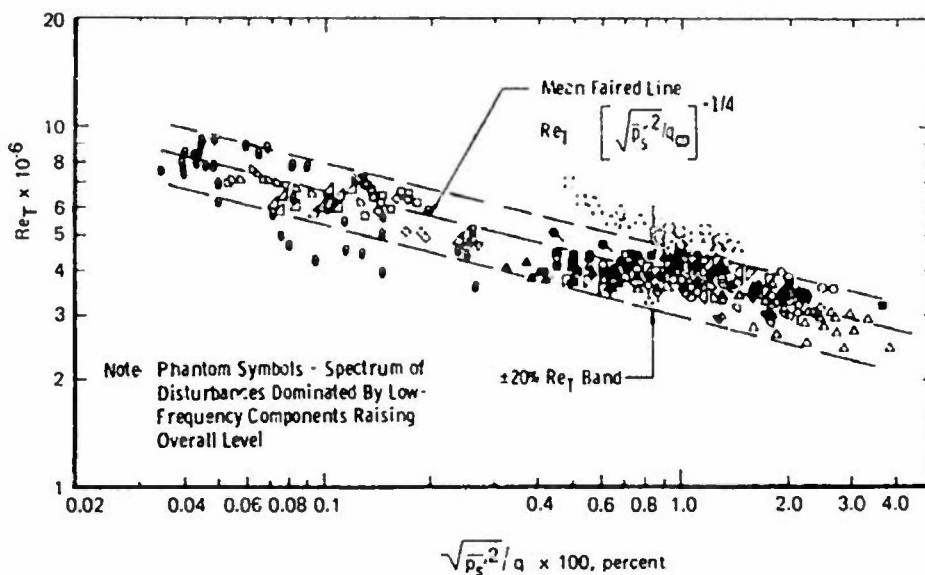


Fig. 11 Correlation of transition Reynolds number on  $10^\circ$  cone (from ref. 18)

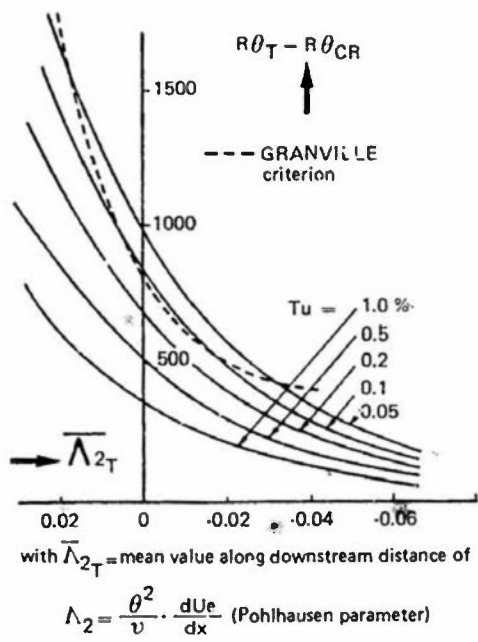


Fig. 12 Estimated effect of tunnel turbulence on transition (from ref. 30)

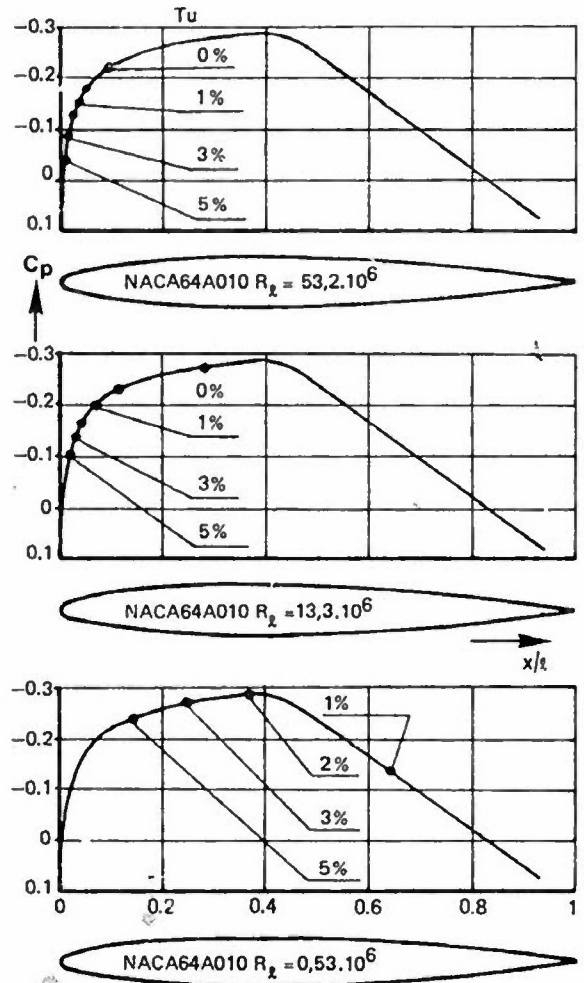


Fig. 13 Example of tunnel turbulence on transition location of some typical airfoils (from ref. 14a)

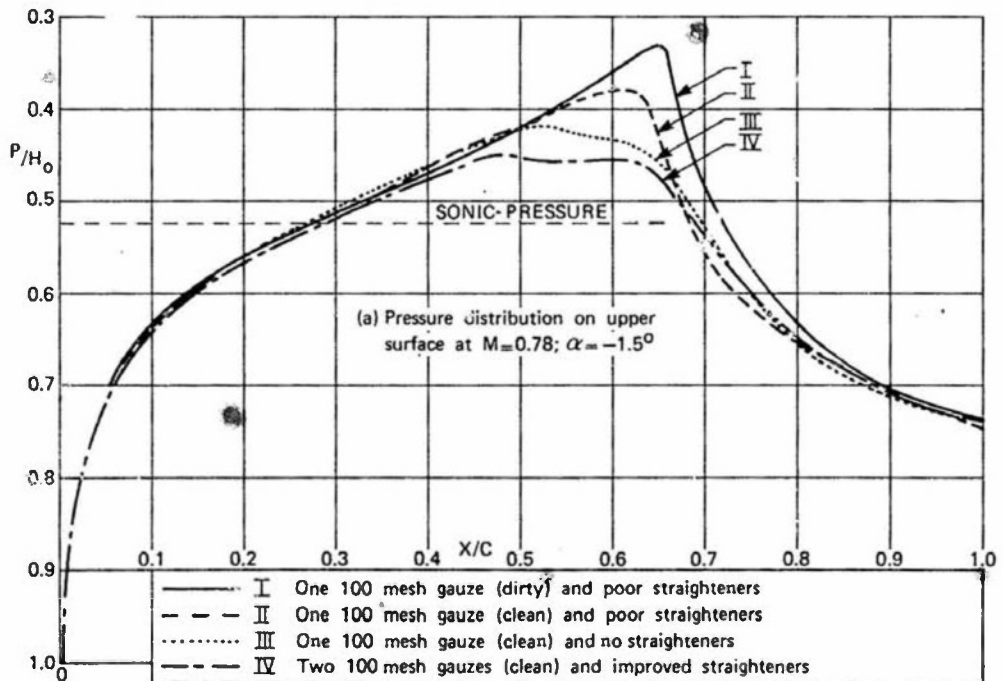


Fig. 14 Effect of flow quality on pressure distribution (from ref. 20)

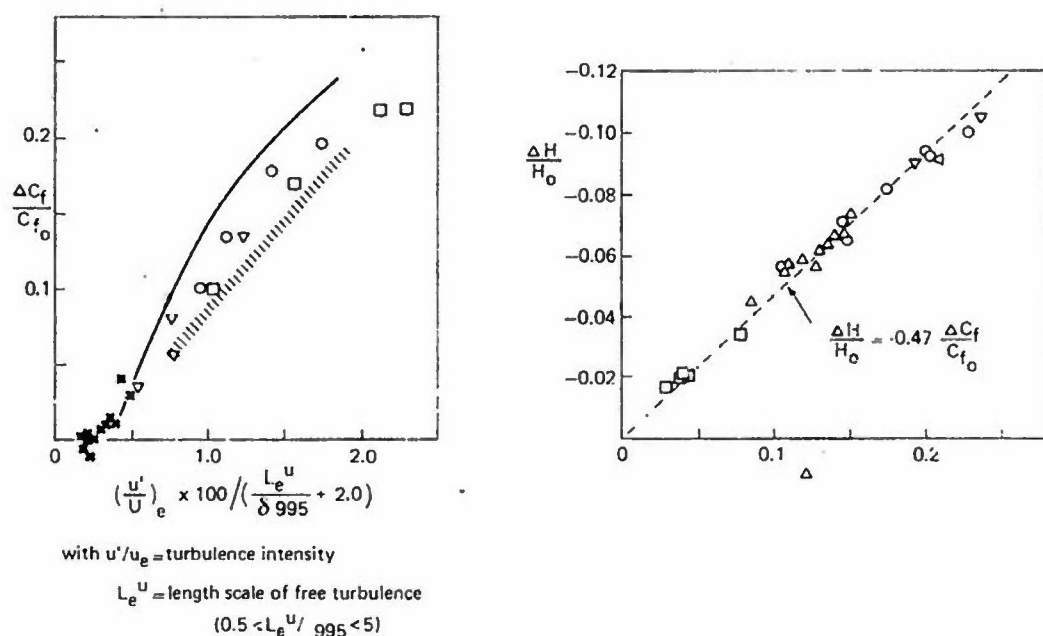


Fig. 15 Influence of free stream turbulence on flat plate turbulent boundary layer development (from ref. 31)

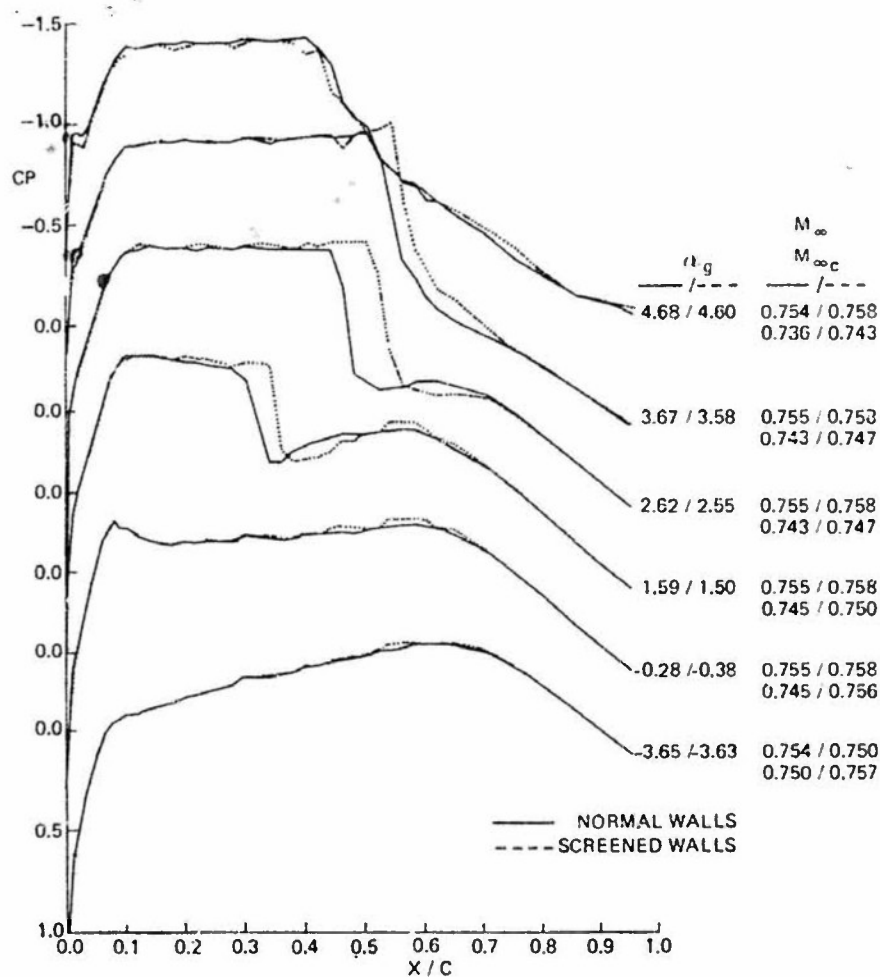


Fig. 16 Influence of flow quality on supercritical airfoil (from ref. 23)

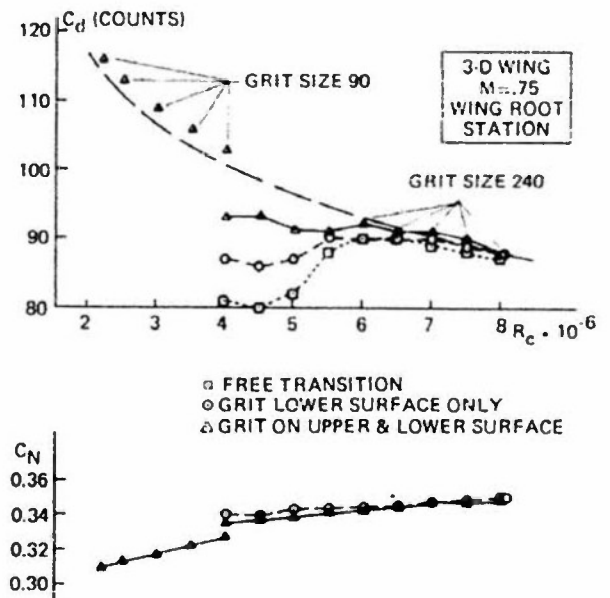
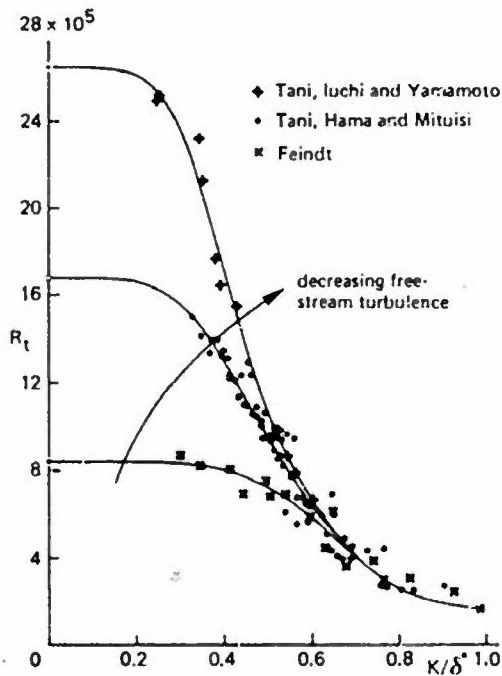
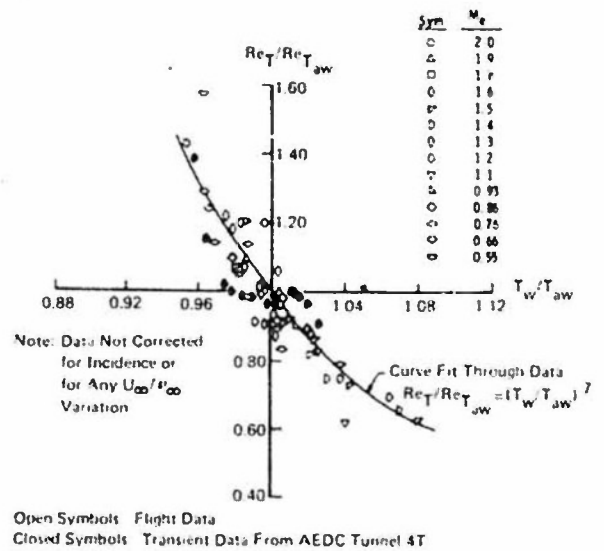
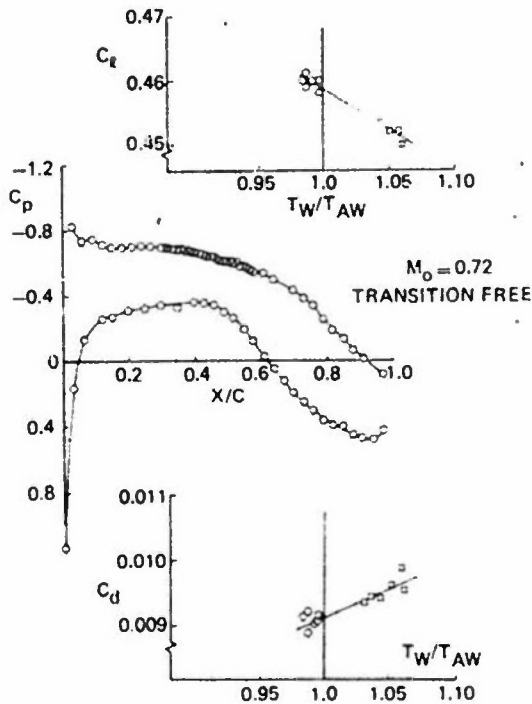


Fig. 18b Drag and lift variation with Reynolds number for two transition strips (from ref. 27)

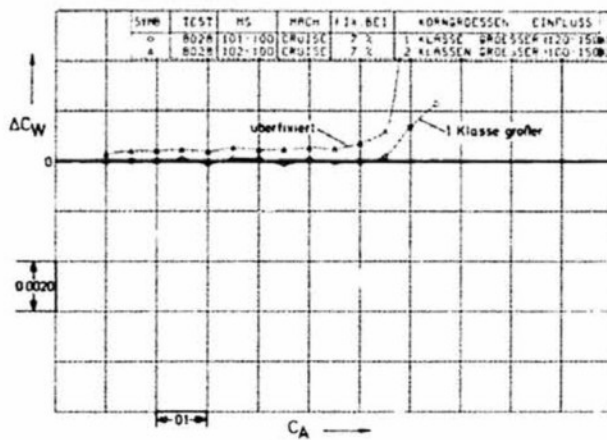


Fig. 19a Effect on drag ( $C_D$ ) of over-fixation (from ref. 27)

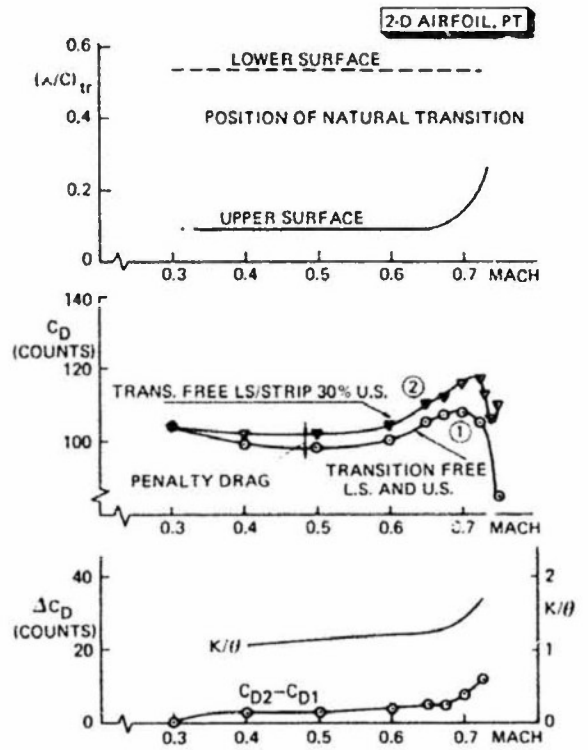


Fig. 19b Effect on drag ( $C_D$ ) of a strip in an already turbulent boundary layer (from ref. 27)

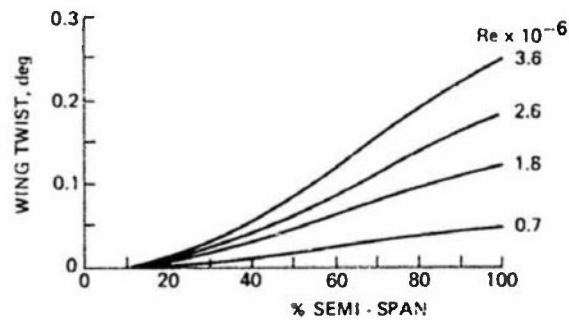


Fig. 20 Estimated wing twist as a function of Reynolds number (ONERA M-5 model, Mach = .84, lift = 0.4) (from ref. 7)



## SECTION 2.3.2 TECHNIQUES FOR BOUNDARY LAYER TRIPPING AND CONTROL

by

Dr G.P. Russo  
Experimental Gasdynamics  
Istituto di Aerodinamica  
Università degli Studi di Napoli  
80125 Napoli, Italy

### 2.3.2.1 TRANSITION FIXING

The simulation in wind tunnel tests of the higher Reynolds numbers experienced in high subsonic or transonic flight is usually achieved by artificial fixing of transition on the model either in the same position as expected in flight, close to the leading edge, or in an aft position to control the boundary layer scale at the shock location or, alternatively, at the trailing edge (see Sections 2.2.1, 2.2.2 and 2.2.4 of this report).

The methods adopted to fix premature transition can be classified under two main headings:

- a) Boundary layer tripping devices, which are solid or fluid obstacles put inside the boundary layer to increase local turbulence and provoke premature transition; these can introduce a more or less pronounced increase in drag.
- b) External means influencing the turbulence level of the stream ahead of the model; these do not introduce parasite drag but are generally scarcely controllable.

In the first category may be classified, following Schlichting (Ref.1), two-dimensional (cylindrical) devices (spanwise wires, ridges and grooves), three-dimensional (point-like) obstacles (cylinders or air jets normal to the surface of the model) and distributed roughness strips (balloons or carborundum grains).

In the second category fall both devices influencing the turbulence of the whole tunnel stream (a grid across the tunnel or simply the unidentified sources of turbulence generating the poor quality of the flow) and devices producing a local increase of turbulence just ahead of the model (a flat plate or a wire parallel to the leading edge).

Other methods of boundary layer manipulation such as suction (Refs. 1,2 and 3) or heat removal or addition (Ref.1) are not applied in current industrial practice.

#### A) Boundary layer tripping devices

Two-dimensional and three-dimensional obstacles essentially differ in the mechanism of producing instability in the laminar boundary layer (Ref.4): two-dimensional obstacles produce spanwise vortices while three-dimensional obstacles produce streamwise horseshoe vortices.

As far as classification of tripping devices is concerned, care must be taken in achieving the desired type of trip: a spanwise row of obstacles with too narrow gaps and/or a too small height/diameter ratio will behave more as a two-dimensional than as a three-dimensional trip; a strip of distributed roughness will act as a rough-surface two-dimensional trip if particle distribution is too dense and as a lot of random three-dimensional obstacles if particles are sparse.

The problem is to find a tripping device of minimum dimensions producing effective transition at the trip location without modifying appreciably the potential flow nor giving rise to prohibitive parasite drag making thus misleading the extrapolation of wind tunnel results; the procedure must furthermore be easily reproducible to warrant reliable results; the device should not be damaged by prolonged tests and lastly should be easily removable giving back unaltered conditions of the surface.

The minimum size of the trip is difficult to predict with great accuracy and is a function of the Reynolds and Mach numbers. Thus, if the minimum trip is to be used, a preliminary experiment is required to determine its size and, furthermore, the size should be changed as the conditions of the experiment are modified.

For instance, an increase in the angle of attack, and hence a variation of the position of the stagnation point on an airfoil, makes the upper surface trip less effective and the under surface trip more effective, Fig.1 (Ref.5). Since it would be a time-consuming, and therefore expensive, procedure to develop different transition strips for different test conditions, it is a practice to select a compromise configuration that will originate zones of overfixing as the angle of attack is changed.

Overfixing, in fact, is believed to be always better than underfixing since, Fig.2 (Ref.6), it is expected that overfixing produces only small drag increases while underfixing provokes a rearward displacement of the transition point giving rise to strong variations in drag.

The experimental results reported in Figs. 3 (Ref.6), 4 (Ref.7), 5 (Ref.8) show that the drag increase due to the use of trips one or two grits more than the minimum is of few counts.

#### i) Two-dimensional trips

The use of a two-dimensional trip, as a wire glued to the wall of the model and perpendicular to the stream, is confined to 2-D model configurations. As the diameter of the wire is increased the point of transition moves progressively upstream from the point of natural transition towards the position of the wire (Ref.9). A frequently used characteristic parameter is the ratio between wire diameter and displacement thickness, the transition point reaching a position close behind the wire when this ratio is of the order of magnitude one.

An empirical law for the determination of the relative position of transition point and trip in terms of the height of the roughness element has been given by Dryden (Ref.10). A corresponding critical Reynolds number, based on wire diameter and free stream flow conditions, equal to 700 has been calculated by Winter and coworkers (Ref.11) as a result of a correlation of many experimental data in the range of subsonic speeds up to  $M=0.9$ . At supersonic speeds the critical value increases exponentially with Mach number (Fig.6). Krämer (Ref.12) finds a Reynolds number equal to 900 for a fully effective trip but states that also in this case a minimum distance remains between the position of the transition point and the position of the wire such that the difference between the corresponding Reynolds numbers is  $2 \cdot 10^4$ .

In the case of flat cross sections (rectangular ridges) the value of the critical Reynolds number is considerably larger, whereas for sharp elements it becomes smaller. Ridges may consist of a series of wires stuck to the surface or of strips of plastic material formed between pieces of adhesive tape which are subsequently removed. This method is used in preference to strips of tape because it is possible to produce ridges with sharp edges which are more effective for a given height. After prolonged running the corners of the ridge may become rounded, and it then needs to be replaced if its effectiveness is to be maintained.

Sometimes it is the practice to use multiple wires or ridges in succession: in general these are preferred to single elements since their size can be smaller and consequently the disturbances produced in the main stream are not so severe.

A method of provoking transition, recently developed in England (Ref.6), makes use of stripes of alpha-numeric transfer characters as produced for graphic art work (Letraset). The material, being very thin and self-adhesive, can be built up in layers to produce a very regular transition band with the required thickness.

#### ii) Three-dimensional trips

A spanwise row of isolated excrescences can be used to fix transition. The regions of turbulent flow behind these spread laterally downstream and transition across the whole span is achieved when the regions of turbulence formed downstream of the excrescences unite. This delay in the formation of a uniformly turbulent layer precludes the use of the technique if it is required to fix transition very close to the leading edge. In some cases the method has advantages in that the effect of the excrescences is believed to be quite independent of the direction of the flow in the boundary layer.

The experimental data collected by Braslow (Ref.13) show that the critical value of the roughness Reynolds number, based on the velocity at the height of the roughness and the height of the roughness, is a function of the ratio between the diameter 'd' and the height 'k' of the roughness. For  $d/k=1$  the roughness Reynolds number goes from 600 to 700 (Fig.7) and is practically independent of Mach number at low speed.

Several methods are available for constructing the excrescences: one is to insert short lengths of wire protruding from the surface of the model, a variant is the use of small discs (Refs.14 and 15) or spherical particles glued or soldered on the surface of the model.

A transition band obtained by cutting a self-adhesive tape in a saw-tooth shape has been tested at the ONERA in Modane (Refs. 15 and 16). The tests showed that the minimum thickness required to obtain transition is larger than that required for a distributed roughness strip giving rise to a larger parasite drag.

A new type of transition band has been developed at the RAE (Ref.6) consisting of a very thin strip of metal foil through which a single row of small holes is punched using a sewing machine. The edges of these holes are ragged and form minute "coronets" whose size can be controlled by using different sizes of needle. These "coronets" are considered as combining the trip height control of ballotini with the effectiveness of sharp irregular carborundum particles and giving furthermore a superior control of density distribution as compared to distributed roughness trips.

Chordwise wires or plastic strips contouring the leading edge produce a turbulent boundary layer by lateral contamination of the laminar boundary layer (Ref.17). This procedure is advantageous since it does not induce perturbations in the potential flow and is more effective than other tripping methods at high angles of attack, see Fig.8 (Ref.7). An example of the measured velocity profiles on an airfoil downstream of longitudinal wires is reported in Fig.9 (Ref.18).

To overcome the difficulty of selecting the minimum useful size of the disturbance, which is a function of the particular experiment, a technique is sometimes used in which the size of the disturbance can be varied simply during the experiment from outside the tunnel. A row of holes is drilled across the span, and the disturbance is created by allowing a small quantity of air to flow from these into the boundary layer. If  $m$  denotes the rate of mass flow of air injected into the boundary layer per unit span and  $m_B$  the corresponding boundary layer flow then the drag increases with  $m$  up to a constant value when  $m/m_B > 0.015$ , Fig.10 (Ref.7).

This is probably the most elegant way of producing transition since the size of disturbance can be varied by controlling the air flow. It is, however, of limited application to general models on account of the pipework involved, Fig.11 (Ref.7).

Potter proposes in Ref.19 the use of vortex generators as trips assuming that the extra drag be not worse than that caused by other conventional trips. The problems involved are the lack of data on the development of transition downstream of the device and the spanwise non uniformity.

### iii) Distributed roughness.

A narrow band of the model surface is roughened by coating it with a minimum thickness of an adhesive (epoxy resin or lacquer) and dusting it with carborundum, sand or ballotini of known average grain size.

Provided that the roughness be sparsely distributed (a too dense roughness would act as a two-dimensional trip), transition moves very close to the roughness when a critical roughness Reynolds number,  $Re_{k,cr}$ , is attained. Experimental investigations have determined that this critical value is equal to 600 (Ref.20). This value is constant, except at the low values of the length Reynolds number,  $Re_x$ , at subsonic speeds. At low values of  $Re_x$ , less than  $10^5$ , resulting from either a decrease in tunnel unit Reynolds number or a decrease in the distance of the roughness band from the leading edge, the value of  $Re_{k,cr}$  increases above 600. The value of  $Re_{k,cr}$  remains constant up to approximately  $M=2$ , thereafter it begins to increase.

The magnitude of the disturbance is usually smaller when distributed roughness is used than for a two-dimensional trip. Grit-type trips offer another advantage: they make possible to optimize transition by selecting the minimum local grit size along the span, see Fig.12 (Ref. 21).

Ballotini and carborundum grains are the most used roughness materials as ballotini can be graded down to quite small diameters with a small variation in particle size and carborundum is readily available and shows superior effectiveness in provoking transition due to the resulting sharp and irregular surface of the strip.

Since the concept of "sparse" distribution is quite vague the need is felt to compare the quality of the obtained strip with some standard test specimens of proved effectiveness in order to warrant a good repeatability of the strips in different tests or in the case of replacement of a damaged strip.

## B) External means

A high level of turbulence in the stream will cause premature transition on a model by lowering the critical Reynolds number. The unsolved problem is the exact correlation between intensity of turbulence and location of transition on a model since also the scale of turbulence may play an important role on the response of the boundary layer (Ref.19).

### i) Increasing turbulence of the whole wind tunnel stream

Otto (Ref.22) made a systematical investigation of the effects of a grid, suspended across the wind tunnel ahead of the test section, on the measured aerodynamic forces on a model. He found a simple correlation, valid for low speeds, between intensity of turbulence and turbulence factor, defined as the ratio "effective Reynolds number/test Reynolds number". Although similar effects could be expected in a high speed wind tunnel the technique would result in an excessive increase in the power needed to drive the tunnel.

It would also be possible to use the inherent high level of turbulence of a tunnel to simulate higher Reynolds numbers; this feature that causes a particular tunnel to be a poor facility for transition research would make it suitable for viscous simulation. It is doubtful if such an environmental trip, which could be rather desirable being free of inherent drag, may be used with confidence.

### ii) Devices increasing local turbulence ahead of the model

A wire can be suspended near and parallel to the leading edge such that the model be in the turbulent wake of the wire. The method is not successful in supersonic flows as large

disturbances are propagated into the main stream whilst only a narrow wake is produced. Furthermore the position of the wire must be changed if the incidence is altered by a large amount.

Occasionally turbulent flow in the boundary layer over the whole surface of the model has been produced by supporting a flat plate ahead of it. Although valuable in certain experiments, the technique has the objections that it is restricted to symmetrical airfoils at zero incidence and that the turbulent boundary layer produced on the model is relatively thick.

### 2.3.2.2 TRANSITION DETECTION

In order to control the effectiveness of a transition fixing device in the whole envelope of test conditions (angle of attack, Mach number etc.) reliable methods are required to check that a true turbulent boundary layer has been generated at the desired location.

The methods adopted to detect transition can be divided in two classes:

a) Methods relying on the measurement of thermofluid-dynamic quantities inside the boundary layer; the inception of turbulence is detected from theoretically well known features such as velocity profile, thickening of the boundary layer, increase of turbulence level and of acoustic noise. The adopted techniques are measurements of stagnation pressure profiles with Pitot tubes, measurements of intensity of turbulence with hot-wire or Laser-Doppler anemometers, visualization of compressible boundary layers with optical methods, detection of pressure fluctuations with stethoscopes or piezoelectric sensors.

b) Methods based on the detection of the increase of mass, momentum and energy diffusion taking place at the model surface once transition to turbulent boundary layer has been achieved.

The most used technique is surface flow visualization with oil flow or with sublimating or evaporating substances. Not broadly used in industrial practice, but nevertheless promising in a laboratory environment, are measurements of temperature recovery factor with thermocouples, hot films, liquid crystals and thermography.

#### A) Boundary layer measurements

##### i) Velocity profiles and total pressure measurements.

These methods are based on the marked difference existing between velocity profiles in laminar and turbulent boundary layers. Velocity profiles at different chordwise stations are measured with a single Pitot tube traversing the boundary layer normally to the model surface or, alternatively, with a rake of Pitot tubes. The procedure relying on point measurements is time consuming; furthermore the presence of the Pitot tube may alter the behaviour of the boundary layer.

A simpler procedure consists in measuring the total head in the proximity of the surface with a Preston tube (Ref. 23). Transition is detected by a chordwise exploration of the boundary layer: the transition point is characterized by a sudden increase of the total head. Alternatively a total head exploration can be made at a distance from the wall slightly smaller than the expected turbulent boundary layer thickness; in this case a sudden decrease of the total head will indicate transition.

##### ii) Turbulence measurements

The onset of a high level of turbulence, typical of transition, can be directly measured with a fast response anemometer such as a hot-wire or a Laser-Doppler anemometer. Both anemometers give point measurements and are therefore most suited for the exploration of two-dimensional models; both require sophisticated electronic circuitries and data reduction procedures. The Laser-Doppler anemometer is a non-intrusive diagnostic tool but requires flow seeding.

An alternative approach is the detection of increased acoustic noise in the zone of transition using surface stethoscopes or piezoelectric gauges (Refs. 23 and 24).

##### iii) Optical methods

In compressible flows, especially supersonic flows, optical techniques are particularly useful in giving information about transition since they visualize the modification of the law of boundary layer thickening typical of transition. Shadowgraphy, Schlieren method, interferometry and, recently, holography all have been used successfully.

An interesting advantage of shadowgraphy is that transition can be detected easily because the position of maximum rate of change of the density gradient is farther from the surface in a laminar boundary layer than in a turbulent boundary layer of similar momentum thickness, so that a bright line marking this position in the flow dips towards the surface as transition occurs (Ref. 25).

Optical methods have the obvious advantage of being non-intrusive but have the serious disadvantage of giving only integrated results along the light path; their use must be therefore confined to two-dimensional or axially-symmetric fields.

## B) Diffusion based methods

### i) Methods based on momentum diffusion (wall shear stress)

The use of non volatile liquid films is based on the principle that the film moves in the direction of the surface shear stress on the model. It is of most value in showing the presence of any separation region or in indicating the surface streamlines. Also transition can be seen as the surface shear in a turbulent region may be sufficient to remove the liquid there, whilst it remains in a laminar region.

Alternatively, during the time before the liquid is swept away from a turbulent region, it is sometimes possible to see a difference in the wave pattern on the surface of the liquid there, compared with a laminar region: the wavelength in the laminar region being larger than that in the turbulent region. This method can be used in intermittent tunnel tests.

The viscosity of the liquid must be chosen according to tunnel speed and test duration: maximum viscosity being required for continuous supersonic wind tunnels. For low speeds tunnels the most suitable liquids, in ascending order of viscosity, are: kerosene, light Diesel oil, light transformer oil. In order to obtain a better contrast a pigment is added: white pigments, as titanium dioxide or china clay, on black models; a black powder (lampblack) on light models; fluorescent pigments, to be observed with ultraviolet light, irrespective of model colour. An additive, as oleic acid with titanium dioxide, is usually used to control the size of paint flocs. Heavy oils suitable for high speed are fluorescent and good contrast is obtainable by viewing the film in ultraviolet light.

### ii) Methods based on mass diffusion (evaporation and sublimation)

The most used methods in wind tunnel work are based on the differential rate of mass diffusion (evaporation and sublimation). If the surface of the model is coated with a thin film of a liquid or a sublimable solid the turbulent region, due to its higher rate of mass diffusion, causes a higher rate of evaporation or sublimation. The disappearance of the liquid or solid film can be rendered visible with some appropriate artifice.

In the china-clay method, developed at the NPL during the II WW, the model is permanently coated with white china-clay which is sprayed with a liquid (methyl salicylate) having the same index of refraction of the solid particles; the coating appears transparent when moist and the white surface reappears after evaporation.

The liquid film technique is frequently used when a quick indication of transition is required in the course of a wind tunnel test. A volatile oil is wiped on the surface, the film evaporates more quickly in the turbulent region. The indication is clearer on a matt black surface.

In high speed wind tunnels the evaporation technique has been almost completely discarded in favour of sublimation methods where a solution of a suitable solid in a highly volatile liquid is sprayed onto the model. Indication of the state of the boundary layer is then shown by the different rates of sublimation of the solid deposit in different flow regimes.

In continuous supersonic wind tunnels a slow indicator such as azobenzene is used, a rapid indicator such as hexachlorethane is used in intermittent supersonic wind tunnels. A medium indicator like acenaphthene is widely used in subsonic and transonic tests.

Care must be taken not to spray the sublimating substance onto the transition strip whose effectiveness could otherwise be diminished (Ref. 15).

### iii) Methods based on thermal diffusion (temperature recovery factor)

On an adiabatic wall a higher temperature recovery factor is expected if the boundary layer is turbulent than if it is laminar. The position of transition can be thus detected measuring wall temperature provided that conduction in the wall be negligible.

Thermocouples and hot films have been used to detect transition ; since both devices give point measurements their use is not recommended in three-dimensional tests where a too large number of sensors would be necessary.

Liquid crystals and temperature-sensitive paints able to visualize temperature distribution on the model (contact thermography) have been extensively tested at the ONERA (Ref. 26). Both are sensitive only in a quite narrow range of temperatures so that the tunnel temperature must be carefully selected. The tests showed a superiority of temperature-sensitive paints as compared with liquid crystals that are furthermore quite sensitive to mechanical strains.

Alternatively thermography has been used, for instance by Peake and coworkers (Ref. 27) at the NAE, utilizing an infra-red imaging camera coupled to a sophisticated oscilloscope which together produce a real time TV-type display of the infra-red emission from a model surface.

The method has the advantage of not being intrusive and is thus particularly useful when, as in high Reynolds number flows, arrays of impact tubes and also sublimating solutions and oil-flow visualization indicators may themselves introduce sufficient roughness to promote premature transition.

Care must be taken in selecting wind tunnel windows material since both glass and quartz are opaque to the wavelengths of the infra-red emission for which the camera detector is sensitive (Ref. 28).

### 2.3.2.3 CONCLUSIONS

The most used techniques in industrial practice to provoke transition at the desired location on the model rely on narrow strips of sparsely distributed ballotini or carborundum grains. Carborundum is preferred for its sharp irregular shape giving rise to a superior effect in tripping; ballotini are preferred for their closer dimensional control.

A new technique trying to combine these two desirable features has been proposed which makes use of "coronets" produced with a sewing machine on thin metal strips.

Another recently proposed technique makes use of transfer characters (Ketraset) build up in layers of the desired thickness.

Methods based on the increase of the turbulence level of the stream ahead of the model are to be considered not sufficiently reliable.

The two most used techniques to detect transition on 3-D models are both based on surface visualization: the first one makes use of sublimating substances, acenaphthene in high subsonic and transonic tests; the second one makes use of fluorescent oil + ultra-violet light.

An alternative technique, promising for its reversibility, is the visualization of temperature distribution on the surface with an infra-red camera (thermography) or with a temperature-sensitive paint.

For 2-D or axially-symmetrical models more conventional techniques can be used as measurements of velocity profiles with pitot tubes, boundary layer thickness with optical methods, turbulence levels with hot-wire or Laser-Doppler anemometers.

### 2.3.2.4 REFERENCES

1. Schlichting, H.: "Boundary Layer Theory", 7th Ed., 1979, Mc Graw Hill.
2. Bore, C. L.: "On the Possibility of Deducing High Reynolds Number Characteristics Using Boundary Layer Suction", AGARD-CP-84-71, FDP Specialists' Meeting on Facilities and Techniques for Aerodynamic Testing at Transonic Speeds and High Reynolds Number, Göttingen, Germany, 26-28 April 1971, paper 23.
3. Green, J. E.: "Some Aspects of Viscous-Inviscid Interactions at Transonic Speeds and Their Dependence on Reynolds Number", AGARD-CP-83-71, FDP Specialists' Meeting on Facilities and Techniques for Aerodynamic Testing at Transonic Speeds and High Reynolds Number, Göttingen, Germany, 26-28 April 1971, paper 2.
4. Sedney, R.: "A Survey of the Effects of Small Protuberances on Boundary-Layer Flows", AIAA J., vol.11, n.6, June 1973, p.782-792.
5. Elsenaar, A.: "Experiences with Transition Fixation in the High Speed Regime at NLR", NLR Memorandum AC-83-039 C, December 1983.
6. Cross, A. G. T.: "High Reynolds Number Simulation; U.K. Industry Approach", British Aerospace P.L.C. Aircraft Group, Note No.YAD 5079, November 1984.
7. Haines, A. B.: Communication at the 1st Meeting of the AGARD FDP WG09, Bruxelles, 17-18 May 1984.
8. Szodruch, J.: "Transition Fixing Methods Used by MBB, Civil Aircraft Division", 1st Meeting of the AGARD FDP WG09, Bruxelles, 17-18 May 1984.
9. Fage, A.: "The Smallest Size of a Spanwise Surface Corrugation which Affects Boundary-Layer Transition on an Aerofoil", R&M 2556, 1947.
10. Dryden, H. L.: "Review of Published Data on the Effect of Roughness on Transition from Laminar to Turbulent Flow", J.A.S., 20, p.477-482, 1953.
11. Winter, K. G., Scott-Wilson, J. B., Davies, F. V.: "Methods of Determination and of Fixing Boundary Layer Transition on Wind Tunnel Models at Supersonic Speeds", AGARD Memorandum AG 17/P7, Sixth Meeting of the Wind Tunnel and Model Testing Panel, Paris, France, 2-6 November 1954, p.167-191.
12. Krämer, K.: "Über die Wirkung von Stolperdrähter auf den Grenzschichtumschlag", ZFK 9, p.20-27, 1961.
13. Braslow, A. L.: "Review of the Effect of Distributed Surface Roughness on Boundary-Layer Transition", AGARD R-254, April 1960.
14. Chan, Y. Y.: Communication at the 1st Meeting of the AGARD FDP WG09, Bruxelles, 17-18 May 1984.
15. Bouvier, P.: "Recherche d'une Nouvelle Méthode de Déclenchement de la Transition. Écoulement Bidimensionnel. Essai de Septembre 1980 à S3MA", RTI n.0186/1464 GN, January 1981.
16. Bouvier, P.: "Comparaison de Deux Méthodes de Déclenchement de Transition sur une Voilure d'Avion Civile", Note 255 552, 11 June 1981.
17. Michel, R., Sirieux, M.: La Recherche Aeronautique, No.52, 1956.



18. Michel, R.: "Boundary Layer Simulation and Control in Wind Tunnels Activities at ONERA/CERT", 1st Meeting of the AGARD FDP WG09, Bruxelles, 17-18 May 1984.
19. Potter, J. L.: "Review of Requirements and Status of Simulation and Scaling of Transonic Viscous Flows", AEDC-TR-84-23, September 1984.
20. Braslow, A. L., Hicks, R. M., Harris, R. V. jr: "Use of Grit-Type Boundary-Layer Transition Trips on Wind-Tunnel Models", NASA TN D-3579, 1966.
21. Franz, H. P.: "Grenzschicht-Umschlagsteuerung für Start- und Lande-Konfigurationen", Grenzschichtsteuerung durch Transitionsfixierung, DFVLR-Mitt. 84-17, 1984.
22. Otto, H.: "Systematical Investigations of the Influence of Wind Tunnel Turbulence on the Results of Model Force Measurements", AGARD-CP-174, FDP Symposium on Windtunnel Design and Testing Techniques, London, U.K., 6-8 October 1975, paper 48.
23. Nitsche, W., Thünker, R., Haberland, C.: "Untersuchungen zum Experimentellen Nachweis der Grenzschichttransition", Grenzschichtsteuerung durch Transitionsfixierung, DFVLR-Mitt. 84-17, 1984.
24. Van den Berg, B.: "Transition Detection Using Surface Pressure Holes", Grenzschichtsteuerung durch Transitionsfixierung, DFVLR-Mitt. 84-17, 1984.
25. Bradshaw, P.: "Experimental Fluid Mechanics", 2nd ed., Pergamon Press, 1970.
26. Vial, R.: "Comparaison de Deux Méthodes de Déclenchement de Transition sur une Voilure d'Avion Civil à S3MA.", Centre de Modane Avrieux, Document Interne 2-0159 GY, October 1984.
27. Peake, D. J., Bowker, A. J., Lockyear, S. J., Ellis, F. A.: "Non-obtrusive Detection of Transition Region Using an Infra-red Camera", AGARD-CP-224, FDP Symposium on Laminar-Turbulent Transition, Lingby, Denmark, 2-4 May, 1977, paper 29.
28. Thomann, H., Frisk, B.: "Measurement of Heat Transfer with an Infrared Camera", Int. J. Heat Mass Transfer, Vol. 11, pp.819-826, 1968.

#### ACKNOWLEDGEMENTS

My participation to the meetings of the AGARD WG09 has been possible thanks to the financial support of the Italian Ministry of Public Education (MPI 60%) and of the National Research Council (CNR).

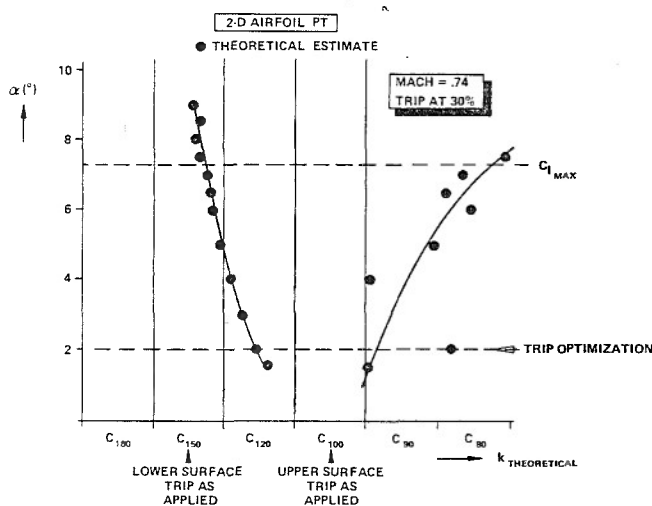


Fig.1-Effect of the angle of attack on the minimum trip size required to fix transition on an airfoil (Ref.5).

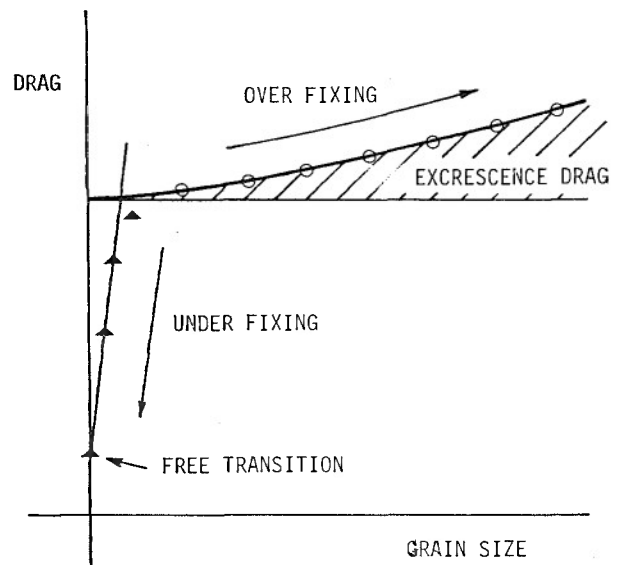


Fig.2-Ideal drag variation with roughness height or grain size (Ref.6).

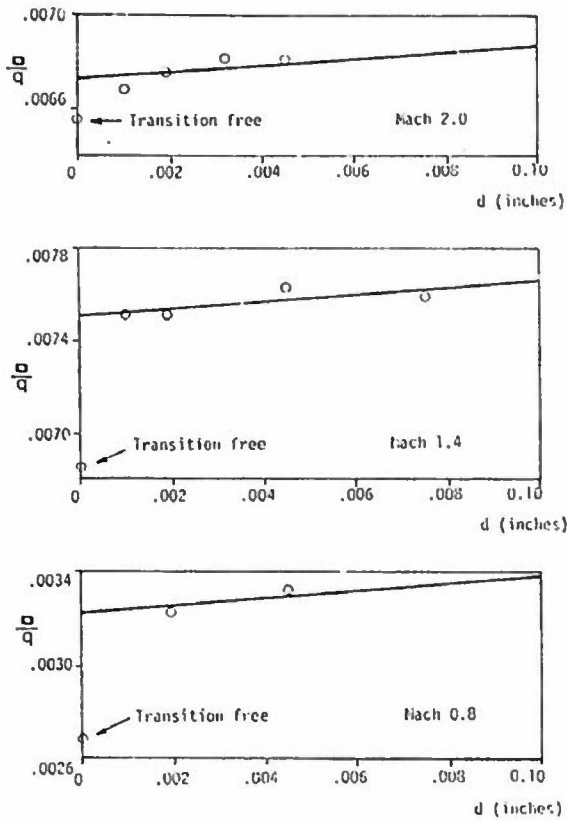


Fig.3-Variation of drag with ballotini grain size for a wing body model (Ref.6).

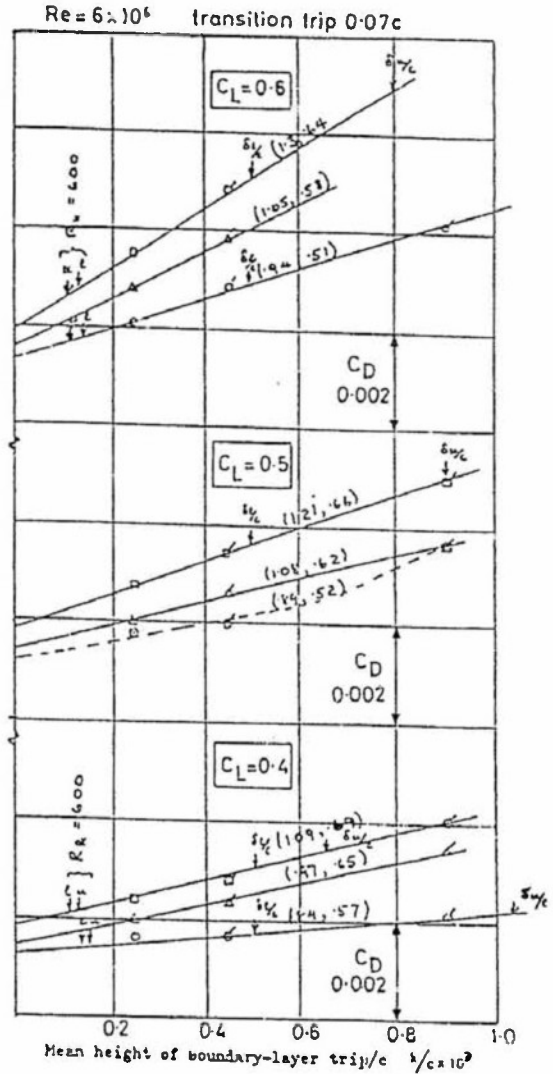


Fig.4-Influence of the height of transition trip on the measured drag (Ref.7).

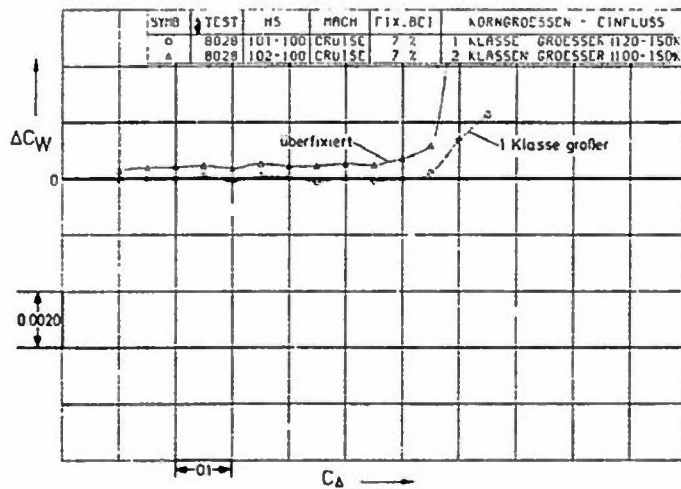


Fig.5-Influence of size of roughness elements on drag (Ref.8).



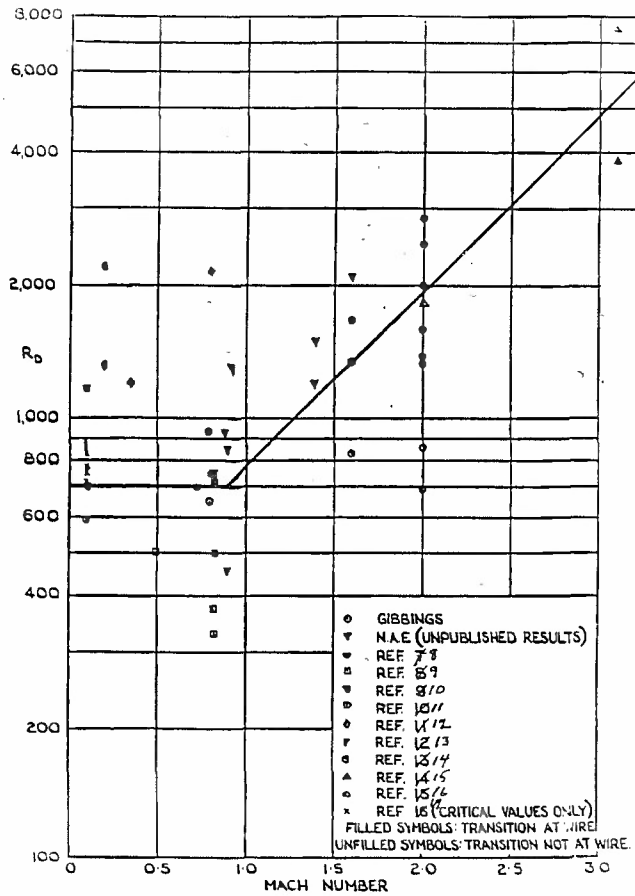


Fig.6-Correlation of results of tests using transition wires (Ref.11).

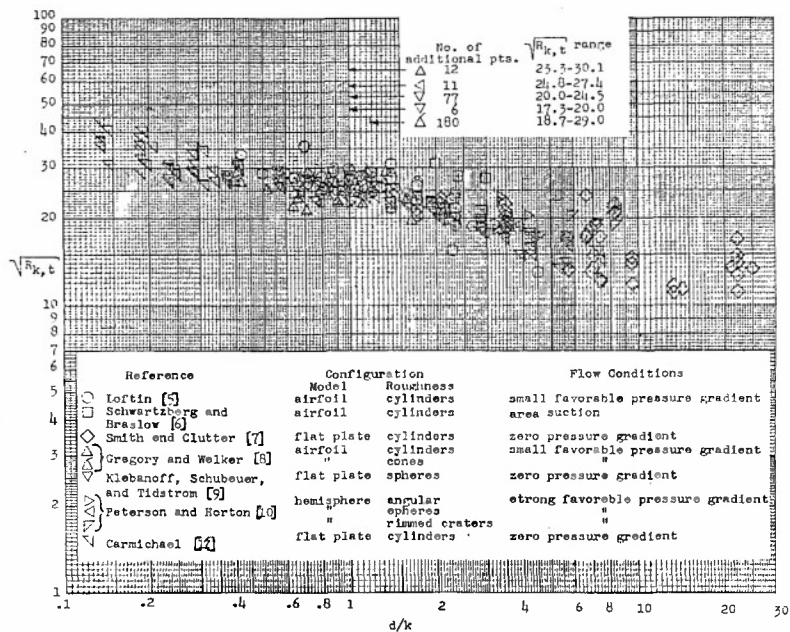


Fig.7-Low speed correlation of 3-D roughness transition data in terms of the local roughness Reynolds number and the roughness shape parameter (Ref.13).

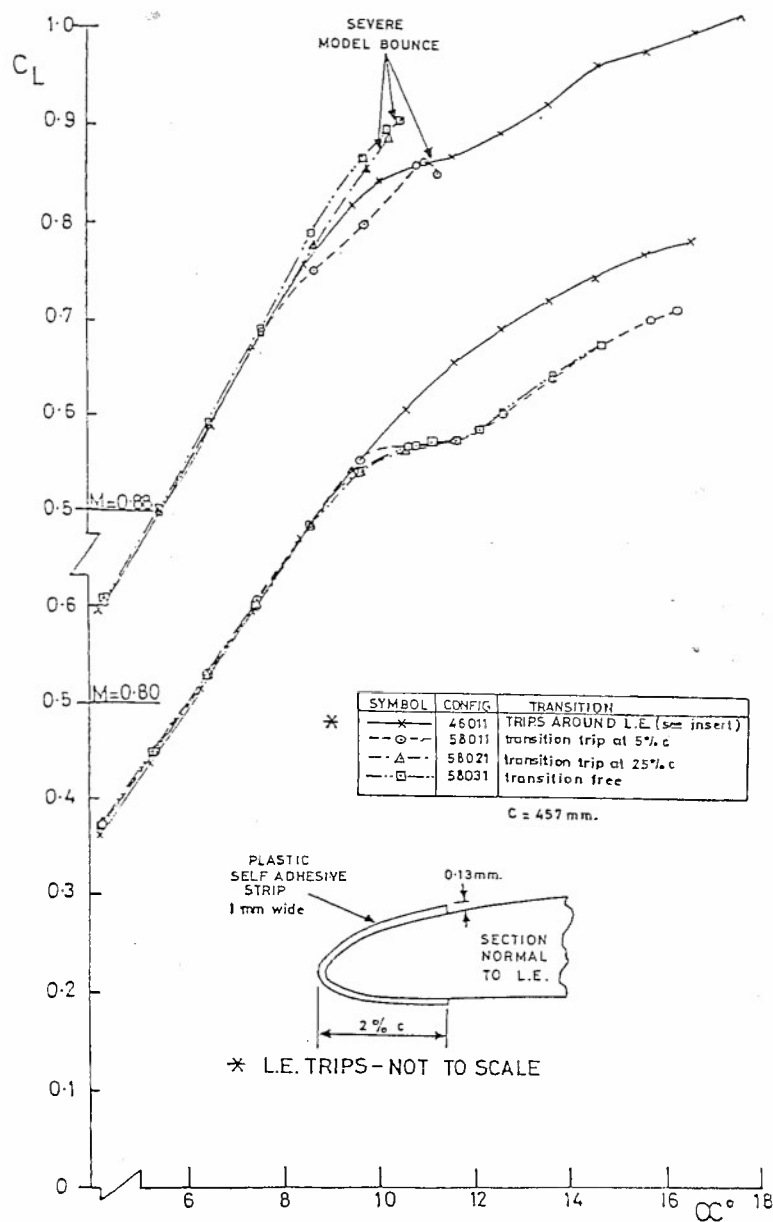


Fig.8-Effect of chordwise trips on transition fixing as compared with spanwise trips (Ref.7).

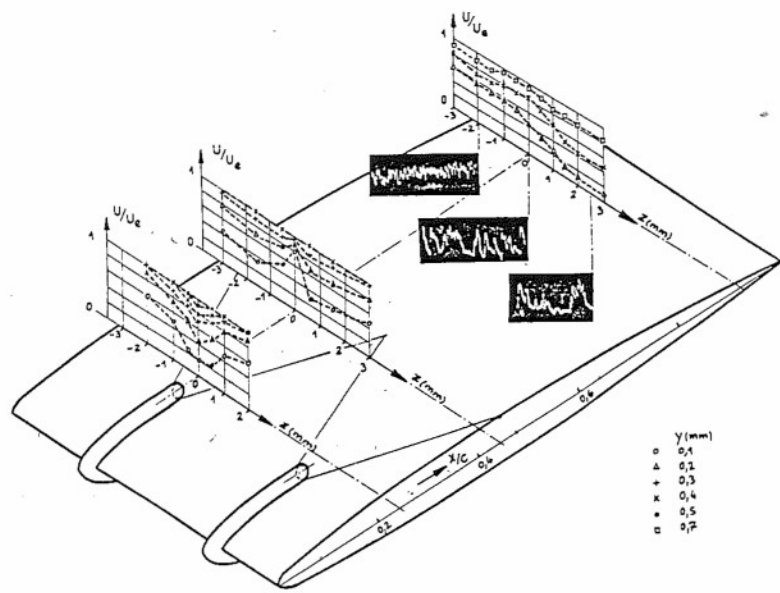


Fig.9-Velocity profiles measured downstream of longitudinal wires (Ref.18).

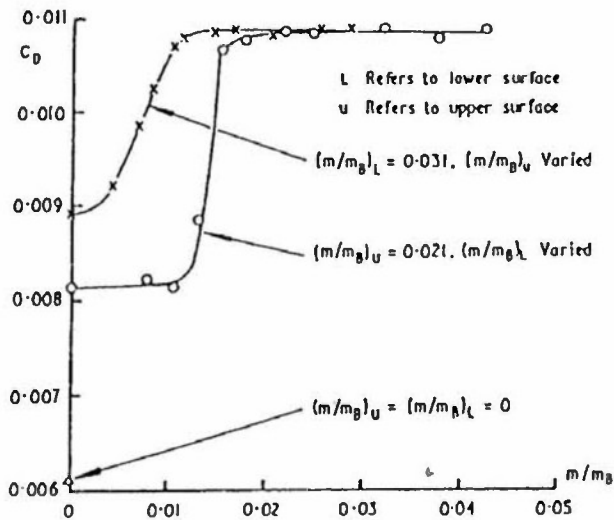


Fig.10-Effect on the drag of air injection from both surfaces of the aerofoil RAE 5225.  $\alpha=0.53^\circ$  ( $c_L=0.3$ ),  $M=0.735$ ,  $Re_c=6 \cdot 10^6$  (Ref.7).

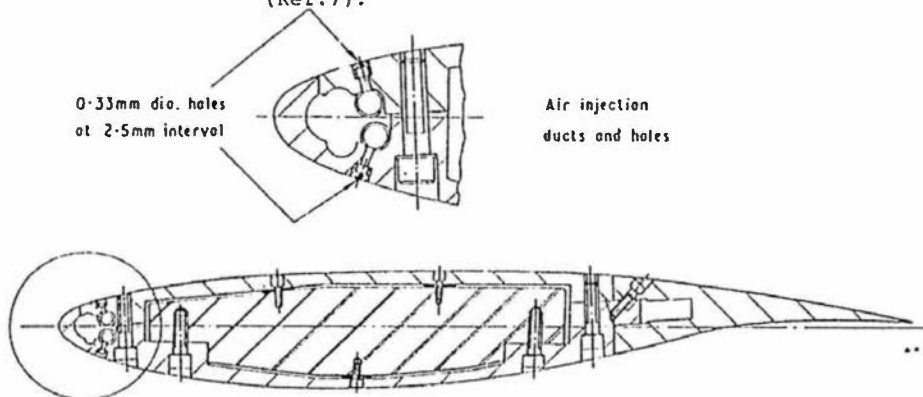


Fig.11-Model RAE 2058 aerofoil equipped with air injection ducts and holes (Ref.7).

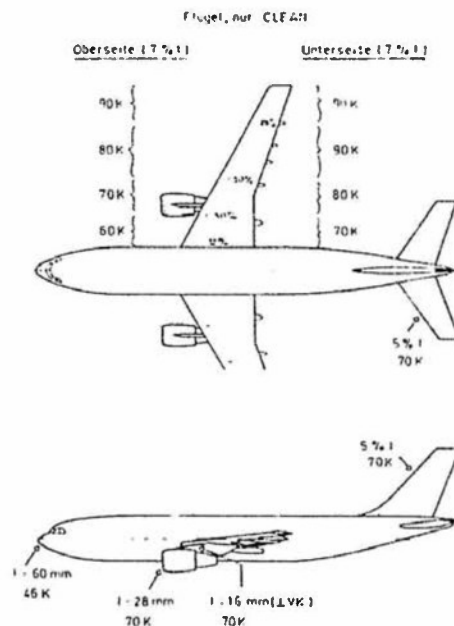


Fig.12-Optimized grit size distribution on an AIRBUS model (Ref.21).

SECTION 2.4  
SUMMARY AND RECOMMENDATIONS  
BY  
Review Committee

The surveys of relatively simple configurations (bodies, high aspect ratio wings and delta wings) all start with a phenomenological distinction between the various flow regimes. Such a distinction is essential for a good understanding of what is really happening. It also clearly shows that a simulation methodology, at least when it is intended to simulate aspects of high Reynolds number flow at wind tunnel Reynolds numbers, can never be general but should always be tuned to a particular flow regime. But besides these differences two basic phenomena seem to be of importance in nearly all cases (as is well known): the influence of the state of the boundary layer (either laminar, transitional or turbulent) and the influence of boundary layer separation on the aerodynamic characteristics. The problem is further aggravated by the fact that boundary layer separation is very often strongly coupled with the upstream history of the boundary layer and hence its state.

The uncertainty with respect to the state of the boundary layer appears to be a very fundamental and almost insuperable limitation of wind tunnel testing and high Reynolds number prediction. In principle, theories are available to predict the transition point for various types of flow (see e.g. fig. 7.8 of section 2.2.4). But it is still very much uncertain how the "theoretical" transition point (in practice always a transition region) is affected by other disturbances like flow quality, temperature effects and surface roughness (see section 2.3.1). Experimental information in this respect is limited to simple flows like flat plates or cones. Similar information for other types of transition processes (attachment line flows, cross flow instabilities, etc.) is missing. The pessimists will argue, in view of these sensitivities, that transition prediction will never be satisfactory. The optimists will plead for more theoretical and experimental work.

If the state of the boundary layer cannot be predicted adequately, it should at least be measured in the wind tunnel. The reviews did not indicate that this is done systematically in routine testing. The sublimation technique for transition detection is still the most widely used. But this technique is time consuming and therefore expensive. There is no doubt however that there is a large market for a transition detection method that can be used routinely in combination with standard force and pressure measurements.

Faced with this situation, it is quite comprehensible that industry very often favours tests with artificially fixed boundary layer transition. The survey reveals that this is particularly true (with some exceptions) for drag evaluation. One is, when proper care is taken in the selection of the transition strip, sure of turbulent boundary layer development and eliminates all unknown and unwanted transition point variations. When the boundary layer is assumed to be turbulent at flight Reynolds number one should expect at least a qualitative correspondence between wind tunnel and flight. Such a qualitative correspondence opens the way to Reynolds number extrapolation, either by theory or experiment.

At this point, however, the second phenomenon of boundary layer separation presents, as is also well known, a potential conflict. At low tunnel Reynolds numbers, with separated flow (or a particular type of separation) the qualitative correspondence is lost when, at flight Reynolds numbers, that separation is absent (or of another type). There are, in principle, two solutions to this problem, apart from high Reynolds number testing. One solution is conservative design such that separations are absent in the wind tunnel or Reynolds-insensitive (salient edges!) at critical areas of the flight envelope. The other solution is to modify the boundary layer development in the wind tunnel in such a way that separation is avoided. The survey shows a number of techniques that are actually used: aft-fixation (to thin the turbulent boundary layer), vortex generators (to energise the boundary layer) and contour modifications (to relief the pressure gradient). It is interesting to note here that the application of these techniques appears to be always limited to one type of flow in relation with a particular aerodynamic characteristic like the determination of buffet boundary, shock-wave drag, afterbody/jet interference, stall characteristics, etc. The flow is often well understood in these cases. One does not necessarily aim for an exact simulation of the flight Reynolds number (as a consequence of practical limitations like the available length of laminar boundary layer development), but it provides at least an indication of the sensitivity for Reynolds number changes. One type of flow appears to be the most popular in this respect: the two-dimensional flow over an airfoil with a substantial region of supercritical flow terminated by a shock wave. This type of flow is known to be Reynolds number sensitive and of great practical significance. But it is also, fortunately, a flow where the aft-fixation technique can be applied due to a substantial region of laminar boundary layer flow. It is an "easy case" for simulation.

Is that the reason why flows with shock-waves near the leading edge (as shown in section 2.4, figs. 5 and 6) have received much less attention? Also still relatively simple flows like the vortex flow on delta wings and the flow on bodies of revolution have not been studied sufficiently from the point of view of the effects resulting from a change in boundary layer development and the subsequent viscous/non-viscid interaction (although some good references can be found in the reviews of chapter 2).

Flows are not always simple and section 2.4 brings us back to the reality of complex configurations. They are defined as "any configuration for which three-dimensional effects become important". And one might add here configurations where interaction occurs between various types of flow. The section makes it very clear that simple recipes don't work here. The best one can do is to try the understand the flow and its sensitivity to boundary layer changes by comparing results with free and variable fixation, by a systematic build-up of a test program starting from simple basic geometries, by evaluating the effects of local modification. It also appears that not the lack of knowledge (although a better understanding is clearly wanted) but costs and the complexity of the flow severely limit the application of simulation methodologies: "For combat aircraft at high incidence the uncertainty of scale effects is such that correction of wind tunnel results to full scale is often not attempted". (Conclusion 6 of section 2.4.)

The final question is then how to proceed with the development of "simulation methodologies". The answer is outside the scope of the review committee. Nevertheless, some recommendations can be given:

1. More experimental information is required with respect to the influence of disturbances (like flow quality, surface roughness, heat transfer) on transition location; the study should not be limited to boundary layers on flat plates or cone surfaces but instead be concentrated on attachment line flows (either along the leading edge or - for free vortex flow - on the delta wing surface), three-dimensional flows (like a body of revolution under incidence) and laminar separation bubbles with and without shocks etc. It should also be attempted to include these effects in boundary layer calculation methods.
2. A number of "building block" experiments are required to study in a fundamental way different types of viscous/non-viscid interactions with respect to the state of the boundary layer (laminar, transitional or turbulent) and its Reynolds number sensitivity. The flow on two-dimensional airfoils with a large region of supercritical flow and an interaction between shock and trailing edge separation is a typical and well documented example of such a "building block". One should look, however, for other kinds of flow as well, like the flow on swept leading edges with shocks, the secondary separation underneath a vortex on a delta wing, separation and subsequent vortex formation on bodies of revolution under incidence, etc. etc.
3. Current theoretical work on so-called strong viscous/non-viscid interaction should be strongly supported. As a first step it is sufficient to prescribe the transition point (if required) in these calculation methods. In the future it might be possible to use more advanced transition prediction methods as described under 1). The "building block" experiments of 2) are essential for the validation of the strong interaction methods.
4. The "building block" experiments will lead to a better understanding of particular details of the flow development as they appear on practical configurations. Of a "building block" experiment does not show a strong sensitivity to viscous changes (state of the boundary layer, Reynolds number) there is no reason to worry. If the flow is sensitive, the "building block" experiment might help to define a "simulation methodology" for that particular type of flow in relation with a particular aerodynamic characteristic (like the application of aft-fixation for buffet boundary prediction).
5. The "building blocks" are only valuable if similar flow phenomena can be identified on an aircraft configuration in the wind tunnel. This requires extensive pressure plotting, possibly skin friction measurements and economical methods to either detect or to fix transition. Where necessary, more refined experimental methods should therefore be developed. Supporting theoretical calculations of the type mentioned under 3) are also essential to identify critical parameters.

## Section 3

## SIMULATION/EXTRAPOLATION METHODOLOGY

by

The Methodology Committee of  
AGARD FDP Working Group 09

C. Armand	France
Y.Y. Chan	Canada
A. Elsenaar	Netherlands
A.B. Haines	United Kingdom
J.L. Potter	United States
E. Reshotko, Chairman	United States
G.P. Russo	Italy

While wind tunnels have now been used for about a century to obtain performance data for vehicles to be used in atmospheric flight, there are still numerous uncertainties and ambiguities in the interpretation of the data and in reliably extrapolating them to flight conditions. These issues have been recently addressed by the AGARD Fluid Dynamics Panel Working Group 09. This section is a report of the Methodology Committee of the working group.

## CONTENTS

## 3.1 INTRODUCTION

## 3.2 GENERAL FRAMEWORK

- 3.2.1 An Outline of the Methodology
- 3.2.2 Experimental Tools - Tunnel and Model Requirements
- 3.2.3 Computational Tools for Simulation Methodologies
- 3.2.4 Empirical Tools

## 3.3 APPLICATIONS

- 3.3.1 Transport-type Configurations
- 3.3.2 Combat Aircraft
- 3.3.3 Slender Bodies

## 3.4 CONCLUSIONS

## SECTION 3.1 INTRODUCTION

by

Professor E. Reshotko  
Dept. of Mechanical and Aerospace Eng.  
Case Western Reserve University  
Cleveland, OH 44106, USA

The simulation problem in wind tunnels can be divided into two parts - far field and near field. The first of these recognizes the finiteness of the wind tunnel as compared to the infinity of the flight domain. Techniques have been proposed for assessing the blockage and interference effects due to the finite dimensions of the wind tunnel. More recently, much attention has been given to the adaptive wind tunnel.

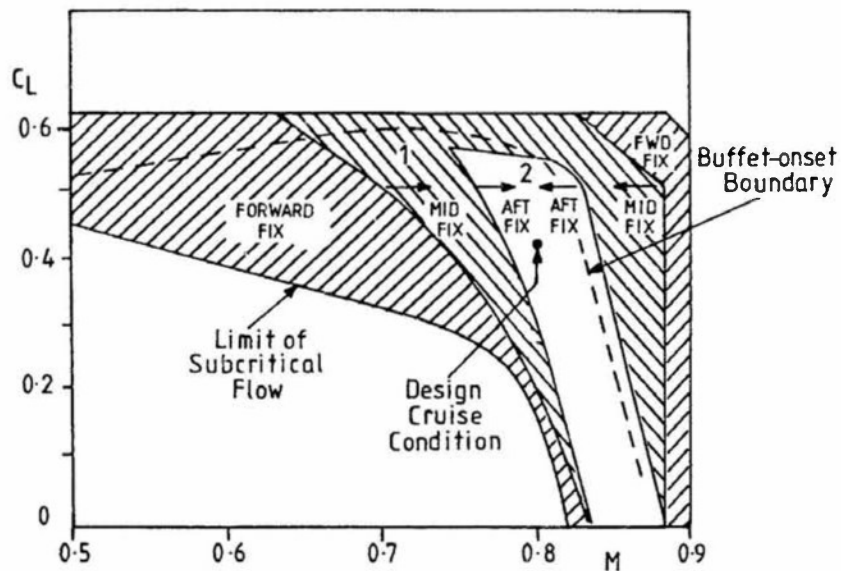
The near field simulation is referred to as viscous or boundary-layer simulation since it involves adjusting the boundary layer conditions on a model in such a way that the results can be reliably corrected to flight Reynolds numbers. This is usually done by some form of boundary layer tripping since transition locations in flight are likely to occur at smaller fractions of chord or fuselage length than in the wind tunnel.

This section of the document presents the basis of a simulation methodology, describes the experimental, computational and empirical procedures that are needed to implement such methodologies, and finally develops detailed methodologies for the three cases of transport-type configurations, combat aircraft configurations and slender bodies or missile shapes. It is of course to be recognized that the methodologies, trips and sealing procedures would be different for each of the flight regimes - subsonic, transonic, supersonic and hypersonic. The emphasis in the activity of the working group is decidedly on the supercritical regime of transonic flight.

A simulation methodology is the underlying rationale for relating wind tunnel results to flight conditions. Such methodologies are not unique, and are in some ways dependent on the phenomenon being simulated. A methodology once chosen, will require the application of boundary layer controls or trips to implement the simulation. The methodology may dictate multiple tests, each with a different trip location. Finally, the wind tunnel results must be analyzed and extrapolated to the conditions of the full scale vehicle in flight. This is accomplished within the dictates of the simulation methodology using computational fluid dynamics (CFD) techniques or well based empiricism. The extrapolability of the test results is an important issue and will be addressed in detail.

The organizing concept underlying any of the methodologies is the correct simulation of each of the flow regimes that might be identified in a lift coefficient (or angle-of-attack) vs. Mach number map for the configuration to be tested. These regimes are defined by the various shock-boundary layer interactions or separations or combinations thereof that might appear. For transport-type configurations there is more or less a single generic map such as that shown in Figure 1. For combat aircraft configurations there are a number of different cases that have to be considered depending on sweep angle, thickness ratio of the wing, leading edge shape, etc., making the situation a bit more complex. In all cases, the attempt is to duplicate the flight pressure distribution as closely as possible in the wind tunnel so that the principal extrapolation will be with respect to Reynolds number. This requires careful attention to reproducing shock locations and the character of the shock-wave boundary-layer interactions through tripping.

In Section 3.2.1, the methodology is developed and elaborated. The remaining portions of Section 3.2 delineate the testing requirements for both tunnels and models as well as describe the present and expected states-of-the-art in computational and empirical techniques that are useful in the implementation of the simulation methodologies. Section 3.3 is devoted to a presentation of the detailed methodologies for the different classes of configuration considered herein.



In Range 1  
2-Point Transition Sweep Possible

In Range 2  
3-Point Transition Sweep Possible

Fig. 1:  $C_L$  vs. Mach number map for transport type configurations. Regions of validity of data with different roughness bands on a wing upper surface.



## SECTION 3.2 GENERAL FRAMEWORK

### SECTION 3.2.1 AN OUTLINE OF THE METHODOLOGY

by

A.B.Haines  
Chief Executive  
Aircraft Research Association Ltd  
Manton Lane, Bedford MK41 5PA, UK

and

A.Elsenaar  
National Aerospace Laboratory (NLR)  
Anthony Fokkerweg 2  
1059 CM Amsterdam, the Netherlands

#### 3.2.1.1 The basic philosophy

##### 3.2.1.1.1 Introduction

This section of the report introduces the philosophy underlying the methodologies to be described in detail in Section 3.3. It should be recognized at the outset that, in practice, the detailed methodology that will be favored for any specific test program is likely to depend on

- (i) the tunnel being used for the tests (see Section 3.2.2),
- (ii) the type of configuration being tested (as illustrated by the differences in approach that will be noted between Sections 3.3.1, 3.3.2 and 3.3.3),
- (iii) the precise aims and requirements of the particular test program.

There is therefore no single methodology that will serve for all tests in all tunnels. However, all the methodologies can be based on a single general philosophy.

In devising the methodologies, there has been no conscious intention to depart from the best of established practice. Rather, the aim has been to place the established techniques on a sounder scientific basis and to exploit not only the accumulated practical experience but also, the rapid advances that have been and are being made in developing theoretical methods and CFD codes for transonic flow calculations. The methodologies also make use of various empirical relations that have been derived from recent experimental research on topics such as shock/boundary layer interaction - see Section 4.5. It is fair to say that the methodologies represent a serious attempt to implement the recommendations of many lectures and reviews that have suggested that by employing wind tunnels and CFD tools in partnership, some of the limitations of both will be alleviated.

There is far more to a simulation methodology than making decisions about whether, how and where to fix transition. Action is required before, during and after the actual tunnel tests. CFD codes should be used ahead of the tests to gain an early idea of the nature of the flow over the model to be tested and of where and how this flow is likely to be subject to uncertain scale effects. This knowledge will help to define the detail of how to control the boundary layer over the model in the tunnel tests. The experimental program should then include an in-depth study of the viscous effects, the aim being to reduce the uncertainties in the final phase after the tests when the data have to be extrapolated to full scale conditions. On the assumption - implicit in this report - that the maximum tunnel test Reynolds number is less than the full scale value, it should be recognized that some extrapolation of the data will probably always be required. Only on rare occasions will it be possible to find a test technique that will provide a complete simulation of the full scale viscous flow in all its important respects.

##### 3.2.1.1.2 Types of scale effect

The simulation methodology has to address two types (1,2) of scale effect:

- (i) "Direct" Reynolds number (or viscous) effects arising as a result of changes in the boundary layer (and wake) development for a fixed or "frozen" pressure distribution. Examples of "direct" effects range from the well known variation of skin friction with Reynolds number for a given transition position to complex issues such as changes in the length of a shock induced separation bubble for a given pressure rise through the shock, and
- (ii) "Indirect" Reynolds number (or viscous) effects associated with changes in pressure distribution resulting from changes with Reynolds number in the boundary layer and wake development. An example of a "indirect" effect, one can note that changes in boundary layer displacement thickness with Reynolds number can lead to changes in supercritical flow development and hence, in shock position and shock strength. Hence, a change in wave drag with Reynolds number at a given  $C_L$  or incidence can appear as an "indirect" viscous effect.

Strictly, this distinction (i, ii) between "direct" and "indirect" scale effect is merely a convenient artifice to simplify the discussion of the effects. It is an artificial distinction because, in practice, the two types of effect are always coupled. When the flow is subcritical and fully attached, one can often safely ignore this coupling because the indirect effects will be relatively small but when shock waves are present and even more when there is a tendency for the flow to separate, this coupling can be very important. In CFD terms, "strong coupling" implies that the flow has to be calculated by a method capable of allowing for strong as well as merely weak interactions between the inner (viscous) and outer (inviscid) flow fields. At

the present time, (1987), such methods are only in the early stages of development and even when they have been developed in the future, it is likely that they will still be too costly and time-consuming to use in routine applications of a simulation methodology. Hence, the boundaries marking the appearance of flow phenomena giving rise to strong interactions are of particular significance in the context of a simulation methodology. While the interactions are weak, one can rely on CFD predictions that can be applied in practice as a guide to the extrapolation from model to full scale but where the interactions are strong, measured trends will have to form the basis for the extrapolation. The aim for a good simulation methodology must be to bring these boundaries, if possible, within the range of the tests. 3.2.1.1.3 Experimental approach.

The approach adopted for the in-depth study of the viscous effects is the central feature of the simulation methodology. Broadly, there are two possible approaches:

- (i) Reynolds number sweeps in which the model is tested over a range of Reynolds number with transition fixed at a position, probably near the leading edge, and close to where it is forecast to occur in flight at full scale Reynolds numbers,
- (ii) With manipulation of the boundary layer to produce a viscous flow behavior closer to that forecast to occur at full scale Reynolds numbers. In practice, at the present time (1987), this implies using the after-fixing technique in which the boundary layer is allowed to remain laminar over the forward part of the surface and transition is then tripped at a position further aft than in flight. In other words, this approach will typically involve a sweep through a range of transition positions.

Whenever possible, both these approaches should be practiced; this will give added confidence in the final extrapolation. Fig 1 presents results (3) from test on a two-dimensional aerofoil over a range of Reynolds numbers and transition positions. In this case, both approaches can be followed successfully: the results with transition fixed at  $0.07c$  or occurring naturally near the leading edge provide a Reynolds number sweep from  $R = 2.3 \times 10^6$  to  $R = 30 \times 10^6$  but if it had been only possible to test at  $R = 2.3 \times 10^6$ , tests with transition fixed at  $0.30c$  would have provided a reasonable simulation of data near  $R = 8 \times 10^6$  and then, one would have had to extrapolate to  $R = 30 \times 10^6$  with the help of CFD predictions which should have been acceptable in this case in view of the fact that the data with transition fixed at  $0.07c$ , are smooth and do not exhibit any sudden discontinuities. This implies that in this case, any boundaries below which coupling between the direct and indirect scale effects are liable to distort the trends against Reynolds number, either do not exist or lie outside the test range.

The results with free transition are included in Fig 1 to illustrate another important general conclusion. The boundary layer manipulation approach can be applied successfully at  $R = 2.3 \times 10^6$  but not  $R > 6 \times 10^6$  clearly because at the higher Reynolds numbers, natural transition has moved forward to near the leading edge and there is therefore no capability to change the transition position. For other wings and/or tunnels, the limiting Reynolds number for application of the manipulation approach would not necessarily be  $R = 6 \times 10^6$ . Indeed, with some pressure distribution, it may not be possible to apply the technique at Reynolds numbers as low as  $R = 2 \times 10^6$  and and only rarely will it be possible at Reynolds numbers above  $R = 10\text{--}15 \times 10^6$  (see the later discussion on the 'flat-plate simulation criterion'). The important point is that the ability to maintain laminar flow over the forward part of the surface places a limit, dependent on tunnel turbulence and wing pressure distribution, on the application of the approach.

In the simple example in Fig 1, it would have been fair to describe the changes with Reynolds number above say,  $R = 8 \times 10^6$  as an extrapolation of the measured trends at lower Reynolds numbers. In general, however, this will not necessarily be true. Even when the changes with Reynolds number arise from indirect scale effects and can be predicted by CFD codes, allowing merely for weak viscous/inviscid interactions, the trends may be far from smooth and monotonic. For example, in terms of the pressure distribution, the changes in boundary layer displacement thickness with Reynolds number, while being smooth in themselves, could lead to notable changes in character in the supercritical flow development, e.g. from a distribution containing a largely isentropic recompression at one Reynolds number to a distribution with two strong shocks at another Reynolds number, as illustrated in the comparison in Fig 2. More seriously, changes involving strong viscous/inviscid interactions or more specifically, changes in transition position and/or mechanism and changes in the nature and position of any boundary layer separation can introduce departures from smooth trends with Reynolds number that can be described in a simplified discussion as 'discontinuities'. Three examples of such discontinuities can be quoted:

- (1) Typically, a Reynolds-number sweep from model to full scale with a forward transition position could include a change from a transition position induced by a roughness band near the leading edge at low Reynolds number to a position induced naturally by contamination of the boundary layer along the leading edge attachment line at high Reynolds number. This change could introduce discontinuous changes, not only in drag but also in the way the flow breaks down at high  $C_L$ . At low Reynolds number, this breakdown could be due to a laminar separation upstream of the roughness band, while at high Reynolds number, it could be due to a turbulent separation. An example of such a change is shown in Fig 3.
- (2) On many wings at moderate  $C_L$  and the lower transonic Mach numbers with a peaky pressure distribution over the upper surface, a laminar separation can be present at low Reynolds numbers upstream of any traditional transition fixing device. An increase in Reynolds number initially postpones the appearance of this separation to higher values of  $C_L$  but ultimately, the tendency for the flow to separate in this way is completely suppressed. The trends with Reynolds number at the higher Reynolds numbers when the flow is attached are clearly liable to be different from those at lower Reynolds numbers when the separation is present. In a simplified presentation, one can say that the changeover occurs at a 'critical' Reynolds number,  $R_{crit}$ , denoted in Section 3.3.2 (methodology for tests on combat aircraft for which this point is particularly important) as  $R_{critF}$  where F implies a separation on the forward surface.

- (3) A change with Reynolds number in the nature of the viscous flow development near the wing trailing edge. Historically, this is the leading example of a change likely to interrupt a smooth trend with Reynolds number and it is the one that has received most attention. A separate 'rear separation' initiated close to the trailing edge is frequently observed in low Reynolds number testing on advanced wing designs but the hope is that, with many of these designs, this separation would not be present at full scale Reynolds numbers. To quote the terms introduced (4) by Pearcy, there will be a change at some Reynolds number from a class B flow (rear separation capable of extending forward with  $C_L$  and/or Mach number and of interfering with the development of any other separation such as a shock-induced separation bubble) to a class A flow (no separation near the trailing edge until a shock-induced separation bubble has extended rearward and burst). Again, in a simplified presentation, one can say that this changeover occurs at a critical Reynolds number,  $R_{crit}$ , which, when there is a need to differentiate from (ii) above, will be written as  $R_{critR}$ , R referring to a rear separation. It has generally been accepted that the possibilities for substantial scale effects are much greater with class B flows. Recent thinking (5,6,7) has however emphasised that with many wings, the scale effects are significant even when the flow is of the class A type. Also, on the other hand, recent evidence suggests that on many modern advanced wings, any rear separation tends to remain limited in extent and not to increase notably with  $C_L$  or to interact with the flow further forward. Nevertheless, the presence of a rear separation will always reduce the circulation around the wing and will, for several reasons, increase both the wave drag and the viscous drag at a given  $C_L$ . Also, if, on a three-dimensional wing, it is only present over part of the span, it can modify the spanwise position at which major flow breakdown first occurs with increase in  $C_L$  and, as a result, can completely change the subsequent development of the flow breakdown. In these circumstances, the extrapolation to full scale could certainly not be described as an extrapolation of the measured trends. A simulation methodology that brings  $R_{critR}$  within the effective range of the tests is therefore highly desirable.

Reverting to the two approaches for the in-depth study of the viscous effects in the actual tests, the first approach, i.e. Reynolds number sweeps, strictly can only be practised in a variable pressure (or temperature) tunnel. The available test Reynolds number can be further extended by testing a complementary half model to a different scale, typically 1.4 to 1.8 x the scale of the basic complete model. One would not expect to be able to create a single curve of say  $C_D$  against R at a given  $C_L$  directly from the measured results for the two models but by overlapping the test Reynolds number ranges for the two models, the trends through the half model data can be used as a basis for extrapolating the results for the complete model up to the maximum test Reynolds number for the half model. Even when the tests are being made in an atmospheric tunnel, tests on a complementary half model can still be helpful in establishing trends with Reynolds number but since there is then no overlap in the data, great care has to be taken in interpreting the comparison in view of the inherent doubts about the absolute accuracy of half model data. Clearly, the case for exploiting the second approach, i.e. manipulating the boundary layer by after-fixing, will be greater if the tests are being made in an atmospheric tunnel.

#### 3.2.1.1.4 Effective Reynolds number; simulation scenarios

The aim with boundary layer manipulation is to extend the effective Reynolds number range of the tests up to values near to and if possible, beyond the full scale Reynolds number. One can define the effective Reynolds number as the Reynolds number that would be needed if transition were fixed in the generally (forward) position forecast for transition in flight at full scale Reynolds number to produce the same viscous flow behavior as that observed in the tunnel tests with aft transition. The required conversion between Reynolds number and transition position is obtained from CFD calculations, ideally for the 3D wing-body combination but realistically at the very least, for an equivalent two-dimensional aerofoil, and depends on what simulation criterion is chosen as a basis for the conversion. This important question as to what criterion to choose is addressed later but making the assumption that an appropriate choice can be made, it is now possible to present the simulation/extrapolation scenario in diagrammatic form.

Five possible scenarios are shown in Figs 4-8. To describe each of these in turn:

- (1) Fig 4:  $R_{crit} < R_{flight} < \text{maximum test effective } R$   
This is the simplest case: The results suggest that no rear separation or other strong viscous/inviscid interaction will be present in flight and it has proved possible to test with a transition position ( $x_T^*$ ) that should give, in terms of the chosen simulation criterion, full simulation of the flight behavior: no extrapolation required.
- (2) Fig 5:  $R_{flight} < R_{crit} < \text{maximum test effective } R$   
This is really a subdivision of case 1 but interpretation of the data is more uncertain. On paper, the conclusion is the same as for case 1, i.e. full simulation of flight has been achieved in the tests and no extrapolation is necessary. However, this conclusion rests critically on whether one can trust the CFD codes/separation criteria in forecasting that in terms of a rear separation, results for  $R_{test}$ ,  $x_{T_{test}}^*$  are equivalent to those for  $R_{flight}$ ,  $x_{T_{flight}}^*$ .
- (3) Fig 6:  $R_{crit} < \text{maximum test effective } R < R_{flight}$   
Some extrapolation required - from maximum effective R to  $R_{flight}$  but this should be manageable on the basis of the trends from CFD calculations including merely weak viscous/inviscid interactions.
- (4) Fig 7:  $\text{Maximum test effective } R < R_{crit} < R_{flight}$   
Real uncertainty is now creeping in: the extrapolation from maximum test effective R to a forecast  $R_{crit}$  has to be on the basis of an extrapolation of the measured trends and then, from  $R_{crit}$  to  $R_{flight}$  on the basis of the trends in CFD calculations. It should be noted that  $R_{crit}$  cannot, and must not be derived as the values of R at which the extrapolation of the measured data intersects the CFD predictions. This would be tantamount to saying that theory is capable of forecasting the flight results and that there is no need for the tunnel tests.  $R_{crit}$  must be obtained by use of the empirical relations and techniques discussed in Section 3.2.4 or by intelligent extrapolation of the measured trends and then the CFD codes must be used merely to establish the trends between  $R_{crit}$  and  $R_{flight}$ .

- (5) Fig 8: Maximum test effective  $R < R_{flight} < R_{crit}$ . This is really a subdivision of case 4 but the extrapolation is even more uncertain because neither the measured nor calculated results will be capable of giving any precise guidance as to the quantitative consequences of the fact that a rear separation (etc) is still expected to be present in flight.

It must be stressed that Figs 4-8 are only diagrammatic and simplified. The real situation could be much more complicated. Some general points should be noted:

- (i) The pictures have been drawn on the basis that a discontinuous change in the direction of the trend with Reynolds number occurs at  $R_{crit}$ ; in real life, it is much more likely that the change in direction occurs gently and smoothly over a range of Reynolds number.
- (ii) The pictures imply that the changes with  $R$  that occur beyond  $R_{crit}$  are linear and monotonic. This is not necessarily true and the later discussion, for example about the possible use of shock position as a simulation criterion, will contain evidence that the variation of shock position with Reynolds number can be in either direction and one can envisage results for a given aerofoil in which the shock can move forward or rearward with changes of Reynolds number above  $R_{crit}$ , the direction being a function of Reynolds number.
- (iii) The range of transition positions available to the test engineer will be subject to various limitations, e.g.
  - (a) the ability to maintain laminar flow back to the desired transition position. This will depend on the tunnel turbulence, acoustic noise spectrum and the pressure distribution over the wing surface.
  - (b) the need to ensure a turbulent boundary layer/shock interaction.
  - (c) the need to avoid any local interaction between the transition trip and the flow near the shock.
  - (d) the need to minimize, as far as possible, any significant disturbance to the supercritical flow development over the forward part of the surface.

Limitations (b,c) dictate that the furthest aft acceptable transition position in the tunnel tests will be at least  $0.10c$  and probably  $0.15c$  ahead of the position of the shock.

- (iv) The chosen simulation criterion is used for both the variable plotted up the ordinate scale and for the conversion of the model test Reynolds number into an effective Reynolds number; however, the value of  $R_{crit}$  is not necessarily related to the chosen simulation criterion as this criterion may have no relevance to the flow phenomenon creating strong viscous/inviscid interaction at Reynolds numbers below  $R_{crit}$ .
- (v) There is no reason in principle why a given set of model test data should not be in one scenario for one simulation criterion and in a different scenario for another criterion. Experience is lacking as to whether this situation is liable to occur often in practice and whether, if so, it leads to serious problems in knowing how to extrapolate. If this situation arises, it would reinforce the early message that to be successful in applying the methodology, one must understand the nature of the flow over the configurations being tested.
- (vi) As implied by Fig 1, a similar presentation to Figs 4-8 could be tabled for most of the aerodynamic coefficients, e.g.  $C_L$ ,  $C_D$ ,  $C_m$ , with the conversion to effective Reynolds number based on whatever is considered to be the most relevant simulation criterion, even though these coefficients are themselves unlikely to be treated as possible simulation criteria.

### 3.2.1.1.5. Simulation criteria

Turning now to the choice of simulation criterion, this may be regarded as the vital crux issue in the definition of the whole methodology. There is no clear consensus as to what to choose and probably, there is no single criterion that will serve for all test programs. The correct choice will always depend on the objectives of the particular test program and it will probably always be prudent to interpret the data on the basis of more than one criterion. In view of the widely different capabilities of likely potential users of the methodologies, it may be helpful to put forward several possible criteria at different levels of refinement:

- (a) a zero-level criterion: easy to apply, not dependent on the particular configuration under test,
- (b) a first order criterion representing the overall integrated scale effect on the pressure distribution or more probably, some leading feature of the pressure distribution, such as shock position or shock strength.
- (c) a second order criterion based on the local viscous effects in some particularly sensitive local region.

To develop these ideas in more detail:

- (a) the zero-level criterion  
At this level, the proposal is to use a simple 'flat plate simulation criterion' provided in Fig 9. This criterion is based on the requirement that the boundary layer momentum thickness at the trailing edge of a flat plate is the same for the tunnel test Reynolds number and aft transition



location and for the effective Reynolds number and transition at the leading edge (clearly, a different criterion would have to be used for any application in which extensive laminar flow was expected in flight)

Fig 9 has been derived (7) using simple incompressible boundary layer relations to provide a zero-order approximation to the direct scale effect. It is clearly simple to apply in converting test Reynolds numbers with aft transition to effective Reynolds number, but it knows nothing about the pressure distribution over the test model, the presence of shock waves or incipient separations etc. It is only of use in converting the Reynolds numbers and hopefully, in defining whether full simulation has been achieved in the test range of Reynolds numbers and transition positions. It will play no part in the extrapolation procedure beyond the effective Reynolds number (if this extrapolation is required) or in the assessment of  $R_{crit}$ . Perhaps surprisingly, however, present evidence suggests that this simple criterion (due to Elsenaar) is remarkably good as a guide to the conversion from the model test Reynolds number (with aft transition) to an effective Reynolds number

- (1) for the data plotted in Fig 1, the criterion yields an effective Reynolds number of  $R = 6.1 \times 10^6$  for the tests at  $R = 2.3 \times 10^6$  with transition at 0.30c; the measured data suggest that the 'true' value may be about  $R = 8 \times 10^6$ ,
- (2) for tests (7) on another aerofoil at NLR, the criterion yields  $R = 10.6 \times 10^6$  and actual measured data showed good agreement with the pressure distributions at  $R = 12.5 \times 10^6$ ,
- (3) for the early NASA data (8) that highlighted the simulation problem in transonic flow, the criterion yields  $R = 14 \times 10^6$  and the measured data shows a satisfactory correlation at  $R = 16 \times 10^6$ ,

Despite these encouraging indications, there is no reason in principle why this zero-order criterion should be reliable when considering conditions near and downstream of the foot of the shock; it is more likely to succeed when the major scale effects are associated with conditions near the trailing edge. In other words, the values of effective Reynolds number derived using the zero-order criterion may be a good guide when considering drag and rear separation tendencies but may not be appropriate when considering the growth of a shock-induced separation bubble. Nevertheless, it is felt worth including this zero-order criterion in the methodology because of its inherent simplicity.

Fig 9 also offers support for the earlier assertion that the aft-fixing technique cannot, in general, be applied at Reynolds numbers above about  $R = 10 \times 10^6$ . Figure 1 in Section 3.2.2 shows that in conditions of near-zero pressure gradient, transition Reynolds numbers in the range  $3 \times 10^6 < R_{tr} < 5 \times 10^6$  are achieved in most existing larger transonic tunnels and the consequences of not being able to achieve higher values are shown by the boundaries plotted in Fig 9. In practice, the attainable values of  $R_{tr}$  may be somewhat lower than  $R_{tr} = 3 \times 10^6$  because of many modern advanced wings, there will be an adverse pressure gradient over the forward upper surface ahead of the shock in the design condition.

(b) First-order simulation criterion

'First order' in this context implies that the criterion is chosen in an attempt to represent the overall viscous effects on the complete pressure distribution rather than a specific local viscous effect. In the future, it may become possible to use a manipulation technique, e.g. distributed suction (9,10), surface cooling (11), or changes in the model shape, that will produce the full scale pressure distribution in the model tests but, at the present time, as noted earlier, the only tool that is generally available is the aft-fixing technique which clearly is not capable of achieving this ideal objective. Rather, the aim must be to reproduce those features of the pressure distribution that have most impact on the aerodynamic characteristics, e.g. features such as shock strength and shock position. Past experience suggests that often, in practice, shock position is particularly sensitive to scale effect, e.g. to quote from Kraft in section 4.8:

"unequivocally, the highest priority for a proper simulation in a transonic wind tunnel test is that the model scale test must reproduce the full scale location of the shock wave".

Shock position must therefore be a leading candidate for a first-order simulation criterion. This is not a surprising conclusion: most of the early examples (12,13) of serious scale effect were associated with significant differences in shock position between model and full scale. Indeed, the diagrammatic pictures in Figs 4-8 were drawn with shock position very much in mind as the simulation criterion. One of these figures, Fig 7, is reproduced again in Fig 10 with the ordinate scale now labeled 'shock position'. The starting point for creating this figure in practice is to undertake CFD calculations for a range of Reynolds numbers with  $x_{TR_{flight}}$  and for a range of transition positions for  $R_{model\ test}$ . From these calculations, one finds the value of  $R_{effective}$  which produces equivalence (for the chosen first order simulation criterion) between  $(x_{TR_{flight}}, R_{effective})$  and  $(x_{TR_{model\ test}}, R_{model\ test})$  for each of the transition positions used in the model test. The measured shock positions for different  $x_{TR}$  at  $R_{model\ test}$  are then plotted at these values of  $R_{effective}$  to produce the measured trend and a comparison of the measured and calculated trends will help to substantiate the predictions of  $R_{crit}$ . These matters are discussed in more detail in Section 3.2.1.1.6 below.

However, before accepting shock position as the obvious first choice for a first-order simulation criterion, some reservations must be expressed, viz:

- (i) in general, the major errors in shock position will occur when the tests are being made with forward transition and Reynolds numbers below  $R_{crit}$ . They occur either because a rear separation is present or possibly because, at the lower Reynolds numbers, a shock-induced separation bubble has extended to the trailing edge. In other words, the serious scale effect arises from a strong interaction between the viscous and inviscid flow fields and therefore would not be predicted by a CFD method only capable of allowing for weak

interactions. Such methods might therefore be predicting much smaller changes in shock position with Reynolds number and/or transition position and conversion to an effective Reynolds number on the basis of such calculations might be misleading,

- (ii) also, Fig 10 may be misleading in suggesting that above  $R_{crit}$ , the trend with Reynolds number is for the shock to move slowly rearward with increase in Reynolds number. At a given incidence, this may be true but at a given  $C_L$ , which is, in general, the more reliable basis for assessing scale effects, the direction of the trend may be in either direction (see Figs 11a,b). This is because the trend at a given incidence can be offset to a greater or lesser extent by the effects of a change in incidence to maintain a given  $C_L$ : at high Reynolds number, there is more rear loading and hence, less incidence is required to maintain a given  $C_L$  and on some wings, this can result in a forward movement of the shock at a given  $C_L$ . As a consequence, it is possible, in principle, for the model test data to simulate the results at more than a single Reynolds number.
- (iii) following on from (ii), it is quite possible to find examples such as that shown in Fig 11c, where there is little change in shock position with Reynolds number. This does not mean that there is no scale effect: as can be seen, there is still a significant change in shock strength with Reynolds number at a given  $C_L$ . It simply means that there will be examples, even when the flow is supercritical, where shock position is not an appropriate simulation criterion.

These reservations about the use of shock position as a simulation criterion do not reflect on the potential value of plotting shock position as a function of Reynolds number or transition position converted to effective Reynolds number on the basis of say, the zero-order criterion. Such graphs will often be one of the best ways of assessing the values of  $R_{crit}$  as being the value of Reynolds number at which the measured trends depart from the trends calculated by methods allowing for weak viscous/inviscid interactions.

In practice, shock strength may be a better simulation criterion than shock position. Experience suggests that it may always show a decrease with Reynolds number at a given  $C_L$ , i.e. Figs 4-8 in format would still apply but with shock strength increasing from top to bottom of the figures.

Shock position and/or shock strength are naturally appropriate criteria only when the flow is supercritical. When the flow is subcritical, e.g. on the wing lower surface, the most obvious advance from the zero-order criterion is to use the calculated non-dimensional momentum thickness at the wing trailing edge as the criterion. In this way, allowance is made for the effects of the pressure distribution on the overall viscous effect.

This list of shock position, shock strength and non-dimensional momentum thickness at the trailing edge is by no means exhaustive of the criteria that might be suggested. For example, the non-dimensional boundary layer displacement thickness at 0.90c is another parameter in regular use (14). Even if full simulation in terms of one or more of the parameters is achieved, some extrapolation will still be needed. The virtues of using shock position and shock strength as the criteria are that the subsequent extrapolation has merely to cope with the direct scale effects; adequate simulation of the indirect effects has already been obtained.

#### (c) Second-order local simulation criteria

Despite the last remark under (b) above, one can argue that ideally, the simulation criterion should be related to a direct scale effect. Strictly, in the context of uncertain scale effect needing a simulation methodology, it is the direct scale effects that are the more important. As noted above, even when the gross scale effect is apparently an indirect effect, this has become important because the indirect effect, e.g. a change in shock position, has been magnified by an interaction with a direct effect such as a change with Reynolds number in the separation characteristics.

A list of local simulation criteria related to the direct scale effects is tabled below (the first has already been mentioned under (b)):

- (i) the non-dimensional momentum thickness at the trailing edge-relevant for the conversion of drag data,
- (ii) the non-dimensional length,  $L_{sep}/c$ , of the shock-induced separation bubble expressed as a function of either the boundary layer momentum thickness (Fulker & Ashill, 5) or displacement thickness and shape factor (Stanewsky, 6) immediately ahead of the shock,
- (iii) the parameter,  $(\delta^*/c) \times (H_{i1}-1)$ , proposed in Section 4.5 as a means of correlating the shock upstream influence, and possibly relevant also to the state of the boundary layer approaching the trailing edge and also possibly to the development of the shock-induced separation bubble.

To reiterate, the above local simulation criteria are related to the direct viscous effects. To apply them in practice, one also needs to allow for the indirect effects and unless these are trivial, this complicates the procedure. Nevertheless, considerable success (5) has attended the use of (ii) as a means of predicting buffet onset boundaries at high Reynolds numbers and this is important since this is often a leading test objective, particularly for subsonic transport aircraft. When  $R < R_{crit}$ , i.e. when a rear separation is present, the indirect effects certainly cannot be dismissed as trivial and further, it is conceivable (4) that there is then a significant interaction between the development of the rear and shock-induced separations. Strictly, therefore, one needs a further local simulation criterion to cover the effects of a rear separation when present. There is no reason in principle why any of the first-

order or second-order criteria listed above should be appropriate (although, as noted, (iii) above could be relevant). Methods exist - see Section 3.2.4 - for predicting the onset of a rear separation but more than this is needed. The requirement is for a simulation criterion to reflect the severity of the separation and thus, the consequences on shock position,  $C_L$ ,  $C_D$ , etc. It is possible that having obtained some evidence from the measured test data as to where the flow tends to separate, computed values of  $H_{ij}$  at a position just upstream of this point of separation may be a suitable criterion. Another possibility would be to use the pressure at the wing trailing edge (15). While it is true that comparisons of computed and measured trends in the variation of  $C_{pTE}$  with any appropriate variable will undoubtedly be useful as a means for judging whether the prediction of the value of  $R_{crit}$  is reliable, it is felt that existing CFD codes may not be equal to the challenge of using  $C_{pTE}$  as a simulation criterion for the conversion to an effective Reynolds number. Further research is needed before clear guidance can be given on what is the best criterion to cover conditions where a rear separation is present. In the meantime, it is hoped that the procedure proposed in Section 3.2.1.1.6 below will serve to bypass this problem.

One final comment about the terminology: a second order criterion should not be regarded as a refinement of a first order criterion. A second order criterion attempts to match some detailed feature of the pressure distribution thought to be relevant to a particular direct scale effect, whereas a first order criterion attempts to match the model and full scale pressure distributions in an average sense and thus, when applied successfully, should largely eliminate the indirect scale effects, leaving the test engineer with the problem of estimating all the direct effects. Use of any criterion will tend to suggest that an aft movement of transition at the model test Reynolds number will be equivalent to an increase in effective Reynolds number with a given transition position but there is no reason why, in principle, all the criteria should predict precisely the same effective Reynolds number. In practice, one should choose the criterion that appears to be most relevant in the context of the aims of the particular test program and one should attempt to obtain the closest approach to full simulation in respect of this criterion; in other respects (and often even in this primary respect), the test data will have to be extrapolated to full scale to allow for the likely lack of full simulation.

### 3.2.1.1.6 Use of Simulation Criteria

The words 'simulation criteria' are perhaps unfortunate. They convey the impression that by manipulating the boundary layer to obtain a specified value of a simulation criterion, one can reproduce the full scale viscous flow behavior in the actual model tests and there is no need for any extrapolation. In fact, this will only be true in very rare cases; in general, irrespective of which simulation scenario (1-5, see Section 3.2.1.1.4) applies, some extrapolation will always be necessary. Let us consider each scenario in turn:

- (1) Scenario 1: Fig 4:  $R_{crit} < R_{flight} < \text{maximum test effective } R$ .  
Apparently, in this case, no extrapolation is required but even here, one has to be wary. The precise conversion of a model test Reynolds number to an effective Reynolds number may depend on which simulation criterion has been chosen and so, data which can be taken as applying to  $R_{flight}$  on one criterion may correspond to some other Reynolds number on a different criterion. The correct tactics here are to convert to the effective Reynolds number on the basis of the criterion that appears to be the most relevant to the objectives of the test program and then to use the measured data for the transition position,  $x_{T, test}$ , giving the closest approach to effective  $R = R_{flight}$  as the approximate first order results for  $R_{flight}$ . Calculations of the pressure distributions, wave drag, viscous drag etc are then made for  $(x_{T, test}, R_{test})$  and  $(x_{T, flight}, R_{flight})$  and differences between these results as corrections to obtain improved, second-order results for flight at full flight at full scale Reynolds numbers, these corrections being in a sense, an 'extrapolation' to full scale. Obviously, if the conversion from the model test Reynolds number to an effective Reynolds number proved to be the same whatever simulation criterion were used, there would be no corrections and no 'extrapolation' but this is unlikely. At the very least, a check should always be made to establish whether there is a need to correct the viscous drag - by comparing the profile drag for  $(x_T, R)_{model\ test}$  and  $(x_T, R)_{flight}$  estimated by some 'data sheet' approach.
- (2) Scenario 2: Fig 5:  $R_{flight} < R_{crit} < \text{maximum test effective } R$ .  
Again, at first sight, no extrapolation is required but there are two additional problems. First, as noted above, many of the possible simulation criteria will not necessarily apply when  $R < R_{crit}$  and this creates uncertainty as to whether one can rely on the conversion to an effective Reynolds number and hence, on whether one is choosing the correct test data to simulate the behavior at  $R_{flight}$ . A simulation criterion such as shock position is likely to be far more sensitive to both transition position and Reynolds number when, for example, a rear separation is present. This does not necessarily mean that the values of effective Reynolds number deduced by using CFD codes that ignore strong viscous/inviscid interactions are incorrect but clearly, it would be somewhat coincidental if they were precisely correct. Some reassurance would be obtained if the test results suggest that as transition is moved rearward, the rear separation disappears at about effective  $R = R_{crit}$ ; but even this is not a very precise check because, in practice, the rear separation does not suddenly 'disappear'; there is merely a gradual change from a separation with reverse flow to a development with a very thick boundary layer ahead of the trailing edge. In view of the uncertainty over whether one can convert successfully to an effective Reynolds number in this range below  $R_{crit}$ , there is little point in using more than the zero-order simulation criterion unless one is studying specific developments such as the growth of a shock-induced separation bubble.

The second problem is that because  $R_{flight} < R_{crit}$ , one cannot use CFD codes that merely allow for weak viscous/inviscid interactions in the manner described for scenario 1 to derive an 'extrapolation' to full scale from the results for effective  $R = R_{flight}$ . Again, some reassurance may be obtained by treating  $R_{crit}$  as  $R_{flight}$  and applying the same procedure as for scenario 1. If  $R_{crit}$  is not too far beyond

$R_{crit}$ , this approach may be a guide to whether the corrections in the 'extrapolation' are likely to be trivial or not.

Fortunately, customers will not demand the same accuracy in results that fall into scenario 2 as for cases in scenarios 1, 3 or 4: an optimum design for a transport aircraft is unlikely to cruise in flight with separated flow over part of the surface and for a combat aircraft, where this might be true, required accuracy standards, e.g. in  $C_D$  are, in any case, less stringent. Nevertheless, the procedure for scenario 2 has been described in some detail because it is a stepping stone to what is required in the more important scenario 4.

- (3) Scenario 3: Fig 6:  $R_{crit} < \text{maximum test effective } R < R_{flight}$ .  
Clearly, some extrapolation is required in this case but perhaps surprisingly, this is the scenario for which the final corrected results are least sensitive to any uncertainties in the conversion to effective Reynolds number on the basis of a simulation criterion. Assuming that one is quite sure that  $R_{crit} < \text{maximum test effective } R$ , one should then use the results for the furthest aft transition position (i.e. maximum test effective  $R$ ) as the first order basic data and then convert to  $R_{flight}$  following the trends in the predicted computed data, i.e. applying corrections based on the differences between the computed results for  $(x_{T, \text{furthest aft}}, R_{\text{model test}})$  and  $(x_T, R)_{flight}$ .

It follows that, in this case, (and also for scenario (1)), the conversion to an effective Reynolds number on the basis of a simulation criterion plays no part in either the choice of the model test data that give the closest approach to full scale or the correction of these data to obtain the best possible simulation of full scale. This does not mean that simulation criterion will probably have been used ahead of the tests to define the range of transition positions that should be covered in the tests, subject to the limitations set out under (iii) in Section 3.2.1.1.4. Also, computed and measured trends with effective Reynolds number should be plotted as in Fig 6 and comparison of these trends is helpful in checking that the predictions of  $R_{crit}$  are reasonable. Finally, different criteria should be used to establish that the data fall into scenario 3 in more than one respect; as noted earlier, this does not necessarily follow and it may be found that, in other respects, the data fall into scenario 1 (or 2) and simulation will have been achieved in the test range. Different procedures may have to be adopted for the extrapolation of the data to meet different test objectives.

- (4) Scenario 4: Fig 7: Maximum test effective  $R < R_{crit} < R_{flight}$ .  
In this case, the extrapolation is much more uncertain. The difficulties arise from the fact that  $R_{crit}$  lies outside the test range or in other words, a rear separation (or some other coupled strong viscous/inviscid interaction) is still present in the results obtained with the furthest aft transition position that will satisfy the limitations listed in Section 3.2.1.1.4. The general recommendation as to how to proceed is clear: extrapolate the measured trends to  $R_{crit}$  and then follow the computed trends from  $R_{crit}$  to  $R_{flight}$ . This sounds simple but in practice, to be successful, it places great reliance on the accuracy of the conversion to an effective Reynolds number which directly controls the slope of the measured trends which are extrapolated until effective  $R = R_{crit}$ . Strictly, since  $R < R_{crit}$ , the conversion to an effective Reynolds number should preferably be based on a simulation criterion related to local conditions near the trailing edge. As noted in Section 3.2.1.1.5, further research is needed before one can recommend such a criterion with confidence. Use of the other criteria listed in Section 3.2.1.1.5, including the zero-order criterion, may, coincidentally, still give a reasonable slope for the measured trends against effective Reynolds number but whether it is acceptable to continue the extrapolation up to effective  $R = R_{crit}$  must be open to considerable doubt. Despite these reservations, it will always be worthwhile to use the zero-order simulation criterion in view of its simplicity and to extrapolate the measured results to  $R_{flight}$  in this straightforward manner, via extrapolate the measured trends to effective  $R = R_{crit}$  and then follow the computed trends from  $R_{crit}$  to  $R_{flight}$ : this will give a first approximate idea of the flight results.

It is possible that a better procedure, could be derived as follows:

- (i) choose shock position, shock strength,  $C_D$ ,  $C_{pTE}$  and/or any other feature of the measured results that is sensitive to the presence of the rear separation,
- (ii) plot both the measured and predicted computed variation of these parameters against transition position (note: transition position not effective Reynolds number),
- (iii) compare the measured and computed trends and if thought sensible and appropriate, plot the differences,  $\Delta X_s$ ,  $\Delta M_s$ ,  $\Delta C_D$ ,  $\Delta C_{pTE}$ , against transition position,
- (iv) estimate the values of  $R_{crit}$  not merely for the flight (in general, forward) transition position but also for the transition positions used in the model tests and plot against transition position,
- (v) extrapolate the curve in (iv) without regard for the fact that one would not be able to test with a further after transition position until one finds  $R_{crit} = R_{\text{model test}}$ ,
- (vi) extrapolate the curves in (iii) by a similar amount to that found necessary in the extrapolation in (v) and if the procedure is sound, it should be found that these curves are reaching an asymptote at the end of the extrapolation. As noted in the discussion on scenario 2, one should expect  $\Delta X_s$ , etc. to reach the asymptote gradually rather than abruptly. One should not force the asymptotic values to zero because this would be tantamount to accepting the computed values to be correct at  $R > R_{crit}$ ,
- (vii) finally, the values at  $R_{flight}$  are obtained by adding the asymptotic values of  $\Delta X_s$  etc. to the predicted computed values.



The above is a plausible procedure but it must be admitted that experience in its use is lacking. The general aim with the boundary layer manipulation approach is to bring the measured data, if possible, within scenarios (1,2,3); further development of the theoretical methods is probably needed to give confidence in a methodology such as that described above for coping with results for three-dimensional test configurations that fall into scenario 4.

- (5) Scenario 5: Fig 8: Maximum test effective  $R < R_{flight} < R_{crit}$ . This is even more difficult than scenario 4 and probably,  $R_{crit}$  is too far outside the test range for the extrapolation to be performed to any close accuracy. Fortunately, the customer for such a case would not expect close accuracy and quite possibly, would have lost interest in the results having found that a rear separation or similar feature was likely to be present in flight at full scale Reynolds numbers (note - this reasoning is not necessarily true for a combat aircraft when it may still be sensible to be interested in a design flying with the flow separated over the upper (or lower) surface of a deflected trailing edge maneuver flap). The best approach for scenario 5 is merely to use the zero-order simulation criterion and to extrapolate the measured results to effective  $R = R_{flight}$ .

### 3.2.1.1.7 Use of Reynolds number sweeps

The discussion in Section 3.2.1.1.6 has concentrated on the boundary layer manipulation approach. However, when the tests are being made in a variable pressure tunnel, there is an additional degree of freedom that can be exploited to enhance confidence in the final result. The five possible scenarios, as discussed in Section 3.2.1.1.4, still apply but, as noted in Figures 4-8, the maximum effective Reynolds number is now simply the maximum true Reynolds number for a particular model configuration provided that the Reynolds number sweep is performed with a transition position similar to that forecast for flight at full scale Reynolds number. As noted on the figures, half models can and should be used to exploit the tunnel capabilities to the full but it is important to preserve an overlap in test Reynolds number between the half model and complete model tests. This is because the half model test should not be expected to provide absolute data but should be viewed as a dedicated experiment with a specific aim of investigating detailed Reynolds number effects (16).

In many variable pressure tunnels, it is possible to change the Reynolds number by a factor of about 2.5 for a given model and then, by use of the half model, to obtain a further increase by a factor of between 1.6 and 2, according to the configuration geometry and Mach number range of the particular tests. In other words, a Reynolds number sweep over a range of between 4:1 or 5:1 should be possible but this may still be somewhat less than could be achieved in  $R_{effective}$  in favorable cases by use of the boundary layer manipulation approach. One might find that the results are in scenario 3 with aft fixing or scenario 4 with a Reynolds number sweep but the significance of this point could be offset by the fact that some of the uncertainties of being in scenario 4 would be less important with a Reynolds number sweep where the data are being plotted against true test Reynolds number rather than a somewhat problematic effective Reynolds number. Also, in practice, the boundary layer manipulation approach is subject to various limitations, particularly when applied to the moderate or small aspect ratio wings of combat aircraft (see section 3.3.2). The weak and strong points of the two techniques are summarized in Table 3.2.1.1. The important point with the Reynolds number sweep is whether it has covered a range sufficient to include the likely value of  $R_{critR}$  and  $R_{critF}$  as discussed in Section 3.2.1.1.3. The general procedure is to extrapolate the measured trends from the Reynolds number sweep up to  $R_{critR}$  or  $R_{critF}$ , whichever is appropriate, and then to follow the trends from the CFD calculations. There may of course be examples where the range of a Reynolds number sweep with forward transition can be extended further towards full scale Reynolds number by use of the boundary layer manipulation approach but one is more likely, in a variable pressure tunnel, to reach a condition at maximum pressure where it is impossible to obtain a large extent of laminar flow. Even if no extension of the range is possible, it may still be useful to use both approaches because, if one can establish that the trends in relation to true Reynolds number in the Reynolds number sweep and effective Reynolds number in the transition sweep are the same, it will obviously greatly increase confidence in the interpretation of the test data.

### 3.2.1.2. Creation of the Full Methodology

The discussion has now reached the point where the important concepts in the above philosophy can be assembled into a full methodology. The steps in the recommended general methodology can be set out briefly as follows:

#### STEP 1

Ahead of the tests, learn about the tunnel, the model and the test objectives. Identify the important design/operating conditions. In the references below to CFD calculations, it is assumed that at the design/operating conditions for which these calculations are made, the flow is either completely attached or only includes local separations near the leading edge or trailing edge or at the foot of the shock up to the point when these separations develop in a dramatic fashion. Conditions beyond buffet onset are therefore excluded even though the flow under such conditions is of major concern in tests on a combat aircraft.

#### STEP 2

Ahead of the tests, apply CFD codes allowing for weak viscous/inviscid interactions to learn as soon as possible about the flow over the model to be tested and whether and how this flow is likely to be subject to significant scale effects of either the direct (change in boundary layer development) type. These calculations are made for the design/operating conditions identified in (1).

Ahead of the tests, apply the zero-order simulation criterion (see Section 3.2.1.1.5 and Fig 9) to gain a first idea of whether it is likely to be possible to find a transition position in the model tests that will simulate the full scale behavior.

Finally, ahead of these tests, calculate the values of  $R_{crit}$  below which a strong viscous/inviscid interaction such as a rear separation or a laminar separation near the leading edge is predicted to occur with the forecast transition position for flight at full scale Reynolds number.

### STEP 3

Start the tests with a general coverage of the whole test envelope to find whether the results are critically dependent on the state of the boundary layer, e.g. test with both transition fixed and free or with two alternative transition positions.

### STEP 4

Include in the tests an in-depth study of the viscous effects either by undertaking Reynolds number sweeps (in a variable density tunnel) or by manipulating the boundary layer, e.g. by a sweep through a range of transition positions (in an atmospheric tunnel). Wherever possible, both approaches should be practised. Also, whenever possible, extend the Reynolds number sweep to higher Reynolds numbers by testing a complementary half model, the tests on the complete and half model being arranged to overlap in a certain range of Reynolds number. The boundary layer manipulation approach is employed for two reasons:

- (i) to simulate, as far as possible, the full scale viscous flow behavior in the model tests,
- (ii) to include, if possible,  $R_{crit}$  in the test range of effective Reynolds number.

### STEP 5

After the tests, take the results from the Reynolds number sweeps and plot appropriate parameters, e.g. shock position, shock strength,  $C_D$  etc at a given  $C_L$  against Reynolds number. Plot both the measured and computed results. Comparison of the measured and predicted trends will provide a check on the predicted values of  $R_{crit}$  and may lead to revised estimates of  $R_{crit}$ . If the tests (including the tests on any complementary half model) have extended to beyond  $R_{flight}$ , the results are directly applicable to full scale conditions; if, as is more likely in general, the tests do not extend up to  $R_{flight}$ , the results have to be extrapolated by extending the measured trends to  $R_{crit}$  and then following the computed trends from  $R_{crit}$  to  $R_{flight}$ , care being taken to remember that it is unlikely that any sharp discontinuous change in the slope of the trends occurs at  $R_{crit}$ .

After the tests, the measured results from tests using the boundary layer manipulation approach should be plotted against an effective Reynolds number defined as the Reynolds number that would be needed if transition were fixed at the position for flight at full scale Reynolds number to produce the viscous flow behavior obtained in the model tests with after transition. The conversion to an effective Reynolds number should be based on either the zero-order simulation criterion (see Section 3.2.1.1.5 and Fig 9) or whatever first order or second order criteria that appear to be particularly relevant to the test objectives.

Compare the measured trends against effective Reynolds number with the computed trends against Reynolds numbers in results such as shock position, shock strength,  $C_D$  and  $C_{pTE}$ . These characteristics are chosen because they are particularly sensitive to the extra viscous effects which occur below  $R_{crit}$ . This comparison between measured and predicted trends provides a check on the estimates of  $R_{crit}$ .

Use the graphs produced in (8) to identify which is the relevant scenario of the five discussed in Section 3.2.1.1.4 (see Figures 4-8). Remember to check on the basis of more than one simulation criterion.

### STEP 6

Implement the extrapolation procedure for the appropriate scenario as described in Section 3.2.1.1.6. The procedures as described may appear laborious but remember that the full procedure will probably only be followed to provide the best possible extrapolation for the important design/operating conditions identified in (1).

The procedure as described above is set out in much more detail in the methodologies in Section 3.3. It will be realized that in order to introduce the philosophy in a reasonably clear manner, various gross simplifications have been made in the outline above. Phrases such as 'testing with a certain transition position' suggest that the test configuration is merely a two-dimensional aerofoil. However, to extend the methodology to the high aspect ratio wing of a subsonic transport is not difficult (see Section 3.3.1). For the lower aspect ratio wing of a combat aircraft (Section 3.3.2) there has to be much more emphasis on the complex flow patterns that can be encountered but the same philosophy can still be followed in principle. In all cases, the recipe for success is:

- (a) Understand the nature of the flow over the test configuration.
- (b) Cover as wide a range of Reynolds number or effective Reynolds number as possible.
- (c) Be guided by past experience but do not necessarily repeat what one did with the previous design. It all depends on whether the flow is precisely the same; even if the two designs come from the same family, this is unlikely to be true, e.g. both the maximum effective Reynolds number and  $R_{crit}$  could be different and the results for the two wings could be in different scenarios.
- (d) Unless one is absolutely sure, avoid short cuts and simplifications.

## REFERENCES

1. Hall, M. G. Scale effects in flows over swept wings.  
AGARD CP 83-71 April 1971
2. Elsenaar, A. AGARDOGRAPH on 'Reynolds number effects'.  
Chapter 1. To be published.
3. Elsenaar, A. Experiences with transition fixing in the high speed regime at NLR.  
Grenzschicht Steuerung durch Transitionfixierung.  
DFVLR Mitteilung 84-17 October 1984
4. Pearcey, H. H.  
Osborne, J.  
Haines, A. B. The interaction between local effects at the shock  
and rear separation - a source of significant  
scale effects in wind tunnel tests on aerofoil and wings.  
AGARD CP 35, Paper 11 September 1968
5. Fulker, J. L.  
Ashill, P. R. A model of the flow over swept wings with shock  
induced separation.  
RAE TR 83088 1983
6. Stanewsky, E. Interaction between the outer inviscid flow and the boundary layer on  
transonic airfoils.  
Dissertation, TU-Berlin (D 83) 1981  
(also Z. Flugwiss. Weltraumforsch. 7 (1983),  
Heft 4, pp 242-252)
7. Elsenaar, A. Private communication.
8. Blackwell, A. Effect of Reynolds number and boundary layer transition location on shock  
induced separation.  
AGARD CP 35, Paper 21 September 1968
9. Green, J. E. Some aspects of viscous-inviscid interactions at transonic speeds and their  
dependence on Reynolds number.  
AGARD CP 83, Paper 2 April 1971
10. Bore, C. L. On the possibility of deducing high Reynolds number characteristics using  
boundary layer suction.  
AGARD CP 83, Paper 23 April 1971
11. Reshotko, E. Drag reduction by cooling in hydrogen fueled aircraft.  
J. Aircraft, Vol 16, No 9, p 584 1979
12. Loving, D. L. Wind tunnel flight correlation of shock induced separated flow.  
NASA TN D 3580 1966
13. Cahill, J. F. Simulation of full scale flight aerodynamic characteristics by tests in  
existing transonic wind tunnels.  
AGARD CP 83, Paper 20 April 1971
14. Boppe, C. W. Future requirements of wind tunnels for CFD code verification.  
AIAA 86-753  
1st Aerodynamic Testing Conference,  
West Palm Beach March 1986
15. Khan, M. M. S.  
Cahill, J. F. New considerations on scale extrapolation of wing  
pressure distributions affected by transonic shock induced separation.  
NASA Contractor Report 166426 March 1983
16. Boersen, S. J.  
Elsenaar, A. Half-model testing in the NLR high speed wind  
tunnel HST: its technique and application.  
AGARD CPP 348 August 1983

TABLE 3.2.1.1

## RELATIVE MERITS OF MANIPULATION (BY AFT FIXATION) AND REYNOLDS NUMBER SWEEPS

SIMULATION BY BOUNDARY LAYER MANIPULATION	EXTRAPOLATION FROM REYNOLDS NUMBER SWEEPS
1a APPLICABLE FOR ALL WIND TUNNELS (PROVIDED $Re_c \geq 2 \times 10^6$ & PROBABLY $\leq 12 \times 10^6$ )	APPLICABLE ONLY FOR VARIABLE DENSITY TUNNELS 1b
2a MAY BY-PASS 'CRITICAL EVENTS', e.g. DISAPPEARANCE AT $Re_{crit}$ OF REAR SEPARATIONS FORECAST NOT TO OCCUR AT FLIGHT REYNOLDS NUMBER; UNDER CERTAIN CONDITIONS (SEE 3a) POSSIBLE TO MATCH FLIGHT PRESSURE DISTRIBUTIONS; ONLY LIMITED EXTRAPOLATION (e.g. FOR DRAG) REQUIRED	THEORY IS REQUIRED TO PREDICT 'CRITICAL EVENTS' IN REYNOLDS NUMBER RANGE BEYOND TUNNEL CAPABILITIES AND TO PREDICT TRENDS AFTER THE CRITICAL EVENT 2b
3a A REGION OF LAMINAR FLOW AHEAD OF THE SHOCK REQUIRED; THEREFORE ONLY APPLICABLE FOR CERTAIN REGIONS IN $C_L$ - M PLANE	CONTINUOUS INFORMATION IN $C_L$ - M NUMBER PLANE 3b
4a UNCERTAINTY INTRODUCED BY VALIDITY OF THE SIMULATION CRITERION; MAXIMUM SIMULATED REYNOLDS NUMBER DEPENDS ON CHOICE OF CRITERION AND PRESSURE DISTRIBUTION, HENCE, $C_L$ AND M	EXTRAPOLATION ERROR DEPENDS ON 4b TUNNEL REYNOLDS NUMBER RANGE RELATIVE TO FLIGHT REYNOLDS NUMBER AND ON WHETHER 'CRITICAL EVENTS' OCCUR OUTSIDE TEST RANGE.
5a THREE-DIMENSIONAL EFFECTS COULD CAUSE DIFFICULTIES NEAR ROOT AND TIP	THREE-DIMENSIONAL EFFECTS DO NOT 5b REPRESENT AN ADDITIONAL PROBLEM BUT COULD ACCENTUATE DIFFICULTY OF 2b
6a REQUIRES A NUMBER OF TUNNEL RUNS WITH VARIABLE TRANSITION STRIP SIZE AND LOCATION; SHOCK WAVE POSITION MUST BE MONITORED RELATIVE TO STRIP LOCATION TO AVOID SPURIOUS EFFECTS IN REGIONS WITH SUPERSONIC FLOW	REQUIRES A NUMBER OF TUNNEL RUNS 6b TO ADAPT TRANSITION STRIP SIZE TO REYNOLDS NUMBER; SPURIOUS TRANSITION STRIP EFFECTS RESTRICTED TO LEADING EDGE REGION BUT MIGHT STILL BE SIGNIFICANT

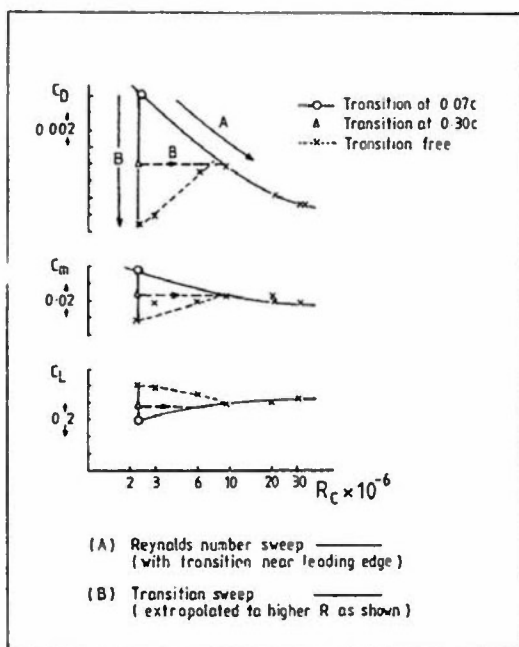


FIG. 1. EXAMPLE OF TWO SIMULATION APPROACHES  
2D AEROFOIL TESTS AT DESIGN CONDITION

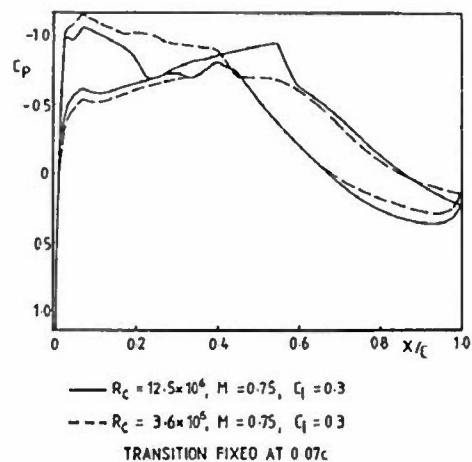


FIG. 2 EFFECT OF REYNOLDS NUMBER ON  
PRESSURES AT GIVEN  $C_L$ ,  $M$ .

2D AEROFOIL TEST AT NLR

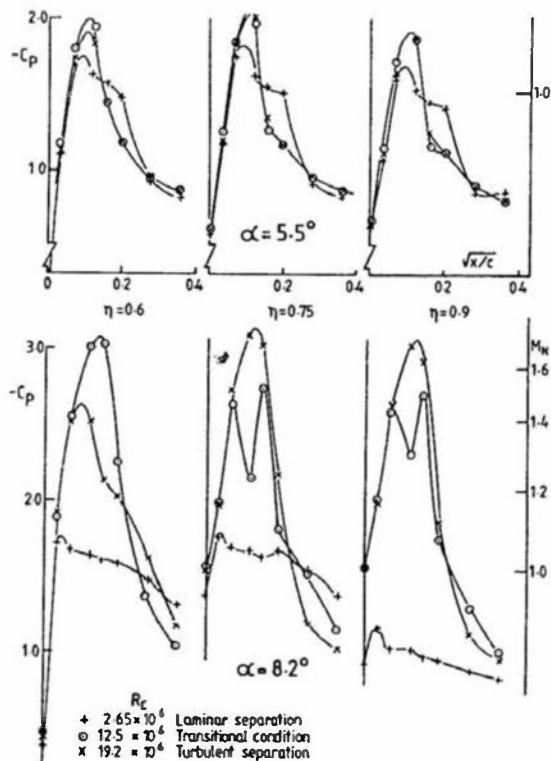


FIG. 3. EFFECT OF REYNOLDS NUMBER ON PRESSURE  
DISTRIBUTION NEAR LEADING EDGE

Combat aircraft model:  $42.2^\circ$  leading edge sweep. Test in RAE 8'x8' tunnel.

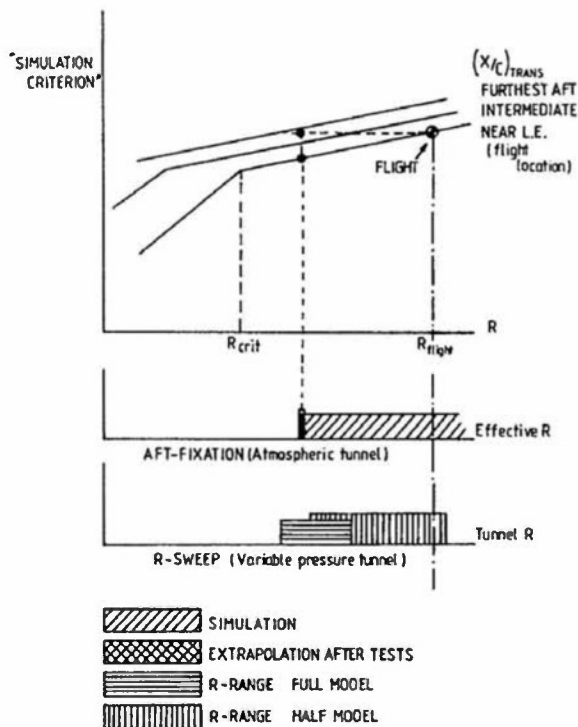
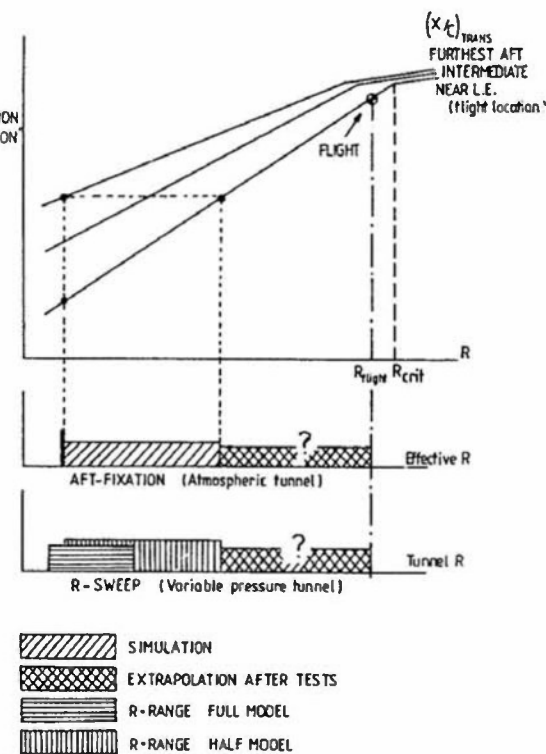
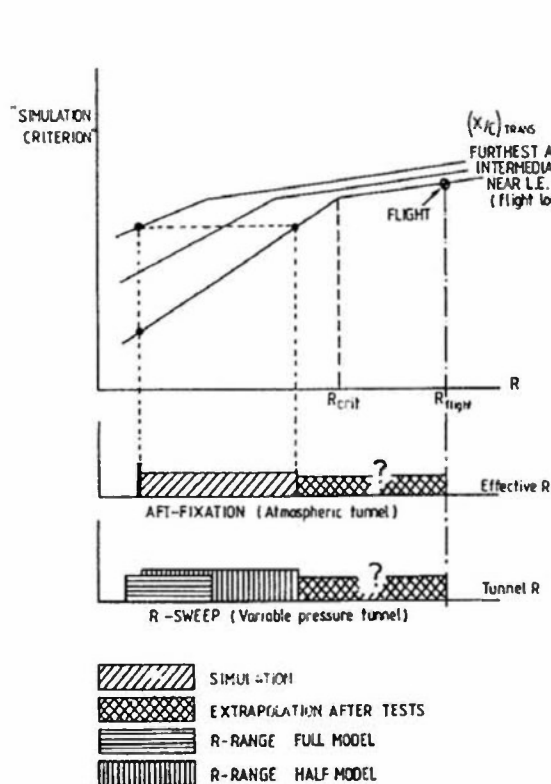
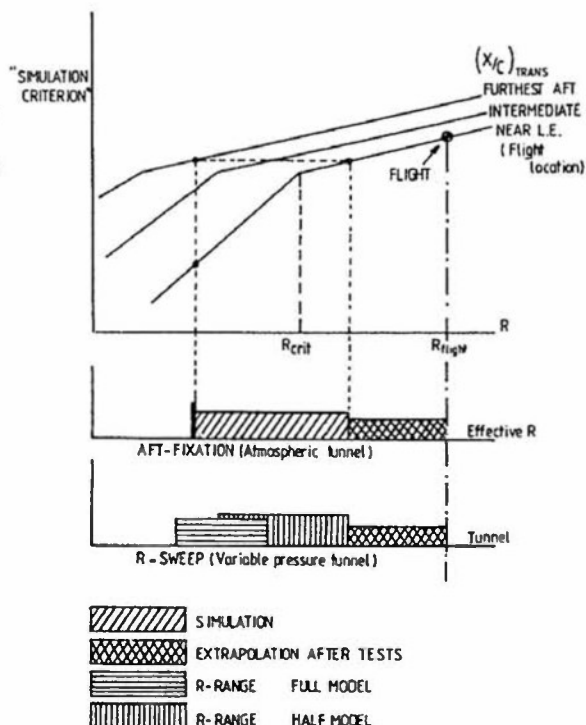
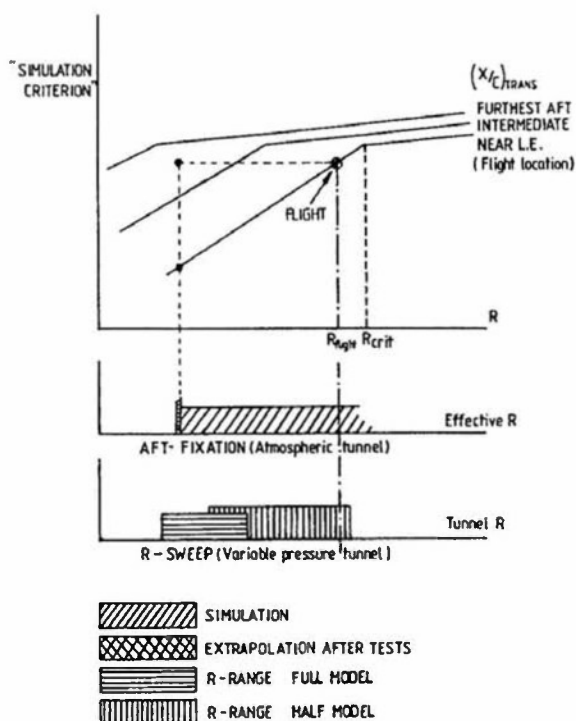


FIG. 4 SIMULATION SCENARIO 1



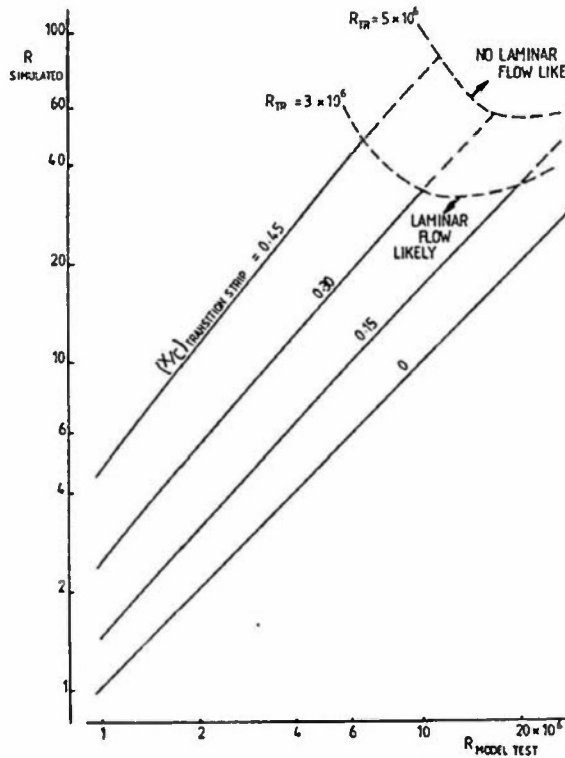
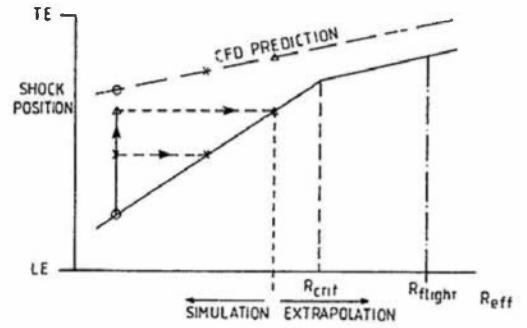


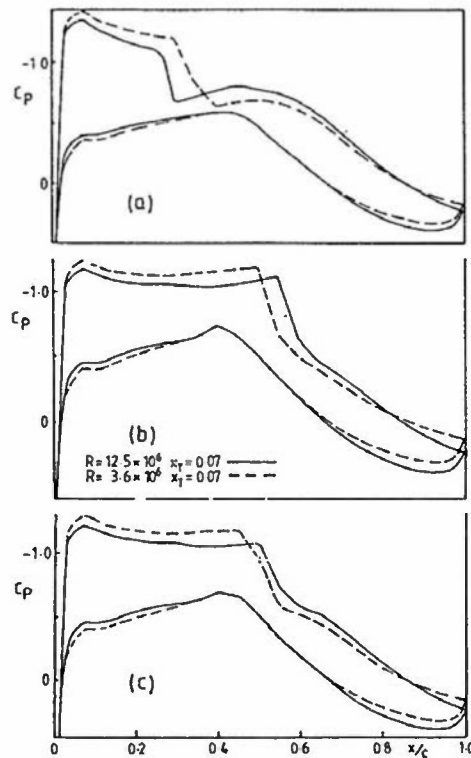
FIG. 9 ZERO LEVEL SIMULATION CRITERION  
(EQUIVALENT  $\theta$  AT T.E. OF FLAT PLATE)



○ — — — — — AFT TRANSITION DATA REPLOTTED AS  $x_{TR, SHOCK}$  DATA AT  $R_{eff}$ , CONVERSION TO  $R_{eff}$  BASED ON EQUIVALENCE OF CFD PREDICTIONS FOR  $(x_{TR, FLIGHT}, R_{eff})$  AND  $(x_{TR, AFT}, R_{model test})$

EXTRAPOLATION SHOULD BE BASED ON MEASURED TREND UP TO  $R_{crit}$  AND THEN ON CFD TREND FROM  $R_{crit}$  TO  $R_{flight}$

FIG. 10 USE OF SHOCK POSITION AS  
SIMULATION CRITERION  
(DIAGRAMMATIC)



NOTE: (a) shock moves forward with  $R$   
(b) shock moves rearward with  $R$   
(c) shock does not move with  $R$

FIG. 11 a,b,c. EFFECT OF REYNOLDS NUMBER AND  
TRANSITION POSITION AT A GIVEN  $C_L$ ,  $M$ .



## SECTION 3.2.2 EXPERIMENTAL TOOLS: THE TUNNEL AND THE MODEL

by

A.B.Haines  
Chief Executive  
Aircraft Research Association Ltd  
Manton Lane, Bedford MK41 8PA, UK

and

A.Elsenaar  
National Aerospace Laboratory (NLR)  
Anthony Fokkerweg 2  
1059 CM Amsterdam, The Netherlands

The aim of this short section of the report is to draw attention to experimental factors that can have a significant impact on the details of the methodology to adopt for a particular test program in a particular tunnel.

First and foremost, the methodology and in particular, the choice of approach to the in-depth study of the viscous effects is likely to depend on the test Reynolds number and on whether it is possible to vary the Reynolds number by changing the tunnel stagnation pressure (or temperature). If the tests are being made in a variable density tunnel, Reynolds-number sweeps will tend to be the preferred option; if the tests are being made in an atmospheric tunnel, manipulation of the boundary layer to produce a closer representation of the full-scale boundary layer behavior will be the only possible approach unless one is prepared to test more than one model to a different scale. Whenever possible, both approaches should be practised but nevertheless, the type of tunnel will dictate the preference. Reynolds number, is however, not the only significant parameter. The stream turbulence and noise level are also important, as shown in Section 4.8. The required standards of tunnel flow quality and data accuracy were set out in the report (1) of an earlier Sub-Committee of the AGARD Fluid Dynamics Panel. For convenience, however, let us summarize the main issues that can affect the success of applying either approach to the study of the viscous effects.

### 1 Reynolds-number sweeps

Clearly, the first requirement is to be able to test ideally over a Reynolds-number range that is significant in the context of extrapolation from model to full scale. This implies that the tests are being made in a variable density tunnel with an appreciable range of stagnation pressure (or temperature).

The interpretation of the results is not necessarily straightforward. Some of the apparent Reynolds number effects may be pseudo-Reynolds number effects (2, 3, 4). These can arise from changes with the stream unit Reynolds number in the empty tunnel flow calibration (static pressure, Mach number and flow angle), stream turbulence, acoustic noise spectrum or wall interference characteristics. In the past, the existence of these possible effects has not always been recognized, thus leading to confusion in the assessment of the true Reynolds-number effects. It is therefore essential that the tunnel flow calibration, stream quality and wall interference is measured at all test Reynolds numbers and the pseudo-Reynolds number effects identified and, if possible, eliminated from the model test data. In particular, one should assess whether there are any significant effects due to changes in

- (a) empty tunnel stream buoyancy and flow angle,
- (b) the calibration of the mean stream static pressure in terms of a reference pressure, e.g. in a plenum chamber around a ventilated test section. This can be especially important when making measurements of the drag of part of a complete model, e.g. on a fuselage afterbody (2),
- (c) the acoustic noise spectrum. Some experiments by Benek (5) and Weeks & Hodges (6) have suggested that boundary layer development for a given transition position can be relatively insensitive to sound waves but it is generally accepted that a realistic requirement (7) is for the level of  $\sqrt{\overline{p_s^2}}/q$  to be near 0.5% and for the value of the parameter  $[nF(n)]^\dagger$  to be near 0.002 at the relevant value of  $n$  for all test Reynolds numbers; otherwise, apparent changes with  $R$  in particular, the model buffeting response may not be genuine.
- (d) the stream turbulence. The ideal requirement (1) is for the rms-value of the  $u$ -component to be as low as 0.1% or even 0.05% for experiments in laminar flow but it is unlikely that this requirement is met in most transonic tunnels; values of 1% may be more typical (8). The effect of the stream turbulence may be far greater than generally appreciated. It appears that if the stream turbulence is notably greater than 0.1%, there may well be a need for correcting the Reynolds number to an 'effective Reynolds number' before plotting the data from a Reynolds-number sweep. The difficulty is that the 'effective Reynolds number' may depend on what feature of the test data is being considered. To quote some statements from the literature:
  - (i) 'even 0.1% rms  $u$ -component fluctuation causes somewhat more than 0.1% increase in flat-plate skin friction' (1),
  - (ii) 'free-stream turbulence may need to be less than 0.1% for the uncertainty in 'effective' Reynolds number to be less than 5%', (9)
  - (iii) 'an increase in free-stream turbulence level of 1% can have an effect on the conditions for separation-onset very similar to the effect of increasing Reynolds number of 60 to 70%' (9).



Conclusions such as (iii) above have sometimes led to the suggestion that large increases in stream turbulence may be a means of simulating high Reynolds number conditions but this suggestion should be resisted. High stream turbulence could provoke other spurious effects and also, it is not equivalent to an increase in Reynolds number in all respects, e.g. it gives an increase in skin friction, analogous to the effect of a reduction in Reynolds number.

- (e) the wall interference characteristics. A change in the stream unit Reynolds numbers leads to a change in the wall boundary layer thickness and hence, for a transonic tunnel with slotted or perforated walls, a change in the effective wall porosity. A fallacy in some past testing practice has been to determine wall interference by testing models of different scale at different stagnation pressures adjusted to achieve the same chord Reynolds number and then assuming that the wall interference corrections for all the tests is that needed to produce the same corrected data for all the models. This assumption can be invalid because the wall interference can, in principle, change with stagnation pressure and hence, model test data corrected making this assumption can contain a pseudo-Reynolds number effect.

This list may not be comprehensive but it should be sufficient to indicate that success in applying the Reynolds-number sweep approach can be critically dependent on knowing and allowing for various possible deficiencies in flow quality.

## 2 Boundary layer manipulation

At the present time, 'boundary layer manipulation' generally implies testing at a given Reynolds number and a number of different artificially fixed transition positions. The methodology as outlined in Section 3.2.1 is designed to suit test chord Reynolds numbers broadly in the range  $2 \times 10^6 \leq Re_c \leq 10^7$ . At lower Reynolds numbers, e.g.  $Re_c \leq 10^6$  it is likely that whatever the transition position, the boundary layers will be too thick to permit an adequate simulation of the full scale viscous flow over a wing of modern design. At higher Reynolds numbers, e.g.  $Re_c = 15 \times 10^6$  it is likely that transition will inevitably occur close to the wing leading edge.

The essential requirements, therefore, for this approach to be practised successfully are that the wing chord Reynolds number be in the range quoted above and that the transition Reynolds number in the facility is high enough for the transition position to be under the control of the test engineer, subject to the constraints set by the model geometry and the pressure distributions over the surface of the model. Fortunately, the transition Reynolds numbers in a near-zero pressure gradient in most of the leading transonic tunnels have been determined from tests on a 10° cone (8,10). The values lie in the range  $2.5 \times 10^6$

$\leq Re_T \leq 7.5 \times 10^6$  with a clear correlation established between  $Re_T$  and  $\sqrt{p_s^2/q}$  as shown in Fig 1, which

contains some values from flight tests with the same 10° cone. These values of  $Re_c$  appear to be sufficient to permit the boundary layer manipulation approach to be practised in most and probably all of these facilities for model test conditions where there are no significant adverse pressure gradients over the part of the surface where one is hoping to maintain laminar flow. The more important question is likely to be the extent to which these values of  $Re_T$  are degraded in an adverse pressure gradient.

It is interesting to note that these respectable values of  $Re_c$  are achieved despite the turbulence levels which are probably at least 0.5% fluctuation in u-component for most of these facilities. Pate (11) in reviewing all the available evidence, concludes that for the turbulence levels commonly obtained in transonic facilities, the stream noise level is usually the dominant factor in determining  $Re_T$ . This is not to say that the turbulence levels are unimportant. As noted above in the discussion on Reynolds-number sweeps, the effects of turbulence level can be considered as a modification of the effective Reynolds number and this appeared to be confirmed by the analysis of the correlation of drag data for a C-SA model tested in various transonic facilities (12). These issues are however far from resolved at the present time.

Turning from features of the tunnel flow to the design of the model, the test engineer in applying the methodology has to know

- (i) the shape of the model relative to the full scale aircraft or missile. Generally, models of transport aircraft are manufactured to a geometry that includes an allowance for the aeroelastic distortion of the full-scale aircraft in 1 g cruising flight. For combat aircraft, practices vary according to the test requirements; it may be thought more appropriate to attempt to reproduce the aeroelastic distortion in flight at selected points on the maneuver boundary. Another issue that is likely to be more important in the future is whether the model should continue to be scaled from the full scale vehicle geometry or whether the aim should be to reproduce the same non-dimensional displacement surface as on the full scale aircraft. Obviously, this can only be achieved for one particular design test condition but it could still produce a closer simulation to the full scale viscous flow in other conditions than if the full scale non-dimensional geometry had been retained. The justification for this tentative suggestion lies in the fact that with advances in wing design, the supercritical flow development over the forward wing upper surface has become more sensitive to small changes in section shape. Hence, changes in displacement thickness with Reynolds number can have a significant effect (13). Under these circumstances, it could be more accurate to use theory to allow for the changes of viscous effects with Reynolds numbers for a given displacement surface than to expect theory to be capable of predicting the changes in supercritical flow development with Reynolds number for a given non-dimensional geometry. This point should ideally be studied by CFD calculations before committing the model manufacture.
- (ii) The extent to which the excrescences present on the full scale aircraft have been represented on the model.

- (iii) The surface finish of the model. It is general practice to assume making drag estimates that the models have surfaces that are aerodynamically smooth but the requirements for this to be acceptable become more stringent with increase in test Reynolds number. The earlier AGARD recommendation (1) is that for tests involving boundary layer measurements, the criterion should be  $u_\tau k/\nu < 5$  where  $k$  is the surface roughness.

Finally, any methodology that relies on a comparison of measured test data with the results of CFD calculations as an essential element of the procedure for extrapolation to full scale must depend for its success on the accuracy of the test data and hence, on issues that strictly, are unrelated to the viscous flow effects. Good testing practice should be followed in all respects, e.g. the test data should be corrected for the effects of empty tunnel flow buoyancy, model support tares, mean tunnel flow angle (by testing the model erect and inverted) and any swirl in the tunnel flow if yaw is achieved by the pitch-roll technique. One of the most vital issues for the extrapolation of drag data is to determine the model angle-of-attack to an accuracy of 0.01° or better and thus, to know mean flow angle to this accuracy at all test Reynolds numbers. It has to be accepted that in most transonic tunnels, the flow angle will vary across the span of the wings of the model by far more than 0.01° thus affecting the effective twist of the wings\* but the crucial reason why one needs to know the angle-of-attack to 0.01° or better is that, in general, the internal balance measures normal and axial force and  $C_N$  and  $C_A$  have then to be resolved to obtain  $C_L$  and  $C_D$ . At  $C_L = 0.5$ , a typical cruise  $C_L$  for a transport aircraft, an error of  $\Delta\alpha = 0.01^\circ$  implies an error of 0.0001 in  $C_D$ .

\*Frequently, particularly when the tests are being made in a tunnel with a closed working section, the model wing is manufactured with a twist distribution modified to offset the spanwise variation in incidence induced by the wall interference, thus producing an effective twist in agreement with the full scale aircraft. It is more difficult to apply this idea to offset the variation across the tunnel in the empty tunnel flow angle calibration.

## REFERENCES

- 1 Wind tunnel flow quality and data accuracy requirements.  
AGARD Advisory Report No 184 November 1982
- 2 AULEHLA, F  
EBERLE, A Reynolds number effects on transonic shock location.  
AGARD CP-335, Paper no 4 September 1982
- 3 BINION, T W Jr  
KRAFT, E M A review and an update of the FDP Specialists meeting (London) on wall interference in wind tunnels.  
AGARD CP 348, Paper no 6 September 1983
- 4 BINION, T W Jr Pseudo Reynolds number effects.  
AGARDograph on Reynolds number effects, Chapter 2, To be published
- 5 BENEK, J A Effects of acoustic and vortical disturbances on the turbulent boundary layer at freestream Mach number 0.5.  
AEDC-TR-77-73 1977
- 6 WEEKS, D J  
HODGES, J An experimental investigation of the influence of acoustic disturbances on the development of a turbulent boundary layer.  
ARC CP no 1155 1978
- 7 MABEY, D G Flow field stability and model vibration in wind tunnels at subsonic and transonic speeds.  
ARC CP no 1155 1971
- 8 DOUGHERTY, N S Jr  
STEINLE, F W Transition Reynolds number comparisons in several major transonic tunnels.  
AIAA 74-627 July 1974
- 9 GREEN, J E On the influence of free stream turbulence on a turbulent boundary layer, as it relates to wind tunnel testing at subsonic speeds.  
RAE TR 72201  
AGARD-R-602 October 1972
- 10 DOUGHERTY, N S Jr  
FISHER, D F Boundary layer transition on a 10-degree cone; wind tunnel/flight data correlation.  
AIAA-80-0154 January 1980
- 11 PATE, S R Effects of wind tunnel disturbances on boundary-layer transition with emphasis on radiated noise: a review.  
AIAA-80-0431 March 1980
- 12 TREON, S L  
STEINLE, F W  
HAGERMAN, J R  
BLACK, J A  
BUFFINGTON, R J Further correlation of data from investigations of a high subsonic speed transport aircraft model in three major transonic wind tunnels.  
AIAA-71-291 March 1971

NOTATION

$k$	Surface roughness
$n$	Reduced frequency
$\sqrt{\overline{p_s^2}}$	rms value of fluctuating static pressure
$q$	Dynamic pressure
$Re_c$	Reynolds number based on wing chord
$Re_T$	Transition Reynolds number
$u_\tau$	Shear-stress velocity
$\nu$	Kinematic viscosity

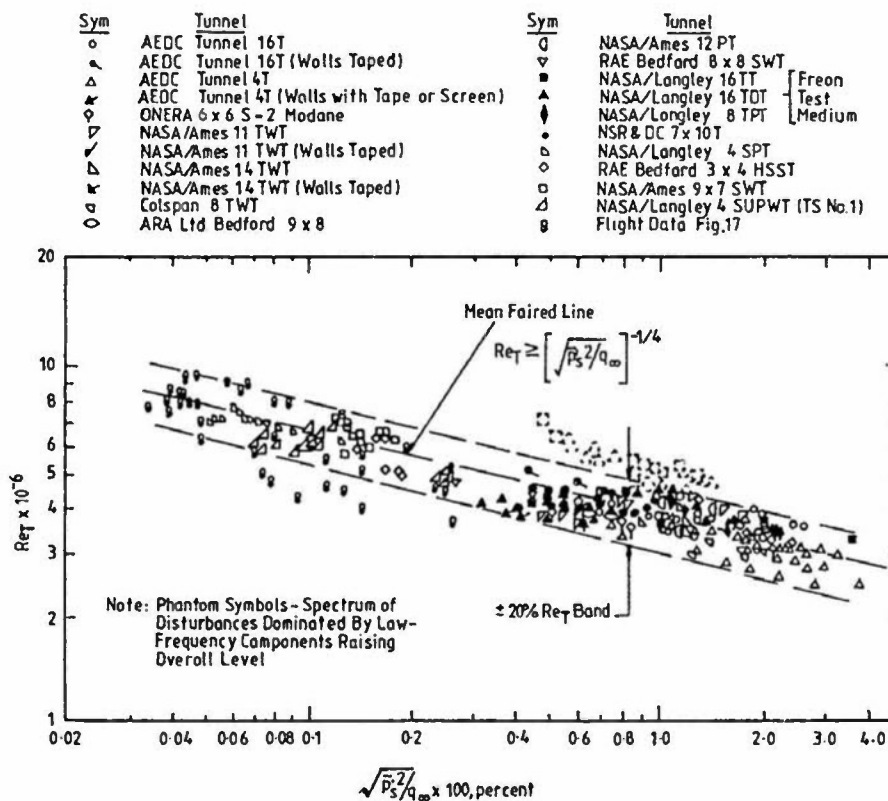


FIG.1 TRANSITION REYNOLDS NUMBERS DEDUCED FROM TESTS WITH 10° CONE  
(Ref.10)

### SECTION 3.2.3 COMPUTATIONAL TOOLS FOR SIMULATION METHODOLOGIES

by

Dr Y.Y.Chan  
National Research Council of Canada  
Montreal Road  
Ottawa, Ontario K1A 0R6, Canada

#### 3.2.3.1 Introduction

To predict full scale phenomenon from tests with a scale-model in the wind tunnel, it is necessary to preserve the relative magnitude of the forces acting on the model so that the resulting flow is dynamically similar. Because of the limited performance of the testing facilities, scaling of the ratio of the viscous force to the inertia force is always a difficult problem. At transonic speeds, this problem is accentuated by the sensitivity of the external inviscid flow to the perturbation of the condition at the surface. Thus the displacement effect due to the growth of the boundary layer along the body directly influences the development of the outer flow. The existence of the shock wave situation over part of the body induces additional complication as the shock interacts with the shear layer and alter the local flow structures. Large efforts have been made for better understanding the interactive components of the flow and deriving techniques for proper reproduction of the flow fields. These can be exemplified by the pioneering works of Haines, Holder and Pearcey<sup>(1)</sup> to the accumulative contributions of the High Reynolds Number Wind Tunnel working group (HIRT) of the AGARD Fluid Dynamics Panel<sup>(2,3)</sup> and the workshop on High Reynolds Number Research of NASA<sup>(4)</sup>. For current simulation practices and criteria for achieving adequate simulations, a thorough review is given in Chapter 2 of this report.

During the past decade, the rapid development of the digital computer and computational fluid dynamics (CFD) have made their impact in aerodynamic testing and simulations. The importance of computers and CFD in complementing the wind tunnel operation and testing programs has been discussed by Haines<sup>(5)</sup> and later demonstrated by Whitfield et al<sup>(6)</sup>. For viscous simulations or scale effects, Haines pointed out that by applying CFD to allow for the inadequate test Reynolds number, the ability to forecast the aerodynamics of the full scale aircraft could be increased. This was shown by Loving<sup>(7)</sup> with the well known case of transonic scale effects on the wings of the C-141; CFD was able to provide the correct extrapolation of the wind tunnel data to the full scale Reynolds number in excellent agreement with the flight data. Haines also showed an example of direct simulation of the local flow; if a rear separation was likely to happen in the experiment, CFD could be used to find the aft fixing location to give the same boundary layer thickness at the foot of the shock as at full-scale Reynolds number with forward transition. Further applications of computational methods for estimations of simulation conditions can also be found in Chapter 2.

The augmentation of wind tunnel simulations by CFD is limited at present by the latter's capabilities. It is known that CFD cannot yet cost effectively provide a complete flow field about a complicated configuration. However, CFD is well capable to generate efficiently flow fields over components of the configuration. In Section 3.2.1, the role of computation in a test program is established and the applications of the computational results to design and checking of the test are discussed. With this understanding, the present state of flow computations that could be implemented for viscous flow simulations is examined. The prediction of transition which is vital for flow simulation is reviewed in Section 4.3 and will not be included in the present discussions.

Computation of viscous flows at high Reynolds numbers have been advanced greatly as a branch of CFD for both two and three dimensional flows, shock wave interactions and moderate separations can be treated. These are accomplished by the developments of viscous-inviscid interaction theory, Navier-Stokes technology and turbulence modelling. A number of comprehensive reviews on these topics have recently been published. The 1980 81 AFOSR-HTTM-Stanford Conference has covered a broad spectrum of turbulent shear flows<sup>(10)</sup>. External aerodynamic flows have been reviewed by Marvin with emphasis on turbulence modelling<sup>(11)</sup>. Interactive flows have been discussed by a number of authors<sup>(12,13,14,15,16,17)</sup>. The analytical aspects of the interactive flows have been presented by Messiter<sup>(18)</sup> on the interactive theory in general and by Adamson and Messiter<sup>(19)</sup>, Melnik<sup>(12)</sup> on shock wave-boundary layer interaction in particular. For three-dimensional boundary layers, computational methods have been reviewed by Smith<sup>(20,21)</sup> and Cebeci<sup>(22)</sup>, while turbulence modelling can also be found in Marvin<sup>(11)</sup>. The full Navier-Stokes methods have been comprehensively reviewed by Mehta and Lomax for transonic flows<sup>(23)</sup>.

The present section is not intended to be a comprehensive review of the computational methods for viscous flows. It is rather to examine the capabilities of the methods which could be applied to the design and checking of experimental simulations. With references to the cited reviews, in particular References 11, 12 and 16 which contain extensive bibliographies, a summary is given on the computations of viscous aerodynamic flows. Important features of the flow field are discussed and their computational results are demonstrated by typical examples. Some original papers used in the discussions are also listed as direct references.

#### 3.2.3.2 SCALING OF TURBULENT BOUNDARY LAYERS AT HIGH REYNOLDS NUMBER

It is well known that the turbulent boundary layer has a composite structure. At large Reynolds numbers, a two layer structure is developed<sup>(12,24,25)</sup>. The outer layer is essentially independent of viscosity, except through its indirect influence on the skin friction and the total thickness of the layer. The inner layer is dominated by the shear stress and is independent of the free stream velocity and the thicknesses. Matching the inner and outer velocity profiles leads to the logarithmic skin friction law. The length scales in terms of the thicknesses of the outer and the wall layers respectively are given by

$$\frac{\delta}{L} = O(\epsilon), \quad \epsilon = O(\ln Re)^{-1}$$

$$\frac{\delta^+}{L} = O(\epsilon \hat{\epsilon}), \quad \hat{\epsilon} = (\epsilon^2 Re)^{-1} = \epsilon^{-2} e^{-1/\epsilon}$$

where  $\epsilon$  is the basic parameter characterized by the large Reynolds number limit and  $\epsilon$  is the ratio of the thicknesses of the inner and outer layers. The wall layer is exponentially thin compared to the total boundary layer thickness and hence is not influenced, to the lowest order, by the pressure gradient except when the flow is separated or the pressure gradient is very large. For transonic flow, the weak interaction of the viscous-inviscid flow is governed largely by the displacement effect of the boundary layer<sup>(12,16)</sup>; thus for flow simulations, the thickness of the outer layer (or the boundary layer as a whole) is the basic parameter that should be reproduced in principle in model testing.

When the streamwise pressure gradient becomes very large, as occurs at the shock wave, or at the trailing edge or at incipient separation, strong viscous-inviscid interaction takes place. These local interactions in small regions are dominated by the outer layer which behaves approximately as an inviscid rotational flow. This allows the interactions to be analyzed analytically revealing the parameters controlling the local flow development<sup>(12,18)</sup>. For example, the flow similarity for the shock wave-boundary layer interaction expressed in terms of pressure coefficient has been shown to be<sup>(12)</sup>

$$C_p = C_p(x, y; Re, M_\infty, \gamma, \pi, \delta) = C_p(\tilde{x}, \tilde{y}; K_1, \pi)$$

where

$$\tilde{x} = \frac{x}{(\gamma + 1) M_\infty^2 \delta \epsilon^{1/2}}, \quad \tilde{y} = \frac{y}{\delta};$$

$$K_1 = \frac{M_\infty^2 - 1}{(\gamma + 1) M_\infty^2 \epsilon}$$

$K_1$  is the viscous transonic similarity parameter and  $\pi$  is the effective profile shape. Flows with the same values of  $K_1$  and  $\pi$  are thus similar. The results of these analyses have been applied by Khan and Cahill<sup>(26)</sup> to the correlations of the trailing edge pressure coefficients for both attached and separated flows with strong interactions. The correlation can be employed for extrapolation of wind-tunnel data on a wing to full scale Reynolds numbers (see Section 2.2.2.6). It should be noted that the scalings of  $x, y$  and the parameter  $K_1$  depend on  $\epsilon$  and  $\delta$ . Thus for simulations of the strong interaction, it is necessary to reproduce both the boundary layer thickness  $\delta$  and the profile shape at the interaction region. The techniques commonly used to achieve a close reproduction of these parameters in the tests are "aft-fixing"<sup>(27,28)</sup> and boundary layer control<sup>(29)</sup>. Discussions of these and other methods and their applications can be found in Sections 2.2.2 and 2.2.4. For transonic flows the zonal shock-boundary layer interaction may have a bigger influence on the flow field than the global weak interaction. Thus simulations of strong interaction must be emphasized and the parameters properly reproduced.

### 3.2.3.3 VISCOUS FLOW COMPUTATIONS

Methods for solving boundary layer equations, both in integral and differential approaches are highly developed<sup>(10,13)</sup>. In the former case, the computational efficiency is a great asset especially for three dimensional flows or interactive flows requiring iterations between the external flow and the boundary layer. The choice of the auxiliary equations to complement the momentum integral equation is critical for the development of the method and the lag-entrainment approach has generally been accepted<sup>(30)</sup> and used in transonic flow computations<sup>(12,16)</sup>. The essence of this method is the use of the turbulent kinetic energy equation that considers the turbulent structure explicitly. Thus the parameters affecting the turbulence development such as extra rates of strain and free stream turbulence can be taken into account.

In the differential approach, the equations are written in finite difference form and the difference equations are then solved by efficient numerical algorithms. The computation starts at an initial station and proceeds in the downstream direction according to the parabolic nature of the equations. Since the equations are solved directly without assuming parametric relations between the unknown quantities as in the integral methods, the differential methods in principle are more flexible in applications.

The use of Reynolds averaged equations requires the supplementary information of turbulent shear stresses for closure of the computational system. This information is derived by relating the unknown to the mean-velocity field or the mean-turbulent field with algebraic relations or transport equations<sup>(10,11)</sup>. The former is the eddy viscosity model and the latter utilizes the equations or high order correlations such as the turbulent kinetic energy and the dissipation. The added equations, however, are no self-contained as they consist of correlations of higher order, which are usually unknown. Thus it is necessary to relate the unknowns to the known field quantities and evaluate the relations from experimental data. The range of application of the turbulence model would, therefore, be affected by the conditions at which the experimental data have been taken and the sensitivity of the chosen parameters to these conditions.

At transonic speeds, the weak interaction due to the displacement of the external flow by the boundary layer can be treated readily by conventional boundary layer calculations. The rate of growth of the boundary layer provides the inner boundary conditions for the inviscid flow calculations. An iterative process is thus required for the solution of the complete flow field. For strong interactions at the shockwaves and at the trailing edge of the airfoil, the interactive flows can be treated locally as the affected regions have limited extent at high Reynolds numbers. The local results are then incorporated into the global computational procedure. This approach has been commonly used in calculating the flow field over transonic airfoils or wings with attached flow<sup>(12,16)</sup>.

If the pressure distribution is prescribed, the boundary layer equation is singular at the separation point and the direct method fails there. However, with either the displacement thickness or the surface shear stress prescribed, the separation point is regular and the computation can proceed through the separation region. Coupled with an external inviscid flow calculation, the inverse method can adequately compute the flow field with a shallow separation region such as the leading edge separation bubble or moderate separation at the trailing edge<sup>(14)</sup>.

A further development in the interactive methods is the thin layer Navier-Stokes approach, the first order form of which reduces to a boundary-layer-like system with the normal pressure gradient included. The solutions of the viscous and inviscid flows are



matched with overlapping computational domains. The approach is therefore uniformly valid for the interactive flows discussed above<sup>(15)</sup>.

For gross separations, the thin layer interaction approach fails and solution of the Reynolds averaged Navier-Stokes equations is required. The elliptical nature of the system with the computing region covering a large portion of the flow field leads to long computing time. For high Reynolds number flows with turbulent wall layer, turbulence modelling is again required for the closure of the Reynolds averaged form of the equations. Like the other differential methods for turbulent boundary layers, this exact solver cannot completely escape the empiricism and the limitations imposed from the closure models<sup>(23)</sup>. To increase the computational efficiency, the Navier-Stokes equations are parabolized by neglecting the streamwise diffusion terms and the thin layer techniques can then be applied<sup>(31)</sup>.

The discussion above applies in general to both two- and three-dimensional flows. In the latter case, the additional degree of freedom increases the complexity of the flow structure and hence the solution procedure. The nature of the equations along and normal to the external stream directions becomes hyperbolic and the zone of influence has to be considered in the computational algorithms. Turbulence modelling is extended to include the additional components of the stress tensor. The computational effort is thus more demanding and more costly<sup>(20,22)</sup>. For the same reason, the experimental observations and measurements of three-dimensional flows are far fewer than those of two-dimensional ones, thus the nature of the flow is less well understood especially at separations<sup>(32,33)</sup>.

### 3.2.3.4 COMPUTATIONAL CAPABILITIES

The aerodynamic flows in order of complexity and the computational methods required for their simulations are summarized in Figure 1. In the figure, the broad arrow drawn in the direction of the computational level for each column indicates that similar or better results can be obtained at a higher level. The present capabilities of the computational methods as outlined in the last section are now further discussed through the flow characteristics delineated in the figure. Viscous-inviscid interactions as an inherent characteristic of transonic flows will be emphasized. The assessment is based on published comparisons between computations and experimental data. For flow simulations, it is ideal if the complete flow field about the configuration can be reproduced as a whole. However, because of the Reynolds number limitation of the testing facilities, multiple simulations with each designed for reproduction of a local interaction may be necessary as recommended in Section 2.4. Thus the components of the interactive flows will be first discussed, then followed by the complete flow field. The free-stream turbulence effects on the development of the boundary layer will also be included in the discussion as the former is an intrinsic property of all wind tunnels. (See Section 2.3.1.5).

#### 3.2.3.4.1 Two-Dimensional Flows

##### 3.2.3.4.1.1 Attached Flows

The most essential requirement of a computational method is its ability to predict boundary layer development at the desired Reynolds number. Since most of the computational methods, both differential and integral, involve a number of empirical inputs which are derived from experimental data collected at certain range of Reynolds numbers, the first test of the methods is thus to examine their applicability at different Reynolds numbers. In the case of differential methods, a critical test of Reynolds numbers extended from 11.7 to 314 million with significantly different values of skin friction, providing excellent testing conditions for this case. As shown in Figure 2, the predictions from a number of methods with turbulent models of different complexity follow the data trend well enough to provide estimates of Reynolds number effects. Additional examples have been given by Horstman et al<sup>(34)</sup>.

Integral methods, as exemplified by the  $\lambda$ -entrainment approach, work well for moderate Reynolds numbers but have not yet been tested to such a high Reynolds number as the above example. The correlation coefficients in the method are derived from data of moderate Reynolds numbers. High Reynolds number data are thus urgently needed for extending the validity of this method<sup>(35)</sup>.

One may conclude that for attached boundary layer flows, their development can be adequately computed by the existing codes in the differential or integral forms for the range of Reynolds numbers interesting for flow simulations. Models that affect closure through the mean-turbulent-field equations appear to be more generally applicable.

##### 3.2.3.4.1.2 Leading Edge Separation Bubbles

For transonic airfoils at off design conditions, steep compression may occur at the leading edge region. If the Reynolds number is large, the boundary layer becomes rapidly turbulent close to the leading edge and is better prepared to sustain the adverse pressure gradients. However, if the Reynolds number is low enough for the boundary layer to remain laminar, separation may occur and a separation bubble is formed. The separation bubble affects the downstream development of the boundary layer and changes the local pressure distribution significantly. Thus for proper simulation, it is necessary to know whether the separation bubble would be formed under experimental conditions.

A shallow separation region such as the separation bubble has been treated by the inverse boundary layer method coupled to an inviscid calculation. The inverse methods have employed both integral and differential forms<sup>(36,37)</sup>. For the leading edge separation, the boundary layer is laminar and undergoes transition to turbulent flow prior to reattachment to the surface. Proper models of transition for the free shear layer are required as part of the computational procedure. The success of the prediction method is shown in Figure 3 taken from Gleyzes, Cousteix and Bonnet<sup>(38)</sup>. The experimental data have been obtained on a 200 mm chord ONERA LC100D airfoil. The separation occurred at quarter chord at  $Re_c = 2.2 \times 10^6$  and a low free stream turbulence intensity of 0.4%. The pressure distribution and the variations of the boundary layer properties are well predicted over the separation region. The example shown is for low speed flows, however cases at transonic speeds are also given in the paper. Similar success can be found in Davis's paper for the differential method<sup>(37)</sup>.

##### 3.2.3.4.1.3 Shock-Boundary Layer Interaction

The strong interaction of the shock wave and the boundary layer is an intrinsic feature of transonic flows. The analytical results of the asymptotic analysis of a normal shock interaction with the boundary layer on a flat plate, as discussed in Section 3.2.3.2, can be used for scaling of the local flow parameters if the interaction does not induce separation. For interactions with local separation, the Navier-Stokes equations or the thin layer approximation are required for the solution of the flow field. Specially designed experiments have been performed to provide a precise check on computational predictions and input for turbulence modelling<sup>(39)</sup>. Results have been presented by Marvin for the Navier-Stokes solutions<sup>(11)</sup> and are reproduced in Figure 4. The shock wave was formed inside a circular test section and interacted with the wall boundary layer. The upstream Mach number of the shock was 1.41 and the local Reynolds number 37 million. Separation in this test case was small. The pressure rise through the interaction is correctly predicted by the computations. The boundary layer developments, as shown here by the skin friction distributions and the velocity profiles,

indicate that the turbulence models with mean-turbulent field yields better results than those with mean-velocity field. The well predicted pressure rise regardless of the turbulence modelling is a result of the inviscid dominated nature of the outer layer as discussed in the previous section.

In the thin layer approach, the viscous flow computation is coupled to a transonic inviscid code and the solution is obtained by a semi-inverse global iteration process allowing for flow separation<sup>(39)</sup>. Computational results for one of the special experiments by Marvin<sup>(38)</sup> have been given by LeBalleur<sup>(39)</sup> and are reproduced here in Figure 5. The shock wave-boundary layer interaction took place on a symmetrical 18% circular arc airfoil at zero incidence. With the transonic small disturbance code for the inviscid flow computation, the results agree well with the experimental data in the lower Mach number case involving a small separation region. For large shock-induced separation, only qualitative agreement is obtained. The variations of the boundary layer properties over the interaction region are also shown for the higher Mach number case with flow separation well predicted. Note that the Navier-Stokes results are also shown in the figure for comparison. The over-prediction of the pressure rise for both the Navier-Stokes and the thin layer solutions is due to the fact that the computations predict a strong, nearly normal shock while the experiment indicates the presence of a weak oblique shock. It has recently been shown that if the downstream condition corresponding to the experimental flow field is imposed, an oblique shock is predicted and the experimental pressure rise is recovered<sup>(40)</sup>.

#### 3.2.3.4.1.4 Trailing Edge Flows

At the vicinity of the trailing edge of an airfoil, the streamline curvature and the normal pressure gradients are no longer small and the interaction with the inviscid flow is moderate for attached flows and strong for separated flows. For attached flow the asymptotic analysis delineates the local flow structure explicitly and provides corrections for the computations of weak interactions<sup>(12)</sup>. For flows with separation, the Navier-Stokes method or its thin layer approximation are again required for the solution of the flow field. The Navier-Stokes computations shown by Horstman and their comparisons with data from experiments specially designed to examine the trailing edge flows are particularly illustrative<sup>(41)</sup>. Some typical results are shown in Figure 6 taken from this reference. The test configuration consisted of a forebody and a rear section to which different trailing edge models could be attached. The trailing edge model shown in the figure has the form of the upper rear quadrant of an 18% thick circular arc airfoil. Data were obtained at Mach number of 0.7 and Reynolds number of 40 million per meter. A small separation zone was obtained close to the trailing edge. The displacement thickness variation in the trailing edge region shows the well known sharp discontinuity in slope as the nonslip condition changes to the wake condition. The trend of the experimental data is well predicted, as well as the details of the flow field in the forms of velocity profiles and turbulent shear stress profiles. It is also shown that for attached flows, turbulence modelling has a secondary role in the interaction as indicated by the asymptotic analysis. For separated flows, however, turbulence modelling becomes important, the velocity should now be scaled by the square root of the maximum shear stress and the upstream history of the turbulence development must be taken into account<sup>(42)</sup>.

The thin layer interactive approach is well suited for treating the trailing edge flow with or without separation as discussed in the previous section. The result from an interactive method coupling the Euler solution and the inverse boundary layer approach is also shown in the figure<sup>(43)</sup> and is in good agreement with the data. The direct boundary layer computation using the measured pressure distribution fails to reach the level of the data as the trailing edge is approached. This failure has indeed been observed in many classical test cases<sup>(30)</sup>.

#### 3.2.3.4.1.5 Flows Over Airfoils

The complete flow field over an airfoil can be constructed by adding the zonal strong interactions to the overall weak interactions or by a global consideration covering the whole airfoil and wake. The former approach is commonly used for airfoil computations with attached flow and is exemplified by the methods developed by Melnik<sup>(12)</sup>, Lock<sup>(16)</sup> and Stanewsky<sup>(44)</sup>. The approaches of these methods are basically similar and are different mainly due to the selection of the strong interaction modules incorporated into the computation. All give excellent predictions of pressure distribution and the variation of boundary layer displacement over the airfoil. The aerodynamic coefficients are well predicted up to the trailing edge separation. Some typical computational results for pressure distributions and boundary layer properties taken from Reference 12 are shown in Figure 7.

The thin layer method that treats all interactions in a global form also predicts accurate results for the example given above. Since the method is applicable to moderately separated flow, it can in principle be used to determine the maximum lift coefficient. The Navier-Stokes method can also be applied beyond the inception of separation. As an example, the aerodynamic coefficients computed by this method are shown in Figure 8. The results from the interactive method, for both the lift curve and the drag polar, follow the experimental data closely. The results from the Navier-Stokes solutions, however, are less satisfactory. The discrepancy of the latter may be due to the fact that the computations were performed assuming free boundaries at the wind-tunnel test conditions and no adjustments were allowed for the wall interference correction<sup>(40)</sup>. Recent advances of the interactive methods and improvement of the overall accuracy can be found in the excellent lecture note by Lock<sup>(17)</sup>.

From the above discussions on two-dimensional flow computations, we may observe that all methods predict the experimental data trends well enough to provide accurate estimation of viscous effects for flow simulations. Both integral and differential methods of solution are well developed. For turbulence modelling, eddy viscosity is sufficient for most conditions. However, the mean-turbulent-field closure is needed as extra strain rates become large. Methods for computing viscous-inviscid interactions, which is an inherent feature of transonic flows, are also developed. The thin layer method can readily treat moderate separated flows and shock wave boundary layer interactions. For flows with strong separation such as that induced by shock waves and at the trailing edge, the Navier-Stokes method is required.

#### 3.2.3.4.2 Three-Dimensional Flows

Computational methods for three-dimensional flows are less developed than the corresponding ones in two-dimensions. The complexity of the flow field requires additional effort both in formulation and computation. The concepts and techniques discussed in the last section for two-dimensional flows are in principles, with some generalizations, applicable to the three-dimensional cases. Care, however, must be taken for the unique characteristics of three-dimensional flows especially at separation.

For attached flows, the computational methods, both integral and differential are well developed. The performance of some of these methods have been assessed by comparison with experimental data of Van den Berg and Elsenaar<sup>(45)</sup> for flows over an infinite swept wing. Although the test flow of the experiment was incompressible, the experimental conditions resembled those encountered on real wings. Thus the data has been used by various investigators for evaluation of computational results. For this test, a streamwise adverse pressure gradient was imposed on the flow that led to separation. The computational results from both integral and differential methods taken from Smith's review<sup>(21)</sup> are shown in Figure 9. All predictions from direct methods show good agreement with the experimental data when the cross flow is small or moderate but they fail as the cross flow becomes large. Improving the turbulence modelling for the differential methods from isotropic eddy viscosity to full Reynolds stress model only improve the results slightly<sup>(11)</sup>. It has been shown by Cousteix<sup>(46)</sup> and Smith<sup>(21)</sup> that the rapid thickening of the boundary layer and the large skew rate at the rear portion of the flow required interactive treatment. Interactive calculations using inverse boundary layer methods yield excellent agreement with the experimental data in the same manner as the trailing edge flow discussed in the previous section.

With the patching approach, the interactive flow over a transonic wing has been calculated for attached flows<sup>(16)</sup>. The thin layer matching approach of LeBalleur has been extended to an infinite swept wing with quasi-three-dimensional separation and shock-wave boundary layer interactions<sup>(15)</sup>. The Navier-Stokes method has also been employed to compute a full three-dimensional flow over a 45-degree swept, 10% thick circular arc airfoil at zero incidence and spanning a wind tunnel test section<sup>(23)</sup>.

Similarly, as for the planar wing, boundary layer flows over a fuselage can be calculated up to the separation region<sup>(47)</sup>. The flow developed along the wing-body junction is considered as a corner flow problem in which the secondary-flow is generated by Reynolds stress gradients and the lateral skewing of the shear layer. The Navier-Stokes method is required for the solution, a parabolized version is given by Arnal in which turbulence modelling is also examined<sup>(48)</sup>.

The three-dimensional separation is more complicated than the two-dimensional one. It is governed not by a simple algebraic condition as in the two-dimensional case but by the differential relations of the limiting streamlines, the singular solutions of which define the separation points or lines. For open separations, the separated shear layer inevitably rolls up into a free vortex. For simulating three-dimensional separated flow, Navier-Stokes methods are required and a typical example has been given by Fujii and Kutler on the separated vortical flow over a delta wing at high angles of attack<sup>(49)</sup>. Another example including both closed and open separations has been given by Mehta, in which the transonic flow field on the boattail of an axisymmetric body at an angle of attack has been computed<sup>(23)</sup>. Both examples demonstrate the capabilities of the Navier-Stokes technology for simulations of complex flow fields.

The present computational capability for three-dimensional flow is still short of the objective of predicting viscous effects in transonic flow on complete aircraft configurations. However, the progress in component flow computations will provide us with building blocks for complete flow simulations in the future.

### 3.2.3.4.3 Unsteady Flows

When the flow past a body is time dependent, the governing equations become hyperbolic, and the solutions are obtained by marching in time. The unsteady flows commonly encountered in a wind tunnel are mostly oscillating in nature, the boundary layer is thus periodic with an imposed mean flow. The methods of solution of the boundary layer equations can again be integral or differential. The former is exemplified by the method of Cousteix et al<sup>(50)</sup> and the latter is given in some details by Telsonis which includes turbulence modelling<sup>(51)</sup>.

For an oscillating airfoil in transonic flow, the weak interaction has been considered for low reduced frequencies by patching the unsteady inviscid solution with the steady boundary layer solution<sup>(52)</sup>. A more general approach has used the unsteady boundary layer solution and the matching conditions for the viscous-inviscid interaction flows<sup>(15,53)</sup>. The interactive computational results of a pitch oscillating airfoil is shown in Figure 10, taken from LeBalleur<sup>(15)</sup>. The interactive computations greatly improve the inviscid solutions and agree well with the experimental data, especially for the unsteady pressure peak at the shock wave. The Navier-Stokes methods are most suited for computation of unsteady flows with separations. In Mehta's review, examples are given for wing buffeting with oscillatory shock waves and separations, and for the aileron buzz<sup>(23)</sup>. The buffet boundary of an airfoil at high lift condition is also well predicted.

### 3.2.3.4.4 Free Stream Turbulence

The airflow in a wind tunnel always contains small amount of unsteadiness generated in the tunnel circuit in forms of velocity and pressure fluctuations. The most direct effect from these disturbances to the flow past a model is on boundary layer transition, the detailed discussion of which can be found in Chapter 4. The effects on the development of the turbulent boundary layer have been treated by Timme<sup>(54)</sup> and Green<sup>(55)</sup>. It has been shown that the free stream turbulence causes increased boundary layer growth with associated increment in surface skin friction and fuller velocity profiles. The reduction of the shape factor has a similar effect to an increase of Reynolds number. However, the thickening of the boundary layer works against the requirements of small thicknesses, both for the displacement effect and for the shock wave-boundary layer interaction at higher Reynolds numbers.

In computations of the turbulent boundary layer development, the free stream turbulence can be taken into account if the mean-turbulent field modelling is used. The capabilities of these methods in predicting the increases of skin friction due to free turbulence have been examined in the 1980-81 Stanford Conference (Vol. III of Ref. 8, test case 0211). All methods predict much the same values but are low in comparison with experimental data used for assessment. This suggests that the turbulence modelling may not be adequate or the correlation parameters need further adjustment for computations of this complex turbulent flow. Thus better understanding of turbulence field interactions is necessary for further improvement of the computational methods.

### 3.2.3.5 Viscous Flow Computations for Wind Tunnel Tests

The capabilities of the computational methods for viscous flow simulations have been examined in the last section. Because of the requirement of high accuracy in aerodynamics tests, e.g. one count for relative drag (see Section 3.2.2), only computations for fully attached flow can be accepted with confidence at present. For flows with moderate separations, the development of the methods is less complete and the computations can only be considered for estimation of the trend of variations of the flow parameters.

Within the present limitations, the role of computations for flow simulations in a wind tunnel test program is defined in detail in Section 3.2.1 on simulation methodology. When a test program is initiated and the ranges of the test parameters specified, computations are carried out to simulate the flow field within the range of interest. Computational results may include pressure distributions, boundary layer development and drag at Reynolds numbers of the full scale aircraft and of the test model. These serve to define, for example, the positions and heights of transition trips, forward fix position and location of the peak suction near the leading edge and aft fix position for producing proper boundary layer thicknesses at the shock or for relieving near separations. During the test, computations are performed for direct comparison with the test results. Any serious disagreement could indicate viscous effects not allowed in the computations and adjustments of the test conditions such as forward or aft fix positions might be required. Finally, the test data obtained are then converted to the full scale condition in procedures recommended in Section 3.2.1 with computations providing for the difference between values of flow parameters at full scale Reynolds number and at model test conditions. Direct extrapolation of test data to full scale conditions by computations alone must be treated with care and reservation in view of the strict requirement of accuracy.

Since wind tunnel tests always cover a number of parameters over wide ranges, large amounts of computation may be required to generate the required information. Thus the computational efficiency is an important factor for the operation to be practical. For the present generation of computers, the methods based on the interactive theory are most suitable. The inviscid flow field is generated mostly by the full potential code at present. In view of the rapid development of the Euler code, the inviscid computations will soon be replaced by the latter in the near future.



### 3.2.3.6 CONCLUDING REMARKS

In the brief review of the computational capabilities for viscous flows, it has been shown that the methods of solution of the governing equations have been well developed. Turbulence modelling is adequate for simple flows, though further verifications and developments are still needed for complex flows. Interactions of viscous and inviscid flows, which is a basic characteristic of transonic flows are properly formulated and analyzed.

Attached flows can be predicted accurately for a wide range of Reynolds numbers. Flows with moderate separations near the leading or the trailing edges and the shock wave-boundary layer interactions can be treated by the interactive methods. Methods for two-dimensional flows are better developed while three-dimensional and unsteady flow methods are showing rapid progress. In general, computations can be applied to simple configurations or components of a complex configuration.

The interaction of computational simulations with wind tunnel test programs has effectively augmented the capabilities of these tests. The information provided by computations is now essential for design and checking of the test and for interpretation and extrapolation of the results. Due to strict requirement of accuracy in aerodynamic tests, applications of computation are limited, at present, to simulations of attached flows. For complex flow simulations, especially with flow separation, further development is needed in better understanding the physical nature of the flow and its modelling. In view of the rapid progress of computational methods<sup>(8,9)</sup>, these will certainly be achieved in the near future.

### 3.2.2.7 REFERENCES

1. Haines, A.B.  
Holder, D.W.  
Pearcey, H.H.      Scale Effects at High Subsonic and Transonic Speeds and Methods for Fixing Boundary-Layer Transition in Model Experiments.  
British Aeronautical Research Council, R&M 3012, September 1954.
2.      Facilities and Techniques for Aerodynamic Testing at Transonic Speeds and High Reynolds Numbers.  
AGARD CP-83-71, April 1971.
3. Panikhurst, R.C.      Technical Evaluation Report on AGARD Specialist's Meeting on Facilities and Techniques for Aerodynamic Testing at Transonic Speeds and High Reynolds Number.  
AGARD AR-37-71, October 1971.
4.      High Reynolds Number Research — 1980.  
NASA CP-2183, December 1980.
5. Haines, A.B.      Computers and Wind Tunnel: Complementary Aids to Aircraft Design.  
Aeronautical Journal, July 1977, pp. 306-321.
6. Whitfield, J.D.  
Pate S.R.  
Kimzey, W.F.  
Whitfield, D.L.      The Role of Computers in Aerodynamic Testing.  
Computers and Fluids, Vol. 8, 1980, pp. 71-99.
7. Loving, D.L.      Wind Tunnel — Flight Correction of Shock-Induced Separated Flow.  
NASA TN D-3580, 1966.
8. Chapman, D.R.      Computational Aerodynamics Development and Outlook.  
AIAA Journal, Vol. 17, No. 12, December 1979.
9. Kutler, P.      A Perspective of Theoretical and Applied Computational Fluid Dynamics.  
AIAA Journal, Vol. 23, No. 3, March 1985, pp. 328-341.
10. Kline, B.J.  
Cantwell, B.J.  
Lilley, G.M.      1980-81 AFOSR-HTTM-Stanford Conference on Complex Flows.  
Vol. I, II & III, Stanford University, 1981.
11. Marvin, J.G.      Turbulence Modeling for Computational Aerodynamics.  
AIAA Journal, Vol. 21, No. 7, July 1983, pp. 941-955.
12. Melnik, R.E.      Turbulent Interactions on Airfoils at Transonic Speeds — Recent Developments in Computation of Viscous-Inviscid Interactions.  
AGARD CP-291, February 1981.
13. Cebeci, T.  
Stewartson, K.  
Whitelaw, J.H.      Calculation of Two-Dimensional Flow Past Airfoils.  
In Numerical and Physical Aspects of Aerodynamic Flows II, Ed. T. Cebeci, Springer-Verlag, New York, 1984.
14. McDonald, H.  
Bailey, W.R.      A Survey of Recent Work on Interacted Boundary-Layer Theory for Flow with Separation.  
In Numerical and Physical Aspects of Aerodynamic Flows II, Ed. T. Cebeci, Springer-Verlag, New York, 1984.
15. LeBalleur, J.-C.      Numerical Viscous-Inviscid Interaction in Steady and Unsteady Flows.  
In Numerical and Physical Aspects of Aerodynamic Flows II, Ed. T. Cebeci, Springer-Verlag, New York, 1984.
16. Lock, R.C.  
Firmin, M.C.P.      Survey of Techniques for Estimating Viscous Effects in External Aerodynamics.  
In Numerical Methods in Aeronautical Fluid Dynamics, Ed. P.L. Roe, Academic Press, New York, 1982.

17. Lock, R.C. Prediction of the Drag of Wings at Subsonic Speeds by Viscous/Inviscid Interaction Techniques. In Aircraft Drag Prediction and Reduction, AGARD Report 723, 1985.
18. Messiter, A.F. Boundary-Layer Interaction Theory. Transactions of the ASME, Vol. 50, December 1983, pp. 1104-1113.
19. Adamson, T.C. Jr. Analysis of Two-Dimensional Interactions Between Shock Waves and Boundary Layers. In Annual Review of Fluid Mechanics, Vol. 12, 1980.
20. Smith, P.D. The Numerical Computation of Three-Dimensional Boundary Layers. In Three-Dimensional Turbulent Boundary Layers, Ed. H.H. Fernholz and E. Krause, Springer-Verlag, New York, 1982.
21. Smith, P.D. Direct and Inverse Integral Calculation Methods for Three-Dimensional Turbulent Boundary Layers. Aeronautical Journal, May 1984, pp. 155-159.
22. Cebeci, T. Problems and Opportunities with Three-Dimensional Boundary Layers. AGARD R-719, May 1984.
23. Mehta, U. Reynolds Averaged Navier-Stokes Computations of Transonic Flows — The State of the Art. In Transonic Aerodynamics, Ed. D. Nixon, AIAA, 1982.
24. Mellor, G.L. The Large Reynolds Number Asymptotic Theory of Turbulent Boundary Layers. International Journal of Engineering Sciences, Vol. 10, 1972, pp. 851-873.
25. Goldberg, U. Scaling and Modeling of Three-Dimensional Pressure-Driven Turbulent Boundary Layers. AIAA 83-1695, July 1983.
26. Khan, M.M.S. New Considerations on Scale Extrapolation of Wing Pressure Distributions Affected by Transonic Shock-Induced Separation. NACA CR-166426, March 1983.
27. Blackwell, J.A. Jr. Preliminary Study of Effects of Reynolds Number and Boundary-Layer Transition Location on Shock-Induced Separation. NASA TN D-5003, January 1969.
28. Haines, A.B. Further Evidence and Thoughts on Scale Effects at High Subsonic Speeds. AGARD CP-174, Wind Tunnel Design and Testing Techniques, 1974.
29. Stanewsky, E. Interaction Between the Outer Inviscid Flow and the Boundary Layer on Transonic Airfoils. Zeitschrift für Flugwissenschaften und Weltraumforschung, Vol. 7, No. 4, July-August 1983, pp. 242-252.
30. Green, J.E. Prediction of Turbulent Boundary Layers and Wakes in Compressible Flow by a Lag-Entrainment Method. Weeks, D.G. British Aeronautical Research Council R&M No. 3791, 1973.
31. Rubin, S.G. A review of Marching Procedures for Parabolized Navier-Stokes Equations. In Numerical and Physical Aspects of Aerodynamic Flows, Ed. T. Cebeci, Springer-Verlag, New York, 1982.
32. Williams, J.C. III Incompressible Boundary-Layer Separation. In Annual Review of Fluid Mechanics, Vol. 9, 1977.
33. Topak, M. Topology of Three-Dimensional Separated Flows. Peake, D.J. Annual Review Fluid Mechanics, Vol. 14, 1982.
34. Horstman, C.C. An Evaluation of Several Compressible Turbulent Boundary Layer Models: Effects of Pressure Gradient and Reynolds Number. Kussoy, M.I. AIAA Paper 78-1160, 1978.
35. South, J.C. Report of the Panel on Theoretical Aerodynamics. Thames, F.C. In High Reynolds Number Research — 1980, NASA CP-2183, December 1980.
36. Gleyzes, C. A Calculation Method of Leading-Edge Separation Bubbles. Cousteix, J. In Numerical and Physical Aspects of Aerodynamic Flows II, Ed. T. Cebeci, Springer-Verlag, New York, 1984.
37. Davis, R.L. Analysis of Transitional Separation Bubble on Infinite Swept Wings. Carter, J.E. AIAA-85-1685, July 1985.
38. Reshotko, E. Experiments Planned Specifically for Developing Turbulence Models in Computations of Flow Fields Around Aerodynamic Shapes. Marvin, J.G. In Numerical Methods and Wind Tunnel Testing, AGARD CP-210, June 1976.
39. LeBalleur, J.-C. Numerical Studies in High Reynolds Number Aerodynamics. Peyret, R. Computers and Fluids, Vol. 8, 1980, pp. 1-30.
40. Viviand, H. Advances and Opportunities in Transonic-Flow Computations. Ballhaus, W.F. Jr. In Numerical and Physical Aspects of Aerodynamic Flows, Ed. T. Cebeci, Springer-Verlag, New York, 1982.
41. Deiwert, G.S. In Numerical and Physical Aspects of Aerodynamic Flows, Ed. T. Cebeci, Springer-Verlag, New York, 1982.
42. Goorjian, P.M. In Numerical and Physical Aspects of Aerodynamic Flows, Ed. T. Cebeci, Springer-Verlag, New York, 1982.
43. Holst, T.L. In Numerical and Physical Aspects of Aerodynamic Flows, Ed. T. Cebeci, Springer-Verlag, New York, 1982.
44. Kutler, P. In Numerical and Physical Aspects of Aerodynamic Flows, Ed. T. Cebeci, Springer-Verlag, New York, 1982.

41. Horstman, C.C.

Numerical Simulation of Turbulent Trailing Edge Flows.  
In Numerical and Physical Aspects of Aerodynamic Flows II, Ed. T. Cebeci, Springer-Verlag, New York, 1980.

42. Johnson, D.A.  
King, L.S.

A Mathematically Simple Turbulence Closure Model for Attached and Separated Turbulent Boundary Layers.  
AIAA Journal, Vol. 23, No. 11, November 1985, pp. 1684-1692.

43. Whitfield, D.L.  
Swaffort, T.W.  
Jacocks, J.L.

Calculation of Turbulent Boundary Layers with Separation and Viscous-Inviscid Interaction.  
AIAA Journal, Vol. 19, No. 10, October 1981, pp. 1315-1322.

44. Stanewsky, E.  
Nandan, M.  
Inger, G.R.

The Coupling of Shock Boundary Layer Interaction Module with a Viscous-Inviscid Computation Method.  
In Computation of Viscous-Inviscid Interaction, AGARD CP-291, 1981.

45. Van den Berg, B.  
Elsenaar, A.

Measurement in a Three-Dimensional Incompressible Turbulent Boundary Layer in an Adverse Pressure Gradient Under Infinite Swept Wing Conditions.  
National Aerospace Laboratory, Netherlands, TR 72092U, 1972.

46. Cousteix, J.  
Houdeville, R.

Singularities in Three-Dimensional Turbulent Boundary-Layer Calculations and Separation Phenomena.  
AIAA Journal, Vol. 19, No. 8, August 1981, pp. 976-985.

47. Hirschel, E.H.

Three-Dimensional Boundary-Layer Calculations in Design Aerodynamics.  
In Three-Dimensional Turbulent Boundary Layers, Ed. H.H. Fernholz and E. Krause, Springer-Verlag, New York, 1982.

48. Arnal, D.  
Cousteix, J.

Numerical Study of Corner Flows.  
In Three-Dimensional Turbulent Boundary Layers, Ed. H.H. Fernholz and E. Frause, Springer-Verlag, New York, 1982.

49. Fujii, K.  
Jutler, P.

Numerical Simulation of the Viscous Flow Fields Over Three-Dimensional Complicated Geometries.  
AIAA Paper 84-1550, June 1984.

50. Cousteix, J.  
Houdeville, R.  
Javelle, J.

Méthodes de calcul des couches limites instationnaires.  
In Boundary Layer Effects on Unsteady Airloads, AGARD CP-296, 1981.

51. Telionis, D.P.

Unsteady Viscous Flows.  
Springer-Verlag, New York, 1981.

52. Houwink, R.

Unsteady Viscous Transonic Flow Computations Using the LTRAN2-NLR Code Coupled with Green's Lag-Entrainment Method.  
In Numerical and Physical Aspects of Aerodynamic Flows II, Ed. T. Cebeci, Springer-Verlag, New York, 1984.

53. Rizzetta, D.P.  
Yoshihara, H.

Oscillating Supercritical Airfoils in the Transonic Regime with Viscous Interactions.  
In Boundary Layer Effect on Unsteady Airloads, AGARD CP-296, 1981.

54. Timme, A.

Effects of Turbulence and Noise on Wind-Tunnel Measurements at Transonic Speeds.  
In Fluid Motion Problems in Wind Tunnel Design, AGARD R-602, April 1973.

55. Green, J.E.

On the Influence of Free Stream Turbulence on a Turbulent Boundary Layer. As it Related to Wind Tunnel Testing at Subsonic Speeds.  
In Fluid Motion Problems in Wind Tunnel Design, AGARD R-602, April 1973.

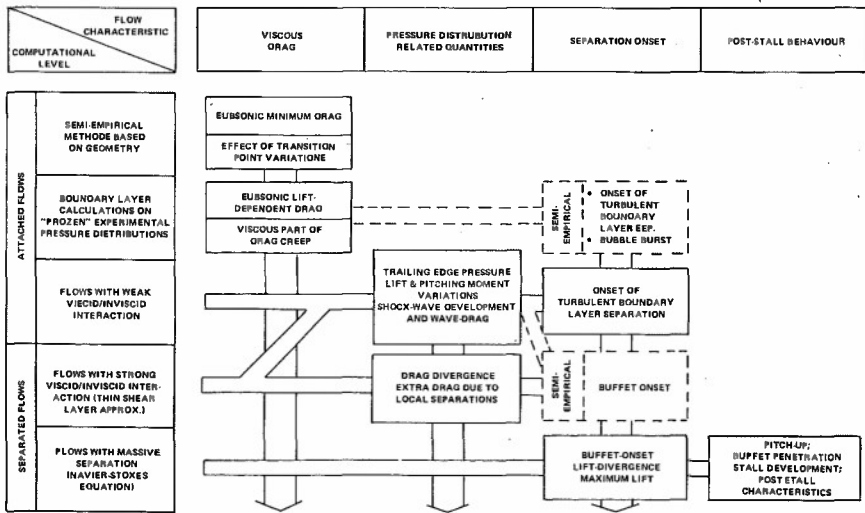


FIG. 1: HIERARCHY OF COMPUTATIONAL METHODS FOR TRANSONIC VISCOUS FLOW SIMULATIONS

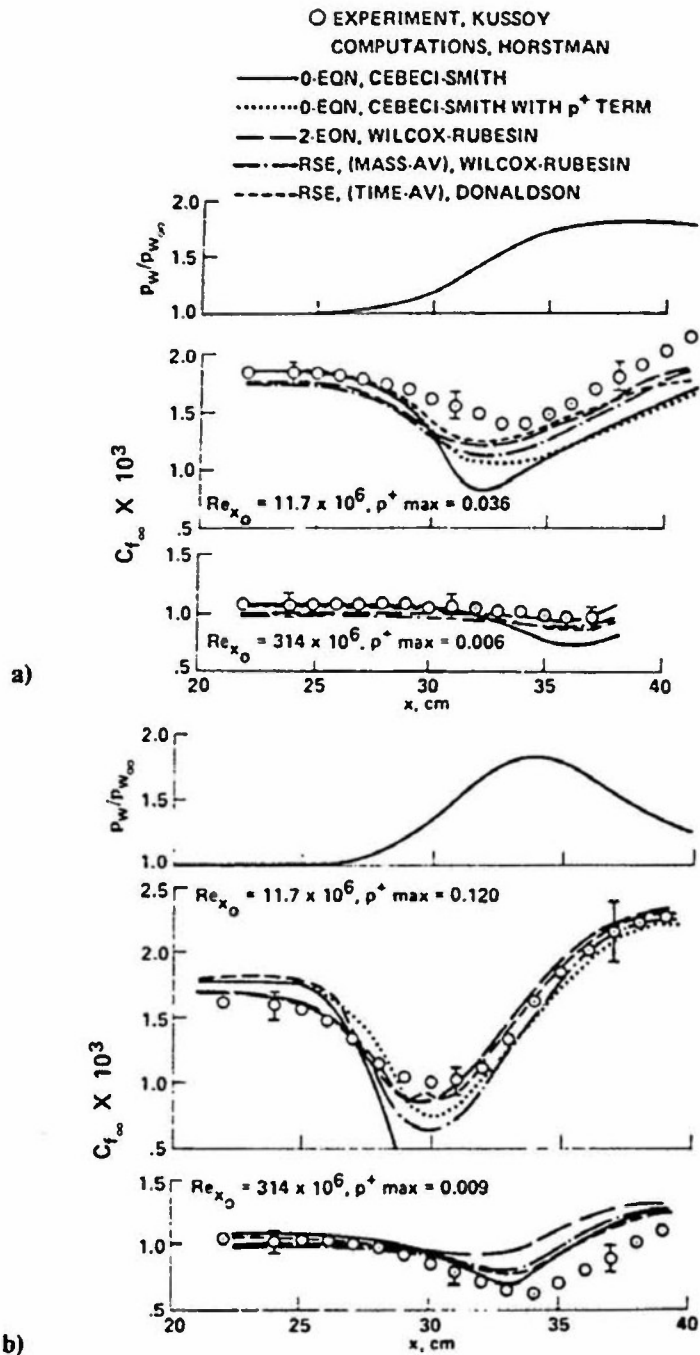
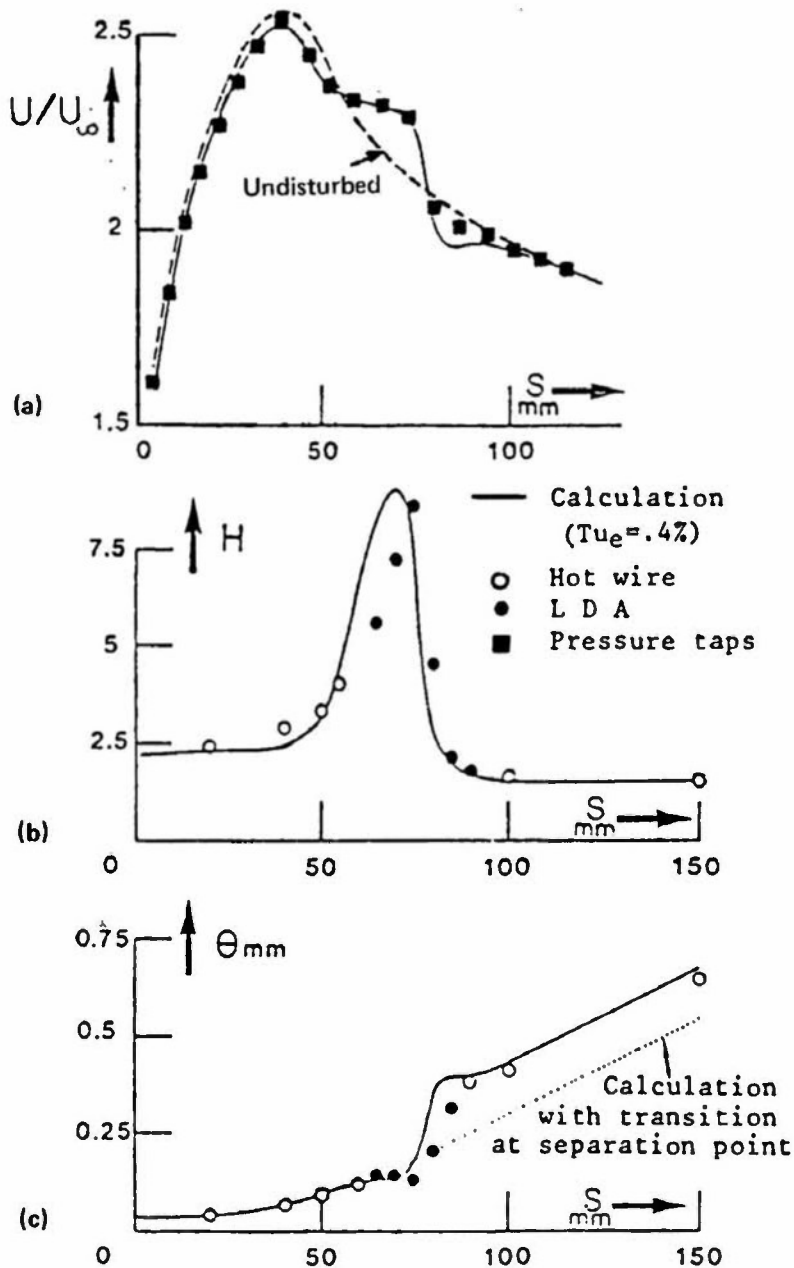


FIG. 2: COMPUTATIONS OF SKIN FRICTION FROM COMPRESSIBLE TURBULENT BOUNDARY LAYER CODES WITH DIFFERENT TURBULENCE MODELS AT HIGH AND MODERATE REYNOLDS NUMBERS,  $M_\infty = 2.3$ , (a) ADVERSE PRESSURE GRADIENT FOLLOWED BY RELAXATION; AND (b) ADVERSE PRESSURE GRADIENT FOLLOWED BY A FAVOURABLE ONE. (REPRINTED FROM REFERENCE 11)



**FIG. 3: COMPUTATIONS OF SEPARATION BUBBLE WITH AN INVERSE METHOD ON ONERA LC100D AIRFOIL AT  $Re_c = 2.2 \times 10^6$ , TURBULENCE INTENSITY = 0.4%, (a) VELOCITY DISTRIBUTION; (b) FORM FACTOR VARIATIONS; (c) MOMENTUM THICKNESS VARIATIONS; EXPERIMENTAL DATA FROM THE AUTHORS. (REPRINTED FROM REFERENCE 36)**

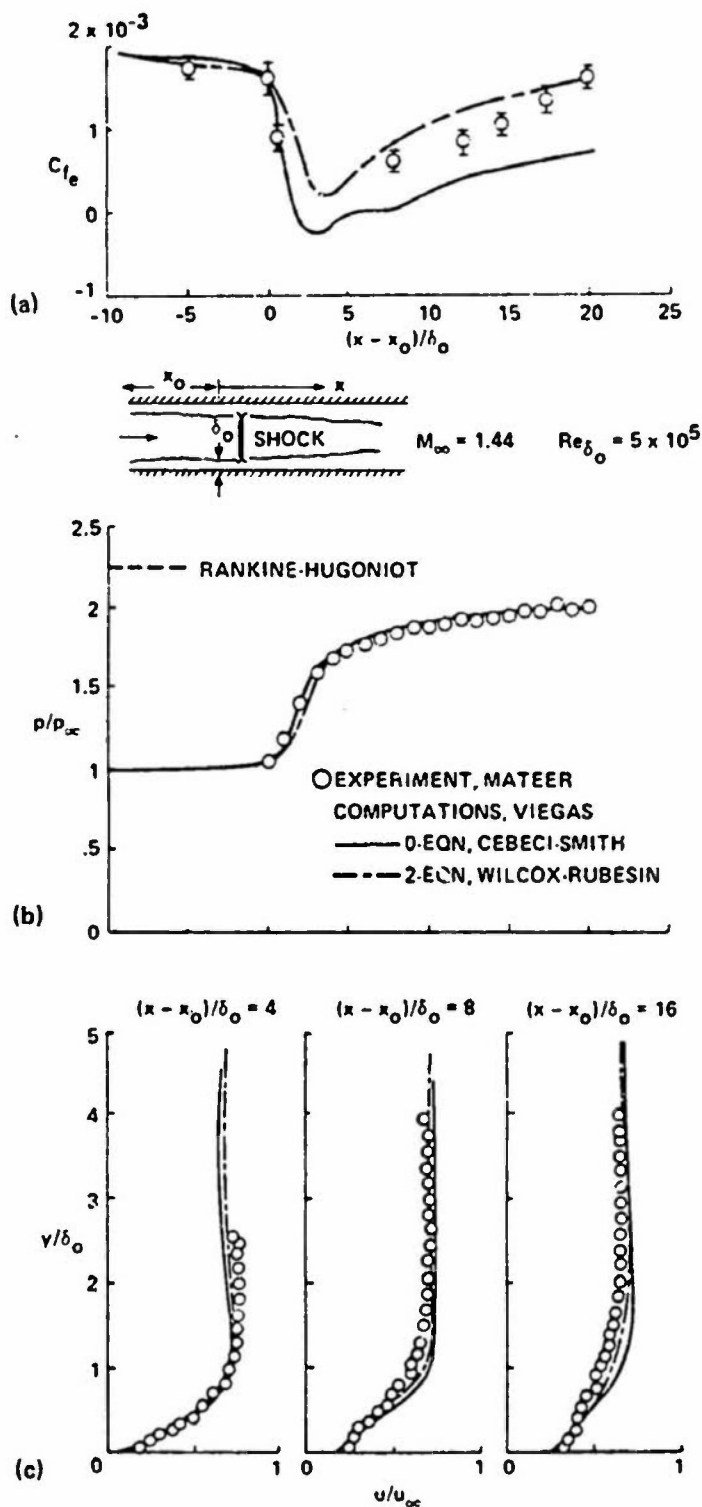


FIG. 4: COMPUTATIONS OF TRANSONIC NORMAL SHOCK WAVE-BOUNDARY LAYER INTERACTION AT  $M_\infty = 1.44$ ,  $Re_{x_0} = 37 \times 10^6$ , (a) WALL PRESSURE; (b) SKIN FRICTION; (c) VELOCITY PROFILES. (REPRINTED FROM REFERENCE 11)

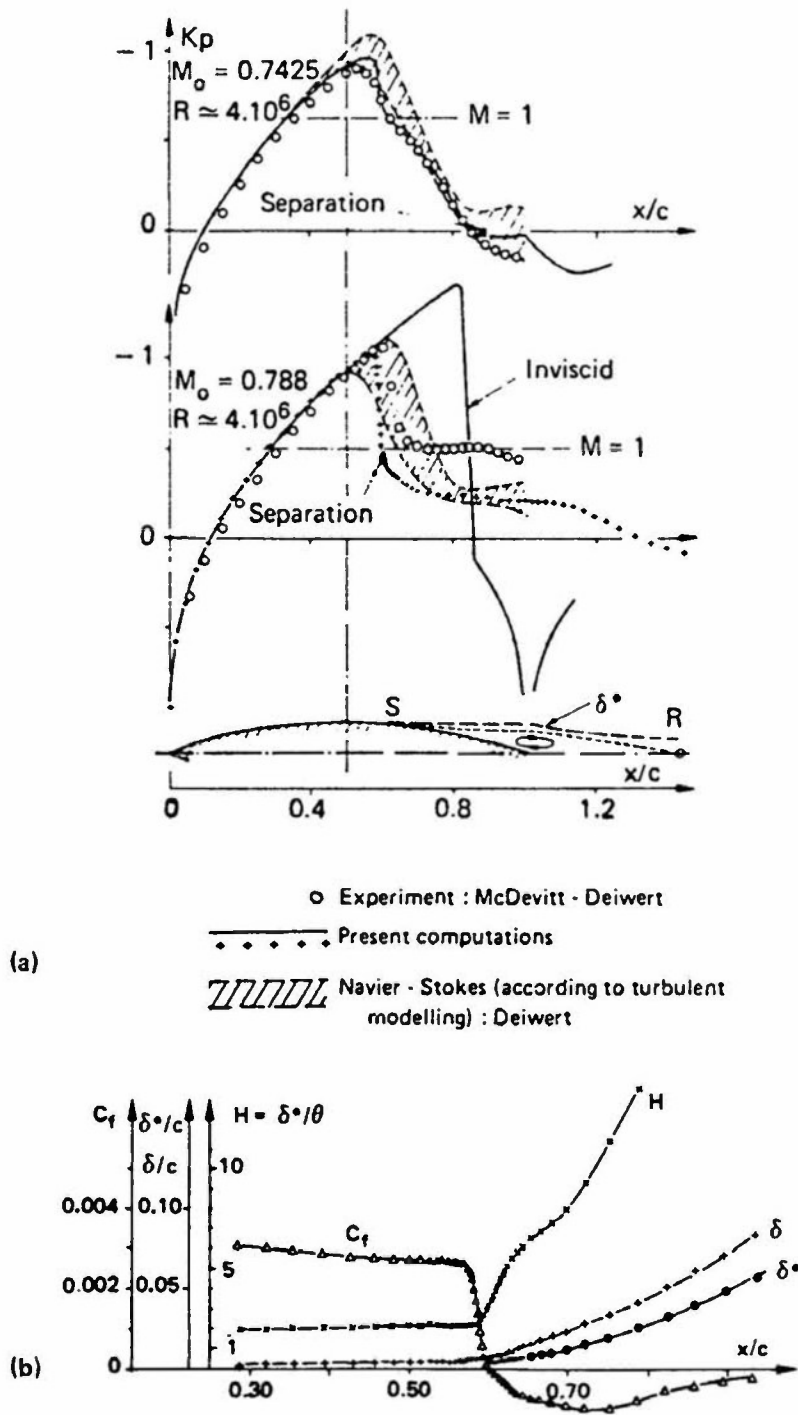


FIG. 5: COMPUTATIONS OF SHOCK WAVE-BOUNDARY LAYER INTERACTION ON AN 18% CIRCULAR ARC SYMMETRICAL AIRFOIL AT  $Re \simeq 4 \times 10^6$ , (a) PRESSURE DISTRIBUTIONS AT  $M_\infty = 0.7245$  AND  $0.788$  RESPECTIVELY; (b) VARIATIONS OF BOUNDARY LAYER PROPERTIES FOR  $M_\infty = 0.788$ . (REPRINTED FROM REFERENCE 39)

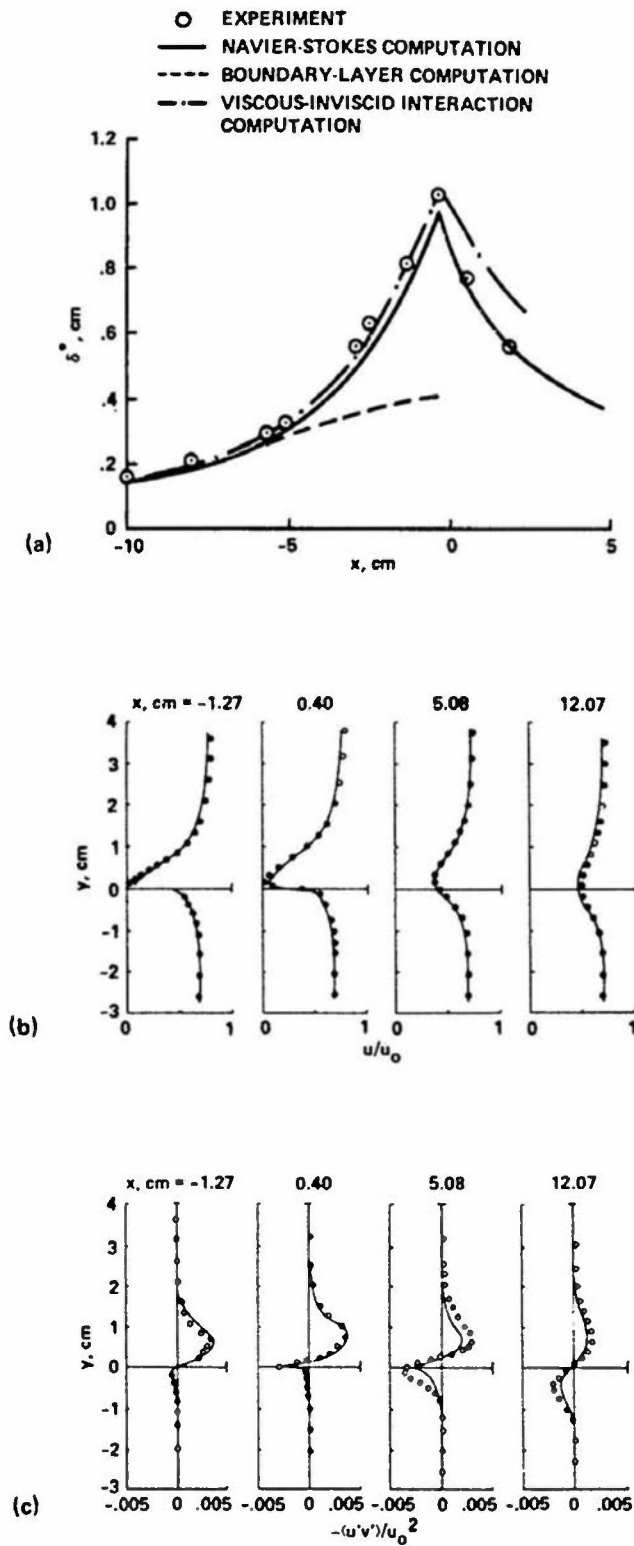


FIG. 6: COMPUTATIONS OF TRAILING EDGE FLOW ON AN UPPER REAR QUADRANT OF AN 18% CIRCULAR ARC AIRFOIL AT  $M_\infty = 0.7$ ,  $Re = 4 \times 10^7/m$ , (a) DISPLACEMENT THICKNESS DISTRIBUTION; (b) MEAN VELOCITY PROFILES; (c) TURBULENT SHEAR-STRESS PROFILES. (REPRINTED FROM REFERENCE 41)



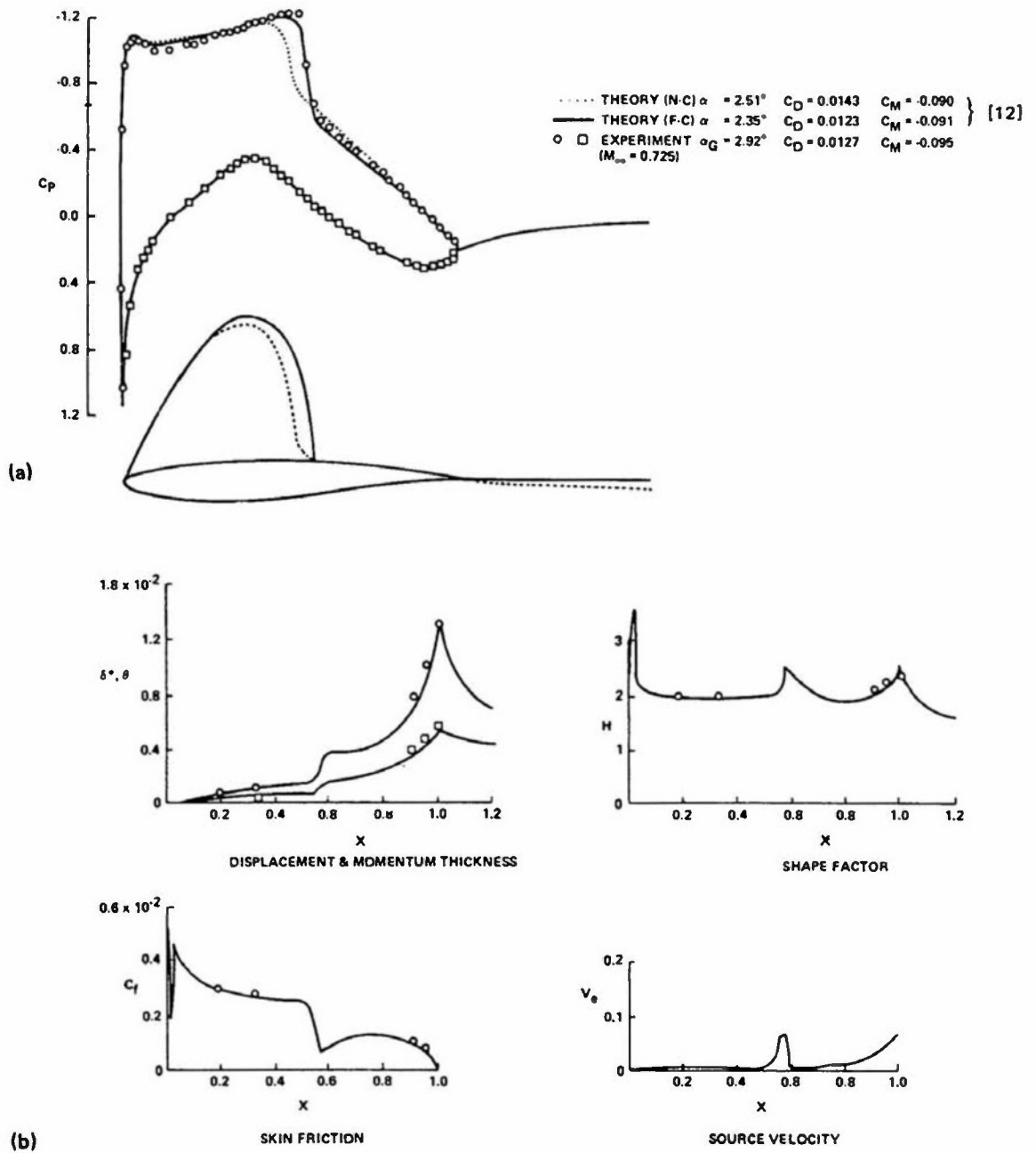


FIG. 7: COMPUTATIONS OF FLOWS OVER RAE 2822 AIRFOIL AT  $M_\infty = 0.728$ ,  $C_L = 0.743$ ,  $Re = 6.5 \times 10^6$ , (a) PRESSURE DISTRIBUTION ( $X_T = 0.03$ ); (b) BOUNDARY LAYER DEVELOPMENTS ( $X_T = 0.11$ ). (REPRINTED FROM REFERENCE 12)

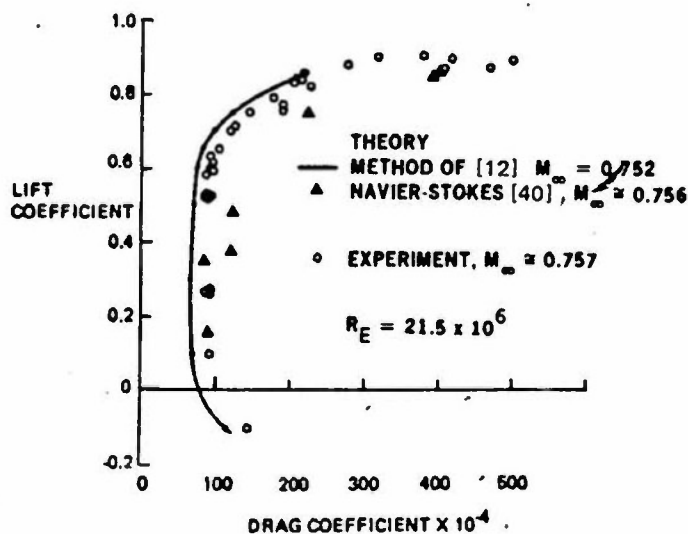
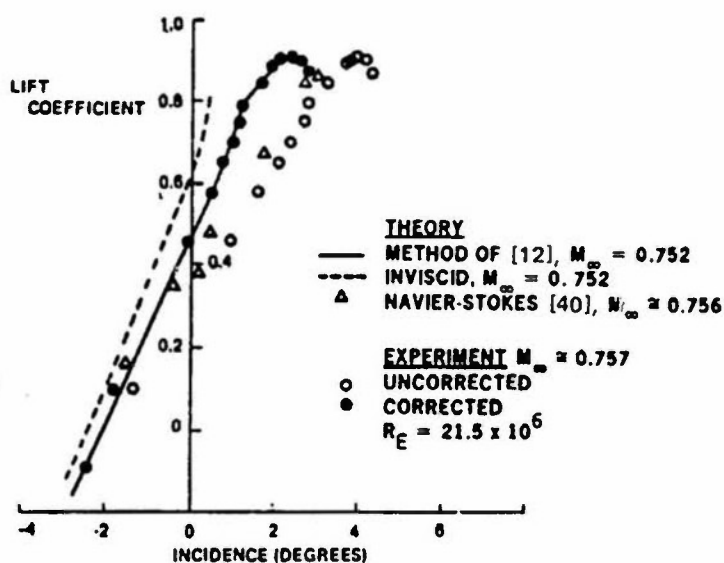


FIG. 8: LIFT CURVE AND DRAG POLAR FOR G&K 75-06-12 AIRFOIL AT  $Re_c = 21.5 \times 10^6$  (REPRINTED FROM REFERENCE 13)

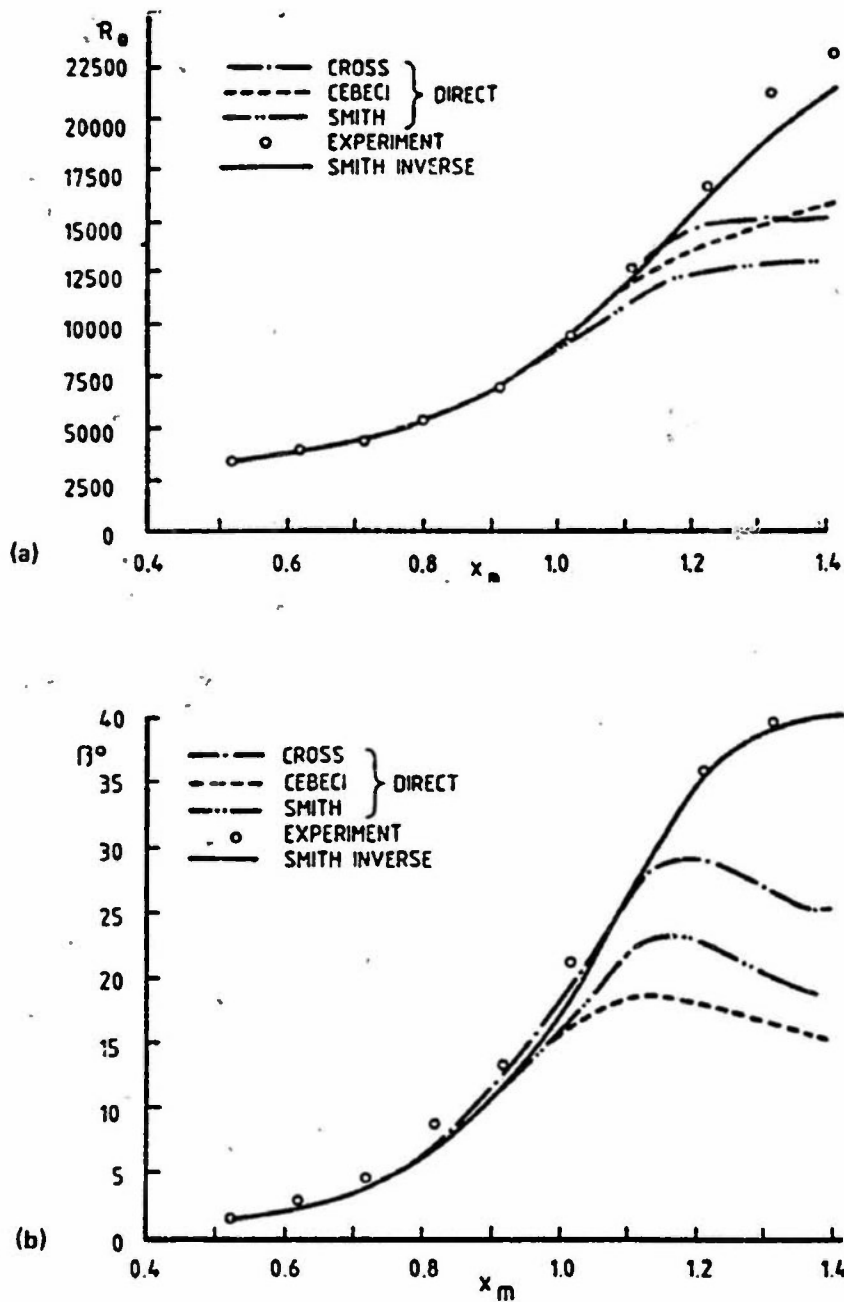


FIG. 9: COMPUTATIONS OF THREE-DIMENSIONAL BOUNDARY LAYER FLOW ON AN INFINITE SWEEPED PLATE WITH ADVERSE PRESSURE GRADIENT, (a) MOMENTUM THICKNESS; (b) LIMITING STREAMLINE ANGLE. (REPRINTED FROM REFERENCE 21)

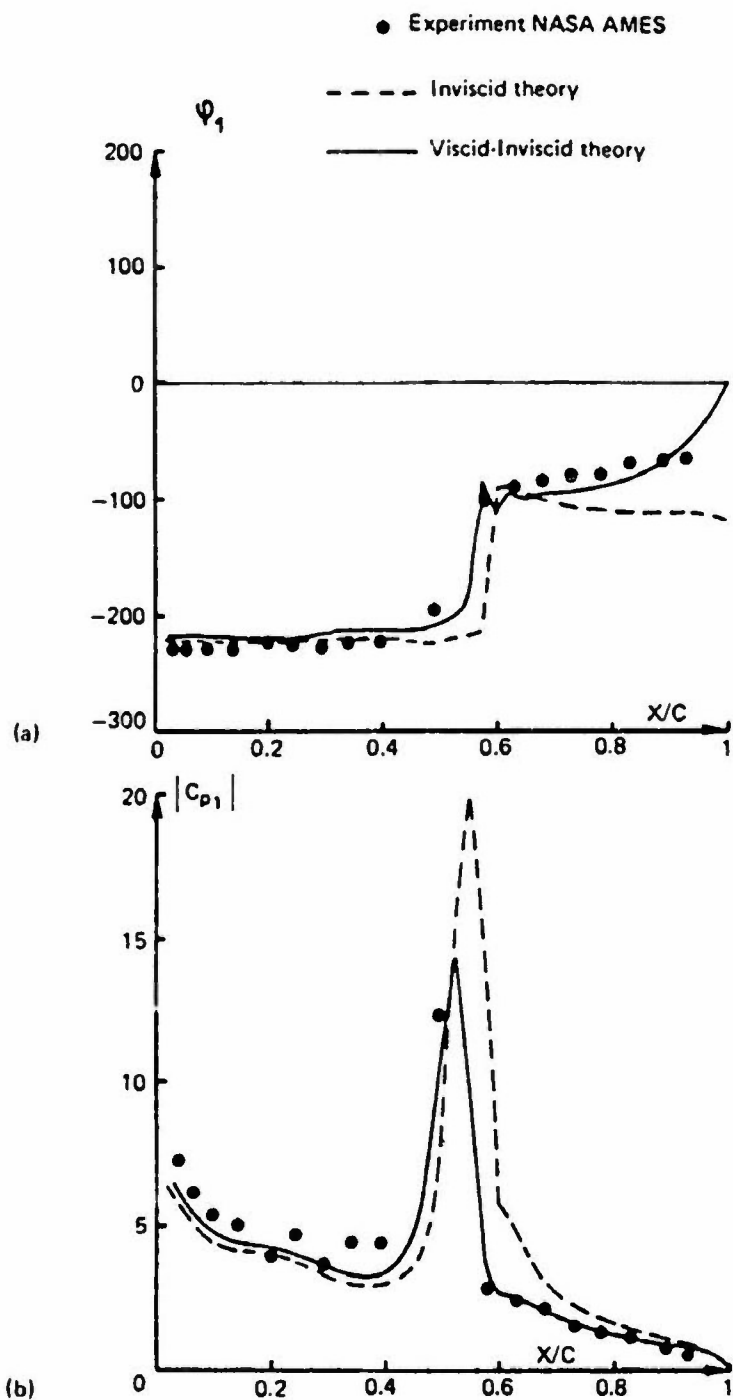


FIG. 10: COMPUTATIONS OF UNSTEADY FLOWS OVER NACA 64A010 AIRFOIL, FIRST HARMONIC, PITCH OSCILLATIONS AT  $M_\infty = 0.8$ ,  $\alpha = 0^\circ$ ,  $Re = 12 \times 10^6$ ,  $k = 0.40$ , (a) PHASE ANGLE; (b) MAGNITUDE OF UNSTEADY PRESSURE DISTRIBUTIONS. (REPRINTED FROM REFERENCE 15)

## SECTION 3.2.4 EMPIRICAL TOOLS FOR SIMULATION METHODOLOGIES

by

A.Elsenaar  
National Aerospace Laboratory (NLR)  
Anthony Fokkerweg 2  
1059 CM Amsterdam, The Netherlands

and

A.B.Haines  
Chief Executive  
Aircraft Research Association Ltd  
Manton Lane, Bedford MK41 8PA, UK

### LIST OF SYMBOLS

$c$	local airfoil chord
$c_f$	local skin-friction coefficient
$C_L$	lift-coefficient
$C_D$	drag-coefficient
$C_{DW}$	wave drag contribution to total drag-coefficient
$H_{11}$	local incompressible shape factor in streamwise direction
$L$	typical length scale, defined in text
$M_\infty$	free-stream Mach number
$M_1$	Mach number ahead of shock
$n$	amplification factor in linear stability theory
$p$	local static pressure
$R$	Reynolds number (subscript refers to local conditions)
$T_u$	turbulence level of the wind tunnel
$U_e$	local free-stream velocity
$u_\tau$	skin-friction velocity
$x$	distance along airfoil chord in streamwise direction
$\delta_1^*$	boundary layer displacement thickness in stream-wise direction
$\delta_2$	boundary layer displacement thickness in cross-wise direction
$\bar{\Lambda}$	average value of Pohlhausen parameter $\frac{\theta^2}{\nu} \cdot \frac{dU_e}{dx}$
$\theta$	boundary layer momentum thickness
$\nu$	kinematic viscosity
$TE$	subscript, refers to trailing edge conditions
$AL$	subscript, refers to attachment line conditions
	subscript, refers to onset of instability
$T$	subscript, refers to transition location

### INTRODUCTION

For the application of a simulation/extrapolation methodology a detailed understanding of the relevant viscous effects is essential. Prior to the actual wind tunnel tests theoretical calculations, using some of the methods as described in section 3.2.3, will be made. When during the actual wind tunnel tests experimental results become available, a major part of the analysis will also be based on a comparison of theory and experiment. Additionally, theory can be applied using experimental data (e.g. pressure distributions, transition locations) as input values. As outlined in section 3.2.1 different levels of sophistication are possible here. The required level of sophistication will depend on the complexity of the problem, the availability of additional information and the available time or other resources. However, as discussed in section 3.2.3 even the most sophisticated computational methods today cannot describe all aspects of the flow development. This is particularly true for details of the flow development that involve boundary layer transition and/or separation.

For that reason this section attempts to describe the "empirical tools" that can be used to supplement the theoretical calculations or the experimental information. Most of these "empirical tools" are taken directly from chapter 4. For the convenience of the user, they are presented in an operational way by distinguishing between "input", "supporting calculations" and "method(s)". In each case only the principle of the method is briefly indicated; for details, one must refer to chapter 4, where the methods are described in more depth.

Also, in many cases, alternative relations can and will be used depending on existing practice and experience of a particular design team. Where possible, in addition to a "simple method" a more sophisticated method has been specified (indicated between []). In some cases the more sophisticated method is almost identical to a complete numerical simulation. In that respect the present set of "empirical tools" is open-ended. On the one hand, new experimental information will become available in the future to refine or extend the "empirical tools" as used at present. On the other hand, the ever increasing sophistication in flow modelling through computational methods will eventually supersede most empiricism.

TOPIC 1: TRANSITION PREDICTION

## INPUT

- . measured or calculated pressure distributions
- . Reynolds number (tunnel, flight)
- . leading edge geometry and wing planform
- . turbulence level of wind tunnel ( $T_u$ )
- . measure of surface roughness

## SUPPORTING CALCULATIONS

- . 2D or quasi 3D boundary layer calculations
- . [full 3D boundary layer calculations, the choice depending on the configuration and test aims]

## METHOD(S)

- . In sections 4.3.3.1.2 and 4.3.3.2.2, simple criteria are specified for the prediction of transition due to
  - leading edge contamination  
eg  $R_{\theta,AL} > 100$  where  $R_{\theta,AL}$  is the Reynolds number based on the momentum thickness of the boundary layer along the leading edge attachment line.
  - Tollmien-Schlichting streamwise instability  
eg  $R_{\theta T} - R_{\theta S} > f(\Lambda, T_u)$   
where  $R_{\theta S}$  is the momentum thickness Reynolds number for neutral stability and  $\bar{\Lambda}$  is a mean value of the Pohlhausen parameter, averaged over the length from  $x_0$  to  $x_T$ , this parameter being a function of the streamwise pressure gradient and the momentum thickness (see figure 7 in 4.3). This approach is effectively an extension by ONERA/CERT (Michel et al, ref.1) of the wellknown Granville criterion in order to allow for the effects of tunnel stream turbulence.
  - cross-flow (CF) instability  
eg  $R_{\delta 2T} > \phi(H_{11}, T_u)$   
where  $\delta_2$  is the displacement thickness of the cross-flow profile of the boundary layer.

The application of these criteria for flight and tunnel Reynolds numbers will yield graphs similar to Figure 18 of section 4.3. Use of the criteria merely requires output from integral boundary layer calculations.

The reader is referred to section 3.3.3 for the prediction of the various types of transition in the special case of elongated bodies at incidence.

- . [Sophisticated: stability calculations based on calculated boundary layer profiles from finite difference calculations will provide amplification factors for both Tollmien-Schlichting (TS), Cross-flow (CF) and Görtler instabilities. If they exceed a certain level  $n = f(T_u)$ , it is assumed that transition will occur.  
eg  $n_T = -8.43 - 2.4 \ln T_u$  (section 4.3.3.1.2)  
as proposed by Mack (ref.2), v. Ingen (ref.3) and Michel et al. (ref.1) on the basis of flat-plate data.  
This relation has not yet been fully validated for general use but it appears to predict the general trends even when pressure gradients are present. In making predictions of transition position in flight, it should be satisfactory to take  $n = 9$  as a standard value.  
There is some evidence that there can be an interaction between the TS and CF instabilities but further research is needed to establish a proven relation for this effect (see, for example ref. 4 and 5).  
Compressibility is not thought to have a large effect on the critical values of  $n$  but it is most important that the calculations for the TS instability should be made using compressible stability theory].

A word of warning is needed at this point. The criteria/methods given above suggest that the position of transition depends solely on the shape of the surface, the pressure distribution over the surface and the turbulence intensity. Effects due to tunnel noise, known to have some influence, are not represented. Moreover, in some experiments a correlation is observed between transition location and the tunnel unit Reynolds number as discussed in detail in section 3.3.3. This correlation has not yet been explained satisfactorily in terms of physical meaningful parameters. Depending on further studies, changes to the predictions methods may be needed.

- . Additionally, the likelihood of relaminarisation can be estimated from a criterion based on

$$\frac{v}{U_e} \frac{dU_e}{dx} \text{ or } \frac{v}{\rho U_e^3} \frac{dp}{dx}$$

(Launder & Jones, ref.6; Patel & Head, ref.7)

- . Transition can also occur in a laminar separation bubble (see TOPIC 2). Its precise location (only relevant for detailed calculations) can also be calculated by means of an amplification method (see v. Ingen, section 4.6).

TOPIC 2: SEPARATION IN LEADING EDGE REGION

## INPUT

- . calculated pressure distributions
- . Reynolds number (tunnel, flight)
- . leading edge geometry and wing planform
- . transition locations (TOPIC 1)

## SUPPORTING CALCULATIONS

- . 2D or quasi 3D boundary layer calculations
- . [coupled viscous-inviscid strong interaction methods]

## METHOD(S)

The problem is very similar to the prediction of maximum lift at low speed. Some phenomena that can be observed in the leading edge region are

- . laminar separation  
to be estimated from boundary layer calculations based on inviscid pressure distributions.
- . bubble bursting  
(eg Horton (ref.8); see also v. Ingen, section 4.6.3)  
[More refined methods require calculations based on viscous-inviscid strong interaction with an empirical transition location; see TOPIC 1 and also v. Ingen, section 4.6.2 and 4.6.3].
- . turbulent boundary layer separation  
A method for the prediction of turbulent boundary layer separation is required for conditions where  
(a) transition occurs as a result of contamination along the wing leading edge attachment line, or  
(b) the flow reattaches downstream of a laminar separation bubble.  
Separation can possibly be estimated by finding whether  $C_p$  approaches zero in a turbulent boundary layer calculation using the inviscid pressure distribution as input. Use of a measured experimental pressure distribution can lead to misleading results because of the 'pressure relief' in the pressure distribution approaching separation; see section 4.6.6. Prediction is particularly difficult for cases where a laminar separation bubble is present because of uncertainties in the boundary layer characteristics at reattachment, see section 4.6.4.
- . shock-induced leading edge separation.  
When the velocities in the leading edge region (and perpendicular to isobars) are locally supersonic, a very complex interaction between the (possibly laminar) boundary layer and shock can be present. This type of flow is not well understood at present.

Some investigations have suggested that a particular value of maximum local Mach number could serve as a suitable criterion but this approach cannot be recommended in view of the fact that for different types of geometry, maximum values ranging from 0.8 to 1.8 have been observed. The fact that this range can extend as low as 0.8 is proof in itself that a maximum local Mach number is not a satisfactory criterion. Research is needed to establish a better criterion which must take account of the severity of the adverse pressure gradient aft of the peak velocity.

TOPIC 3: SHOCK WAVE BOUNDARY LAYER INTERACTION

## INPUT

- . measured and/or calculated (3D) pressure distributions
- . Reynolds number
- . wing geometry
- . upstream boundary layer development (TOPICS 1 and 2)

## SUPPORTING CALCULATIONS

- . 2D or (quasi) 3D boundary layer calculations
- . [coupled viscous-inviscid (strong) interactions methods]

## METHOD(S)

- Completely attached flow  
Conventional turbulent boundary layer calculations can be used to estimate the boundary layer development underneath the shock but the calculations can be refined by revising the discontinuous pressure rise (inviscid) at the shock by a pressure gradient defined by the upstream interaction or influence length,  $L_{upstream}$ , given by a relation of the form

$$L_{upstream} / c = \text{constant} \times \delta_1^* / c \times (H_{11} - 1)$$

(Stanewsky, section 4.5.3.)

where  $\delta_1^*$  and  $H_{11}$  are the boundary layer displacement thickness and incompressible shape factor immediately upstream of the interaction zone.

Fig. 17 of section 4.5 suggests that 67 is an appropriate value for the constant in the above relation.

It follows that manipulation of the boundary layer to give the same value of  $\delta_1^* / c \times (H_{11} - 1)$  in the model tests as under full scale conditions would yield full simulation as regards the upstream influence.

## (h) Shock-induced incipient separation

Research has shown that the onset of incipient separation is only weakly dependent on viscous effects.

Fig. 27 of section 4.5 presents this dependence in the form of a graph of shock-upstream Mach number,  $M_1$ , for incipient separation as a function of  $H_{11}$ . It is thought that this relation will apply for swept shock waves up to angles of sweep of at least  $30^\circ$  provided  $M_1$  is always taken as the local Mach number component normal to the shock front.

## (c) Growth of shock-induced separation bubble

Various methods, based on correlations of experimental data, exist for prediction of the length,  $L_{sep}$ , of a shock-induced separation bubble.

Notable amongst these are

- (i) Fuiker & Ashill's correlation (ref.9) in the form

$$L_{sep}/\theta_1 = f(M_1, R/\theta_1)$$

where  $\theta_1$  = boundary layer momentum thickness immediately upstream of the shock interaction zone.

- (ii) Stanewsky's correlation (section 4.5) in the form

$$L_{sep}/\delta_1^* = f(M_1, \delta^*/R)$$

With  $R$  the average upper surface contour radius between shock and trailing edge.

Note: the conditions of the turbulent boundary layer at reattachment are very uncertain (see the discussion by Stanewsky in section 4.5.5). Additional empirical information is required for the accurate prediction of the boundary layer further downstream. Sufficient experience has not yet been gained in the use of the above relations to know whether, in general, they lead to significantly different predictions or whether their use is completely inconsistent with the use of  $\delta_1^*/c \times (H_{11}-1)$  parameter. Clearly there is no a priori reason why all these approaches should be compatible. In the methodologies described in §§ 3.2.1, 3.3.1 and 3.3.2, the emphasis is placed on the Fuiker-Ashill approach, largely because this offers a means of also predicting when the shock-induced separation bubble suddenly extends to the trailing edge, see (d) below. It is not clear at present whether the relations for  $L_{sep}$  continue to apply when a rear separation as well as a shock-induced separation bubble is present: existing evidence suggests that this is true in many but not in all cases.

[A more sophisticated approach would require a (local) application of the Navier-Stokes equations or a coupled viscous-inviscid strong interaction method. In both cases, considerable uncertainty is introduced by the difficulty in choosing an appropriate turbulence model.]

## (d) Extension of shock-induced separation bubble to the trailing edge.

Prediction of the complete flow breakdown from the shock to the trailing edge is an important aspect of the simulation scenario: this condition is a guide to buffet-onset. For values of  $M_1 < 1.4$ , Fuiker & Ashill's correlation suggests that flow breakdown occurs when the shock-induced separation bubble has extended to a point, 'R', denoting the start of the relatively rapid pressure rise ahead of the trailing edge. At higher values of  $M_1$ , they suggest that flow breakdown occurs when reattachment behind the bubble is predicted to occur at a point upstream of 'R' and they provide a method for predicting the distance ahead (see Fuiker & Ashill, ref.9). This empirical method has only been validated to date for a particular class of pressure distributions and for conditions where the sweepback of the shock front is not greater than about  $25^\circ$ . Further refinement of the method will probably be required to widen its range of applicability.

[Calculation methods based on viscous-inviscid strong interaction approach or on the Navier-Stokes equations contain in principle all elements for a proper treatment but application of these methods is at present limited to 2D flow and even then, the accuracy of the results depends on the accuracy of the turbulence model in the separated region of the flow.]

#### TOPIC 4: TURBULENT TRAILING EDGE SEPARATION

##### INPUT

- . either measured or calculated pressure distributions
- . Reynolds number
- . wing geometry
- . the upstream boundary layer development (TOPICS 1 to 3)

##### SUPPORTING CALCULATIONS

- . 2D or (quasi) 3D boundary layer calculations
- . [NS or coupled viscous-inviscid strong interaction methods]

##### METHOD(S)

The prediction of trailing edge separation is a complex problem that has not yet been solved satisfactorily. The present state-of-the-art is discussed by van Ingen in sections 4.6.5 to 4.6.7 and it appears that there are a number of empirical approaches to prediction which become progressively more difficult and uncertain as one increases incidence and/or Mach number to conditions where first, the flow becomes supercritical and then, the shock wave becomes strong enough to induce a separation bubble. Extension of this bubble to the trailing edge has been discussed above under topic 3(d); the present paragraph is concerned with the prediction of a separation of the turbulent boundary layer close to the trailing edge as a separate phenomenon but still possibly influenced by the presence of a shock-induced separation. With a substantial separation bubble underneath the shock, the trailing edge separation will depend critically on the upstream history of the boundary layer. Strictly speaking, separation



defined by a vanishing skin friction. But from the discussion by van Ingen in § 4.6 it becomes clear that the application of this definition is far from easy. The general approach is to calculate the development of the turbulent boundary layer and to apply various empirical criteria for prediction of separation-onset such as

- (a) the skin friction  $C_f$  decreasing below a certain (small) value,
  - (b) shape factor  $H$ , increasing above a certain value at a certain distance ahead of the trailing edge
  - (c) a critical value of  $\Theta_{TE}/U_e \cdot dU_e/dx$  (see van Ingen, section 4.6.6.2) where  $U_e$  is the local velocity outside the boundary layer.
  - (d) a shape factor correlation (see van Ingen, section 4.6.6.3 and also defined by Kline, ref.10).
- The turbulent boundary layer calculations can be based on either measured or calculated pressure distributions but if measured pressure distributions are used, misleading results will be obtained unless one departs from the measured distribution ahead of the trailing edge where, if a separation is present, it will introduce some 'pressure relief' (see van Ingen, section 4.6.6). When using a measured pressure distribution, it should be paired to an estimated value of the trailing edge pressure, this value being obtained preferably from an inviscid-viscous iterative calculation. If the turbulent boundary layer calculations are being based on a calculated pressure distribution, this should always be obtained by a method that allows for at least weak viscous-inviscid interactions. When a substantial separation bubble is present underneath a shock, the predictions of behaviour near the trailing edge will clearly depend critically on the upstream history of the boundary layer. There should be proper allowance if possible for the separated region through, for example, an inverse boundary layer calculation prescribing  $C_p = 0$ . These methods may fail when the shock is relatively far aft because the boundary layer profile at the likely separation point may not yet have recovered to an equilibrium shape for a turbulent layer. The possible interaction between a shock-induced separation bubble and a rear separation is not sufficiently understood for reliable simple prediction methods allowing for this interaction to be available.

[Calculation methods based on viscous-inviscid strong interaction or on the Navier-Stokes equations contain in principle all elements for a proper treatment of the problem. However, the accuracy of the results depends critically on the validity of the selected turbulence model in the region of flow separation]

#### TOPIC 5: VISCOUS DRAG SCALING

##### INPUT

- . main features of geometry (wetted area, wing thickness/chord etc)
- . Reynolds number
- . transition location (TOPIC 1)
- . pressure distributions and precise wing geometry (not necessary for method (i))

##### SUPPORTING CALCULATIONS

- . 2D, quasi 3D or full 3D boundary layer calculations with weak viscous-inviscid interactions
- . 2D boundary layer calculations with allowance for strong viscous-inviscid interactions.
- . [3D boundary layer calculations with allowance for strong viscous-inviscid interactions]

##### METHODS

- . In increasing order of refinement:
  - (i) Form factors, e.g. from DATCOM or RAeS Data Sheets, in combination with a flat plate skin friction law,
  - (ii) Simple boundary layer calculations, e.g. by the integral lag-entrainment method of Green in combination with a wake-relation, eg Squire and Young. These methods exist for 2D and quasi 3D flows.
  - (iii) More advanced coupled viscous-inviscid interaction methods for 2D or quasi 3D flows, e.g. Melnik et al (ref.11), Lock & Williams (ref.12) and Davis & Carter (ref.13). These methods are capable of coping with local boundary layer separations.

[Sophisticated:

- (iv) As (iii) but extended to the general case of a swept three-dimensional wing]

#### TOPIC 6: WAVE DRAG SCALING

##### INPUT AND SUPPORTING CALCULATIONS

- . Reynolds number
- . calculated pressure distributions with allowance for viscous-inviscid interactions
- . wing surface curvature distributions
- . [for some methods, complete flow field calculations]

##### METHOD(S)

The changes with Reynolds number in the boundary layer displacement thickness and separation characteristics can lead to changes in the shock strength and shock position and hence, wave drag for a given  $C_p$ . A method is therefore required for estimating the wave drag for a given shock strength and shock position. Simple first order methods applicable to the flow over both 2D sections and swept 3D wings are given by Lock (ref.14,15,16). These relate the wave drag to the local surface curvature at the foot of the shock. For a 2D section,

$$C_{D_W} = \frac{1}{c \kappa_W} F(M_\infty, M_{10})$$

$$\text{where } F(M_\infty, M_{10}) = 0.243 \frac{1 + 0.2 M_\infty^3}{M_\infty} \cdot \frac{(M_{10} - 1)(2.0 - M_{10})^4}{M_{10}(1 + 0.2 M_{10}^2)}$$

where  $\kappa_W$  = surface curvature at foot of shock

$M_\infty$  = free stream Mach number

$M_{10}$  = local Mach number ahead of the shock and close to the surface

For a swept 3D wing,

$$C_{D_W} = \int_{\text{body}}^1 \frac{c(\eta)}{c} C_{D_W}(\eta) d\eta$$

where  $c(\eta)$  = local chord

$\eta = y/s$

$s$  = semi span,  $\bar{c}$  = mean chord

$$\text{and } C_{D_W}(\eta) = \frac{\cos^4 \Lambda_s}{c \kappa_W} F(M_\infty \cos \Lambda_s, M_{10}^*)$$

where  $\Lambda_s$  = sweep of the shock front at  $\eta$

$M_{10}^*$  = Mach number component normal to the shock at its foot.

More elaborate methods are available for estimating the wave drag based on an integration along the forward surface of the shock. The above formulae for  $C_{D_W}$  are likely to be unreliable when the shock is in, or is located just downstream of, a region of  $C_{D_W}$  discontinuous or rapid variation of surface curvature; in due course, the formulae will be revised to cope with this situation.

[Sophisticated: wave drag obtained directly as an output from calculations of the flow by methods based on solutions of the full Euler equations with coupled viscous-inviscid interactions or the Navier-Stokes equations.]

#### REFERENCES

1. Michel, R  
Arnal, D  
Coustols, E  
Stability calculations and transition criteria in two- and three-dimensional boundary layers  
2nd Symp. IUTAM on Laminar-Turbulent Transition - Springer Verlag (1984)
2. Mack, L.M  
Transition and laminar instability Jet Propulsion Lab. Publication 77-15 (1977)
3. J.L. van Ingen  
Transition, pressure gradient, suction, separation and stability theory  
AGARD CP 224 (1957)
4.  
F-111 Natural Laminar Flow Glove Flight Test Data Analysis and Boundary Layer Stability Analysis  
NASA CR - 166051 (1984)
5.  
Hybrid Laminar Flow Control Study - Final Technical Report  
NASA- CR- 165930 (1982)
6. Launder, B.E.  
Jones, W.P.  
On the prediction of laminarisation  
ARC-CP 1036 (1969)
7. Patel, V.C.  
Head, M.R.  
Reversion of turbulent to laminar flow  
J. Fluid Mech., Vol 34, part 2 (1968)
8. Horton  
A semi-empirical theory for the growth and bursting of laminar separation bubbles  
ARC- CP-1073 (1969)
9. Fulker, J.L.  
Ashill, P.R.  
A model of the flow over swept wings with shock induced separation  
IUTAM Symposium "Turbulent Shear-Layer/ Shock-Wave Interactions", Palaiseau, France (1985)  
see also: RAE TR 83088 (1983)

10. Kline, S.J. Contribution to round table discussion "Computation of viscous-inviscid interactions", AGARD CP-291 (1980)
11. Melnik, R.E.  
Chow, R.R.  
Mead, H.R.  
Jameson, A. An improved viscid/inviscid interaction procedure for transonic flow over airfoils  
NASA CR 3805 (1985)
12. Lock, R.C.  
Williams, B.R. Viscous-Inviscid Interactions in External Aerodynamics  
Progress in Aeronautical Sciences,  
Pergamon Press (1985)
13. Davis, R.L.  
Carter, J.E. Analysis of Airfoil Transitional Separation Bubbles
14. Lock, R.C. Prediction of viscous and wave drag at high subsonic speeds by viscous-inviscid interaction techniques  
AGARD R-723 (1985)
15. Lock, R.C. The prediction of the drag of aerofoils and wings at high subsonic speeds.  
Journal of the Royal Aeronautical Society (June/July 1986).
16. A method of determining the wave drag and its spanwise distribution on a finite wing in transonic flow.  
ESDU TDM 83022 (1983)

## SECTION 3.3 APPLICATIONS

### SECTION 3.3.1 TRANSPORT-TYPE CONFIGURATIONS

by

A.B.Haines

and

A.Elsenaar

#### 3.3.1.1 Introduction

Various reasons can be advanced for treating transports as a separate, distinct class of aircraft for the purpose of defining a detailed viscous simulation methodology. For example,

- (i) the wings are typically of high aspect ratio ( $A \geq 6$ ), limited sweepback ( $\Lambda_{LE} < 40^\circ$ ) and moderate thickness/chord ratio, eg  $0.08 < t/c < 0.15$ ,
- (ii) the most scale-sensitive viscous phenomena tend to appear near and outboard of mid-semi-span where the flow can often be regarded as quasi-two-dimensional - see Fig 1. Much of the past research on scale effect in transonic flow is therefore relevant,
- (iii) many model test programmes for subsonic transports concentrate merely on the limited  $C_L$  -  $M$  region covering the likely cruise conditions and extending up to but not beyond the buffet-onset boundary. There will of course be exceptions to this general statement: in some cases, the programmes will have to cover a wider test envelope in order to obtain loading data for the aircraft structural engineer and to provide a guide to the stability and control characteristics up to the design diving speed.

In general, therefore, both the geometry and the transonic flow development will be simpler than for the combat aircraft configurations considered later in §3.3.2. This does not mean that the task of defining a suitable viscous simulation methodology for a subsonic transport aircraft is a simple task. The difficulties in simulating the full scale flow can still be formidable and the accuracy requirements for the test data can often be very stringent. For example, the customer for the tests may often demand a relative accuracy of  $\Delta C_D = 0.0001$  (ie 1 'drag count') or better, when comparing two competing wing designs for a given application or when determining the incremental effects of say, the nacelle installation, the flap track fairings, a tip winglet or a wing-body fairing. Despite the fact that one is considering a restricted class of wing geometry, one should resist any temptation to say that once one has tested one wing design, one merely has to apply the same detailed practice to the next design. Even if the two designs bear a family resemblance, the differences are likely to be significant in the present context. In the first test programme on a new configuration, one should apply the full methodology as described below; short cuts should not be taken; each new configuration should be treated on its merits.

Before describing the methodology in detail, a few general points are worth noting:

- (a) the methodology is concerned with the flow over the wing. Scale-sensitive viscous effects may also be present in the flow over the rear fuselage of a subsonic transport but these are discussed in §3.3.3,
- (b) an implicit assumption throughout is that on the full scale aircraft in flight, transition is likely to occur near the wing leading edge. Future aircraft designs may however seek to exploit extensive laminar flow over the forward part of the wing upper and lower surfaces; detailed changes to the methodology will then be required,
- (c) the methodology can be applied most effectively when testing a model with extensive pressure plotting facilities. When these are not available, it will be essential to conduct surface flow visualisation tests; even when pressure distributions are measured, flow visualisation is highly desirable as an aid in interpreting the pressures. The fundamental message underlying all the detailed methodologies: to be successful, know your flow and appreciate the nature of the viscous effects that may be present in the model tests.

#### 3.3.1.2 The Detailed Methodology

##### STEP 1 : Collection of relevant information

The test engineer should start by collecting the relevant information about the tunnel, the model and the aims and requirements of the particular test programme. The important issues regarding the tunnel and the model are discussed in §3.2.2.

The objectives for a test programme on a model of a subsonic transport aircraft are likely to include

- (i) cruise drag - often required to an accuracy of  $\Delta C_D = 0.0001$  or better as regards the increment in drag between two configurations of the same model or ideally, as between one model and another in the same family. Realistically, one cannot expect to achieve better than  $\Delta C_D = \pm 0.0005$  for the extrapolated absolute drag of the full scale aircraft and many organisations may regard this as a highly optimistic target,

- (ii) the buffet-onset boundary - generally required to a relative accuracy of 0.01 in  $C_L$  at a given Mach number,
- (iii) pressure distributions - required to an accuracy of  $\Delta C_p = 0.01$  for checking computer codes and for performance verification but better than this, eg ideally  $\Delta C_p = 0.001$  for assessing the effects of small changes in configuration,
- (iv) stability and control data including the effects of ailerons, spoilers, airbrakes, tailplane, fin, elevator and rudder with pitching moments, for example, determined to an accuracy of better than  $\Delta C_m = \pm 0.0010$ ,
- (v) lift-curve slope to an accuracy of certainly better than 5% for gust analysis.

To achieve these standards of accuracy and repeatability, the Mach number should be held constant in a polar for drag data to an accuracy of  $\Delta M = \pm 0.001$  or better and the angle-of-attack should be known to an accuracy of better than 0.01°. Many other factors have to be addressed with care: balance design and calibration, tunnel stream humidity, wall interference and model support interference. These may appear irrelevant in the context of a viscous simulation methodology but if they are not addressed with care, the successful application of the methodology will be compromised.

The customer for the tests should indicate the  $C_L$  -  $M$  region for which he is most interested in obtaining a good viscous simulation of the full scale flow behaviour. This could take the form of a picture such as that shown in Fig 2, viz three primary design or cruise conditions and a target buffet-onset boundary. Points A-F could then be selected as the conditions for the calculations in Step 2. It should be emphasised that Fig 2 is only intended to be a typical illustration: not every subsonic transport will have to meet a specification with three operational cruise conditions and, in some cases, one would not be able to ignore low  $C_L$  conditions, particularly for aircraft with underwing nacelle installations.

#### STEP 2 : Preparatory calculations

Calculations should be made by the most advanced theoretical method conveniently available to obtain the wing pressure distributions, boundary layer development and, if possible, the wave drag and viscous drag at the important operational conditions identified in Step 1. Calculations should be made for both the full scale aircraft at a typical flight Reynolds number and for the model at a representative test Reynolds number.

The complexity of the configuration chosen for these calculations will depend on the capabilities of the test establishment. It would be unrealistic to suggest that one needs to use a code/grid suitable for calculating the flow over the complete aircraft and at the other extreme, it is possible that useful guidance could be obtained from calculations for two-dimensional flow. Ideally, however, the calculations should be made for at least the three-dimensional wing-body configuration or preferably, the wing-body-nacelle installation, bearing in mind that the addition of the nacelles, whether underwing or on the aft-fuselage, can modify the shock pattern over the wing upper surface at a given  $C_L$  as well as introducing serious viscous effects on the wing lower surface.

Strictly, to compare with the measured data and to provide a reliable extrapolation of the viscous effects to full scale conditions, the CFD codes used for these calculations should be capable of allowing for: strong viscous-inviscid interactions such as a laminar separation near the wing leading edge, a shock-induced separation bubble and a rear separation ahead of the wing trailing edge but such codes have not yet been developed for general use. Even when, in the future, they have been developed, it is probably unrealistic to suggest that they should be used in a general viscous simulation methodology except as a means of checking some specific point of overriding importance in a particular case. In practice, the nature of the CFD code used in this step 2 in the proposed methodology will always be subject to the cost and timescale constraints of the testing establishment and the customer. Writing in 1987, it is however reasonable to propose that the calculations should be made using an Euler code with allowance for at least weak viscous-inviscid interactions. The restriction to weak interactions is not such a serious drawback as might appear at first sight: divergence between trends in the measured and computed data will frequently serve as a guide to where strong viscous interactions are present in the measured data, and this knowledge will help in the intelligent extrapolation of the data to full scale conditions. Indeed, the methodology, as written later, eg in Step 5.3, takes deliberate advantage of the fact that the strong viscous-inviscid interactions are not allowed for in the calculations.

Predictions should be made of the position of natural transition for both the full scale aircraft and the model, applying criteria (see §3.2.4) for

- (i) transition due to contamination along the wing leading edge attachment line,
- (ii) transition due to cross-flow instability,
- (iii) transition due to Tollmien-Schlichting instability as in two-dimensional flow,
- (iv) transition due to Görtler instability.

For most transport aircraft, except for those designed specifically to exploit laminar flow, transition will tend to occur at or near the leading edge as a result of mechanism (i) or because of joints in the wing surface. In most model tests at reduced Reynolds number, however, natural transition is likely to be induced by mechanism (ii) or (iii) and so, whenever there is a favourable, neutral or only slightly adverse pressure gradient, transition is likely to occur much further aft than in flight. In many cases in the model tests, natural laminar flow will be maintained back to the shock and the results with natural transition will then be unrepresentative of the full scale viscous behaviour which contains a turbulent boundary layer/shock interaction.

If the tests are being made in a variable pressure tunnel, the calculations of pressure distribution and boundary layer development should be repeated for various Reynolds numbers in the test range (extended, if thought appropriate, by the use of a supplementary half-model as described in §3.2.1). Also, whenever the intention is to use the boundary layer manipulation approach, ie aft-fixing, the calculations should be repeated for a range of transition positions at the model test Reynolds number. These transition positions should all lie ahead of the predicted natural transition position and should range from a typical 'forward fix' position at say, 0.05c (but see (i) below) back to a position about 0.15c ahead of the shock front, marking the rearward extent of the region of supercritical flow as determined in the calculation for natural transition.

The general aim of these calculations is to give the model test engineer an early indication of the likely pressure distributions over the wing at the primary test conditions of operational interest and, in particular, an appreciation of where and how the flow is likely to be scale-sensitive. Specifically, the calculations will indicate

- (i) a suitable position for a forward transition trip. This should be as near the leading edge as possible in order to reduce uncertainty in the interpretation of the drag data but it should be recognised that it will be difficult to provoke transition in a strongly favourable pressure gradient. Also, if the calculations indicate that there is a peak suction close to the leading edge, the trip should not be located near or immediately downstream of this peak suction. There are two main reasons for this recommendation:
  - (a) the outgoing expansion waves from near this peak suction are lost if the region is allowed to be immediately ahead of the forward facing step introduced by the transition trip. This can lead to a significant change in the subsequent supercritical flow development. These effects are illustrated in Fig 3,
  - (b) placing the trip in a steep adverse pressure gradient immediately behind the peak suction can lead to undue thickening of the boundary layer and thus, possible extra problems such as a premature rear separation - see Fig 3.

Experience has shown that if this recommendation is ignored, there will be a lack of repeatability in the test data,

- (ii) the probable range of positions at which transition can be tripped in the model tests and still achieve the primary aim of ensuring a turbulent boundary layer/shock interaction with no local interference between the trip and the flow at the foot of the shock. As explained in §3.2.1, testing with an aft trip is a means of extending the effective range of the effective test Reynolds number and the range of possible transition positions can be translated into a range of effective Reynolds number by using the zero-level simulation criterion introduced in §3.2.1.1.5 and plotted in Fig 9 of §3.2.1 reproduced here for convenience as Fig 4. The effective Reynolds number is defined as the Reynolds number that would be needed if transition were fixed in the (generally forward) position forecast for flight at full scale Reynolds number in order to produce the same viscous flow behaviour as in the model tests with aft transition, this correspondence being judged on the basis of the chosen simulation criterion,
- (iii) whether a rear separation is likely to be present in the model tests and, if so, the extent to which this can be eliminated by changes in Reynolds number and/or transition position in the available test range. Methods for predicting a rear separation are discussed in §3.2.4. The Reynolds number (or effective Reynolds number) above which the rear separation is forecast not to occur is denoted by  $R_{crit}$  in the subsequent discussion,
- (iv) whether - and this is a remote possibility for design/operational conditions such as A-F in Fig 2 - there is likely to be a laminar separation ahead of a suitable forward trip position. If so, the Reynolds number above which this is forecast not to occur, is denoted as  $R_{critf}$ ,
- (v) the required transition trip heights for various Reynolds number/transition positions. General experience suggests that these should be slightly greater than those that would be predicted<sup>1</sup> by Braslow and Knox on the basis of the calculated thickness of the laminar boundary layer at the chosen transition positions but the actual values for any particular tunnel are likely to depend on the stream turbulence and the values for any particular wing design depend on the upstream history of the boundary layer. General experience appears to suggest that the height of an aft fix has to be somewhat greater if the pressure gradient upstream of the trip is favourable than when it is adverse, ie the effect of the gradient on the stability of the laminar boundary layer is more important in general than its effect on the thickness of the boundary layer.

A study of the results of (ii,iii,iv) will provide a forecast of which simulation scenario (§3.2.1) is likely to apply at the operating conditions identified in Step 1. To summarise:

- 1  $R_{crit} < R_{flight}$  and test range of R or effective R includes  $R_{flight}$ : scenario 1
- 2  $R_{crit} > R_{flight}$  but test range of R or effective R includes  $R_{flight}$  and  $R_{crit}$ : scenario 2
- 3  $R_{crit}$  within test range of R or effective R but range insufficient to include  $R_{flight}$ : scenario 3
- 4  $R_{crit}$  forecast to be less than  $R_{flight}$  but both  $R_{crit}$  and  $R_{flight}$  beyond test range: scenario 4
- 5  $R_{crit}$  forecast to be higher than  $R_{flight}$  and both  $R_{crit}$  and  $R_{flight}$  beyond test range: scenario 5.

It should be noted that, at this stage, these deductions from the calculations are only forecasts for a limited number of conditions. The actual transition positions to be used in the tests (apart from the initial forward fix) will be based on the measured data obtained in Steps 3 and 4 and eventually, the placing of the data in different simulation scenarios for the purpose of extrapolation to full



scale is likely to be based on the first-order or second-order simulation criteria discussed in 53.2.1. For the present, however, there is no need to become involved in such complications. The simple approach outlined above will be sufficient to alert the test engineer as to the viscous flow problems he is likely to encounter in the actual tests.

The above description of the proposed procedure for Step 2 is somewhat simplified. Stating that the calculations should be made for a certain transition position,  $x_T$ , suggests that one can - and should - trip transition at the same  $x_T$  at all positions across the span. This may well be possible with a forward trip at say, 0.05c, but with an aft trip, one must allow for the likely changes in shock position near the root and tip. A typical shock pattern over the wing upper surface near, for example, the buffet-onset boundary at the cruise Mach number (point E) was shown in Fig 1. Natural transition is likely to be induced in the tunnel test ahead of or as a result of the pressure-rise through the inner forward and outboard shocks and it is clear that the range of  $x_T$  available for manipulating the boundary layer is limited near the root and tip. For the high aspect ratio wings of most subsonic transports, these restrictions may not be too important since, as noted in Fig 1, the most significant viscous effects in the cruise and up to buffet-onset are likely to be found near mid-span (apart from local effects in the wing-body junction).

#### STEP 3: Initial datum tests with forward fixed and with free transition

Note: in practice, it is possible that, for convenience, the tests in both Steps 3 and 4 will be conducted in a single tunnel entry; when describing the methodology, it is useful, however, to keep the distinction between Steps 3 and 4. It also serves as a warning against the frequent practice, to be deprecated, of customers omitting Step 3, either on cost grounds or because "they know what to expect". As observed earlier, experience with earlier configurations can only serve as a guide; the detail is always liable to change with a new configuration.

The first move should be to apply a forward fix of the appropriate height at the position chosen on the basis of the calculations in Step 2. This trip should be a narrow band of ballotini, carborundum or serrated tape ('hande crantee') or a set of air jets, according to the experience or preference of the individual test establishment. The tests should then start with a check, usually by means of a sublimation test with say, acenaphthene, on the effectiveness of the trips on both the upper and lower surfaces. One should check the effectiveness in various operating conditions, eg

- (a) some or all of the typical operational design or cruise conditions, eg A, B, C in Fig 2, as chosen for the CFD calculations in Step 2,
- (b) conditions near buffet-onset at similar Mach numbers, these conditions being chosen by on-line monitoring of the test data,
- (c) if necessary, other conditions where there is any reason to doubt the effectiveness of the transition fixing, either because of a lower test Reynolds number, eg at low Mach number in an atmospheric tunnel, or a more favourable pressure gradient or a thicker boundary layer.

It is worth noting that if the acenaphthene is sprayed over the whole wing surface, including the region upstream of the transition trip, a 'good fix' implies that some small 'turbulence wedges' are visible immediately downstream of the trip, whereas if the acenaphthene is only sprayed on the wing aft of the trip, the aim should be to obtain a clear indication with no wedges. Obviously, one should apply the smallest trip that will produce these results; otherwise, the presence of the trip may lead to an unnecessary increase in drag.

Tests should then be made with and without this forward trip over the full range of  $C_L$  and Mach number: note: the full range including conditions at low Mach number and not simply the region around the points chosen for the CFD calculations.

The aims of the test with the forward trip can be summarised as follows:

- (i) To establish the absolute drag levels free from any uncertainty due to an unknown extent of laminar flow and thus, by comparison with predictions for conditions where the flow is fully attached and subcritical, to provide some check that the measured data have been corrected successfully for the support tares, tunnel wall interference, buoyancy effects etc. Unexplained discrepancies may indicate that there are local viscous problems, eg in a wing-body junction, and surface oil flow visualisation tests should then be made to check whether these can be identified. If such effects are present, they could be scale-sensitive and this point should be borne in mind in the later stages of the methodology.
- (ii) To compare with the results of the CFD calculations in Step 2. Any serious disagreement, eg in shock position, could indicate that viscous effects, eg a rear separation, not allowed for in the CFD calculations, is present in the measured data. In other words, the tests with the forward trip are being made at a Reynolds number below  $Re_{crit}$  - at least, for these particular operating conditions. If so, this would confirm the need for further tests, as described in Step 4, involving either a Reynolds number sweep or a transition position sweep at a given model test Reynolds number. If the tests are being made on a model without pressure plotting facilities, the comparison between measured and predicted shock positions would have to be based on the evidence from surface flow visualisation tests. Also, a surface flow visualisation test with oil either applied to the wing ahead of the test or perhaps, preferably, emitted from holes in the wing surface during the test, provide the clearest indication of whether a rear separation is present or not.
- (iii) To find how the shock position varies with  $M$  and  $C_L$  and thus, to gain some idea of the likely  $C_L - M$  ranges in which one can test with a further aft transition position and still obtain a turbulent boundary layer/shock interaction. As noted earlier, the shock position is likely to vary somewhat across the span of the wing.

- (iv) To study the nature of the pressure distributions aft of the shock and, in particular, to note how the pressures at different chordwise positions vary with  $C_L$  and Mach number. These curves provide another means of possibly identifying whether a rear separation is present - see Fig 5, for example, reproduced from the original reference<sup>2</sup> by Haines, Pearcey and Osborn, which introduced the concept of class A and class B flow separations.

The test with free transition is included largely for diagnostic purposes and to provide a guide as to what can be attempted in the in-depth study of viscous effects in Step 4. For example, it will show:

- (i) whether laminar flow can be maintained back to the outboard shock,
- (ii) whether the generally relatively weak forward shock, if present on the inner wing, is strong enough to provoke transition,
- (iii) whether a rear separation is still present; if so, this almost certainly implies that it will be present at the model test Reynolds number, whatever transition fixing practice is adopted,
- (iv) the furthest aft shock position likely to be achieved at a given incidence (but not necessarily at a given  $C_L$ ) and Mach number at the test Reynolds number and, therefore, the extent to which the shock positions observed in the forward fix test are providing a conservative guide to the transition positions that can be chosen for the tests in Step 4. Note: an aft movement of transition will lead to a thinner boundary layer at the shock and at the trailing edge and hence, a further aft shock position at a given incidence. In general, however, fixing transition ahead of the shock will still result in the shock being slightly further forward than in the transition-free test.

The actual data from the transition-free test can provide a very misleading idea of the full scale performance. In particular, as illustrated in Figs 6a,b,

- (i) an aft movement of transition with increase in Mach number at a given  $C_L$  as the supercritical region extends rearwards, can completely mask<sup>3</sup> the presence of a drag-creep prior to the start of the steep drag-rise, and
- (ii) an aft movement of transition with increase in incidence, again in sympathy with a rearward extension of the supercritical region, can give<sup>4</sup> spuriously high values of lift-curve slope which could be misleading for gust analysis.

In theory, it might be possible to correct the transition-free data for the effects of these movements of transition but, in practice, any suggestion that this should be done in routine testing, would be impracticable. Hence, in general, for a transport aircraft, the transition-free data should not be used for the quantitative forecasts of the full-scale behaviour; they are being obtained merely to help the test engineer in the understanding of the viscous effects in the transition-fixed data. There may be exceptions to this general recommendation, eg some establishments and customers believe that because the boundary layers will be thinner in a transition-free test, the results from such a test may provide the most reliable indication of the full-scale hinge moments for a trailing edge control or the full-scale values of  $C_{m_0}$ .

#### STEP 4: In-depth study of viscous effects

Testing a model of a subsonic transport at Reynolds numbers in the range  $2 \times 10^6 < R < 6 \times 10^6$  with transition tripped in a forward position, as in the initial datum tests in Step 3, is unlikely to provide an adequate simulation of the full scale viscous effects. None of the viscous simulation criteria are likely to be satisfied. There is therefore a need for further tests to study the viscous effects and to assist in the extrapolation to full scale. There are two approaches - either conduct Reynolds number sweeps if possible or manipulate the boundary layer which, at present, implies conducting a sweep through a range of transition positions at a given Reynolds number. Whenever possible, both approaches should be practised; they are described in detail in Steps 4a and 4b below.

The in-depth study has three main aims:

- (i) to provide 'trends' in the measured data that can be compared with 'trends' in the CFD data from Step 2 and which together, can be used in the extrapolation of the data to full scale,
- (ii) to produce a closer simulation in the actual tests of the full-scale viscous flow behaviour,
- (iii) to eliminate, as far as possible within the tests, any premature rear separation or other strong viscous-inviscid interaction not expected to be present in flight at full scale Reynolds numbers.

#### STEP 4a: Reynolds number sweep

Tests should be made with transition fixed in the forward trip position selected for the tests in Step 3 for a range of Reynolds numbers. This is of course only possible if the tests are being made in a variable pressure tunnel. The range of available test Reynolds number can be extended by use of a second model to a different scale, eg a half-model. In many variable pressure tunnels, it is possible to change the Reynolds number at a given Mach number by a factor of about 2.5 for a given model and then, by use of a half model, to obtain a further increase by a factor of between 1.6 and 2, according to the geometry of the particular configuration and the Mach number requirements of the particular tests. In other words, a Reynolds number sweep over a range of 4:1 or 5:1 should be possible. By use of the two models, a Reynolds number range can be obtained even in an atmospheric tunnel, but this is less satisfactory because it may never be possible to link the data, particularly the drag data from the two models, to form a single curve against Reynolds number. In a variable pressure tunnel, it is



possible to obtain an overlap between the Reynolds number ranges for the complete and half model tests and then, it is possible to extend the complete model data to higher Reynolds number by following merely the trends of the half-model data.

These tests will concentrate primarily on the  $C_D$  -  $M$  area of most interest to the customer, i.e. the area around the design/operational conditions identified in Step 1, but there will always be a case for widening the range and to include, for example, conditions at relatively low Mach number and low  $C_D$  as a check on the absolute drag levels. It is important that the data are computed and corrected appropriately for effects which, if undetected, would contaminate the data as pseudo-Reynolds number effects. One particular point that should be highlighted is that the roughness band or trip heights should always be changed to suit the test Reynolds number; otherwise, one will 'overfix' at the higher Reynolds numbers and introduce a significant drag penalty that is difficult, on present knowledge, to estimate accurately.

Sufficient test Reynolds numbers should be included to establish the trends with reasonable accuracy. If possible, while the tests are in progress, these measured trends should be compared with the predicted trends. Any serious divergence between the predicted and measured trends should be identified and diagnosed, as to whether they are due to viscous effects and, if so, what viscous effect and where on the wing. In particular, the data should be studied to establish whether there is any sign of a rear separation ahead of the trailing edge on either wing surface or of a separation near perhaps 0.7c on the wing lower surface. It may be possible to recognise the presence of such separations fairly readily from the on-line plotted data either by comparing measured and predicted shock positions or by creating plots of the form shown in Fig 5 or directly from the evidence of surface oil flow tests. Sufficient test Reynolds numbers should then be included to identify whether these effects disappear in the test range of Reynolds number: these will provide a direct indication from the measured results of the values of  $R_{crit}$ , these being probably a function of Mach number and  $C_D$ . These values are likely, at the present time, to be more reliable than any values derived from the CFD calculations and prediction techniques discussed in §3.2.4.

#### STEP 4b: Manipulation of the boundary layer

Tests should be made with one or more aft trips covering a range of different transition positions with transition induced by a trip of an appropriate minimum height deduced from the calculations in Step 2. Obviously, the natural transition positions observed in Step 3 provide an indication of the furthest aft transition positions that can be achieved in the model tests at a given Mach number and  $C_D$ , but the limitations are somewhat more severe in that the positions for these aft trips have to be chosen

- (i) to ensure a turbulent boundary layer/shock interaction,
- (ii) to avoid any local interaction between the trip and the flow near the shock,
- (iii) to minimise, as far as possible, any serious disturbance to the supercritical flow development over the forward part of the wing surface, and naturally
- (iv) to ensure that one can claim that there is completely laminar flow ahead of the trip at all conditions of interest; otherwise, there will be difficulties in interpreting the drag data.

Illustrations of the problems that may arise if (i,iii) are ignored, are shown in Figs 7,8. In both cases, the flow decelerates ahead of the trip and then accelerates over the top of the roughness band. If the trip is too close to the shock, as in Fig 7, the interaction leads to the development of a second (and spurious relative to full scale) supercritical region downstream of the trip, which eventually merges with the region further forward to create a single supercritical region but with a shock both stronger and lying further downstream than if the interaction with the trip had not been present. This leads to an increase in wave drag and indeed, as can be seen in Fig 7, the existence of this form of interaction can often be readily recognised from a study of the drag polar. The correct conclusion is that a condition such as that illustrated in Fig 7 lies outside the range of validity of tests with that particular trip. It does not meet requirements (i,iii), i.e. the point lies below boundary AA - see Fig 9. To avoid this form of interaction, the trip should be at least 0.15c ahead of the shock. Bearing in mind that, as noted earlier, the shock position will tend to move aft in many cases as the transition position is moved rearward, a rough-and-ready guideline is that an aft trip should be at least 0.10c ahead of the shock position observed with a further forward trip.

The interaction between a trip and the supercritical flow development is not always as severe as that illustrated in Fig 8. It tends to be most noticeable in cases where, without the interference from a trip, the supercritical flow development contains a largely isentropic recompression to a weak shock; the presence of a trip can introduce a local expansion followed by a shock loading, once again, to an increase in wave drag. In such cases, the test engineer should consider whether he can reduce this interference by a change in position, height or width of the roughness band but if this is not possible, one must eliminate the excess wave drag from the results by fairing out the hump in the drag polar (see Fig 7). More scientifically, one should consider whether, in this particular case, one should test transition-free and accept the need for a limited but still significant number of sublimation tests to determine the transition position over the full wing surface. This may be acceptable for cases where any shock waves are still relatively weak and one can thus tolerate a laminar boundary layer/shock interaction.

In practice, with a model of a subsonic transport, one should attempt to obtain an upper surface transition sweep with at least 3 points on the sweep, viz

- (a) the forward trip already tested in Step 3,
- (b) a 'mid' trip at aay, 0.15c for which, to obtain valid data, it may be necessary to limit the tests to a Mach-number range above say, ( $M_{design} - 0.1$ ),
- (c) a 'rear' trip at aay, 0.25 - 0.30c with the tests limited to say, ( $M_{design} - 0.02$ ).

If possible, there should be on-line monitoring of significant features of the pressure distributions, eg shock positions, to ensure that these tests with aft fixes cover somewhat more of the  $C_D$  -  $M$  plane

than the area in which the data are expected to be valid data satisfying the requirements set out above. As indicated in Fig 9, the range of validity is, in fact, a corridor between two boundaries corresponding to

- (i) when the shock waves move aft with increase in Mach number to a position about 0.15c behind the trip. As already noted, this boundary can be recognised from a study of the drag polars; typically, as the shock passes over the trip, the drag can be increased by the local interference by an amount that can be in the range  $0.0001 < \Delta C_D < 0.0005$  - see Fig 7,
- (ii) when the shock wave moves forward after the flow has separated and hesitates about 0.15 - 0.20c behind the trip. This second boundary must, by definition, lie beyond the buffet-onset boundary. It can generally be recognised from a study of the  $C_L - \alpha$  and  $C_m - \alpha$  curves as an increase in lift-curve slope and a nose-down change in pitching moment over a limited range of incidence, these effects being associated with a hesitation in the forward movement of the shock with incidence as it approaches the trip from the rear under the influence of the more severe separation. Fig 10 presents an illustration of the complex interactions that can ensue in such a condition. The variation of shock position with incidence at a given Mach number is presented for 4 stations across the span; for all stations, the shock begins to move forward above about  $\alpha = 4^\circ$  but at two of the stations, the shock is held behind the roughness band sited at 0.15c for an appreciable range of incidence above  $\alpha = 6^\circ$ . As a result, the nose-up change in  $C_m$  which appeared at about  $\alpha = 4^\circ$  is reversed by a nose-down change above about  $\alpha = 7^\circ$ . The study of the pressure distributions has therefore shown that this nose-down change is due to the local interaction being discussed and is likely to be completely unrepresentative of the full scale behaviour. The real conclusion is that upper boundary of the range of validity of the tests with this particular trip passes through about  $\alpha = 6.2^\circ$  at this Mach number but this would of course be fully adequate to cover buffet-onset which is likely to occur near  $\alpha = 4^\circ$ . The details of this particular example are of course peculiar to this particular example; to reiterate, the important general point to remember is that it is often possible to recognise the boundary marking the upper limit of the range of validity of the measured data with a given transition trip by a detailed study of the reasons underlying an increase in lift-curve slope and a nose-down change in  $C_m$  relative to the general trends.

As noted earlier, the aft transition trips will have to be brought forward towards the leading edge at both the tip and root in order to stay ahead of the shock front - see Fig 1.

The required number of trips, their position and the test Mach number range for which they are capable of providing valid data, will depend on the wing design; the suggestions (a,b,c) above reflect design practice at the time of writing; they may change in the future but it is hoped that the general principles are clear after referring to the diagrammatic picture in Fig 11. The aim should be to obtain an adequate sweep with, if possible, more than two points on the sweep and extending as far aft as possible. If a rear separation is still present with the furthest aft transition position, the only further step that could be taken in the tests to eliminate this separation, would be to consider whether it is desirable or feasible to modify the shape of the model in the region affected by this separation and retest. At the present time, the general feeling is that this idea should only be applied in a research experiment and it is certainly too soon to put forward a precise methodology based on this idea, to use in routine testing. One of the potential difficulties is that the modified shapes will generally include a blunt base. The depth of this base should be limited to about 0.006c; otherwise, any advantage gained from the suppression of a rear separation could be nullified by the introduction of a base drag term with an uncertain extrapolation to full scale.

In practice, tests 'with one or more aft fixes' will frequently have to include more than a sweep of transition positions. Experience has shown that, for some wing designs, a trip of greater height is needed to fix transition effectively at buffet-onset (eg point D in Fig 1) than in the cruise (eg point B in Fig 1). No general guidance can be given on this point but it is essential that one should determine and use the minimum roughness band height that is effective in these two conditions. Otherwise,

- (a) using a trip that is effective (but only just effective) in the cruise, and is ineffective at buffet-onset, may give a spuriously optimistic  $C_L$  for buffet-onset at a given Mach number and also, a lift-curve slope that is too high approaching buffet-onset and hence, a spuriously pessimistic result in the context of gust analysis, and
- (b) using a trip that is effective at buffet-onset may imply using a trip that is larger than that required for the cruise and thus, may give pessimistic results for cruise drag.

It is therefore necessary or, at least, highly desirable to test with both types of trip but this comparative exercise would probably only have to be undertaken with one or, at the most, two transition locations. For a subsonic transport, particularly at the design/operational conditions identified in Step 1, the upper surface is likely to be far more important than the lower surface in the context of uncertain scale-sensitive viscous effects. The flow over the lower surface should not however be ignored and, with many advanced wing designs, a transition-sweep on the lower surface will also be a desirable part of the test programme in order to establish, for example, trends in the data at effective Reynolds numbers below a value of  $Re_{crit}$  related to a flow separation due to a steep adverse pressure gradient near say, 0.7 chord. If the wing carries an underwing nacelle installation, local scale-sensitive flow separations are likely to be present - at least until the design is finally optimised and it may not be easy to alleviate these by manipulation of the boundary layer; the local pressure distributions may not be conducive to any aft-movement of transition. This is an area that requires further research before a definitive methodology can be proposed.

STEP 5: Consolidation of measured data

In the description below, it is assumed that it has been possible to employ both the Reynolds number sweep and boundary layer manipulation approaches; if not, the amendments to the text should be obvious.

The procedure can be conveniently described under six headings:

STEP 5.1: Confirmation of ranges of test validity

The test engineer should establish from a study of the measured pressure distributions, supported by evidence from the flow visualisation tests, the  $C_L$  -  $M$  ranges for which the data from the tests with aft transition trips can be accepted as valid data, satisfying the requirements set out at the start of Step 4 and what, if any, corrections should be applied to these data to account for possible interaction between the trips and the supercritical flow development. The test engineer is then able to create a diagram such as Fig 11. Reference to this diagram will define the data that can be used to produce the 'transition sweeps' to be plotted in Step 5.2.

STEP 5.2: Plotting of 'measured trends' against  $R$  or effective Reynolds number

The valid measured data should be cross-plotted to produce trends against Reynolds number (from the Reynolds number sweeps) and against transition position/effective Reynolds number (from the transition sweeps). The conversion from transition position to effective Reynolds number should still be based at this point on the zero-level simulation criterion introduced earlier and plotted in Fig 4. This zero-level criterion is based on the requirement that the boundary layer momentum thickness at the trailing edge of a flat plate should be the same for the aft transition position at the model test Reynolds number as for the flight transition position at the effective Reynolds number, "zero-level" therefore implies that the conversion does not depend on the geometry of the particular wing or on the particular  $C_L$  and Mach number. The criterion is therefore very simple to apply; its use can be entirely justified on this argument but it should be stressed that experience in its use is very limited. The first-order criteria (in which there is more experience) discussed later in Step 5.5, are likely to be more accurate but they are more difficult to apply. The trends to be plotted are likely to depend on the aims and requirements of the particular test programme but, for a transport aircraft, the most useful trends to plot are likely to include

- (i)  $C_D$  at a given  $C_L$  and Mach number at, for example, the design/operational cruise conditions identified in Step 1 and at other conditions which would appear to help in the understanding of the data,
- (ii) the position of the shock at a given  $C_L$  and Mach number, probably for a number of spanwise stations,
- (iii) similarly, the strength of the shock, the 'strength' being defined as the value of the Mach number component normal to the shock at a position just upstream of the shock,
- (iv) the strength of the shock at conditions on the buffet-onset boundary where this boundary has been determined either from the divergence of trailing edge pressures, wing root bending moment or accelerometer signals or, less satisfactorily, from breaks in the lift and pitching moment data,
- (v) the length of the shock-induced separation bubble at  $C_L$ ,  $M$  conditions between separation-onset and buffet-onset, both for a given  $C_L$  and for a given shock strength at a given Mach number,
- (vi) the lift-curve slope at conditions selected for gust analysis,
- (vii)  $C_{m_0}$  and any other features in the pitching moment data judged to be significant,
- (viii)  $C_{DTE}$  at a given  $C_L$  and Mach number, again at several spanwise stations,
- (ix) when appropriate, the chordwise and spanwise extent of any rear separation, again as a function of  $C_L$  and Mach number.

The list above is not necessarily fully comprehensive.

These 'measured trends' should be compared on the same graphs with the 'computed trends' in respect of (i,i,i,i,viii) viz, drag, shock position, shock strength and trailing edge pressure.

In cases where a Reynolds number sweep has been extended by use of a half-model, the measured trends from the tests on both models should be plotted on the same graph but no attempt should be made to force the results artificially into a single curve. This applies particularly to the drag data where there may be many reasons of technique why the absolute accuracy of the half model data may be open to question. When the Reynolds number sweeps are being performed in a variable pressure tunnel, the hope must be that there is a range of Reynolds number in which there is an overlap between the complete and half model data. This will provide confidence that one can extend the trends from the complete model test by following the shape of the trends from the half model tests - see Fig 12. Even when there is no overlap, the extension should still be possible in many cases but will be uncertain if the value of  $R_{crit}$  which, in theory, marks a discontinuity in the slope of the trends, is near or just beyond the range of the complete model test.

STEP 5.3: Derivation of  $R_{crit}$ 

$R_{crit}$  is defined as the value of Reynolds number above which any strong viscous-inviscid interactions present at model test Reynolds number but not allowed for in the CFD calculations in Step 2, disappear as the Reynolds number is increased with transition in the (forward) forecast position for flight at full scale Reynolds numbers. In the context of subsonic transport aircraft, the most likely example of this type of viscous-inviscid interaction is a rear separation on the wing upper surface. There are however other possibilities, eg a local separation on the wing lower surface some distance ahead of the trailing edge near possibly 0.7c, a local separation in the wing-body junction or near a flap track fairing, a separation in the wing-body junction or, more generally, in the gully flow between the wing and a pylon-mounted underwing nacelle or finally, a laminar separation near the leading edge. The effects of a rear separation can lead to

- (a) a lack of full pressure recovery at the trailing edge,
- (b) a reduction in circulation around the sections affected and hence, an increase in incidence and thus, in general, shock strength to maintain a given  $C_L$ ,
- (c) the possibility of an interaction with the growth of a shock-induced separation bubble.

It cannot be emphasised too strongly that a small rear separation can, as a result of (a,b) lead to increases in drag that are significant for a subsonic transport. Effects of type (c) can affect the buffet-onset boundary, particularly when the shock is far aft at Mach numbers beyond design, eg at position F in Fig 2.

An early appreciation of whether rear separations are likely to be present in the model tests was obtained from the CFD calculations in Step 2 but, as noted in §3.2.4, the prediction of a rear separation is an uncertain process at the present time. A clearer idea can be obtained from a study of surface oil flow patterns and of the experimental data as plotted in Step 5.2. For example, the comparisons between the measured and predicted trends in drag, shock position, shock strength and trailing edge pressure may appear as shown diagrammatically in Figs 11a-d. If the results were as shown in Fig 13, all these pictures would give a clear idea of  $R_{crit}$  (from a Reynolds number sweep) or effective  $R_{crit}$  (from a transition sweep) but, in practice, they will not be as clear; the sudden discontinuities in slope at  $R_{crit}$  will, in practice, be smeared over a range of Reynolds number and, on many wings, the rear separation is likely to disappear at different values of  $R_{crit}$  at different stations along the span. Experience suggests that the shock position and drag pictures in Fig 13 will provide the best guidance; probably, the trailing edge pressure picture will be the least reliable because of the difficulties in predicting the values accurately.

If  $R_{crit}$  occurs within the test range, confirmation that the value of  $R_{crit}$  has been derived correctly, can be obtained by a study of the 'Pearcey plots' (Fig 5) discussed earlier and the trends (ix) above, which have probably been obtained, in part at least, from the Pearcey plots. In theory,  $R_{crit}$  can depend on both  $C_L$  and Mach number but on some recent wing designs - and this may be a foretaste for the future - there appears to be a tendency for  $R_{crit}$  to vary little with  $C_L$ . Also, the position of the rear separation, when it occurs, appears to vary little with  $C_L$ .

If the data from the Reynolds number and transition sweeps appear to indicate different values for  $R_{crit}$  and effective  $R_{crit}$ , this would suggest that the zero-order simulation criterion is inadequate in this context. As explained in §3.2.1, it is difficult to find a simulation criterion specifically tuned to rear-separation prediction but if, as suggested above, this separation tends to occur at a certain chordwise position, it is possible that the value of  $H$ , the boundary layer shape factor, derived from the calculated pressure distribution, for a position just upstream of where the flow is observed to separate in the tests, would be a suitable criterion. In other words, the values of effective Reynolds number would then be based on the requirement that the calculated values of  $H$  at the appropriate chordwise position are the same for (test  $x_T$ , test  $R$ ) and for (flight  $x_T$ , flight  $R$ ). This suggestion may be an unjustified refinement of the practice of calculating  $H$  at a position one boundary layer displacement thickness ahead of the trailing edge - a practice that appears to have been used with some success in the UK. It should be noted that, in applying these ideas,  $R_{crit}$  should always be approached in the calculations from attached flow conditions, ie from  $R > R_{crit}$ . Other simulation criteria are discussed later in Step 5.5.

#### STEP 5.4: Identification of simulation scenario

The five possible simulation scenarios were introduced earlier in the description of Step 2. To reiterate for convenience:

- Scenario 1 :  $R_{crit} < R_{flight}$  and  $R_{flight}$  within test range of  $R$  (in a Reynolds number sweep) or effective  $R$  (in a transition sweep)
- Scenario 2 : As 1 but  $R_{crit} > R_{flight}$
- Scenario 3 :  $R_{crit} < R_{flight}$ ,  $R_{crit}$  within test range but  $R_{flight}$  beyond test range
- Scenario 4 :  $R_{crit} < R_{flight}$  and both  $R_{crit}$  and  $R_{flight}$  beyond test range
- Scenario 5 : As 4 but  $R_{crit} > R_{flight}$

The scenarios differ therefore in whether  $R_{crit} < R_{flight}$  or  $R_{crit} > R_{flight}$  and in whether  $R_{crit}$  and  $R_{flight}$  lie within or outside the model test range of  $R$  or effective  $R$ . The problems regarding the prediction of  $R_{crit}$  have already been discussed in Step 5.3 and so the new issue is whether the test range includes  $R_{flight}$ . Clearly, it is only on rare occasions that a Reynolds number sweep will include  $R_{flight}$  (this is indeed the reason for the present study) but the ideal aim of the boundary layer manipulation approach is to bring  $R_{flight}$  within the test range of effective  $R$ , ie to achieve scenario 1 (or 2). If this cannot be achieved, the next hope is that  $R_{crit}$  has been brought within the test range, ie scenario 3; failing this, one has to accept that the tests are in scenario 4 or 5 and that the uncertainties in the extrapolation to full scale are necessarily greater. All the evidence needed to identify which scenario applies has been assembled in Steps 5.2 and 5.3 - provided that one can rely on the conversion from transition position to effective  $R$ , being based on the zero-level criterion. If the test engineer then finds that the tests are in scenarios 1, 2 or 3 by a sizeable margin, this should be sufficient to proceed to the extrapolation in Step 6, but if it appears that the tests are in scenarios 4 or 5 (or even in 3 if the identification appears marginal or open to doubt), one should proceed to Step 5.5 and consider whether the data would be in a different scenario if a different simulation criterion were used in the derivation of  $R_{eff}$ .

#### STEP 5.5: Effect of choice of simulation criterion

By definition, at an effective  $R = R_{flight}$ , one should have eliminated the sources of major scale effect by manipulating the boundary layer to obtain a good simulation of the full scale viscous flow behaviour. However, as noted earlier, the zero-level simulation criterion, which was selected merely on the grounds of convenience and simplicity, is unaware of the wing geometry and the actual pressure



distribution over the wing. This criterion may therefore fail to be sufficiently accurate for the difficult and uncertain cases identified at the end of Step 5.4.

The scale effects that have to be eliminated if possible can be of two types:

- (i) 'direct' effects - the response of the boundary layer (and wake) development to a given pressure distribution,
- (ii) 'indirect' effects - the response of a pressure distribution to changes in the boundary layer development.

The broad aim of the boundary layer manipulation approach is to obtain a better simulation of (i) and thus, hopefully, also attain simulation in respect of the indirect effects (ii). Success can be judged by means of the various simulation criteria proposed in §3.2.1.

- (a) shock position
- (b) shock strength
- (c) the non-dimensional boundary layer momentum thickness at wing trailing edge
- (d) the non-dimensional length of shock-induced separation bubble
- (e) the boundary layer shape factor at a position close to the trailing edge on the upper surface or at any other position where separations are anticipated.

For perfect simulation, all these criteria should be satisfied but, in practice, employing the transition-sweep approach, this is unlikely to be achieved. This can cause difficulties but they should not be exaggerated. One should remember that the realistic aim is not to achieve complete simulation in all respects; rather, it is to produce a set of experimental data that can be extrapolated reliably to full scale conditions. Even if it is possible to obtain effective  $R = R_{flight}$  in the range of the model tests, some extrapolation of the data is always required (except in the trivial case where it has been possible to test with  $x_{T,flight}$ ,  $R_{flight}$ ). The aim should be to start the extrapolation from a datum condition that either minimises the corrections to be applied in the extrapolation phase (Step 6) or, at least, improves the reliability of these corrections. One should therefore choose the simulation criterion(s) that appear to be most relevant to the quantity being extrapolated. (a,b) are major features of the pressure distribution; if these are simulated correctly, the indirect scale effects will be minimised. (c,d,e) are local criteria and if these are simulated, some specific direct effects are minimised. (a,b,c) are relevant to the extrapolation of drag, lift-curve slope and pitching moment; (d) to the prediction of the full scale buffet-onset boundary and (e) to the existence of a rear separation as already discussed in Step 5.3.

To obtain the best results from applying the simulation methodology, the test engineer is strongly advised to consider these other criteria for all cases other than those for which it has been possible to decide conclusively in Step 5.4 that the results lie in scenarios 1 or 3. To comment on each of criteria (a-d):

#### (a) Shock position

Most of the available literature suggests that shock position should be the most important and suitable criterion. Clearly, lack of agreement in shock position between model and full scale can have a large effect on drag, lift and pitching moment data. However, experience suggests that when there are appreciable differences in shock position, this is due to the fact that the model tests are being made at an effective Reynolds number lying below  $R_{crit}$ . Above  $R_{crit}$ , the changes in shock position at a given  $C_L$  with Reynolds number or effective Reynolds number (ie transition position) may often be relatively small and not necessarily in a monotonic direction. Shock position is therefore an excellent parameter to choose when seeking guidance as to whether the tests are being made at  $R < R_{crit}$  or not but it may not be a good simulation criterion because of its relative insensitivity above  $R_{crit}$ . The computed trends in shock position with Reynolds number, as plotted in Step 5.2, will indicate whether it is worth considering shock position as a simulation criterion; where this appears appropriate, the picture for shock position should be replotted against a new effective Reynolds number, defined on the basis that according to the CFD calculations, the shock position is predicted to be the same for (test  $x_T$ , test  $R$ ) as for (forward forecast flight  $x_T$ , effective Reynolds number). This graph will provide a 'second opinion' on which is the appropriate simulation scenario and on whether the measured and predicted trends appear to come into agreement at a value of  $R_{crit}$  that is plausible in the light of all the other evidence.

#### (b) Shock strength

The effects of Reynolds number or transition position on the shock strength, as predicted by the CFD calculations, allowing only for the weak viscous-inviscid interactions, are likely to be clearer (ie in general, monotonic, in the sense that an increase in Reynolds number or aft movement of transition will reduce the shock strength for a given  $C_L$  and Mach number as a result of the extra rear loading), than for shock position. Although lack of simulation in shock strength may often, at first sight, appear less dramatic than lack of simulation in shock position, the effects of a lack in simulation in shock strength may be much more powerful. Shock strength is, for example, a primary variable, both when considering drag creep and also, the length of a shock-induced separation bubble and hence, buffet onset. Shock strength may therefore be a very suitable criterion to use in practice. Once again, the trends plotted in Step 5.2 should be replotted against a new effective Reynolds number using shock strength as the criterion and this provides a 'third opinion'.

#### (c) Non-dimensional boundary layer momentum thickness at trailing edge, $\theta_{TE}$

This is an obvious extension from the zero-level criterion and could be a suitable criterion for the wing lower surface, where there is unlikely to be any shock wave at the conditions identified in Step 1 or on the upper surface where the flow is subcritical or merely contains a large isentropic

recompression.  $\theta_{TE}$  is in fact an appropriate criterion irrespective of whether the flow is subcritical or supercritical because it is the most relevant parameter for assessing the viscous conditions at the trailing edge and hence, the overall circulation, and thus, the shock strength and position. It is, of course, unlikely that  $\theta_{TE}$  will have been measured in the model tests and so one can merely use  $\theta_{TE}$  in an analogous manner to the other criteria as a means of converting the transition position to an effective Reynolds number. In principle, one could perhaps create a 'measured trend' by calculating  $\theta_{TE}$  from the measured pressure distribution, but such calculations would only be meaningful above  $R_{crit}$  and the effort hardly seems worthwhile in a standard routine methodology, where there is no attempt to include strong viscous-inviscid interactions in the calculations.

As noted earlier in the description of Step 4, the flow over the lower surface, although often less important in the present context, cannot be ignored. The need to consider both surfaces brings certain difficulties. First, the range of transition positions that can be covered in the model tests at a given  $C_L$  and Mach number is unlikely to be the same for the two surfaces. Second, even if tests at the same (aft), transition position have been possible, the corresponding effective Reynolds number is liable to be different - unless the zero-order simulation criterion has been used. Superficially, it may seem attractive to test with different transition positions on the two surfaces such that, according to the chosen simulation criterion, eg  $\theta$  on the two surfaces at or near the trailing edge, the two values of  $R_{eff}$  are the same. This would however be a very laborious procedure to apply in practice. The relative transition positions needed to achieve this identity are likely to vary with  $C_L$ . A better procedure would be:

- (i) convert to an effective Reynolds number using whatever is the favoured simulation criterion for the upper surface and establish trends for a given transition position on the lower surface - and preferably, the furthest aft transition position. These trends will form the basis of the first-order corrections deduced in the extrapolation procedure in Step 6,
- (ii) deduce second-order corrections by plotting trends, for a given transition position on the upper surface and preferably furthest aft transition position, ie highest possible test  $R_{eff}$  for the upper surface, against an effective (lower surface)  $R_{eff}$  derived by using  $\theta_{TE}$  for the lower surface as a simulation criterion.

It should be possible to apply this procedure successfully when both surfaces are in scenarios 1 or 3, ie  $R_{crit}$  within the test range of effective Reynolds number. If a flow separation is still present on the lower surface at  $R_{eff} > R_{crit}$  on the upper surface, there must be some additional uncertainty in the correction procedure. In really difficult cases, this uncertainty could possibly be assessed by deriving the first-order corrections (i) above from the data with two alternative transition positions on the lower surface and comparing the results.

#### (d) Non-dimensional shock-induced separation bubble length

This is a relevant simulation criterion when considering buffet-onset. In general, with the high-aspect-ratio wings of most subsonic transports, buffet onset at high subsonic speeds occurs when the shock-induced separation bubble extends back to the wing trailing edge over a significant part of the span. Scale effect on the bubble length comprises:

- (i) an indirect effect - the effect of Reynolds number on the shock strength at a given  $C_L$  and Mach number, and
  - (ii) a direct effect - the effect of Reynolds number on the bubble length for a given shock strength and pressure distribution ahead of the shock.
- (i) has already been addressed when considering shock strength as a simulation criterion and so to obtain a further independent assessment of how to convert from transition position to an effective Reynolds number, one should consider (ii), ie the bubble length ( $\vartheta_B$ ) for a given shock strength ( $M_s$ ). Prediction methods for  $\vartheta_B$  are discussed in §2.5 and noted in §3.2.4. One favoured method at the present time (1987) is that due to Fulker and Ashill<sup>5</sup> who use a relationship of the form

$$\vartheta_B/\theta_s = F(M_s, R_{\theta_s})$$

where  $\theta$  = boundary layer momentum thickness  
and the suffix 's' relates to conditions immediately upstream of the shock.

The increases of  $\vartheta_B$  with  $M_s$  as observed in the measured results in the  $C_L$ -range between separation-onset and buffet-onset at various free-stream Mach numbers have already been plotted in Step 5.2. These results can be cross-plotted to provide 'measured trends' in  $\vartheta_B$  with transition position converted to an effective Reynolds number on the usual basis, viz that according to the CFD calculations of the pressure distributions and boundary layer development and the chosen prediction method for  $\vartheta_B$ , the bubble length is the same for (test  $x_T$ , test R) and for (forecast flight  $x_T$ , effective R). As with the previous simulation criteria, these measured trends should be compared with computed trends based on the calculated pressure distributions and boundary layer development. In this case, however, any serious disagreement between the measured and computed trends does not necessarily indicate that the test effective Reynolds numbers lie below  $R_{crit}$ . There are at least three possible explanations for any serious discrepancy, viz

- (a) the measured and computed pressure distributions ahead of the shock and, hence, the values of  $\theta_s$  and  $R_{\theta_s}$  are different,
- (b) the chosen prediction method for  $\vartheta_B$  does not apply for the particular pressure distribution/wing design, or

- (c) the test effective Reynolds numbers are genuinely below  $R_{crit}$  and there is an interaction between a rear separation and the growth of the shock-induced separation bubble (this can occur if the shock is relatively far aft but it does not necessarily occur in every case when the two separations are present).

A study of the measured pressure distributions should show which of (a,b,c) applies in any particular case. Further evidence is obtained from a correlation of the measured buffet-onset boundaries and the development of the bubble. The analysis<sup>5</sup> of Fulker and Ashill suggests that buffet onset should

#### STEP 6: Extrapolation of data to full scale

Complete viscous simulation is unlikely to be achieved in the actual tests and hence, extrapolation of the data to full scale conditions is a vital element in the complete simulation methodology. Extrapolation is needed even when, by use of the boundary layer manipulation approach, the results have been brought within scenario 1. This is because the value of the effective test Reynolds number, ie the transition position that corresponds with  $R_{flight}$  is likely to depend on which simulation criterion is being applied and so, no set of data is a perfect simulation in all respects. The only real exception to this general statement is provided by the case where it has been possible to extend a Reynolds number sweep far enough to include  $R_{flight}$  but, as noted earlier, this is an unlikely eventuality.

The general rule is that the measured trends should be extrapolated if necessary to  $R_{crit}$  and then, one should rely on the computed trends from  $R_{crit}$  to  $R_{flight}$ . The precise procedure will depend on which simulation scenario is applicable and the description below begins with some general remarks as to how to proceed in each scenario. The procedure is then set out in more detail for leading test objectives for a subsonic transport such as cruise drag and buffet onset and then, finally, extrapolation of other aspects of the results are discussed more briefly.

#### STEP 6.1 General procedure

##### (i) Scenario 1 (boundary layer manipulation approach)

Convert the transition position to an effective Reynolds number using what appears to be the most relevant and suitable simulation criterion for the quantity to be extrapolated and find what transition position leads to  $R_{eff} = R_{flight}$ . The measured results (interpolated if necessary) for this transition position form the starting point for the extrapolation which is needed even in this case. As already noted, full simulation will not necessarily have been achieved at  $R_{eff} = R_{flight}$ . Even if there is full simulation of all the major features of the pressure distribution, it would be a coincidence if the skin friction drag were the same at  $(x_T, R)_{test}$  and  $(x_T, R)_{flight}$ . This extrapolation is achieved by use of the following equation:

$$X_1 \text{ at } (x_T, R)_{flight} = \text{Measured } X \text{ at } (x_T, R)_{test,1} + \text{Computed } (X \text{ at } (x_T, R)_{flight} - X \text{ at } (x_T, R)_{test,1}) \quad (6.1)$$

where  $X_1$  = extrapolated value using procedure for scenario 1 and the suffix test,1 indicates that  $x_T$  has been chosen in the appropriate manner for scenario 1, ie  $x_T$  to give  $R_{eff} = R_{flight}$ .

It is worth noting that, although the conversion to  $R_{eff}$  has been used in identifying that the results are in scenario 1 and in defining the starting point for the extrapolation, the final extrapolated result  $X_1$  does not depend on whether the conversion has been accurate or not.

##### (ii) Scenario 2

This is similar to scenario 1 in the sense that the test range of  $R$  or  $R_{eff}$  is sufficient to cover  $R_{flight}$  but the extrapolation, if, as is likely, the data have been obtained by the boundary layer manipulation approach, is more difficult and uncertain because  $R_{crit}$  is forecast to be higher than  $R_{flight}$ . To assume that one can use exactly the same procedure as in scenario 1, is effectively equivalent to assuming that the consequences of the rear separation (or whatever is the strong viscous-inviscid interaction that is present at  $R < R_{crit}$ ) are the same at  $(x_T, R)_{test}$  for  $R_{eff} = R_{flight}$  as at  $(x_T, R)_{flight}$ . The only clue readily available to the test engineer as to whether it is safe to act on this assumption is provided by a comparison of the values of  $R_{crit}$

- (i) as deduced from the CFD calculations for various Reynolds numbers with  $x_{T,flight}$ , and
- (ii) as deduced either from the CFD calculations for various transition positions at  $R_{test}$  converted to  $R_{eff}$  by the chosen simulation criterion or from the study in Step 5.3 of the measured trends.

For convenience, in the later discussion and in Fig 16, the second value (ii) is described as the "effective  $R_{crit}$ ", this description implying that  $R_{crit}$  has been derived from a study of trends plotted against  $R_{eff}$ .

These two values of  $R_{crit}$  should, in theory, be the same but if this is achieved in practice, it would be a striking vindication of the choice of simulation criterion and hence, one needs a methodology that will cope both for cases (situation 1, Fig 16) where this agreement is achieved and for cases where it is not (situations 2 and 3, Fig 16). It should be stressed that the methodology as written below (and similarly, the methodology for scenarios 4 and 5) has been devised as a response to this challenge but it is not yet (1987) supported by practical experience. It is hoped that it will be used in the future and refined or modified later in the light of experience.

If the two values of  $R_{crit}$  obtained from (i,ii) are in reasonable agreement (situation 1, Fig 16), it is appropriate to continue to use the extrapolation procedure proposed for scenario 1. If, however, the values of  $R_{crit}$  and effective  $R_{crit}$  differ substantially (thus implying that the chosen simulation criterion is not successful in resolving issues regarding the rear separation), a different procedure is needed. In an extreme case (situation 2, Fig 16), one might find that, whereas the measured

results may suggest that at  $R_{eff} = R_{flight}$ ,  $R_{eff} < R_{crit}$ , the CFD results may suggest that with the forecast flight  $x_T$ ,  $R_{flight} > R_{crit}$ . The appropriate procedure for this case is

$$X_2 \text{ at } (x_T, R)_{flight} = \text{Measured } X \text{ at } (x_T, R)_{test,2} + \text{Computed } (X \text{ at } (x_T, R)_{flight} - X \text{ at } (x_T, R)_{test,2}) \quad (6.2a)$$

where the suffix '2' indicates that  $x_T$  chosen to give  $R_{eff} = R_{crit}$  (as deduced from the measured data).

This is an unusual example of the general rule that one should accept measured data up to  $R_{crit}$  and then extrapolate from  $R_{crit}$  to  $R_{flight}$  according to the computed trends - unusual in the sense that, in this case, the 'extrapolation' is to a lower Reynolds number. The aim of this procedure is to eliminate the effects of the rear separation present in the measured results at  $R_{eff} = R_{flight}$ , the argument for removing them being based on the fact that, according to (i), no rear separation should be present at  $(x_T, R)_{flight}$ .

In the general case (situation 3, Fig 16), where effective  $R_{crit} \neq R_{crit}$  and where both are higher than  $R_{flight}$ , it is possible that an acceptable procedure is to calculate both  $X_1$  and  $X_2$  and then to link them by an equation which, on the simplest basis, would take the form

$$X_{1/2} = k X_1 + (1 - k) X_2 \quad (6.2b)$$

$$\text{where } k = \frac{R_{crit} - R_{flight}}{\text{Effective } R_{crit} - R_{flight}}$$

Note: This equation is proposed in the expectation that, in general,  $R_{crit} < \text{Effective } R_{crit}$  but, if future experience shows that  $R_{crit}$  can be higher than effective  $R_{crit}$ , this proposal may have to be recast.

This equation effectively assumes that, as in the diagrammatic presentation in Fig 16, the measured trend in  $X$  below  $R_{crit}$  is linear. In practice, this is unlikely to be true, i.e.  $R_{crit}$  will not mark an abrupt discontinuity in slope; the form of the equation for  $X_{1/2}$  will then have to be changed in sympathy with the shape of the measured trend.

It is therefore possible to propose a procedure for scenario 2 but the uncertainty in the results will remain because

- (i) for all three cases listed above, the assumption is made that, whatever approach is successful in reconciling the effects of transition and Reynolds number on the occurrence or not of the strong viscous-inviscid interaction, is equally successful in reconciling the effects of this interaction - an unproven assertion, and
- (ii) the procedure for  $X_{1/2}$ , in particular, depends on the CFD predictions of  $R_{crit}$  but, as noted in §3.2.4, this task is far from easy at the present time.

Fortunately, the customer will, in general, not demand the same high standard of accuracy in the extrapolated results if they lie in scenario 2 as in scenarios 1 or 3 but one should not dismiss scenario 2 as being of no practical interest. The designer may be prepared to accept a wing design for which, even in the cruise condition, there is a limited rear separation over part of the span. However, in the relatively near future, routine CFD calculations may be able to handle such situations and then, some of the difficulties implied in the above procedure for scenario 2 will fade away.

### (iii) Scenario 3

Extrapolation in scenario 3 is virtually as simple as in scenario 1 despite the fact that  $R_{eff} = R_{flight}$  appears to lie outside the test range. It is much easier than in scenario 2 because the test range extends beyond  $R_{crit}$  and so, the extrapolation procedure can be closely similar to that employed in scenario 1, viz

$$X_3 = \text{Measured } X \text{ at } (x_T, R)_{test,3} + \text{Computed } (X \text{ at } (x_T, R)_{flight} - X \text{ at } (x_T, R)_{test,3}) \quad (6.3)$$

where suffix 3 indicates that  $x_T$  chosen to give  $R_{eff} = R_{crit}$ .

Again, as with scenario 1, it is worth noting that the final value  $X_3$  does not depend on the accuracy of the conversion to  $R_{eff}$ .

### (iv) Scenario 4

Extrapolation in scenario 4 is significantly more difficult: both  $R_{crit}$  and effective  $R = R_{flight}$  lie outside the test range and while it is easy to say that the measured trends should be extrapolated to  $R_{crit}$  and then, one should follow the computed trends from  $R_{crit}$  to  $R_{flight}$ , this may be difficult to achieve in practice to the required accuracy.

If the data have been obtained in a Reynolds number sweep, the main difficulty lies in the possibly gross extrapolation required in the measured trends if  $R_{crit} \gg \text{maximum } R_{test}$ . At least, in this case, there will not be the same uncertainty in the value of  $R_{crit}$  that is present in the boundary layer manipulation approach but one still has to allow, to the best of one's ability, for the measured trends to come into line with a curve parallel to the computed trends over a range of Reynolds number outside the test range. The equation for the extrapolation in this case (Reynolds number sweep) is



$X_4 = \text{Extrapolated measured } X \text{ at } R = R_{\text{crit}}$

+ Computed ( $X \text{ at } R_{\text{flight}} - X \text{ at } R_{\text{crit}}$ )

(6.4a)

If the data have been obtained by the boundary layer manipulation approach, the extrapolation of the measured trends is more difficult because one is extrapolating into a range that does not exist correlate with when the bubble has extended back to near a point  $R$  corresponding to the start of the final steep pressure-rise to the trailing edge. In other words, the further extension of the bubble beyond  $R$  to the trailing edge occurs suddenly. This conclusion is supported by a fair amount of experimental evidence but has really only been validated for a fairly limited class of pressure distributions containing an identifiable point  $R$  some distance downstream of the shock (see Ref 5 for certain qualifications of this statement). If the measured data for the test wing do not support the conclusion and if there is a significant discrepancy between the measured and computed trends, it is likely that either (b) or (c) is the explanation and then, reference to the conclusions based on the other criteria will help to decide between (b) and (c). It is important to establish whether or not the prediction method for  $R_B$  applies: when it does, the method can be used in Step 6 for the extrapolation to full scale.

Use of  $R_B$  as a simulation criterion is very useful, in the context of prediction of buffet onset, in establishing whether the test range of transition positions includes a position for which the effective Reynolds number =  $R_{\text{flight}}$  and, if so, what transition position provides this simulation. In other words, it is a means of deciding whether, in this particular context, the tests are in scenario 1 (or 2) or, on the other hand, whether they are in scenarios 3, 4 (or 5); it may not help greatly in resolving an uncertainty between scenarios 3 and 4 because, as noted in the previous paragraph, it is not immediately obvious as to whether a divergence between the measured and computed trends implies that  $R_{\text{eff}} < R_{\text{crit}}$ .

#### STEP 5.6: Identification of cases where extrapolation in Step 6 may be judged unnecessary

It was emphasised in the introduction to §3.3.1 that one should not adopt short cuts in applying the methodology and that each new configuration should be treated on its merits. Nevertheless, there will be occasions where one is merely seeking to compare two very similar designs or to determine the increments due to a change in configuration not expected to affect the standard of viscous simulation in the tests. There will therefore be occasions when there is a natural hope that one can use the measured test data without having to implement the extrapolation procedure in Step 6 below. This short cut should however only be adopted when

- (i) one is only interested in comparative or incremental data.
- (ii) the test data are in simulation scenarios 1 or 3, ie maximum test effective  $R > R_{\text{crit}}$ ,
- (iii) if they are in scenario 3, the extrapolation of the range to cover  $R_{\text{flight}}$  is relatively trivial so that one either knows or at least can assume that the likely changes in the results in this range are similar for the two configurations being compared.

Even when it is permissible to omit Step 6, the procedure is not entirely straightforward. It will be easier if one can rest content with the data obtained with the furthest aft transition position of the tests (if in scenario 3) or for the transition position giving  $R_{\text{eff}} = R_{\text{flight}}$  (scenario 1), ie with the data contained in the  $C_L - M$  corridor between the two limits of test validity discussed earlier and illustrated in Fig 11. If data are required over a wider range of Mach number (or  $C_L$ ), care has to be taken in patching together the data from the several tests with different transition trips. For example,

- (i) in creating  $C_D - M$  curves at constant  $C_L$  over the full flight envelope, one has to allow for the changes in skin friction due to the different extents of laminar flow. Strictly, one should apply corrections based on the values of  $C_{D_V}$ , viscous drag derived from the CFD calculations,
- (ii) the buffet-onset boundary should be taken as the envelope of the boundaries obtained with say, the forward, mid and rear trips - see Fig 14,
- (iii) the spurious effects on  $C_L$  and  $C_m$  immediately beyond the upper limit of validity for any particular aft trip should be ignored. In the real, full scale flow, the shock wave will move progressively forward with increase in incidence and would not exhibit the hesitation behind the trip. The only advice that can be offered on this point (and there will be nothing better in Step 6) is to fair from the  $C_L$  and  $C_m$  data with the aft trip to the data obtained with the mid trip and then, beyond the limit of validity of the mid band, to fair to the data with the forward trip. Tests<sup>6</sup> on half models over a wide range of Reynolds number in the RAE 8 ft x 8 ft tunnel provide some support for this apparently rash procedure as illustrated in Fig 15.

One particularly important point to remember is that when comparing results for two wing designs, for which a further aft trip has to be used on the later, more advanced wing B to achieve a model test effective Reynolds number greater than  $R_{\text{crit}}$ , ie scenario 3 rather than scenario 4, than for the earlier wing A, but one cannot test wing A with this further aft trip (possibly because the shock wave on A is not sufficiently far aft), one must compare the results with the different transition positions and include a correction for the change in  $C_{D_V}$  due to the different extent of laminar flow; similarly, changes in lift-curve slope due to the different extents of laminar flow should be allowed for when deriving the buffet boundary. This is likely to be a much more accurate procedure than using the results for the same transition position for which the data for wing B could include an uncertain increase in  $C_D$  due to the effects of a rear separation or whatever strong, viscous-inviscid interaction that is leading to the conclusion that  $R_{\text{eff}} < R_{\text{crit}}$ .

It must be reiterated that to obtain, in particular, the drag data to the required accuracy, one should use the complete methodology including Step 6. Step 5.6 should only be substituted when there are severe constraints in timescale and/or cost. It is hoped that, in the future, it will become accepted practice, even in routine testing, to accept the need for extrapolation and for the confidence in the CFD methods to grow so that they can be accepted with assurance for this purpose. Physically - transition positions aft of the shock would not be possible in practice and, even if they were, the data could not be regarded as a simulation of full scale at any Reynolds number. A possible unproven procedure was put forward in §3.2.1. Setting this procedure out again in the context of a subsonic transport (note: many of the actions will have already been undertaken in earlier steps):

- plot the measured and predicted computed variation in any parameters sensitive to the presence of a rear separation against transition position (note: transition position rather than  $R_{eff}$ ). Suitable parameters would be shock strength, shock position, drag and possibly  $C_{PTE}$
- if possible, then plot the differences between the measured and computed trends, i.e. plot  $\Delta X_s$ ,  $\Delta C_D$  and  $\Delta C_{PTE}$  against transition position,
- estimate the values of  $R_{crit}$  for the different transition positions and plot against transition position. This sounds simple but there will again be possible difficulties as with scenario 2 due to the fact that different approaches to the prediction of  $R_{crit}$  may not yield the same values,
- extrapolate the curves in (c) without regard to the fact that one would not be able to test with a further aft transition position; extrapolate until  $R_{crit} = R_{test}$
- extrapolate the curves in (b) by a similar amount to that found necessary in (d) and hopefully, these curves of  $\Delta X_s$ ,  $\Delta X_s$ ,  $\Delta C_D$  and  $\Delta C_{PTE}$  will reach an asymptote (generally, a non-zero asymptote) at the end of this extrapolation,
- there are then two possible approaches: either use the relation

$$X_4 = \text{Asymptotic value of } \Delta X + \text{Computed } X \text{ at } (x_T, R)_{flight} \quad (6.4b)$$

or perhaps with more certainty, the relation

$$\begin{aligned} X_4 = & \text{Measured } X \text{ at } (x_T, R)_{test, 4} \\ & + (\Delta X_{asymptote} - \Delta X_{furtherst \text{ aft } x_T}) \\ & + \text{Computed } (X \text{ at } (x_T, R)_{flight} - X \text{ at } (x_T, R)_{test, 4}) \end{aligned} \quad (6.4c)$$

where suffix 4 indicates further aft  $x_T$  in test.

#### (v) Scenario 5

This brings together the problems of scenarios 2 and 4 and is even more difficult because, probably, a considerable extrapolation of the measured trends is now needed to reach  $R_{crit}$ . There is probably little point in the boundary layer manipulation approach of including any refinement beyond the zero-level criterion, extrapolating the measured trends to the forecast  $R_{crit}$  and  $x_{Tflight}$  and using a modified form of the second of the relations above in (iv,f) for the final extrapolation, i.e.

$$\begin{aligned} X_5 = & \text{Measured } X \text{ at } (x_T, R)_{test, 5} \\ & + \text{Extrapolated measured } (X \text{ at } R_{crit} - X \text{ at furthest aft } x_T) \\ & + \text{Computed } (X \text{ at } (x_T, R)_{flight} - X \text{ at } (x_{Tfurthest \text{ aft}}, R)_{test}) \end{aligned} \quad (6.5)$$

where suffix 5 indicates furthest aft  $x_T$  in test range.

Fortunately, customers would not expect or require close accuracy from results in scenario 5.

This description of the general extrapolation procedure for the different scenarios illustrates why it is highly desirable to perform an extended Reynolds number sweep or to adopt the boundary layer manipulation approach to bring the data into either scenario 1 or scenario 3. To achieve scenario 3 rather than 4, i.e. to bring  $R_{crit}$  within the test range, is a more important aim than striving for complete viscous simulation in the tests, which is probably unattainable.

### STEP 6.2: Extrapolation of specific leading test objectives

#### (a) Cruise drag

The measured values of  $C_D$  at the operational cruise/design conditions identified in Step 1 were plotted against Reynolds number (from the Reynolds number sweeps) or effective Reynolds number (from the transition sweeps) in Step 5.2. At that stage, the zero-level simulation criterion was being used for the conversion to effective Reynolds number, but the plots for shock position and shock strength, with these parameters chosen as simulation criteria, are also highly relevant to the prediction of full scale cruise drag for conditions where there is supercritical flow over the wing upper surface. These graphs of shock position and shock strength are likely to provide the best indication of whether  $R_{eff} = R_{flight}$  in the model test range but the  $C_D$  graphs themselves, possibly replotted against  $R_{eff}$  obtained through the use of one of these other criteria, may give the clearest idea of  $R_{crit}$  as deduced from the measured results. These graphs may be sufficient to identify which simulation

scenario applies in the context of cruise drag and then, the full scale drag can be obtained by applying the relevant procedure and relations from Step 6.1 and by adding some additional corrections, viz

$$C_{Dflight} = \text{Measured } C_D \text{ at } (x_T, R)_{test, n} \\ + \text{Extrapolated measured trend in excess } C_D \text{ between } (x_T, R)_{test, n} \text{ and } R_{crit} \\ + \text{Computed } \{C_D \text{ at } (x_T, R)_{flight} - C_D \text{ at } (x_T, R)_{test, n}\} \\ - \Delta_{TR} C_D + \Delta_E C_D$$

where

- (i) the suffix 'n' indicates the scenario,
- (ii) the second term only exists for scenarios 4 and 5,
- (iii) the words 'excess drag' are used to describe the extra drag associated with the strong viscous-inviscid interaction present at  $R < R_{crit}$  and determined in principle as described in Step 6.1. The variation of this excess drag with Reynolds number will also, in practice, include the scale effect on the drag contribution due to any local separation, eg in a wing-body junction or a wing-pylon junction in a wing-mounted propulsion installation,
- (iv) the values of  $(x_T, R)_{test}$  that are used as the starting point for the extrapolation are given below:

Scenario	Reynolds number sweep	Transition sweep
1	$R_{flight}$	$x_T$ to give $R_{eff} = R_{flight}$
2,3	$R_{crit}$	$x_T$ to give $R_{eff} = R_{crit}$
4,5	Highest test R	Furthest aft $(x_T)_{test}$

- (v) the calculation of the third term can be performed most accurately by splitting  $C_D$  into three component terms

$$C_D = C_{DW} + C_{DV} + C_{Di}$$

where  $C_{DW}$  = wave drag coefficient

$C_{DV}$  = viscous drag coefficient

$C_{Di}$  = vortex-induced drag coefficient

Methods for predicting  $C_{DW}$  and  $C_{DV}$  from the calculated pressure distributions are described in §3.2.4. Unless the maximum test R or the maximum effective R is far below  $R_{crit}$ , the change in  $C_{Di}$  in the extrapolation is unlikely to be large. The dominant contribution may well be the change in  $C_{DW}$  but this can be minimised (and hence, its accuracy improved) if the shock position and shock strength in the flow over the wing upper surface are similar at  $(x_T, R)_{flight}$  and  $(x_T, R)_{test, n}$ ; hence, the advantage of using these quantities as simulation criteria. It has been assumed throughout that the computed trends will be obtained by methods allowing merely for weak viscous-inviscid interactions; when the methods are capable of allowing for a limited rear separation, the accuracy of the procedure will be improved as in many cases, the values of  $R_{crit}$  will be lower, thus implying less uncertain extrapolation of the measured trends if the data are in scenario 4 (or 5),

- (vi) in the fourth term,  $\Delta_{TR} C_D$  is the estimated increase in  $C_D$  in the model tests due to the presence of the transition trip,
- (vii) in the fifth term,  $\Delta_E C_D$  is the estimated increase in  $C_{Dflight}$  due to the presence of roughness and excrescences on the full scale aircraft but not represented on the model,
- (xiii) the whole equation does not include any corrections for non-viscous related effects that may contribute to the extrapolation from model test to full scale, eg jet effects, intake spillage effects, aeroelastic effects etc. Also, one should stress that the procedure as described is concerned with the viscous effects in the flow over the wing; the viscous effects on the drag of the rear fuselage are considered separately in §3.3.3.

#### (b) Buffet onset

As noted under (d) in Step 5.5, buffet onset for most subsonic transports at high subsonic speeds occurs when the shock-induced separation bubble extends back to the wing trailing edge over a significant part of the span. Methods exist for predicting the growth of this bubble with increase in shock strength - see §4.6 and 3.2.4. The analysis in Step 3.5 will have shown whether the trends in the measured data are consistent with forecasts by one of these methods and, if not, whether this is due to:

- (i) an interaction between the bubble and some other strong viscous-inviscid interaction such as a rear separation present at  $R < R_{crit}$ , or
- (ii) a failure of the data to support the assumptions of the chosen prediction method.

The description in Step 5.5 used the method<sup>5</sup> of Fulkner and Ashill as an example of a prediction method. According to this approach, the bubble extends to the trailing edge when

$$M_s^* = F(R_{\theta_s}, \theta_s)$$

where  $M_s^*$  = shock strength on buffet-onset boundary,

$\theta_s$  = boundary layer momentum thickness immediately ahead of the shock,

$$\theta_s = \frac{\theta_s}{x_R - x_s}$$

and  $x_R$  is the chordwise position of the start of the final pressure-rise to the trailing edge.

If the measured data appear to be consistent with the fundamental assumptions of this method, a relatively simple approach to the extrapolation of the buffet-onset boundary to flight at full scale Reynolds numbers can be developed as follows:

- (i) choose an appropriate spanwise position to represent the 'significant part of the span' where the separation has extended from the foot of the shock to the trailing edge at buffet onset (this could vary with Mach number),
- (ii) for this station, the measured trends in  $M_S^*$  at a given Mach number which have already been plotted in Step 5.2 against Reynolds number (from the Reynolds number sweeps) or transition position (from the transition sweeps) should be compared with predicted trends based on the above relation, the values of  $R_\theta$  and  $\bar{\theta}_s$  derived from the measured data and the charts of Ref 5,
- (iii) in cases where there is reasonably close agreement between the measured and predicted trends, the values of  $M_S^*$  on the full scale buffet-onset boundary can be derived from the relation

$$M_S^* \text{ for } (x_T, R)_{\text{flight}} = \text{Measured } M_S^* \text{ for } (x_T, R)_{\text{test},6} + \text{Predicted } (M_S^* \text{ for } (x_T, R)_{\text{flight}} - M_S^* \text{ for } (x_T, R)_{\text{test},6}) \quad (6.6)$$

where the suffix 6 denotes the  $(x_T, R)_{\text{test}}$  which is found to give the closest approach to  $M_S^*$  for  $(x_T, R)_{\text{flight}}$ .

A zero value for the second term implies that, in this respect, full simulation has been achieved in the test with  $(x_T, R)_{\text{ig}}$ . Experience suggests that this may often be possible.

In cases where the trends are not in good agreement and where it is believed that this is because  $R_{\text{test}} < R_{\text{crit}}$ , one should use the extrapolation procedures described in Step 6.1 with the parameter  $M_S^*$  for buffet-onset used as the simulation criterion, ie for the conversion of transition position to effective Reynolds number. It should be noted that an interaction does not always occur between a shock-induced and a rear separation even when both are present; it is more likely to occur when the shock is relatively far aft when, if present, the interaction will probably reduce the value of  $M_S^*$  for a full separation from the foot of the shock to the trailing edge.

- (iv) the full scale  $C_L$  for buffet onset at a given Mach number can then be obtained through the relation

$$C_L \text{ for } (x_T, R)_{\text{flight}} = \text{Measured } C_L \text{ for } (x_T, R)_{\text{test},6 \text{ or } 7} + \Delta C_{L\text{indirect}} + \Delta C_{L\text{direct}} \quad (6.7)$$

where

- (a) when there is good agreement between the measured and predicted trends, use test,6 defined as above under (6.6),
- (b) when there is a serious interaction with a rear separation, use test,7 where the suffix 7 implies that the data have been taken not from the test that gives the closest approach to  $M_S^*$  for  $(x_T, R)_{\text{flight}}$  but from the test at either the highest test Reynolds number (in a Reynolds number sweep) or the highest effective Reynolds number (in a transition sweep). In practice, this may be found to be an academic distinction,
- (c)  $\Delta C_{L\text{indirect}}$  represents the indirect scale effect, ie the change in  $C_L$  for a given  $M_S$  between  $(x_T, R)_{\text{test},6 \text{ or } 7}$  and  $(x_T, R)_{\text{flight}}$ ,
- (d)  $\Delta C_{L\text{direct}}$  represents the direct scale effect, ie the change in  $C_L$  due to the change in  $M_S^*$  between  $(x_T, R)_{\text{test},6 \text{ or } 7}$  and  $(x_T, R)_{\text{flight}}$ .

In practice, it may often be possible to combine  $\Delta C_{L\text{indirect}}$  and  $\Delta C_{L\text{direct}}$  in a single term but it was felt preferable to set the procedure out in this form to emphasise that there are two separate effects.  $\Delta C_{L\text{indirect}}$  can be estimated with the aid of the plots created in Step 5.5 using shock strength as a simulation criterion;  $\Delta C_{L\text{direct}}$  can be obtained either from the CFD calculations for  $(x_T, R)_{\text{flight}}$  or probably to the required accuracy from the measured results, remembering that one should use the value of  $(dC_L/dM_S)$  immediately below the buffet-onset boundary.

Both  $\Delta C_{L\text{indirect}}$  and  $\Delta C_{L\text{direct}}$  are likely to be functions of Mach number. The total correction may only be of the order of 0.05 in  $C_L$  but, nevertheless, is sufficient to justify care in extrapolation.

### (c) Lift-curve slope

The values of lift-curve slope, particularly in the incidence range encompassing cruise and buffet onset, are frequently required for gust analysis. Clearly, these values could be extrapolated to full scale following the general guidance in Step 6.1 but this is an area where it may be unwise to break with past experience. The most important lesson from the past is that, if possible, there should be no change in transition position on either wing surface in the range of incidence over which one is taking the slope. Hence, the measured values should not be taken from a transition-free test or from a nominally transition-fixed test in which transition has moved forward (or aft) of the band over part of the incidence range in question. The normal practice is to test with the furthest aft transition

position that safely meets this requirement, then correct the values of lift-curve slope by standard data sheets for any difference in transition position between wing upper and lower surface and then, finally, to apply contingency factors based on past experience for the extrapolation to the full scale aircraft. This may sound very crude compared with the procedure proposed for cruise drag and buffet onset but before one could justify the use of a more refined technique, such a technique would have to be applied first to the data from the past on which present practices are based. The contingency factors mentioned above have to cover more than viscous effects, eg there may be significant aeroelastic effects: hence, to refine the extrapolation of the viscous effects and then to apply the same contingency factors would not necessarily improve the accuracy of the final results.

#### (d) Pitching moments

Failures to predict the full scale pitching moments have, in the past, provided the most embarrassing and well-publicised examples justifying the need for a more reliable simulation methodology. It is therefore clear that, whenever possible, one should extrapolate  $C_m$  in the manner proposed in Step 6.1, ie in a manner similar to that described in detail for cruise drag. It should be recognised however that this places an even greater demand on the accuracy of the CFD methods. A method for 2D flow will not, in general, be sufficient because the pitching moments for the 3D wing-body will depend on the spanwise loading and the spanwise variation of the sectional effects. Also, the method must be capable of allowing for at least weak viscous-inviscid interactions because the pitching moments are sensitive to the pressure distributions very close to the leading and trailing edges, ie the regions that depend greatly on the viscous effects. Nevertheless, use of existing CFD methods and the extrapolation procedures of Step 6.1 should be sufficient to avoid the gross errors of the past - at least in the  $C_L$  -  $M$  area up to buffet onset. These errors probably occurred because of a failure to simulate the shock position and a lack of recognition that the test data were in scenario 4, ie  $R_{test} < R_{crit}$ .

Prediction of the pitching moments beyond the upper boundary of the  $C_L$  -  $M$  corridor in which valid data can be obtained with the furthest aft trip is however far more difficult. This was discussed earlier in Step 5.6. As explained earlier, this boundary lies beyond buffet onset - see Fig 11, but the pitching moments can still be very important in the context of the wing structural loads. At the present time, it is not possible to suggest an extrapolation procedure involving the use of CFD in these extreme conditions - hence, the somewhat arbitrary procedure recommended in Step 5.6. However, another possibility for a subsonic transport with a wing of high aspect ratio would be to develop a methodology based on the analysis<sup>7</sup> of Khan and Cahill as described in §4.8 which has suggested that, for some wings at least,

- (i) the relation between shock position and trailing edge pressure in the presence of an extensive flow separation, is independent of  $(R, x_T)$ ,
- (ii) the shape of the variation of  $C_{p_{te}}$  with Mach number and incidence can be collapsed onto a single curve of  $C_{p_{te}}$  against a transonic similarity parameter,  $K$ , which depends on  $(R, x_T)$  through the inclusion of the local skin friction coefficient immediately ahead of the shock, and
- (iii) the location of this curve relative to the  $C_{p_{te}}$  and  $K$  axes can be forecast again as a function of  $(R, x_T)$ .

Evidence is needed on the success of this method when applied to a wide range of independent wing designs.

As noted earlier in Step 3, it is fairly general practice to use transition-free data for the values of  $C_{m_0}$  - at least up to the Mach number at which a shock-induced separation is present at  $C_L = 0$ . The justification for this practice is that with natural transition, the boundary layer thicknesses will be smaller than if any trip is present. Strictly, this justification is arguable unless it has been shown that the boundary layer thicknesses are similar to those on the full scale aircraft in flight. At the very least, calculations of the boundary layer development should be made so that the test engineer and the customer are aware of the implications of the established practice and whether these differ from one wing design to another.

#### (e) Spoiler/airbrake effectiveness and loads

Raising a spoiler acting as a lateral control or an airbrake is likely to lead to a marked forward movement of the shock and, as a result, it may be impossible to practise any boundary layer manipulation approach. Also, transition is liable to be invoked by the pressure-rise ahead of the spoiler and possibly at the wing leading edge on one of the surfaces. Testing with an aft trip may of course be possible with the spoiler closed but to retain this test as the datum for a series with different spoiler deflections may give misleading results at small spoiler deflections. The general recommendation must therefore be to perform all the spoiler tests including the datum at the maximum possible test Reynolds number with either a forward trip or, at the most, a mid trip as described in Step 4b. These tests will provide increments due to spoiler deflection, consistent from the standpoint of transition position but possibly still misleading at small spoiler angles, because the flow in the test with the spoiler closed does not simulate the full scale flow. It may therefore be preferable to link

- (a) the results for the spoiler closed extrapolated to  $(x_T, R)_{flight}$  as described earlier, and
- (b) the results for the spoilers deflected as measured in the tests.

No refined extrapolation technique can be justified, bearing in mind that

- (i) there can be large aeroelastic effects not represented in the model tests,
- (ii) these data do not have to be obtained to the same close accuracy as those discussed earlier.



### 3.3.1.3 Concluding Remarks

The detailed methodology as described here has been based on much past experience and an appreciation of how the advances in CFD can be exploited to place the methodology on a more scientific basis.

It is hoped that the methodology has been set out in a way that will stand the test of time; with experience, the detail may change but the general framework should remain. As noted at the end of §3.2.1, successful use of the methodology will depend on

- (i) good knowledge at all stages of the detailed flow over the test configuration,
- (ii) the ability to test over a wide range of either Reynolds number or effective Reynolds number,
- (iii) the realisation that each new wing design or configuration has to be treated on its merits, and
- (iv) short cuts should be avoided unless one is absolutely sure.

It is recommended that, to gain experience, the proposed methodology should be applied for a significant period in parallel with whatever is the established practice. Any large differences in the extrapolated results should be assessed to find whether the reasons justify departure from existing practice: in other words, the methodology that has been set out above should do better, being on a sound scientific basis, but it will still have to prove itself in the future.

### REFERENCES

- 1 Braslow, A L, Knox, E C, Simplified Method for Determination of Critical Height of Distributed Roughness Particles for Boundary-Layer Transition at Mach Numbers from 0 to 5, 1958, Langley Aeronautical Laboratory NACA TN 4363.
- 2 Pearcey, H H, Osborne, J, Haines, A B, The Interaction Between Local Effects at the Shock and Rear Separation - a Source of Significant Scale Effects in Wind-Tunnel Tests on Aerofoils and Wings, 1968, AGARD CP 35.
- 3 Elreenaar, A, AGARDograph on Reynolds number effects. To be published.
- 4 Henne, P A, Dahlin, J A, Peavey, C C, Gerren, D S, Configuration Design Studies and Wind Tunnel Tests of an Energy Efficient Transport with a High-Aspect-Ratio Supercritical Wing. 1982, NASA Contractor Report 3524.
- 5 Fulke, J L, Ashill, P R, A Study of the Factor Influencing Shock-Induced Separation on Swept Wings, 1983, RAE TR 83088, also 1985, Turbulent Shear-Layer/Shock-Wave Interactions, IUTAM Symposium, Palaiseau, France.
- 6 Weeks, D J, An Investigation of Scale Effects on the Transonic Flow over Swept Wings, Part 1: Measurements on a Model of a Transport-Aircraft Configuration, 1976, RAE TR 76158.
- 7 Khan, M M S, Cahill, J F, New Considerations on Scale Extrapolation of Wing Pressure Distributions Affected by Transonic Shock-Induced Separation, 1983, NASA Contractor Report 166426.

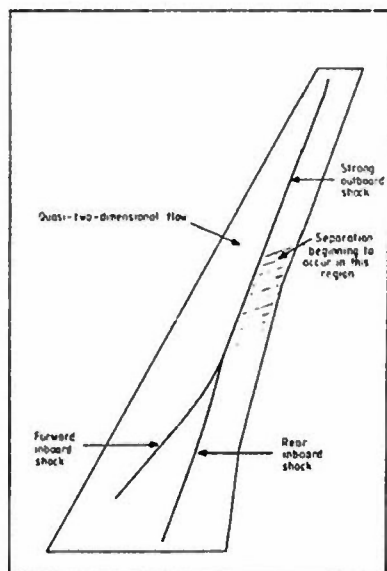


FIG 1 TYPICAL TRANSPORT AIRCRAFT WING SHOCK PATTERN  
(BUFFET ONSET AT DESIGN MACH NUMBER)

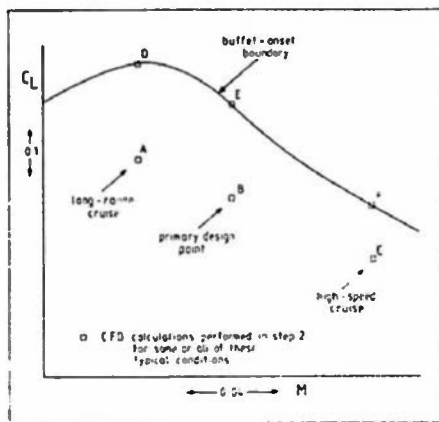


FIG 2 STEP 1: CHOICE OF OPERATING CONDITIONS FOR  
PREPARATORY CFO CALCULATIONS IN STEP 2  
(Typical illustration)

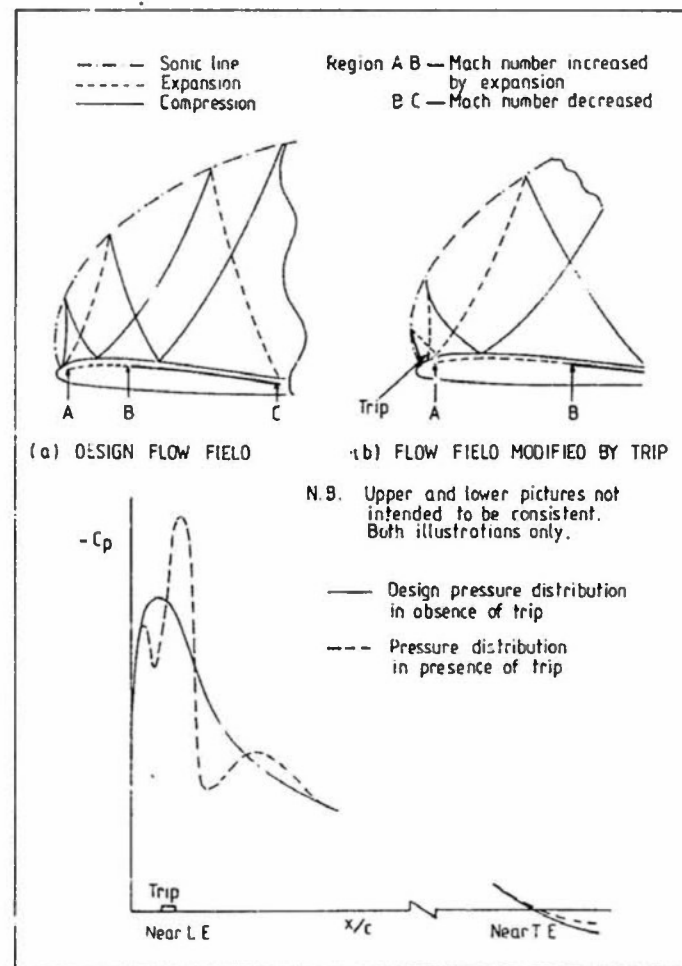


FIG 3 POSSIBLE EFFECTS OF TRIP IF PLACED NEAR TO PEAK  
SUCTION POSITION  
(Diagrammatic)

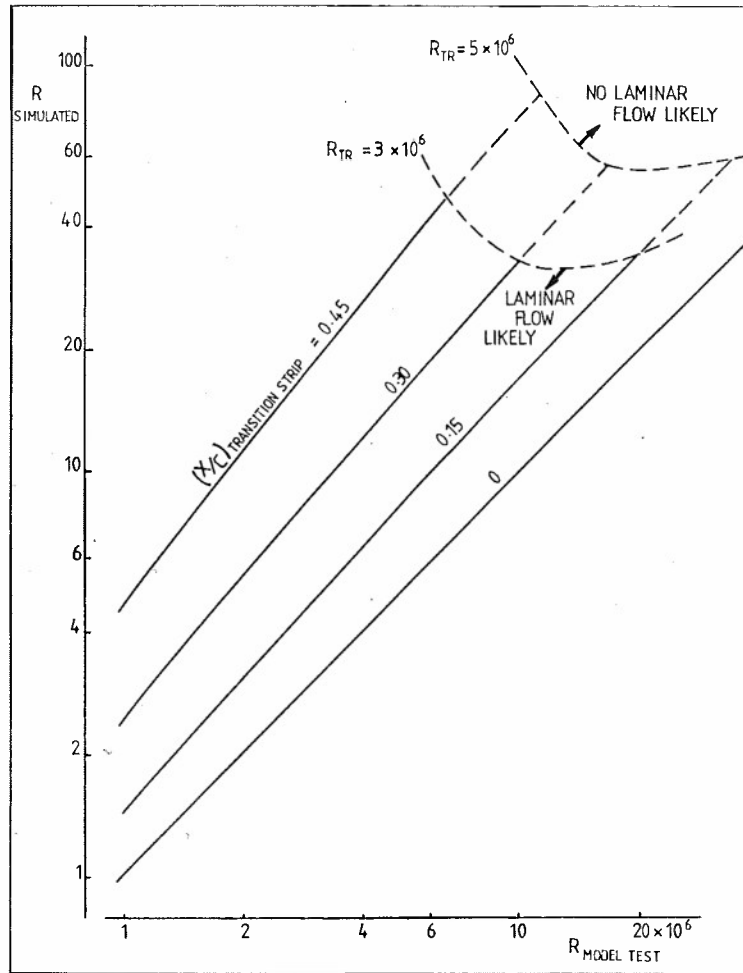


FIG 4 ZERO LEVEL SIMULATION CRITERION  
(Equivalent  $\theta$  at T.E. of flat plate)

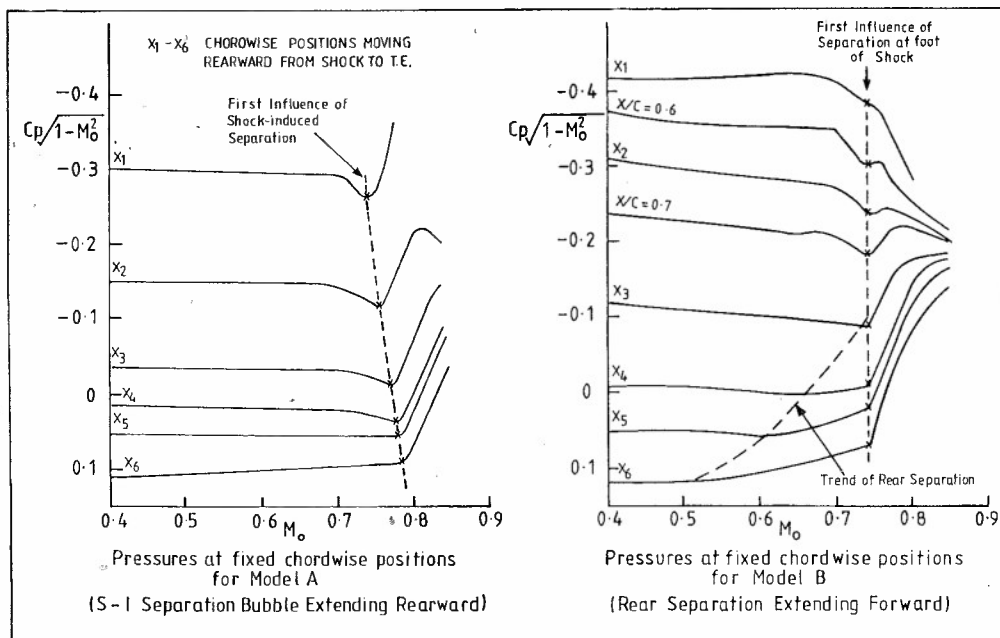


FIG 5 'PEARCEY PLOTS' TO IDENTIFY 'A' AND 'B' TYPE FLOW SEPARATION



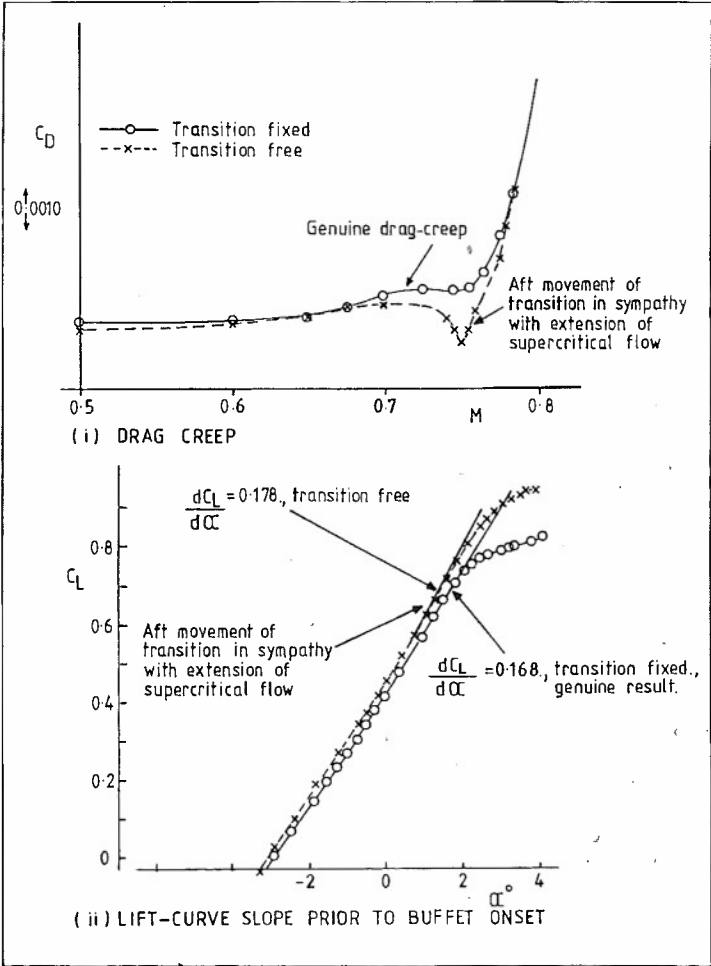


FIG 6 EXAMPLES OF SPURIOUS RESULTS WITH FREE TRANSITION

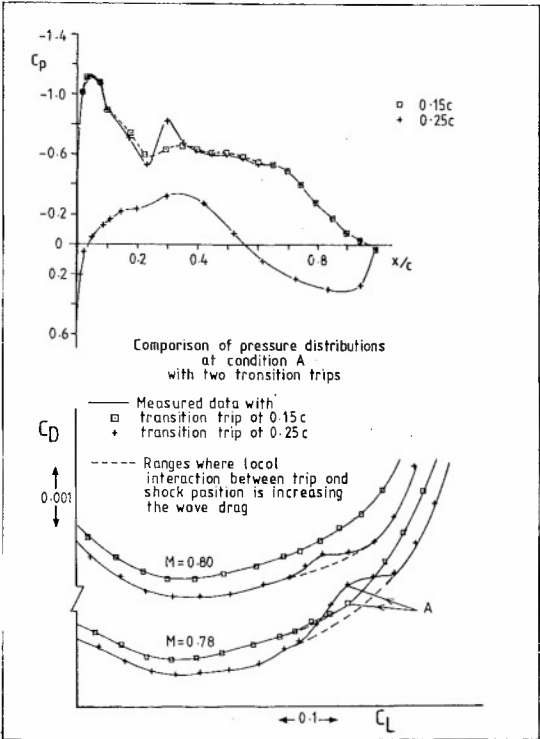


FIG 7 ILLUSTRATION OF UNCERTAINTY IN DRAG DATA DUE TO TRIP-SHOCK INTERFERENCE

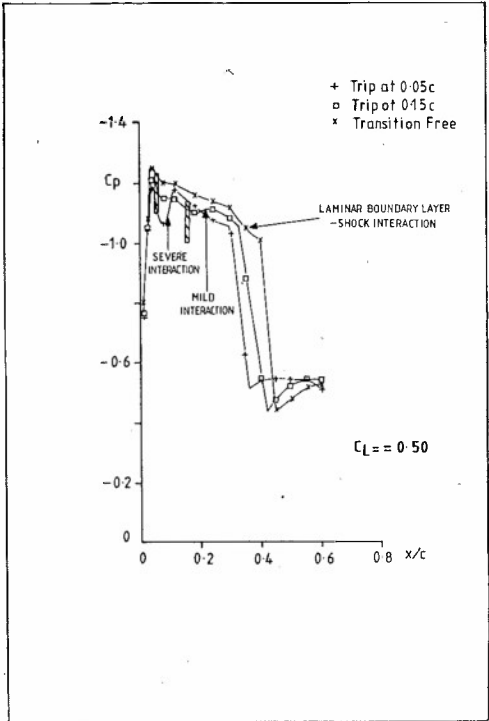


FIG 8 TRIP INTERFERENCE WITH SUPERCRITICAL FLOW DEVELOPMENT

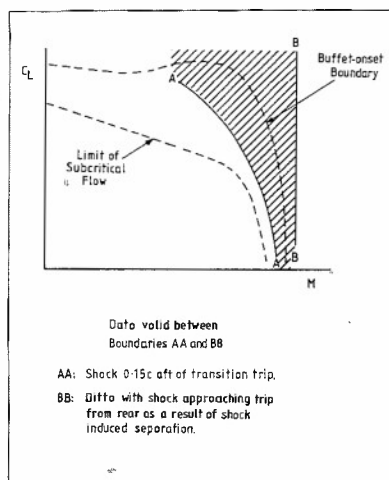


FIG 9 RANGE OF VALIDITY OF DATA WITH AN AFT TRIP

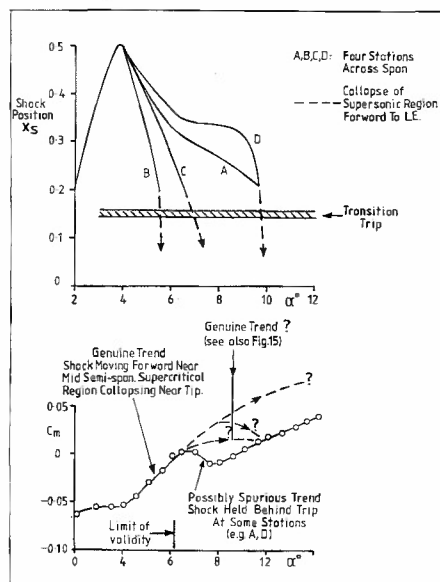


FIG 10 UPPER LIMIT OF VALIDITY OF DATA WITH AFT TRIP

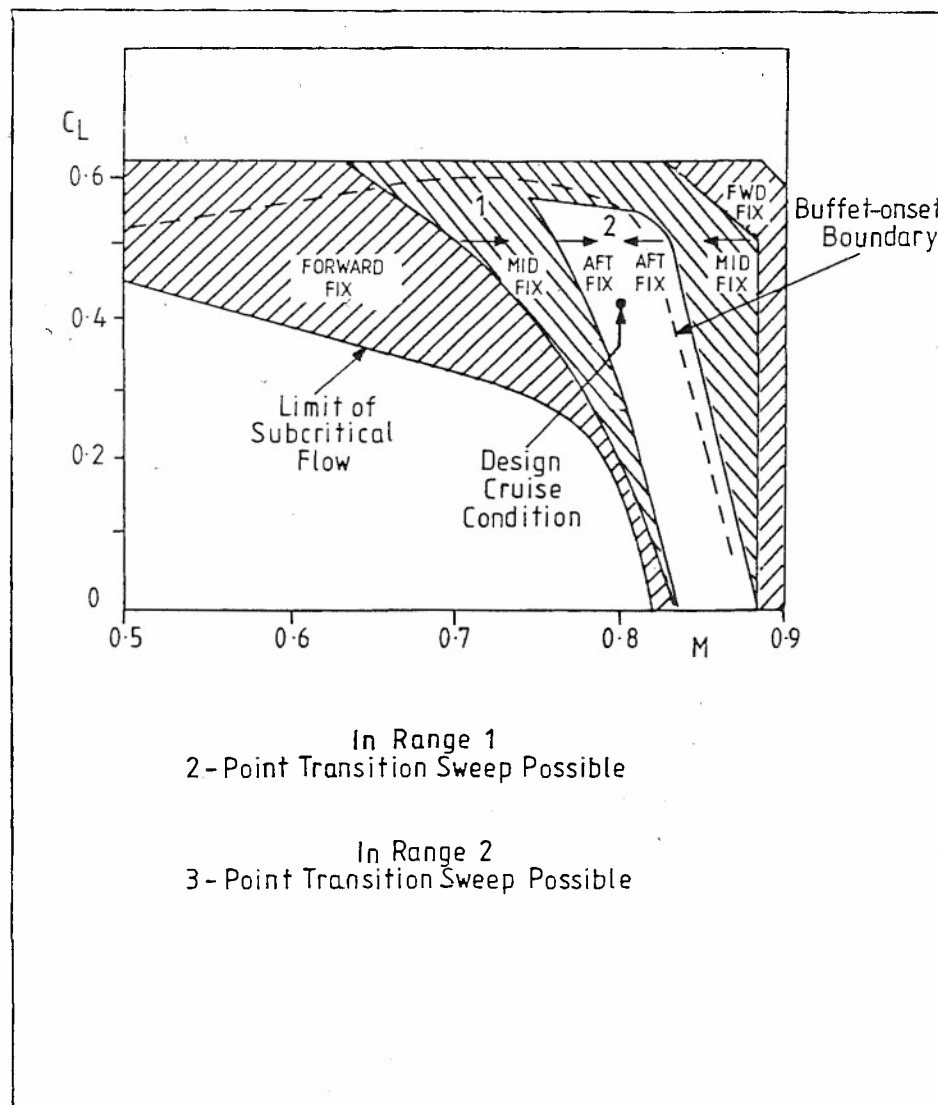


FIG 11

USEFUL RANGES WITH DIFFERENT TRIPS

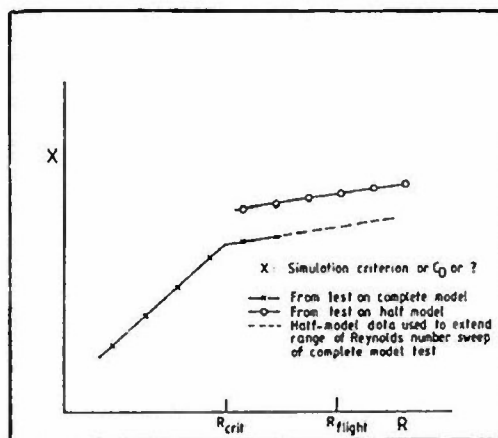


FIG 12 EXAMPLE OF USE OF HALF-MODEL DATA TO EXTEND R-SWEEP  
Without half-model : Scenario 3  
With half-model : Scenario 1

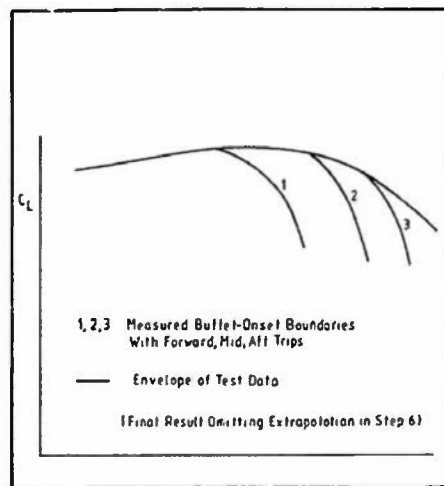


FIG 14 CONSOLIDATION OF BUFFET ONSET DATA (STEP 5.6)

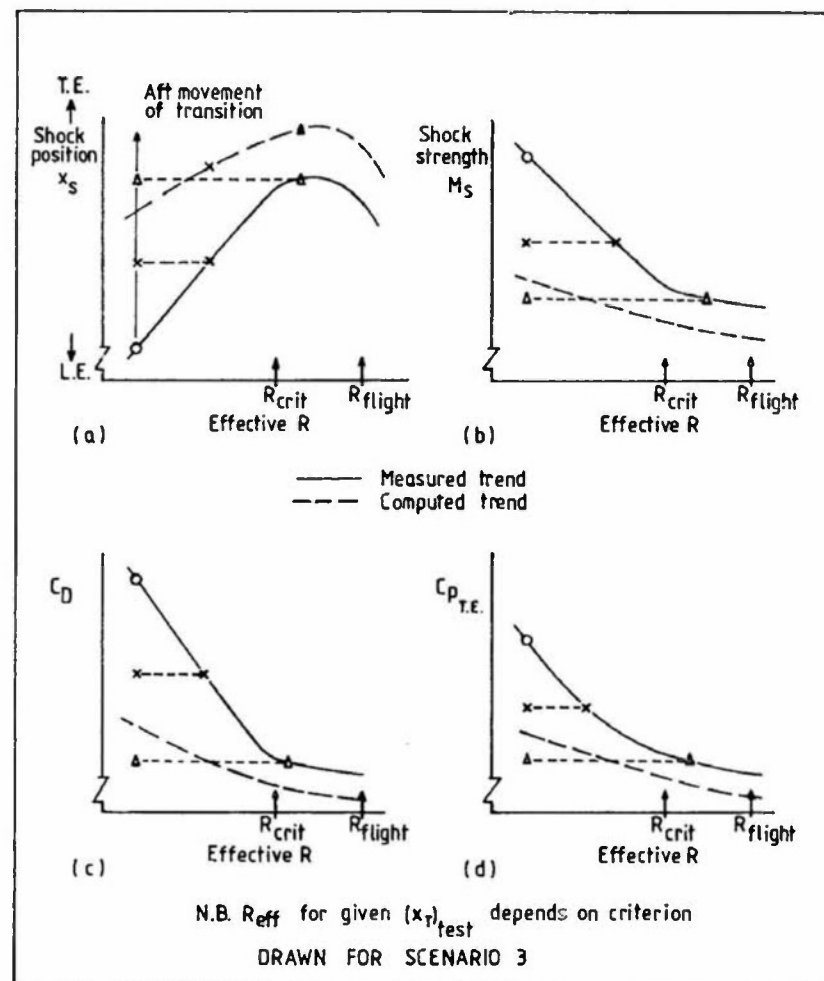


FIG 13

USE OF DIFFERENT CRITERIA TO DETERMINE  $R_{crit}$  AND TO IDENTIFY SIMULATION SCENARIO

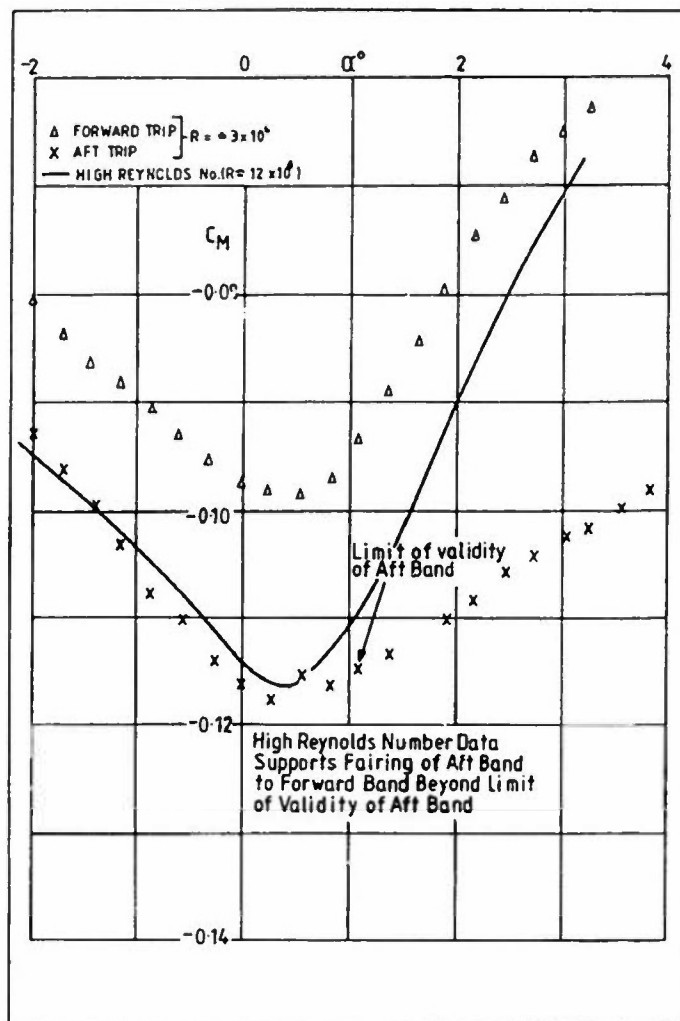


FIG 15 CONSOLIDATION OF PITCHING MOMENT DATA  
(BASED ON 'WEEKS' DATA FROM  
RAE 8ft x 8ft TUNNEL TESTS)

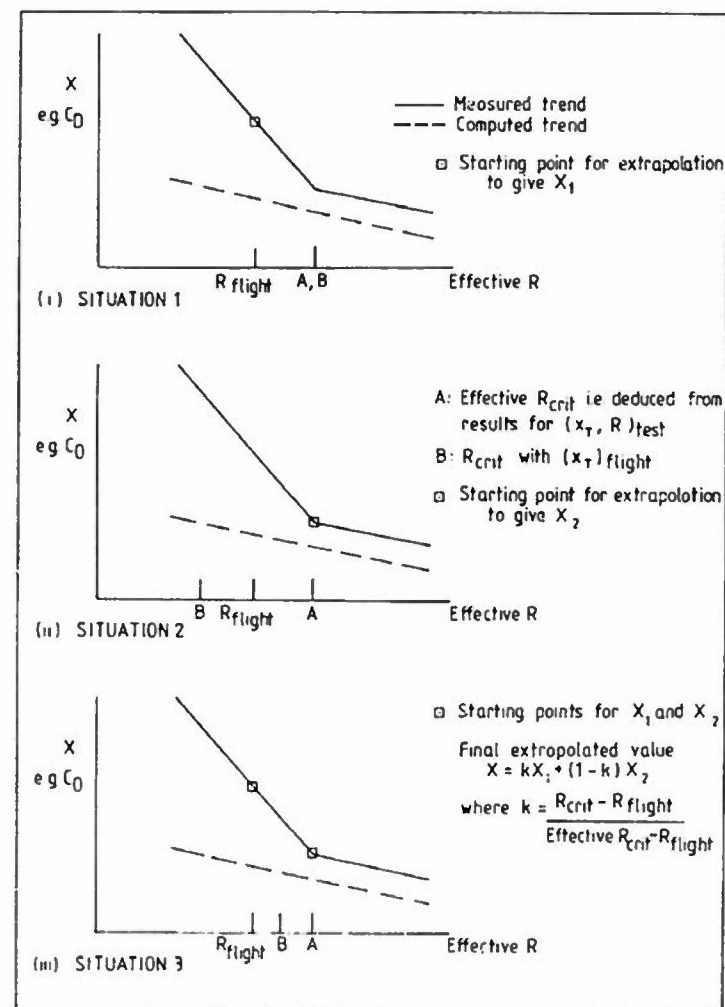


FIG 16 EXTRAPOLATION PROCEDURE FOR SCENARIO 2  
(SEE TEXT FOR STEP 6.1)

## SECTION 3.3.2 COMBAT AIRCRAFT

by  
A.B.Haines

### 3.3.2.1 Introduction

There are many reasons why combat aircraft configurations present a difficult challenge to the drafting of a general simulation methodology. For example,

- (i) There is a wide range of possible configurations as illustrated in Fig 1. While it is true that nearly all the combat aircraft shown in this figure have wings of moderate or low aspect ratio and moderate or high sweepback, the aspect ratio varies between about 1.5 up to 5.0 and the leading edge sweepback from 40° to 70°. Wing thickness/chord ratio can vary from about 0.035 for an aircraft designed to give good supersonic performance up to 0.10 or more for a trainer or strike aircraft. At present, there is a trend towards aircraft with thin wings of either delta or cranked delta planform but clearly, the methodology has to be capable of coping with any of the possible designs. It is wrong to think in terms of a single detailed methodology: to imagine that there is one preferred transition-fixing technique or one style of extrapolation that will suit all possible designs is obviously an illusion.
- (ii) Since, in nearly all cases, the wings are of low or moderate aspect ratio, the link with what happens in two-dimensional flow is much less tenable than for a transport aircraft and often, three-dimensional effects or at least, variations across the span become paramount.
- (iii) Compared with the subsonic transport aircraft discussed in §3.3.1, the geometry of a combat aircraft can be very complex and often, different types of flow can exist over different parts of the configuration.

To list some of the complicating features:

- (a) the thicker wing designs frequently have a fair number of control stations across the span and thus, there can be a considerable spanwise variation in, for example, the wing leading edge radius,
- (b) some aircraft incorporate variable sweep and thus, a whole spectrum of different types of flow can be encountered with a single design. Also, variable sweep can imply a crank in the leading edge of the inner wing,
- (c) on designs with wings having a cranked delta planform, the flow patterns can be determined by the change in leading edge sweepback somewhere near mid-semi-span,
- (d) many aircraft layouts are close-coupled and thus, the flow over one surface can be greatly influenced by the interference from another surface, eg the flow over the main wing can be influenced by the presence of a canard, an inboard wing leading edge extension (LERX or strake) or a vortex flap ahead of the wing leading edge,
- (e) the wings of some aircraft are fitted with fences, vortex generators or other devices to control the stall,
- (f) many future aircraft are likely to use manoeuvre flaps at both the wing leading edge and trailing edge; these will be deflected down for high-lift conditions and up in the high speed dash,
- (iv) The model tests have to cover a wide range of operating conditions and there are many 'design points' at widely different  $C_L$  and Mach number,
- (v) Unlike the model tests for a transport aircraft, where the main interest lies in the range up to buffet onset, where the flow is essentially attached, the main concern in model tests for a combat aircraft may often lie in what happens beyond buffet-onset in conditions where there may be large areas over which the flow has separated and for which, as a result, the use of CFD at the present time is severely limited.

For all these reasons, the emphasis in this methodology, compared with that for the transport aircraft, must lie less on comparisons between measured and calculated results and more on how to react to different types of flow. Once again, the methodology in §3.3.2 addresses primarily the flow over the wing (and other lifting surfaces) in the presence of the fuselage. There may also be problems in viscous flow simulation over the afterbody and these are considered briefly in §3.3.3.

### 3.3.2.2 The detailed methodology

#### STEP 1 : Collection of relevant information

The most likely objectives for a model test programme for a combat aircraft include

- (a) Drag in long range cruise and loiter conditions where the flow is likely to be subcritical - required to relative accuracy of ideally,  $\Delta C_D = 0.0002$ ,
- (b) Drag in sustained manoeuvre and high speed dash conditions where the flow will be supercritical

and significant wave drag may already be present - required to a relative accuracy of  $\Delta C_D = 0.0005$ ,

- (c) Stability and control characteristics in these conditions, with and without various external store loads,
- (d) The buffet-onset boundary as a guide to the approach to usable lift conditions - to an accuracy of perhaps  $0.02 \ln C_L$ ,
- (e) The usable lift boundaries and an indication of what characteristic is likely to define the usable lift boundary, eg pitch up, nose slice, wing drop, wing rock, heavy buffet, loss of directional stability etc. The effects of manoeuvre flaps,
- (f) Post-stall behaviour at high incidence, particularly at low and moderate Mach numbers,
- (g) Aircraft loads over the full flight envelope,
- (h) External store installed loads and release characteristics,
- (j) The nature of the flow separations and how they develop and the detailed surface pressure distributions - to an accuracy of  $\Delta C_p = 0.01$  for checking computer codes and better than this for assessing the effects of small changes in design.

To achieve the required standards of accuracy and repeatability, the Mach number in a polar should be held constant to  $\Delta M = 0.002$  or better and the tunnel test should provide  $\alpha$ -traverses at constant  $\beta$  with  $\beta$  held constant and  $\beta$ -traverses at constant  $\alpha$  with  $\alpha$  held constant to an accuracy of  $\pm 0.05^\circ$ . The customer should provide the important design/operational conditions for the configuration under test. Holt and Probert,<sup>1</sup> in describing the design of a wing for a combat aircraft, noted that, for their design exercise, there were 5 design points corresponding to sustained manoeuvre at Mach numbers of  $M = 0.9, 0.8, 1.2$  and  $0.6$  and a low  $C_L$  sea level dash condition at  $M = 0.94$ . These were 5 conditions at which the pressure distributions and flow fields could be calculated but, in the model test, there will be great interest in how the flow developed beyond these conditions.

The geometry of the wing will provide an early indication to the tunnel test engineer of the type of flow breakdown to be expected at high  $C_L$  at various Mach numbers in the test range. It is helpful to list six broad categories, viz

- I     Thick wing, moderate sweepback and aspect ratio  
(t/c)<sub>outer wing</sub> > 7%,  $\Lambda_{LE} < 45^\circ$   
 $2.5 < A < 4.5$   
eg Harrier, AV8B, Tornado at intermediate sweep
- II    Thin wing, moderate sweepback and aspect ratio  
(t/c)<sub>outer wing</sub> < 7%,  $\Lambda_{LE} < 45^\circ$   
 $2.5 < A < 4.5$   
eg F-4 Phantom, Jaguar
- III   Thin wing, round LE, no LE/TE manoeuvre devices deflected, high sweepback, low aspect ratio  
(t/c)<sub>outer wing</sub> < 6%,  $\Lambda_{LE} > 50^\circ$   
 $A < 3$   
eg Fairey Delta, Mirage F1-C
- IV    Thin wing, round LE, LE/TE manoeuvre devices deflected, high sweepback, low aspect ratio  
(t/c)<sub>outer wing</sub> < 6%,  $\Lambda_{LE} > 50^\circ$ ,  $A < 3$   
eg EFA, Rafale,  
likely to be a common type in the future
- V     Thin wing, sharp LE, high sweepback, low aspect ratio  
(t/c) < 4%,  $\Lambda_{LE} > 50^\circ$
- VI    Thin wing, swept forward  
(t/c)<sub>outer wing</sub> = 5%,  $\Lambda_{LE} = -30^\circ$

The test engineer should attempt to place the configuration under test in one of these categories. This will not always be easy because they are not six absolutely distinct classes. For example, a cranked delta wing could exhibit the flow features of both II (outer wing) and III (inner wing), compounded at high  $C_L$  by features of IV.

## STEP 2 : Preparatory calculations

If the test wing is in class V, this step should be omitted but, in all other cases, calculations should be made for all except wings of class V by the most advanced theoretical method conveniently available of the wing pressure distributions, boundary layer development and, if possible, the wave drag and viscous drag for at least some of the important design/operational conditions identified in Step 1. It is suggested that these should include

- (i) a sustained manoeuvre condition at the primary design Mach number, eg  $M = 0.8$  for wings of class I, or  $M = 0.9$  for wings in the other classes,
- (ii) a sustained manoeuvre condition at a lower, operationally important Mach number, eg  $M = 0.65$  and, if possible, higher incidences at this Mach number to study the flow around the leading edge,

- (iii) a high speed dash condition at relatively low  $C_L$  and high subsonic speed, eg  $M = 0.90$  to  $0.95$ .

For wings of class IV, the calculations for (1,ii) would ideally cover more than one setting of the manoeuvre flaps. The calculations should be made for both the full scale aircraft at flight Reynolds numbers and for the model at a representative test Reynolds number - and more than one model test Reynolds number if the tests are being made in a variable density tunnel.

The complexity of the configuration chosen for the calculations will depend on the capabilities of the test establishment and/or customer. It would be unreasonable to suggest that one always needs to use a code/grid capable of handling the complete aircraft but, at the other extreme, calculations for two-dimensional flow will be of only limited value, possibly merely giving a qualitative idea of sensitivity to viscous effects. Realistically, the calculations should, if possible, be made for at least the three-dimensional wing-body configuration and, if the design includes a canard surface, the code should be capable of allowing for the interference of the canard flow field.

Strictly, to compare with the measured data and to provide a reliable extrapolation of the viscous effects to full-scale conditions, the CFD codes should allow for strong viscous-inviscid interactions such as a laminar separation near the wing leading edge, a shock-induced separation bubble and a rear separation ahead of the trailing edge. Ability to predict the existence of such effects is, of course, a vital element in any methodology but again, as with the complexity of the configuration, it would be unrealistic to suggest that the codes to be used in a general methodology should be capable of allowing for all the effects of such interactions. Writing in 1987, it is realistic to suggest that the calculations should be made by an Euler code with allowance for weak viscous-inviscid interactions. The restriction to weak viscous-inviscid interactions is not as serious as might appear at first sight. Divergence between the measured and the predicted calculated results and, in particular, divergence between the trends with Reynolds number and/or transition position, can be used as a means of identifying where and when strong viscous-inviscid interactions are present in the measured data; this knowledge will help in devising an intelligent extrapolation of the data to full scale conditions. In other words, the methodology as written attempts to take advantage of the fact that the strong interactions are not allowed for in the calculations of wing pressure distributions.

Predictions should be made of the position of natural transition for both the full scale aircraft and the model, employing criteria for

- (i) transition due to contamination along the wing leading edge attachment line,
- (ii) transition due to cross-flow instability,
- (iii) transition due to Tollmien-Schlichting instability as in two-dimensional flow,
- (iv) transition due to Görtler instability.

With a combat aircraft and particularly a small combat aircraft, one cannot rule out the possibility that, under cruise conditions at least, there may be a significant extent of laminar flow, even on the full scale aircraft. The chances of this occurring are greatest for an aircraft with a thin wing (ie a relatively sharp leading edge) flying at relatively low Reynolds number (ie a small aircraft flying at high altitude). Also, assuming a smooth surface, the chances will be greater near the wing tip where, because of the small chord, it is more likely that  $Re < 90$ , thus eliminating the possibility of transition due to mechanism (i). Calculations suggest for example that, for the Harrier GR Mk V, some laminar flow might be possible near the wing tip at flight altitudes such as 30,000 ft. Often, in practice, at high incidence, when, at the lower Mach numbers at least, the laminar boundary layer will separate near the leading edge but, at high Reynolds numbers, this would merely lead to a short separation bubble followed by a reattachment, ie there is an additional mechanism for transition.

The calculations of pressure distributions and boundary layer development for the higher Mach number conditions should be repeated for various transition positions at a representative (generally maximum) model test Reynolds number. These transition positions should all lie ahead of the predicted natural transition position and should range from a typical 'forward fix' position at say, 0.05c to a position about 0.15c ahead of the forward, inboard/outboard shock front - see Fig 2, as obtained in the calculations with natural transition. If the tests are being made in a variable pressure tunnel, the calculations of the pressure distributions and boundary layer development should also be repeated for several Reynolds numbers in the test range.

The general aim of these initial calculations is to give the model test engineer an early appreciation of the flow likely to occur over the model test configuration at least in the  $C_L - M$  domain where the flow is substantially attached, and qualitatively, by intelligent extrapolation, outside this range. Specifically, the calculations will indicate:

- (i) a suitable position for a forward transition trip. This should be as near to the leading edge as possible to reduce uncertainty in the interpretation of the drag data but it should be recognised that tripping is difficult in a strongly favourable pressure gradient. This is particularly unfortunate in the case of tests on a model of a combat aircraft because there is a strong probability that, at the lower transonic Mach numbers, the flow breakdown at high incidence will be initiated by a laminar separation near the leading edge. Strictly, therefore, it is highly desirable, in principle, to trip the boundary on or very close to the leading edge but, to date, no satisfactory method for doing this has been devised. Plastic strips wrapped round the leading edge and normal to the leading edge have been tried but the results suggest that these strips introduce other effects unrepresentative of the full scale flow. In general, therefore, (but not necessarily for wings of class V), one should use the results of the calculations to suggest a suitable position for a conventional forward trip near say, 0.05c. For the reasons noted in 53.3.1, this should not be located near or immediately downstream of any peak suction close to the leading edge; also, for wings of class IV, the trip should not be located near the hinge of the leading edge manoeuvre device.



- (ii) whether it should be possible to fix transition in a further aft position and still ensure a turbulent boundary layer/shock interaction. As indicated by the nature of the shock patterns in Fig 2, this may not be possible near the root and tip of the wing of a combat aircraft, but, as implied in §3.2.1, an aft movement of transition in the important region near and outboard of mid-semi-span, could still be extremely valuable as a means of extending the effective Reynolds number range of the tests. In this context, the effective Reynolds number is defined as the Reynolds number that would be needed with the (probably far forward) transition position forecast for flight at full scale Reynolds numbers to produce the same viscous flow behaviour as in the model tests with the aft transition position, this equivalence being judged on the basis of some chosen simulation criterion. Use of this technique on a model of a combat aircraft will be more limited than on a subsonic transport wing of high aspect ratio. This follows from the wing planform (Fig 1) and the likely shock patterns (Fig 2) but the calculations should show that use of the approach is possible at high subsonic and transonic speeds except on wings of category V.
- (iii) whether there is likely to be a laminar separation near the leading edge and, if so, the Reynolds number,  $R_{crit}$ , beyond which this would be forecast to disappear. Such a separation could well be present in the model tests at, for example, the sustained manoeuvre condition at  $M = 0.6$  and possibly at similar  $C_L$  up to say,  $M = 0.9$ , dependent on the wing section shape for most combat aircraft wing planforms.
- (iv) whether a rear separation is likely to be present and over which part of the span and again, the Reynolds number  $R_{crit}$ , above which this would be expected to disappear. Such a separation could well occur in the model tests with wings of category I and almost by definition, will occur on wings of category III, IV where some separation is likely to occur on the surfaces of the trailing edge manoeuvre flap within the  $C_L$ -range of the usable flight envelope.
- (v) the required trip heights for various test Reynolds number/transition positions. General experience suggests that these should be slightly greater than those that would be predicted by Braslow and Knox<sup>2</sup> on the basis of the calculated laminar boundary layer thickness at the chosen transition positions but the actual values for any particular tunnel are likely to depend on the stream turbulence.

The results of these CFD calculations will therefore provide a first guide as to which simulation scenario (§3.2.1) is likely to apply at the important design/operational conditions identified in Step 1: the deduction as to which scenario is relevant depends on a comparison of

- (i) the maximum test  $R$  or  $R_{eff}$ ,
- (ii)  $R_{crit}$  and  $R_{crit}$ , and
- (iii)  $R_{flight}$

### STEP 3 : Initial datum tests with fixed and free transition

Armed with the knowledge from Step 2, a forward fix of the appropriate height should be applied to the model at the chosen position (possibly varying slightly across the span, being nearer to the leading edge at wing tip and root). This trip should be a narrow band of Ballotini, carborundum, serrated tape ('bande crantée'), isolated pyramids, strips of 'letraset' or preferably, a set of air jets, according to the experience and preference of the individual test establishment.

The tests should start with a check on the effectiveness on both wing surfaces of the trips in provoking transition. This is usually achieved by means of a sublimation test with say, acenaphthene. One should check the effectiveness in

- (a) the sustained manoeuvre condition at the primary design Mach number,
- (b) a low  $C_L$  cruise or high speed dash condition,
- (c) if thought necessary, at any other condition where there is reason to doubt the effectiveness of the transition fixing, eg because there is a lower test Reynolds number, a more favourable pressure gradient or a thicker wing boundary layer.

The remarks in §3.3.1 about how to conduct a sublimation test still apply. Both wing surfaces should be checked.

Tests should then be made with and without the forward trip over the full test range of  $C_L$  and Mach number. If the aircraft has a canard surface, these initial tests will have to be made with and without the canard.

The tests with a forward trip will provide

- (i) a means of checking that the drag values have been corrected successfully for the effects of support tares, wind tunnel wall interference, buoyancy effects etc. This can be done by comparing the measured values for subcritical Mach numbers with simple predictions without being confused by doubts about the extent of laminar flow on the model,
- (ii) a comparison with the results of the CFD calculations made in Step 2. Any serious disagreement, eg in shock position, could be an indication that some viscous effects, eg a rear separation, not allowed for in the calculations, are present in the experimental data. One must admit however that this would not be conclusive unless confirmed by a study of the pressure distributions over the rear of the wing surface and/or surface oil flow patterns. The hesitation arises on account of the complex geometry of a combat aircraft: compared with a transport aircraft, there is less certainty that any existing theoretical method with allowance for only weak viscous interactions will place the shock in the correct position,

- (iii) an indication of how the shock strength and position vary with  $C_L$  and Mach number,
- (iv) the data from which one can construct the diagrams for flow development with  $C_L$  and Mach number discussed below in Step 4. These diagrams serve as a guide to the nature of the flow breakdown at high incidence over the test Mach number range.

The test with free transition is included to indicate

- (i) whether laminar flow can be maintained back to the inboard forward and outboard shocks of a typical shock pattern, Fig 2; if not, the ability to manipulate the boundary layer by aft fixing will be limited,
- (ii) whether a rear separation is still present; if so, it will clearly be present whatever transition fixing technique is employed,
- (iii) whether there is any separation on the lower surface that can be alleviated or suppressed by thinning the boundary layer by removing the forward trip. Such separations are often difficult to detect by merely studying a single pressure distribution obtained with a single boundary layer state.

In general, as with a model test on a transport aircraft, it would be unwise to accept transition-free data as a reliable guide to the full scale behavior. Strictly, one should always test with a turbulent boundary layer/shock interaction unless the flow is believed to be laminar back to the shock in flight and also, the drag data are difficult to interpret if the transition position is free to move with  $C_L$  and/or Mach number. On the other hand, there may be occasions when the transition-free data can be used for more than diagnostic purposes, eg

- (a) at high  $C_L$  and the lower transonic Mach numbers when the flow breakdown is initiated by a separation ahead of the trip, in general - but see later in Step 6 - the presence of the forward trip will not achieve any improved simulation at full scale and may actually have an adverse effect by thickening the boundary layer and accentuating a tendency to a rear separation; hence, transition-free data may be preferred,
- (b) as already noted, on some combat aircraft, it may be possible to maintain laminar flow back to the shock on the full scale aircraft.

#### STEP 4 : In-depth study of flow development in model tests

The results from the tests in Step 3 should be studied to identify the nature of the flow breakdown at various Mach numbers in the test range. At least six broad types of flow breakdown at high  $C_L$  can be identified and often, more than one type can be present at a given Mach number and  $C_L$ . They are illustrated in Figs 3-8.

They can be described briefly as follows:

Type A Leading edge vortex separation from wing apex (or from a strake or LERX - (Fig 3) wing leading edge intersection)

This type of flow separation would be expected to occur on a wing of type V, irrespective of the Mach number at subsonic and supersonic speeds. The final flow breakdown will result from the vortex lifting off the surface or bursting. Little scale effect in symmetric flight would be expected up to this incidence. However, there can be detailed changes with Reynolds number in the position of the separation of the outward flow below the primary vortex and hence, in the formation and characteristics of the secondary vortex. These can become more significant in yawed flight when, even more significantly, the changes in effective sweep of the port and starboard wing leading edges may affect the formation of the primary vortices. Hence, even for this type A flow breakdown, it would be wrong to assume, without any evidence from the measured results, that there is no significant scale effect to investigate.

Type B Vortex separation from near the leading edge occurring first on the outer wing and (Fig 4) extending in with increase in incidence (or first near mid-semi-span and then extending in and out).

This type of flow would be expected to occur at low Mach numbers, eg  $M = 0.4$ , on the wings of many combat aircraft models, particularly those of type III. The flow is similar to that in type A but significant scale effect is now likely with the appearance of the separation and its extension inwards being delayed with increase in Reynolds number. If the wing aspect ratio is high enough ( $A > 2$ ), flow breakdown occurs when part of the wing lies completely outboard of the vortex.

Type C Shock-induced separation behind highly swept shock situated ahead of say,  $0.2c$ . (Fig 5)

This type of flow would be expected to occur at high lift on the wings of most combat aircraft at Mach numbers below  $M = 0.8$  and to persist up to higher Mach numbers on wings that are thin and/or highly sweptback. If the sweep of the shock front is more than about  $25^\circ$ , it will be a three-dimensional separation rolling up into a vortex which will move inboard with increase in incidence. Flow breakdown occurs when the flow over the top of the vortex fails to reattach to the surface and/or a significant part of the wing lies outboard of the vortex.\* Subsequently, at higher incidence, it is possible for a supersonic region to re-establish itself around the outer wing leading edge. If the

---

\*This would not apply if the outboard wing had a supersonic trailing edge

shock sweep is 25° or less, the shock-induced separation will extend rearward as a bubble similar to what happens in two-dimensional flow. In the context of viscous simulation, this distinction between a vortex and a bubble separation may not be too important in respect of the methodology to be adopted in the tunnel test but could affect the extrapolation procedure (see Step 6). This type of separation does not necessarily occur first near the tip; for a highly twisted wing, it can appear first near mid-semi-span.

**Type D** Shock-induced separation behind a moderately swept shock outboard of the intersection of 3 (Fig 6) shocks in a 3-shock pattern, ie shock near mid-chord, eg  $0.3 < x_s < 0.55c$ .

This type of flow would be expected to occur at high lift on most modern combat aircraft wings of types I, II at Mach numbers near the primary design manoeuvre condition, eg  $M = 0.8$  for I or  $M = 0.88$  for II. When the separation bubble extends to the trailing edge, the shock moves forward. The flow breakdown can extend either inward, outboard or forward and this development could be very scale-sensitive.

**Type E** Shock-induced separation behind a slightly swept shock located fairly far aft, (Fig 7) eg  $0.6 - 0.8c$ .

With most wings of types I and II, the flow breakdown changes from type D to type E with increasing Mach number above the primary design value, eg between  $M = 0.85$  and  $0.90$  for wings of type I or above  $M = 0.90$  for II. Also, a deflection of a rear manoeuvre flap on a wing of type IV can lead to this type of flow separation, ie there can be a strong shock aft of the flap hinge in addition to the main shock system further forward.

The distinction between D and E lies not simply in the position of the shock inducing the separation: with E, there is little tendency for the shock to move forward as a result of the separation. This is partly because, after a relatively small divergence of the trailing edge pressure, the flow at the trailing edge becomes supersonic and also partly because the flow at near-sonic Mach numbers is highly three-dimensional.

**Type F** Rear separation (usually in association with C, D or E). (Fig 8)

Rear separation can occur immediately ahead of the trailing edge and extend progressively forward with increasing incidence or can be induced by a steep pressure rise on the surface of a deflected manoeuvre flap. It may also be observed at Mach numbers below design, aft of a high peak suction at the position where the main shock will be located at the design Mach number.

Assuming that the tests are being made on a model with extensive pressure plotting facilities, diagrams such as those illustrated in Figs 9-13 can then be created. These diagrams are more complicated than those discussed in §3.3.1 in the methodology for tests on models of subsonic transport aircraft. They have to cover the full  $C_L - M$  domain with emphasis on the region beyond separation-onset. In the absence of pressure plotting data, some of the boundaries can still be defined with the help of evidence from surface oil flow visualisation tests. Four  $C_L - M$  boundaries are shown plotted as full lines; these indicate

- 1 the first appearance of supercritical flow,
- 2 the first appearance of a shock-induced separation bubble,
- 3 the first development of a complete separation from the foot of the shock to the trailing edge
- 4 the first major break (in an adverse sense) in the  $C_L - \alpha$  or  $C_m - C_L$  curves.

Additional boundaries plotted as dashed lines indicate when the shock moves aft of positions such as  $0.30c$  or  $0.55c$ , these shock positions being determined for the point on the span where the shock strength is at its greatest.

All the diagrams in Figs 9-13 are presented twice. The hatched areas on the left-hand figures are labelled with the letters A-E, indicating the relevant type of flow breakdown as listed above; the hatched areas on the right-hand figures indicate the  $C_L - M$  regions where a rear separation appears to be present; in the cross-hatched areas, this rear separation is really a shock-induced separation which, for example, for a wing of category IV, could be sited on the surface of a deflected manoeuvre flap.

Diagrams such as those illustrated in Figs 9-13 provide the background for the in-depth study of viscous effects in Step 5. Arguably, not all the detail is strictly necessary but it is possible to claim that even boundary 1 marking the appearance of supercritical flow is relevant in the context of a viscous simulation methodology. Failure to simulate the full scale shock positions in the  $C_L - M$  (or  $\alpha - M$ ) corridor between boundaries 1 and 2 can have a profound effect on the subsequent flow breakdown at higher incidences. The most likely effects at reduced Reynolds numbers are that the rear shock (see Fig 14) is further forward and the forward shock is more swept than at full scale Reynolds numbers and that, as a result, the point of intersection of the shocks in the typical 3-shock pattern, as shown in Fig 14, is further inboard. Simulation of the correct full scale position of this intersection is however an important requirement. The maximum shock strength and hence, the likely spanwise position for the initial appearance of a shock-induced separation bubble on boundary 2 will tend to lie just outboard of this intersection point. A discrepancy, relative to full scale in this position can lead<sup>3</sup> to a completely different subsequent development of the flow beyond boundary 2, see Fig 16, and later discussion in Step 5b. Even if these effects on the flow breakdown do not materialise, lack of simulation of the shock strengths and positions in the range between boundaries 1 and 2 is likely to affect the wave drag and viscous drag at the design/operating conditions identified in Step 1 and so, in this sense, boundary 1 can mark the beginning of significant scale-sensitive

viscous effects. On the other hand, boundary 1 also marks the lower boundary of the range in which some manipulation of the boundary layer through aft fixing should be possible.

In practice, the flow patterns may be much more complicated than that sketched in Fig 2. Two types of flow separation may internet, eg the occurrence of a laminar separation near the leading edge may trigger the appearance of a rear separation ahead of the trailing edge. Particularly with wings of classes III and IV, two separate shock systems can be present, each lending to their own particular viscous effects. The boundaries as plotted in Figs 11 and 12 for these wings are likely to be determined by the forward system at Mach numbers up to about  $M = 0.85$  for wings III or  $M = 0.80$  for wings IV and by the rear system at higher Mach numbers.

The scene is now set to define the issues that should, if possible, be explored in further tests in Step 5. These issues can be summarised as follows:

- (a) the success or otherwise of the calculations in Step 2 in forecasting the strengths and positions of the shock waves at the important design/operating conditions identified in Step 1. Any serious disagreement between the calculated results and the measured data from the tests in Step 3 with forward transition can indicate that strong viscous/inviscid interactions not allowed for in the calculations are present in the measured data, eg a rear separation on the upper surface or a separation near  $0.7c$  on the lower surface. If so, this could affect the extrapolation to full scale conditions; further tests are therefore needed to confirm their presence and to establish trends in the measured data with Reynolds number and/or transition position,
- (b) in the Mach-number range for which it has been established that the flow breakdown is of type B, it is likely that, in the model tests, there is a laminar separation ahead of any possible position for a forward transition trip whereas, at full scale Reynolds numbers, transition will occur ahead of a separation of the turbulent boundary layer. If so, extrapolation of data to full scale is likely to be difficult and unlikely to be a simple extrapolation of any measured trends; even so, further tests in Step 5 may still be useful,
- (c) in the Mach-number range for which it has been established that the flow breakdown is of type C, the separation triggering the breakdown will tend to have occurred near the forward transition trip. The test data may therefore be misleading because of a local interaction between the trip and the shock and so, further tests are desirable with some change in the trip - even if it is only a small change,
- (d) in the Mach-number range for which it has been established that the flow breakdown is of type D, the detailed development of the flow separation with increase in  $C_L$  or incidence beyond boundary 2 is sensitive to the variation in shock strength (and hence, shock sweep) along the length (spanwise) of the outboard shock; it therefore depends on the viscous effects discussed under (a) above and (e) below and further tests should be made - and are possible in this case - to establish 'measured trends',
- (e) any rear separation present in the model tests but not forecast to occur in flight can have a major impact on the development of the final flow breakdown, particularly if the rear separation is only present over part of the span. Locally, where there is a rear separation, the shock wave will probably be too far forward and, as a result, the shock sweep will be increased and shock strength reduced outboard of this region and vice-versa inboard. It is therefore quite possible for the flow breakdown to start at the wrong spanwise position and to spread in the wrong direction, relative to what would happen under full scale conditions. No simple correction, eg  $\Delta C_L$  for model to full scale, could allow for this sort of scale effect and hence, further tests in an attempt to eliminate this rear separation are highly desirable.

#### STEP 5: Additional tests to explore viscous effects

The study of the flow patterns and data from the tests in Step 3 will have identified the areas of the  $C_L - M$  plane where further tests to study the viscous effects should be conducted if possible. There are two approaches: either

- (i) to conduct Reynolds number sweeps if the tests are being made in a variable density tunnel or if two models to a different scale are available, or
- (ii) to manipulate the boundary layer to obtain a better simulation of the full scale boundary layer behaviour.

Whenever possible, both approaches should be practised.

This in-depth study has three main aims:

- (i) to provide trends in the measured data that can be compared with trends in the CFD data from Step 2 and which, together, can be used in the extrapolation of the data to full scale,
- (ii) to produce a closer simulation in the actual tests of the full scale viscous flow behaviour,
- (iii) to eliminate, as far as possible within the tests, any premature rear separation or other strong viscous-inviscid interaction not expected to be present in flight at full scale Reynolds numbers.

#### STEP 5a: Reynolds number sweeps

Tests should be made at two or more additional test Reynolds numbers with transition fixed in the forward trip position selected for the tests in Step 3. The height of any roughness band used to fix transition should be varied to suit the test Reynolds number and checks should be made at each



Reynolds number to check that transition is not occurring ahead of the band and that the band is effective in promoting transition.

The tests should be made over the full  $C_L$  -  $M$  range but particular attention should be paid to

- (i) the results at high  $C_L$  in the Mach-number range in which the flow breakdown is of type B,
- (ii) the results in areas where a rear separation is evident,
- (iii) changes in shock position for a given  $C_L$  and Mach number in the region where the flow is substantially attached (except possibly for a rear separation).

Trends in the measured data that could usefully be plotted against Reynolds number include:

- (i) in regions where the flow breakdown is of type B, the value of  $C_L$  at which the curve of  $(-C_p)_{\max}$  with  $C_L$  for a particular spanwise position shows a pronounced break, thus indicating the appearance of a significant laminar separation,
- (ii) the chordwise position of  $(-C_p)_{\max}$  in this  $C_L$  -  $M$  region, if this shows any significant variation with Reynolds number,
- (iii) the local  $C_L$  at a given incidence,
- (iv) the shock position, shock sweep and shock strength for a given  $C_L$ , Mach number and spanwise position,
- (v) the extent, both spanwise and chordwise, of any rear separation present at a given  $C_L$  and Mach number. The extent of the rear separation can be judged on the basis of plots of the form originally suggested by Pearcey - see Fig 5 in §3.3.1.

As regards (iv), the trends should be compared with those predicted by the CFD calculations in Step 2. Any serious divergence between the measured and predicted trends should be identified and diagnosed to establish whether they are due to viscous effects and, if so, the nature of these effects.

#### STEP 5b : Manipulation of the boundary layer

The ideal approach - and one that may be possible in the future - would be to suck through the model surface to reduce the boundary layer thickness but, at present, the established technique is to allow the boundary layer to remain laminar over the forward part of the wing surface and then to trip the boundary layer in a position that is further aft than the forecast natural transition position in flight at full scale Reynolds numbers.

Tests should be made whenever possible with one or more alternative transition trip positions on the wing upper surface (and also possibly on the lower surface, dependent on whether there are any significant separations on the lower surface in likely operational conditions). These trip positions have to be chosen

- (i) to ensure a turbulent boundary layer/shock interaction,
- (ii) to avoid any local interaction between the transition trip and the flow near the shock,
- (iii) to minimise, as far as possible, any serious disturbance to the supercritical flow development over the forward part of the wing surface,
- (iv) to ensure that there is a laminar boundary layer back to the trip at all conditions of major interest; otherwise, there will be difficulties in interpreting the drag data.

To achieve (i,ii) the trip should be at least 0.15c ahead of the shock which probably implies at least 0.10c ahead of the shock positions observed in the tests in Step 3 with a forward trip.

These requirements, coupled with the fact that obviously, it is not possible to maintain a laminar boundary layer beyond the positions observed in the tests in Step 3 with natural transition, can pose serious limitations on the use of the aft-fixing technique on a model of a combat aircraft. Tests at high subsonic speeds on wings of type I offer the best prospects, eg the boundaries in Fig 9 indicate that the shock is aft of 0.3c at  $M > 0.80$  and aft of 0.55c at  $M > 0.90$ , although even in this case, these positions refer to stations near mid-semi-span; near the root and tip, as shown by Fig 7, the shock could be further forward. With wings of types III and IV, where there is a clear need to produce a thinner boundary layer ahead of a rear shock, it may still not be possible to move transition aft because of the adverse pressure gradients associated with either shock waves or part-span vortex flows present over the forward part of the wing surface - see Figs 15(a,b).

On the other hand, it is worth pointing out that  $R_{\text{flight}}$  for a combat aircraft will be less than for most transport aircraft and hence, a relatively small movement of transition may be sufficient to give the required simulation. It would be wrong, therefore, to conclude that little can be achieved by changing the position of the transition trip. Three positive suggestions can be made:

- (i) test with a small change, either forward or rearward, in the position of the 'forward trip',
- (ii) test with one or more aft trips in an attempt to create a 'transition sweep' for as much of the  $C_L$  -  $M$  envelope as possible,
- (iii) test with an aft trip applied in a different direction (spanwise) compared with the aft trips in (ii).

Each of these proposals addresses the simulation problems in specific, but different, parts of the  $C_L$  -  $M$  plane. To explain the aims of each proposal in more detail:

(i) A small change in forward trip position

The aim is to explore whether, and to what extent, flow breakdowns of types B and C, ie high incidence or  $C_L$  at the lower Mach numbers in the transonic range, are sensitive to the precise location of the transition trip. Such sensitivity is a real possibility because one can distinguish between three situations and a small change in trip location can easily shift the results for a given  $C_L$  and Mach number from one situation to another. These situations can be described as follows:

- (a) The shock wave (or more generally, the adverse pressure gradient inducing a laminar separation) lying a little way upstream of the trip. In this situation, the trip will not prevent the separation of the laminar boundary layer but there is some evidence to suggest that the presence of a roughness band slightly downstream of the point of separation will encourage the separated boundary layer to reattach. If so, the flow will contain a small, relatively unimportant closed laminar separation bubble and it can be argued that this is likely to be more representative of what might happen at full scale Reynolds numbers than if the bubble had been allowed to extend progressively rearward with increase in incidence. Nevertheless, the quantitative interpretation of such data could be difficult.
- (b) The shock sited very close to the trip - in practice, this means that the shock will be immediately aft of the trip. As noted earlier, this will result in the shock being stronger and slightly further aft than it would have been if the interaction between shock and trip had not been present.
- (c) The shock lying say, 0.10 - 0.15c downstream of the trip, thus satisfying the requirements specified earlier. Some interference to the supercritical flow development may still, however, be caused by the trip and it may still be valuable to find the effect of changing the position (and/or the height) of the trip.

This proposal, therefore, can be regarded as an aid to the diagnostic interpretation of the data. Comparison of the results with the different trip positions should add to the confidence of the test engineer in his interpretation of any particular set of results.

(ii) Several aft trips to create a 'transition sweep'

This was a main theme in the methodology for model tests for a transport aircraft. With a typical combat aircraft, the limitations are more severe and the interpretation of the comparative results more difficult. Nevertheless, for the wing of class I that produced the diagrams in Fig 9, tests with a trip at say, 0.15c, should be possible for Mach numbers of  $M = 0.80$  and above and with a trip at say, 0.40c at Mach numbers of  $M = 0.90$  and above. These chordwise positions apply to the mid-semi-span region on the wing upper surface; it will not be possible to move the trip as far aft on either the inner or outer wing.

The ideal aims of these tests with aft trips are

- (a) to achieve  $R_{eff} = R_{flight}$  within the range of the transition sweep,  $R_{eff}$ , as defined earlier, is the Reynolds number that would be needed with the (generally, forward) transition position forecast for flight at full-scale Reynolds numbers to produce the same viscous flow behaviour as in the model tests with an aft trip, the equivalence being judged on the basis of some chosen simulation criterion,
- (b) to eliminate any strong viscous-inviscid interaction such as a rear separation or a separation near 0.7c on the lower surface present in the model tests with forward transition but not expected to be present in flight at full-scale Reynolds numbers.

If these two aims are achieved, the results will lie in simulation scenario 1 as defined in §3.2.1, ie  $R_{crit} < R_{flight}$  and  $R_{flight}$  within the test range of effective Reynolds number.

If only (b) is achieved, the results will be in scenario 3, ie  $R_{crit}$  within test range but  $R_{flight} >$  maximum test effective  $R$ .

(b) is perhaps the more important objective because, if  $R_{crit}$  lies beyond the test range of effective Reynolds number, the results will lie in scenario 4 (or 5) and extrapolation of the test data to full-scale Reynolds numbers will be difficult.

Even if it is believed (eg from the results of the CFD calculations in Step 2) that  $R_{flight}$  is within the possible test range, one should not go to great trouble to test at precisely  $R_{eff} = R_{flight}$ : the transition position needed to achieve this identity is likely to vary with  $C_L$  and Mach number and also, there is the added difficulty with a combat aircraft wing that the identity cannot be defined with precision in view of the likely variation across the span. It is preferable simply to test with two or more different transition positions going as far aft as possible at any Mach number and paying particular regard to the design/operational conditions identified in Step 1 and to the position on the span where the flow breakdown is initiated as incidence is increased. Fortunately, as noted earlier, this is the part of the span where the maximum movement of transition should be possible and still meet the requirements set out above.

The trends in the data for a given  $C_L$ , Mach number and spanwise position should then be plotted against transition position or preferably  $R_{eff}$ . As in §3.3.1, the conversion to  $R_{eff}$  can be based on various different simulation criteria, eg

- (i) the simple, 'zero-level' criterion plotted in Fig 4 of §3.3.1. This zero-level criterion is based on the requirement that the boundary layer momentum thickness at the trailing edge of a flat plate should be the same for the aft transition position at the model test Reynolds

number as for the flight transition position at the effective Reynolds number. This criterion is simple to apply but can, at best, be only approximate since it does not depend on the particular wing geometry or pressure distribution,

- (ii) shock position,
- (iii) shock strength,
- (iv) the non-dimensional boundary layer thickness at the trailing edge of the real wing,
- (v) the boundary layer shape factor at a position close to the trailing edge.

It will be realised at this point that unless it has been possible to make the tests in a variable pressure tunnel, the derivation of  $R_{eff}$  using simulation criteria (ii-v) has to be based on the results of CFD calculations such as those performed in Step 2. This is one very good reason why it is certainly simpler and probably preferable merely to use the zero-level criterion for the conversion to  $R_{eff}$  when testing a model of a combat aircraft. Also, as noted in the discussion in §3.3.1, the final extrapolated data will not depend on whether the conversion to  $R_{eff}$  has been strictly accurate or not in all cases where the desirable aim of bringing the data into scenarios 1 or 3 has been achieved. If the data are still in scenario 4 (or 5), the uncertainty about the conversion is only one of several reasons why the extrapolation is necessarily difficult.

The trends in the measured data having been plotted against  $R_{eff}$  should then be compared with the corresponding trends in the computed data. Differences between the trends should be studied to establish whether they are due to strong viscous-inviscid interactions not allowed for in the calculations (if so, the disappearance of a difference in trend beyond a certain value of  $R_{eff}$  would be a check on more direct predictions of the value of  $R_{crit}$ ) or whether it is merely an indication that the available codes for the calculations cannot handle the complex geometry of the configuration under test.

#### (iii) Aft trip in a different spanwise direction

It is likely that, in most tests, the best simulation of the full scale flow in the  $C_L - M$  region up to buffet-onset, ie up to boundary 3 in Fig 9, for example, is achieved with the furthest aft trip that one can use at a given  $C_L$  and Mach number. This certainly applies in the range where the flow breakdown is of type D because then, the strongest shock is likely to be just outboard of the point of intersection of the 3 shocks and this is just where the trip can be at its furthest aft position. However, it is quite possible that the change from a forward trip to this aft trip will have led to a subsequent flow breakdown beyond boundary 3 that is less representative of the full scale behaviour. It is probable that, on the outer wing towards the tip, it will not be possible to move the transition trip so far aft and still meet the requirements set out earlier, eg 0.15c ahead of the shock. For example, the "0.35c trip" in Fig 16 was actually brought forward to 0.2c at the tip for this reason. As a result, the shortfall in local  $R_{eff}$  relative to local  $R_{flight}$  is likely to be greater near the tip than near mid-semi-span and hence, one may have a situation where  $R_{eff} > R_{crit}$  locally near mid-semi-span but  $R_{eff} < R_{crit}$  near the tip. The presence of say, a rear separation near the tip but not near mid-semi-span could then trigger a flow breakdown starting from near the tip and spreading inwards, whereas in flight at full-scale Reynolds numbers - and ironically, with the forward trip at model test Reynolds numbers - it could spread forward from the position of the outboard shock at buffet onset - see, for example, the comparison shown in Fig 16.

Faced with results such as those shown in Fig 16, it is difficult to know how, in the tests, to obtain a better simulation of the full scale behaviour. This example suggests however that one possible idea for a technique to simulate full-scale flow breakdown of type D (and possibly, types C and E also) is to choose trip positions across the span and thus, a trip direction spanwise such that  $(R_{full\ scale} - R_{eff})^*$  is independent of spanwise position, outboard of the expected point of initial flow breakdown at full scale Reynolds numbers. Effectively, this means the outer wing where the local Reynolds number is small, is allowed to call the tune and with this aft trip,  $R_{eff}$  near mid-semi-span will be less than that achieved in the best aft trip test in (ii). The two aft trips, one for buffet-onset and the other for buffet penetration, are compared diagrammatically in Fig 17.

Even accepting the above concept in principle, there is still at present considerable uncertainty about how to apply it in practice. For example, the suggestion that  $(R_{full\ scale} - R_{eff})^*$  should be maintained constant<sup>\*</sup> across the span of the outer wing is only one possible suggestion introduced primarily to explain the concept in principle. In practice, it may be preferable to think in terms of choosing an aft trip direction that will

- (i) give the same shock sweep inboard and outboard of the point of initial flow breakdown as forecast for the wing in flight at full scale Reynolds numbers at buffet onset,
- (ii) if any rear separation is present, ensure that its effects on pressure recovery at the trailing edge, local circulation and shock position as judged from a comparison of the measured and predicted trends with  $R_{eff}$  in these respects, are reasonably uniform across the span of the outer wing.

As with the proposal to test with a slightly different position for a forward trip, this test with an aft trip in a different direction will at least serve a diagnostic purpose. Even if it does not give a better simulation, it will at least alert the test engineer as to whether the results and, in particular, the flow breakdowns of type D are sensitive to the precise location of the transition trip. If they are and especially, if the shock fronts at buffet-onset are always parallel to the transition trips, as has been noted in certain combat aircraft model tests, the test engineer will appreciate the need to be cautious about whether he has achieved a realistic simulation.

<sup>\*</sup>Note: These values of Reynolds numbers are based on the mean chord; they are not values of local Reynolds number.



To summarise, it is vital to avoid, as far as possible, any effect that leads to a relative change in boundary layer behaviour at one part of the span compared with another. The chances of achieving this aim are greatly improved if it has been possible completely to eliminate any rear separation that would not be present at full scale Reynolds numbers. When this has not been achieved with aft-fixing, consideration should be given to whether it can be achieved by any other technique for manipulating the boundary layer. This is particularly important in the case of wings of class IV, Fig 12, where a separation may be present at high lift over the upper surface of a trailing edge manoeuvre flap but where it is not possible to test with an aft transition position because of the flow over and behind the leading edge manoeuvre flap. It is doubtful whether it would be desirable or feasible to modify the shape of the rear surface to obtain a better simulation of the full scale behaviour. The real need is to reduce the boundary layer thickness upstream of the rear manoeuvre flap and since this reduction is needed at a clearly defined position, it should be possible to consider achieving this aim, either by use of vortex generators or, preferably, by means of suction through an appropriately located slot. Further research is needed before one can define such a methodology in detail.

The discussion above regarding both Steps 5a and 5b has concentrated on the flow over the wing upper surface. However, with a typical combat aircraft, similar and/or additional problems can exist on the lower surface. For advanced wings designed to carry a high degree of rear loading, there is always a risk of a flow separation on the wing lower surface in a steep adverse pressure gradient near 0.7c. Also, in the high speed dash condition, the manoeuvre devices will be deflected upwards, thus introducing the possibility of a separation over the lower surface of the rear manoeuvre flap. Hence, the case for studying the effects of Reynolds number and transition position on the flow over the lower surface can be as strong as for the upper surface. The tests in Step 3 with and without a forward trip will have confirmed or otherwise the need for such tests and whether a 'transition sweep' can be attempted on the lower surface.

Combat aircraft are frequently expected to carry a multitude of external stores below the wing lower surface, eg on underwing pylons. Even the bare pylons without the stores can introduce local areas of separated flow on the wing lower surface. Reynolds number sweeps may still be useful but transition sweeps may not be feasible because the presence of the pylons may dictate that transition occurs near the leading edge. It is doubtful whether any extra tests can be proposed in this context; the problem has to be addressed in the extrapolation procedure in Step 6.

Reverting to the upper surface, the discussion above has not mentioned wings of class V, ie thin, highly swept wings with a sharp leading edge or wings of class VI, ie sweptforward wings. For class V the flow separations on such a wing will tend to occur at the wing leading edge, irrespective of Mach number or Reynolds number. There may however still be some scale effect on any secondary separation outboard of the primary vortex, Fig 3, and to check on this point, an extra test can be made with a trip located on a ray from the wing apex (or when appropriate, a strike/wing leading edge intersection) lying between the line through the inflexion in the surface streamlines and the line marking the secondary separation. If the test shows a marked difference in the results, the data from this test will probably be the better guide to the full scale behaviour. This point is particularly important when considering flight at  $\beta \neq 0$ .

Finally, all the above description of Steps 4 and 5 has assumed implicitly that the tests are being made on a model of an aircraft with a sweptback wing of types I-V; some of the detail but not the overall philosophy would have to be changed if the tests were made on a model with a sweptforward wing of type VI. One of the most significant differences in detail is revealed by the boundaries plotted in Fig 13: even with the help of a canard surface and appreciable shaping of the fuselage, it is likely that supercritical flow will tend to appear first on the inner rather than outer wing. Similarly, flow breakdown will tend to start on the inner wing and the risk of a premature rear separation, ie  $Re_{eff} < Re_{crit}$  is greater on the inner wing. The effects of a rear separation can be compounded by the high sweptforward of the wing trailing edge. The need for a transition sweep in order to increase the test range of  $Re_{eff}$  is therefore highly desirable and it should not be assumed that this is not required simply because the local Reynolds number is relatively high on the part of the wing subject to the strong viscous-inviscid interaction. The ability to undertake such a sweep is probably greater than for a sweptback wing but this may be a premature judgement since, to date, there is only limited experience in testing models of sweptforward wings and further research in this area could be helpful.

#### STEP 6 : Extrapolation of data to full scale

This is a vital step in the methodology. Past practice with model test data for combat aircraft has generally been to correct for the established smooth trends with Reynolds number in quantities such as skin friction drag and lift-curve slope but to accept the rest of the data as being the best that one can obtain from a test in a tunnel at reduced Reynolds number. It has, of course, been recognised that test data containing either a laminar separation near the leading edge or a rear turbulent separation, will be subject to scale effect but there has been no accepted procedure for attempting a quantitative extrapolation to full scale. The general aim has merely been to devise the best transition-fixing technique to suit the particular configuration under test (as in Step 5 above) and to conduct a Reynolds number sweep whenever possible and to extrapolate the measured trends from this sweep.

In view of the complex nature of the flow over a combat aircraft in many conditions of operational interest, it may often be difficult to adopt a more carefully reasoned scientific approach but this description of current practice hardly rates as a viscous simulation methodology. Complete viscous simulation is unlikely to be achieved in the actual tests, whatever techniques are employed, and so extrapolation to full scale should be a vital step in the full methodology. Extrapolation is needed even when it has been possible to extend the test range to cover  $Re_{eff} = Re_{flight}$  (scenario 1): it is unlikely that any one set of test data satisfies this identity in all respects.

It is easy to set out the broad principles of an extrapolation procedure. Essentially, the aim should be:

- (ii) at the lower transonic Mach numbers where, at moderate and high  $C_L$ , there is a risk that, in the model tests, there is a laminar separation near the wing leading edge, extrapolate if necessary the measured trends from a Reynolds number sweep up to  $R = R_{critF}$  and then, extrapolate 'the computed trends from  $R_{critF}$  to  $R_{flight}$ ;
- (iii) at Mach numbers where there is a rear separation or some other strong viscous-inviscid interaction on the rear of either surface, extrapolate the measured trends (from a Reynolds number sweep) to  $R = R_{critR}$  or (from a transition sweep) to  $R_{eff} = R_{critR}$  and then follow the computed trends to  $R_{flight}$ .

However, to apply these principles in practice is not as simple and straightforward as might appear. For example

- (a) they offer no help if the tests are being made in an atmospheric tunnel and if the model test  $R$  is less than  $R_{critF}$ . The real need is for a technique to create a turbulent boundary layer ahead of the point where the laminar boundary layer is separating in the model tests. This is an area for future research but, in the meantime, a comparison of the measured and computed results at the model test Reynolds number and of the computed forecasts at the full-scale Reynolds number may provide some qualitative guidance;
- (b) there will be cases where the model test data are being obtained at a Reynolds number or effective Reynolds number less than both  $R_{critF}$  and  $R_{critR}$ ; in such cases, the measured trends should, if necessary, be extrapolated to whichever is the higher of  $R_{critF}$  and  $R_{critR}$  with appropriate discontinuities at whichever is the lower;
- (c) the values of  $R_{critF}$  and  $R_{critR}$  are likely to vary with spanwise position,  $C_L$  and Mach number. The phrase "extrapolation of the measured trends up to  $R_{crit}$ " has to be interpreted as meaning extrapolation until  $R_{crit}$  has been reached over virtually the whole span at a given Mach number and  $C_L$ .

In principle, values of  $R_{critF}$  and  $R_{critR}$  can be determined

- (i) from predictions of transition position and flow separation on the basis of the calculated pressure distributions - see §3.2.4;
- (ii) by extrapolation of the measured trends in a Reynolds number sweep; and
- (iii) in the case of  $R_{critR}$ , by an extrapolation of the difference between the measured and predicted trends to find where these differences tend to zero.

Diagrammatic pictures illustrating the use of (iii) for determining  $R_{critR}$  are presented in Figs 18a-d. If the pictures in practice were as clear as those shown in Figs 18a-d, these would provide a good support tool to predictions by the direct method (ii). However, it is unlikely that, in practice, they will be as clear: the changes in slope at  $R_{critR}$  are likely to be smeared over a range of Reynolds number rather than appearing as sudden discontinuities. For  $R_{critF}$ , the pictures for shock position and  $C_D$  will probably provide the best guide; for  $R_{critF}$ , the value of  $C_p$  at a position close to the leading edge will be the most sensitive parameter.

None of these methods (i,ii,iii) can be regarded as fully reliable at the present time for a combat aircraft in view of the three-dimensional nature of the flow over a complex configuration. Probably, the safest course is to adopt (ii) but use of (ii) for  $R_{critF}$  poses a stringent test on the accuracy of methods to predict the pressure distribution around the leading edge of three-dimensional wings of complex geometry. Fortunately, errors in predicting  $R_{critF}$  and  $R_{critR}$  may not be too serious in their effects on the final end-result of the extrapolation of the model test data to full scale conditions.

The extrapolation procedure is now discussed in detail for some of the most likely objectives for model tests for a combat aircraft.

#### A Drag (ignoring scale effects on flow over fuselage afterbody)

One of the most likely objectives for a model test on a combat aircraft is to determine the aircraft drag in the cruise, high speed dash and sustained manoeuvre conditions identified in Step 1. In most of these conditions, the flow will be supercritical and the extrapolation has therefore to allow for changes with Reynolds number in wave drag as well as the more obvious changes in viscous drag. In principle, one should apply the procedure already described in detail in the methodology for subsonic transports in §3.1.2. However, the three-dimensional nature of the complex flow patterns over typical combat aircraft wings adds to the difficulties in applying this procedure in practice.

Nevertheless, in principle

$$\begin{aligned}
 C_{Dflight} &= \text{Measured } C_D \text{ at } (x_T, R)_{test, n} \\
 &\quad - \text{excess } C_D \text{ at } (x_T, R)_{test, n} \\
 &\quad + \text{Computed } [C_D \text{ at } (x_T, R)_{flight} - C_D \text{ at } (x_T, R)_{test, n}] \\
 &\quad - \Delta_{TR} C_D + \Delta_F C_D
 \end{aligned}$$

where

- (i) the suffix 'n' denotes the scenario,  
 (ii) the datum condition 'test,n' for the start of the extrapolation depends on which scenario is relevant:

Scenario 1 :  $R_{crit} < R_{flight}$  and  $R_{flight}$  within test range of  $R$  or  $R_{eff}$   
 Scenario 2 : As 1 but  $R_{crit} > R_{flight}$   
 Scenario 3 :  $R_{crit} < R_{flight}$ ,  $R_{crit}$  but not  $R_{flight}$  within test range of  $R$  or  $R_{eff}$   
 Scenario 4 :  $R_{crit} < R_{flight}$  but both  $R_{crit}$  and  $R_{flight}$  outside test range  
 Scenario 5 : As 4 but  $R_{crit} > R_{flight}$ .

Scenario	Datum test,n	
	Reynolds number sweep	Transition sweep
1	$R_{flight}$	$R_{eff} = R_{flight}$
2,3	$R_{crit}$	$R_{eff} = R_{crit}$
4,5	Highest test $R$	Furthest aft $(x_T)_{test}$

Note: the second term in the equation therefore only exists when the test data are in scenarios 4 or 5. Even when the data have been brought within scenario 1 by means of a transition sweep, it will still be necessary to activate the extrapolation procedure because the third, fourth and fifth terms will still be present, e.g. it would be merely coincidental if the skin friction drag were the same in flight as in the model test at  $R_{eff} = R_{flight}$ .

- (iii) the words "excess drag" refer to the  $\Delta C_D$  believed to be associated with the strong viscous-inviscid interaction at  $(x_T, R)_{test,n}$  not allowed for in the CFD calculations. Graphs such as those in Fig 18 have to be constructed and extrapolated to  $R$  (or  $R_{eff} = R_{crit}$ ) and then, the excess  $C_D$  at  $(x_T, R)_{test,n}$  for scenarios 4 and 5 has to be determined as the difference between the measured and computed trend in  $C_D$  between  $(x_T, R)_{test,n}$  and  $R_{crit}$ . The need to predict this term accounts for why extrapolation is more difficult in scenarios 4 and 5.
- (iv) the calculation of the third term can be performed most accurately by splitting  $C_D$  into three component terms

$$C_D = C_{DW} + C_{DV} + C_{Di}$$

where  $C_{DW}$  = wave drag coefficient,

$C_{DV}$  = viscous drag coefficient

$C_{Di}$  = vortex-induced drag coefficient.

Methods for predicting  $C_{DW}$  and  $C_{DV}$  are described in 53.2.4 but it should be stressed that, to date, these have only been validated for wings of low or moderate sweepback up to say, 40° - 45° sweep. It should be remembered that these methods are based on an approach originally developed for predicting the drag of two-dimensional section and it would be unreasonable to expect that they would still be applicable for say, a slender delta wing,

- (v) in the fourth term,

$\Delta_{TR} C_D$  is the estimated increase in the measured  $C_D$  due to the presence of the transition trip,

- (vi) in the fifth term,

$\Delta_E C_D$  is the estimated increase in  $C_{Dflight}$  due to the presence of either roughness or excrescences on the aircraft but not represented on the model.

The equation does not include any corrections for other effects that do not properly form part of a viscous simulation methodology but which, nevertheless, can contribute to the extrapolation from model to full scale, e.g. jet effects, intake spillage effects, aeroelastic effects.

To give a single illustration of why, in practice, application of the procedure can be more difficult for a combat aircraft wing than for the high aspect ratio wings of the typical subsonic transport, one can refer in general terms to the likely shape of the  $C_D - R_{eff}$  or  $C_D - R$  curves. Any feature approaching a 'discontinuity' in these curves for a high aspect ratio wing or a two-dimensional aerofoil can be regarded as a clue as to where some strong viscous-inviscid interaction is disappearing (or possibly appearing) with increase in Reynolds number. It is more difficult to make such a judgement for a section of a moderate aspect ratio wing: a 'discontinuity' may merely indicate a significant change in the supercritical flow pattern over the section as a result of a change with Reynolds number in possibly, merely, the indirect scale effects, i.e. the progressive change in boundary layer displacement thickness with Reynolds number. Such a change would be expected to occur, for example, for a section lying between the full-scale and model test positions of the intersection of the 3 shocks in the flow patterns in Fig 17. Admittedly, the subsequent spanwise integration of the values of local  $C_{DW}$  and  $C_{DV}$  may largely eliminate such a 'discontinuity' but this point is just one example of another of the difficulties: there is so much spanwise variation in all respects that it may be difficult, in practice, to identify the reasons for differences between the measured and computed trends with Reynolds number.

## B Buffet onset and subsequent flow breakdown

The extrapolation procedure depends on which type of flow breakdown has been observed:

Type A : Leading edge vortex separation from wing apex (or defined position near wing root)

Little significant scale effect would be expected at least up to the incidence when the vortex lift off the surface and/or bursts. Therefore, up to this incidence, one should use whatever has been judged to be the best set of test data from Steps 3 and 5 with no further correction but with, possibly, some reservations about the lateral characteristics.

Further research is needed to clarify whether there are significant scale effects in the final flow breakdown characteristics.

Type B : Separation from near leading edge, spanwise extent initially incidence-dependent.

This is likely to be a laminar separation in the model tests and its appearance and growth with incidence will vary appreciably with Reynolds number up to  $R_{crit}$  when it is replaced by a turbulent separation. The ability to extrapolate is therefore heavily dependent on the ability to predict transition and the occurrence of laminar or turbulent separation near the leading edge. In cases where it has been possible to undertake a Reynolds number sweep, one should

- (i) extrapolate the measured trend with Reynolds number in the value of  $C_L$  for the separation-onset at a given spanwise station and Mach number up to the predicted value of  $R_{crit}$  for this station,
- (ii) estimate the change in  $C_L$  for separation-onset likely to occur at  $R_{crit}$  as a result of the change from a laminar separation to a turbulent separation with transition at what is likely to be close to the full scale position for this incidence and Mach number,
- (iii) predict, eg on the basis of the methods in 53.2.4, possible changes in  $C_L$  for separation-onset at a given spanwise station and Mach number with increase in Reynolds number from  $R_{crit}$  to  $R_{full}$  scale,
- (iv) create, on the basis of (i,ii,iii), an idea of the spanwise development of the separation with  $C_L$  at full scale Reynolds number and compare with the corresponding developments in the model tests. If, at some point in a Reynolds number sweep, a similar development occurred but at a lower  $C_L$ , it would be possible to apply a  $\Delta C_L$  correction to the test data obtained in this particular test but it is unlikely that, in general, one will be able to find such a set of data. It is more probable that one will find examples where the separation near the leading edge has been delayed so much by an increase in Reynolds number that the flow breakdown is related to a rear rather than a leading edge separation.

At the present time, it is uncertain whether any satisfactory methodology can be developed to deal quantitatively with the extrapolation for this type of flow breakdown. The steps described above may, however, represent a start towards devising such a procedure or, at least, showing the order of the uncertainty.

Type C : Shock-induced separation behind a highly swept shock.

Figs 9 and 10 show that the increase,  $\Delta C_L$ , in  $C_L$  between boundary 2 (separation-onset) and boundary 3 (separation back at the trailing edge) can be quite considerable when the flow breakdown is of type C. At the present time, there is no established method for predicting the likely scale effect on  $\Delta C_L$ . Any success in predicting  $\Delta C_L$  in terms of the shock strength and the boundary layer thickness ahead of the shock by a method such as that proposed by Fulker and Ashill might be purely coincidental, in view of the fact that the reattachment process for a separation induced by a highly swept shock is entirely different from what happens in two-dimensional flow. The three-dimensional separation behind a shock swept at more than about  $25^\circ$  initially rolls up into a part-span vortex and 'separation back to the trailing edge' corresponds with when this vortex bursts, lifts off the surface or moves so far inboard that a complete flow separation from near the leading edge back to the trailing edge can exist outboard of the vortex. Prediction of  $\Delta C_L$  involves more than just the prediction of when these phenomena occur: there is also the question of how much extra lift is carried by the wing as a result of the suction on the wing surface below the vortex. Some evidence suggests that, with increase in Reynolds number, this vortex flow enervates less of the wing surface, implying a reduction  $\Delta C_L$  with Reynolds number. On the other hand, it is arguable that, as the separation extends back to the trailing edge, eg between  $(\alpha_x - 0.5^\circ)$  and  $(\alpha_x + 1.5^\circ)$  in Fig 5, the separation loses its vortex character and becomes more analogous to a bubble separation and if one then chooses to apply a method such as Fulker and Ashill, it would be found that  $\Delta C_L$  between boundaries 2 and 3 increases with Reynolds number. On present knowledge, therefore, prediction of the 'direct' viscous effects is very uncertain; if a rear separation is present in the model tests, this merely adds to the uncertainty.

The best procedure that can be suggested at the present time is as follows:

- (1) extrapolate the measured trends<sup>2</sup> with  $R_{eff}$  in the 'indirect' viscous effect, ie the value of  $C_L$  for the shock strength that corresponds to separation-onset at a given spanwise station up to  $R_{crit}$  and then, extrapolate from  $R_{crit}$  to  $R_{full}$  scale using

<sup>2</sup>from a Reynolds number sweep and/or transition sweep; despite the far forward shock position, a change of even 0.05 in transition position may still be significant.

CFD calculations of the wing surface pressure distribution. Assuming that the shock strength for separation-onset can be treated as independent of  $R_{eff}$  (the measured trends will provide a check on this point), this prediction of the 'indirect' effect will give a correction  $\Delta C_{L2}$  to apply to the  $C_L - M$  boundary 2,

- (ii) extrapolate to  $R_{full}$  scale, the measured trends against  $R_{eff}$  in the lift increments  $\Delta C_{L3}$  from boundary 2 to boundary 3 and  $\Delta C_{L4}$  from boundary 3 to boundary 4,
- (iii) add  $\Delta C_{L2}$ ,  $\Delta C_{L3}$  and  $\Delta C_{L4}$  to produce a full scale estimate of boundary 4 and similarly for boundary 3 and interpret the scale effect on the aerodynamic characteristics on the basis of these lift increments.

Type D : Shock-induced separation behind a shock near 0.3 - 0.5 chord.

For this type of flow breakdown, full scale buffet-onset values, ie boundary 3, can, in theory, be predicted as described in §3.3.1.2, but the results on which to establish a measured trend may be more limited. Also, because there is no region where the flow can be described as quasi-two-dimensional, developments, at the critical spanwise station where the shock-induced separation occurs first, in the incidence range in which this separation is extending back to the trailing edge, may be modified by what is happening at neighbouring stations. Nevertheless, there is some evidence that for flow breakdowns of type D on at least wings of class 1, it is still possible to apply the Fulker and Ashill method with as much success as for transport wing configurations. More experience and more research are however needed.

At the present time, therefore, the recommended procedure is as follows:

- (i) predict the buffet-onset boundary 3 by applying the procedure of §3.3.1.2, Step 6b starting if possible from the measured results with an aft trip of type (iii), Fig 17,
- (ii) assume that what happens beyond this corrected full scale boundary 3 is similar to that observed in the test with aft trip (iii).

Type E : Shock-induced separation behind a shock at 0.6 - 0.8c.

One can distinguish between two possible situations:

- (a) a pure type E flow breakdown related simply to the development of a separation induced by a far aft, relatively unswept shock,
- (b) a more complex type E flow breakdown developing out of a situation at lower values of  $C_L$  where, even in the absence of a strong shock wave, there is a rear separation over the same part of the wing surface, eg over the surface of a rear manoeuvre flap in the case of a wing of class IV.

For (a), it can be argued that the extrapolation to full scale Reynolds numbers merely has to allow for the change in the indirect viscous effect, ie the change in the shock strength for a given  $C_L$  and Mach number. The changes due to the direct viscous effects should be trivial because, for these aft shock positions, the shock-induced separation bubble is likely to extend to the trailing edge immediately after separation-onset. As previously, the indirect viscous effect can be estimated by comparing the results of CFD calculations for full scale and model test Reynolds numbers and transition positions.

For (b), no extrapolation procedure can be put forward with any certainty. The main difficulty lies in the fact that model test results suggest that a rear manoeuvre flap can be effective, even when the flow is fully separated over one surface. In other words, one has to devise an extrapolation procedure for conditions in which even the full scale flow contains a rear separation. The indirect effects can be allowed for by extrapolating the measured rather than the predicted trends and, in this case, extrapolating the measured trends all the way to  $R_{full}$  scale but further research - and study of any flight-tunnel comparisons - is needed before one can say with confidence that this is sufficient.

### C Manoeuvre flap effectiveness

The assessment of a manoeuvre flap design and the determination of how to optimise the settings of the flaps to suit flight at different conditions are likely aims for model tests on a combat aircraft. An extrapolation procedure is therefore required for predicting the scale effect on the flap effectiveness, ie  $\Delta C_L$ ,  $\Delta C_m$  and  $\Delta C_D$  due to flap deflection. One should however resist the temptation to devise a procedure for the direct extrapolation of these quantities. It is preferable to treat the wing with the manoeuvre flap at different settings as distinct configurations and to extrapolate the results for each configuration separately. This recommendation is based on the fact that it is quite possible for a change in flap setting to alter, not merely the magnitude, but also the very nature of the scale effect. For example, recalling the discussion in Step 4 of the likely scale effect for different types of flow pattern, it is possible to visualise a situation<sup>3</sup> in which in manoeuvring flight at say,  $M = 0.65$ ,

- (i) the scale effect with the flap at 0° is mostly related to the disappearance with increase in Reynolds number of a laminar separation and its replacement by a turbulent separation either near the leading edge or, more probably, spreading forward from the rear with increase in incidence,
- (ii) the scale effect with the flap deflected down at say, 10° is related to the effect of Reynolds number on the development of a shock-induced separation bubble on the upper surface near, say, 0.15c and also the indirect scale effect associated with the extent to which a



thick boundary layer is capable of suppressing the expansion in the flow over the upper surface around the knuckle of the rear flap at, say,  $0.7 - 0.8c$ ,

- (iii) the scale effect with the flap at intermediate settings, eg  $5^\circ$ , can contain all these effects interacting with each other.

It is clearly unreasonable to expect any simple rules-of-thumb for the variation of  $\Delta C_L$ ,  $\Delta C_m$  and  $\Delta C_D$  due to flap deflection with Reynolds number to succeed in such a situation. The need is to understand the nature of the flow at each flap setting and to extrapolate each configuration as if it was a new wing design. The general dictum "know your flow" is crucial.

### 3.3.2.3 Some particular examples of practical interest

The general methodology for a combat aircraft, as set out above, has addressed some of the complexity of the flow over a typical clean configuration but has still, for the sake of clarity, omitted some of the complication likely to be encountered in practical applications of the methodology. For example, on a real project, the flow - and, in particular, the viscous effects - may be controlled by some local feature of the aircraft geometry or by the interaction of the flow fields over close-coupled surfaces. To quote four typical examples:

- (1) On several aircraft projects<sup>4</sup>, the usable lift characteristics have been enhanced by the use of some form of leading-edge device near or outboard of mid-semi-span, eg a sawtooth, a notch or a small fence. The common feature of these devices is that they provide a 'fix' to the flow pattern. Some sources of scale effect are thereby eliminated, eg whatever the Reynolds number, part-span vortices will tend to form outboard and inboard of the 'fix'. On the other hand, experience has shown that Reynolds number can affect the optimum spanwise position for such a fix and if there are more than one, the spanwise distance between them. Prediction of whether such changes are likely to occur should be based on the in-depth study of the flow patterns in Step 4 and devising a procedure in Step 6 to suit the observed flow phenomena.
- (2) On several aircraft projects, the usable lift has been enhanced by the fitting of a leading-edge chord extension or strake at the wing root. The flow patterns over a wing/strake combination can be very complicated<sup>5</sup> but, in some respects, they may be less sensitive to changes in Reynolds number than the apparently simpler flow pattern over the wing without the strake. The basic wing leading edge/chord extension or strake intersection serves to position several major features of the flow pattern. Also, the effect of the strake on the flow over the rear wing upper surface tends to reduce the risk of a rear separation occurring even at low Reynolds number. On the other hand, the flow under the vortex shed by the highly swept strake leading edge can separate at high incidences and this development can interact with any area of flow separation on the outer wing: a general methodology may not be able to cope with such a complex situation.
- (3) Many combat aircraft are now fitted with a canard surface and, in some respects, the canard flow field has similar effects to the flow over a leading-edge chord extension at the wing root. For example, typical effects of the canard flow field include a reduction in the loading on the inner wing and hence, less risk of a rear separation; also, the rear shock will be weaker and the forward shock will tend to originate from near the intersection of the wing leading edge and the edge of the canard wake. As a result, the intersection point of the 3-shock pattern (Fig 2) will be further out than on the wing without canard at the same incidence and Mach number and thus, the likely spanwise extent of the area of flow separation on the outer wing will be less. All these features should reduce the likely scale effect between model and full scale and improve the ability to apply the methodology. On the other hand, the flow over the canard surface itself may contain scale-sensitive viscous effects which may add to the complication by interacting with the flow over the main surface.
- (4) Finally, combat aircraft are required to carry a multitude of stores which are often mounted on underwing pylons. Even the bare pylons without the stores can result in local separations on the wing lower surface near the pylons. Arguably, the local Mach numbers in the wing-pylon junctions are often so high that scale effects and the consequences would not be expected, but it is still possible that these effects will be relieved by an increase in Reynolds number. This adds a further element of uncertainty but the advice must still be to apply the principles of the general methodology to the local situation, viz know your flow and use CFD methods to guide the extrapolation whenever possible.

### 3.3.2.4 Concluding Remarks

Devising a viscous simulation methodology for model tests of a combat aircraft design is more difficult than for a subsonic transport. The geometry is more complicated and hence, more difficult to model for a CFD calculation; the flow patterns are more complex and can contain various interacting features; there is more interest in the development of the flow beyond the buffet-onset boundary; the ability to manipulate the boundary layer in the model tests is more limited. Nevertheless, one should not be too depressed; in many cases, there may be relatively little scale effect and, in general, the transition positions required to give  $Re_{eff} = Re_{flight}$  will be further forward than for a subsonic transport and hence, relatively small changes in transition position may give a useful lead.

The emphasis in the methodology as described in §3.3.2.2 rests on the in-depth study of the flow patterns and, in particular, the identification of the scale-sensitive viscous effects in the flow patterns over the model under test. The description of these flow patterns and of how, in principle, to construct a methodology to meet the various possible situations, is based on much past experience and on an awareness of the advances in CFD methods. However, it must be stressed that some of the detail in the proposed methodology has not yet been validated in practice. To be fully successful:

- (i) the test engineer must be fully aware of the type of flow over the test configuration,
- (ii) the CFD methods may have to be developed further to cope with the complicated geometry and complex flow, and
- (iii) better methods than aft-fixing may be needed to manipulate the boundary layer in the model tests in order to prevent an unrepresentative laminar separation and to obtain a better simulation of the boundary layer thickness ahead of a region of the surface where separations are expected to occur both in the model tests and in flight at full-scale Reynolds numbers.

It is recommended that, to gain experience, the proposed methodology should be applied for a significant period in parallel with whatever is the established practice. Any large differences in the extrapolated results should be assessed to find whether the reasons justify departure from existing practice: in other words, the methodology that has been set out above should be better, being on a sound scientific basis, but it will still have to prove itself in the future.

#### REFERENCES

- 1 Molt, D R, Probert, B, Some Particular Configuration Effects on a Thin Supercritical Variable Camber Wing, 1980, Paper No 15, AGARD-CP-285.
- 2 Braslow, A L, Knox, E C, Simplified Method for Determination of Critical Height of Distributed Roughness Particles for Boundary-Layer Transition at Mach Numbers from 0 to 5, 1958, Langley Aeronautical Laboratory NACA TN 4363.
- 3 Haines, A B, Viscous Simulation Scenario for Military Aircraft and Components, 1984, Unpublished.
- 4 Haines, A B, Aerodynamic Interference - A General Overview, 1983, Paper No 9, AGARD Report 712.
- 5 Moss, G F, Some UK Research Studies of the Use of Wing-Body Strakes on Combat Aircraft Configurations at High Angles of Attack, 1978, Paper No 4, AGARD-CP-247.



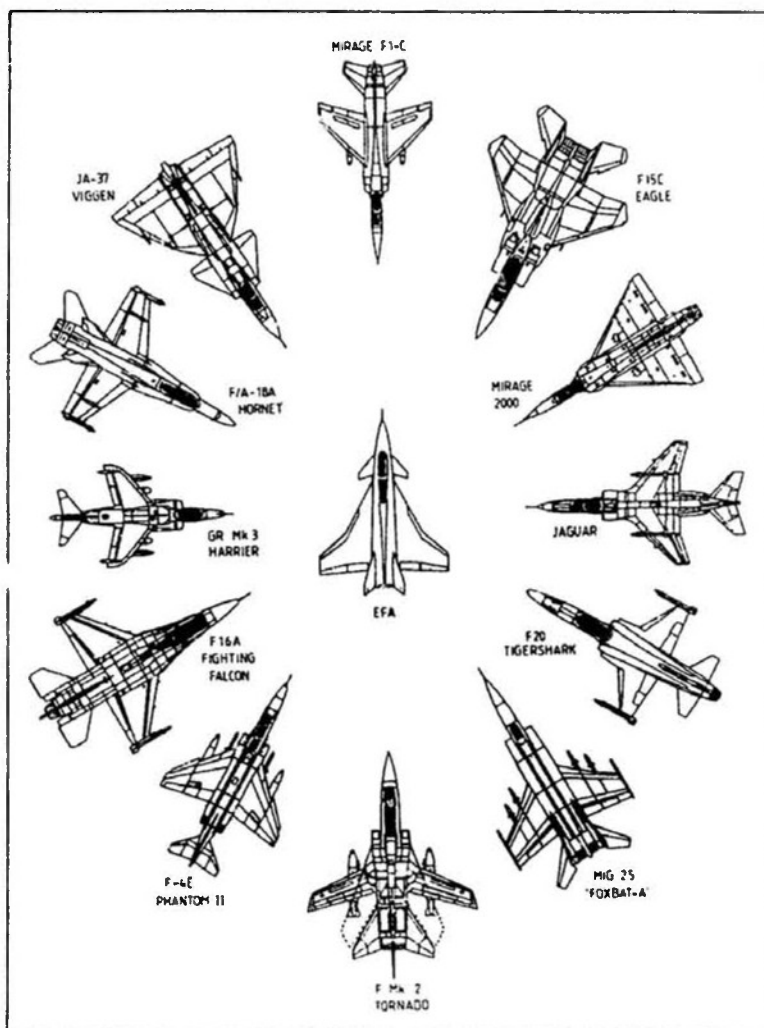


FIG 1 A VARIETY OF WING PLANFORMS FOR COMBAT AIRCRAFT

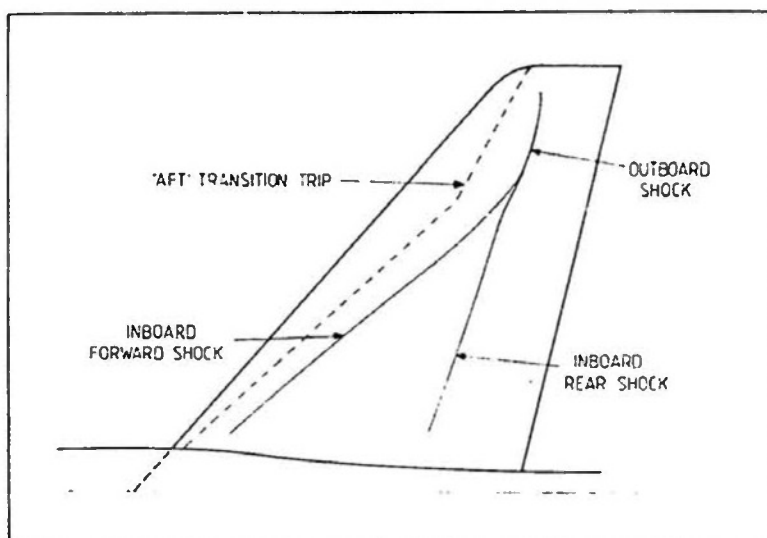


FIG 2 TYPICAL SHOCK PATTERN : COMBAT AIRCRAFT WING

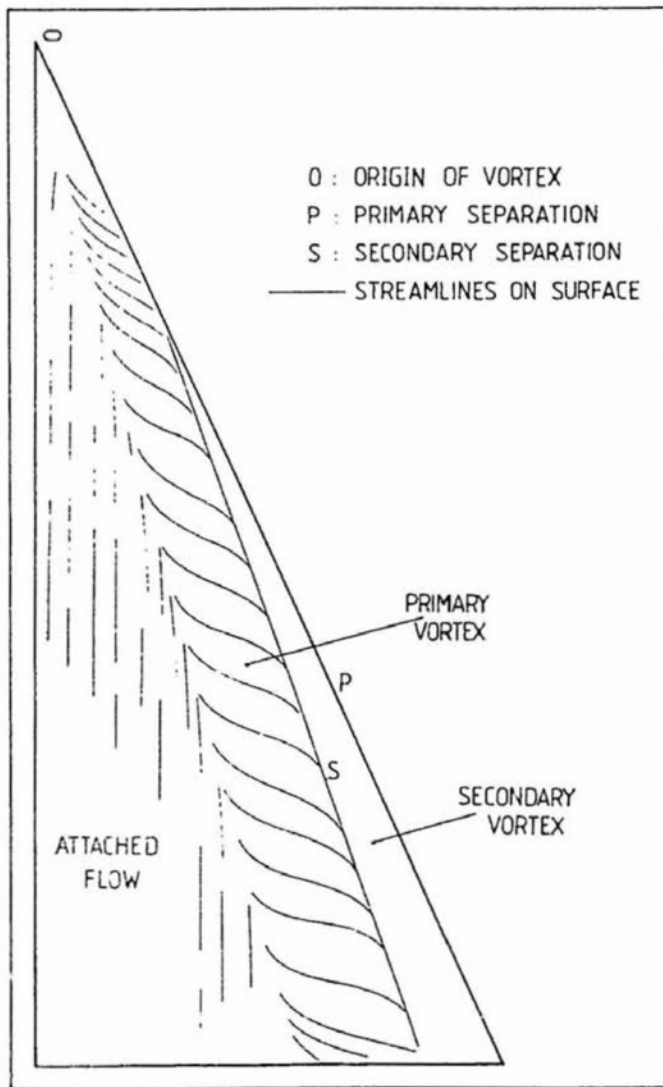


FIG 3

TYPE A FLOW DEVELOPMENT

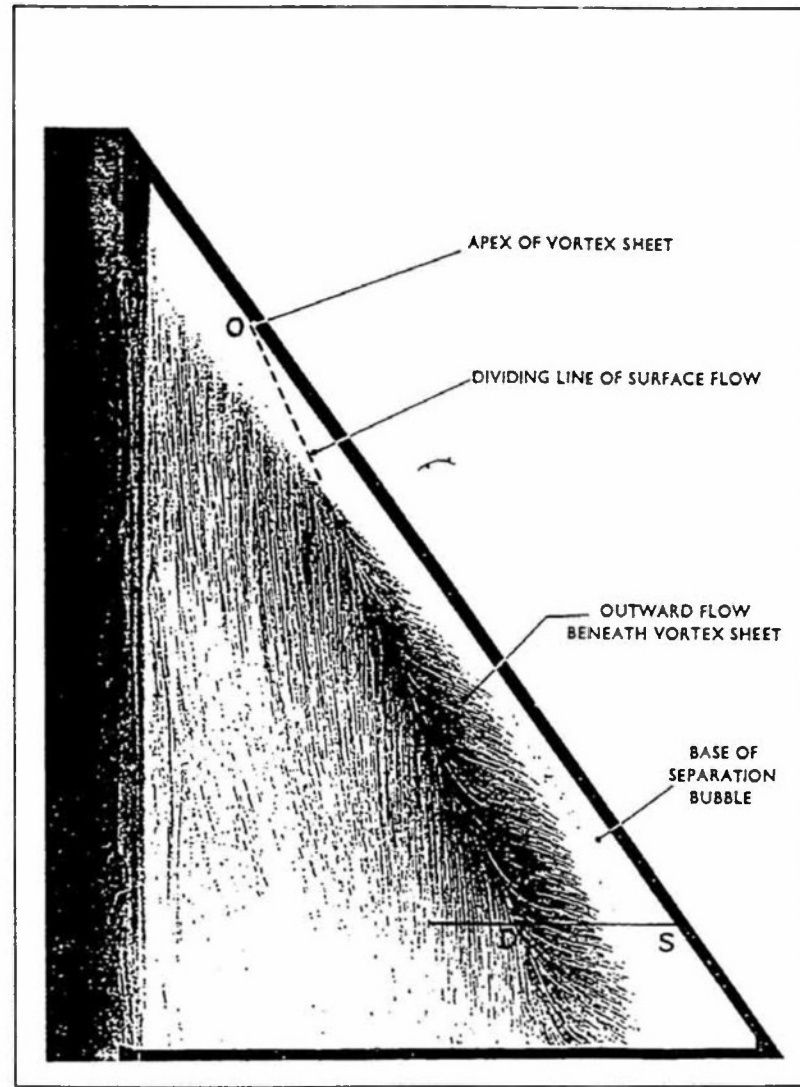


FIG 4

TYPE B FLOW DEVELOPMENT

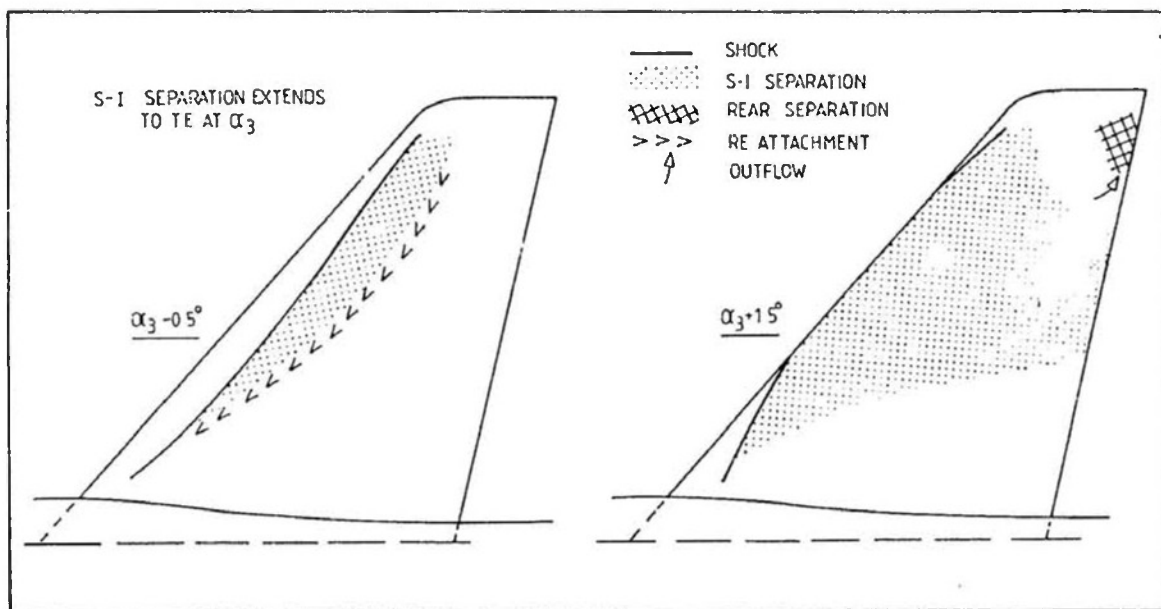


FIG 5

TYPE C FLOW DEVELOPMENT

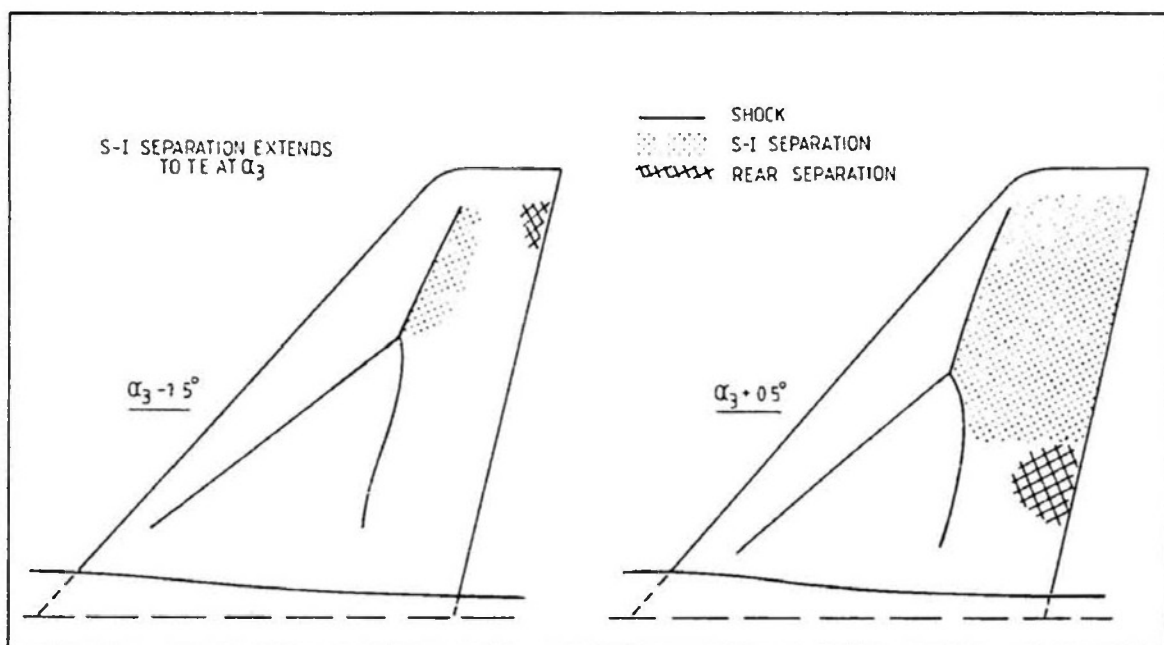


FIG 6

TYPE D FLOW DEVELOPMENT

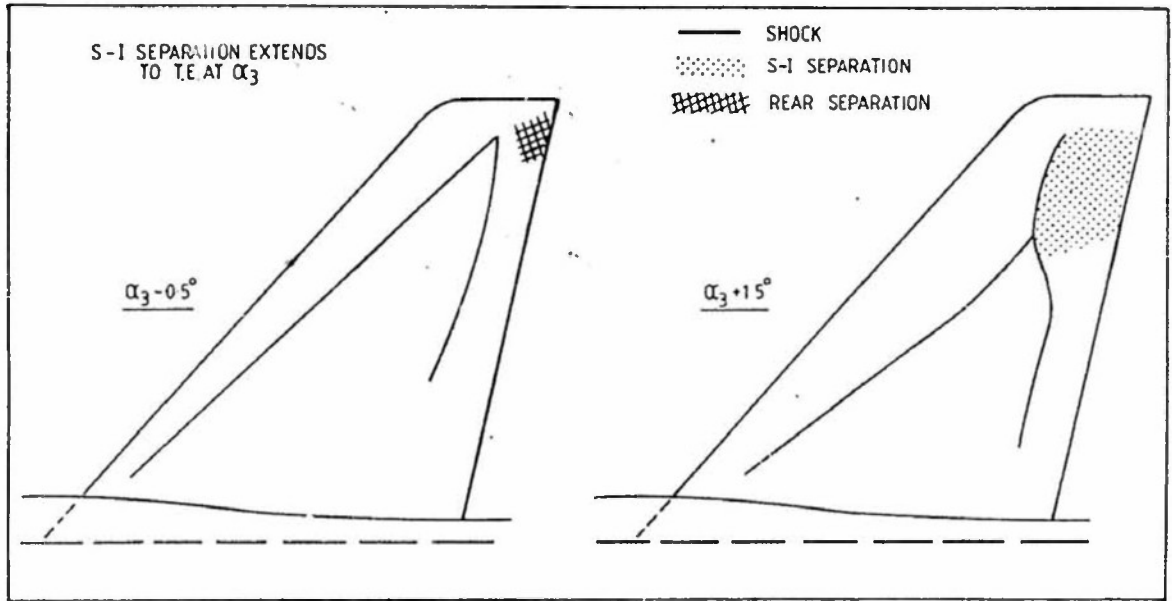


FIG 7

TYPE E FLOW DEVELOPMENT

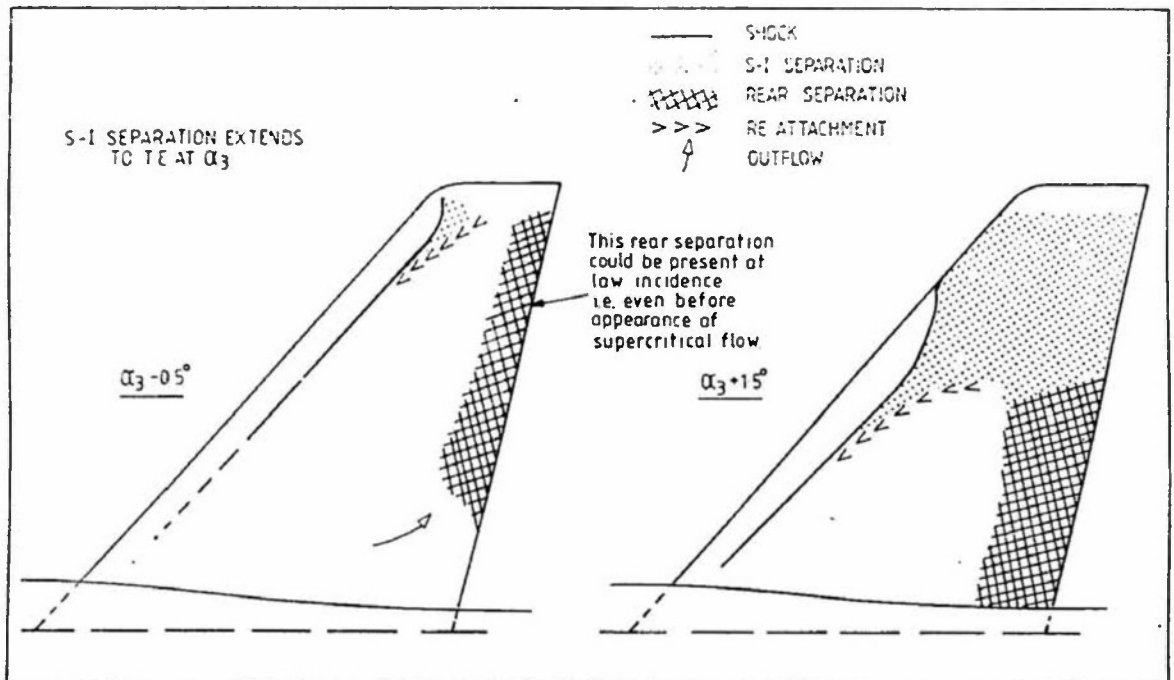
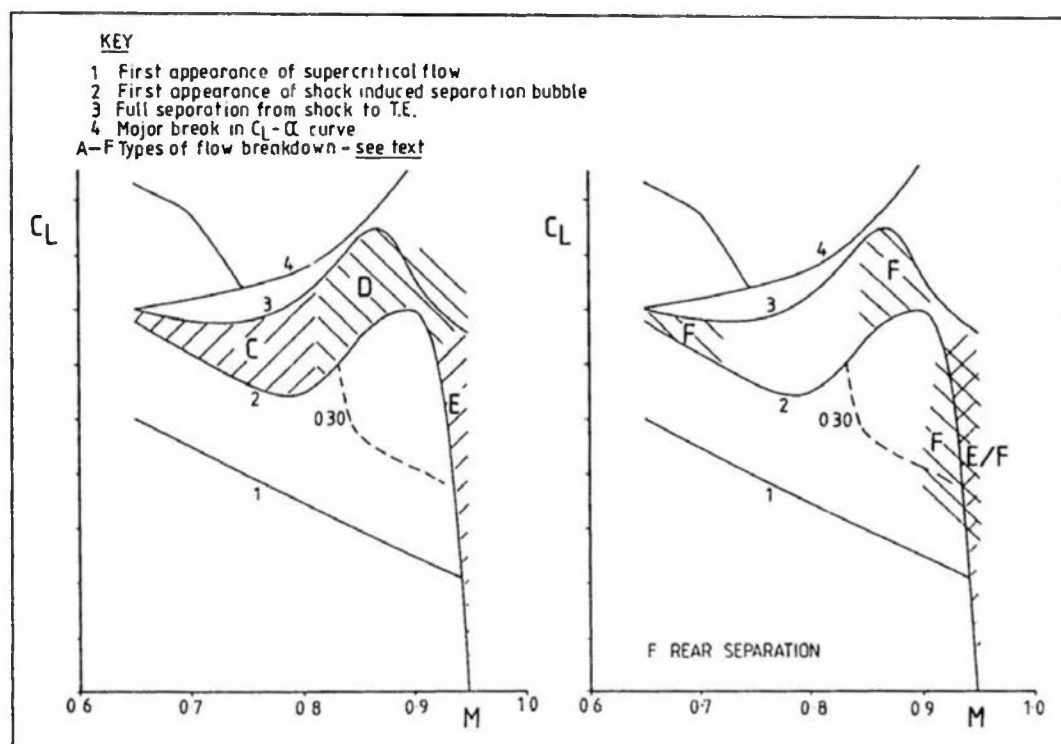
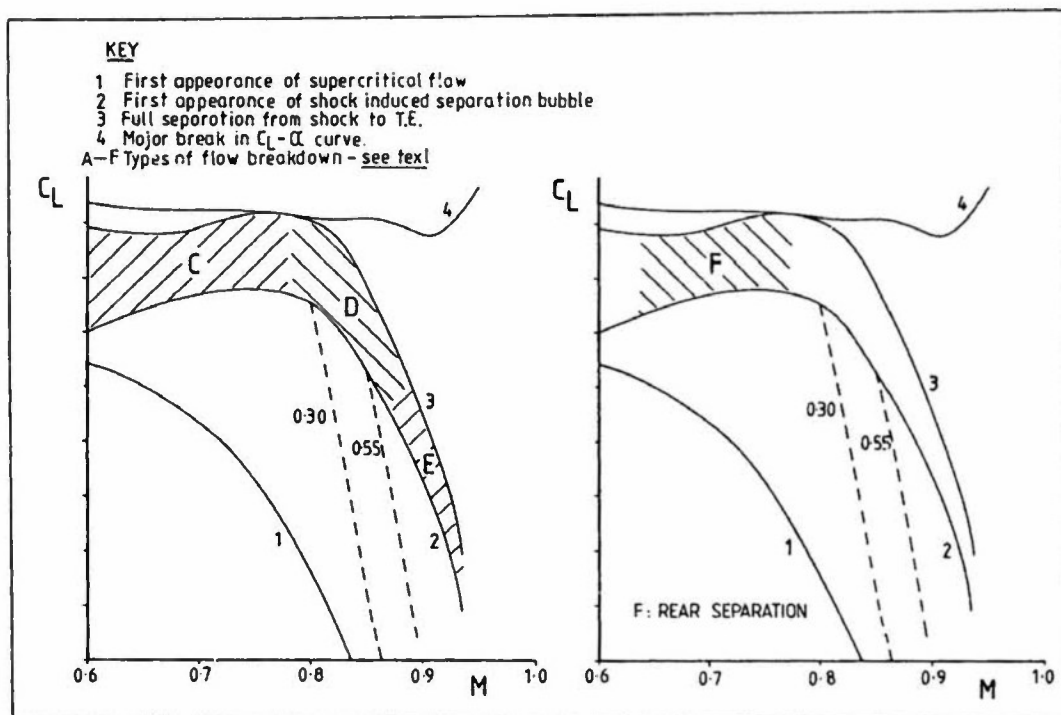


FIG 8

TYPE F FLOW DEVELOPMENT (PROVOKED BY PRESENCE OF TYPE C)



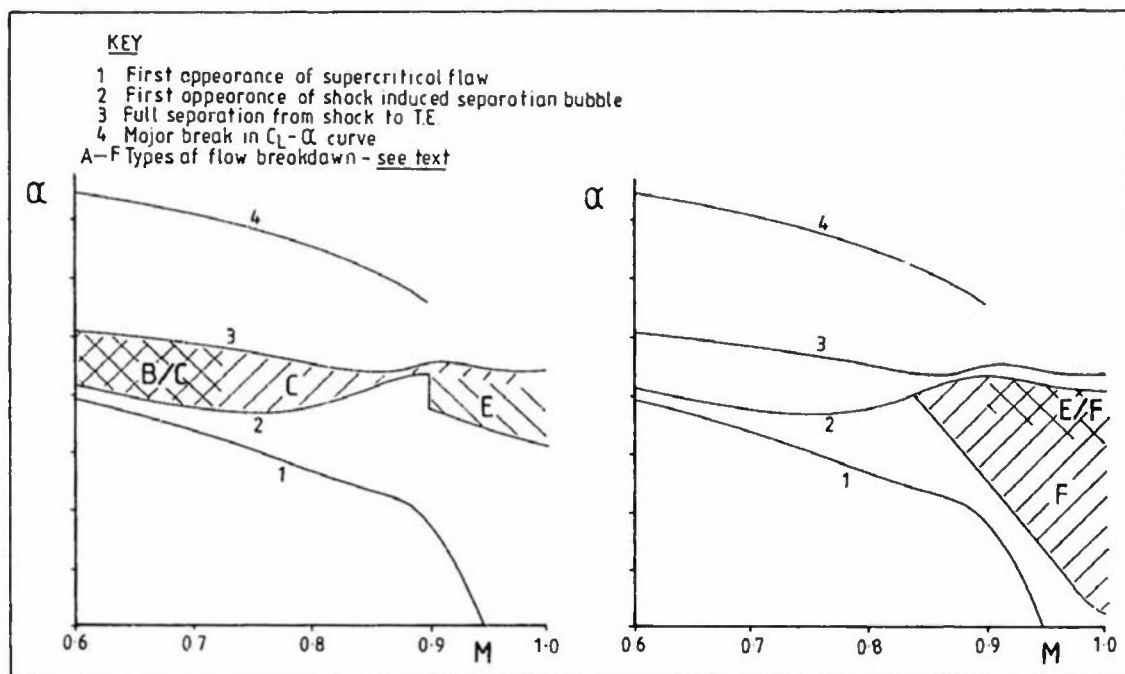


FIG 11

FLOW DEVELOPMENT : WING CLASS III

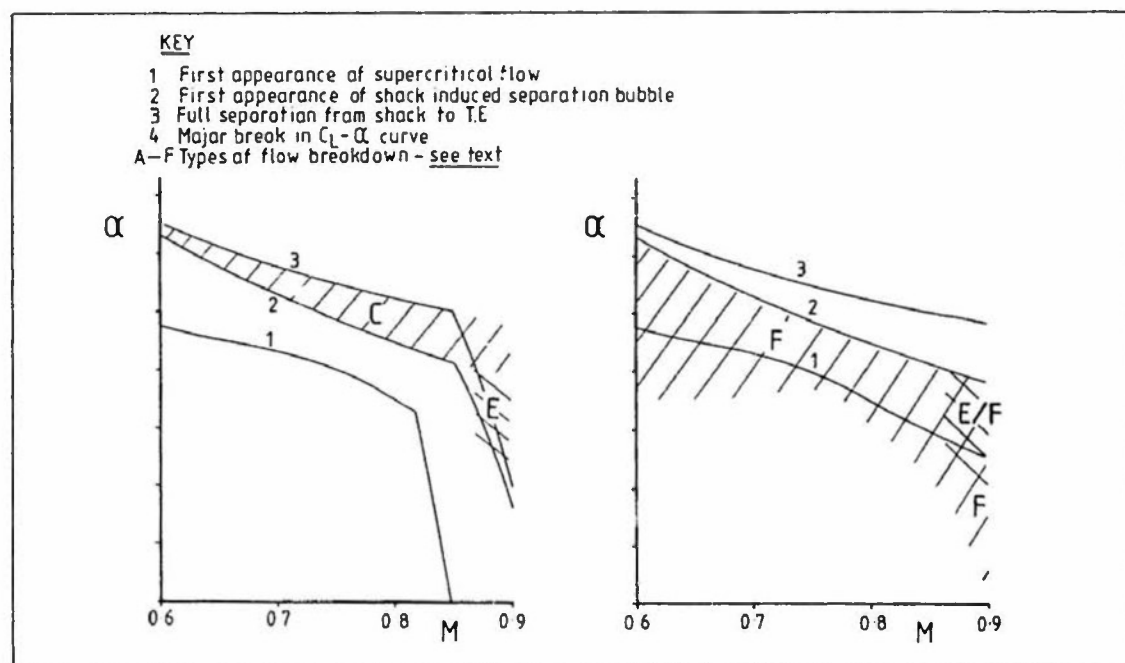


FIG 12

FLOW DEVELOPMENT : WING CLASS IV

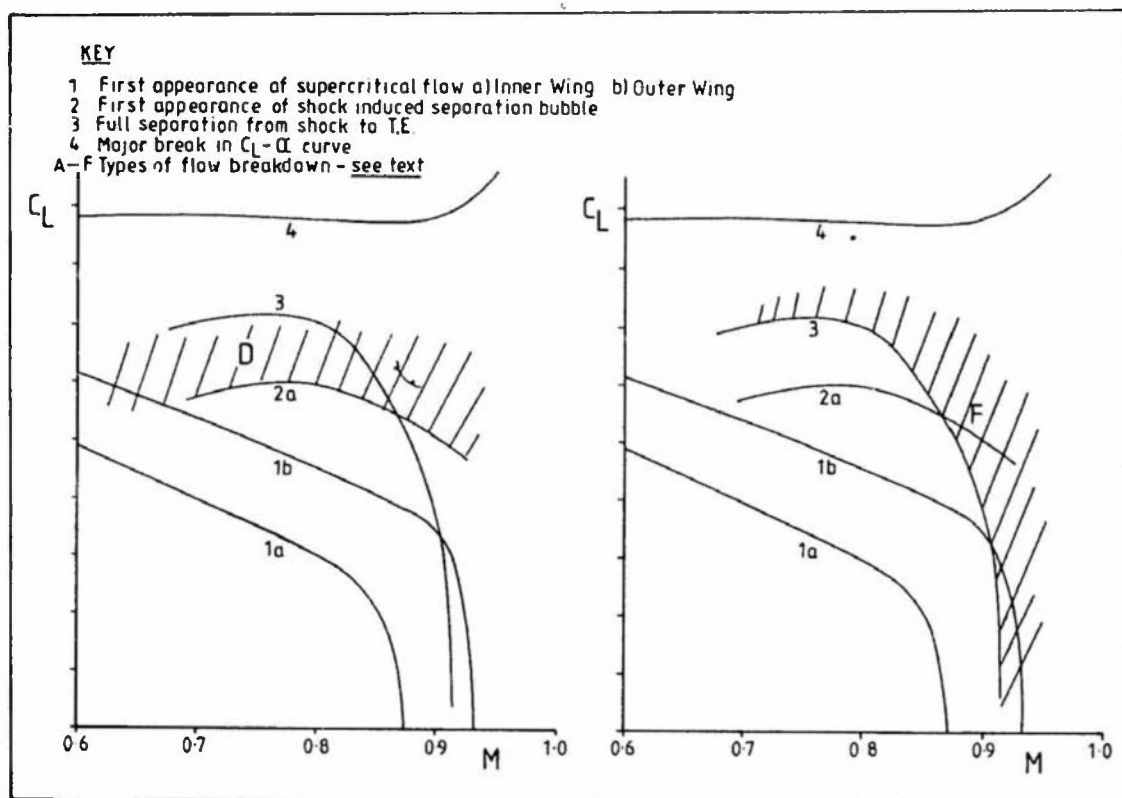


FIG 13

FLOW DEVELOPMENT : WING CLASS VI

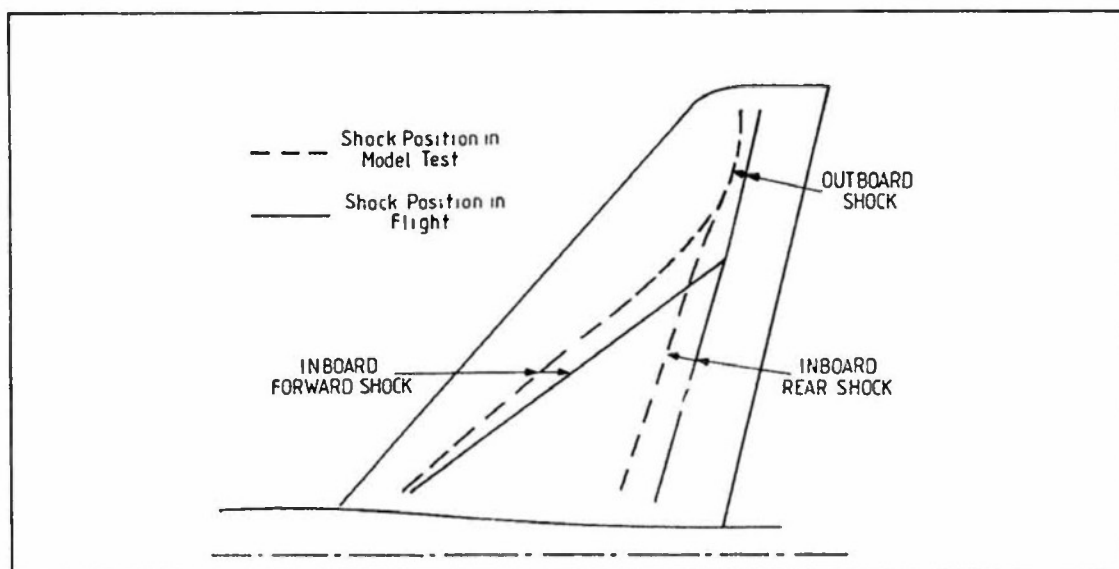


FIG 14

DIAGRAMMATIC ILLUSTRATION OF VISCOUS EFFECTS ON FLOW PATTERN D



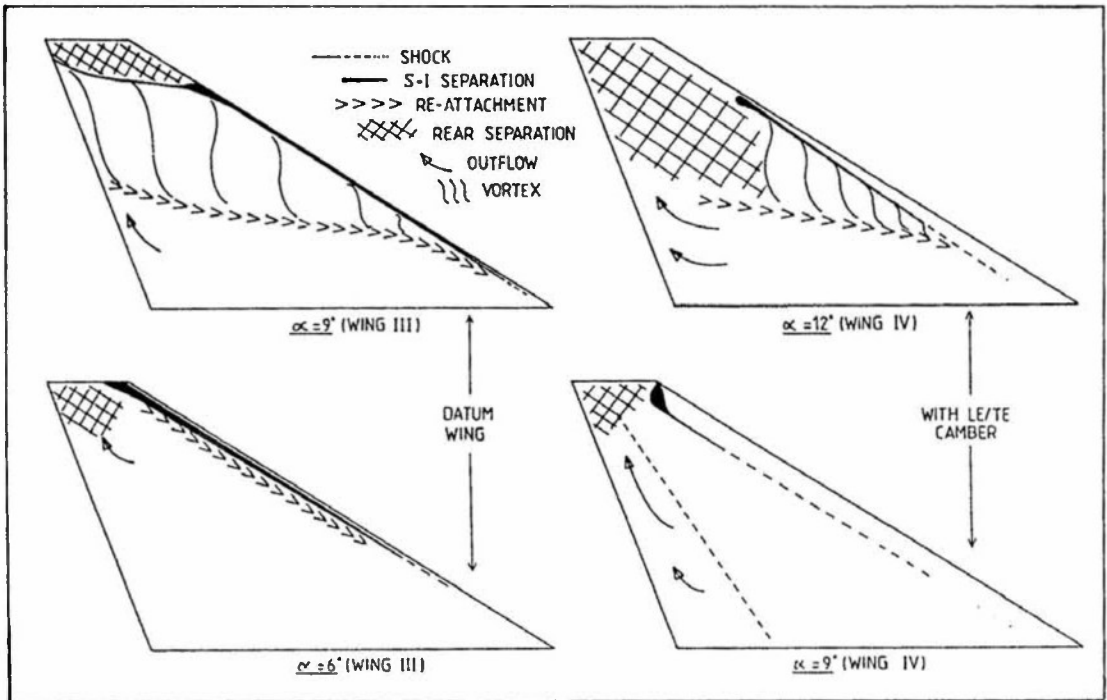


FIG 15a

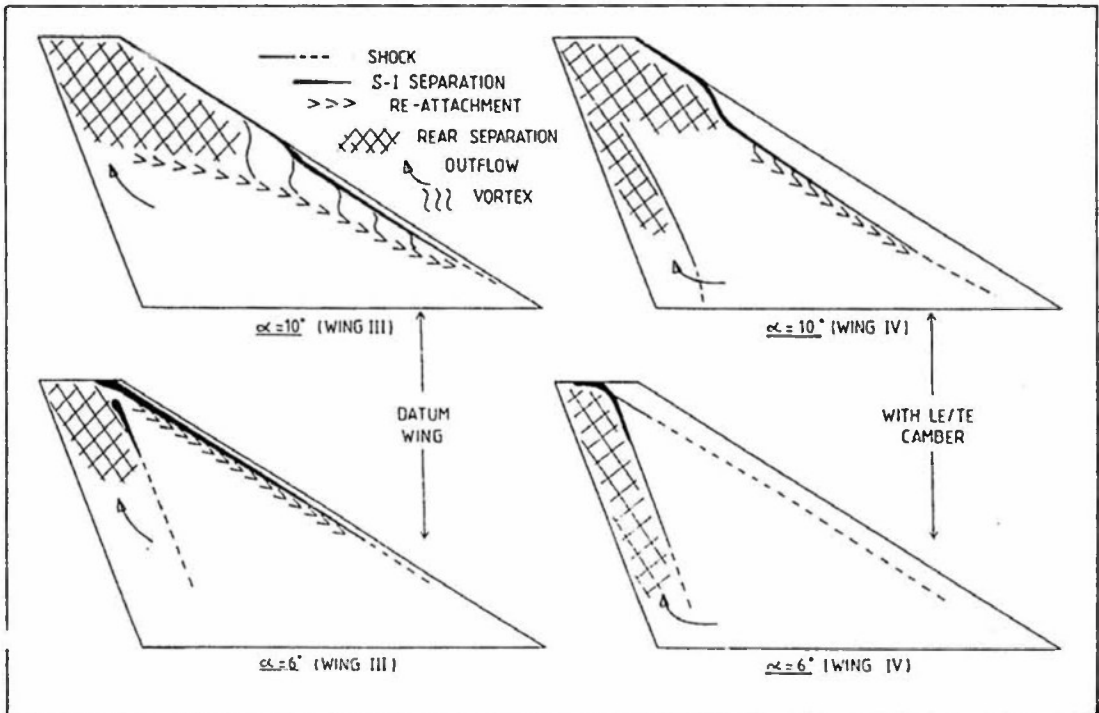
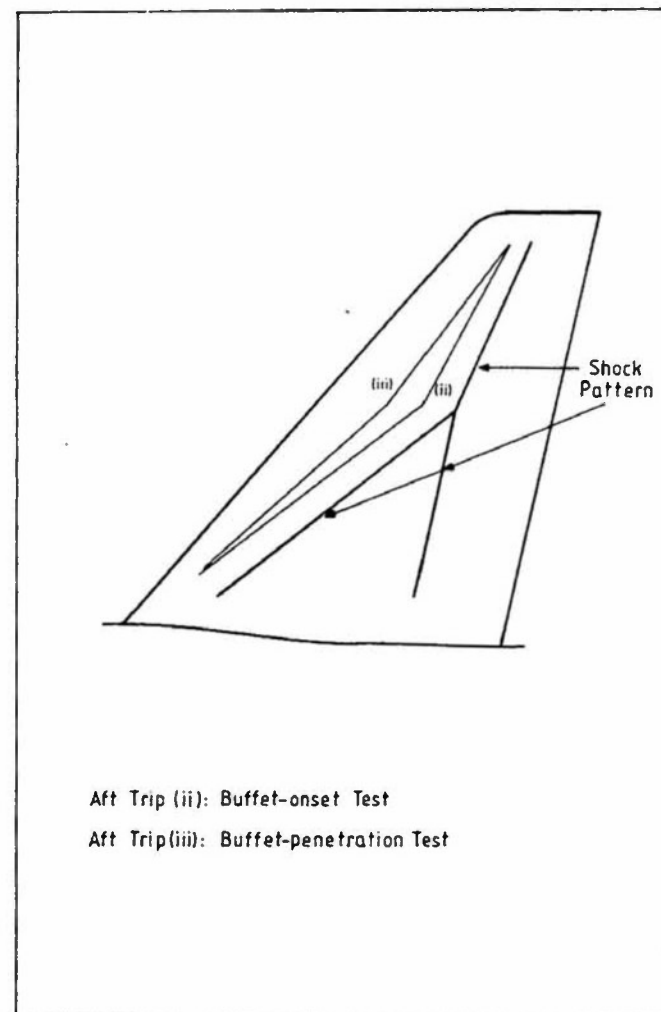
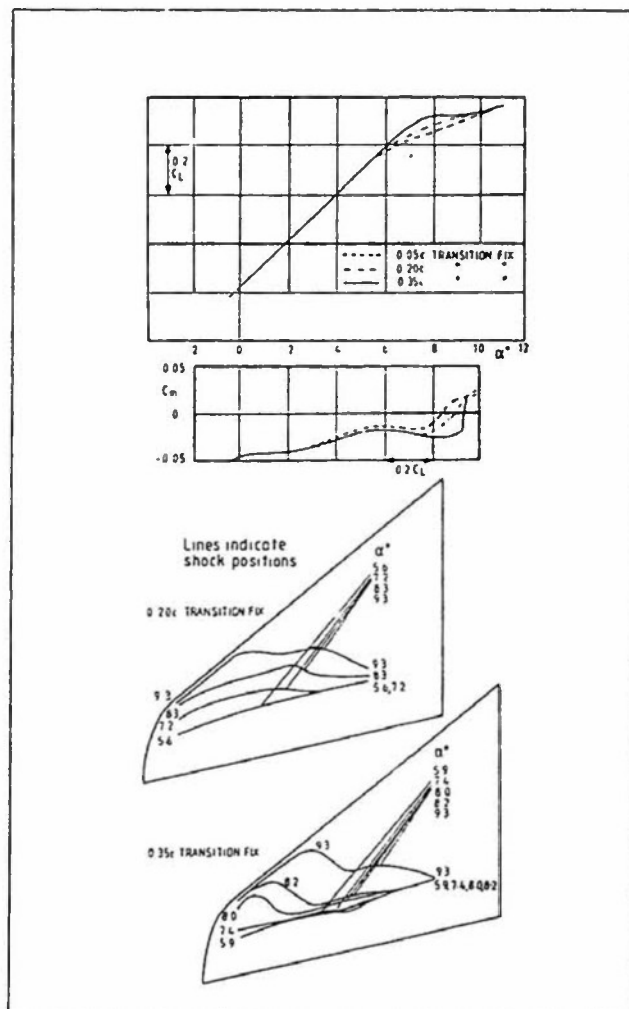
COMPARISON OF FLOW OVER WINGS III AND IV :  $M = 0.80$ 

FIG 15b

COMPARISON OF FLOW OVER WINGS III AND IV :  $M = 0.90$



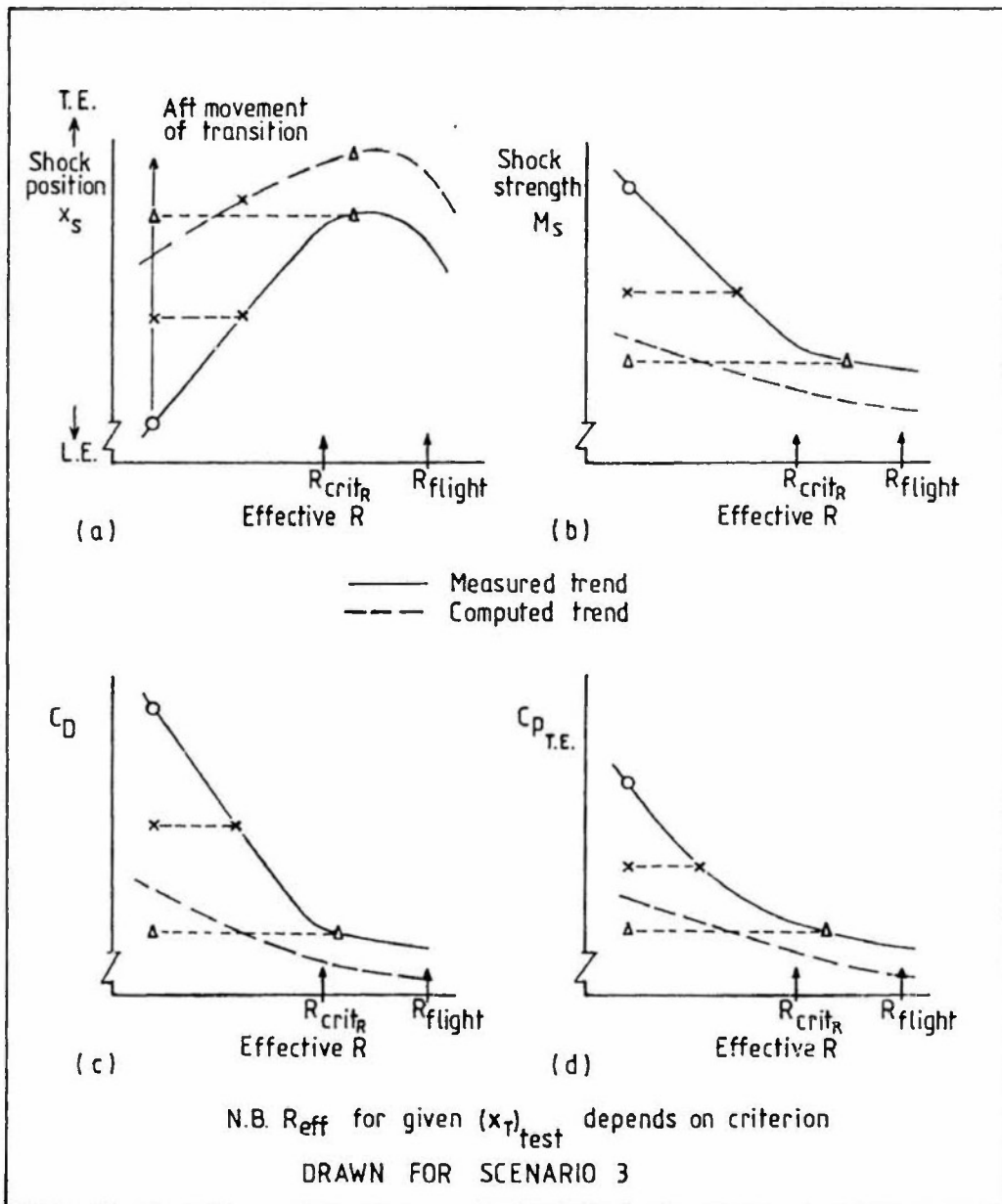


FIG 18

USE OF DIFFERENT CRITERIA TO DETERMINE  $R_{crit}$   
 AND TO IDENTIFY SIMULATION SCENARIO

### SECTION 3.3.3 MISSILES, FUSELAGES AND SIMILAR BODIES

by

Dr J.L.Potter  
200 Sheffield Place  
Nashville, TN 37215, USA

#### NOMENCLATURE

$C_L$	lift coefficient
$C_{N0}$	normal force coefficient
$C_y$	side force coefficient
$D$	base diameter of a body
$d$	local body diameter
$H$	boundary layer shape factor, $\delta^*/\theta$
$k$	roughness height
$M$	Mach number
$p$	spin rate, radians/sec
$R$	body radius
$Re$	Reynolds number
$\bar{Re}$	$Re_{ext}/(Re_{ext} @ T_w=T_{aw})$
$Re_d$	Reynolds number defined by Eqs. (1-3)
$T$	temperature
$\bar{T}_w$	$T_w/T_{aw}$
$U$	freestream velocity
$V$	$U \sin \alpha$
$W$	$U \cos \alpha$
$x$	coordinate along windward attachment line
$y$	coordinate along surface in circumferential direction from windward attachment line
$\alpha$	angle of attack
$\delta$	boundary layer total thickness
$\delta^*$	displacement thickness
$\nu$	kinematic viscosity
$\theta$	momentum thickness

#### Subscripts

$aw$	adiabatic wall
$crit.$	designates critical Reynolds number (see Sect. 4.2)
$D$	based on maximum afterbody diameter
$d$	based on local body diameter
$e, \delta$	edge of boundary layer
$eff.$	designates effective Reynolds number (see Sect. 4.2)
$k$	at the roughness
$s$	at separation
$t$	at beginning of transition
$w$	wall
$x$	based on streamwise length
$\infty$	freestream
$o$	at the attachment line
$1$	upstream of shock or trip
$2$	downstream of shock or trip

#### 3.3.3.1 INTRODUCTION

The flows about elongated bodies are discussed in the context of simulation and scaling in Ref. 1. With that as a point of departure, the present discussion is confined to the practice of tripping laminar boundary layers at locations on models selected with the goal of imulating higher Reynolds numbers. This goal normally is associated with sub-scale testing in wind tunnels under size and unit Reynolds number limitations that prevent duplication of full-scale Reynolds numbers of the aircraft or missile under study.

The thorough discussion of the goals and principles of test planning presented in Section 3.2.1 should be read as a part of this introduction. Even though the specific flow features selected for primary attention in the effort toward determining aerodynamic characteristics at flight Reynolds numbers may be different when missiles instead of wings are considered, the principles are unchanged.

It should be noted that hypervelocity re-entry bodies are not included in this discussion, although some of the comments could apply equally to those missiles. Thus, Mach numbers are assumed to vary from subsonic up to low supersonic values.

In contrast to airplane test programs, the missile designer often can match full-scale flight Reynolds numbers in wind tunnels and often can use actual prototype airframes rather than sub-scale models. In such cases, tripping normally is not necessary or desirable. Lift and drag, including lift nonlinearity at angle of attack, and control effectiveness frequently are the aerodynamic characteristics of most interest. Detailed data such as pressure distribution or boundary layer transition and separation locations are never obtained from flight tests on many tactical missiles.

The review of possible flow phenomena and the effects of Reynolds number illustrated, e.g., in Refs. 1 and 2, suggests that many of the strategies developed mainly in testing airfoil and wing models may also be appropriate when missile and fuselage shapes are involved. These include "forward fixing," "aft fixing," and "free-transition" testing. See, e.g., Sections 3.2.1 and 3.2.2 of this report and also Ref. 3. Inasmuch as airplane configurations are well covered in other parts of this document, missiles of airplane-like design are not discussed in this Section. In particular, the techniques for transonic testing of wings and airfoils are not discussed, in deference to the detailed coverage in the earlier Sections. Conditions more typical of missiles, such as higher Mach numbers, axisymmetric or elongated shapes, and the possibility of very high angles of attack are assumed. The latter conditions may bring about a need for an arrangement of boundary layer trips that is peculiar to missile testing. Bodies of revolution and similar elongated shapes at high angles of incidence often are strongly affected by the separated vortical flows on their lee sides. Consideration of this latter type of flow has led to use of longitudinal as well as circumferential trip placements. Many examples of this practice have been reported, e.g., Ref. 4.

It seems impossible to write an unconditional, step-by-step program that will always lead to an accurate prediction of full-scale aerodynamic coefficients on the basis of sub-scale wind tunnel data. What follows has to be looked upon as a general outline wherein it is hoped that the philosophy and technical approach are useful guides for test engineers.

### 3.3.3.2 DEFINING DESIRED BOUNDARY LAYER CHARACTERISTICS

The ultimate purpose of the testing program is assumed to be the prediction of full-scale flight aerodynamic coefficients or related information. Therefore, a provisional plan leading to that goal is necessary to guide the steps taken in the test program. The plan may be altered by results obtained in the course of testing, but it is needed nevertheless.

The configuration and the operating condition to be simulated obviously influence the procedure to be followed. If a relatively simple ogive-cylinder at low angles of attack is involved, little effect of freestream Reynolds number on overall normal force coefficient would be anticipated, provided that the boundary layer is largely turbulent, and overall axial force coefficient would be expected to follow a trend with Reynolds number dictated by the applicable skin friction equation. However, extrapolation of a trend determined by data for low Reynolds number may be hazardous if large angles of attack are involved. This is illustrated in Fig. 1, from Ref. 5, where there is an apparent reversal of trend of  $C_{NO}$  with Reynolds number. (Reynolds number is based on freestream conditions and afterbody diameter.) This arises because of the interdependence of local flow separation, pressure distribution, transition location, and vortex formation. Figure 1 presents a subsonic case; at significantly higher Mach numbers the situation could be different because shock waves may also interact with the boundary layer. The  $(\alpha, M_\infty)$  boundaries where these asymmetries may occur are altered at higher Mach numbers, as shown in Fig. 2 which is taken from Ref. 6.

A particularly thorough discussion of the variations in aerodynamic loads on ogive-cylinders in subsonic flow that were brought about by changing Reynolds number and incidence has been given in Ref. 7. It is brought out that not merely the laminar or turbulent state of the boundary layer but also the location of transition is important in determining the separation boundaries, and that critical (i.e., transitional) Reynolds numbers, based on a reference dimension,  $Re_p$ , may be much different for stations on a tapered nose where local

body diameter,  $d$ , and local crossflow Reynolds number based on  $d$  will be variable and lower than  $Re_p$ . This is illustrated by Fig. 3 from Ref. 7. The possibilities for different distributions of loading and Reynolds number/ $\alpha$  responses are suggested by Fig. 3 when it is remembered that crossflow drag coefficients and locations of separation on cylinders are strongly influenced by laminar-to-turbulent transition which depends on local Reynolds numbers and pressure gradients.

Because of the complex interdependence of transition and separation boundaries and the resulting load distribution, it would seem especially important to match relative flight transition locations when testing in wind tunnels. Noting that a range of vehicle attitudes may exist in flight and that transition boundaries will, in general, change with each combination of roll/yaw/pitch, it is apparent that an extended test program will be required if a thorough investigation of all possibilities is carried out. To be completely rigorous, the test planner will have to estimate the transition boundary for each vehicle attitude of possible interest so that appropriate boundary layer tripping can be done.

A carefully considered decision has to be made regarding whether it is desired to produce the asymmetric aerodynamic loading that may occur when a smooth, slender cylindrical body experiences a range of Reynolds numbers and angles of incidence. An alternative obviously is the suppression or elimination of these rather complex and possibly troublesome effects of transition/separation by placing suitable trips and, if needed, separation-fixers or mini-strakes on the body. The latter presumably would be done only if the full-scale vehicle also would be so equipped. In this discussion it is assumed that only tripping is planned and that it will be done for the purpose of simulating full-scale viscous phenomena, not necessarily to eliminate the viscous-flow effects such as those illustrated in Refs. 5-7 and elsewhere. When these effects are viewed from the position of the designer of the full-scale vehicle, it seems clearly advantageous to incorporate features in the configuration to encourage symmetrical separations. This would tend to minimize out-of-plane forces and lead to more predictable aerodynamics, cf. Ref. 8. Again it is emphasized that the present discussion concerns simulation through boundary layer management, not elimination or suppression of natural phenomena that will be encountered in flight.

One hears occasional remarks that no evidence of these asymmetrical flows has been seen in flight tests. In many cases this may result from analyzing free-flight by fitting measured motion with equations of motion that do not make provision for the necessary out-of-plane components. Other reasons may be relatively rapid changes in angles of incidence and roll, as well as changing Reynolds and Mach numbers typical of missile flights, or the influence of trajectory control systems working to oppose forces that would drive the vehicle off course. Spin-stabilized missiles or ones that are spun slowly only to minimize effects of misalignments should be less likely to exhibit the type of asymmetric forces that are caused by imperfections in body contour. The present discussion ignores asymmetric forces due to flow or body "defects," although it is obvious that they may occur. The presence of canards or other protuberances near the nose also will modify the leeside flow. However, in principle, there would seem to be no reason not to expect these asymmetric flow phenomena under appropriate conditions in flight as well as in wind tunnels.

Testing of aircraft models with such features as nacelles, external stores, inlets, and propellers or rotors presents special problems that cannot be easily handled. The effects of interfering flows as well as scale have to be considered, and the susceptibility of the particular measurements to boundary layer effects is important. The usual requirement would appear to be the thinnest possible turbulent boundary layer ahead of stations where separation may occur on the components deemed sensitive to scale effect, but the thickening of the boundary layer resulting from tripping when local Reynolds numbers are very low may be more harmful than the consequences of accepting a laminar layer for which  $\delta^*/(\text{critical local dimension})$  is closer to the full-scale value. Of course, it is sometimes possible by aft tripping to achieve the desired boundary layer state at a lower  $\delta/x$  in the wind tunnel than the corresponding ratio in flight. That may seem undesirable, but it could be useful in studies of the Reynolds number sensitivity of the data.

The case of bodies with non-circular cross sections also deserves mention. Examples of aerodynamic data on such bodies may be found in Refs. 9-11, among others. Figures in Ref. 9 illustrate some of the flow patterns that must be kept in mind when planning boundary layer trip placements. Very strong effects of a trip wire on yawing moment at higher angles of attack are illustrated in Ref. 10, but it is quite possible that the so-called trip wire served to fix separation and enforce symmetry of leeside vortices. The potential for this dual effect of trips should be recognized because, as stated earlier, it is important to distinguish between trips and strakes or salient edges when deciding what should be simulated in testing.

If a fuselage or nozzle-afterbody test is being conducted, several factors have to be considered. First, it must be noted that a fuselage forebody may be similar to the ogive-cylinder already discussed insofar as effects of flow separation at high angle of attack



are concerned. Thus, scaling procedures would also be similar. A fuselage with an upswept afterbody usually will be strongly affected by flow separation, even at low angle of attack. In some cases, the location of separation will be fixed by salient edges, i.e., the situation where flow separation is fixed at sharp discontinuities in the body surface. Then, the effects of changes in Reynolds number usually are small if the boundary layer is turbulent upstream of separation. If the body contour is rounded, so that a salient edge is not presented, the simulation is more critical. The laminar or turbulent state of the boundary layer and the relative thickness should be duplicated or approached to the degree possible upstream of the area in question. Recalling that separation is largely dictated by the pressure gradient, given that the boundary layer is laminar or turbulent (cf. Refs. 12-16) it would seem to follow that assuring the full-scale boundary layer state (laminar or turbulent) and relative displacement thickness ( $\delta^*/R$ ) are most important in scale model testing where separation is the main concern. When it is not feasible to approximate relative thickness, the effort normally will be directed to minimizing thickness.

Testing of complete aircraft models at large angles of attack is done to determine post-stall behavior, which can be a critical safety consideration. When vortices off of the fuselage and/or nacelles, and the wing wake blanket the tail surfaces, as may happen at angles above stall, loss of tail effectiveness can occur. Therefore, there is more than academic interest in the flow over fuselages and similar bodies at high incidence.

Duplicating boundary layer shape factor,  $H$ , has been given as a criterion when separation is studied. If a requirement of a fully-developed turbulent boundary layer is imposed, as is typical, then if the tripping is not done too close to the separation, the full-scale shape factor often can be approached. For some distance ( $\approx 20\delta$ ) downstream of trips,  $H$  is elevated because  $\delta^*/\delta$  may be raised and  $\theta/\delta$  lowered by the trips. An example from Ref. 17 is shown in Fig. 4. Aft tripping to achieve lower displacement thickness should not be done too near to the expected shock wave or separation point, say no less than  $20\delta$  distant.

These considerations have been briefly discussed to indicate the analytical approach that should be taken in planning a series of experiments leading toward prediction of full-scale aerodynamics of missiles, fuselages and similar bodies. Much more could be written, but it is not feasible to cover all of the many types of simulation problems that may be encountered. Scale effects on airfoils and wings have received particular attention (see, e.g. Refs. 2 and 18-20). When the desired scale-model boundary layer characteristics have been defined, based upon careful analysis of predicted full-scale conditions and appropriate simulation parameters, the test plan may be written. Rarely can all of the suggested criteria for simulation be satisfied. Compromises usually have to be accepted, and in those circumstances the criteria serve as goals.

### 3.3.3.3 STEPS IN A GENERAL TEST PLAN

To a large extent, these steps are consistent with Section 3.2.1 and other earlier discussion. Therefore, as already recommended, these parts of this report may be read for added insight, even if interest is confined to missile or fuselage shapes.

Step 1 - Collection of relevant information. This includes:

- (i) test conditions;
- (ii) tunnel flow characteristics;
- (iii) dimensioned model drawings;
- (iv) Model surface roughness and mounting details that may affect test data;
- (v) information on any differences between the model and the full-scale vehicle, including gaps, excrescences, and similar features;
- (vi) scope of instrumentation and flow visualization to be used in the test.
- (vii) selection of critical points or lines in the flight envelope. These conditions provide a focus for the simulation effort. Usually they will follow from the design requirements of the aircraft or missile, and they may be defined in the  $(C_L, M_\infty)$  or  $(\alpha, M_\infty)$  and altitude space.

Step 2 - Prediction of major differences in viscous effects between wind tunnel and flight, using CFD and empirical tools available. See Section 4.

These differences generally stem from differences in transition location and/or separation. Boundary layer thickness and shape factor, as well as transition location may be of concern. With the use of criteria for predicting the location of transition, estimates must be made for both the full-scale and the wind tunnel cases corresponding to the operational points identified in Step 1. Most readers probably will agree that this step can



only result in approximate and uncertain estimates at the current state of the art unless there has been prior experience with closely similar conditions. A brisk argument is likely to arise if any specific procedure is advocated. At this time most effort is being devoted to the  $e^n$  methodology, but it is not in wide use for test planning.

Sometimes full-scale Reynolds numbers are great enough and/or construction of the vehicle skin is rough enough to justify the assumption of full-scale transition very near the nose. Then, if there has been prior experience with similar tests in the particular wind tunnel involved, the wind tunnel engineers usually will have enough empirical knowledge to make good estimates for the wind tunnel case. Determination of transition location on the wind tunnel model is one of the first test objectives recommended. At this stage the concern is on the differences between flight and tunnel. Prior to flight tests, the greater uncertainty usually pertains to the full-scale case. This subject is discussed again later.

### Step 3 - Primary experimental assessment of viscous effects at tunnel conditions.

This may involve the following:

(a) Free-transition testing --- This is helpful for determining what trip size and placement to use, if any at all, and it will contribute to a better estimate of full-scale transition location. The measurements to be made in this phase of testing will be determined by overall test objectives. Pressure or heating rate distributions are more indicative of local flow conditions and boundary layer state. If only forces are measured, transition and separation locations must be found by either boundary layer probing or use of a technique for making transition and separation visible. The latter may include shadow or schlieren photography systems, the application of a coating to the model that responds to transition and separation, or thermo-optical devices that locate transition and separation by sensing the variations in surface temperature corresponding to laminar and turbulent or separated flow heating rates. Obviously, the applicability of these techniques is dependent on the test conditions and model. Density gradients and aerodynamic heating rates are usually inadequate to give good results from techniques dependent on those quantities at subsonic or even transonic Mach numbers. Discussions of transition detection methods are contained in Refs. 21-23 and various other sources. Separation usually will be detected by the same techniques.

(b) Tests with fixed transition --- Transition is fixed at the estimated flight locations and the measurements of Part (a) are repeated. (Trip selection is discussed in a later section.) Flow visualization is again important. Differences in separation locations and extent found in Parts (a) and (b) should be noted and related to both boundary layer conditions and the other measured data. Under transonic conditions, shock positions may differ between Parts (a) and (b), and this also should be noted. Especially in the case of configurations with canards, strakes, or other components providing interfering flows that may cause upstream transition, it may be concluded that the addition of trips did not bring about any change in the overall aerodynamic coefficients. In such an event, further testing with boundary layer tripping may not be necessary.

The purpose of Steps 3 and 4 is to define a "baseline" trend of the desired data as Reynolds number changes, or at least a baseline condition which provides the point of departure for Reynolds number scaling. It hardly needs to be emphasized that this baseline trend must be truly a result of change in Reynolds number of the flow over the model and not a result of changes in flow quality or tunnel wall interference that accompanied the change in freestream unit Reynolds number. Testing over a range of Reynolds number (Re sweeps) with more than one trip location and/or roughness height may be necessary to properly define a baseline.

A word of caution may be in order if an airframe with fins or strakes is being tested. The question of trips for those components should not be overlooked, and it may be especially critical if deflected aerodynamic control surfaces are involved. Relative or nondimensional boundary layer thicknesses, as well as their laminar or turbulent state, are likely to influence results. If there are gaps between surfaces, the ratio of  $\delta^*/(\text{gap width})$  may be significant. Testing with a fully laminar boundary layer may be considered when the thinnest local boundary layer is desirable for simulating flows over surfaces where boundary layer thickness is not negligible in comparison to the model dimension area in question. However, it is important to remember that laminar boundary layers separate more readily than turbulent layers, and that may be the primary consideration.

At this stage, additional CFD results may be helpful because it would now be possible to compare the measured data with computations. If trends and/or absolute values are in agreement, this knowledge may be used in planning further testing.

#### Step 4 - - - Study in depth of viscous effects for selected critical conditions.

There are two approaches to this step that may be taken individually or in combination depending upon the particular circumstances. Two determining factors are the spatial extent over which transition can be controlled on the wind tunnel model and the degree of certainty with which full-scale transition and separation are predictable. Testing costs are another factor likely to be important in determining how thoroughly this step is studied. However, it is not the purpose to address economic concerns here. Two sub-steps are suggested.

(4a) Boundary layer manipulation to approximate the key condition(s) predicted for full-scale Reynolds number - - - The key condition(s), singular or plural, may be, e.g., boundary layer transition location, possibly with implications for leeside vortices; or boundary layer thickness and shape factor immediately upstream of a shock wave, a base, or an inlet. Criteria for predicting separation, such as given in Refs. 12-16, are often useful in deciding how to proceed in this step if one is dealing with airfoils. However, similar criteria have not been developed for bodies such as typical missiles, fuselages, and similar bodies at angles of incidence. Calculations can be made for these latter bodies, but the processes known to the writer are too lengthy and complex to be popular for test planning at this time. As shown by many experiments, separation along these bodies occurs at varying circumferential positions along the length even though angle of incidence is fixed, cf. Ref. 1 and listed sources therein.

Step 4a differs from Step 3 in that it is directed to simulation of full-scale viscous effects at critical locations on the model, in contrast to the direct attempt to match only the relative transition location as done in Step 3. Differences in results may lead to identification of significant problems in simulation and enable the experimenters to plan Step 4b.

(4b) The next recommended step is testing with transition locations based on study and comparison of the results from Steps 3 and 4a. This phase of testing is intended to provide the data for extrapolation to the flight Reynolds number. If it is believed that the best simulation will result from fixing transition at the relative location predicted for full-scale flight, then that should be done and the data taken for the full range of Reynolds number. If it is believed that relative boundary layer thickness and/or shape factor at a critical location are the significant factors, then transition fixation should be done with that objective. When resources are sufficient to allow the extra effort, both approaches are recommended as a way to assess criticality of these factors.

#### Step 5 - - - Consolidation of data

The data should be analyzed in depth to evaluate the apparent degree of simulation and the likelihood that a solid baseline trend with Reynolds number has been defined. Attention must be paid to issues already highlighted, such as the extent to which the applicable simulation parameters have been matched with predicted flight values and the possibility that spurious effects have arisen because of deficiencies in testing capabilities. The measured data should be examined for evidence of the predicted trends, particularly for changes with Reynolds number that indicate whether  $Re_{eff}$  is greater or less than  $Re_{crit}$  for important aerodynamic phenomena. (This topic is elaborated on in Section 3.2.1 and later.) Unexpected trends naturally will need analysis if they are revealed. Questions of utmost interest are:

Do the data and calculations agree well enough to suggest that the full-scale viscous flow has been adequately simulated, and has a sound base for any necessary extrapolation been laid down? If not, why?

#### Step 6 - - - Prediction of full-scale aerodynamic coefficients

At this point the experimental data for use in the planned extrapolation should be in hand. If it has been possible to obtain data defining a baseline trend which is thought to be suitable for straightforward Reynolds number scaling, it remains to account for transition and shock wave movements, skin friction coefficient, and displacement thickness variation with increasing Reynolds number. A safe baseline trend is one which is not expected to undergo discontinuous or unpredictable change with Reynolds number such as could result from a major movement of transition or separation locations. In many cases, this will be provided by the data collected in Step 3. In more complex problems, study and comparison of the data from Steps 3 and 4 is required in order to establish the baseline trend.

Awareness of potential pitfalls in the extrapolation is essential. If it is thought that Steps 3 and 4 have not led to a secure baseline, special tests to explore possible trend

breakdowns may be justified. An example would be a test of a model with the critical parts fabricated to contours simulating the reduced displacement thickness that would correspond to a greater Reynolds number. Although this artifice would reveal high Reynolds number pressure coefficients and flow separation, some experimental data such as total drag would have to be adjusted to account for the low Reynolds number skin friction present.

Because many wind tunnel tests do not include simulated propulsive units or associated inlet and exhaust flows, it is important to account for these features of the full-scale vehicle in arriving at full-scale aerodynamic coefficients. Differences in boattail and base pressures are likely when jet-on and jet-off conditions are compared. This is not altogether a viscous-flow problem, but there may be a significant interaction between the inviscid and viscous phenomena in this case.

The possibility of useful support from computational fluid dynamics (CFD) should not be ignored in any of the steps. If either the actual result from the tunnel or at least the trend with Reynolds number can be matched by CFD, then the way to extrapolate to higher Reynolds number is clear. Even in such an event, though, the assurance of no surprise in continuing a sub-scale or computed trend has to be thoughtfully examined. If there is reason to doubt that an unchanging trend with increasing Reynolds number has been established at this point in the program, further effort to estimate full-scale results will obviously depend on the experimenter and his resources.

### 3.3.3.4 BOUNDARY LAYER TRANSITION

It is important to recognize that boundary layer transition on inclined, smooth cylindrical bodies may come about in different ways, depending principally on angle of attack and Reynolds number. These modes are (1) separated shear layer instability, (2) attachment-line contamination, (3) cross-flow instability, and (4) streamwise-flow instability. Any one of these may prevail under circumstances to be described. The final mode listed has received by far the most attention, but it remains an unresolved issue in fluid dynamics despite the effort spent on its study. Possibly the best known approach for predicting transition that grows from streamwise instability is the  $e^n$  method (see Section 4.3). This has some appeal because of its close relation to stability theory. Unfortunately,  $n$  has to assume a wide range of values to fit experimental data, cf. Refs. 24 - 26. Reference 24 deals with wings, while Refs. 25 - 26 concern bodies of revolution. Reference 25 is a source of detailed experimental data and comparison with results of the  $e^n$  method for predicting boundary layer transition on a body of revolution in a subsonic wind tunnel at  $\alpha = 0$ . The results are reasonably good for the subsonic axisymmetric body studied. Reference 26 presents data from subsonic testing of a series of bodies with different nose shapes and zero angle of attack. Comments in Refs. 24 and 26 sum up the status of the  $e^n$  method at this time.

For any particular set of two-dimensional or swept-wing data with similar stream disturbance levels and spectra, the  $e^n$  method for estimating the beginning of transition works reasonably well; however, even within a given data set, the value of  $n$  may vary significantly, evidently depending upon currently uncontrollable variations in disturbance field or receptivity. (Ref. 24)

Of the four models that did not exhibit laminar separation, the results did not show a single unique ratio between the measured flow properties in the transition regions and the computed spatial amplification ratios obtained by linear stability theory. On Model 3, the range of amplification factors that correlates with the onset of transition lies between  $e^8$  and  $e^{12}$ . The corresponding range for Model 4 is from  $e^9$  to  $e^{11}$  and on Model 6 from  $e^{10}$  to  $e^{12}$ . The data taken for Model 8 indicate that a nearly constant value of  $e^7$  correlates well with data at the onset of transition. (Ref. 26)

Data in Ref. 24 show that even in free flight the value of  $n$  may have to vary 20-30% from the mean to fit experimental observations on one airfoil with modest changes in angles of attack and unit Reynolds numbers.

The best-known alternative procedure for predicting transition is that described in Sect. 4.3 where the Pohlhausen parameter and free-stream relative turbulence intensity are the basis for finding a value of  $Re_{\theta}$ . However, none of the current predictive methods account for the often profound influence on transition that seems to accompany changes in unit Reynolds number.

A major and little understood obstacle to better predictive methods for all of the modes of transition is represented by the phenomenon called the unit Reynolds number effect (for lack of a better designation). This is not the place to attempt an exhaustive discus-

sion of this topic, but it is necessary to bring it up because there is often reluctance to recognize the role of the unit Reynolds number when transition prediction procedures are proposed. Although there are reports of experiments wherein it is said that  $Re_{et}$  was constant as  $(U/v)_e$  changed, and there is reason to believe that sound provides a major source of the apparent unit Reynolds number effect in supersonic wind tunnels, there is no satisfactory explanation yet for the free-flight and subsonic wind tunnel experiments wherein  $Re_{et}$  varied with  $(U/v)_e$ . Inability to deal with this factor in transition predictions is a major obstacle.

Figure 5 from Ref. 27 gives the data for a sharp cone of 10-deg apex-angle tested in flight on a F-15 airplane. As such, it probably represents the best reference for the flight case in the range of Mach number shown. It is important to note that  $T_w = T_{aw}$  and  $\alpha = 0$  deg for all of the F-15 cone data in Fig. 5.

The cone on the F-15 at subsonic Mach numbers had a streamwise pressure gradient, unlike the constant-pressure distribution of fully supersonic flow. Also of some interest is the general increase in  $(U/v)_e$  that accompanied increasing  $M_e$ . The latter condition tends to merge the influences of each of those parameters when data scatter is also involved.

A pronounced influence of unit Reynolds number  $(U/v)_e$  has been found in other free-flight data, whereas the F-15 flight data are inconclusive on that issue, cf. Ref. 27. References 28 and 29 present flight data showing very strong effects of changing unit Reynolds number. Figure 6 illustrates this with data from Ref. 28, and Fig. 7 shows the results from a large number of flights analyzed and reported in Ref. 29.

The significance of the temperature ratio  $T_w/T_{aw}$  in regard to transition is shown in Fig. 8 from Ref. 30. There are gaps and some data that appear inconsistent with the general trend in Fig. 8. Therefore, extrapolation and interpolation of the curves is not recommended. For small changes of  $T_w/T_{aw}$  from unity, linear stability theory appears to be a good qualitative guide to the effect upon  $Re_{et}$ , but when  $T_w/T_{aw} \ll 1$ , great uncertainty exists, cf. Ref. 30.

The enormous difficulty of transition analysis is indicated in Fig. 9 where the data of Figs. 5-7 are combined with other free-flight data (Refs. 31-34) for sharp, right-circular cones. There is little doubt that the unit Reynolds number and the wall temperature ratio effects contribute to the extremely broad ranges of  $Re_{et}$  shown in Fig. 9. Other possible sources of variability, such as measurement accuracy, definition of transition, surface finish, angle of attack, etc. are, of course, obvious. However, the principal obstacles to our understanding are believed to be represented by  $(U/v)_e$  and extreme values of  $T_w/T_{aw}$ . At this time, with one exception, there is no satisfactory analytical method for accounting for either of these factors. The exception is the influence of  $T_w/T_{aw}$  when that ratio is near enough to unity. It then is qualitatively predicted by linear stability theory. Fortunately, this allows analysis of most transonic flight cases.

It seems possible that the particular character of the disturbance that causes transition in a given case is the product of the combination of environmental factors present. These include both free-stream and surface factors. The unit Reynolds number, or something related thereto, apparently is an environmental factor that can influence the disturbance, its growth, or the receptivity of the boundary layer to destabilization. The net effect of this influence may be dependent upon the particular set of circumstances.

If there were evidence that  $Re_{et}$  is constant for the same physical configuration at equal  $M_e$ ,  $T_w/T_{aw}$ , and  $(U/v)_e$  in different wind-tunnel or free-flight environments, then the problem would be simpler. Unfortunately, that does not appear to be true. Although the qualitative effects of the known variables generally appear to be consistent, the value of  $Re_{et}$  resulting from their combined actions seems to depend on the test body and its disturbance environment in ways not yet understood. Until the questions such as those posed by Figs. 8 and 9 are answered, no method for estimating full-scale transition Reynolds number can be viewed with any confidence. Unless there is experience with similar designs in the same flow environment, rather wide uncertainty bands will have to be assumed. (Also see discussion in Ref. 35.)

It has already been noted that transition may be brought about by different flow processes when a body is at an angle of attack or yaw. As discussed in several papers by Poll (Refs. 36-40), attachment line contamination and cross-flow transition are associated with missile shapes at angles of attack. Laminar separation bubbles may trigger transition even at zero incidence if flow turning angle is too large in some region, or it may occur at angle of attack when the cross flow encounters adverse pressure gradients. Poll (Refs. 37 - 38) has given comprehensive descriptions of these modes and provided methods for estimating the corresponding transition Reynolds numbers. His studies have dealt with incom-



compressible flow, in greater part, but he has indicated how compressible-flow attachment-line contamination may be analyzed in Refs. 36, 39 and 40.

In brief, the criteria given by Poll (Ref. 37) for a right circular cylinder, in terms of body diameter,  $d$ , and freestream unit Reynolds number,  $(U/v)_{\infty}$ , are:

- For the separated shear layer mode of transition - - -

$$(U/v)_{\infty} d = 1 \times 10^6 \times \tan \alpha / \{(1 + 3.3 \tan^2 \alpha) \cos \alpha\} \quad (1)$$

- For the attachment-line contamination mode - - -

$$(U/v)_{\infty} d = 1.1 \times 10^6 \times \tan \alpha / \cos \alpha \quad (2)$$

- For the cross-flow instability mode - - -

$$(U/v)_{\infty} d = 1.45 \times 10^5 \times (1 + 3.3 \tan^2 \alpha) / \sin \alpha \quad (3)$$

If an angle of attack of, say, 10 deg is assumed, one sees that transition in the separated shear layer mode is predicted when  $Re_d = 162,400$ . When  $Re_d = 197,000$ , attachment-line contamination causes transition and precludes laminar separation on that portion of the body downstream of the attachment-line transition, because the boundary layer has become turbulent before it separates. Cross-flow instability, predicted if  $Re_d > 10^6$ , also would not be observed when the local flow has been made turbulent at the attachment line. The streamwise mode of transition for axial flow occurring (usually) when  $Re_{ex} > 2 \times 10^6$  on bodies such as those under discussion, will become a factor on the downstream portion of the body when angle of attack is small enough for axial flow to dominate. Even though Eqs. (1-3) are not presented with a lower limit on angle of attack, it is reasonable to assume a lower limit at the angle where the flow does not separate, i.e., predominately axial flow exists. However, that is somewhat ambiguous because of the circumferential variation of conditions at even small angles of attack. Alternately, one would look for a lower limit based upon a Reynolds number characterizing the flow.

If a tapered body is under consideration, transition could occur in different modes along the body at one angle of attack. (Note that local angle of incidence is not equal to  $\alpha$  if body radius is not constant with  $x$ , i.e., the body is tapered.) At an angle of attack, streamwise transition would not occur at a constant  $x$  all around the circumference, it would be found at slightly greater  $x$  on the windward area and at much reduced  $x$  on the lee side of typical missile bodies. The possibility of transition occurring in varying ways at varying locations, with corresponding changes in separation locations and pressure distributions, over relatively small ranges in angle of attack can cause complex Reynolds number and Mach number dependence of typical missile shapes at higher angles of attack. See Ref. 36 for further discussion.

The influence of unit Reynolds number may be less of a problem in the non-streamwise modes because spatial movement of transition in the lateral direction is restricted. For example, separation is strongly influenced by pressure gradient, and separated shear layer transition occurs a relatively short distance after separation. Even though unit Reynolds number apparently affects the length of laminar flow from separation to transition (Potter, Ref. 41), this length sometimes is relatively short compared to body length, and the practical importance may depend upon the effect on vortex formation. That is, if reattachment occurs, followed by turbulent separation, the dependent aerodynamic forces may be different than they would be if laminar or transitional boundary layer separation occurs. The complexity of the processes of transition and separation on an inclined, tapered, cylindrical body should encourage experimenters to take the time to explore the effects of several different boundary layer manipulation schemes. In that way, the potential variations in the aerodynamic coefficients can be revealed and the implications evaluated for the full-scale case.

The different modes of transition that may occur are illustrated in Fig. 10 from Ref. 37. This figure strongly suggests that when angle of incidence is not zero, transition may occur in any of the four modes discussed, depending upon the values of the cross-flow and the streamwise Reynolds numbers. Even though  $Re_{ex}$  may be greater than  $Re_d$ , it may not be high enough for the axial streamwise-flow mode of transition to dominate. Clearly, if trips are applied to cause transition near the nose at zero incidence, these boundaries would be altered. If tripping is done for a test program, the experimenters must evaluate the effect of trips on these various modes of transition in order to produce the effect wanted in their test.

The understanding of transition and related separation phenomena on bodies of revolu-

tion at angles of attack is a recent and evolving development in aeronautics. The views on this subject expressed by Lamont (Ref. 7) contrast markedly with those of Ericsson and Reding (Ref. 42).

As a summary of this Section, it is suggested that transition in the near-axial streamwise mode be predicted by the procedures described in Section 4.3, with the added proviso that some departure from the prediction be anticipated as unit Reynolds number varies. This has the effect of placing a broadened uncertainty band around the predicted  $Re_{ext}$ , and it appears that the band also must be wider at supersonic Mach numbers. Of course, if experimental transition data for similar configurations and flow conditions are available, they certainly should be considered in addition to the prediction methods.

It also has been shown that unit Reynolds number affects transition in separated laminar shear layers, but the range of uncertainty that can be created is limited by the relative shortness of the separation bubble in many cases. Thus, if the location of separation is predicted satisfactorily, the precise location of transition may not be critical. The writer is unaware of any evidence of significant unit Reynolds number influence on transition arising from attachment-line contamination or cross-flow instability.

### 3.3.3.5 RAPIDLY SPINNING BODIES

A special category is created by spin-stabilized bodies where Magnus forces may be affected by boundary layer conditions. Sturek's experiments (Refs. 43 - 44) have nicely demonstrated the effect of high spin rate on transition location and side force on supersonic, sharp cones with 10-deg half-angles. Figure 11 shows that the circumferential distribution of  $x_t$  (beginning of transition) is rotated in the direction of spin, with moderate change in shape. Figure 12 shows that boundary layer configuration had a strong influence on side-force coefficient,  $C_y$ , that coefficient being decreased in magnitude when the windward boundary layer was changed from laminar to turbulent flow. Sturek concludes that

The Magnus force is extremely sensitive to boundary layer configuration. The Magnus force is greatest for the boundary layer configuration that has the greatest difference in thickness of the boundary layer from the wind to the lee side. (Ref. 43)

In Ref. 44 he also remarks that

Close agreement for Magnus force between experiments conducted at different test facilities, especially at tunnel operating conditions which yield laminar or transitional boundary-layer configurations, should not be expected due to the extreme sensitivity of the Magnus force to boundary layer configuration. (Ref. 44)

These results clearly show that correct simulation of full-scale viscous flow is also required in testing spin stabilized bodies. The referenced investigation concerned supersonic flows and incidences less than cone half-angle. With no tripping, laminar flow existed almost to the base of the cone on its windward attachment line. However, natural transition to turbulent flow occurred early on the lee side, suggesting that free shear layer transition was involved. Spin induced streamline curvature and an influence of spin on separation and vortical flow come to mind as possible factors in this type of flow.

### 3.3.3.6 TRIP SIZING AND PLACEMENT FOR STREAMWISE-FLOW MODE OF TRANSITION

The procedures described in Refs. 45-49 are applicable for this problem. Anyone responsible for determining trip size and placement probably is familiar with these methods, so they are not reviewed here. The referenced works all pertain to the streamwise type of transition, i.e., not attachment line or cross-flow.

If two-dimensional boundary layer calculation methods are used, it is necessary to apply the Mangler transformation to obtain the boundary layer characteristics for equal edge-of-boundary layer conditions on a body of revolution. In the case of a supersonic, sharp-nosed cone, it will be recalled that

$$\delta_{\text{cone}} = \delta_{\text{flat plate}}/\sqrt{3}$$

for a laminar boundary layer. For a right circular cylinder,

$$\delta_{\text{cylinder}} = \delta_{\text{flat plate}}$$

In both cases, for these relations to hold, the boundary layer thickness must be much less than body radius. Relations for other noses or nose-cylinder bodies usually lie between those shown above.

It is obviously undesirable to locate trips where the local thickening of the boundary layer, or shock and expansion waves that may be associated with boundary layer trips are likely to unduly affect pressure distribution on the model. The undue effect, of course, refers to changes not a consequence of a naturally turbulent boundary layer. Critical areas on missile models will include those places on the airframe where relatively large pressure gradients exist, e.g., nose-body junctures, boattails, and near separation lines. One also must avoid locations where transition due to a laminar separation has already occurred upstream or where relaminarization will occur downstream. If there is any doubt on these issues, the result of the trip needs to be studied by use of a technique for making transition visible on the model.

The usual trips consist of narrow bands of carborundum grit, micro-spheres, or small shapes such as triangles or disks that are sometimes preferred by certain groups. These three-dimensional elements are arrayed in either random, "sparse" bands or ordered rows, with the elements staggered so as to assure that the boundary layer fluid immediately downstream of the trips does not have much lateral nonuniformity. That is, the wakes of the roughness elements have merged a short distance downstream. This is a consideration when the trips have to be placed near the station where turbulent flow is wanted. In terms of effectiveness alone, there is evidence that a single row of trip elements is as effective as a multi-row band of equal height for Mach numbers up to roughly 2. (Personal communication from D. W. Sinclair and W. T. Strike, Jr., Calspan Corp./AEDC Divn.) It is important to bear this latter point in mind when using the methods of Refs. 45-49. Very little data exist on direct and systematic comparisons of different trip element shapes, so that it is often assumed incorrectly that average height is the sole determinant of trip effectiveness. There is evidence that two-dimensional trips are more effective than three-dimensional ones in subsonic flow and that the situation is reversed in supersonic flow (Ref. 46). Nevertheless the most used type of trip has three-dimensional, i.e., distributed roughness. Gas jets have been used, but the advantage of controllable effective disturbance is usually not regarded as worth the extra complication and cost or the disadvantage of fixed location on a model.

The change from essentially axial flow on an elongated body at small angle of attack to nearly cross flow at large angle of attack should be noted. In discussing transition modes at an angle of attack on the order of 10 deg, reference has been made to a streamwise Reynolds number based on axial distance  $x$ . However, all of the remarks about the non-streamwise modes have referred to a Reynolds number based on local body diameter. When angle of attack is great enough, so that streamwise flow becomes crossflow, it too should be described in terms of  $d$  instead of  $x$ . However, the angle at which this change occurs is not immediately obvious. It is affected by body shape, flow conditions, and even location on the body. As angle of attack increases, raising the value of  $Re_d$  defined in Eqs. 1-3, an angle is reached where the separated shear layer mode is activated. After that occurs, for all greater angles,  $Re_d$  is the controlling parameter. Conversely, if  $Re_{ex}$  exceeds the predicted critical value for the axial streamwise mode of transition, that form of transition would be expected regardless of  $Re_d$ . If one visualizes a long, cylindrical body of revolution whose angle of attack is gradually increased from zero, at first, transition occurs on the aft portion where the value of  $Re_{ex}$  for axial-flow transition is exceeded. Then, as angle of attack increases, transition in the axial, streamwise mode moves forward on the leeward and more slowly rearward on the windward surfaces. At that point, the lateral or cross-flow modes are activated and when the critical  $Re_d$  is exceeded, separated shear layer transition occurs. This may happen forward of the station of axial-flow transition, so that a sudden forward movement of transition could occur at the angle of attack where the separated-shear-layer mode comes into play. As angle of attack increases further, raising  $Re_d$ , attachment-line contamination becomes the controlling mode over much of the body. Separated-shear-layer transition could linger near the nose where local body diameter may be small, keeping  $Re_d$  below the threshold for attachment-line contamination. By examining the values of  $Re_d$  and  $Re_{ex}$  for each angle of attack and varying longitudinal distances from the nose of the body, and simultaneously estimating separation boundaries, one can construct a conceptual framework of the modes and locations of transition as angle of attack and unit Reynolds number change. This is a necessary step prior to deciding trip size and location if trips are going to be used.



### 3.3.3.7 TRIP SIZING AND PLACEMENT FOR LATERAL MODES OF TRANSITION

For convenience and to distinguish from axial flow, the non-streamwise modes are loosely referred to as lateral modes here. The effect of a trip upon the free-shear-layer and attachment-line boundaries shown here in Fig. 12 has been discussed in Ref. 37. An important consideration when planning a test program is the achievement of the desired boundary layer characteristics without introduction of unintentional flow modifications such as salient edges which may fix separation. To that end, one has to estimate the probable shock wave and separation fronts along the body for the ranges of angles of attack, Mach numbers, and Reynolds numbers to be covered. Careful study of Refs. 5-7 and 36-38 as well as Section 2.2.1 of this report should be helpful.

After the assessment of the modes of transition, trip locations may be determined. Most trip sizing procedures involve a form of Reynolds number based upon boundary layer properties at the roughness element or at least a boundary layer thickness at that location on the body. Boundary layer calculations should be carried out so that the required trip height can be found.

The design of trips for missile shapes which are to be tested at angles of attack may be based upon Refs. 38-39 insofar as attachment-line transition is concerned. It would seem a good plan to bring about that mode of transition, if a turbulent boundary layer is wanted, because it involves trips well removed from separation and shock locations and it is no problem to select the position for the trips. However, relatively large trips may be necessary to cause transition far forward on the attachment line of tapered bodies, resulting in excessive thickening of the boundary layer. It should be noted that an acceptable trip for the leading edge of an airfoil or wing poses the same difficulty.

For example, for tripping attachment-line boundary layers on bodies of revolution, Poll uses the criterion,

$$Re_k = (W/v)_k \quad k = 550 \quad (4)$$

when

$$R_* = \sqrt{U_\infty d \cos \alpha / (G v_* \tan \alpha)} \quad (5)$$

$$> 245.$$

(Note that  $W_\infty = U_\infty \cos \alpha$ ,  $V_\infty = U_\infty \sin \alpha$  and  $G = (d/V_\infty) (dVe/dy)_{y=0}$  where  $U_\infty$  is the freestream total velocity.) For applications in compressible flow, the kinematic viscosity is based upon a reference temperature,

$$T_* = T_e + 0.10 (T_w - T_e) + 0.60 (T_r - T_e). \quad (6)$$

These conditions are said to produce transition at either 2-D or 3-D roughness elements on a right cylinder at angle of attack.

In view of the relatively low critical values of  $Re_d$  for the lateral modes of transition, it is inferred that natural (untripped) transition will occur even on forward portions of typical missile and fuselage models after angle of attack is increased to only moderate levels. It has already been noted that sudden forward movement of transition may then occur and the experimenter should be watchful for related changes in separation and aerodynamic coefficients.

### 3.3.3.8 REFERENCES

1. Potter, J. L., "Comments on Simulating Higher Reynolds Numbers in Wind Tunnel Testing: Missiles, Fuselages, and Similar Bodies," Section 2 of this report.
2. Potter, J. L., "Review of Requirements and Status of Simulation and Scaling of Transonic, Viscous Flows," AEDC-TR- 84-23, September 1984.
3. Elsenaar, A., "Experiences With Transition Fixation in the High Speed Regime at NLR," Nationaal Lucht-En Ruimtevaartlaboratorium Memorandum AC-83-039 U, December 30, 1983.
4. Barger, R. L. and Sawyer, W. C., "Investigation of Flow Characteristics Over Missile Bodies at Supersonic Speeds," NASA Technical Paper 1579, November, 1979.

5. Lamont, P. J., "Pressures Around an Inclined Ogive Cylinder with Laminar, Transitional, or Turbulent Separation," AIAA Journal, Vol. 20, November 1982, p. 1492.
6. Nielsen, Jack N., "Nonlinear Flow Phenomena at High Angles of attack and Recent Advances in their Prediction," In AGARD-CP-336, Sept. 1982.
7. Lamont, P. J. "The Effect of Reynolds Number on Normal and Side Forces on Ogive-Cylinders at High Incidence, AIAA Paper 84-1799, 1985.
8. Rao, D. M. "Vortical Flow Management for Improved Configuration Aerodynamics - Recent Experiences." In AGARD- CP-342, July 1983.
9. Daniel, D. C. and Zollars, G. J., "Experimental Aerodynamic Studies of Missiles With Square Cross Sections," In AGARD-CP-336, Sept. 1982.
10. Carr, P. C. and Gilbert, W. P., "Effects of Fuselage Forebody Geometry on Low-Speed Lateral-Directional Characteristics of Twin-Tail Fighter Model at High Angles of Attack," NASA Technical Paper 1592, Dec. 1979.
11. Erickson, G. E. and Brandon, J. M., "Low-Speed Experimental Study of the Vortex Flow Effects of a Fighter Forebody Having Unconventional Cross-Section," AIAA Paper 85-1798, 1985.
12. Stratford, B. S., "Flow in the Laminar Boundary Layer Near Separation," Aeronautical Research Council Reports and Memoranda No. 3002, 1957.
13. Stratford, B. S., "The Prediction of Separation of the Turbulent Boundary Layer," Journal of Fluid Mechanics, Vol. 5, January 1959, p. 1.
14. Curle, N. and Skan, S. W., "Approximate Methods for Predicting Separation Properties of Laminar Boundary Layers," Aeronautical Quarterly, Vol. VIII, Part III, August 1957.
15. Townsend, A. A., "The Behaviour of a Turbulent Boundary Layer Near Separation," Journal of Fluid Mechanics, Vol. 12, Part 4, April 1962, pp. 536-554.
16. Van Ingen, J. L., "On the Calculation of Laminar Separation Bubbles in Two-Dimensional Incompressible Flow," In AGARD-CP-168, 1975.
17. Klebanoff, P. S. and Tidstrom, K. D., "Mechanism by Which a Two-Dimensional Roughness Element Induces Boundary- Layer Transition," Physics of Fluids, Vol. 15, No. 7, July 1972, pp. 1173-1188.
18. Haines, A. B., "Possibilities for Scale Effect on Swept Wings at High Subsonic Speeds," Facilities and Techniques for Aerodynamic testing at Transonic Speeds and High Reynolds Number, AGARD-CP-83, August 1971.
19. Hall, M. G. "Scale Effects in Flows Over Swept Wings," Facilities and Techniques for Aerodynamic Testing at Transonic Speeds and High Reynolds Number, AGARD-CP-83, August 1971.
20. Stanewsky, E., "Interaction Between the Outer Inviscid Flow and the Boundary Layer on Transonic Airfoils," Zeitschrift fur Flugwissenschaften und Weltraumforschung, Vol. 7, No. 4, July - August 1983, p. 242.
21. Merzkirch, W. F., Flow Visualization, 1st ed., Academic Press, New York, 1974. 22. Maltby, R. L., ed., "Flow Visualization in Wind Tunnels Using Indicators." AGARDograph 70, 1962.
23. (a) Flow Visualization, T. Asanuma, ed., McGraw-Hill Book Co., New York, 1979.  
(b) Flow Visualization II, W. F. Merzkirch, ed., Hemisphere Publishing, New York, 1982.  
(c) Flow Visualization III, W.-J. Yang, ed., Hemisphere Publishing, New York, 1985.
24. Hefner, J. N. and Bushnell, D. M., "Status of Linear Boundary-Layer Stability Theory and the  $e^n$  Method, With Emphasis on Swept-Wing Applications," NASA Technical Paper 1645, April 1980.
25. Meier, H. U. and Kreplain, H. P., "Experimental Investigation of the Boundary Layer Transition and Separation on a Body of Revolution," Z. Flugwiss. Weltraumforsch., 4, Heft 2, 1980, p. 65.

26. Power, J. L.. "Drag, Flow Transition, and Laminar Separation on Nine Bodies of Revolution Having Different Forebody Shapes," David W. Taylor Naval Ship Research and Development Center Report 77-0064, December 1977.
27. Fisher, D. F. and Dougherty, N. S., "Flight and Wind Tunnel Correlation of Boundary Layer Transition on the AEDC Transition Cone," AGARD CP-339, February 1983.
28. Potter, J. L., "Boundary Layer Transition on Supersonic Cones in an Aeroballistic Range," AIAA Journal, Vol. 13, March 1975, p. 270.
29. Beckwith, I. E., and Bertram, M. H., "A Survey of NASA Langley Studies on High Speed Transition and the Quiet Tunnel," TM X-2466, July 1972, NASA.
30. Potter, J. L., "Review of the Influence of Cooled Walls on Boundary Layer Transition," AIAA Journal, Vol. 18, August 1980, p. 1010.
31. Merlet, C. F. and Rumsey, C. B., "Supersonic Free Flight Measurements of Heat Transfer and Transition on a  $10^\circ$  Cone Having Low Temperature Ratio," NACA TN D-951, 1961.
32. Rumsey, C. B. and Lee, D. B., "Measurements of Aerodynamic Heat Transfer and Boundary Layer Transition on a  $15^\circ$  Cone in Free Flight at Supersonic Mach Numbers Up to 5.2," NACA TN D-888, 1961.
33. Rumsey, C. B. and Lee, D. B., "Measurements of Aerodynamic Heat Transfer and Boundary Layer Transition on a  $10^\circ$  Cone in Free Flight at Supersonic Mach Numbers Up to 5.9," NACA TN D-745, 1961.
34. Potter, J. L., "Boundary Layer Transition on Cones Near Mach One." AIAA Journal, Vol. 12, No. 4, April 1974, pp. 570- 571.
35. Morkovin, M. V., "Bypass Transition to Turbulence and Research Desiderata," NASA CP-2386, May 1984.
36. Poll, D. I. A., "Some Effects of Boundary Layer Transition on Slender Axi-symmetric Bodies at Incidence in Incompressible Flow." In AGARD-CP-336, Sept. 1982.
37. Poll, D. I. A., "On the Effects of Boundary Layer Transition on a Cylindrical Afterbody at Incidence in Low Speed Flow," The Aeronautical Journal of the Royal Aeronautical Society, October 1985, p. 315.
38. Poll, D. I. A., "Some Observations of the Transition Process on the Windward Face of a Long Yawed Cylinder," Journal of Fluid Mechanics, Vol. 150, 1985, p. 329.
39. Poll, D. I. A., "The Development of Intermittent Turbulence on a Swept Attachment Line Including the Effects of Compressibility," The Aeronautical Quarterly, Vol. XXXIV, February 1983, p. 1.
40. Poll, D. I. A., "Transition in the Infinite Swept Attachment-Line Boundary Layer," The Aeronautical Quarterly, Vol. XXX, Nov. 1979, pp. 607-628.
41. Potter, J. L., "Transition from Laminar to Turbulent Flow in Separated Shear Layers," AIAA Journal, To be published.
42. Ericsson, L. E. and Reding, J. P., "Aerodynamic Effects of Asymmetric Vortex Shedding from Slender Bodies," AIAA Paper 85-1797, 1985.
43. Sturek, Walter B. "Boundary Layer Studies on a Spinning Cone," AIAA Paper 72-967, 1972.
44. Sturek, Walter B. "Boundary-Layer Distortion on a Spinning Cone," AIAA Journal, Vol. 11, No. 3, March 1973, pp. 395-396.
45. Braslow, Albert L. "Effect of Distributed Granular-Type Roughness on Boundary-Layer Transition at Supersonic Speeds With and Without Surface Cooling." NACA RML 58A17, March 1958.

See also AGARD Rept. 254, April 1960, and "Use of Grit- Type Boundary-Layer Transition Trips on Wind-Tunnel Models." NASA TN D-3579, September 1966.

46. Potter, J. Leith and Whitfield, Jack D., "Effects of Slight Nose Bluntness and Roughness on Boundary-Layer Transition in Supersonic Flows." Journal of Fluid Mechanics, Vol. 12, Pt. 4, April 1962, pp. 501-535.
47. Braslow, Albert L. and Knox, Eugene C., "Simplified Method for Determination of Critical Height of Distributed Roughness Particles for Boundary-Layer Transition at Mach Numbers from 0 to 5." NACA TN 4363, September 1958.
48. Lyons, W. C. and Levensteins, Z. J., "The Determination of Critical Roughness Height for Boundary Layer Transition," NOL TR 61-87, October 1962.
49. Van Driest, E. R. and Blumer, C. B., "Boundary Layer Transition at Supersonic Speeds: Roughness Effects with Heat Transfer," AIAA Journal, Vol. 6, Nov. 4, April 1968, pp. 603- 607. See also Journal of the Aerospace Sciences, Vol. 29, Aug. 1962, pp. 909-916.

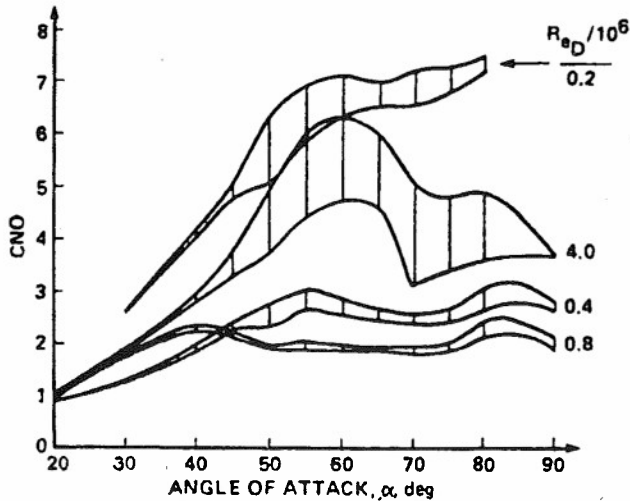


Fig. 1. Example of variation of normal force with Reynolds number and angle of attack. (From Ref. 5.)

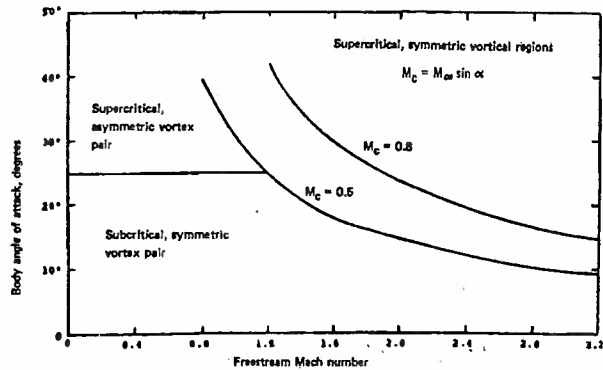


Fig. 2. Approximate boundaries for various types of vortices. (From Ref. 6.)

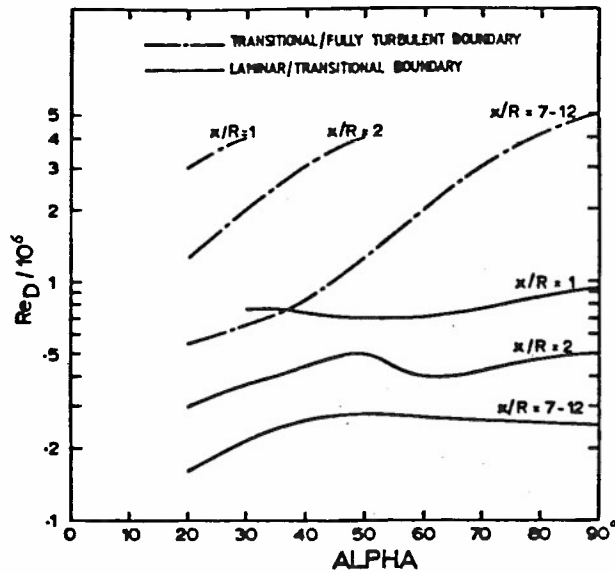


Fig. 3. Boundary layer transition locations along an ogive-cylinder. (From Ref. 7.)

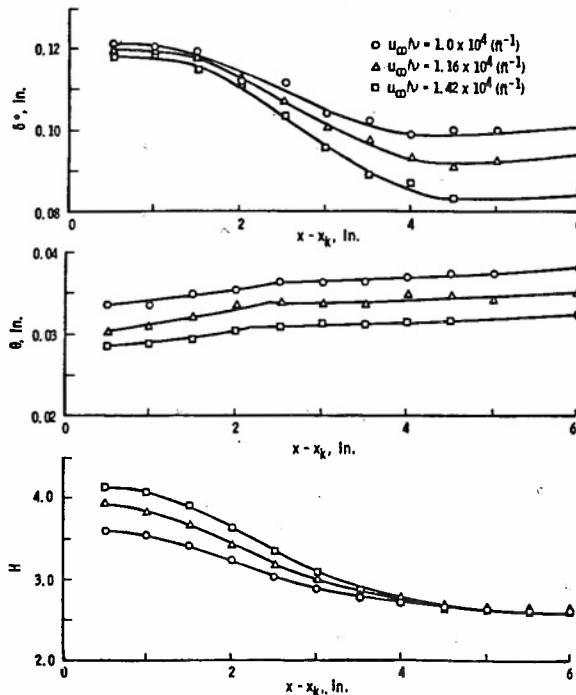


Fig. 4. Distribution of boundary layer parameters downstream of 0.066-in.-diam roughness elements at  $x_k = 2$  ft. (Ref. 17.)

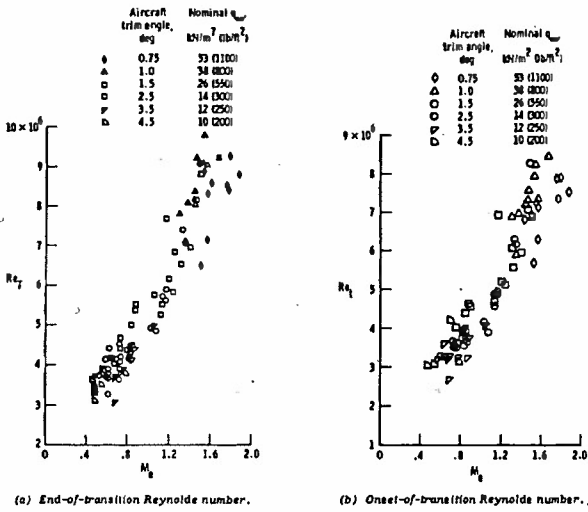


Fig. 5. F-15/AEDC Cone transition Reynolds number as a function of Mach number. (From Ref. 27)

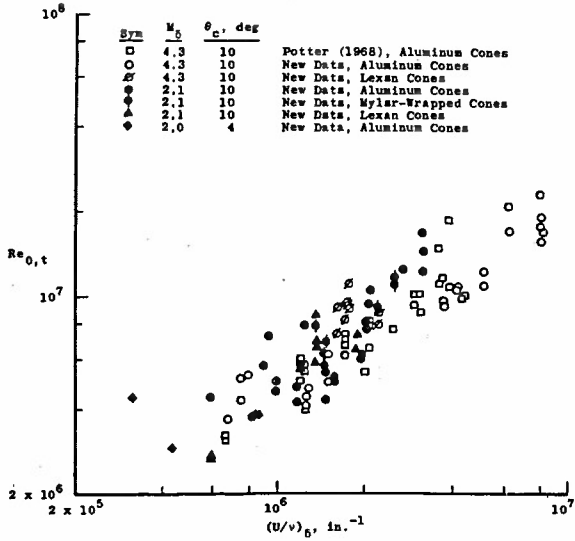


Fig. 6. Boundary layer transition on cones in an aeroballistics range: AEDC data. (From Ref. 28.)

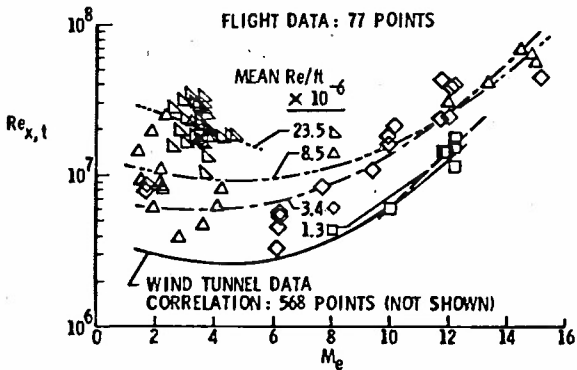


Fig. 7. Boundary layer transition on cones in flight: NASA data. (From Ref. 29.)

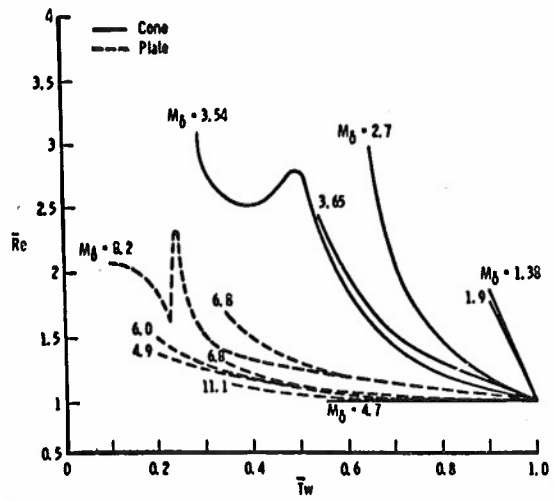


Fig. 8. Experimental effect of wall cooling on transition Reynolds numbers at various Mach numbers. (From Ref. 30.)

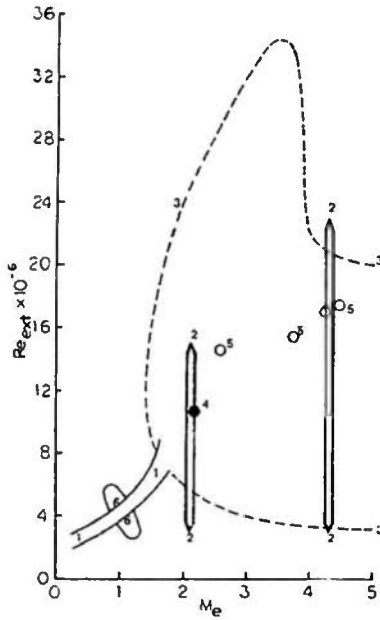


Fig. 9 Collection of free-flight, sharp-cone boundary layer transition data: unit Reynolds numbers and wall temperature ratio variable. 1 - Ref. 27, 2 - Ref. 28, 3 - Ref. 29, 4 - Ref. 31, 5 - Refs. 32-33, 6 - Ref. 34.

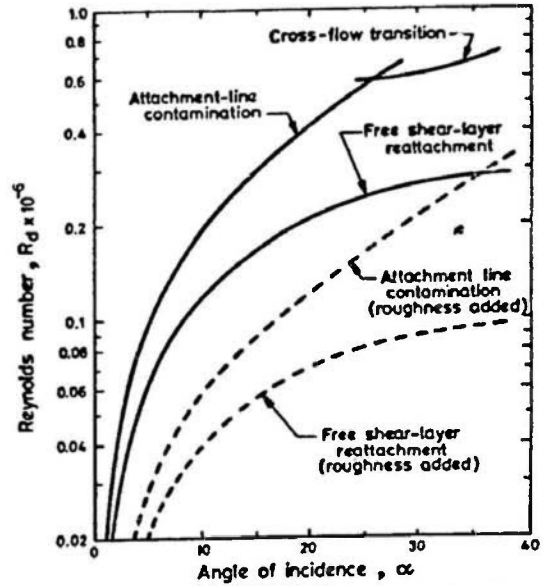


Fig. 10 The effect of roughness on free-shear-layer and attachment-line transition. (From Ref. 37.)

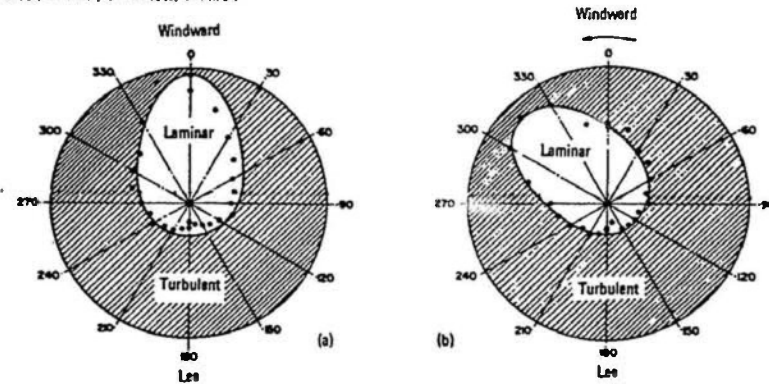


Fig. 11. Boundary layer transition on a sharp, 10-deg half-angle cone at  $M_\infty = 2$  and 4-deg angle of attack: (a) no spin, (b) 20,000 rpm. From Ref. 43.

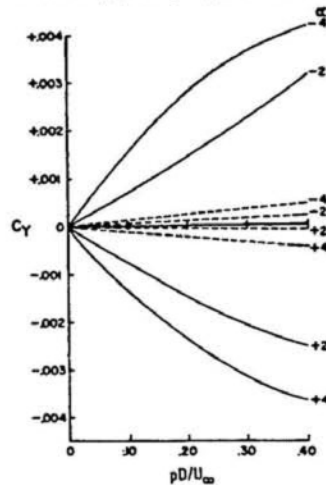


Fig. 12. Side force on a sharp, 10-deg half-angle cone at  $M_\infty = 2$ : —  $Re_{\infty x} = 1.8 \times 10^6$  (laminar on windward side, turbulent on lee side), ---  $Re_{\infty x} = 6 \times 10^6$  (naturally turbulent on both sides). From Ref. 43.



## SECTION 3.4 CONCLUSIONS

by

Professor E. Reshotko  
Dept. of Mechanical and Aerospace Engineering  
Case Western Reserve University  
Cleveland, OH 44106, USA

In Section 3 of this document, the underlying rationale and the detailed simulation methodologies developed by the Methodology Committee of AGARD FDP Working Group 09 have been presented. It is a first step in the attempt to codify and systematize the best of our simulation capabilities to date and to provide the framework for further improvements. By gathering the expertise of the acknowledged leaders of this craft, we have in effect developed an expert system. Such methodologies and their successors will be an essential component of the sophisticated wind tunnel testing and evaluation procedures to which we aspire. The fact that these methodologies are now written down makes them available to the larger wind tunnel testing community and should lead to an overall improved confidence in the test results for the increasingly complex configurations that we seek to evaluate.

The presented methodologies are ones that try to maximize the amount of information that is best obtained through wind tunnel testing. Computational and empirical techniques are used to augment and extend the measurements rather than to replace them. As stated earlier, methodologies are not unique. But we believe that the best methodology is one that optimally captures and synthesizes the contributions of testing, computation and evaluation. The construction of these methodologies even by the experts involved many iterations. Assuming that the process of developing a methodology is convergent, the authors of this section do not believe that the presented methodologies are yet in their final form. Rather one should view the document as a loose-leaf notebook wherein methodologies can be augmented or replaced as improvements are made.

It should also be realized that the presented methodologies are subject to validation, and will in all likelihood be improved as a result of subjecting them to validation. To be complete, the validation of a methodology should include the comparison of model test results from wind-tunnels extrapolated to flight conditions with results obtained from the full size vehicle in atmospheric flight. Even if such validation is difficult to arrange, they will be well worth the effort.

The implementation of the near field simulation methodologies such as developed herein together with the development and implementation of more refined techniques of far field simulation through the assessment or elimination of tunnel wall interference effects can bring on a new era in sophisticated wind tunnel testing. It will enable obtaining the additional decimal place in performance evaluation that is becoming increasingly important in the development of aircraft for supercritical transonic flight.

## SECTION 4

PHYSICAL ASPECTS OF BOUNDARY LAYER SIMULATION AND  
ASSOCIATED RESEARCH REQUIREMENTS

by

The Research Committee of WG-09

Prof. C. Ciray, Turkey  
 A.G.T. Cross, U.K. \*  
 Prof. J.L. van Ingen, The Netherlands  
 Dr. E.M. Kraft, U.S.A.  
 Dr. R. Michel, France  
 J.D. Peterson, U.S.A.\*  
 Dr. E. Stanewsky, F.R.G.  
 Dr. J. Szodruch, F.R.G.\*

\* Joined the Research Committee after completion  
 of their assignment in the Review Committee

## SUMMARY

The improvement of full-scale transonic performance prediction, especially under off-design conditions, requires boundary layer simulation and control in low Reynolds number wind tunnel tests. The physics of the flow associated with such a viscous simulation are reviewed and research needed to verify the results of the present study and to fill the gaps in our knowledge are outlined. In the approach to the subject, the Committee first identified flow phenomena critical in the present context, distinguishing between phenomena involving the direct interaction between the outer inviscid flow and the boundary layer and phenomena primarily affecting the boundary layer development without having a direct influence on the outer flow. The former include shock boundary layer interaction, trailing edge flow, classical (low speed) separation and vortex flows including the formation of wing vortices, vortex breakdown and asymmetrical vortex shedding. It is attempted to establish for these phenomena dominant viscous and outer inviscid flow parameters, i.e., parameters that must be duplicated in a low Reynolds number simulation process. The implementation of such a process requires, in addition, the understanding and predictability of the boundary layer development as it occurs naturally on a given aerodynamic surface or as it evolves under the influence of the wind tunnel environment or by boundary layer manipulation. Accordingly, relevant aspects of the laminar and turbulent boundary layer development,

including non-equilibrium boundary layers and free and forced transition, environmental effects and potential boundary layer manipulation techniques, are reviewed.

## CONTENTS

- 4. Physical Aspects of Boundary Layer Simulation and Associated Research Requirements
  - 4.1 Introduction
  - 4.2 Critical Flow Phenomena
  - 4.3 Boundary Layer Development and Transition
  - 4.4 Development and Analysis of Turbulent Non-equilibrium Boundary Layers
  - 4.5 Shock Boundary Layer Interaction
  - 4.6 Classical Separation, Trailing Edge Flows and Buffeting
  - 4.7 Vortex Flows
  - 4.8 Environmental Effects on Transition and Boundary Layer Characteristics
  - 4.9 Boundary Layer Manipulation
  - 4.10 Summary of Research Requirements and Conclusion

## SECTION 4.1 AND 4.2

## INTRODUCTION AND CRITICAL FLOW PHENOMENA

by

E. Stanewsky

Institut für Experimentelle Strömungsmechanik  
 Deutsche Forschungs- und Versuchsanstalt  
 für Luft- und Raumfahrt e.V.  
 D-3400 Göttingen, FRG

## 4.1 Introduction

The physics of the flow associated with boundary layer simulation procedures in low Reynolds number wind tunnel tests are not at all well understood. This applies to details of the flow phenomena or developments which dominate viscous/inviscid interactions on aerodynamic surfaces, and hence must be "simulated", as well as to the effect of any boundary layer manipulating device on the characteristics of the boundary layer as compared to its natural transition counterpart. Furthermore, only sparse information is at hand concerning the sensitivity of specific flow phenomena or the global flow development about a given aerodynamic configuration to viscous effects, i.e., to changes in Reynolds number or transition point location. Knowing the latter is important since it determines the "need to simulate".

The present scope of work, derived from these deficiencies, can be expressed as follows:

- Review the physics associated with the simulation of high Reynolds number flow and, in particular, determine viscous and outer inviscid flow parameters that dominate viscous/inviscid interaction crucial to the simulation process.
- Define needed research to improve the understanding of the flow physics associated with boundary layer simulation, including research needed to identify and account for wind tunnel environmental effects on the boundary layer simulation.
- Define experiments and/or CFD exercises needed to establish the sensitivity of relevant flow phenomena or flow developments to viscous effects.

The task was approached by first identifying (local) flow phenomena or flow developments believed to be sensitive to changes in the Reynolds number, or, more general, to changes in the initial boundary layer properties, where initial refers here to the boundary layer properties just upstream of its first encounter with severe outer flow developments, such as, for instance, a shock wave. Phenomena

critical in that sense are depicted in Figure 1 of Section 4.2 together with those parameters which may affect the initial boundary layer development. In the present sections we will treat the phenomena summarized in this figure discussing

- physical aspects relevant to the viscous simulation process, identifying, where possible, dominant viscous and outer inviscid flow parameters, and
- future research, recommending experiments needed for a better understanding of the physics underlying viscous simulation.

The aspect of the sensitivity of the flow to viscous changes will, naturally, be part of these considerations.

## 4.2 Critical Flow Phenomena

Critical flow phenomena in the present sense, Figure 1, are those that contribute, due to their effect on the interaction between the outer inviscid flow and the boundary layer, to deviations between low Reynolds number wind tunnel and full-scale flight results. (In a wider sense, these are phenomena which we are not able to compute with sufficient accuracy.) Hence, in order to gain a deeper insight into the physics of the overall simulation

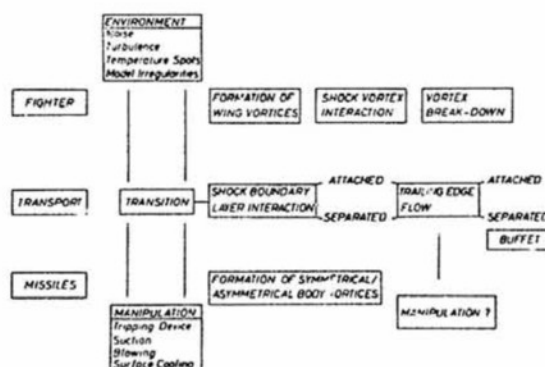


Figure 1: Critical flow phenomena

process, one must try to better understand the critical viscous/inviscid interaction phenomena, especially the strong interactions, characterized by large adverse pressure gradients, since only the latter are likely to be sensitive to viscous changes. This leads in essence to the study of the development of the boundary layer, distinguishing between the "initial" development as dependent on configurational and environmental parameters and the development due to the imposed outer flow field. The latter may, in turn, be strongly dependent on the development of the viscous layer (see Figure 1 of Section 4.5). Note, that only if this is the case, one has to be concerned.

In the following paragraphs, the flow phenomena defined as critical are briefly addressed adhering to the sequence given in Fig. 1. The aim is to demonstrate why these phenomena are considered critical for the viscous simulation process; their in-depth treatment is, of course, left up to the individual sections of the Working Group report.

**Boundary Layer Development and Transition:** For any viscous simulation process it is essential to be able to predict the state of the boundary layer - laminar or turbulent - and characteristic boundary layer parameters upstream of a "critical" outer flow obstacle, such as, for instance, a shock wave, at full-scale as well as wind tunnel conditions. The former is required to provide the magnitude of the (dominant) boundary layer parameter to be duplicated in the low Reynolds number environment of the wind tunnel, the latter is needed to establish that parameter on the wind tunnel model. Determining the boundary layer development means to predict the laminar development, transition, be it free or forced, and, of course, the turbulent development of the viscous layer. The difficulty of the task is exemplified in Figure 2 [1] by considering the numerous parameters influencing transition. If, for instance, transition fixing is required on the wind tunnel model, as is generally the case, the influence of the transition forcing device on the subsequent boundary layer development, including not only its

effect on the boundary layer growth parameters but also on turbulence level and structure, must be known and accounted for in any computational procedure.

In Section 4.3 the state-of-the-art in predicting the boundary layer development, including free and fixed transition, up to critical flow conditions is reviewed, deficiencies outlined and needed research recommended. Section 4.3 is supplemented by a discussion of non-equilibrium boundary layers in Section 4.4.

**Boundary layer manipulation:** In low Reynolds number wind tunnel tests, the experimental determination of transition, especially in routine testing, is essential for several reasons: It is needed for the accurate prediction of full-scale drag, the identification of areas where a tripping device can still be placed and the verification of the effectiveness of a transition fixing agent in promoting transition at the location of the trip. The latter is, unfortunately, dependent on the freestream conditions, Figure 3[2]. If transition must be artificially enforced, the following requirements should be met:

- The outer flow field must not excessively be disturbed and the effect of the transition fixing agent on the subsequent boundary layer development must be known.
- The turbulent boundary layer generated should be as close to a natural transition boundary layer as possible.
- The disturbance due to the tripping device should be (remotely) adjustable so that it can be optimized for any freestream condition considered, where optimization means having transition occurring at the location desired with "zero" drag penalty.

Transition detection and the "optimum" transition forcing is thus a crucial part of the viscous simulation process. The topic is treated in Section 4.9 considering various means of transition fixing and detecting and their influence on the boundary layer development. Also discussed here are devices which are designed to either delay the onset of transition or to alter the already turbulent boundary layer in order to control critical viscous/inviscid interactions. The latter is, of course, part of the direct simulation process.

**Shock boundary layer interaction:** If one considers an airfoil (or a large aspect ratio wing), the upper surface boundary layer, generally turbulent, will at off-design conditions first enter the shock boundary layer interaction region. The shock will, dependent on its strength, either only thicken the boundary layer or cause a direct or indirect separation. In a direct separation the viscous layer

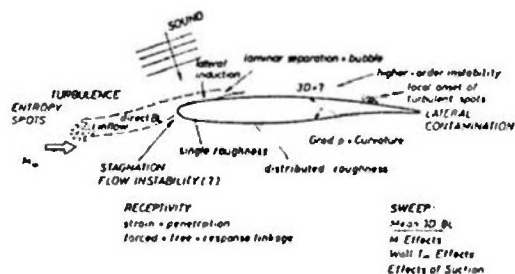


Figure 2: Typical transition issues in external flows [1]

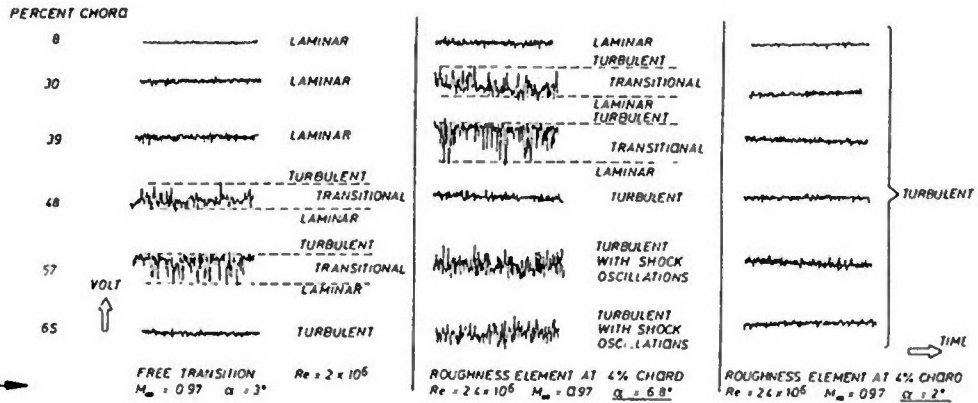


Figure 3b: Surface-hot-film signals for laminar, transitional and turbulent boundary layers on a sheared wing

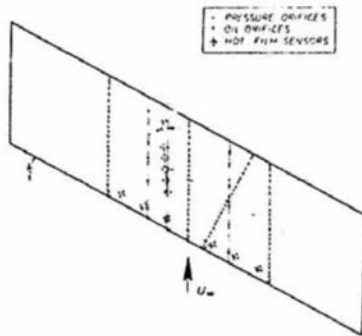
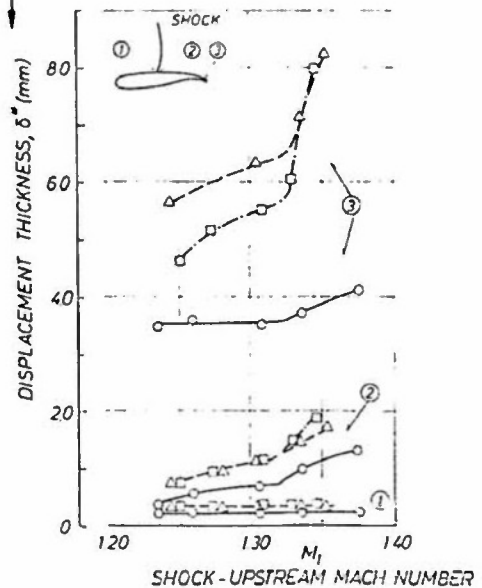


Figure 3a: Sheared-wing instrumentation

leaves the surface at the foot of the shock and reattachment may or may not occur upstream of the trailing edge. In an indirect separation the shock wave affects the boundary layer in a way that causes the flow to separate at the trailing edge due to the rear adverse pressure gradient. (For the numerous separation pattern possible see Ref. 4 of Section 4.5.) It is well known that these developments may be highly sensitive to changes in the initial turbulent boundary layer condition which is, in essence, due to the amplification of shock-upstream differences in crucial boundary layer parameters by the shock, Figure 4, Ref. 5 of Section 4.5. Such differences may, for instance, result from differences in the Reynolds number and/or the transition point location. For a "correct" simulation of the overall flow development at full-scale conditions it seems therefore, first of all, necessary to adequately simulate the shock boundary layer interaction process and to ensure that at the downstream face of the interaction dominant boundary layer parameters closely match the ones to be expected at the high Reynolds numbers of

Figure 4: Amplification of differences in the initial displacement thickness, Ref. 4.5.5



AIRFOIL CAST 10-2 / DOA2

$c = 200\text{mm}$

$M_\infty = 0.765$

	$Re \times 10^{-6}$	TRANSITION	$\delta_1^*$
○	1.95	30% c	0.220
△	1.94	7% c	0.340
□	350	7% c	0.350
			mm

- ① Immediately upstream of shock
- ② Downstream of shock (plateau; see Figure 5, Section 4.5)
- ③ At the trailing edge

Note: The  $\delta_1^*$  - values are averages corresponding to the data points of a specific curve

flight. Whether this will result in a sufficiently close approximation of the full-scale trailing edge flow conditions - or whether here further boundary layer manipulation is required - remains, at this point, an open question. The latter is, of course, imperative to the establishment of the correct full-scale shock strength and location in the low Reynolds number wind tunnel tests, hence to the entire simulation process.

All aspects of the physics of transonic shock boundary layer interaction within the present context including future research requirements are discussed in Section 4.5..

**Classical separation and trailing edge flow:** Staying with the example of airfoils and wings, "classical" subsonic separation may occur here on the upper surface close to the leading edge and near or at the trailing edge and on the lower surface in the adverse pressure gradient region of the cove, Figure 5. For a turbulent boundary layer, the occurrence of this type of separation is known to be highly Reynolds number dependent. Laminar separation - although in its position independent of Reynolds number - is of major concern in low Reynolds number wind tunnel tests since it may have a large effect on the downstream turbulent boundary layer development particularly if transition takes place within the domain of the separated region. Especially critical within the present context is, of course, the development of the (turbulent) boundary layer in the trailing edge region and the corresponding conditions under which the flow leaves the trailing edge since circulation, hence the entire outer flow field, is highly dependent on these conditions, Figure 6 [Ref. 5 of Section 4.5]. The boundary layer at the trailing edge (upper and lower side) is, naturally, a product of its history possibly having gone through a transitional leading edge separation and the shock boundary layer interaction process. It should be noted here that the sensitivity of the global flow development to viscous changes is, as mentioned earlier, configuration dependent. This is indicated in Figure 7 [Ref. 5 of Section 4.5] by considering the change in lift coefficient due to a change in transition location for several transonic airfoils. The results stress the need to establish the sensitivity of a given configuration to viscous (or Reynolds number) changes before commencing an elaborate simulation program.

Classical separation and trailing edge flows, including buffeting, are treated in Section 4.6

**Vortex flows:** The primary types of vortical flows of interest here are forebody vortices, wing leading edge vortex flows, vortex break-down and vortex shock interaction. Considering these flows

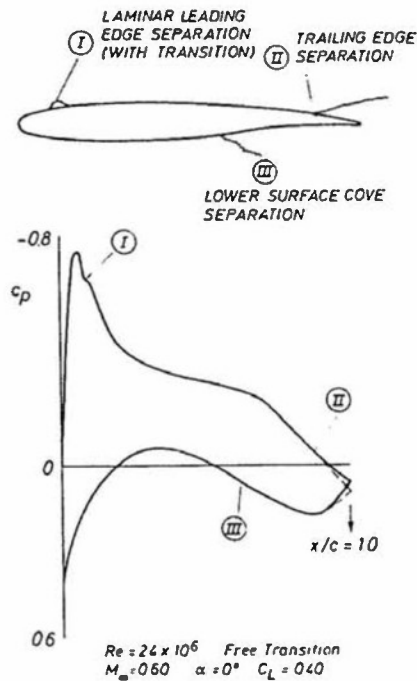


Figure 5: Locations of classical separation. Airfoil CAST 7/DOA1

AIRFOIL CAST 10-2/DOA2  
 $c = 200 \text{ mm}$

$M_\infty = 0.765$      $\alpha$  (or  $M_1$ ) = VARIABLE

	$Re \times 10^{-6}$	TRANSITION	REMARKS
	1.95	30% c	REFERENCE
$\Delta$	1.94	7% c	
$\square$	3.50	7% c	

$$\Delta C_L = [C_L]_{30\%c} - [C_L]_{7\%c}$$

$$\Delta \delta_{TE}^* = [\delta_{TE}^*]_{7\%c} - [\delta_{TE}^*]_{30\%c}$$

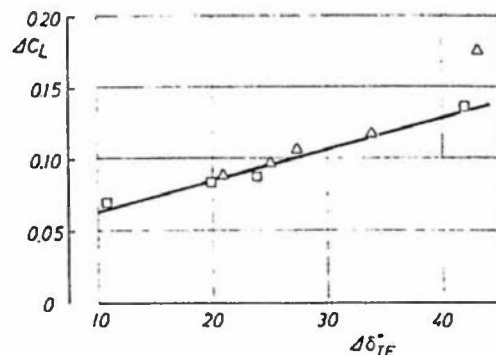
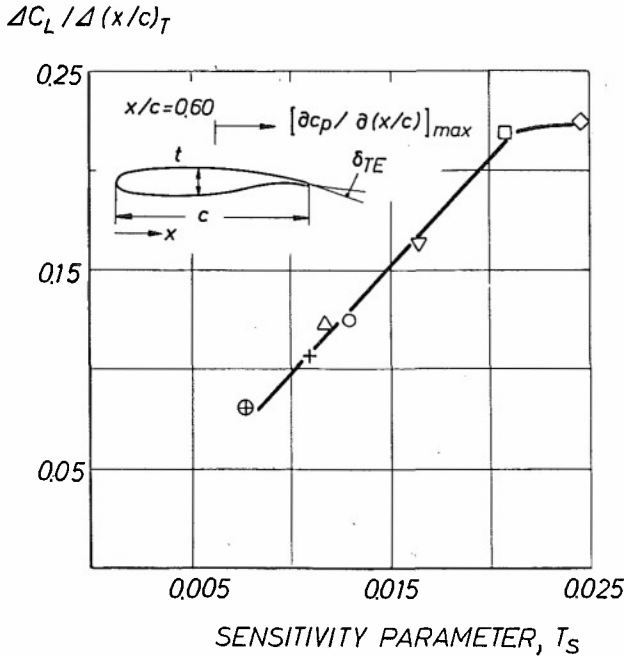


Figure 6: Change in lift coefficient due to a change in trailing edge displacement thickness, Ref. 4.5.5





$$M_\infty = 0.730 \quad Re = 2.4 \times 10^6$$

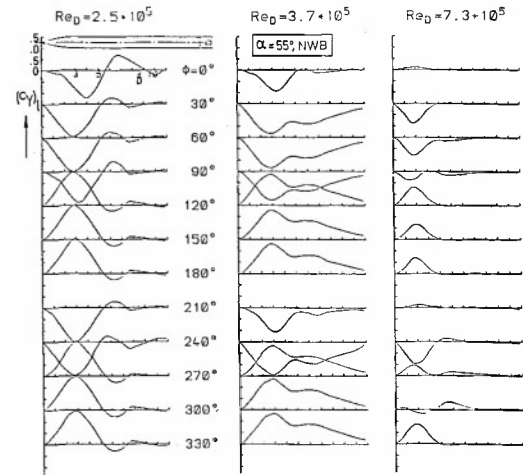
AIRFOIL:  $\circ$  Va2  $\triangle$  T25/1  $\square$  CAST 10-2/DO A2  
 $+$  CAST 7/DO A1  $\nabla$  CAST 12-1/DO A3  
 $\diamond$  DFVLR 48080  $\oplus$  MBB-A1

$$T_S = \delta_{TE}^{1/2} \left[ \partial c_p / \partial (x/c) \right]_{max} (t/c)^2$$

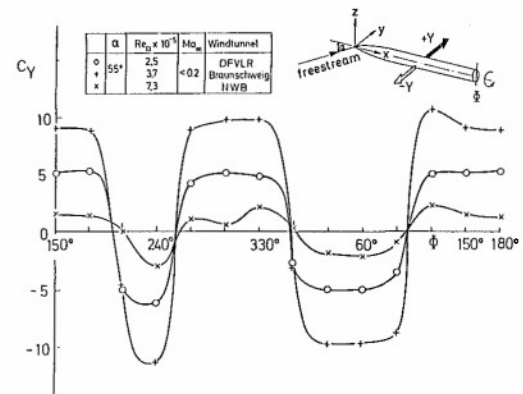
$\Delta C_L / \Delta (x/c)_T =$  Change in lift due to a change in transition location

Figure 7: Sensitivity of transonic airfoils to changes in the shock-upstream boundary layer conditions, Ref. 4.5.5

within the present context of Reynolds number sensitivity and viscous scaling, one must distinguish between configurations where vortices emanate from sharp leading edges, i.e., are fixed by geometry, and configurations where separation and the formation of vortices is pressure gradient induced, hence may develop "anywhere" on a body or a swept wing. The former class of flows is not likely to be very sensitive to viscous changes unless their influence enters via secondary and higher order separations; however, even under these conditions the overall effect is believed to be small. The occurrence of the sustained pressure gradient induced separation and the associated vortex formation and development is, on the other hand, more likely to depend on the upstream boundary layer development, hence may be Reynolds number sensitive. This is demonstrated in Figure 8 [3] where the asymmetrical vortex build-up on a body of revolution at high angles of incidence is seen to be reduced as the Reynolds number is increased. On a rounded leading edge delta wing, the flow situation may be even more complex since here various flow phenomena, possibly sensitive to viscous



Local side force distributions at  $\alpha = 55^\circ$



Roll angle dependence of total side force coefficients

Figure 8: Reynolds number dependence of out-of-plane forces

changes, may be present simultaneously: the primary vortex development, shock wave/vortex or shock boundary layer interaction and conventional trailing edge separation. This complexity makes it difficult to judge the sensitivity of the overall flow development about such configurations to viscous changes so that emphasis must here also be placed on the assessment of the latter for typical vortical flow configurations. Vortical flows are covered in Section 4.7.

**Environmental effects:** Environmental effects are, within the present context mainly of concern in the wind tunnel tests. One may count as environmental effects, naturally, noise, turbulence, temperature spottiness, etc. (see Fig. 2), but also wall interference. The former are especially critical due to their influence on the transition location. Once the boundary layer is turbulent, the influence diminishes and it seems to require relatively large turbulence levels - generally not found in a wind tunnel - to affect, for instance, the shock bound-



ary layer interaction process. Nevertheless, with the ever increasing demand on data accuracy, environmental effects should not, a priori, be treated as negligible. Wall interference, which may affect freestream conditions as well as the overall flow development, must, of course, be accounted for in any simulation process.

Fundamental physical aspects concerning the wind tunnel environment and recommendations for future research activities are covered in Section 4.8.

## REFERENCES

1. Herbert, Th., Morkovin, M.V., "Dialogue on Bridging Some Gaps in Stability and Transition Research", IUTAM Symposium Stuttgart/Germany 1979, Springer-Verlag, Berlin, Heidelberg 1980.
2. Stanswsky, E., Krogmann, P., "Transonic Drag Rise and Drag Reduction by Active/Passive Boundary Layer Control", ACARD Report No. 723, Aircraft Drag Prediction and Reduction, July 1985, pp. 11/1 - 11/41.
3. Hartmann, K., "Experimental Investigation on an Ogive-nosed Body at High Incidence and Different Reynolds Numbers", International Conference on Fluid Mechanics, Beijing, 1987, Peking University Press, Beijing, China.

## SECTION 4.3

## BOUNDARY LAYER DEVELOPMENT AND TRANSITION

BY

Roger MICHEL

ONERA Toulouse Research Center (France)

4.3.1 INTRODUCTION

The principal critical flow phenomena, pointed out in Section 4.2, have been defined as being very sensitive to modifications of the properties of the incoming boundary layer.

Let us, at first, schematize the problem by considering the transonic flow around some profile; the two main critical flow phenomena are the shock-boundary layer interaction region and the downstream separation and trailing-edge flow region.

Two kinds of questions can be asked:

- Do we have to deal with a laminar, transitional or turbulent boundary layer close to the shock? Moreover, what are its characteristics (boundary layer thickness, velocity and fluctuation profiles)? The crucial point concerns, of course, not only the transition but the laminar boundary layer which will become transitional and the turbulent boundary layer which will develop in, a priori, a moderate pressure gradient.

- Considering the fact that the boundary layer is turbulent after the shock wave, what growth will it take in an adverse pressure gradient, especially one strong enough to produce a turbulent separation in the rear part of the profile?

So, in this chapter, we have to analyze the properties of the boundary layer through the three classical aspects of a laminar boundary layer, boundary layer transition and, at last, a turbulent boundary layer. It is not the purpose of the paper to try to give a complete review of either all the work which has been done or the main results in such a great area. It is a matter of simply examining the essential aspects of phenomena and weighted factors as well as opportunities which exist in order to predict the initial characteristics of the boundary as regards to our critical phenomena.

4.3.2 LAMINAR BOUNDARY LAYER DEVELOPMENT

The laminar boundary layer development could just be covered by a statement to the fact that its theoretical treatment is, for all relevant configurations, well in hand. Once the potential flow is given, the number of unknown parameters is equal to the number of equations. Some calculation methods exist; they are sure and precise enough in order to predict the boundary layer development in two- and three-dimensional flows. One can use either field methods solving the local equations of the boundary layer or integral methods involving global equations (see for example CEBECI-BRADSHAW /1/ and COUSTEIX /2/).

However, it must be noticed that the essential aim of boundary layer calculations is to provide us with precise and detailed information, more particularly on velocity profiles, so that one can establish the behavior as regards to laminar stability theory and then apply some transition criterion. To that point, field methods are, a priori, more appropriate. Valid results can, however, be obtained from integral methods by using elaborate closure relationships; usually, an extra global equation is considered as, for instance, the global equation of kinetic energy. Some practical

---

\* Mailing address:  
Residence de la Boisseraie, 25 rue Noulet, 31400 Toulouse, France

aspects will only be developed; they are given from very well known and classic results in order to show up the influence of the essential parameters on the boundary layer development.

In two-dimensional incompressible flows, the self-similar solutions of Falkner-Skan /3/ and Hartree /4/ demonstrate the very sensitivity of the laminar boundary layer and of its velocity profiles to pressure gradients. A classic parameter which is used to show this influence is the Pohlhausen parameter  $\Lambda = \theta^2/\nu \, dU_e/dx$  (where  $\theta$  is the momentum thickness). As will be seen later, this parameter will occur in transition criteria. The evolution of self-similar laminar shape factor and skin friction coefficient with  $\Lambda$  is illustrated in Fig. 1. These results are often used for the closure relationships needed in integral methods.

For transonic flows, at moderate values of Mach numbers, the effect of compressibility is weak, especially as regards to the skin-friction coefficient. On the other hand, the compressibility effect is more considerable on the shape parameter as illustrated through the following formula:

$$H = 2.59 + 0.667 M_\infty^2$$

this formula is valid for a flat plate laminar boundary layer developing on an adiabatic wall.

At last, some observations can be put forward, concerning three-dimensional boundary layers for which there exists a streamwise flow in the direction of the external streamline and a cross-flow in the orthogonal direction. For the streamwise flow, the influence of pressure gradient  $\partial p/\partial x$  is entirely comparable with the one observed in two-dimensional flows. On the other hand, as regards to cross-flow, the effect of negative pressure gradients is very important. In fact, the transverse component of the velocity profile increases considerably with the intensity of this pressure gradient. Here is an essential property for cross-flow instability phenomena and transition which is derived from it.

### 4.3.3 BOUNDARY LAYER TRANSITION

Considering all the research devoted to transition problems, it is very useful to make reference to synthesis papers in which the reader will be able to find all the available bibliography references. Among the most recent reviews, there is the Special Course on Stability and Transition of Laminar Flow /5/ which was held at the von Karman Institute, Rhode St Genese, March 1984. Let us add that in the Special Course on Three-Dimensional Boundary Layers Calculations (V.K. Institute - April 1986) there is also a paper from D. ARNAL /6/ on three-dimensional boundary layers and laminar-turbulent transition.

#### 4.3.3.1 Transition in two-dimensional flows:

##### 4.3.3.1.1 Effective parameters for transition problems in incompressible flows

Three main parameters which have been shown to influence transition Reynolds numbers are the following:

- Pressure gradient (or external velocity gradient):

The pressure gradient acts on the velocity profile and accordingly on the stability properties of the laminar boundary layer; the existence of an inflection point is crucial with respect to the stability problem. Concerning transition, the results follow, qualitatively, those given by the linear stability theory: for negative (respectively positive) pressure gradients, the velocity profiles are stable (respectively unstable) and the transition Reynolds numbers are high (respectively low). The different transition criteria have been set up at first from that effect.

- Surface roughness:

It seems obvious that the surface roughness plays an important role as regards to transition since the boundary layer tripping represents an essential part of the boundary layer simulation and control in wind tunnels. Several results, concerning roughness heights necessary to trip the boundary layer, will be discussed later.

- Free-stream turbulence:

We will examine now some typical results of the influence of free-stream disturbances on transition. On Fig. 2 are plotted different experimental results obtained for a boundary layer in a uniform flow; it shows up the evolution of the transition Reynolds numbers with the external turbulence level,  $Tu$ . At low values of  $Tu$  (say  $Tu < 1/1000$ ), the transition Reynolds number tends towards a constant value, close to 3 million, if we look at the classic experiments of Schubauer-Skramstad /7/ but the results obtained, later on, by Wells /8/ give a higher value.

At low values of the external turbulence rate, it has been shown that aerodynamic sound can control the transition process; Spangler and Wells have investigated the effects of acoustic noise fields of discrete frequencies /9/. The evolution of  $R_{xT}$  with the free-stream disturbance intensity is shown in Fig. 3. It can be observed that high sound levels may be encountered without change in the transition location when sound gives rise to Tollmien-Schlichting waves falling outside the dangerous band in instability theory. If it is not the case, the transition Reynolds number may be dramatically reduced.

#### 4.3.3.1.2 Transition criteria

Empirical transition criteria have been suggested initially to take into account the primary influence of the streamwise pressure gradient assuming implicitly the external turbulence level is low enough so that the experimental results can be plotted on a single curve. The usual transition Reynolds number is based on the momentum thickness. This Reynolds number is correlated to a pressure gradient term such as, for instance, the Pohlhausen parameter or some parameter depending on the shape of the laminar boundary layer velocity profile, as the shape factor  $H$ . Different transition criteria - for instance Michel's criteria /10/ - can be written in terms of such a representation by the use of laminar similarity solutions.

The transition criteria are often used for practical applications, because they are easily introduced in engineering prediction methods such as integral methods. Nevertheless, the problem is that important discrepancies can exist between the various theories (Fig. 4). Moreover, they do not take into account the stability properties of the boundary layer since they could eventually predict the transition point upstream of the critical point, defined in the linear stability theory, which is at variance with the transition process.

A first attempt for considering the stability properties of the boundary layer and the flow history was made by Granville /14/. The experimental results fall on one curve when presented in terms of the difference in momentum thickness Reynolds numbers from the critical ( $x_{cr}$ ) to the transition ( $x_t$ ) point versus an averaged Pohlhausen parameter calculated between  $x_{cr}$  and  $x_t$  (Fig. 5).

So far, among all the different methods, those which provide us with the best capability to predict the transition point are, without doubt, the amplification methods, that is the so-called  $\sigma$  methods which use results from the laminar stability theory by considering the amplification of

Tollmien-Schlichting waves. These methods are based on the observation that transition occurs when the most unstable frequency is amplified by some factor:  $e^9$  for Smith and Gamberoni /15/,  $e^8$  for Van Ingen /16/. The success of such a method lies, in fact, in a judicious choice of the value of the exponential factor.

Therefore, Mack suggests to take into account the effect of the external turbulence level  $Tu$ . The value of the factor  $n$  at the transition location is given by the following relation /17/

$$n_T = -8.43 - 2.4 \ln Tu$$

This relation has been established to fit experimental results of transition for flat plate cases; more generally, it can be applied to flows with pressure gradients.

The application of an  $e^n$  method is, as follows: for a given external velocity distribution, a laminar boundary layer code provides us with the velocity profiles. The laminar stability theory (Orr-Sommerfeld equation) is applied to these profiles at different abscissa. The local amplification rate is then determined for different frequencies and for each of the velocity profiles. Transition will occur when the integration of the local amplification rate gives, for the most unstable frequency, the amplification corresponding to the critical factor  $n_T$ .

Arnal, Habiballah and Delcourt /18/ suggest, for practical applications, a criterion derived from the  $e^n$  method; it is based on velocity profiles of similarity flows. The criterion starts with the envelope curves of amplitude ratio computed for the Falkner-Skan profiles (Fig. 6). Each curve is characterized by a similarity parameter, such as, for instance, the Pohlhausen parameter  $\Lambda$ . The curves of Fig. 6 give for

$$n = \left( \ln \frac{\Lambda}{\Lambda_0} \right)_{max}$$

a relation such as:

$$n = n(R\delta, \text{ or } R\theta, \Lambda)$$

As the critical Reynolds number is itself a function of  $\Lambda$ , and as the value of  $n$  at the transition location depends on the external turbulence level (Mack's relation), one gets a correlation of the form:

$$R\theta_T - R\theta_{cr} = f(\Lambda, Tu)$$

This correlation looks like the one proposed by Granville except that the free-stream turbulence level  $Tu$  is taken into account. It is then sufficient to replace  $\Lambda$  by its averaged value, taken between the critical abscissa and the transition point, to get a transition criterion including the effects of pressure gradient and free-stream turbulence level; it is then applicable to non-similarity boundary layers. The preceding correlation is represented on Fig. 7. The very important influence of the pressure gradient can be clearly observed. Let us notice also the increasing effect of turbulence when going from positive to negative pressure gradients.

As regards to boundary layer simulation in wind tunnels, an important point is to know where transition would occur for flight Reynolds numbers. It is generally assumed that transition will take place close to the leading edge and, very often, the boundary layer is tripped within the first ten percent of the chord. An application of the preceding transition criterion to the CAST 7 profile shows that it is not always the case (Fig. 8). In spite of a rather high value of the lift coefficient ( $C_L = 0.6$ ) negative pressure gradients exist on the forward part of the upper side; downstream to the shock wave, the pressure gradient is equal to zero or slightly negative. This

stabilizing effect gives transitions located further downstream than it could be predicted by using the usual criteria for boundary layer tripping.

#### 4.3.3.1.3 Effect of wall roughness

Only a few results exist as regards to roughness heights below which transition takes place at the same location as on a smooth surface ("natural" transition). Concerning distributed roughness, some Reynolds number  $U_e h/\nu$  close to 120 was identified through experiments conducted by Feindt /19/; there is no influence of the pressure gradient on the value of such Reynolds number (Fig. 9).

A lot of experimental work was done for describing the dependence of the transition point movement on the size of two- and three-dimensional roughness elements. These results can be found in particular in Dryden /20/. When increasing the roughness height (or the free-stream velocity) transition moves gradually upstream for a two-dimensional roughness element (Fig. 10). For a three-dimensional roughness element, the change in the transition location is more abrupt; transition moves quickly forward when the Reynolds number exceeds some critical value corresponding to the roughness height (Fig. 11).

#### 4.3.3.1.4 Effect of compressibility

Considering the problem of transition in transonic and supersonic flows, one of the main difficulties remains in the fact that the available experimental results are most of the time governed by pressure fluctuations induced by the test section walls. Systematic measurements performed on the AEDC cone /21/ showed a quite important scattering of the wind tunnel transition data. The flight transition Reynolds numbers are compared to those obtained in the less "noisy" wind tunnels (Fig. 12); they rapidly moved apart when reaching the supersonic range.

For the range of transonic velocities of our applications, it does not seem, at least in a first analysis, that the Mach number is an essential parameter. Stability calculations indicate only a moderate variation of the critical Reynolds number with respect to the incompressible case. The transition criteria, previously established for incompressible flows, and slightly modified to take into account the effect of compressibility through the involved parameters, could predict with success for some cases, the transition location on an adiabatic wall.

However, more detailed studies of stability for compressible flows performed by Mack /5/ and more recently by Arnal /22/ provided us with results a little bit different from the incompressible ones. At first, at  $Me = 0$ , the two-dimensional waves,  $\psi = 0$ , were only considered; one could then demonstrate that they are the most unstable ones. This is no longer the case in compressible flows; Fig. 13 shows the evolution of the maximum amplification coefficient versus the wave direction,  $\psi$ , for transonic flows /22/; one should notice that the highest amplification corresponds for a non-zero value of  $\psi$  above  $Me = 0.9$ .

Secondly, an important result is that an increase of the Mach number has little effect on the critical Reynolds number; however, the amplification coefficients of the unstable waves are smaller. This property is illustrated on Fig. 12 where, after Arnal, is presented the transition Reynolds numbers obtained with the  $e^n$  method for different values of the exponent  $n$ . For the flat plate case as well as the cone, one gets (Fig. 12) an increase in the transition Reynolds number above the subsonic range. Concerning the cone, it is interesting to notice that the experimental results are obtained for a value of  $n$  close to 10; that last value is in fact the one which has to be considered in incompressible flows at low values of the external turbulence level.

For a non-adiabatic wall, the wall temperature is a very important parameter; there is a stabilizing or destabilizing effect according as the wall temperature is lower or greater than the adiabatic wall temperature. The transition Reynolds number has been estimated to follow a power-type

law,  $T_w-7$ , a result which could be rather well confirmed by Arnal when applying an  $e^n$  method in the flat plate case; but, we must be careful since the effect of non-thermal equilibrium must depend on the pressure gradient in which transition takes place. This effect represents a serious problem for experiments performed in blow-down and in cryogenic wind tunnels since very severe conditions must be respected for fixing the thermal equilibrium of the model.

#### 4.3.3.1.5 Influence of Streamwise Curvature

It is especially in the case of a concave wall that one can observe the influence of a streamwise curvature on the stability of the boundary layer. There is, then, a destabilizing effect of centrifugal forces, which leads to the formation of counter rotating vortices, the axes of which are parallel to the principal flow direction. This instability which was, at first, considered by Gortler /23/, often results in a premature transition. Some essential results are presented here; they are extracted from a more complete review given by Arnal /5/.

From a theoretical point of view, a three-dimensional disturbance is superposed on the basic flow; its form is periodical in the transverse direction. Substituting this form within the continuity and momentum equations, one gets a system of two differential equations for the amplitude functions of  $u$  and  $v$ . For given mean velocity profiles, three parameters arise:

- the Gortler number:  $GL = UeL/v \sqrt{L/R}$
- the wave number:  $\alpha = 2\pi L/\lambda$  ( $\lambda$ : transverse wave length)
- the amplification factor  $K$  (using the temporal theory).

The homogeneous boundary conditions lead to an eigenvalue problem for these three real parameters.

An example of results, obtained by Ragab and Nayfeh /24/, is given on Fig. 14; the temporal amplification rate curves are plotted in a Gortler number-wave diagram for a mean velocity profile of a flat plate boundary layer. One can observe that the neutral curve ( $K = 0$ ) appears to asymptotically approach  $GL = 0.47$  (to which corresponds  $G_0 = 0.25$ ). The same authors computed neutral stability curves for different Falkner-Skan profiles; favorable pressure gradients are stabilizing whereas positive pressure gradients are destabilizing, but this effect diminishes rapidly as the wave number increases.

Concerning the values of the Gortler number at which transition begins, the experimental results are not numerous. Reference is made /5/ to the work of Liepmann /25/, /26/, who investigated the influence of convex and concave curvature on the transition location. The left hand side part of Fig. 15 shows the evolution of  $R()$  taken at the transition point, versus the ratio  $l/R$ .

The effect of a convex wall remains very slight. On the other hand, increasing  $l/R$  decreases notably the transition Reynolds number. Liepmann found that the transition Gortler parameter  $G_{0T} = (Rl) \sqrt{l/R}$  is close to 9 at a very low turbulence level, whereas at higher turbulence levels ( $T = 0.3$  to  $2$ ), the value was about 6. It must be emphasized, however, that Liepmann's data are restricted to slightly curved walls. The dependence on streamwise pressure gradient is certainly small, due to the strong mean velocity profile distortions introduced by the Gortler vortices. In any case,  $G_{0T}$  is about two orders of magnitude greater than the critical Gortler number.

#### 4.3.3.2 Transition in three-dimensional flows:

##### 4.3.3.2.1 Sweptwings - Possible origins of the turbulence

The evolution of the streamwise and cross-flow velocity profiles of the laminar boundary layer which develops on a swept wing is shown in Fig. 16. For a given angle of sweep and angle of attack,



this figure illustrates also the movement of transition as a function of some chord Reynolds number, that is to say the free-stream velocity. It appears that transition may occur through three main mechanisms:

- At low values of the free-stream velocity (or Reynolds number) the transition takes place in the rear part of the wing, in the region of positive pressure gradient. Its movement looks like the one which would be observed on the same airfoil without any angle of sweep. It is governed by the stability properties of the streamwise profile of the laminar boundary layer. This transition shall be called streamwise (instability) transition.

- At higher values of the free-stream velocity, transition rapidly shifts forward and takes place rather close to the leading edge in a negative streamwise pressure gradient. Such a movement is inconceivable in two-dimensional flows, where the accelerated zones stabilize the laminar boundary layer. It is attributable to the stability properties of the cross-flow profile of the boundary layer. This transition shall be called cross-flow (instability) transition.

- At last, for much higher values of the free-stream velocity, the boundary layer which develops on the attachment line can be contaminated by the turbulent structures of large scale coming from the wall on which the wing is fixed: this is the leading edge contamination. Thus, the boundary layer is turbulent all over the whole wing. For such high values of the Reynolds number, relaminarization could not occur very easily.

#### 4.3.3.2 Transition criteria

- Leading edge contamination:

An important parameter is the Reynolds number,  $R_0$ , defined with the momentum thickness of the boundary layer on the attachment line. For infinite swept wing, this Reynolds number depends on the angle of sweep  $\phi$ , on the free-stream velocity  $Q_\infty$ , and on the normal external velocity gradient taken at the leading edge. It is possible to express it in the following form:

$$R_0 = 0.404 \frac{Q_\infty \sin \phi}{\left( \nu \frac{dU_e}{dx} \right)_0^{\frac{1}{2}}}$$

Experimental studies revealed that leading-edge contamination occurs when that Reynolds number exceeds a critical value /27/:

$$R_{0T} = 100$$

For infinite swept wings in incompressible flows, the normal external velocity gradient is

$$\frac{dU_e}{dx} \Big|_0 = 2 \frac{Q_\infty \cos \phi}{r}$$

where  $r$  is the radius of the leading-edge cylinder. So, the Reynolds number beyond which contamination takes place along the attachment line is:

$$\frac{Q_\infty r}{\nu} = \frac{122500}{\tan \phi \sin \phi}$$

This Reynolds number decreases quickly when the angle of sweep increases, as is shown in the following table (the Reynolds number based on the chord of the profile taken in the direction normal to the leading edge is calculated for  $r/c = 1.5\%$ ).

$\phi^\circ$	20	25	30	35	40
$Q_\infty r / \nu$	984 000	622 000	424 000	305 000	227 000
$Q_\infty c / \nu$	$66 \times 10^6$	$41 \times 10^6$	$28 \times 10^6$	$20 \times 10^6$	$15 \times 10^6$

- Streamwise instability:

For this type of instability, a two-dimensional criterion remains valid in three-dimensional flows, provided it is applied along an external streamline. It is possible to use, for instance,  $R\theta_{cr} = R\theta_{cr} = f(\Lambda, Tu)$  where  $\theta$  is the momentum thickness of the streamwise profile and  $\Lambda$  the averaged Pohlhausen parameter calculated along the curvilinear abscissa with this streamwise momentum thickness.

- Cross-flow instability:

Pure empirical criteria have been proposed for characterizing this cross-flow instability type transition by correlating a Reynolds number based on the displacement thickness of the cross-flow profile of the boundary layer:

$$R\delta_2 = \frac{u_e \delta_2}{\nu} \text{ where } \delta_2 = \int_0^\delta \frac{w}{u_e} dy$$

Beasley /28/ proposed that at the point where transition begins, this Reynolds number reaches a constant critical value, close to 150.

A systematic study of the experimental results available in the literature has shown, however, that the cross-flow transitions did not take place for a unique value of  $R\delta_2$  /29/. Various attempts to correlate  $R\delta_2$  with some characteristics of the cross-flow profile have not made it possible to collapse the experimental results. Better results have been obtained by associating the transition Reynolds number,  $R\delta_{2t}$ , with the shape factor of the streamwise profile,  $H$  (Fig. 17).

Coustols and Arnal have also tried to take into account results given by the laminar stability theory, applied to three-dimensional boundary layer, in order to build a second cross-flow transition criterion (see /29/). At a given abscissa, stability properties of different velocity profiles,  $U_e$ , projected in a given direction, (Fig. 18), are studied from  $\epsilon = 0^\circ$  (cross-flow profile) to  $\epsilon = 90^\circ$  (streamwise profile). We then define a Reynolds number  $R\delta_{1\epsilon}$ , based on the displacement thickness of the profile  $U_e$ :

$$R\delta_{1\epsilon} = \frac{1}{\nu} (U_e \sin \epsilon - U_e) dy$$

where  $U_e(y) = U(y) \sin \epsilon + W(y) \cos \epsilon$  and  $U_e$  represents the resultant potential velocity.

Stability calculations revealed the existence of one most unstable direction designated as  $\epsilon_{min}$ . In order to determine that direction, one needs to know the critical Reynolds number. As a consequence, this latter has been represented as a function of either the height of the inflection point of the profile  $U_e$  and of the first derivative of  $U_e$  taken at the inflection point, or some integral parameter if  $U_e$  does not exhibit some inflection point. Moreover, the cross-flow direction was always found to be more stable than the  $\epsilon_{min}$  direction, which varies from  $1^\circ$  to  $5^\circ$ ; this illustrates the concept of "quasi cross-flow instability".

Finally, the criterion for cross-flow (instability) transition has been established from the various experimental data available for swept wings; it is based on a correlation between three parameters (Fig. 19):

- $R\delta_{1\epsilon}$ , taken in the most unstable direction
- the streamwise shape factor parameter  $H$
- the turbulence level  $Tu$

#### 4.3.3.2.3 Application: location of transition on a swept wing

Using the criteria for leading edge contamination, cross-flow and streamwise (instability) transition, a parametric study could be done, in order to show up the combined effect of sweep angle and pressure gradient on transition as function of Reynolds number. The profile that we studied is a sailplane profile (OA P01) defined at the ONERA Aerodynamics Division. The transition location was determined at  $0^\circ$ ,  $20^\circ$ , and  $30^\circ$  of sweep angle. The results are shown on Fig. 20 for the normal angle of attack  $\alpha_n = 1^\circ$ . On the lower surface, where the negative pressure gradients remain moderate, the transition is mainly due to streamwise instability or to leading edge contamination.

Cross-flow instability affects more obviously the upper surface, because of the intensity of the negative pressure gradients and the rapid movement of transition towards the leading edge when giving sweep and increasing the Reynolds number is well evidenced.

Using moreover an "intermittency method" for calculating the transition region (see ARNAL /5/), the boundary layer could be calculated down to the trailing edge. The total momentum thickness (upper + lower surface) obtained at the trailing edge is given in Fig. 21 which clearly indicates the rapid drag increase beyond a certain Reynolds number, strongly dependent on sweep angle.

#### 4.3.3.2.4 Some observations on the stability of three-dimensional boundary layers

A striking aspect related with the stability of three-dimensional boundary layers has been put in evidence through a number of experiments using wall visualization techniques. Figure 22 shows an example of sublimation result obtained on a swept ONERA D airfoil (see /30/) revealing a closely spaced spark pattern nearly aligned with the external streamlines. These streaks indicate a periodical spanwise evolution of the skin friction coefficient. A detailed experimental study, as regards to these streaks, has been undertaken at ONERA/CERT /30/ showing an important evolution in the spanwise direction of the mean velocity profile (and also of the perturbation profiles) measured in the laminar boundary layer (Fig. 23).

The laminar stability theory, extended to three-dimensional boundary layers, allows to verify the existence of these streaks in showing that zero frequency, stationary waves, can be highly amplified in three-dimensional flows. The temporal amplification factor calculated for the station  $X = 0.4$  on the swept ONERA D airfoil is plotted in Fig. 24 as a function of the wave direction  $\epsilon$  for various frequencies /6/. It is clear that the zero frequency is notably amplified, which explains the streaks observed in experiments; in fact, these stability calculations provide us with results in good agreement with experimental values as regards either to the wave length or the amplitude of such a phenomenon /30/.

Figure 22 shows that traveling waves can also be highly amplified: there is a large range of unstable frequencies, the most unstable of which corresponds to 400 Hz (and not to 0 Hz). However, this large range of unstable frequencies is not confirmed by experimental results obtained recently at ONERA/CERT, indicating that only one frequency is amplified in fact; this unstable frequency is most often much lower than for a two-dimensional boundary layer.

A few authors have tried to extend the  $e^n$  method to predict the transition in three-dimensional boundary layers. The extension is not straightforward because the number of parameters determining the most amplified wave increases. Comparisons with experiments have been at first somewhat disappointing, experimental transitions occurring at various values of  $n_T$ , often much higher than for two-dimensional boundary layers (Figs. 25 and 26). However, it could be shown by MALIK and POLL /31/ that strong damping effects can be produced by the streamlines curvature; values of  $n_T$  comparing fairly well with two-dimensional values can be obtained when the curvature terms are introduced in the stability equations.

#### 4.3.4 TURBULENT BOUNDARY LAYER DEVELOPMENT

##### 4.3.4.1 Prediction of turbulent boundary layers

There are a number of calculation methods for predicting the development of "classic" turbulent boundary layers, that is to say without specific additional effects, as external turbulence, wall curvature, or wall temperature, which will be considered later on (for general review and discussion, see for example the conference held at Stanford University in 1968 /32/ and 1980-81 /33/).

Field methods are based on the solution of the local boundary layer equations, using a turbulence model for expressing the turbulent shear stress (mixing length model, transport equations for  $k$ ,  $\epsilon$ ;  $k$ ,  $\epsilon$ ,  $u'v'$ ; and  $k$ ,  $\epsilon$ ,  $u'v'$ ,  $w'v'$  in three-dimensional boundary layers).

The mixing length model often provides us with satisfactory results, but the magnitude of the mixing length  $\ell$  has to be adjusted in some configuration which is the case in strong positive pressure gradients leading to separation.

A two-equation model ( $k$ ,  $\epsilon$ ) represents a very good tool, satisfactory in most cases. In three-dimensional boundary layers, a fundamental question concerns the direction of the turbulent shear stress vector; though it is a classic hypothesis as regards to calculations, a few experiments point out in fact that this direction could be different to the one of the velocity gradient vector. However, one has to say that this problem is not really crucial concerning practical results to which numerical methods lead.

Integral methods /34/ are based on the solutions of the boundary layer integral equations, i.e. the X and Z global momentum equations. They use moreover an auxiliary integral equation (entrainment equation or global kinetic energy equation). The closure relationships are based on representations of the velocity profiles and wall skin friction law which can be based either on empirical results (wall and wakes profiles) or on similarity solutions (equilibrium boundary layers) using, for example, a mixing length model.

In recent developments (Stanford Conference /33/), these closure relationships have been thoroughly analyzed and improved in such a way that integral methods give good results and allow the prediction of turbulent boundary layer with good confidence, even in strong pressure gradients, up to separation.

In incompressible flows, similarity solutions have also been established for turbulent boundary layers, allowing to show the influence of pressure gradients upon the characteristic parameters of the boundary layer. These solutions give the velocity defect profiles of the equilibrium boundary layers by using, for instance, a mixing length model for solving boundary layer equations /35/. The shape factor and the skin friction coefficient are then given by the following formula:

$$H = \frac{1}{1 - G \sqrt{\frac{C_f}{2}}} \sqrt{\frac{2}{C_f}} = \frac{1}{0.41} \ln R\delta^* + D^*$$

where  $G$  and  $D^*$  depend on the shape of the defect velocity profile and are functions of the similarity parameter of the equilibrium boundary layers:

$$\beta^* = \frac{\delta_1}{\epsilon_w} \frac{dp}{dx} \quad \text{or} \quad \frac{\delta_1}{U_e} \frac{dU_e}{dx} \frac{1}{C_f/2}$$

So, skin friction coefficient and shape factor can be represented as a function of the pressure gradient parameter,  $\delta_1/U_e \, dU_e/dx$ , and the Reynolds number  $R\delta_1$ , based on the displacement thickness (Fig. 27).

#### 4.3.4.2 Compressibility effects

##### 4.3.4.2.1 Skin friction coefficient (adiabatic wall)

Several methods, directed or controlled through numerous and well established experimental results, allow to determine correctly the effect of the Mach number on the turbulent skin friction of a boundary layer development on a flat plate, at least in the case of an adiabatic wall. Thus, Fig. 28 taken from Bushnell /33/ provides us with the ratio of the skin friction coefficient at a given Mach number to its value in incompressible flow, for the same value of the abscissa Reynolds number. One can notice that the different methods predict rather well the experimental results; indeed, they show that the skin friction coefficient decreases when the Mach number increases. The effect is not very much dependent to the Reynolds number. It is rather weak for the transonic velocities range which interests us.

##### 4.3.4.2.2 Velocity and temperature profiles

Using a technique which has been widely developed for the laminar case, several variable changes have been proposed; the aim was to collect the velocity profiles of turbulent boundary layers (logarithmic law of the wall and velocity defect profile) on the incompressible curves. The main difficulty consists in the hypothesis on the turbulent shear stress which has to be done; a mixing length scheme has been used; empirical transformations have also been proposed.

As regard to the problem at hand, it does not appear that the shape of the boundary layer velocity profile is very much affected by the compressibility effect. A collection of the experimental velocity profiles obtained until a Mach number equal to 5 has been possible /36/, for the flat plate boundary layer as well as for the velocity profiles close to the separation point (Fig. 29).

A classical result, for the temperature field within the boundary layer in a zero pressure gradient case is that the total temperature is a linear or quasi-linear function of the velocity. This leads to the Crocco relation for the static temperature or to the modified Crocco relation:

$$T = T_w + (T_{ad} - T_w) \frac{U}{U_e} - (T_{ad} - T_e) \frac{u^2}{U_e^2}$$

Combining this relation with a power law for the velocity profile produces the ratio of characteristic thicknesses of the boundary layer, more particularly the parameter  $H = \delta_1/\theta$ , through the use of the formula given in the following section.

It is important to point out that the temperature distribution within the boundary layer is deeply affected when going from zero to non-zero pressure gradient cases.

An example of results obtained through similar solutions of turbulent boundary layers with pressure gradient in compressible flows /37/ is given on Fig. 30. One can observe that the total temperature is not anymore a linear function of the velocity as soon as velocity profiles and shape parameters, corresponding to negative pressure gradient cases as well as positive ones, are considered.

#### 4.3.4.2.3 Wall temperature

Though less critical than for transition, the effect of wall temperature on the turbulent boundary layer can be a problem for tests in blowdown or in cryogenic wind tunnels, because of possible differences between model temperature and equilibrium temperature.

The effect of the wall temperature on the wall skin friction is still uncertain; different results are obtained for example when applying either a reference temperature concept or a mixing length treatment, or when considering some experimental data. However, the effect on the shape parameter is more precise; a formula for flat plate boundary layers is for example:

$$H = 1.4 + 0.4 M_e^2 + 1.22 \frac{T_w - T_{ad}}{T_e}$$

Neglecting the effect of wall temperature on the skin friction, a formula for the displacement thickness leads, for example, to the power law:

$$\frac{\delta_1}{x} = \frac{0.0221 f H}{R_x^{1/6}}$$

where  $f$  is a compressibility function, depending only on the Mach number.

Let us consider now the displacement thickness obtained in nonequilibrium conditions at a given Reynolds number  $R_x$ ; the same displacement thickness would be obtained in equilibrium condition at an "effective Reynolds number"  $R_{x_0}$ :

$$\frac{R_{x_0}}{R_x} = \left( \frac{H}{H_0} \right)^6 = \left( \frac{1.4 + 0.4 M_e^2 + 1.22 \frac{T_w - T_{ad}}{T_e}}{1.4 + 0.4 M_e^2} \right)^6$$

A calculation at  $M_e = 1$  gives the following results:

$T_w/T_{ad}$	0.90	0.95	1	1.05	1.10
$R_{x_0}/R_x$	0.52	0.73	1	1.35	1.80

This concept of effective Reynolds number confirms the severe conditions which should be fulfilled for thermal equilibrium of the models.

#### 4.3.4.3 Specific influences and parameters

##### 4.3.4.3.1 Wall curvature

The longitudinal curvature of the wall (or of the boundary layer streamlines) is an important parameter, which may have a significant influence on the boundary layer development. From fundamental studies of turbulent boundary layers upon concave and convex walls /38/, it has been shown that the turbulence structure is thoroughly modified by curvature (Fig. 31). Concave walls give rise to a dramatic increase of turbulence in the boundary layer, leading rapidly to a complex pattern of Gortler vortices. On the other hand, boundary layers on convex walls contain a much lower level of turbulence than without curvature; this effect could be handled in prediction methods. By analogy with gravity effects, a parameter  $R_j$ , equivalent to a Richardson number, is used for taking into account the curvature in turbulence modeling:

$$R_i = \frac{u/R}{\partial u / \partial y}$$

Essentially, the turbulence length scale is modified by using some function of this Richardson number. For example, with a mixing length scale, the turbulent shear stress expression becomes:

$$u'v' = l^2 \left( \frac{\partial u}{\partial y} \right)^2 F(R_i)$$

where

$F = 1$  for zero curvature ( $R_i = 0$ )

$F > 1$  for concave streamlines

$F < 1$  for convex streamlines

The convex curvature gives rise to a very important decrease in the turbulent shear stress, which is virtually zero in a large part of the external boundary layer.

Field methods and integral methods have been adapted for taking into account the effect of curvature in the development of turbulent boundary layers, especially on convex walls /39/. The main effect is concerned with the entrainment of external fluid by the boundary layer. Various applications and comparisons with experiments have been performed (Fig. 32). It has been shown in particular that taking into account the curvature can improve considerably the prediction of separation when it appears in the curved rear part of wing profiles (Fig. 33).

Contrarily to longitudinal curvature, the transverse curvature does not seem to modify the boundary layer turbulence structure. It acts essentially by the fact that terms which were neglected in the boundary layer approximation, have to be reintroduced in the equations to take into account  $S/R$ . In fact, the effect is not very sensitive for a turbulent boundary layer and can be neglected up to  $\delta/R$  of the order of unity.

#### 4.3.4.3.2 External turbulence

The external turbulence is also a parameter which acts on the turbulence structure and on the boundary layer development. This effect has been studied especially for internal flows in turbomachines, i.e. at high levels of turbulence.

The external turbulence is taken into account in transport equations models, simply as a limiting condition on which depends the distribution of turbulence in the boundary layer. In fact, this entrainment of turbulent external fluid by the boundary layer acts as an augmentation of the turbulence length scale.

Field methods and integral methods have been also adapted for external turbulence /40/. Applications show that there are two main practical effects:

- moderate increase in the wall skin friction,
- modification of the velocity profile: lower value of the shape parameter.

The second effect may be the most important, since it can delay the boundary layer separation, even at somewhat low turbulence levels of wind tunnels (Fig. 34). Detailed results on the effect of external turbulence are given in Section 4.8 on Environmental Effects.

#### 4.3.4.3.4 Wall roughness

It is well known that wall roughness acts on a turbulent boundary layer by giving a shift of the logarithmic law of the wall /41/:



$$\left(\frac{\Delta u}{u}\right) = \frac{1}{k} \log\left(\frac{u_{\tau} h}{\nu}\right) - 3.25$$

The skin friction coefficient increase, due to roughness, is then given by:

$$\sqrt{\frac{2}{Cf_a}} - \sqrt{\frac{2}{Cf}} = \left(\frac{\Delta u}{u}\right)$$

Applications of these formula are shown on Fig. 35: the skin friction coefficient remains equal to a smooth wall coefficient up to a critical height, above which it increases rapidly. The ratio  $h/\delta$  decreases rapidly when the Reynolds number increases. The tolerable roughness height becomes very small, which creates a severe problem for surface finish of models of moderate size tested at high values of the Reynolds number. (The sudden influence of roughness on skin friction, hence drag, has the appearance of a Reynolds number effect).

#### 4.3.4.3.5 Sidewall effects in two-dimensional tests - A warning

The boundary layers developing on the sidewalls in the presence of a two-dimensional model give a convergence effect observed mainly in the regions of strong positive pressure gradients, notably through and after the shock wave in transonic testing. This convergence effect influences the boundary layer development because the momentum balance is no more a two-dimensional boundary layer balance. Momentum thickness and shape parameters can grow more rapidly than predicted by a two-dimensional calculation method. That is a difficult problem which has, for a long time, hindered the verification of prediction methods for turbulent boundary layers going to separation.

#### 4.3.5 CONCLUSIONS - FUTURE RESEARCH REQUIREMENTS

Considering at first turbulent boundary layers, one can reasonably say that numerical codes are available; by this time, they allow to predict, at least for incompressible flows, the development of the whole turbulent boundary layer up to separation. Singularity problems appear of course in the vicinity of the separation, but it is quite easy to get rid of them by considering the inverse mode calculation.

We have not dealt with nonequilibrium boundary layers since this has been done by A.G.T. Cross in Section 4.4. However, questions still have to be answered either as regards to relaxation or when the boundary layer is subject to a quick evolution of the external flow data. An important case concerns the relaxation of the boundary layer downstream of the shock wave and of the separation which might occur; the present turbulence modeling is very arguable. It should probably be very interesting to try to take into account the effects of the streamlines curvature (or more simply of the displacement thickness).

The turbulence modeling in compressible flows must also lead to future research; it would be very useful to obtain more numerous and systematic experimental and fundamental data on the structure of turbulence and more precisely on its thermal aspect. From a practical point of view, the influence of the wall temperature on the turbulent skin friction in the case of a non-adiabatic wall has to be cleared up; for this, experimental results could be obtained through cryogenic wind tunnels. Generally speaking, it would be very fruitful to perform some fundamental research in these tunnels on, for instance, turbulent boundary layers and turbulent skin friction for high values of the Reynolds number.

In three-dimensional flows, the calculation codes provide rather good results as regards to classic boundary layers; but the turbulence modeling is still questionable as regards to the external turbulent zone as well as the viscous sublayer. In paragraph 4.3.4.1, the problem of the direction of the turbulent shear stress has been set up; some efforts have to be accomplished with the three-dimensional turbulence modeling in order to answer, in particular, the question.

In this section, the problem of complex turbulent flows have not been considered such as, for instance, mixing of shear flows (interaction boundary layers-wakes, corner flows, etc.). Let us say that the turbulence modeling plays, of course, an important role; only numerical codes involving transport equations have real chances of success for such problems.

The boundary layer transition imposes a lot of very important questions; future research is required in an experimental as well as theoretical direction. The needs of experimental results are especially critical for the transition in three-dimensional flows; the existing transition criteria have been established from few experimental data and have to be controlled through experiments where the influence of the essential parameters has to be systematically checked. So far, the knowledge of the influence of turbulence and noise on three-dimensional transition is completely insufficient; the same remark can be made in regards to the effects of roughness. Concerning three-dimensional boundary layers, the distinction between the two types of instability is crucial as regards to analysis and prediction of the transition; let us recall that transition can be attributable either to streamwise instability or crossflow instability. However, one has to consider the coupling between these two types of instability; on swept wings, this coupling arises within an intermediate region between strong negative pressure gradients and positive pressure gradients.

For transonic and supersonic flows, one needs coherent and systematic experimental results on transition. The only available data concern uniform flows (cone and flat plate cases); experimental data given on wings for different pressure gradients would be very useful. The main difficulty is that the transition results might be significantly influenced by the aerodynamic noise. Flight tests have to be considered in a way to control the possibility of applications of the existing transition criteria; then, one would have to deal with an environment defined more precisely than with only the external turbulence level  $Tu$ .

The important effect of the wall temperature on the transition has also to be pointed out; this influence has been observed for zero-pressure gradient cases through experiments as well as theoretical results obtained by using the laminar stability theory. In fact, the influence of the wall temperature depends a lot on the pressure gradient; once again, cryogenic wind tunnels could provide us with precious experimental information.

At last, concerning the laminar stability theory and its applications for the transition prediction, one will note that the amplification method is, all things considered, the most promising one for our domains of interest. In spite of the great number of experimental features which are not taken into account through the  $e^n$  method, this technique gives fairly good results, provided the effective parameters are properly introduced into the stability models: oblique waves amplification in two-dimensional compressible flows, curvature effects in three-dimensional flows.

However, these results have to be confirmed with applications and experiments which would be more numerous and more systematic than the ones we have performed so far.

#### 4.3.6 REFERENCES

- /1/ Cebeci, T., and Bradshaw, P. "Physical and Computational Aspects of Convective Heat Transfer," Springer Verlag (1984).

- /2/ Cousteix, J. "Three-Dimensional Boundary Layers - Introduction to Calculation Methods," AGARD FDP VKI Special Course on Computation of Three-Dimensional Boundary Layers (1986).
- /3/ Falkner, W. M. and Skan, S. W. "Some Approximate Solutions of the Boundary Layer Equations," ARC - R&M 1314 (1930).
- /4/ Hartree, D. R. "On an Equation Occurring in Falkner and Skan's Approximate Treatment of the Equations of the Boundary Layer," Cambridge Phil Soc. (1937).
- /5/ "Special Course on Stability and Transition of Laminar Flow," AGARD Paper No. 709 (1984):  
 Arnal, D.: Transition in Two-Dimensional Incompressible Flow  
 Herbert, T.: Non-linear Effects and Secondary Instability  
 Mack, L. M.: Linear Stability Theory  
 Poll, D.I.A.: Transition in Three-Dimensional Flows  
 Reshotko, E.: Environment and Receptivity; Laminar Flow Control - Viscous Simulation
- /6/ Arnal, D. "Three-Dimensional Boundary Layers: Laminar-Turbulent Transition," AGARD FDP VKI Special Course on Computation of Three-Dimensional Boundary Layers (1986).
- /7/ Schubauer, G. B. and Skramstad, H. K. "Laminar Boundary Layer Oscillations and Transition on a Flat Plate," Report NACA 909 (1948).
- /8/ Wells, C. S. "Effects of Free Stream Turbulence on Boundary Layer Transition," AIAA Journal, Vol. 4, No. 1 (1967).
- /9/ Spangler, J. G. and Wells, C. S. "Effect of Free-Stream Turbulence on Boundary Layer Transition," AIAA Journal, Vol. 6, No. 3 (1968).
- /10/ Michel, R. "Determination du point de transition et calcul de la traînée des profils d'aile en incompressible," ONERA Publication No. 58 (1952).
- /11/ Crabtree, L. F. "Prediction of Transition in the Boundary Layer of an Aerofoil," Journal of the Royal Aeronautical Society (1958).
- /12/ Dunham, J. "Predictions of Boundary Layer Transition on Turbomachinery Blades," AGARD Meeting, Boundary Layers in Turbomachines, Paris (1972).
- /13/ Van Driest, E. R. and Blumer, C. B. "Boundary Layer Transition: Free Stream Turbulence and Pressure Gradient Effects," AIAA Journal, Vol. 1, No. 6 (1963).
- /14/ Granville, P. S. "The Calculation of the Viscous Drag of Bodies of Revolution," David Taylor Model Basin, Report 849 (1953).
- /15/ Smith, A.M.O. and Gamberoni, N. "Transition, Pressure Gradient and Stability Theory," Douglas Aircraft Company, Report ES 26 388 (1956).
- /16/ Van Ingen, J. L. "Transition, Pressure Gradient, Suction, Separation and Stability Theory," AGARD CP 224 (1957).
- /17/ Mack, L. M. "Transition and Laminar Instability," Jet Propulsion Lab. Publication 77-15 (1977).
- /18/ Arnal, D., Habiballah, M. and Delcourt, V. "Synthese sur les methodes de calcul de la transition," Rapport Technique No. 11/5018 (1980).

- /19/ Feindt, E. G. "Untersuchungen über die Abhängigkeit des Umschlages laminar-turbulent von der Oberflächenrauigkeit und der Druckverteilungen," Jahrbuch 1956 der Schiffbautechnischen Gesellschaft 50 (1957).
- /20/ Oryden, H. L. "Transition from Laminar to Turbulent Flow," Turbulent Flows and Heat Transfer, High Speed Aerodynamics and Jet Propulsion, C. C. Lin Edition (1959).
- /21/ Oougherty, N. S. and Fisher, O. F. "Boundary Layer Transition on a 10 deg Cone - Wind Tunnel/Flight Data Correlation," AIAA Paper 80-0154 (1980).
- /22/ Arnal, D. and Jelliti, M. "Phenomenes de transition en ecoulement bidimensionnel compressible sur paroi athermane," Colloque sur les Ecoulements Transitoires Compressibles, Poitiers (1986).
- /23/ Gortler, H. "On the Three-Dimensional Instability of Laminar Boundary Layers on Concave Walls," NACA Tech. Memo. 1375, 1954.
- /24/ Ragab, S. A. and Nayfeh, A. H. "On Gortler Instability," Virginia Polytechnic Institute and State University, Blacksburg, VA 24061, 1979.
- /25/ Liepmann, H. W. "Investigations on Laminar Boundary Layer Stability and Transition on Curved Boundaries," NACA Wartime Report W-107, 1943.
- /26/ Liepmann, H. W. "Investigation of Boundary Layer Transition on Concave Walls," NACA Wartime Report W-87, 1945.
- /27/ Poll, D.I.A. "Some Aspects of the Flow Near a Swept Attachment Line with Particular Reference to Boundary Layer Transition," Cranfield Institute of Technology, Co. A. Report No. 7805 (1978).
- /28/ Beasley, J. A. "Calculation of the Laminar Boundary Layer and the Prediction of Transition on a Sheared Wing," ARC R&M 3787 (1973).
- /29/ Michel, R., Arnal, D., and Coustols, E. "Stability Calculations and Transition Criteria in Two- and Three-Dimensional Boundary Layers," 2nd Symp. IUTAM on Laminar-Turbulent Transition - Springer Verlag (1984).
- /30/ Michel, R., Arnal, D., Coustols, E. and Juillen, J. C. "Experimental and Theoretical Studies of Boundary Layer Transition on a Swept Infinite Wing," 2nd Symp. IUTAM on Laminar-Turbulent Transition - Springer Verlag (1984).
- /31/ Malik, M. R. and Poll, D.I.A. "Effect of Curvature on Three-Dimensional Boundary Layer Stability," AIAA Journal, Vol. 23 (1985).
- /32/ "Computation of Turbulent Boundary Layers," 1968 AFOSR-IFP-Stanford Conference.
- /33/ "Complex Turbulent Flows," 1980-81 AFOSR-HTM-Stanford Conference.
- /34/ Cousteix, J. "Integral Methods," AFOSR-HTM Stanford Conference (1981).
- /35/ Michel, R., Quemard, C., and Ourant, R. "Application d'un schema de longueur de melange a l'etude des couches limites turbulentes d'equilibre," N.T. ONERA No. 154 (1969).
- /36/ Michel, R. "Turbulent Boundary Layers at High Speeds," 10th Applied Mechanics Congress, ONERA Publication No. 102, 1960.

- /37/ Michel, R., Quemard, C., and Cousteix, J. "Similarity Solutions for Turbulent Boundary Layers with Pressure Gradients in Compressible Fluid," ONERA, La Recherche Aerospatiale No. 1971-6.
- /38/ So, R.M.C. and Mellor, G. L. "An Experimental Investigation of Turbulent Boundary Layers Along Curved Surfaces," NASA CR 1940 (1972).
- /39/ Cousteix, J. and Houdeville, R. "Methode integrale de calcul d'une couche limite turbulente sur une paroi courbee longitudinalement," ONERA La Rech. Aerosp. No. 1 (1977).
- /40/ Arnal, D. and Michel, R. "Effects of Free-Stream Turbulence on Turbulent Boundary Layers and on Boundary Layer Transition," Euromech 72: Boundary Layers and Turbulence in Internal Flows (1976).
- /41/ Clauser, F. H. "The Turbulent Boundary Layer," Adv. Appl. Mech. 4:1 (1956).

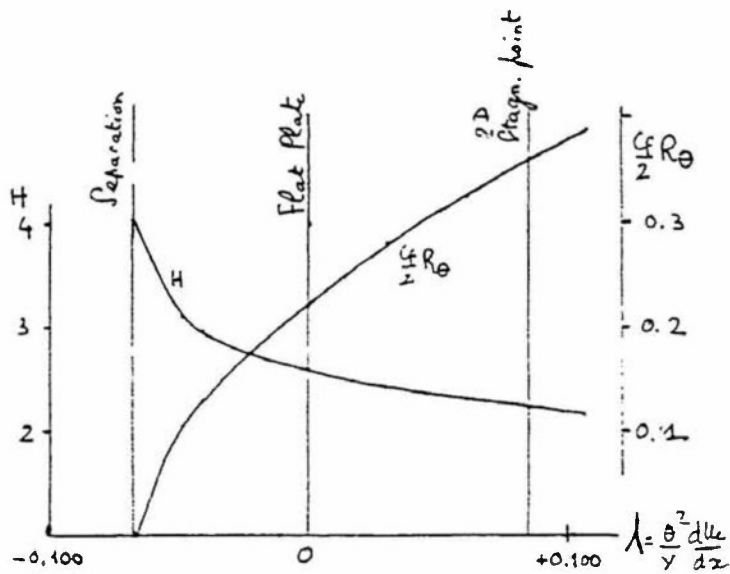


Figure 1. Skin friction coefficient and shape parameter for self similar laminar boundary layers in incompressible flow.

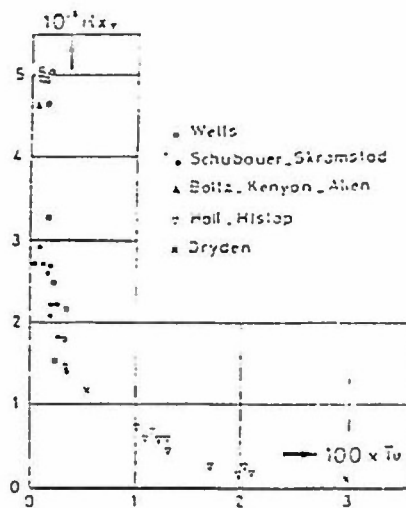


Figure 2. Effect of free-stream turbulence on transition Reynolds number / 5 / (flat plate in incompressible).

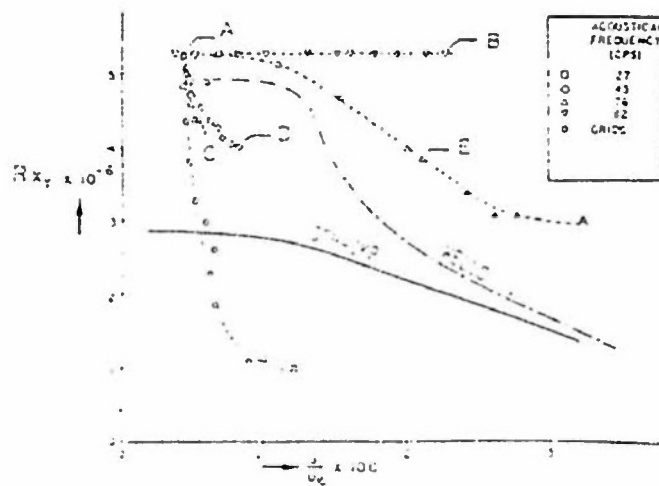


Figure 3. Effect of free-stream disturbances (sound and turbulence) on transition Reynolds number / 9 / (zero pressure gradient, in compressible).

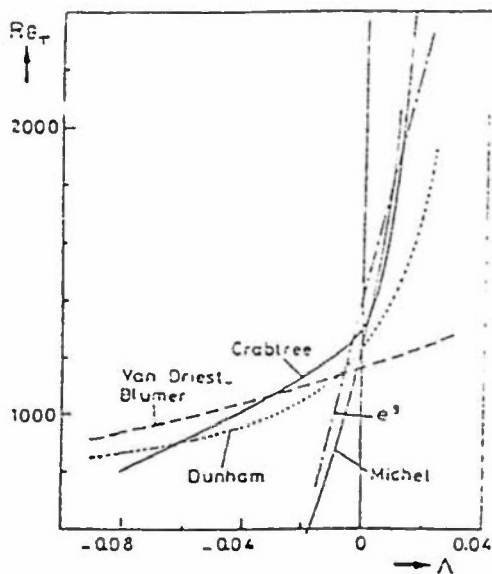


Figure 4. Comparison between some criteria at low values of  $Tu$ .

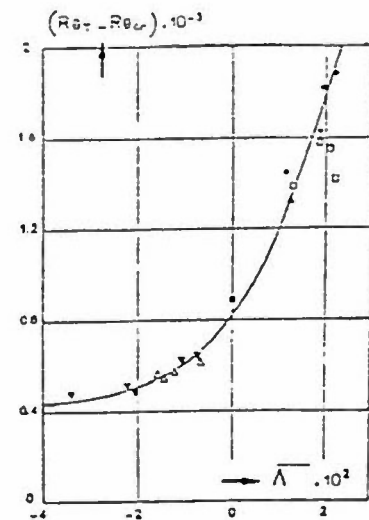


Figure 5. Criterion proposed by GRANVILLE / 14 /.



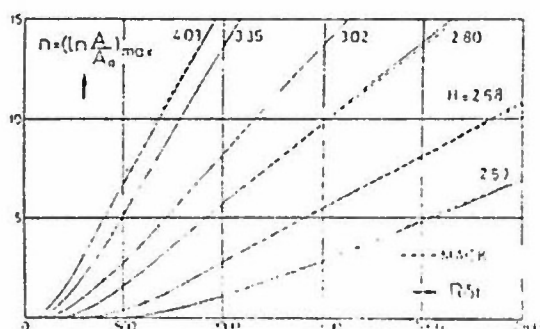


Figure 6. Evolution of  $\eta = (L\eta A / A_0)_{\max}$  for Falkner-Skan family profiles /5/.

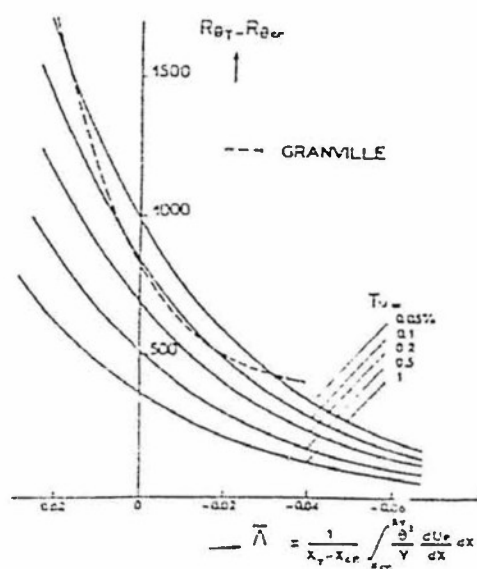


Figure 7. Criterion proposed by Arnal-Habiballah-Delcourt /1d/.

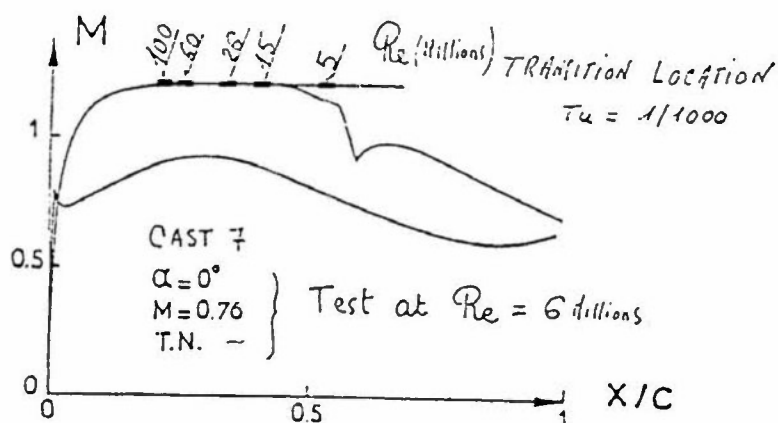
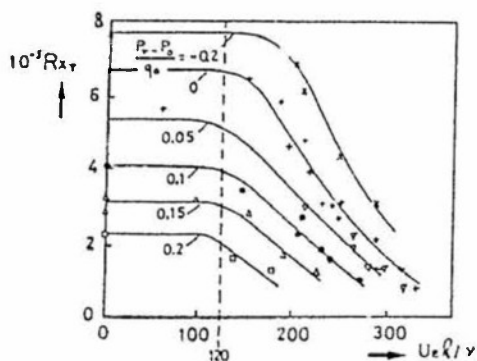
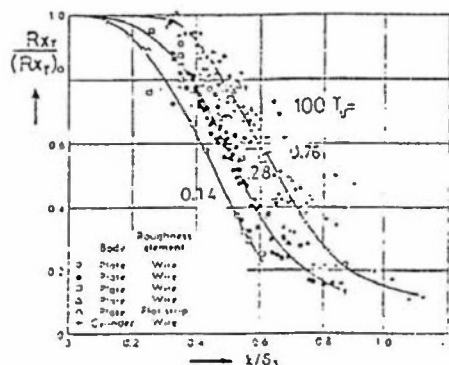


Figure 8. Application of streamrise transition criteria to a wing profile.



**Figure 9.** Influence of pressure gradient and distributed roughness on transition Reynolds number /15/.  
 $U_e$ ,  $P_0$  and  $q_0$  denote velocity, static pressure and dynamic pressure at the test section entrance.



**Figure 10. Ratio of transition Reynolds number with two-dimensional roughness element to that for smooth plate / 20%.**

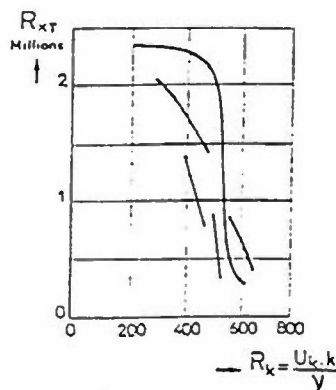


**Figure 11. Three-dimensional roughness elements / 20 /.**

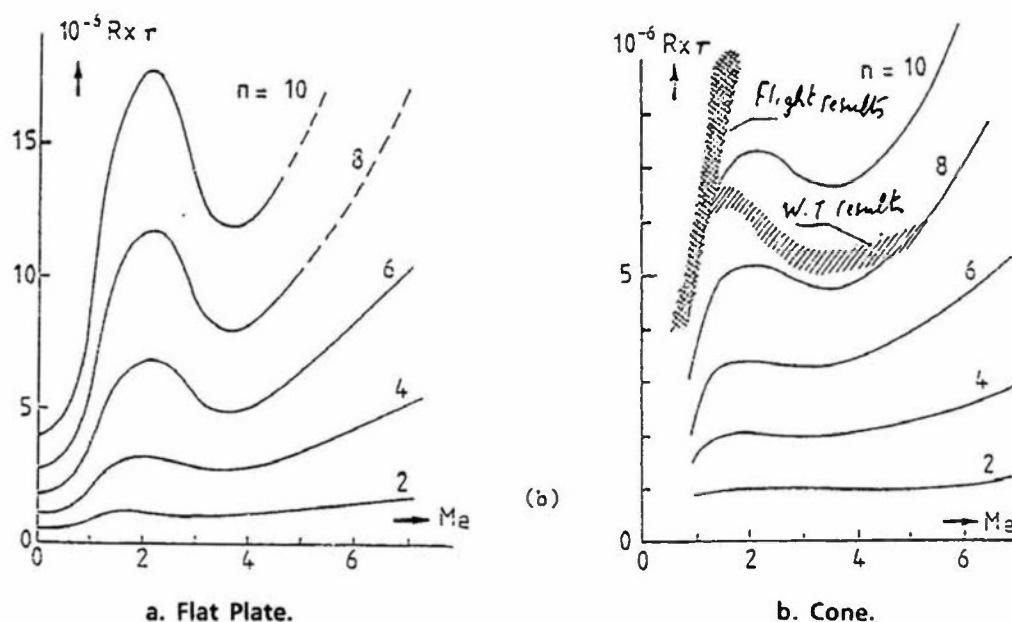


Figure 12. Application of a  $\lambda^n$  transition criteria in transonic and supersonic flows (adiabatic wall).

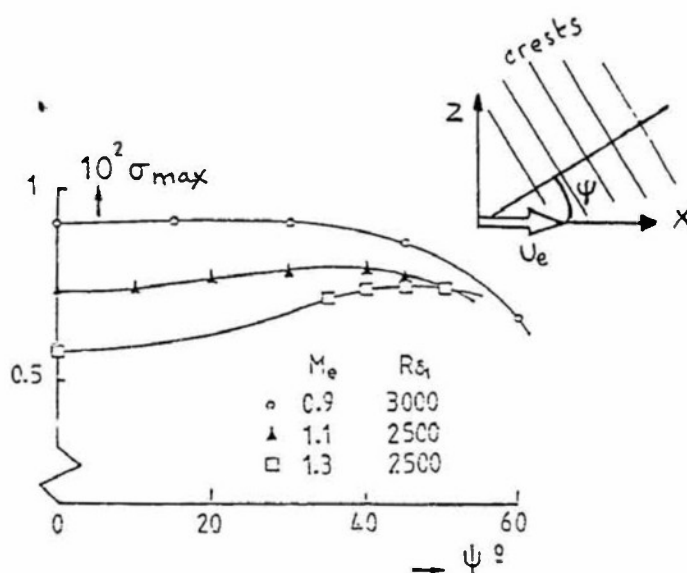
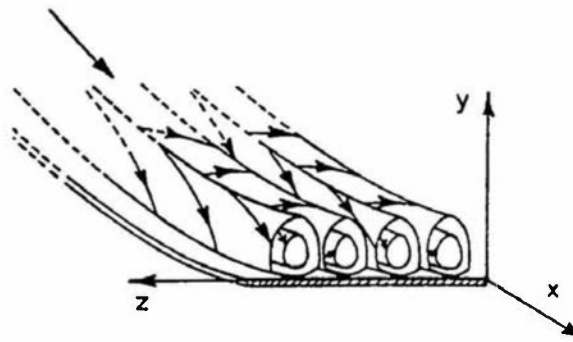


Figure 13. Amplification factor as function of wave direct on a transonic flow (flat plate, adiabatic wall) / 22 /.



GORTLER vortices in flow along a concave wall

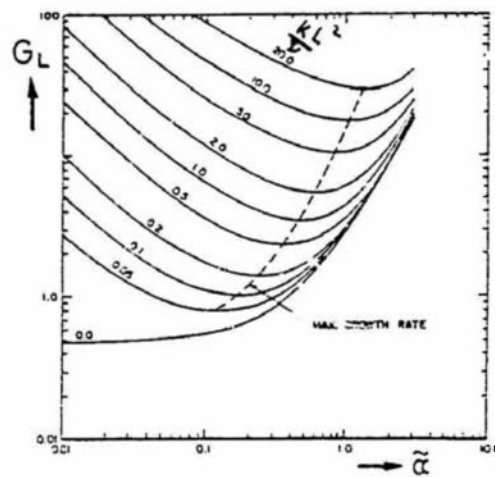


Figure 14. Curves of constant growth rate for the BLASIUS flow along a concave wall (from Arnal / 5 /).

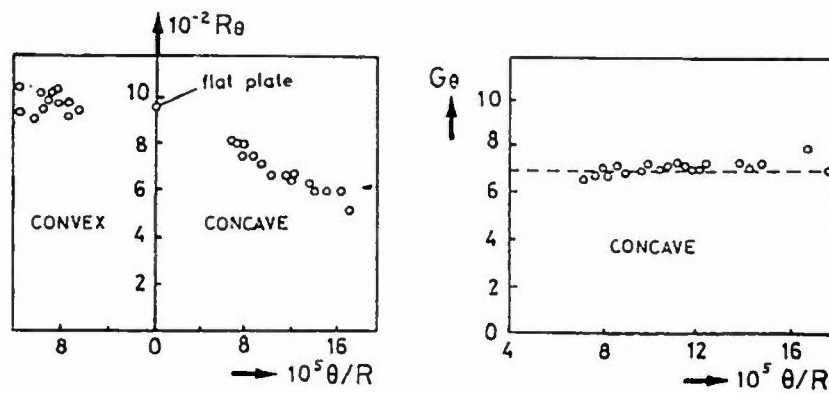


Figure 15. Effect of surface curvature on momentum-thickness Reynolds number and on GORTLER number at the transition location (from Arnal / 5 /).

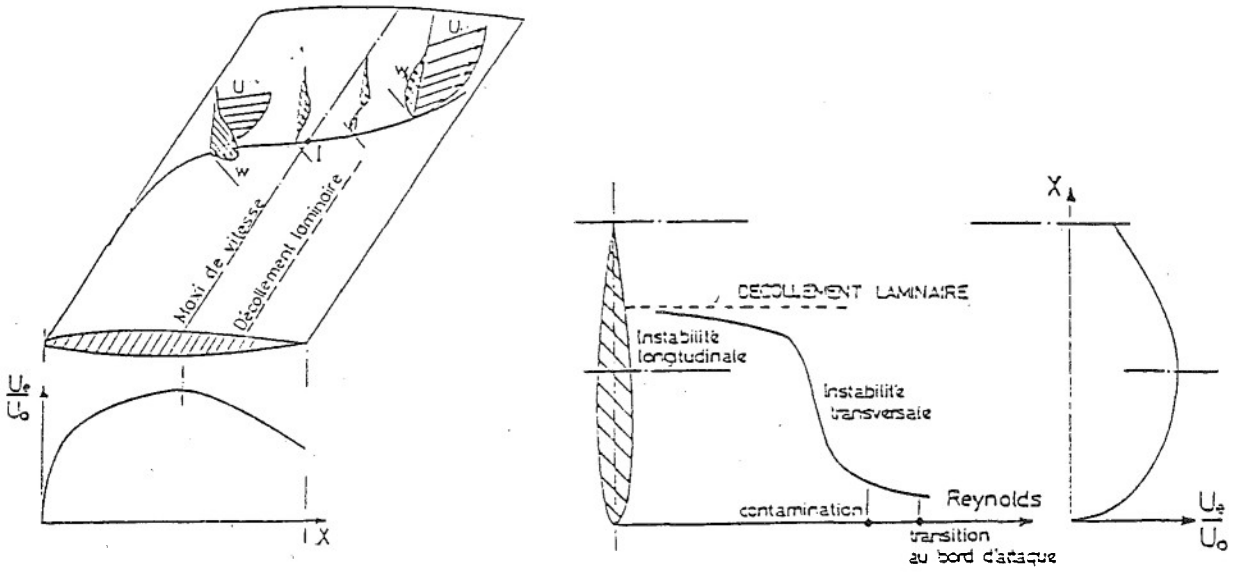


Figure 16. Possible origins of turbulence on a swept wing.

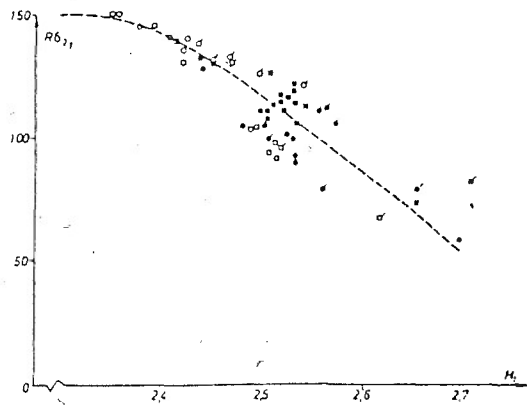


Figure 17. First cross-flow transition criterion  $R\delta_2(H) / 29\%$ .

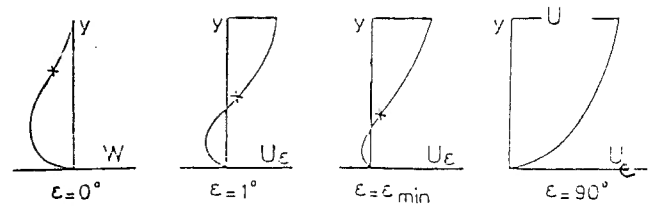


Figure 18. Profiles projected in different directions  $\varepsilon$ .

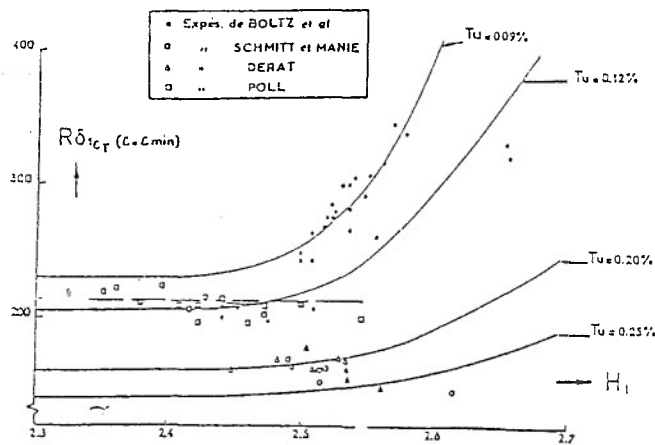


Figure 19. Second cross-flow transition criterion / 29%.

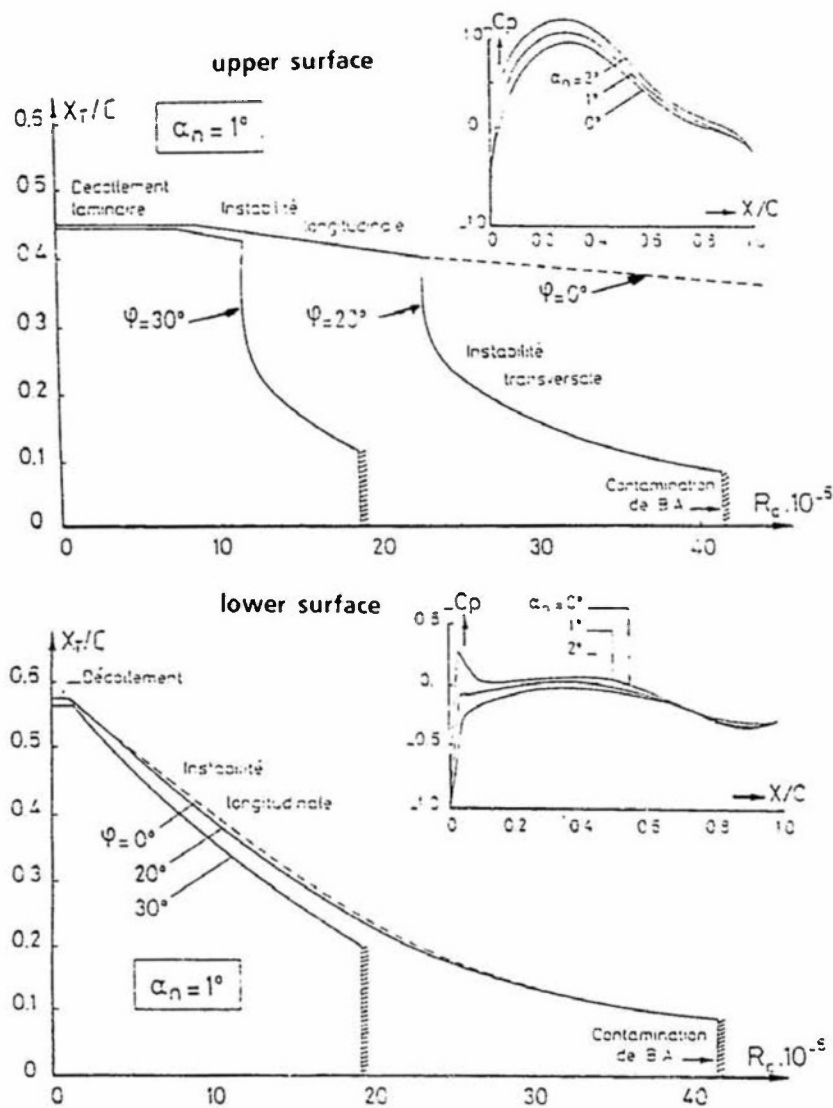


Figure 20. Application of transition criteria to an infinite swept wing (OA PO1 profile).

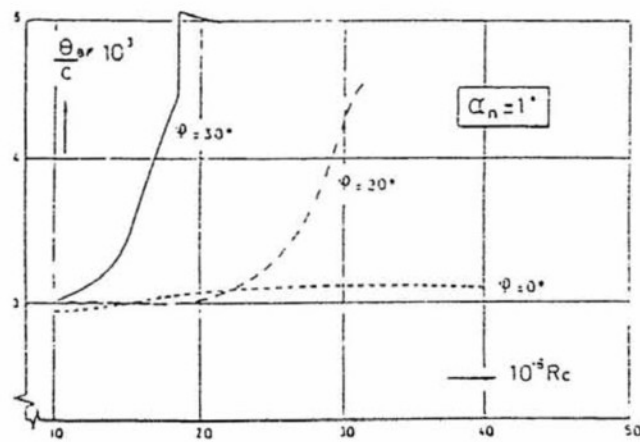
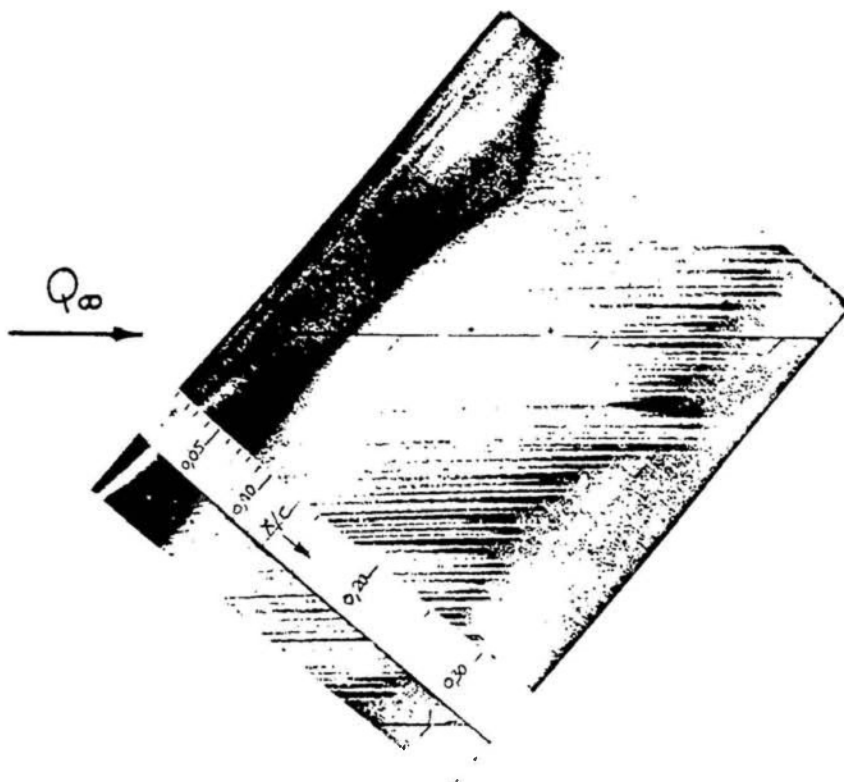
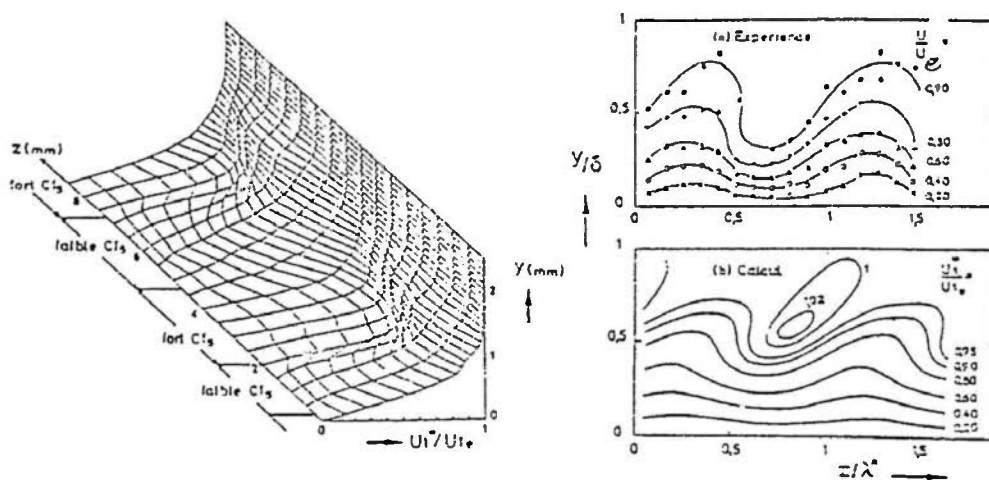


Figure 21. OA PO1 profile: total momentum thickness at trailing edge.



ONERA 0: Swept profile,  $\Psi = 60$  deg,  $\alpha_n = -8$  deg,  $q_\infty = 81$  m/s.

Figure 22. Streaks shown by wall flow visualization /26/.



ONERA 0: Swept profile,  $\Psi = 60$  deg,  $\alpha_n = -8$  deg,  $q_\infty = 48$  m/s,  $X = 0.69$ .

Figure 23. Spanwise evolution of mean velocity in the laminar boundary layer /30/.



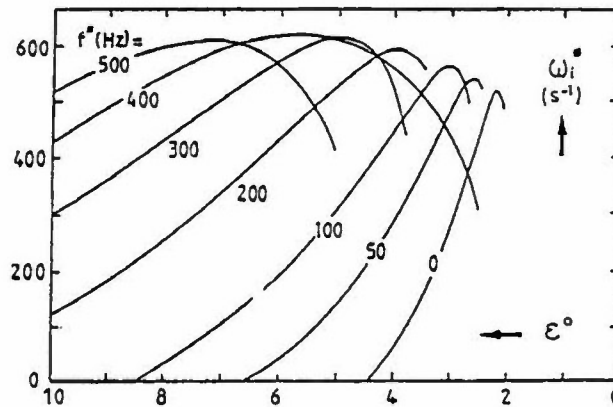


Figure 24. Temporal amplification rate of various frequencies at  $X/C = 0.40$  on ONERA O swept airfoil /6/.  $\Psi = 60$  deg,  $\alpha_n = -8$  deg,  $q_\infty = 48$  m/s.

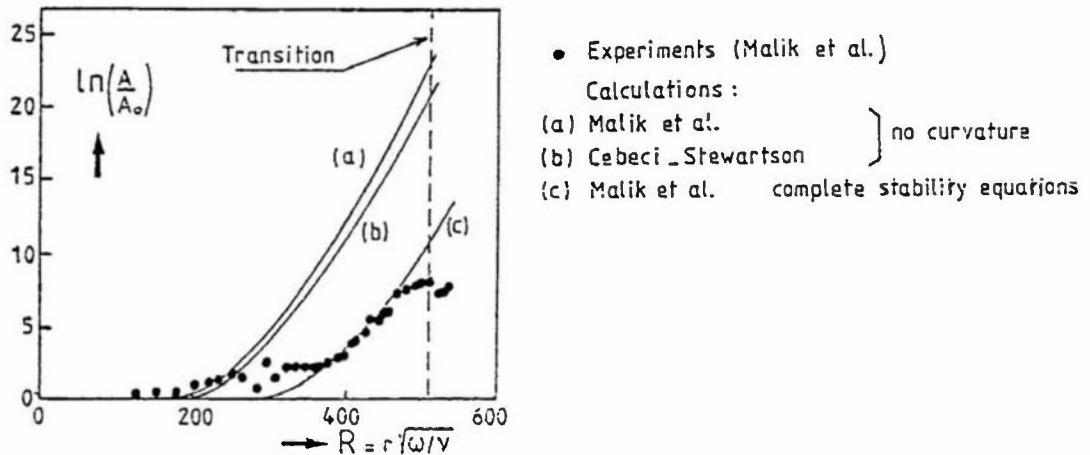


Figure 25. Total amplification rates for stationary waves on a rotating disk /6/.

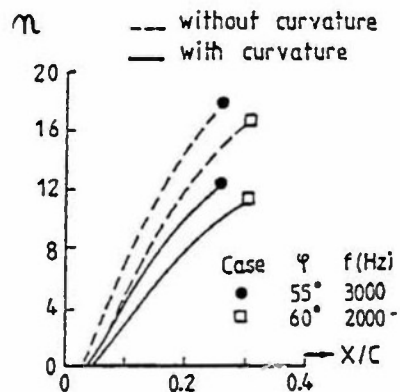


Figure 26. Total amplification rates computed by Malik and Poll /31/. Symbols denote experimental transition points. Poll's yawed cylinder /27/.

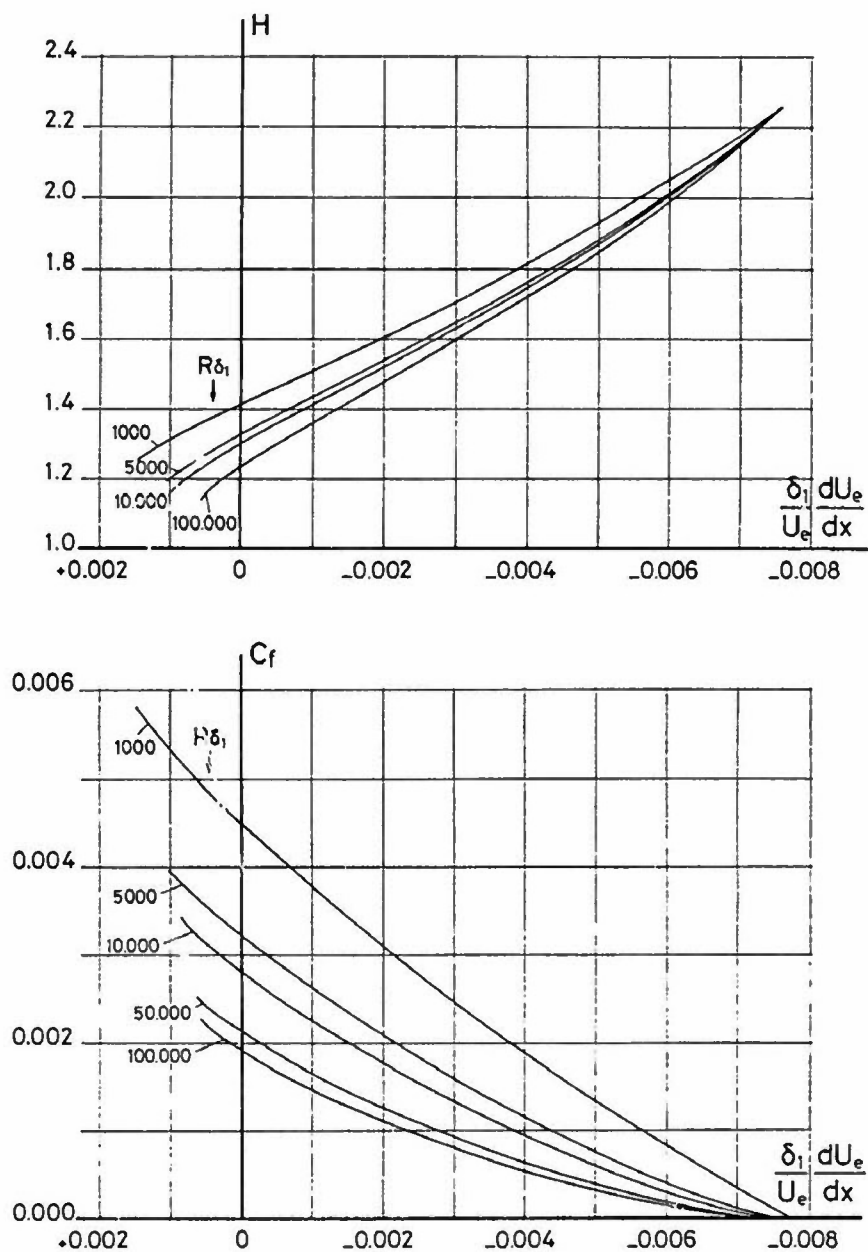


Figure 27. Shape parameter and skin-friction coefficient of turbulent equilibrium boundary layers (incompressible) (mixing length model / 35/.

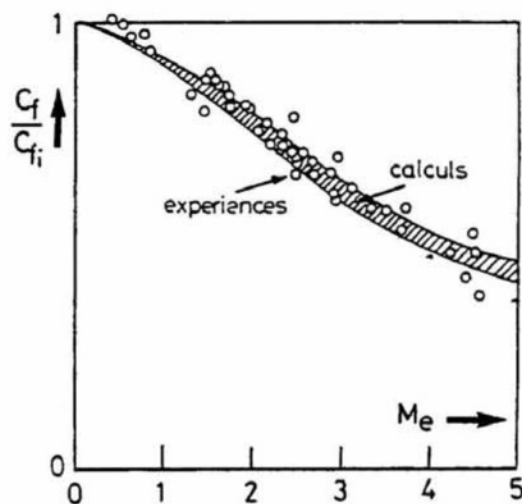


Figure 28. Effect of Mach numbers on flat-plate turbulent skin friction coefficient (adiabatic wall).

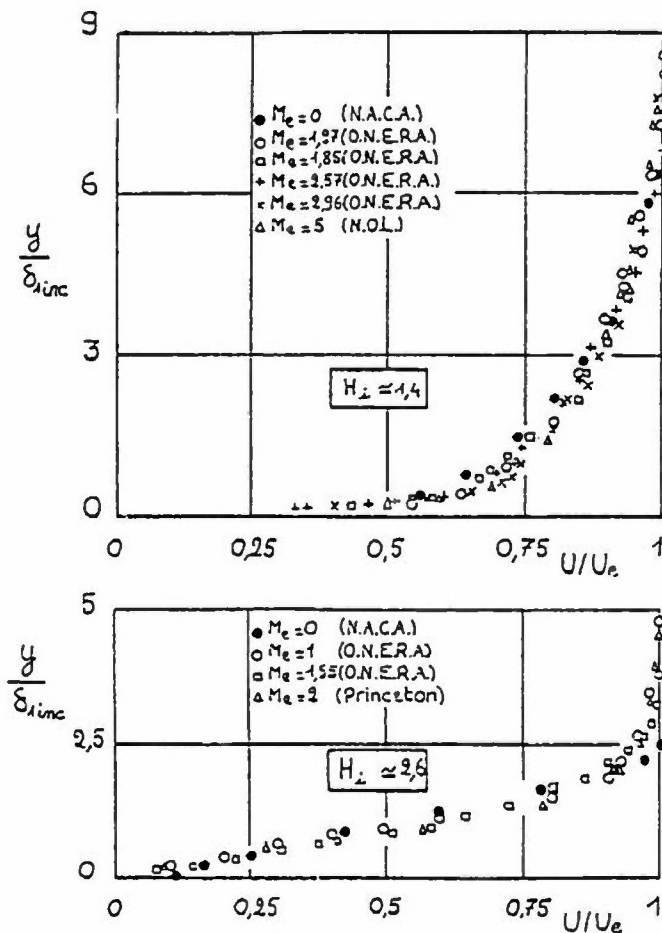


Figure 29. Compressibility effect on turbulent velocity profile / 36 /.

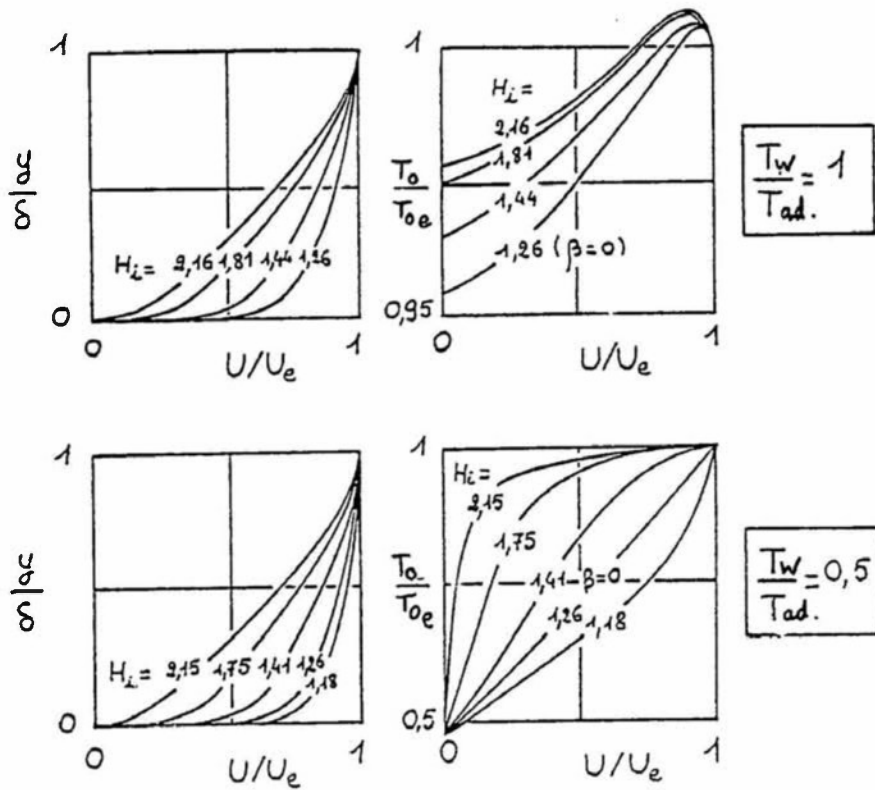


Figure 30. Velocity and total temperature profiles of turbulent boundary layers with pressure gradient / 37 /. ( $M_e = 2$ ,  $R_\delta = 5 \times 10^5$ )

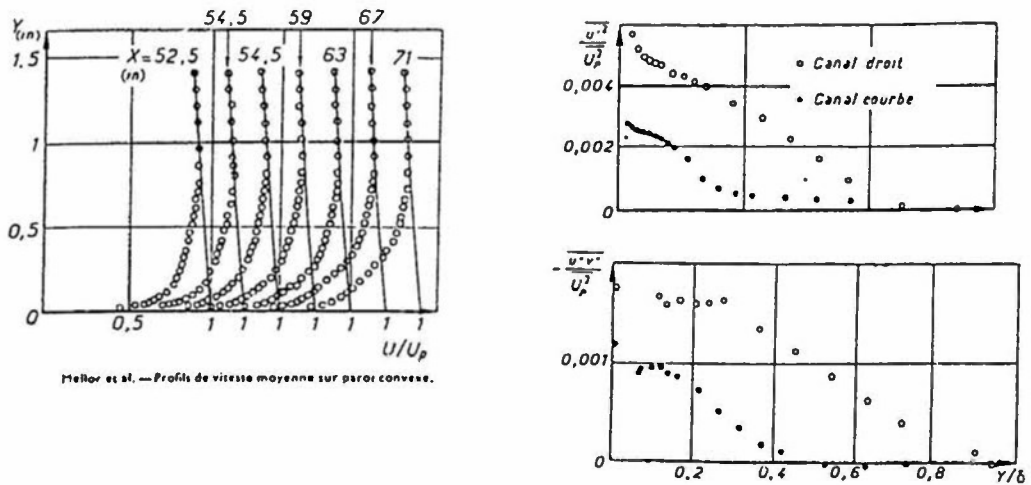


Figure 31. Effect of longitudinal curvature on mean velocity and turbulence profiles in a turbulent boundary layer. (So and Mellor experiments /38/).

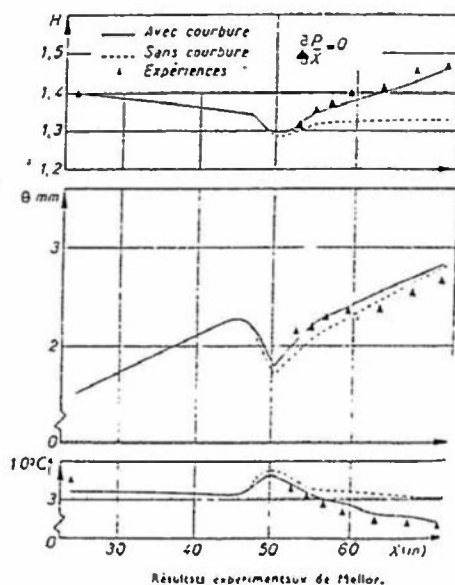


Figure 32. Comparison between experiments and calculation for the development of a turbulent boundary layer on curved walls /39/.

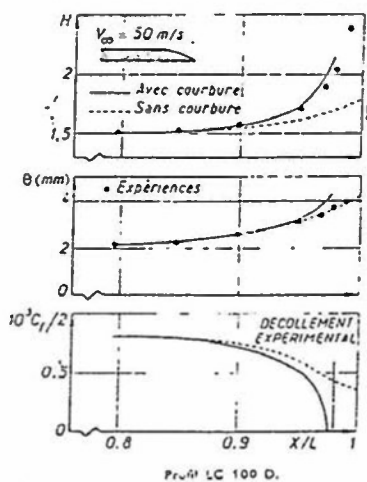


Figure 33. Comparison between experiments and calculation for the development of a turbulent boundary layer on curved walls /39/.

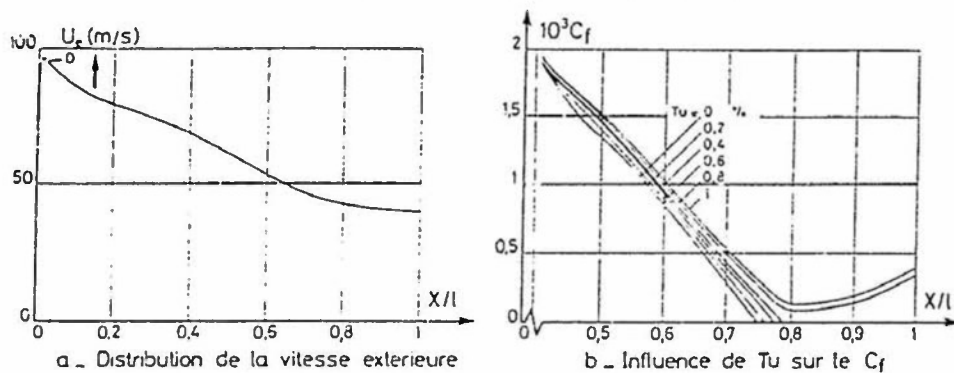


Figure 34. Effect of external turbulence on turbulent boundary layer separation /40/.

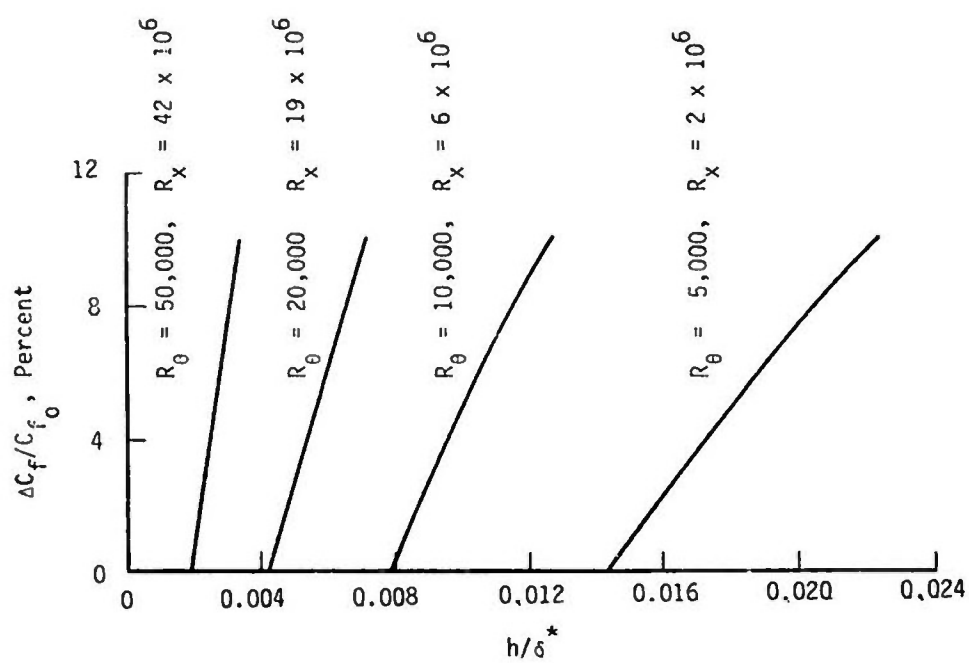


Figure 35. Increase of turbulent skin friction due to surface roughness (flat plate; incompressible flow)

## SECTION 4.4 DEVELOPMENT AND ANALYSIS OF TURBULENT NON-EQUILIBRIUM BOUNDARY LAYERS

by

A.G.T. Cross  
British Aerospace plc  
Military Aircraft Division  
Brough, N. Humberside, HU15 1EQ, UK

### 4.4.1 Introduction

The simulation of flow phenomena involving a boundary layer has already been identified, in Section 4.2, as potentially very sensitive to the upstream state of the incoming layer. The state of the layer in the sense of being laminar, transitional or turbulent is of prime importance and in this context has been dealt with in Section 4.2. However, as turbulent flow is usual at full scale it is a main objective of model tests and worthy of further comment.

For turbulent flow an important consideration is departure from equilibrium as, in these cases the similarity solutions so frequently used in calculations no longer apply. Including non-equilibrium effects in the velocity profile is particularly revealing and is essential for determining the important scale parameters and establishing separation criteria. In this section the turbulent boundary layer is considered specifically in terms of the law of the wall and wake velocity profile which can be used to examine the influence of second order effects including that of departure from equilibrium.

### 4.4.2 Attached Flow

The law of the wall is derived from Prandtl's mixing length hypothesis, the assumption of constant shear stress close to the wall and by matching the law of the wall to the laminar sub-layer. The wall flow is dominated by the wall shear stress with the skin friction coefficient becoming the primary independent variable. The matching of the wall flow with the laminar sub-layer after suitable length and velocity scales are specified results, as shown by Schlichting (Ref. 1), in the Reynolds number dependence of the law of the wall. The wake region away from the wall is dominated, as may be expected, by the external flow inertia rather than wall friction and Coles (Ref. 2) introduced a wake term with a weighting function related to the longitudinal of streamwise pressure gradient.

The law of the wall and wake can be written as,

$$\frac{U}{U_e} = \frac{q}{K} \left[ \ln(Rd q \frac{y}{d}) + A \right] + B \sin^X \left( \frac{\pi}{2} \cdot \frac{y}{d} \right) \quad (4.4.2.1)$$

With the Coles formulation  $X$  takes the value of 2 while the effect of pressure gradient is allowed for in the wake weighting function  $B$ . One of the prime disadvantages with the Coles formulation is that the velocity profile is not fully compatible at the outer edge of the boundary layer where it meets with the external inviscid flow. In order to include such a profile in an integral calculation method it is essential to match the outer edge boundary condition and this requires that,

$$U = U_e \quad \text{when} \quad y = d$$

which in turn requires Coles weighting function to revert to a simple scale factor with a value given by,

$$B = 1 - \frac{q}{K} \left[ \ln(Rd q) + A \right] \quad (4.4.2.2)$$

It is then necessary to reappraise the way pressure gradient is included and Coleman (Ref. 3) suggested making  $X$  a variable. In Reference 4 it was shown by Cross that the wake exponent  $X$  could be related to a departure from equilibrium flow conditions by consideration of the difference between the streamwise pressure gradient parameters of the actual flow and the equivalent equilibrium flow. Thus,

$$X = F(\Pi_r) \quad (4.4.2.3)$$

$$\Pi_r = \left[ \frac{\theta}{U_e} \cdot \frac{dU_e}{ds} \right] - \left[ \frac{\theta}{U_e} \cdot \frac{dU_e}{ds} \right]_{EO} \quad (4.4.2.4)$$

Many studies have been made of boundary layers developing under conditions of equilibrium or self preservation and it is found that they can be characterised by an equilibrium locus relating the shape parameter of the velocity-defect profile to a pressure gradient parameter. The equilibrium locus can be used here to define the equilibrium term of equation 4.4.2.4 and so complete the description of  $X$ . Good results have been obtained using the locus proposed by Green et al (Ref. 5), which after some rearrangement gives,



$$\left[ \frac{\theta}{Q_e} \cdot \frac{dQ_e}{ds} \right]_{EO} = \frac{1.25}{H} \left[ \frac{Cf}{2} - \left( \frac{H-1}{6.432H} \right)^2 \right] \quad (4.4.2.5)$$

Figure 1 is taken from Reference 4 and shows the correlation between optimum values of  $X$ , that is values giving the best fit to experimental data, and the relative pressure gradient parameter  $\Pi_r$ . It can be seen immediately from the figure that for equilibrium flow, that is  $\Pi_r = 0$ , the Coles value still applies and so the velocity profile remains applicable to the wealth of data collected for equilibrium layers for which the original law of the wall and wake is known to work well. However, for very strong pressure gradients, values of  $X$  very different from the Coles value are required and this can be interpreted as a distortion of the profile related to the departure from equilibrium.

In order to show the effect of this non-equilibrium distortion to the law of the wall and wake the experiment of East and Hoxey (Ref. 6) is considered. Figure 2 shows two theoretical velocity profiles compared with the experimental data; one profile for the Coles equilibrium value of  $X$  and one profile using the value determined from Figure 1. In both cases the measured skin friction coefficient and boundary layer thickness were used to construct the theoretical profiles for which the effect of non-equilibrium flow distortion is clearly evident.

When considering velocity profiles for turbulent flow it is informative to examine the nature of the shape parameter relation  $H1 - H$ . The shape parameter  $H1$  was introduced originally by Head (Ref. 7) for entrainment type integral boundary layer calculation while  $H$  is the more commonly known shape parameter. For the revised law of the wall and wake this shape parameter relation is a function of both Reynolds number and pressure gradient with the former effect due to the wall flow and the latter due to that of the wake.

Figure 3 shows the effect on the shape parameter relation of the law of the wall due to varying the Reynolds number at the equilibrium flow condition. The figure shows that the effects of Reynolds number are largely confined to low values of  $H$ . At the equilibrium flow condition separation, as defined by zero skin friction, occurs with  $H = 4$  and the figure shows the Reynolds number effect there to be negligible. This behaviour is due to the disappearance of the logarithmic wall region at separation which leaves only the wake region. The most important consequence of the Reynolds number effect can be seen at the low values of  $H$  where Reynolds number limits the minimum value of  $H$  attainable. This limit plays an important role in flow recovery due to a favourable pressure gradient and is amply demonstrated using the experiment of Chu and Young (Ref. 8). This experiment was for the flow over a flat plate with the suction peak type pressure distribution shown in Figure 4. Figure 5 compares the experimental values of  $H$  with two entrainment integral method predictions; one using the modified law of the wall and wake and one using an empirical shape parameter relation in place of a velocity profile. The limit to the minimum value of  $H$  is clearly seen in the experiment and the law of the wall and wake calculation agrees very well with this. However the calculation using the other method fails to predict this flow feature.

For non-equilibrium flow at constant Reynolds number Figure 6 shows that the distortion of the shape parameter relation due to pressure gradient effects occurs mainly at high values of  $H$ . This is due to the dominance of the wake at these conditions. The main point to notice is that second order pressure gradient effects, that is those in addition to the direct effect in the boundary layer momentum equation, are likely to be important at separation.

#### 4.4.3 Separated Flow

The law of the wall and wake can be applied to fully separated flow though its original development was for attached flow with perhaps incipient separation. This extension is achieved by allowing the friction velocity to have negative values and so model flow reversal close to the wall. The first requirement is to avoid problems with the logarithmic term when the friction velocity goes negative and this is often achieved by taking the modulus of this quantity. A more elegant alternative approach is to recognise that,

$$\text{Ln} q = \frac{1}{2} \text{Ln} (q^2) \quad (4.4.3.1)$$

and so we can put,

$$\frac{Q}{Q_e} = \frac{q}{R} \left[ \frac{1}{2} \text{Ln} (Rd q \frac{y}{d})^2 + A \right] + B \sin^X \left( \frac{\pi}{2} \cdot \frac{y}{d} \right) \quad (4.4.3.2)$$

Figures 7 and 8 show the effect on the shape parameter relation when using the law of the wall and wake for separated flow. The influence of Reynolds number as shown by Figure 7 is relatively small beyond separation in comparison to varying the relative pressure gradient parameter as revealed in Figure 8.

Theoretical results are compared in Figure 9 with the experimental data of Simpson et al (Ref. 9). The theoretical results are calculated for the appropriate experimental Reynolds numbers using, in one case the equilibrium value of  $X$  and in the other the

values of  $X$  determined from the experimental values of pressure gradient parameter. The effect of the relative pressure gradient parameter is clearly evident beyond separation and produces the right effect though the experiment suggests the effect ought to be stronger. Similar results are obtained for the experiment of Hastings and Williams (Ref. 10) and are shown in Figure 10. The results are considered in reasonable agreement with experiment and particularly encouraging considering the velocity profile was developed originally for attached flow.

One potential area for improvement of the velocity profile for separation would be in the equilibrium locus, equation 4.4.2.5, as this could well be expected to be different for attached and separated flow. However later, when three dimensional flow is considered it will become evident that for the positive values of  $\Pi_r$  appropriate to the fully developed separated flow of Figures 9 and 10 there is direct evidence, in the form of Figure 21, for modification of the  $X - \Pi_r$  relation. The evidence is for increased values of  $X$  beyond that given by Figure 1 and this is consistent with the requirement for improved accuracy in the Figures 9 and 10. Further and just as important, the new evidence is not inconsistent with the two dimensional data of Figure 1 as that was based entirely on near zero and negative values of  $\Pi_r$ .

#### 4.4.4 Compressibility

By consideration of the experimental data of Lobb, Winkler and Persh (Ref. 11) Spence (Ref. 12) showed that for Mach numbers up to 8 it was possible to represent the effects of compressibility by writing,

$$Q/Q_e = F(\bar{y}/\bar{d}) \quad (4.4.4.1)$$

$$\bar{y} = \int_0^y (\rho/\rho_e) dy \quad (4.4.4.2)$$

$$\bar{d} = \int_0^d (\rho/\rho_e) dy \quad (4.4.4.3)$$

where equation 4.4.4.1 can be considered an equivalent incompressible velocity profile based on a transformed normal to wall distance  $y$  and a transformed boundary layer thickness  $d$ . Any valid incompressible velocity profile can be substituted for equation 4.4.4.1 but by using the law of the wall and wake we obtain,

$$\frac{Q}{Q_e} = \frac{\bar{q}}{q} \left[ \frac{1}{2} \ln (R\bar{d} \bar{q} \bar{y}/\bar{d})^2 + A \right] + B \sin \left( \frac{\pi}{2} \bar{y}/\bar{d} \right) \quad (4.4.4.4)$$

It can be seen from equation 4.4.4.4 that we have also introduced an equivalent incompressible friction velocity  $q$ . This was introduced following the work of Winter and Gaudet (Ref. 13) who showed that friction velocity and so skin friction, can be related to equivalent incompressible values using the correlation,

$$\bar{q}/q = (1 + .2 Me^2)^{.25} \quad (4.4.4.5)$$

For the particular form of velocity profile considered here, which is additionally dependent on the Spence transformation, a similar correlation was found by Cross (Ref. 14),

$$\bar{q}/q = (1 + .2 Me^2)^{.325} \quad (4.4.4.6)$$

This correlation is shown in Figure 11 and agrees quite well with experiment for two dimensional aerofoil data at transonic and supersonic speeds.

This would normally complete the transformation as the boundary layer thickness can be related to its equivalent incompressible value through equation 4.4.4.3. A more convenient approach, however, involves the shape parameter  $H$ , in addition to the more usual one. Thus by definition we have,

$$H \theta = \int_0^d (1 - Q/Q_e) \rho/\rho_e dy \quad (4.4.4.7)$$

whereas,

$$H \theta = \int_0^d (1 - Q/Q_e) \rho/\rho_e dy \quad (4.4.4.8)$$

and

$$\theta = \int_0^d (1 - Q/Q_e) Q/Q_e \rho/\rho_e dy \quad (4.4.4.9)$$

It will be evident from the equation 4.4.4.2 that the density ratio can be eliminated from equations 4.4.4.7 and 4.4.4.9 by introducing the transformed normal to wall differential element  $dy$ . The combined result for  $\bar{H}$  is independent of density and so the additional shape parameter can be regarded as an equivalent incompressible shape parameter and is particularly useful for assessing separation of the compressible turbulent boundary layer. From equations 4.4.4.3, 4.4.4.7 and 4.4.4.8 we have,

$$\bar{d} - \bar{H} \theta = d - H \theta \quad (4.4.4.10)$$

Further by assuming a quadratic velocity temperature relation in addition to the compressibility transformation of equations 4.4.4.2 and 4.4.4.3 Spence showed that the shape parameter can be transformed to its equivalent incompressible value using,

$$H + 1 = (1 + .2 r Me^2) (\bar{H} + 1) \quad (4.4.4.11)$$

Thus, to complete the transformation the required boundary layer thickness relation can be reduced to,

$$d = \bar{d} [1 + .2 r Me^2 (\bar{H} + 1) / (\bar{H} + H + 1)] \quad (4.4.4.12)$$

Finally, the extension of the law of the wall and wake velocity profile to compressible flow, using the approach just described, is demonstrated in Figures 12, 13 and 14 using the experimental data of References 13 and 15. The figures show that quite good results can be obtained.

#### 4.4.5 Surface Roughness

The law of the wall has the added advantage that surface roughness effects can be included quite naturally. From Schlichting (Ref. 1), using an equivalent sand roughness height  $K_s$  and the data of Nikuradse a law of the wall of the following form could be constructed for the completely rough flow regime.

$$\frac{U}{U_\tau} = \frac{q}{K} \left[ \ln(y/K_s) + a \right] \quad (4.4.5.1)$$

where  $a = 8.5$

By comparing this equation with the standard law of the wall (using  $K = .4$  and  $A = 2.2$  as used by Schlichting) a value of 'a' for hydraulically smooth flow can be determined,

$$a = 5.5 + 2.5 \ln(Rd q K_s/d) \quad (4.4.5.2)$$

and Schlichting compared these two results with Nikuradse's data, Figure 15, for equivalent sand roughness varying from hydraulically smooth through a transitional regime to the completely rough regime. A function that fits this data quite well is

$$a = 1/K [3.4 + (S - 1.2) e^{-2S^2}] \quad (4.4.5.3)$$

where  $S = 1/2 \ln(Rd q K_s/d)^2 \quad (4.4.5.4)$

Comparing Schlichting's form of the law of the wall with the form in equation 4.4.3.2 allows us to replace the constant A of that equation by,

$$A = A_s + A_r \quad (4.4.5.5)$$

where  $A_s$  is the hydraulically smooth flow value and  $A_r$  is an incremental value to allow for surface roughness and is given by,

$$A_r = (1.2 - S) (1 - e^{-2S^2}) \quad (4.4.5.6)$$

One advantage of this form of the equation is that the roughness can be used to determine an equivalent Reynolds Number for hydraulically smooth flow by factoring the actual Reynolds number, i.e.

$$Rd = Rd e^{A_r} \quad (4.4.5.7)$$

Thus for turbulent flow involving roughness, the flow Reynolds number can be corrected to the equivalent smooth surface condition, at least as far as the velocity profile is concerned.

#### 4.4.6 Separation Criteria

Two dimensional separation can be defined as occurring at the point where the velocity gradient in the normal to wall direction is zero at the wall. For the law of the wall and wake this occurs precisely at the point of zero skin friction, providing  $X$  is greater than unity, and this is the obvious criterion for separation. However skin friction is

not always available for an experiment and it is most often that separation is assessed by consideration of the shape parameter  $H$  or  $H'$  when the flow is compressible. At separation the law of the wall vanishes together with Reynolds number dependence and the values of  $H$  or  $H'$  are determined solely by the degree of non-equilibrium flow distortion. In Reference 16 it is shown that at separation for the law of the wall and wake the shape parameter is given by,

$$H = F(X)/(F(2X) - F(X)) \quad (4.4.6.1)$$

where 
$$F(X) = 1 - \frac{2}{\pi} \int_0^{\pi/2} \sin^2 x' dy' \quad (4.4.6.2)$$

This result is presented graphically in Figure 16 which indicates, for the law of the wall and wake at separation, the variation of  $H$  with  $X$ . This figure can then be used in conjunction with Figure 1 to relate separation values of  $H$  to the relative pressure gradient parameter. From these figures it is evident that for equilibrium flow, separation occurs with  $H = 4$ , the Coles value, while  $H$  at separation is reduced significantly below the Coles value as the relative pressure gradient parameter is decreased. The figures also help to explain the apparent inconsistency between current separation criteria based on incipient separation and observations of fully developed separated flow. Thus for trailing edge flows separation criteria based on incipient separation often gives values of  $H$  around 2.0 - 2.2 and Figures 1 and 16 suggests that this is due to the strong adverse pressure gradients of the flow. Once separation is reached however the pressure gradients collapse to give the familiar near constant separated pressure region. In these cases the experiments of Simpson et al and Hastings and Williams indicate separation with values of  $H$  around 4 and Figures 1 and 16 suggest that this is because conditions are not too far from that of equilibrium flow.

We can extend the discussion to shock induced separation if the effect of the shock on the boundary layer is considered simply as that of a very strong adverse pressure gradient. In order to demonstrate that this simplification is valid in the present context, we should ideally consider comparing law of the wall and wake velocity profiles with profile data from experiment. However in the absence of such detailed data, a less rigorous demonstration can be made by performing boundary layer calculations using the proposed velocity profile and comparing results with experiment, in the vicinity of the shock, to see if the correct response to the shock is obtained.

Such a demonstration at least for transonic flow about aerofoils has been carried out using an entrainment integral boundary layer method (Ref. 4) for which closure is obtained using the aforementioned velocity profile. The calculations are for two of the test cases of Cook et al (Ref. 17), for which pressure distributions, skin friction coefficient and shape parameter are shown in Figures 17 to 20. In each case the figures show that the calculated response of the boundary layer to the shock is correctly predicted, both in terms of the skin friction coefficient and the shape parameter  $H$ . Downstream of the shock the agreement is not so good, due partially to a significant normal pressure gradient through the boundary layer which was not modelled by the calculation method. The agreement in the region of the shock suggests that the law of the wall and wake is valid at the shock and consequently it can be expected that the separation correlation of Figure 16 also remains valid.

#### 4.4.7 Scale Parameters

In many experiments the turbulent boundary layer is described simply in terms of the momentum thickness and the shape parameter. The former parameter provides the basic thickness scale of the layer and the latter, strictly the equivalent incompressible value, is an indicator of the boundary layer state. However, in order to fully describe the compressible turbulent velocity profile, using the law of the wall and wake, the following parameters are required,

$$\bar{\delta}, \bar{q}, R\bar{\delta}, \Pi_r$$

where the superscripts are used to denote equivalent incompressible values. Here the boundary layer thickness provides the length scale and the friction velocity, reveals the state of the layer. In addition however, we also have the Reynolds number and a relative pressure gradient parameter the latter of which, as we have already seen, is very important at separation.

In the case of shock boundary layer interactions the pressure gradient parameter may be particularly useful not only for helping to define the upstream boundary layer but also for correlating conditions at the shock itself, even when as already shown this involves separation.

#### 4.4.8 Three Dimensional Flow

The law of the wall can be extended to three dimensions by considering the logarithmic wall region to lie in the direction of the surface streamline or so-called limiting streamline. This interpretation of a three dimensional law of the wall is now quite widely recognised and can be verified by consideration of the experimental data of East and Hoxey (Ref. 6) for highly three dimensional flow and the data of Perz and Elsenaar

(Ref. 18) for sheared wing and plane flow. However the law of the wake cannot be extended quite so easily into three dimensions as it is twisted or skewed throughout its thickness and requires special treatment as described in Reference 19.

As a first step towards extending the law of the wall and wake to three dimensional flow, it was shown in Reference 19 that equation 4.4.3.2 can be applied directly to the magnitude of the velocities in the three dimensional turbulent boundary layer. This ignores the skewed nature of the wake but enables the effect of non-equilibrium flow distortion to be explored in exactly the same way as for the previously discussed two-dimensional case. Thus analysing the experimental data of East and Hoxey together with that of Berg and Elsenaar, optimum values of the wake exponent for three dimensional flow can be correlated against the departure from equilibrium. Figure 21, taken from Reference 19, shows the resulting correlation which can be seen to be in good agreement with the original two dimensional correlation of Figure 1. The agreement between the two correlations suggests merging the results to produce a single correlation and as alluded to earlier, this produces improved results for two dimensional separated flow in addition to a unified theory.

Figures 22 and 23 again taken from Reference 19 show law of the wall and wake profiles fitted to the experimental data of Berg and Elsenaar (Ref. 18). The figures relate to limiting streamline angles of 29 and 35.2 degrees respectively and the later case is a particularly severe test as it is near the condition for a sheared wing form of separation. The main points to notice are that the streamwise flow components are similar to two dimensional velocity profiles and good agreement with experiment is obtained for both the streamwise and crossflow components.

Though the profile of Figure 23 is near separation the value of the shape parameter is only 1.7 and the skin friction is far from zero. This illustrates the important difference between this type of separation and its two dimensional counterpart. The limiting streamline angle is the important additional parameter for three dimensional flow and this should be recognised when assessing the state of three dimensional flows.

#### 4.4.9 Turbulence Model

In dealing with turbulent velocity profiles, discussions so far are consistent with the integral boundary layer calculation method. However, it is also true that the conclusions so far are of a more general nature and care has been taken not to enter a discussion on the relative merits of integral and differential methods, particularly as this can be found elsewhere.

Differential methods are generally, though not always, free of assumptions regarding the velocity profile and the effects of equilibrium, or its departure, results from a consideration of the turbulence structure in the form of a turbulence model. The concept of equilibrium is retained for the 'zero-equation' eddy viscosity models and the high order models are intended when the mean motion and turbulence are not in equilibrium.

It is not intended here to enter a detailed discussion on turbulence models as these have been reviewed before and can be referred to by the reader. However the review of Marvin (Ref. 20) provides a good example and specifically discusses the requirements for external flow aerodynamics. Marvin points out the inadequate use of simple turbulence models for strong shocks with separation and three dimensional flow. It is also pointed out that no single universal turbulence model can be applied with accuracy to the wide variety of flows encountered in computational aerodynamics.

With entrainment integral methods the entrainment closure equation is equivalent to the turbulence model and turbulence history has been introduced successfully using departure from equilibrium based on the turbulent kinetic energy equation. This approach has resulted in the well known lag-entrainment equation of Reference 5. However, even with this refinement the flow downstream of strong shocks still proves difficult, and calculations for highly skewed three-dimensional flow yield similar results to differential methods.

#### 4.4.10 Conclusions

Experimental research involving the turbulent boundary layer now tends to concentrate on the more complex flows involving separation, large normal pressure gradients, shock waves and vortices. On the other hand calculation methods are becoming increasingly available, though developed largely from consideration of simpler flows and the results of earlier experiments. The trend is now to use new experiments as test cases for the computational methods. Given this scenario future experiments must aim to provide a complete description of a flow feature and the relevant boundary conditions.

In this context a full description of the incoming boundary layer is essential and it has been shown that this is very much more than the traditional description based on boundary layer momentum and displacement thickness. By consideration of the law of the wall and wake velocity profile and in particular its most recent developments, important parameters relating to turbulent boundary layer development and separation can be identified. The major points to be noted are summarised below:

- 1 Pressure gradient and the departure from equilibrium or self-preserving flow strongly affects the shape of the velocity profile over a wide range of conditions including separation.



- 2 The effects of pressure gradient directly affect the values of shape parameter attributable to separation. Skin friction is a more direct and so preferred parameter for assessing the state of a layer but if unavailable shape parameter can be used if in conjunction with a relative pressure gradient parameter.
- 3 At separation the velocity profile shape is independent of Reynolds number, though Reynolds number obviously remains important for the upstream development of the boundary layer and so for the determination of the separation position itself.
- 4 At low values of shape parameter Reynolds number has its strongest effect on the turbulent velocity profile and directly determines the minimum attainable values of shape parameter for strongly accelerating flows.
- 5 Compressibility effects can be included as a transformation to enable an equivalent incompressible flow to be considered.
- 6 Surface roughness can be accommodated in terms of its effect on the velocity profile as a Reynolds number correction. This is most likely to be important when extrapolating results to full scale.
- 7 Three dimensional flow introduces the surface or limiting streamline angle as a further important parameter.

#### 4.4.11 List of Symbols

- A Law of the wall constant.
- As Law of the wall constant for hydraulically smooth flow.
- Ar Incremental law of the wall constant for rough flow.
- B Wake scale factor.
- Cf Skin friction coefficient.
- H Shape parameter.
- $\bar{H}$  Equivalent incompressible shape parameter.
- H1 Head's shape parameter =  $[\bar{d}/\theta - \bar{H}]$
- Ks Equivalent sand roughness height.
- K Prandtl's mixing length proportionality constant.
- M Mach number.
- U Streamwise velocity.
- q Non-dimensional friction velocity.
- Rd Reynolds number based on boundary layer thickness.
- r Recovery factor.
- S Natural logarithm of the roughness Reynolds number based on friction velocity and equivalent sand roughness height.
- s Streamwise distance.
- y Normal to wall distance.
- d Boundary layer thickness.
- $\theta$  Boundary layer momentum thickness.
- $\Pi_r$  Relative pressure gradient parameter.
- $\rho$  Density.
- X Wake exponent.

In addition to the tabulated symbols the suffix (e) is used to denote values at the outer inviscid edge of the boundary layer while the superscript (-) is used to denote equivalent incompressible values.

- 1 Schlichting, H. Boundary Layer Theory. Pergamon Press, 1955.
- 2 Editors: Kline, S. J. et al. Proceedings. Computational of Turbulent Boundary Layers. AFOSR-IFP Stanford Conference. 1968.

- 3 Coleman, W. S. Mean Field Development of an Incompressible Fluid in Turbulent Shear Near a Wall.  
BAe Brough Report, unpublished, February 1974.
- 4 Cross, A. G. T. Boundary Layer Calculations using a Three Parameter Velocity Profile.  
BAe Brough Report No. YAD 3428, December 1980.
- 5 Green, J. E.  
Weeks, D. J. and  
Brooman, J. W. F. Prediction of Turbulent Boundary Layers and Wakes in Compressible Flow by a Lag-Entrainment Method.  
RAE TR 72231, January 1973.
- 6 East, L. F. and  
Hoxey, R. P. Low Speed Three Dimensional Turbulent Boundary Layer Data.  
RAE TR 69041, March 1969.
- 7 Head, M. R. Entrainment in the Turbulent Boundary Layer.  
ARC RM 3152, 1958.
- 8 Chu, J. K. and  
Young, A. D. Measurements in Separating Two Dimensional Turbulent Boundary Layers.  
AGARD CP 168, May 1975.
- 9 Simpson, R. L.  
Chew, Y. T. and  
Shivaprasad, B. G. The Structure of a Separation Turbulent Boundary Layer. Part 1. Mean Flow and Reynolds Stresses.  
J. Fluid Mech, Vol. 113, 1981.
- 10 Hastings, R. C.  
and  
Williams, B. R. Studies of the Flow Field near a NACA 4412 Aerofoil at nearly Maximum Lift.  
RAE TM AERO 2026, December 1984.
- 11 Lobb, R. K.,  
Winkler, E. M.,  
and Persh, J. Experimental investigation of turbulent boundary Layers in Hypersonic Flow.  
J. Ae. Sci. 22(1) pp 1 to 9, January 1955.
- 12 Spence, D. A. The Growth of Compressible Turbulent Boundary Layers on Isothermal and Adiabatic Walls.  
ARC RM 3191, June 1959.
- 13 Winter, K. G.  
and Gaudet, L. Turbulent Boundary Layer Studies at High Reynolds Numbers at Mach Numbers between 0.2 and 2.8.  
ARC RM 3712, December 1970.
- 14 Cross, A. G. T. Calculation of Compressible Three Dimensional Turbulent Boundary Layers with particular reference to Wings and Bodies.  
BAe Brough Report No. YAD 3379, November 1979.
- 15 Cook, T. A. Measurements of the Boundary Layer and Wake of two aerofoil Sections at High Reynolds Numbers and High Subsonic Mach Numbers.  
RAE TR 71127, June 1971.
- 16 Cross, A. G. T. The Law of the Wall and Wake at Separation.  
BAe Brough Report No. YAD 5042, November 1983.
- 17 Cook, P. H.,  
McDonald, M. A.  
and Firmin, M. C. P. Aerofoil RAE 2822 - Pressure Distributions, and Boundary Layer and Wake Measurements.  
RAE TM 1725, September 1977.
- 18 van den Berg, R.  
and Elsenaar, A. Measurements in a Three Dimensional Incompressible Turbulent Boundary Layer in an Adverse Pressure Gradient under Infinite Swept Wing Conditions.  
NLR TR 72092U, August 1972.
- 19 Cross, A. G. T. Boundary Layer Calculations and Viscous-Inviscid Coupling. 15th Congress of the International Council of the Aeronautical sciences, paper no. ICAS-86-2.4.1., September 1986.
- 20 Marvin, J. G. Turbulence Modelling for Computational Aerodynamics.  
AIAA Journal, Vol. 21, No. 7, July 1983.



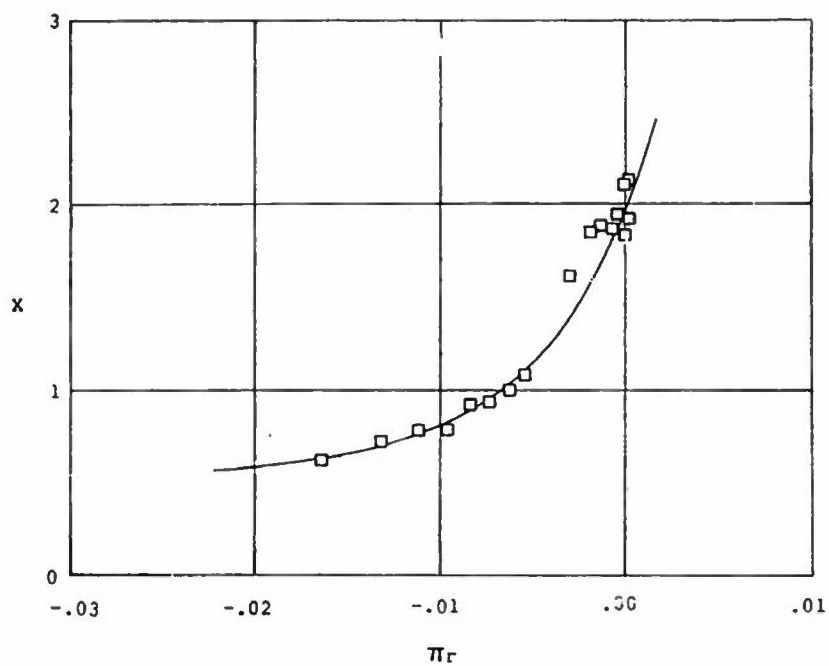


Figure 1. Non-equilibrium flow distortion for two-dimensional flow;  $\square$  experiment; — correlation.

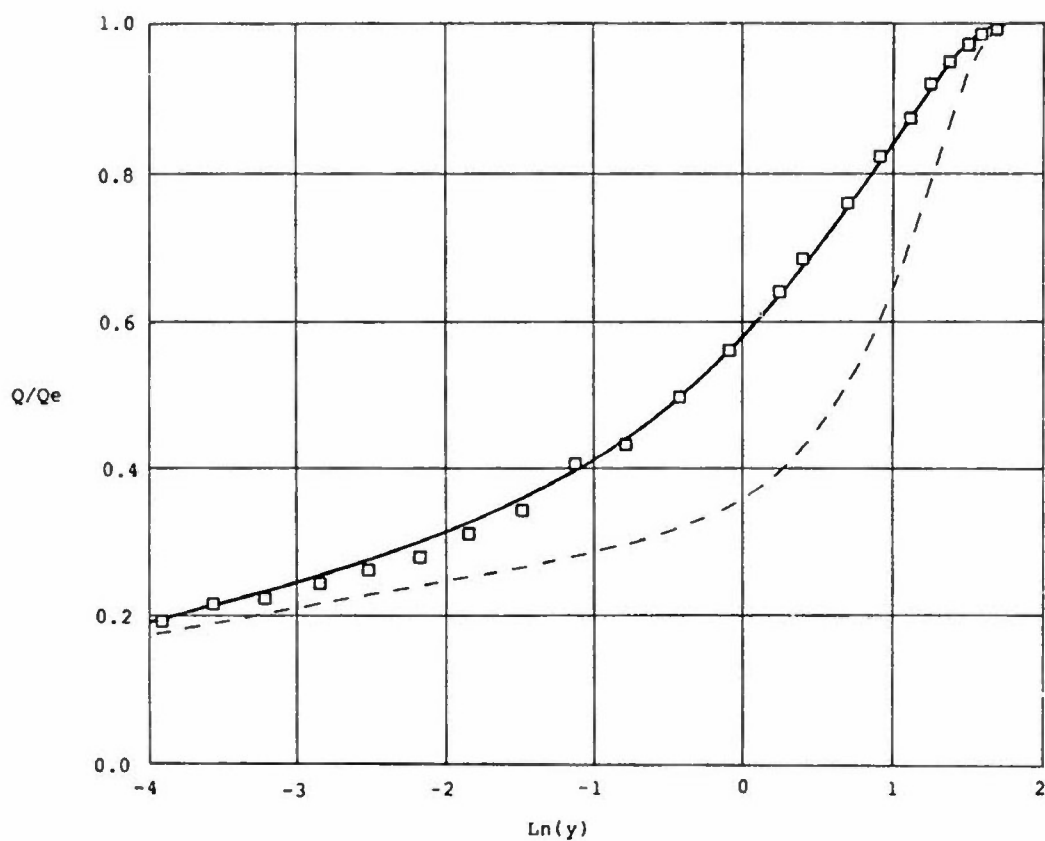


Figure 2. Velocity profiles;  $\square$  experiment; - - - equilibrium flow theory; — general theory.

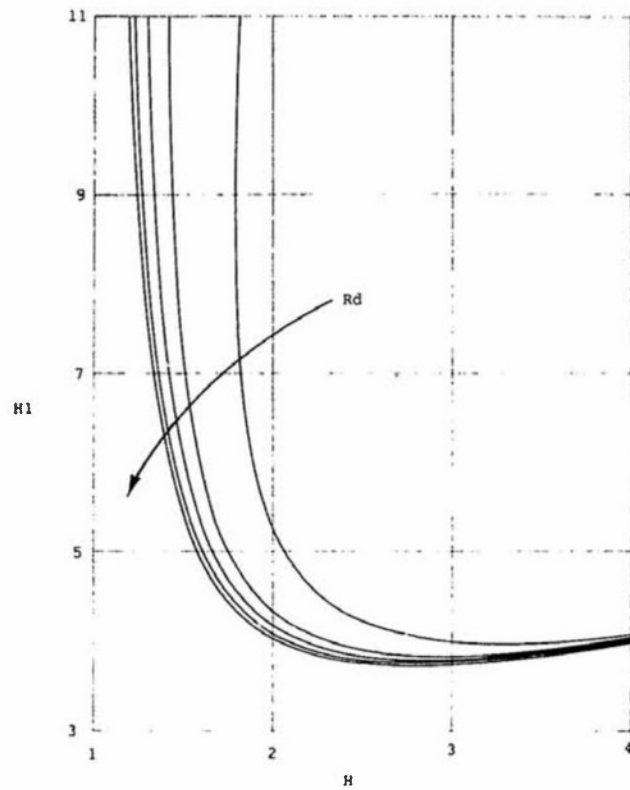


Figure 3. Shape parameter relation. Reynolds number variation for equilibrium flow;  $Rd = 100, 1000, 10000, 1000000, \text{infinity}$ .

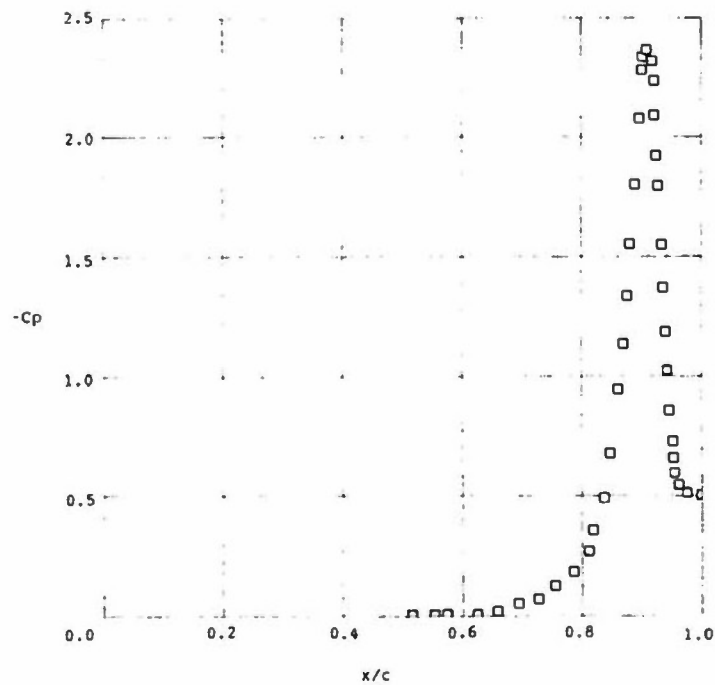


Figure 4. Pressure coefficient distribution;  $\square$  Chu and Young, AGARD CP 166.

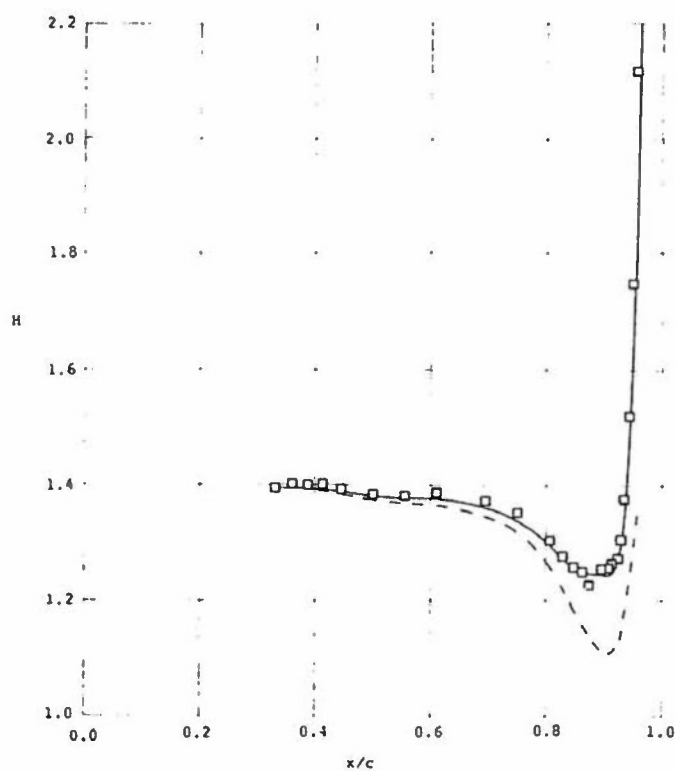


Figure 5. Shape parameter prediction;  $\square$  Chu and Young, AGARD CP 168; — law of wall and wake method; - - - method of Green et al.

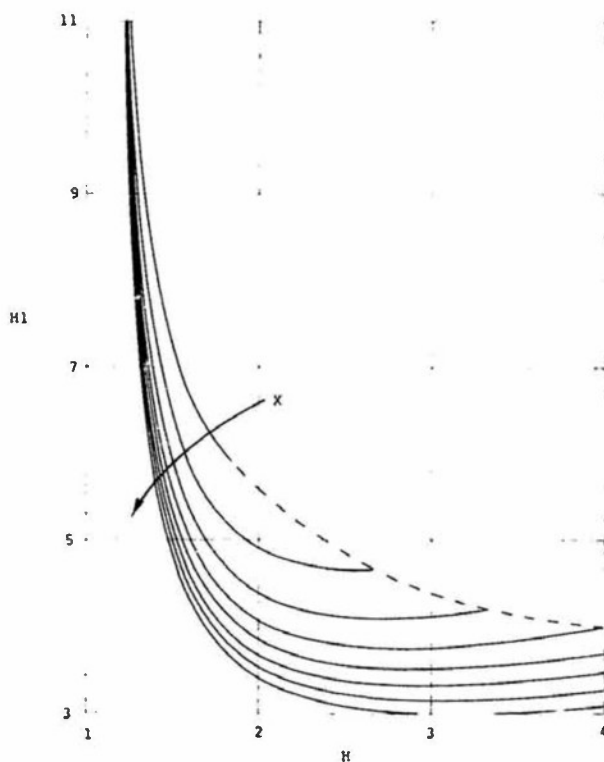


Figure 6. Shape parameter relation. Wake exponent variation at Reynolds number,  $R_d$ , of 1 million; —  $X = .5$  to 4; - - - zero skin friction locus.

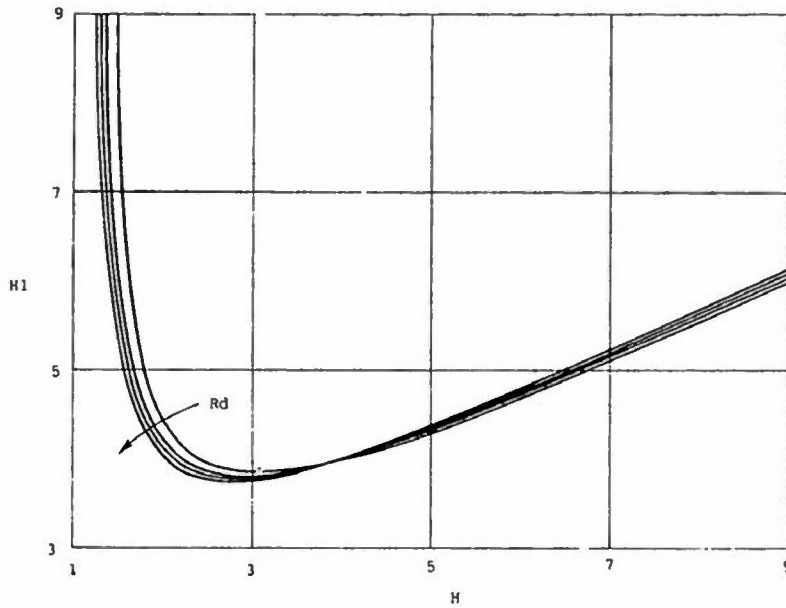


Figure 7. Extended shape parameter relation.  
Reynolds number variation for equilibrium  
flow; —  $Rd = 500, 5000, 50000, \text{infinity}$ .

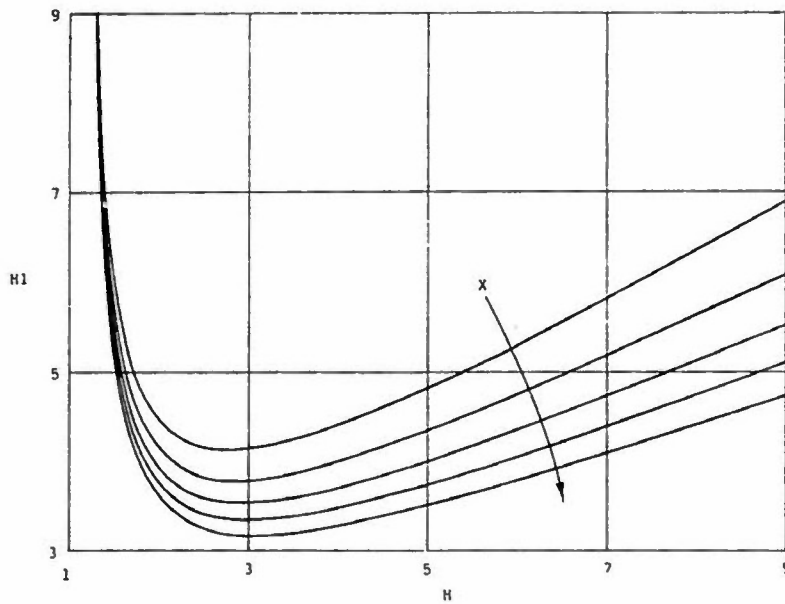


Figure 8. Extended shape parameter relation.  
Wake exponent variation at Reynolds number,  
 $Rd$ , of 50000; —  $X = 1.5 \text{ to } 3.5$

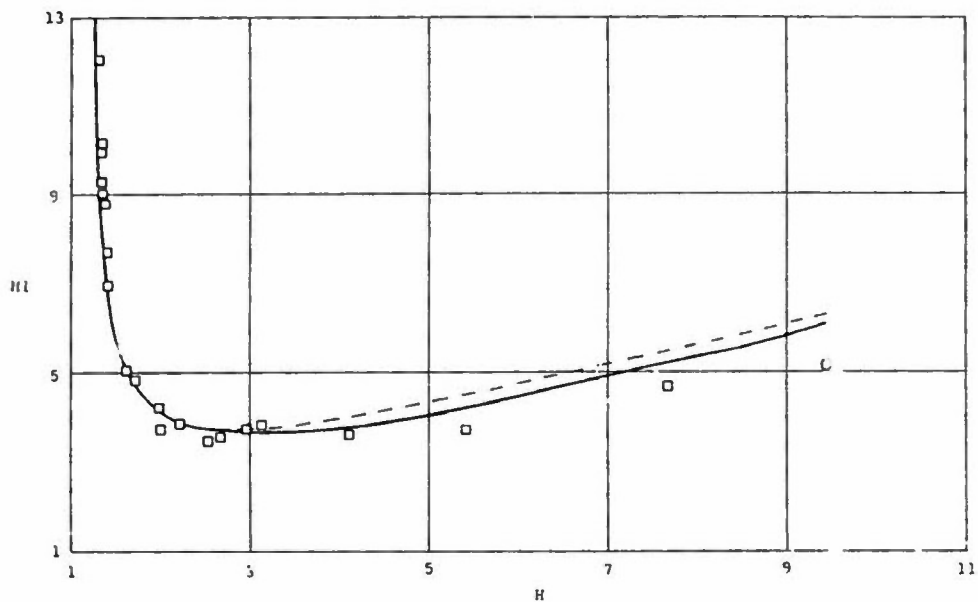


Figure 9. Extended shape parameter relation;  
 □ Simpson et al; - - - equilibrium flow  
 theory; — general theory.

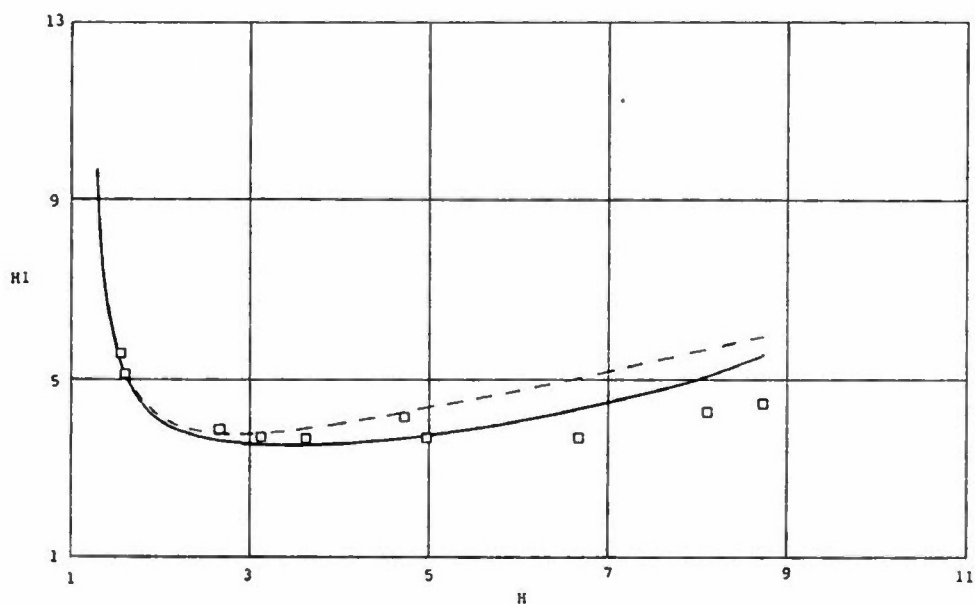


Figure 10. Extended shape parameter relation;  
 □ Hastings and Williams; - - - equilibrium  
 flow theory, — general theory.

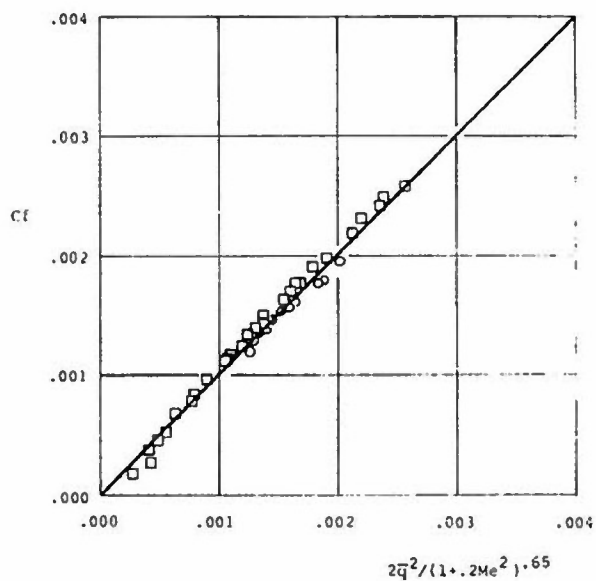


Figure 11. Skin friction correlation;  $\square$  experiment,  $Me = .5$  to  $1.0$ , Cook, RAE TR 71127;  $\circ$  experiment  $Me = .2$  to  $2.8$ , Winter and Gaudet, ARC RM 3712; — theory.

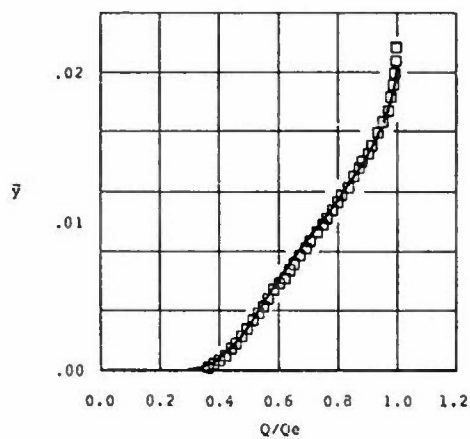


Figure 12a. Transformed compressible velocity profiles;  $\square$  experiment  $Me = .64$ , Cook, RAE TR 71127; — theory.

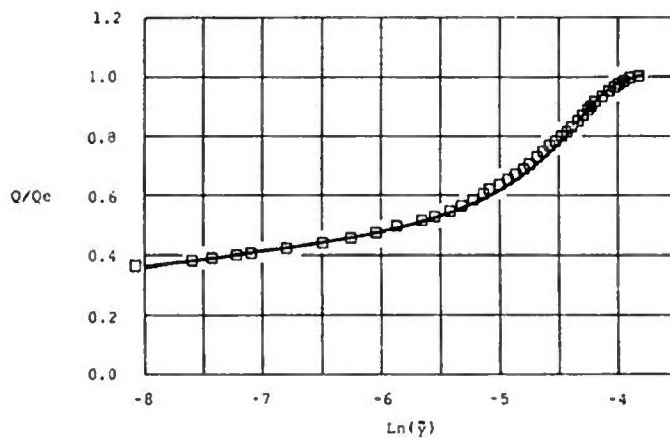


Figure 12b. Transformed compressible velocity profiles, semi-logarithmic plot;  $\square$  experiment  $Me = .64$ , Cock, RAF TR 71127; — theory.

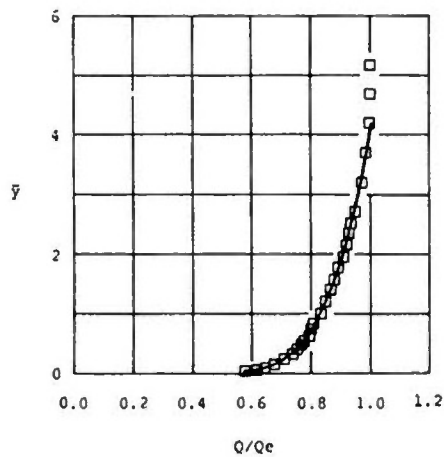


Figure 13a. Transformed compressible velocity profiles;  $\square$  experiment  $Me = 1.4$ , Winter and Gaudet, ARC RM 3712; — theory.

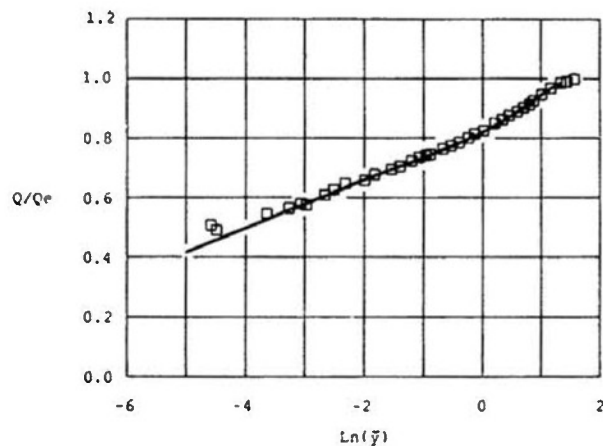


Figure 13b. Transformed compressible velocity profiles, semi-logarithmic plot;  $\square$  experiment  $Me = 1.4$ , Winter and Gaudet, ARC RM 3712; — theory.



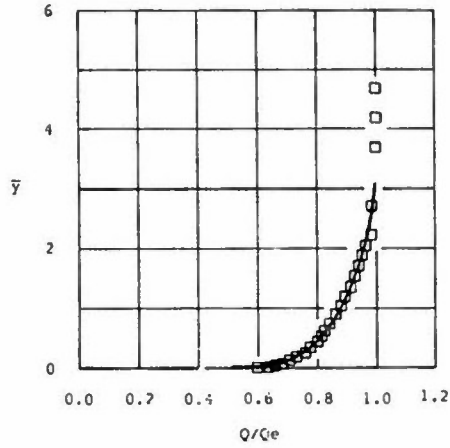


Figure 14a. Transformed compressible velocity profiles;  $\square$  experiment;  $Me = 2.8$ , Winter and Gaudet, ARC RM 3712; — theory.

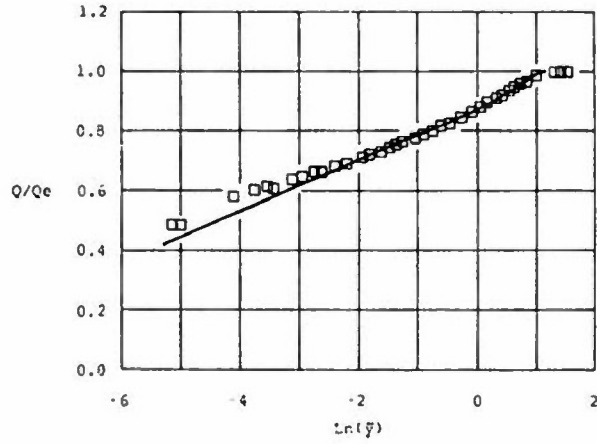


Figure 14b. Transformed compressible velocity profiles, semi-logarithmic plot;  $\square$  experiment;  $Me = 2.8$ , Winter and Gaudet, ARC RM 3712; — theory.

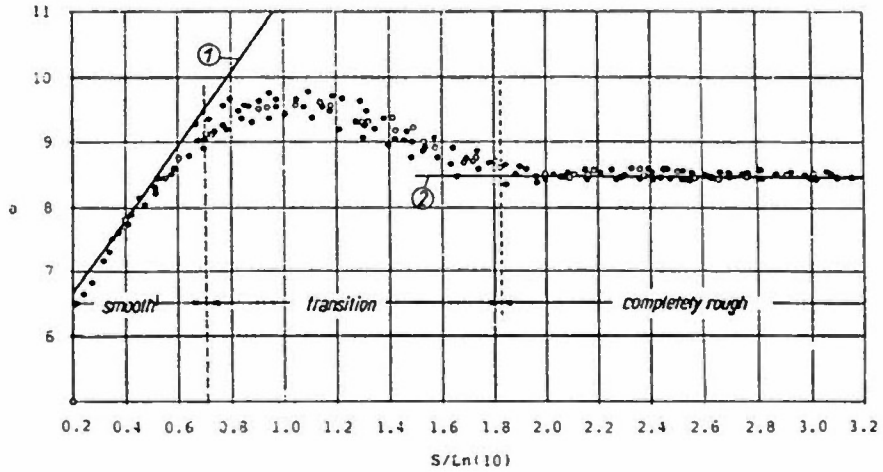


Figure 15. Surface roughness effects. 'a' as a function of 'S' for Nikuradse's sand roughness; curve (1), hydraulically smooth; curve (2), completely rough,  $a = 8.5$ .

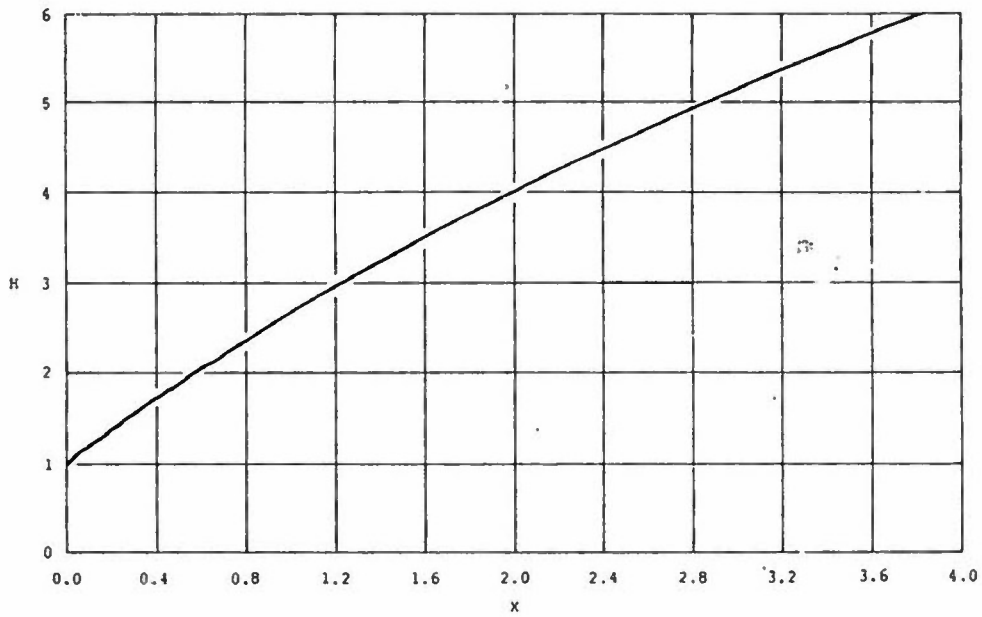


Figure 16. Law of the wake at separation. Shape parameter,  $H$ , for separation as a function of wake exponent,  $X$ .

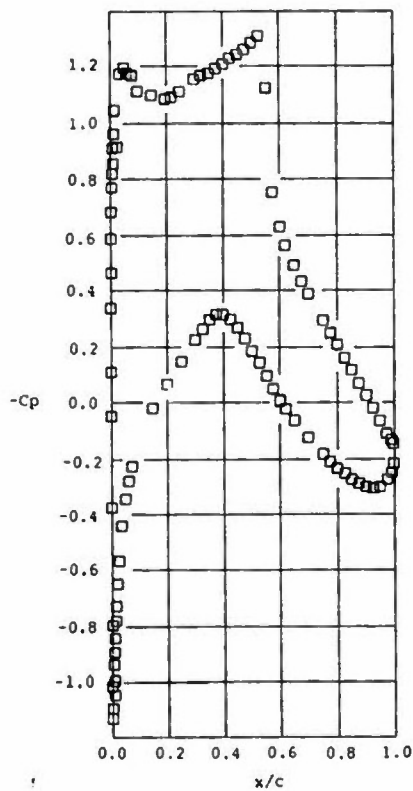


Figure 17. Supercritical aerofoil pressure coefficient distribution, Mach number = .73, Reynolds number = 6.5 million;  $\square$  experiment, CASE 9, Cook, McDonald and Firmin, RAE TM 1725.

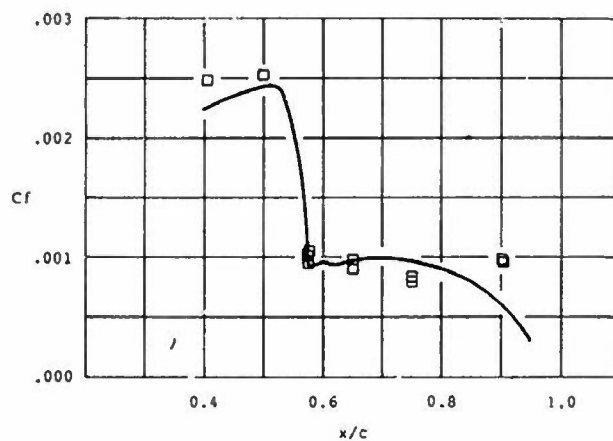


Figure 18a. Skin friction development;  $\square$  experiment, CASE 9, Cook, McDonald and Firmin, RAE TM 1725; — law of wall and wake entrainment integral boundary layer calculation.

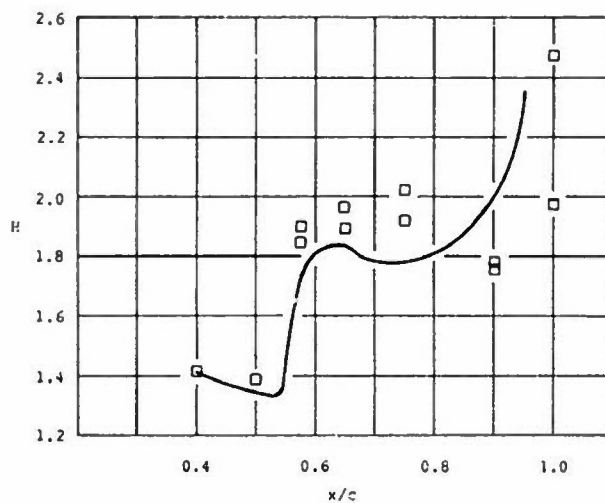


Figure 18b. Shape parameter development;  $\square$  experiment, CASE 9, Cook, McDonald and Firmin, RAE TM 1725; — law of wall and wake entrainment integral boundary layer calculation.

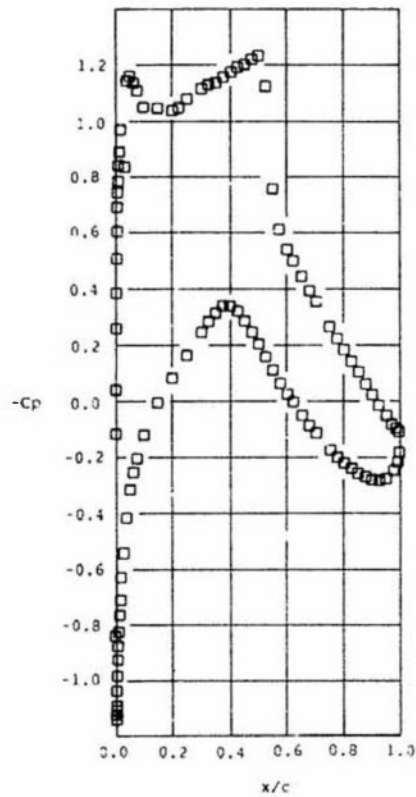


Figure 19. Supercritical aerofoil pressure coefficient distribution, Mach number 1.74, Reynolds number 2.7 million;  $\square$  experiment, CASE 13a, Cook, McDonald and Firmin, RAE TM 1725.

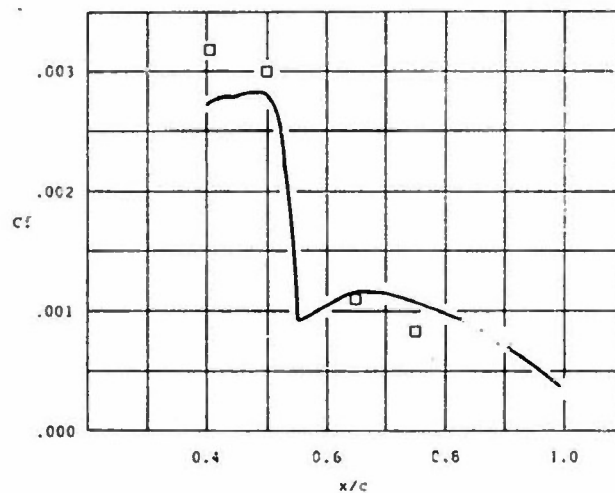


Figure 20a. Skin friction development;  $\square$  experiment, CASE 13a, Cook, McDonald and Firmin, RAE TM 1725; — law of wall and wake entrainment integral boundary layer calculation.

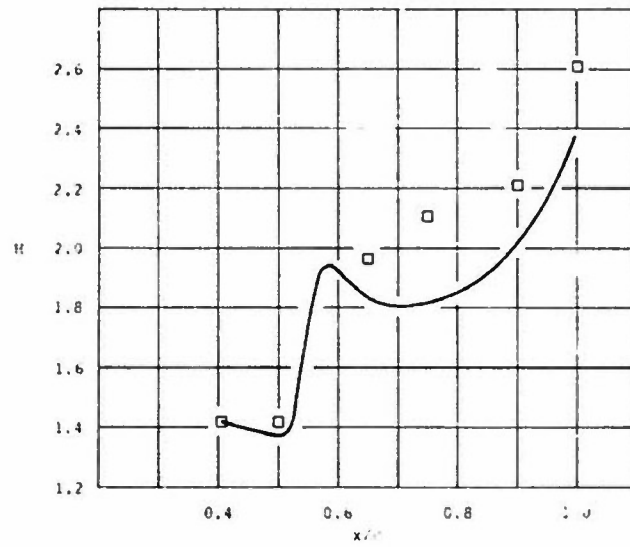


Figure 20b. Shape parameter development:  $\square$  experiment, CASE 11a, Cook, McDonald and Firmin, RAE TM 1725; — law of wall and wake entrainment integral boundary layer calculation.

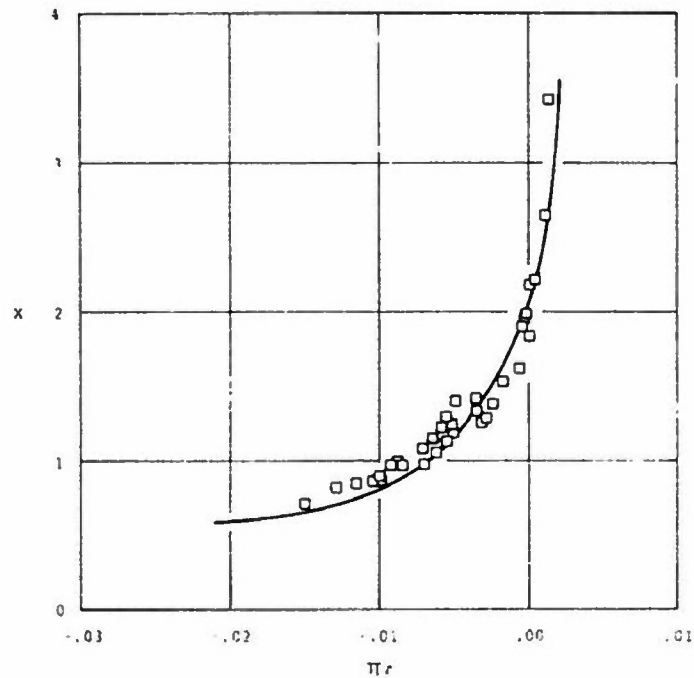


Figure 21. Non-equilibrium flow distortion for three-dimensional flow:  $\square$  experiment; — correlation.

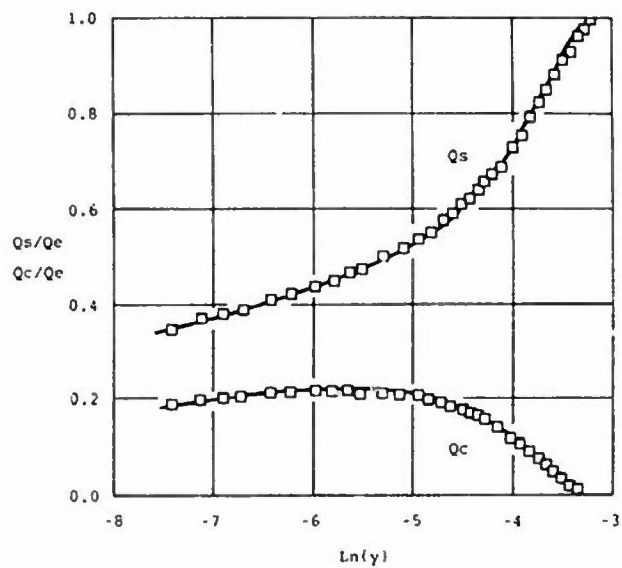


Figure 22. Three-dimensional velocity profiles,  
 $d = 40\text{mm}$ ,  $C_f = .0017$ ,  $Bo = 29.0$  degrees;  
 □ experiment; — theory.

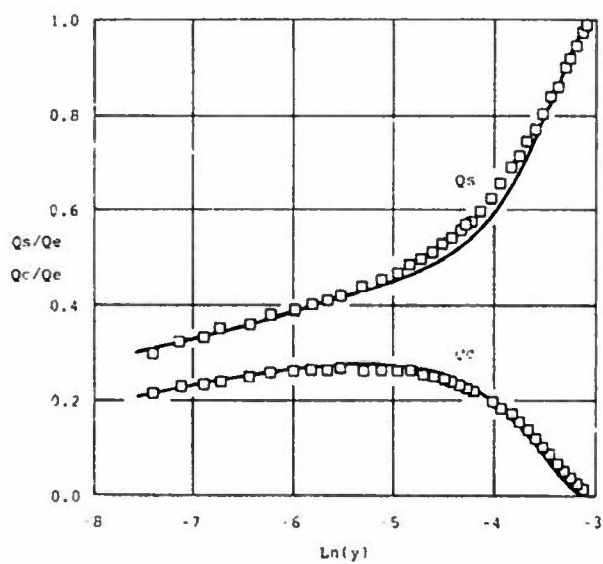


Figure 23. Three dimensional velocity profiles,  
 $d = 48.5\text{mm}$ ,  $C_f = .0015$ ,  $Bo = 35.2$  degrees;  
 □ experiment; — theory.

## SECTION 4.5

## SHOCK BOUNDARY LAYER INTERACTION

by

E. Stanewsky

Institut für Experimentelle Strömungsmechanik  
 Deutsche Forschungs- und Versuchsanstalt  
 für Luft- und Raumfahrt e.V.  
 D-3400 Göttingen, FRG

## SUMMARY

An essential prerequisite for the viscous simulation of the flow about transonic flight vehicles is the "correct" simulation of shock boundary layer interaction. The latter requires that the parameters of the incoming boundary layer dominating the interaction - hence must be duplicated in any simulation process - are known. In the present paper, it is attempted to identify such parameters for the characteristic features of shock boundary layer interaction, namely

- the upstream influence which rules the interactive pressure gradient imposed on the boundary layer,
- incipient separation whose occurrence signals to the designer that the performance boundaries of an airfoil or wing are close,
- the development of the shock-induced separation bubble which leads, possibly in conjunction with rear separation, to the total break-down of the flow, and
- the generation/amplification of turbulence due to the interaction which might have a pronounced influence on any trailing edge flow development.

The upstream influence was, for turbulent interactions, found to be mainly dependent on the viscous parameter  $\delta_1^+ (H_{11} - 1)$ , where  $\delta_1^+$  and  $H_{11}$  are the displacement thickness and the incompressible shape factor, respectively, of the boundary layer immediately upstream of the shock. Incipient separation seems rather insensitive to viscous effects and there is strong evidence that simulating the upstream influence correctly will also result in a sufficiently accurate simulation of incipient separation. For the development of the shock-induced separation bubble with increasing shock strength the momentum thickness immediately upstream of the shock was found to be the dominant viscous parameter. Results obtained at various wind tunnel turbulence levels suggest that turbulence generation within the interaction region is much more powerful than turbulence amplification and that the overall flow development associated with

turbulent shock boundary layer interaction is only affected by freestream turbulence at turbulence levels far in excess of the ones commonly encountered in wind tunnels.

The results of the present study are based in part on rather limited data, especially in the case of three-dimensional flows; they must be verified. To do so and to answer many still open questions, also addressed in the present report, well designed experiments, supplemented by theoretical studies, must be carried out employing realistic transonic configurations with variables being relevant parameters of the incoming boundary layer and the outer inviscid flow.

## NOMENCLATURE

$a$	speed of sound
$a^*$	speed of sound at sonic conditions ( $M_L = 1$ )
$a_t$	speed of sound at stagnation conditions
$c$	airfoil chord
$\bar{c}$	mean aerodynamic chord
$c_f$	skin friction coefficient
$C_L$	lift coefficient
$C_p$	pressure coefficient
$C_p^*$	$C_p$ at sonic conditions ( $M_L = 1.0$ )
$e_f^2$	root mean square voltage (Fig. 43)
$f$	frequency
$H_1$	incompressible shape factor



$H, H_{12}$	shape factor, $\delta^*/\theta$	$x, y, z$	coordinates, generally in streamwise, spanwise and normal direction, respectively, except in Fig. 41 where $y$ ( $v$ ) denotes the normal direction
$H_{32}$	shape factor, $\delta^{**}/\theta$		
$k$	kinetic energy, $0.5 (\bar{u}^2 + \bar{v}^2 + \bar{w}^2)$		
$L_B$	extent of separation bubble	$\alpha, \alpha_g$	geometric angle of attack
$L_D$	downstream interaction length (Fig. 16)	$\alpha_{C_L \max}$	$\alpha$ at maximum lift coefficient
$L_U$	upstream interaction length (Fig. 16)	$\beta_{SF}$	skin friction line angle referenced to undisturbed flow (Fig. 31)
$L^*$	upstream influence $\equiv$ supersonic interaction length (Fig. 7)	$\delta$	boundary layer thickness
$l$	characteristic length	$\delta_w$	wedge angle
$M$	Mach number	$\delta^*$	displacement thickness
$M_L$	local Mach number ( $\hat{=} c_p$ -distribution)	$\delta^{**}$	energy thickness
$p$	static pressure	$\eta$	fraction of span
$p$	total pressure	$\theta$	momentum thickness
$p'$	disturbance pressure, $p - p_1$	$\Lambda$	sweep angle (shock)
$p^*$	$p$ at sonic conditions ( $M_L = 1.0$ )	$\nu$	kinematic viscosity
$Re$	Reynolds number, $U_\infty c / \nu_\infty$	$\tau_w$	wall shear stress
$Re_{\bar{c}}$	Reynolds number, $U_\infty \bar{c} / \nu_\infty$	Subscripts	
$Re_0$	Reynolds number, $u_e^0 / \nu_e$	0	"zero" freestream turbulence (Fig. 42)
Note: $Re$ denotes Reynolds numbers based on freestream conditions, $R$ Reynolds numbers based on local conditions		1	immediately upstream of shock
		2	downstream of shock; kink in the pressure distribution (Fig. 4)
		$\infty$	freestream conditions
$R$	radius of curvature	AD	adiabatic wall conditions
$t$	airfoil thickness	$a$	corresponds to 1 (Fig. 36)
$T_0$	stagnation temperature	$b$	at shock induced separation location (Fig. 36)
$T_w$	wall temperature	$e$	edge of boundary layer
$Tu$	turbulence level	$N$	normal to swept shock
$U_\infty$	freestream velocity	$R$	at reattachment
$\bar{u}$	root mean square velocity fluctuations	$S, s$	parallel to swept shock; conditions at separation (Fig. 4)
$u, v, w$	velocity components; local velocities	TE	at trailing edge

## Superscripts

disturbance due to shock;  
shock-upstream condition  
for incipient separation

Further symbols are explained within the text and figures.

### 4.5.1 Introduction

The flow about lifting aerodynamic surfaces at transonic conditions may - as was already indicated in previous sections - be strongly affected by the interaction of the outer inviscid flow field and the boundary layer. Characteristics of the outer field are shock waves and strong sustained rear adverse pressure gradients. These, with the shock essentially acting as catalyst, tend to thicken the boundary layer and the wake thus reducing circulation due to an effective decambering of the lifting surface. The latter will, in closing the global interaction process, determine the final shock strength and location and the severity of the sustained rear adverse pressure gradients, Figure 1 [1].

Since the interaction process may be sensitive to changes in the Reynolds number or, more general, to changes in the initial boundary layer condition as, for instance, brought about by a shift in the transition point location, its viscous simulation is required in order to determine full-scale flow behavior. An essential prerequisite to the simulation of the global process is then the "correct" simulation of shock boundary layer interaction. The question to be answered regarding the latter - and, in effect, the concern of the present section - is:

- What are the parameters of the incoming boundary layer that dominate shock boundary layer interaction, hence must be duplicated in the simulation process, and, duplicating these parameters,
- to what degree does the boundary layer at the downstream face of the interaction region correspond to the one that would develop at the high Reynolds numbers of flight.

The latter is important since, at the downstream face of the shock boundary layer interaction, the stage is set for the subsequent interaction of the dissipative layer with the rear adverse pressure gradients. One important question is: Must the boundary layer be manipulated once more downstream of the interaction for the correct simulation of trailing edge flow?

In the present section we will mainly consider the interaction of a "normal" shock wave with a turbulent boundary layer as it occurs in transonic flow on the upper surface of an airfoil or wing. However, since detailed information on this type of interaction, especially in three-dimensional flow, is rather limited, recourse will also be taken to shock configurations generated by fins or wedges in a uniform supersonic incoming stream. Before commencing the discussion, it should be noted that in the following presentation essential material is drawn from an AGARDograph by Messrs. Delery and Marvin on two-dimensional shock boundary layer interaction which was just published [2]. The author is especially indebted to Mr. Delery of ONERA for providing him with an early copy of his part of the manuscript of the AGARDograph.

### 4.5.2 General Features of the Interaction

#### 4.5.2.1 Overall boundary layer development

Since the shock wave boundary layer interaction on the upper surface of airfoils or wings is closely coupled with the trailing edge flow development, it seems appropriate to start with a brief qualitative look at the overall interaction involving the shock and the sustained rear adverse pressure gradients and the corresponding response of the boundary layer. If the shock wave is weak, a mere thickening of the boundary layer occurs

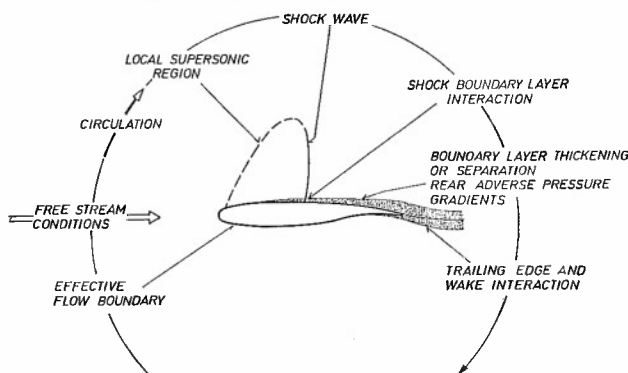


Figure 1: Interaction between shock, rear adverse pressure gradients, boundary layer and wake, Ref. 1

due to the shock with a corresponding spread of the shock pressure jump over several initial boundary layer thicknesses, dependent on shock strength and the condition of the dissipative layer, i.e., whether it is laminar or turbulent, Figure 2a. Downstream of the shock the boundary layer enters, after a period of relaxation, the region of the rear adverse pressure gradients, which cause, dependent on their magnitude, either only a further thickening or a separation of the boundary

layer. In the case of shock-induced separation, with a short separation bubble, a similar development may occur over the rearward part of the lifting surface, Figure 2b. Schlieren photographs depicting some of these flow developments are presented in Figure 3.

In the absence of rear separation, the shock-induced separated region grows downstream with increasing freestream Mach number or angle of attack (increasing  $M_1$ ), initially at a moderate rate until the pressure downstream of the shock fails to establish subsonic conditions, then more rapidly, leading to total separation, Figure 4 [3].<sup>1)</sup> This type of development was designated by H.H. Pearcy et al. as *Type A* flow [4]. Correspondingly, *Type B* flow always includes a trailing edge separation with the extreme being the occurrence of this classical separation prior to the formation of a shock wave or shock-induced separation. In case of the latter, rear separation may spread upstream with increasing Mach number or incidence reaching the foot of the shock before the latter becomes strong enough to generate a direct separation of its own. In praxis, of course, all combina-

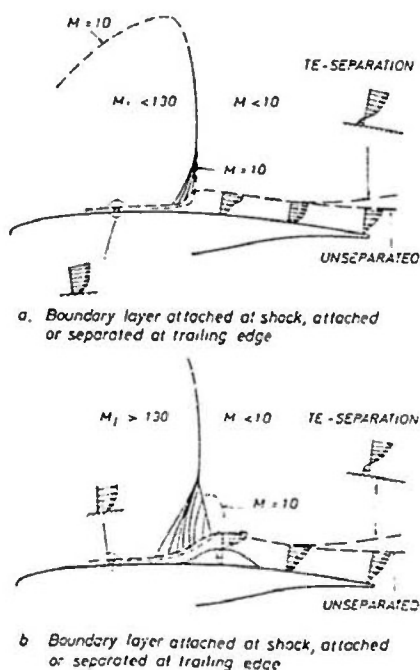
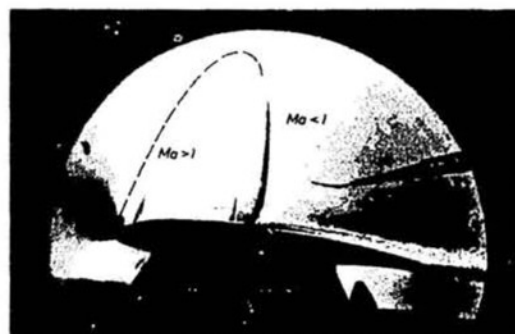
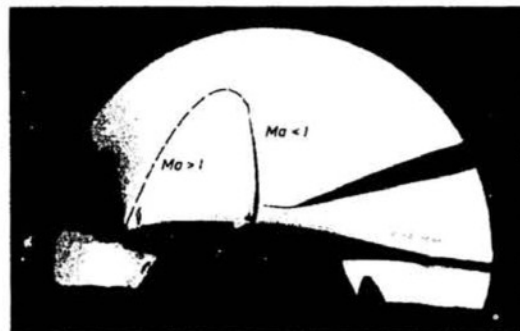


Figure 2: Transonic viscous-inviscid interaction

<sup>1)</sup> Note, that J.L. Fulker and P.A. Ashill define a critical rearward point "R" that, when reached by the separation bubble, signals the rapid growth of the separated region [23]. We will return to this development in Subsection 4.5.5.



b Shock-induced separation,  $\alpha = 5^\circ$ ,  $M_1 = 1.37$



a Attached flow,  $\alpha = 25^\circ$ ,  $M_1 = 1.25$

Figure 3: Schlieren photographs of transonic viscous-inviscid interactions. Airfoil CAST 7,  $M_\infty = 0.765$

tions in the development of rear and shock-induced separation may be found, primarily dependent on the geometry of the aerodynamic configuration [4]. It should be noted that the occurrence of the shock almost always hastens the detrimental rear flow development. These flow developments are, naturally, a challenge to viscous simulation as well as to theoretical assessment.

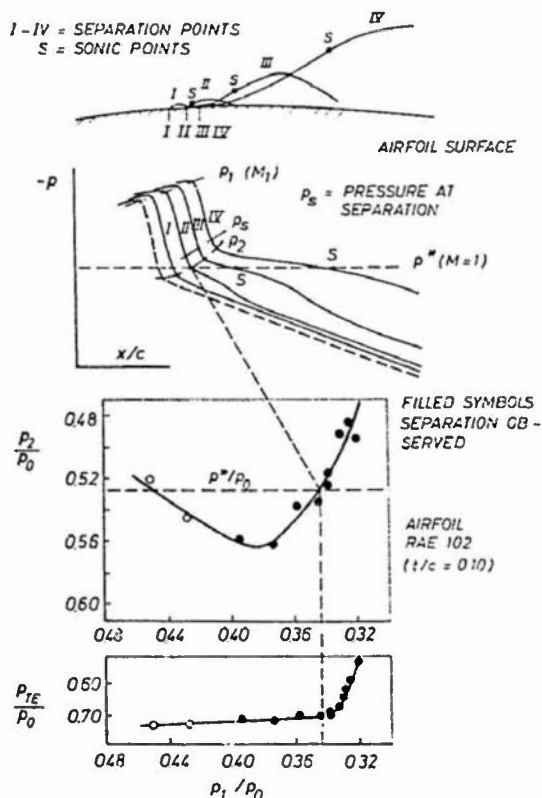
Some quantitative results of the interaction process are shown in Figures 5 and 6 [5]. Figure 5 depicts part of the upper surface Mach number distribution, essential to the interaction, for a shock-upstream Mach number of  $M_1 = 1.30$  and the corresponding chordwise development of characteristic boundary layer parameters. One notices the strong increase in displacement thickness and the appreciable retardation of the boundary layer due to the shock, the relaxation of the dissipative layer in the region of reduced pressure gradients immediately downstream of the shock and the renewed deterioration due to the rear adverse pressure gradients. As indicated by both, the shape parameter  $H_{32}$ , see Ref. 6, and the skin friction coefficient, determined by a law of the wall/law of the wake fit to the measured data [13], separation does not

develop at the shock; however, a trailing edge separation is indicated by the shape parameter  $H_{32}$ .<sup>2)</sup>

If the shock-upstream Mach number is increased, the boundary layer eventually separates at the foot of the shock, Fig. 6. With reattachment taking place not too far downstream, the boundary layer again recovers in the low pressure gradient region before the strong rear adverse pressure gradients take effect. There are two interesting observations to be made concerning the present topic of viscous simulation:

⊙ Development of shock-induced separation

I-IV = SEPARATION POINTS  
S = SONIC POINTS



(b) Behavior of characteristic airfoil pressures

Figure 4: The development of shock-induced separation, Ref. 3

- 2) The use of the skin friction coefficient and the shape factor  $H_{32}$  to determine separation is only an approximation since both parameters are derived from boundary layer profiles measured by a pitot probe [5]. The latter is in the vicinity of separation not a very accurate tool. The shape factor  $H_{32}$  is, furthermore, not unique at separation since turbulent separation is a two parameter event [6]. It is, nevertheless, employed here since only relative changes in the boundary layer development are of primary interest.

1. Compared to the case of Fig. 5 with a tripping device location in 7 % chord, a much thinner boundary layer approaches here - where the roughness element is located at 30 % chord - the shock wave. In spite of this, there seems to be, at nearly the same shock-upstream Mach number ( $M_1 = 1.30$  vs.  $M_1 = 1.31$ ) the same closeness to shock induced separation. The

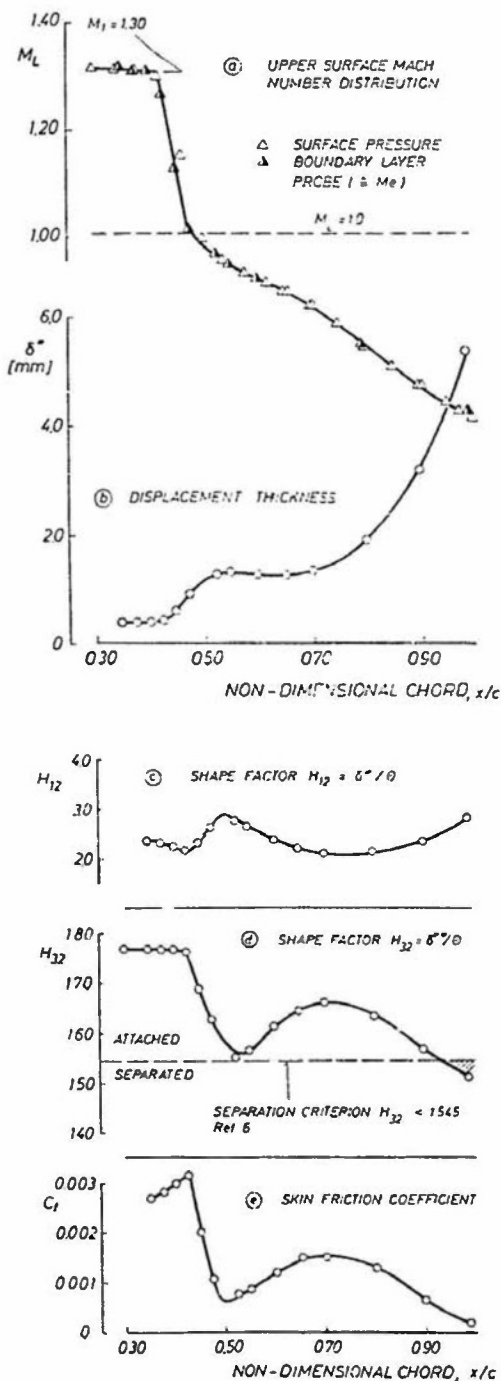


Figure 5: Boundary layer development due to airfoil upper surface interactions, Ref. 5

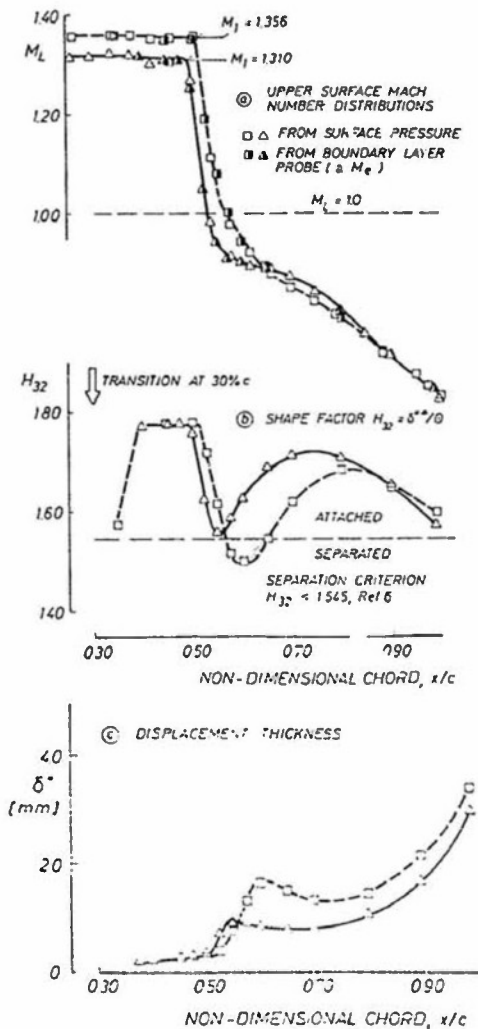


Figure 6: Boundary layer development for two different shock-upstream Mach numbers, Ref. 5

boundary layer development downstream of the shock is, however, distinctly different: The boundary layer recovery is much better and the flow does not separate at the trailing edge in case of the thinner initial boundary layer despite a more rearward shock location, the latter being, of course, a result of the improved conditions at the trailing edge.

2. Considering only the conditions of Fig. 6, one observes that the boundary layer going through the shock-induced separation shows a better overall recovery. It is hypothesized that this is mainly a result of the increased turbulent mixing in the interaction region in the presence of separation. If this holds, certain consequences exist for the viscous simulation process, one of them being related to the initial, i.e., shock-upstream turbulence level: This does not necessarily mean that the incoming turbulence level is of importance, however, if the increased mixing is strongly related to the amplification of the ini-

tial turbulence level - which might be, for instance, dependent on the tripping device employed to force transition - the "correct" full-scale turbulence level must be attained upstream of the shock in order to correctly simulate the rear boundary layer development in the presence of separation. We will return to the subject of interactive turbulence behavior in Section 4.5.6.

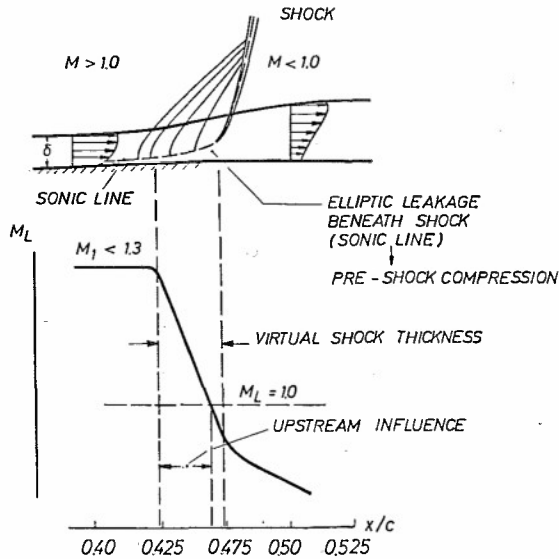
#### 4.5.2.2 Parameters of the Shock Boundary Layer Interaction

##### Upstream influence:

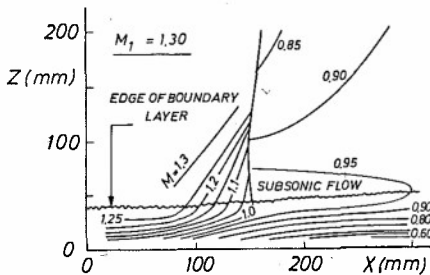
Focussing now on features of the "local" shock boundary layer interaction process, it is desirable to identify first its characteristic structure starting with the attached flow case. Figure 7 shows this structure schematically [2] together with iso-Mach-lines obtained by LDA-measurements in supersonic nozzle flow terminated by a normal shock wave [7]. Characteristically, the pressure rise due to the shock propagates upstream through the subsonic part of the boundary layer. The corresponding flow deceleration causes a thickening of the subsonic layer, bending the sonic line away from the surface thus generating compression waves which propagate through the supersonic part of the flow; the shock discontinuity is thereby replaced by a gradual compression. Note, that the shock acts, where it meets the boundary layer, in most transonic flows as a strong solution to the oblique shock equations with subsonic flow downstream [2].

The upstream influence can now be defined as the chordwise distance between the location where the shock induced pressure rise is first felt and the position where the rise in pressure reaches sonic conditions, Fig. 7a. The magnitude of the upstream influence determines, in an interactive way, the pressure gradient imposed on the boundary layer, thus may considerably affect the further boundary layer development. It is, therefore, seen as an essential parameter in the viscous simulation process whose dependence on initial boundary layer and outer flow properties must be established. Although not of any major consequence to the following discussions, it should be noted that the present definition of upstream influence is, as indicated in Fig. 4, not well suited in the presence of large shock-induced separation bubbles; here, the distance of the pressure rise to separation would be more appropriate.

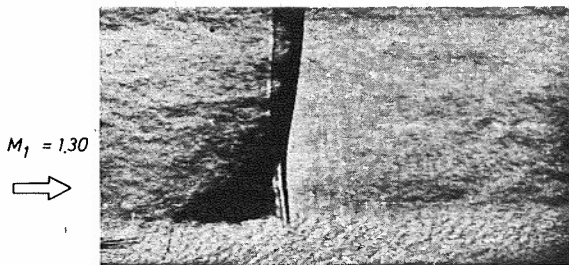
The phenomenon of upstream influence with the spreading of the compression near the wall is a very complex process involving the interplay between different layers into which the interaction region can be divided. Although essential to the complete understanding of the physics of the interaction process, a further discussion



a. Airfoil upper surface shock structure, Ref. 2,5



b. Mach number contours obtained by LDA-measurements in a supersonic nozzle flow, Ref. 7 reported in [2]



c. Schlieren photograph corresponding to Fig. 7b, Ref. 7

Figure 7: Details of transonic shock boundary layer interaction: unseparated flow

here and in the present context is thought superfluous since a detailed treatment is given in the aforementioned AGARDograph on shock-boundary layer interaction [2]. The reader is, furthermore, referred to the original work of Lighthill [8] and Stewartson and Williams [9] on this subject.

#### Incipient separation:

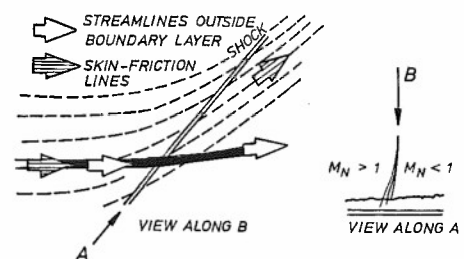
If the strength of an airfoil or wing upper surface shock is increased, either by changing freestream Mach number or angle of incidence, separation will occur at the foot of the shock and will subsequently spread downstream. The onset of separation will essentially set the performance level for a given aerodynamic configuration. It is therefore important

to know exactly when, i.e., at what freestream conditions or shock-upstream Mach number ( $M_1$ ), shock-induced separation is incipient. In the present context it must be established which boundary layer parameters govern incipient separation, hence have to be duplicated in the viscous simulation process.

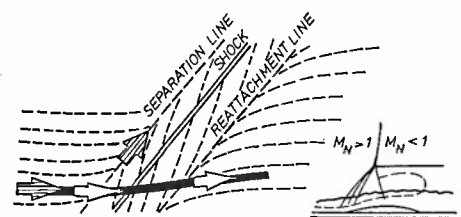
In two-dimensional flow, incipient separation occurs, by definition, when the minimum in the wall shear stress distribution is exactly zero. For lack of skin friction results, a different criterion may, of course, be used, such as the one based on the shape factor ( $H_{32}$ ) distribution where the corresponding minimum is about  $H_{32} = 1.545$ , Figs. 5 and 6.

The exact experimental determination of incipient separation is problematic since direct and highly localized skin friction measurements are still very difficult to conduct and indirect methods, such as the analysis of surface pressure distributions or flow visualization techniques, are not very accurate. This has, in the past, led to some very confusing results. Partly for that reason, one sometimes defines the onset of the "rapid" growth of the shock-induced separation bubble as the onset of significant separation or "effective" incipient separation, a condition that seems easier to be detected.

In three-dimensional swept shock wave turbulent boundary layer interaction, the flow in the plane normal to both the shock wave and the surface considered, resembles, at least for moderate sweep angles, the two-dimensional flow through a "normal" shock, Figure 8 [10][11]. The skin friction lines, however, behave quite differently in three-dimensional flow. This is indicated in Fig. 8 where these lines are presented schematically for a



a. Attached flow



b. Separated flow

Figure 8: Skin friction line pattern beneath a swept shock, Ref. 10



weak unseparated and a strong separated shock boundary layer interaction. Even in attached flow, the skin friction lines are deflected substantially more than the inviscid streamlines; for unseparated flow the skin friction lines do not converge, Fig. 8a. With increasing shock strength, however, a condition will be reached where the skin friction lines just merge into a single common line parallel to the projection of the outer flow shock (view along "B" in Fig. 8). This condition might be defined as "incipient separation". A further rise in shock-upstream Mach number, i.e., shock strength, will result in the skin friction line pattern depicted in Fig. 8b.

*Shock-induced separation:*

At sufficient strength of the shock, the boundary layer separates and a separation bubble develops whose extent depends on the pressure jump imposed on the boundary layer and the initial boundary layer condition, in later stages, of course, also on the severity of the rear adverse pressure gradients. The general structure of the separated interaction field is shown in Figures 9 and 10 for shock-upstream Mach numbers of  $M_1 = 1.5$  [12] and  $M_1 = 1.40$  [7], respectively, the latter being typical of transonic airfoil upper surface Mach numbers at or just prior to total separation, i.e., separation extending from the foot of the shock to the trailing edge. The interaction field is essentially characterized by a lambda system which is composed of, Fig. 9,

- a forward oblique shock ( $C_1$ ) produced by the coalescence of the compression waves resulting from the thickening of the subsonic part of the boundary layer - much in the same way as in attached flow (Fig. 7),
- a quasi-normal shock ( $C_2$ ) which meets  $C_1$  at the triple (bifurcation) point I and
- the outer shock ( $C_3$ ) driving the interaction.

The necessity for this type of shock pattern stems from the fact that  $C_1$  is a weak oblique shock with supersonic flow downstream while  $C_3$  is a strong quasi-normal shock so that there exist behind  $C_1$  and  $C_3$  two different states with different pressures and velocity inclinations. In order to meet the compatibility conditions for these two adjacent flows, a third state is introduced, here through the near normal shock  $C_2$ , which has the same pressure and velocity inclination as the field behind  $C_3$ , but a different velocity level, the latter resulting in the shear layer (vortex sheet) originating at the triple point I.

Comparing Figs. 7b and 10a, it can be seen that the flow pattern observed in separated interactions emerges progressively

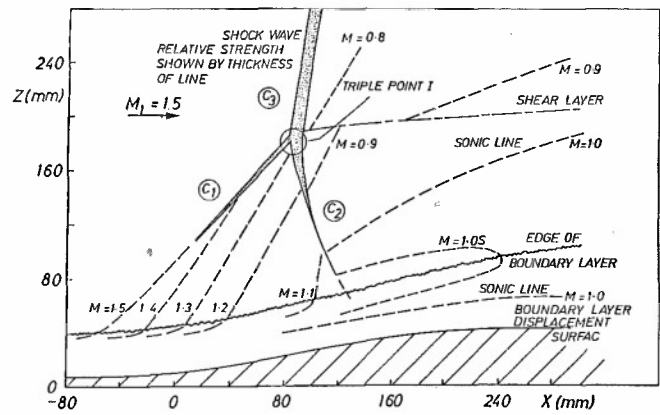
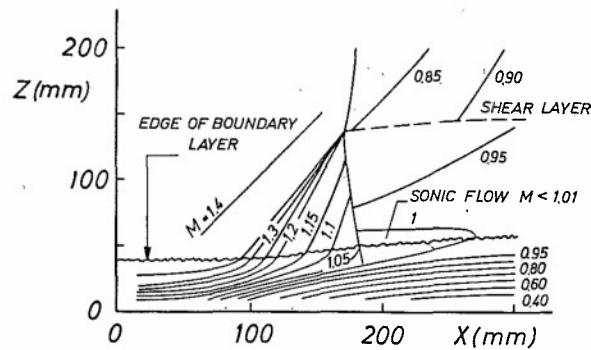
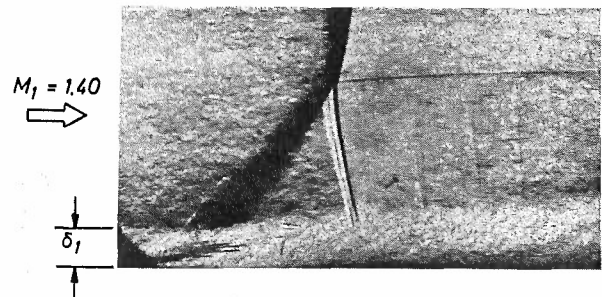


Figure 9: Transonic interaction with large separated region in supersonic nozzle flow, Ref. 12 reported in [2]



a. Mach number contours obtained by LDA - measurements



b. Schlieren photograph corresponding to a.

Figure 10: Structure of transonic shock boundary layer interaction with moderate separation in supersonic nozzle flow, Ref. 7 reported in [2]

from the pattern of unseparated flow. Upstream influence should therefore also be a characteristic feature of shock-induced separation, governed by the same initial boundary layer and outer inviscid flow parameters as in attached interactions. To be added as a characteristic parameter is the extent (or growth rate) of the shock-induced separation bubble. It is to be established which boundary layer parameters essentially rule the development of separation and hence must be duplicated in any viscous simulation procedure.

The characteristic features and developments of transonic shock boundary layer interaction that must be simulated within the overall viscous simulation process can now be summarised to be

- the upstream influence, determining the interactive pressure gradient imposed on the boundary layer,
- inlet separation and
- the development of the shock-induced separation bubble leading, possibly in conjunction with rear separation, to the total break-down of the flow.

The dependence of these features on the initial boundary layer condition and specific outer inviscid flow parameters must be investigated and dominant boundary layer parameters established. In addition, more subtle characteristics, such as the generation and/or amplification of turbulence within the interaction shall be discussed. Finally, current research and future research requirements shall be outlined.

#### 4.5.3 Upstream Influence

The upstream influence is the parameter that determines in an interactive way the pressure gradient imposed on the boundary layer. It may thus have an essential influence on the downstream development of the dissipative layer and must be "correctly" represented in the overall viscous simulation process. It is likely that, at least in the case of unseparated flow, the boundary layer parameters governing the upstream influence are also crucial to the entire shock boundary layer interaction process.

##### 4.5.3.1 Two-dimensional interactions

The upstream influence was defined in 4.5.2 as the chordwise distance between the location where the shock related pressure jump is first felt and the point where the pressure has increased to sonic conditions, Fig. 7. Since the flow development characterized by this parameter is of supersonic nature, it can be assumed that this parameter - or, in the presence of separation, the chordwise distance covered by the pressure rise to separation - is unique to shock boundary layer interaction, i.e., independent of the agent generating the shock and independent of the downstream flow development.

A very thorough investigation of the boundary layer and outer inviscid flow parameters governing the upstream influence was carried out by Delery mainly employing wall mounted "bump" models of the type shown in Figure 11 [2] [14] [15]. The pressure (Mach number) distributions

generated by such arrangements - here on the upper tunnel wall opposite to the bump - are depicted in Figure 12. In the

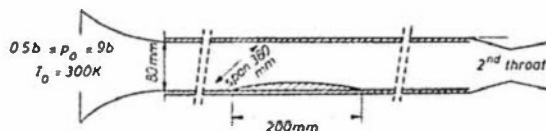
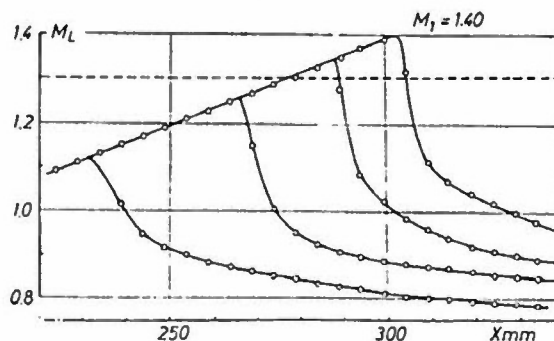
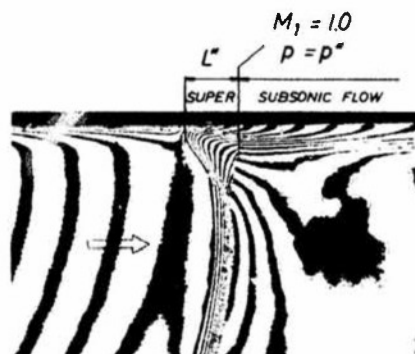


Figure 11: Example of test set-up for basic experiments of Delery, Ref. 2, 15



(a) Upper (bump-opposite) wall Mach number distribution



(b) Interferogram corresponding to the  $M_1 = 1.40$  Mach number distribution

Figure 12: Local transonic Mach number distribution generated by the test set-up of Figure 11, Ref. 2, 15

experiments, this wall Mach number distribution was found to be practically insensitive to changes in the freestream stagnation pressure, the latter being utilized to vary the Reynolds number or, more general, the initial boundary layer conditions, so that the same outer inviscid flow field was maintained while changing the properties of the viscous layer. Furthermore, for the type of pressure distribution considered, i.e., a pressure distribution with a strong acceleration of the flow up to the shock wave, the effect of the favorable pressure gradient on the boundary layer shape factor dominated over the one of the Reynolds number. Thus, it was possible to vary independently the parameters most likely



to have a dominant influence on the upstream or supersonic extent associated with shock boundary layer interaction: The shock-upstream Mach number  $M_1$ , the Reynolds number, based, e.g., on the displacement thickness,  $R_{\delta_1}^*$ , and the (incompressible) shape factor  $H_{i1}$ , the latter also accounting for the history of the boundary layer.

The results obtained with the experimental set-up of Fig. 11 are presented in Figure 13 in form of the normalized interaction length  $L^*/\delta_1^*$  as function of the shock-upstream Mach number  $M_1$  with the Reynolds number  $R_{\delta_1}^*$  as parameter but at a constant shape factor of about  $H_{i1} = 1.20$ . One observes - apart from a moderate data scatter essentially due to the difficulty of accurately determining the exact length  $L^*$  from the wall pressure distributions - in essence an independence of the data on Reynolds number and shock-upstream Mach number. The influence of the former, very pronounced on both, the displacement thickness and the upstream influence  $L^*$ , virtually disappears when one parameter is normalized by the other. The independence on Mach number, present at least up to conditions very close to shock-induced separation ( $M_1 = 1.3$ ), can be explained as follows: Increasing  $M_1$  increases the shock strength and the shock-induced dis-

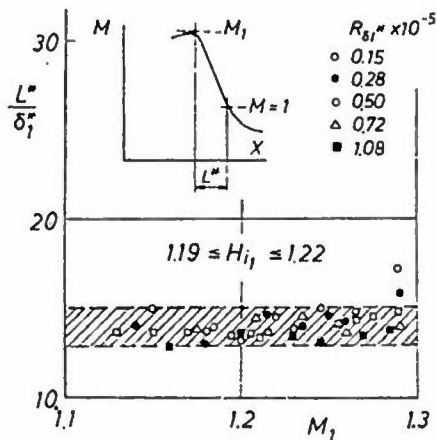


Figure 13: Effect of shock-upstream Mach number and Reynolds number on the supersonic interaction length, Ref. 2

turbance tends to travel further upstream; however, the thickness of the subsonic part of the boundary layer, which roughly scales the extent of the upstream influence, decreases with increasing Mach number, thus compensating the effect of the greater shock strength. From the above observation it may be concluded that, for a given shape parameter, the displacement thickness of the incoming boundary layer,  $\delta_1^*$ , is the proper simulation parameter for the interaction length  $L^*$ .

When the normalization of the upstream influence was applied to a wider range of

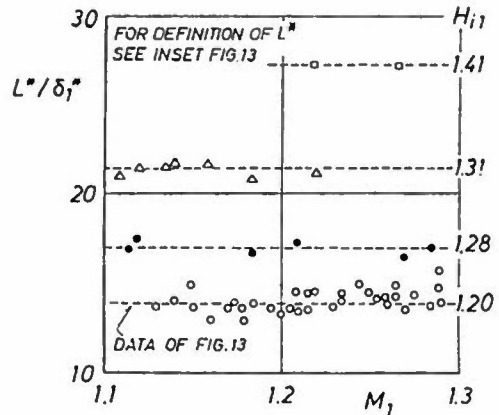


Figure 14: Effect of the incompressible shape factor on the supersonic interaction length, Ref. 2

data obtained in various facilities and with different model configurations, resulting in pronounced differences in the initial boundary layer properties, a large spread of the results was observed [2]. Grouping the  $L^*/\delta_1^*$  values, however, according to the magnitude of the shock-upstream shape factor  $H_{i1}$ , clearly showed a strong dependence of the normalized upstream influence on this boundary layer parameter, Figure 14. One sees that the normalized upstream influence doubles when the shape factor is raised from  $H_{i1} = 1.20$  to 1.40. The reason for this development seems quite simple: A small shape factor means a "full" boundary layer profile with a thin subsonic layer, hence a reduced upstream propagation of the shock associated disturbance.

Inger et al. consider in Ref. 16 the effect of heat transfer on the shock boundary layer interaction process employing a modified version of Inger's existing shock boundary layer interaction solution [17]. This solution requires as input four independent parameters:  $M_1$ ,  $R_{\delta_1}^*$ ,  $H_{i1}$  - already introduced - and the wall to boundary layer edge temperature ratio,  $T_w/T_e$ . By varying one parameter at a time it is shown that the effect of  $T_w/T_e$  on the upstream influence is very small while an appreciable influence of the incompressible shape factor  $H_{i1}$  exists confirming the large effect observed in the experiments discussed above, Figure

15. The shock-upstream shape factor can, of course, be manipulated by changing the wall temperature distribution upstream of the interaction zone, the latter, i.e., the boundary layer manipulation upstream of the interaction, being by the way the main influence of non-adiabatic wall conditions on shock boundary layer interaction, Figure 16.

Within the range of incompressible shape factors and shock-upstream Mach numbers considered, a "normalization" factor for the upstream influence was searched for containing the boundary layer parameters

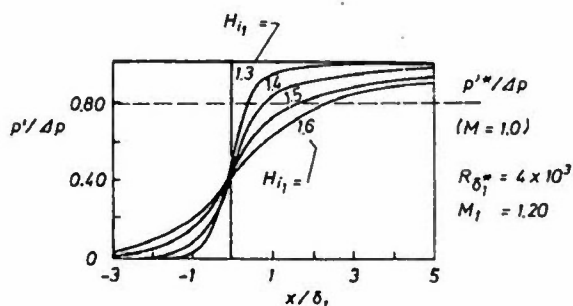


Figure 15: Influence of the shape factor on the supersonic interaction length; theory Inger, Ref. 16

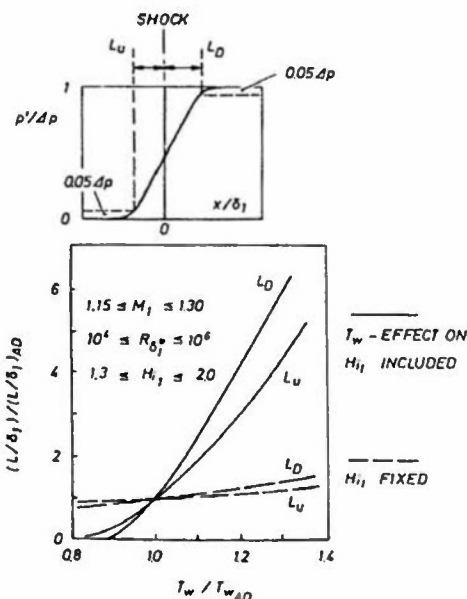


Figure 16: Relative heat-transfer effect on the normalized streamwise interaction extent, Ref. 16

observed to affect the upstream influence most, i.e., the initial displacement thickness and the incompressible shape factor [2]. This led to the purely empirical expression  $(L^*/\delta_1^*)(1/(H_{11}-1))$  which provided a rather satisfactory correlation of the upstream influence with the scatter of the data being no more than 8 percent, Figure 17. The results of Fig. 17 imply that

- for the exact simulation of the full-scale upstream influence, the viscous parameter  $(\delta_1^*/c)(H_{11}-1)$  of the full-scale high Reynolds number flow must be duplicated in the low Reynolds number wind tunnel tests, at least up to the onset of shock-induced separation.

Considering the very simple case of transonic airfoil flow, the feasibility and success of such a viscous simulation will briefly be addressed below.

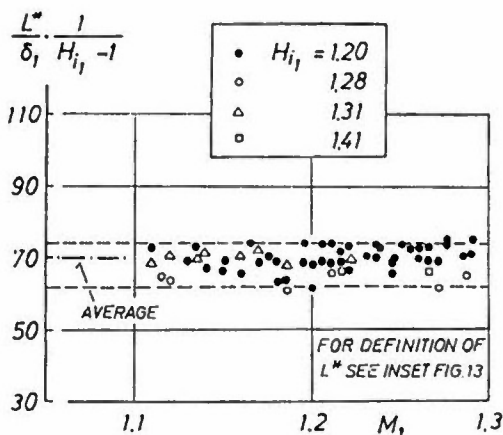


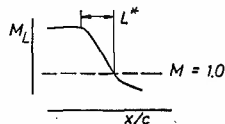
Figure 17: Correlation of the supersonic interaction length (upstream influence) of a transonic shock boundary layer interaction, Ref. 2

The present author has conducted surface pressure distribution and boundary layer measurements on two transonic airfoils for a fairly wide range of initial boundary layer and freestream conditions with emphasis, however, on conditions just prior to and beyond incipient separation [5]. Following the procedure of Delery, the data obtained for these airfoils were analysed with respect to the upstream influence and its dependence on the initial boundary layer conditions. The present results, shown in Figure 18, essentially confirm the data band given in Fig. 17 for the normalized upstream influence at Mach numbers  $M_1 \leq 1.30$ , i.e., prior to shock-induced separation. At higher shock-upstream Mach numbers a strong deviation from the "constant" interaction length occurs, mainly due to the separation bubble delaying the pressure rise to sonic conditions (also see Fig. 4). Note, that when defining the distance to the separation point as upstream influence, the data will again fall within the data-band of Fig. 18, as is indicated by the flagged symbols.

As indicated above, it seems sensible to briefly look at the feasibility and success of simulating high Reynolds number flow by duplicating the viscous parameter just discussed. For this purpose, the transonic flow about the airfoil CAST 10-2 is considered and the results obtained at a Reynolds number of  $Re = 31 \times 10^6$  selected to represent full-scale conditions [5]. Other freestream parameters for this test case are:  $M_\infty = 0.765$ ,  $\alpha = 2^\circ$ ,  $C_L = 0.68$ , i.e., a condition with a relatively strong upper surface shock wave but without shock-induced separation. The pressure distribution corresponding to this condition is shown in Figure 19. For this pressure distribution, the chordwise displacement thickness and the shape factor distributions were calculated by the method of Ref. 18 assuming transition to

AIRFOIL CAST 10-2 ( $c=200\text{mm}$ )				AIRFOIL CAST 7 ( $c=250\text{mm}$ )			
$Re \times 10^{-6}$	TRANS.	$\delta_1^*$	$H_{i1}$	$Re \times 10^{-6}$	TRANS.	$\delta_1^*$	$H_{i1}$
○ 1.95	30% $c$	0.22	1.500	● 2.9	30% $c$	0.27	1.440
△ 1.94	7% $c$	0.34	1.460	△ 2.4	7% $c$	0.42	1.420
□ 3.50	7% $c$	0.35	1.440				(mm)

FLAGGED SYMBOLS:  $L^*$  = PRESSURE RISE TO SEPARATION  
 ○ DENOTES CONDITIONS OF FIG. 19



FOR TYPICAL AIRFOIL  
 PRESSURE DISTRIBUTION  
 SEE FIG. 5 AND 19

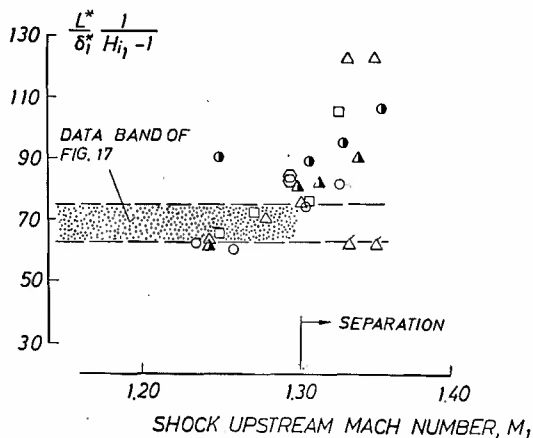


Figure 18: Supersonic interaction length in transonic airfoil flow, Ref. 5

occur, corresponding to the test conditions, at 7 % chord, Figure 20. The shock-upstream value of the viscous parameter, to be duplicated in the low Reynolds number wind tunnel tests, is  $\delta_1^*(H_{i1} - 1) = 0.07$ .

One way of manipulating the initial boundary layer parameters at low Reynolds numbers is, of course, by shifting the (forced) transition region of the boundary layer downstream [19] [20]. This was done in tests with the CAST 10-2 airfoil at a Reynolds number of  $Re = 2.4 \times 10^6$  in steps

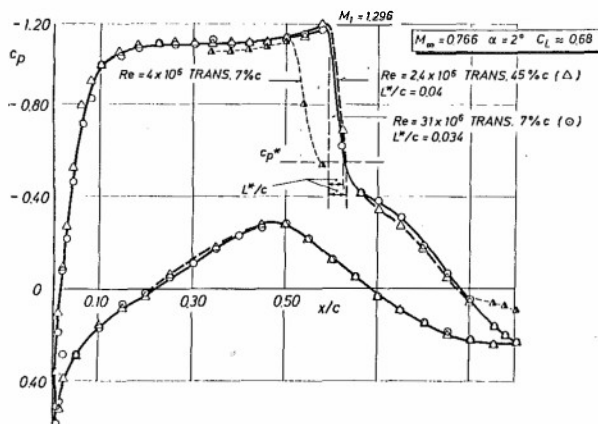
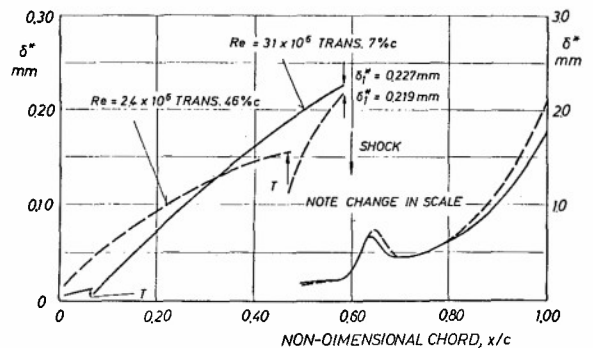
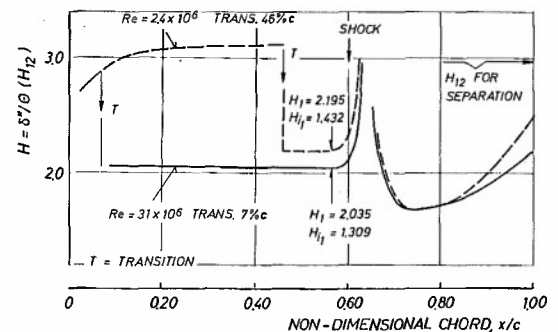


Figure 19: Pressure distributions for widely differing Reynolds numbers but similar viscous parameter  $\delta_1^*(H_{i1} - 1)$ . Airfoil CAST 10-2, Ref. 5



a. Displacement thickness distribution



b. Shape factor distribution

Figure 20: Displacement thickness and shape factor distributions corresponding to the pressure distributions of Fig. 19, Ref. 5, 18

TABLE SHOWING CONDITIONS OF FIGURES 19 AND 20

mm							
$Re \times 10^{-6}$	TRANS.	$c$	$L^*$	$\delta_1^*$	$H_{i1}$	$\delta_1^*(H_{i1} - 1)$	$\frac{L^*}{\delta_1^*} \frac{1}{H_{i1} - 1}$
△ 2.4	45% $c$	200	8	0.219	1.432	0.095	84.5
○ 3.10	7% $c$	172	58	0.227	1.309	0.070	83.5

of the transition strip location of about 15 % chord [5] [20]. The shock-upstream boundary layer condition closest to the high Reynolds number test case was found to be provided by a transition strip location of 45 % chord. Here, a fairly close match in the (calculated) displacement thickness, Fig. 20a, but a less satisfactory agreement in the incompressible shape-factor, Fig. 20b, was attained; the resulting parameter  $\delta_1^*(H_{i1} - 1)$  is 0.095. The discrepancy in this viscous parameter seems to be reflected in the difference in shock upstream influence  $L^*$ , with the normalized interaction length  $(L^*/\delta_1^*)(1/(H_{i1} - 1))$ , however, being about the same, Fig. 19. Despite these differences, there is, as also shown in Fig. 19, a very close agreement between the pressure distributions obtained at such widely differing test conditions. Considering these results, one must keep in mind that the determination of all, viscous and inviscid, parameters involved here is accompanied by certain inaccuracies, experimentally as well as in the computations.

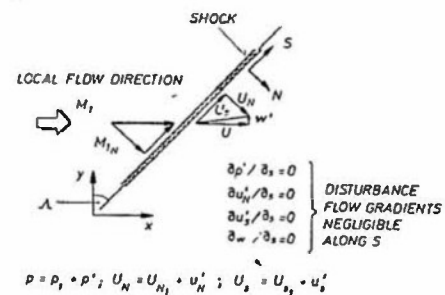
Nevertheless, there seems evidence enough that the duplication of the parameter  $(\delta^*/c)(H_{11}-1)$  leads to a satisfactory simulation of high Reynolds number shock boundary layer interaction prior to separation. More research with very specific experiments is, however, required to confirm the dominance of this parameter and, in particular, to establish the exactness with which this parameter or its components must be duplicated. It is, of course, furthermore necessary to investigate, theoretically and experimentally, how a duplication of this viscous parameter can be achieved. It was already shown by Green [21] that the exact high Reynolds number value of the displacement thickness and the shape factor, which would automatically lead to the correct  $\delta^*(H_{11}-1)$ , cannot be attained simultaneously, at least not by such simple means as manipulating the transition location or other "localized" treatments of the boundary layer. However, there is a chance that the "exact" duplication of the combination of the two crucial viscous parameters is an easier affair, especially for flows with moderate pressure gradients upstream of the shock where the shape factor does not change considerably with chord wise position and is, after tipping, always relatively close to the full-scale value, Fig. 20.

#### 4.5.3.2 Three-dimensional interactions

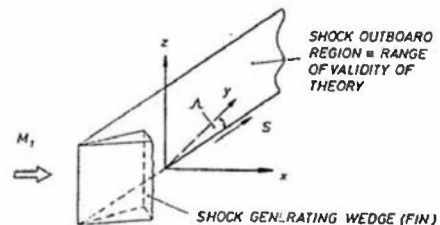
As mentioned in the introduction, only a limited amount of data is available - or amenable to analysis in the present context - on three-dimensional shock boundary layer interactions and the viscous and inviscid parameters ruling these interactions as they occur in transonic (wing) flow. So, one has to rely, at least in a first attempt, somewhat on wedge or fin induced normal shock pattern which bear, however, sufficient resemblance to sheared wing flow to warrant consideration. The uniform incoming supersonic flow generally present in experiments with fins or wedges - as compared to the non-uniform shock-upstream wing flow - is not thought of major influence in the present context. (Relevant experimental results on transonic wing flow which need, however, extensive replotting and, in parts, some boundary layer calculations before analysis are given in References 22 through 25. Some results [24] [25] are incorporated in this report.)

It was already fairly early concluded [26] [27] that for yawed laminar incompressible flow the streamwise flow is independent of the spanwise flow. For turbulent flows, there seems, however, some controversy about the validity - or range of validity - of the so called "independence principle" (named by R.T. Jones [28]). From a rigorous theoretical viewpoint, this principle can, of course, not be strictly true either for compressible flow, where the fluid properties depend on the

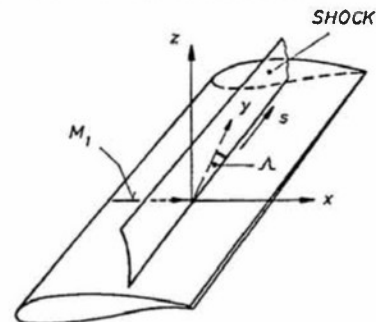
resultant and not the normal component Mach number, or turbulent flows where, in general, the Reynolds stress terms depend on the resultant flow strain and hence cross-couple the normal and tangential momentum equations [29]. In the present context, the independence principle would mean that the interactive flow normal to the shock and the associated upstream influence and increase in displacement thickness as well as the onset of separation (?) are essentially independent of the flow component tangent to the shock, hence of the sweep angle. For the viscous simulation process it means that the viscous and inviscid parameters identified as dominating two-dimensional shock boundary layer interactions are also determinant in three-dimensional flow. The validity of the independence principle and its limits should, therefore, be predominantly considered here.



(a) Three-dimensional shock pattern considered (plan view)



(b) Wedge (fin)-type shock generator



(c) Sheared wing equivalent to mid-span region of large aspect ratio wing.

Figure 21: Three-dimensional shock boundary layer interaction theory: Assumptions and configurations, Ref. 29

Inger has extended his triple-deck theory for two-dimensional shock boundary layer interactions [17] into the three-dimensional domain, considering the impingement of a weak swept shock on a plane turbulent boundary layer [29]. Here, attention is confined to a situation where the shock is straight within a uniform non-interactive inviscid flow field such that the interactive disturbance flow gradients parallel to the shock may be considered negligible, i.e.,  $\delta/\delta_s = 0$ , at least for some moderate distance ahead and behind the shock, Figure 21a. These special conditions are realized, for instance, for sheared-wing shocks in transonic flow, representative of shocks in the mid-span region of a high aspect ratio wing, and in the outboard region of fin-generated shocks, Figs. 21b and 21c. (Regarding the latter, it should be noted that due to the absence of any intrinsic inviscid scale, the disturbance flow is basically conical, i.e.,  $\delta/\delta_r = 0$ , however, it is shown in Ref. 29 that sufficiently far outboard of the fin the conical behavior becomes indistinguishable from the one for  $\delta/\delta_s = 0$ .)

Under the above assumptions, the three-dimensional interaction distinguishes itself from the two-dimensional one - or the "thought" process based on the Mach number component normal to the shock - mainly through turbulence and compressibility effects due to sweep. Considering turbulence, the normal flow ceases to be independent of the tangential component for two reasons: (1) The eddy viscosity of the incoming undisturbed boundary layer depends on the entire resultant flow rather than its normal component and, more important, (2) the corresponding eddy viscosity perturbation due to the shock introduces a tangential or "cross-flow turbulence" effect proportional to  $\sin^2 \Lambda$ , with  $\Lambda$  being the sweep angle [29] (Fig. 21). Compressibility enters via its effect on the wall temperature dependent fluid properties, i.e., density and viscosity at the wall, which are functions of the incoming Mach number,  $M_1$ , rather than the normal component.

Considering the shock upstream influence, the relative importance of compressibility and interactive turbulence due to sweep-back, i.e., essentially the deviation from the (computed) upstream influence assuming full applicability of the independence principle, is demonstrated in Figure 22. This figure indicates that, utilizing the data scatter observed in Fig. 14 at  $H_{11} = 1.20$  as a measure, the independence principle seems to hold up to sweep angles of about  $\Lambda = 30$  degrees. This means that, at least up to these angles between the local flow direction and the shock, (1) two-dimensional results can be transferred to, say, large aspect ratio wings, provided all flow properties are based on the Mach number normal to the shock,  $M_{1N}$ , and (2) the viscous simulation process outlined above for two-dimensional configurations can also be applied to three-dimensional flow.

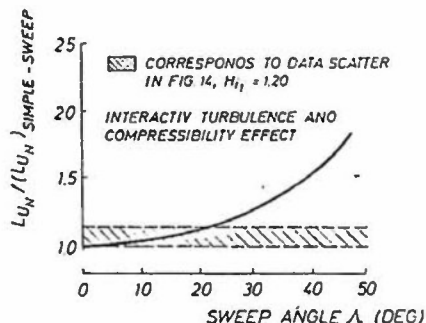
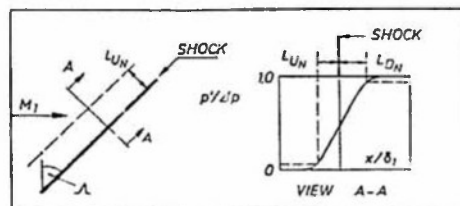


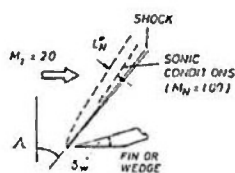
Figure 22: Relative importance of compressibility and interactive turbulence effects due to sweep, Ref. 29

Although the sweep angles are much higher than the ones occurring on large aspect ratio wings and above the limit for the applicability of the independence principle given above, some fin-induced interactions were analysed [30] [31] [32] and the results compared to the two-dimensional data discussed in the preceding section. Figure 23 shows that despite the large sweep angles, the "normal" supersonic interaction length  $L_N^*$  agrees surprisingly well with its two-dimensional counterpart. Regarding the large sweep angles, it should, however, be noted that the supersonic interaction length seems to be less dependent on the conicalness of the flow than the shock-upstream influence  $L_{UN}$ , generally used in the correlation of supersonic interactions [31], since, as indicated in the inset to Fig. 23, the line corresponding to sonic conditions is also slightly conical.

The limited data included for transonic three-dimensional configurations, i.e., the flight data of Ref. 24 and the sheared-wing results of Ref. 25, given in Fig. 23, also confirm the applicability of the viscous simulations parameter  $\delta_1^*$  ( $H_{11} = 1$ ) to swept shock boundary layer interactions.

The analysis of relevant results, especially results of "pure" transonic interactions, with respect to the present objective must be continued in order to verify the findings regarding the viscous simulation parameters discussed above. In addition, there is an urgent need for specially designed experiments to investigate, in detail, characteristic features of three-dimensional transonic shock





NOTE: The compressibility transformation of  $H_1$  is based on  $M_1$

FIN-INDUCED SHOCKS

	$\delta_w^*$	$\Lambda^*$	$M_{1N}$	Ref
○	8	53	1209	30,31
△	8	53	1209	32
▲	10	51	1254	32
□	WING (FLIGHT) DATA (24)			
▽	SHEARED WING DATA (25)			

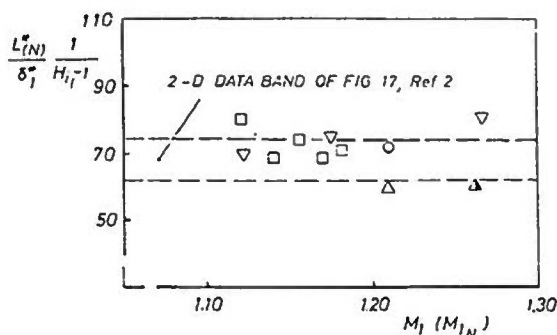


Figure 23: Upstream influence in three-dimensional normal-shock boundary layer interactions

boundary layer interactions and the influence of specific boundary layer and outer inviscid flow parameters, including the shock-upstream Mach number and the sweep angle, on these interactions. At DFVLR Göttingen two experiments, one employing a sheared wing, the other a wedge-type shock generator normal to a flat plate with shock-upstream Mach numbers  $M_1$  typical of transonic wing flow, are being prepared. The experiments, which will include detailed boundary layer measurements, are briefly addressed in Section 4.5.7.

#### 4.5.4 Shock-induced Incipient Separation

The onset of shock-induced separation signals to the designer of transonic aerodynamic vehicles that the performance boundaries, i.e., essentially maximum lift and the buffet boundary, are being approached, more or less rapidly, as the Mach number or angle of incidence is increased. The knowledge of the viscous/inviscid conditions for incipient separation is therefore of considerable importance to the design as well as, in the present context, to the viscous simulation process. It should be kept in mind, however, that there is, of course, a certain margin in the freestream conditions for incipient separation and the onset of total separation, a subject that will be addressed in Section 4.5.5.

#### 4.5.4.1 Two-dimensional incipient separation

Two-dimensional incipient separation occurs, as already pointed out in Section 4.5.2, by definition, when the minimum in the wall shear stress distribution is reached as the Mach number or angle of attack - or, in general, the shock-upstream Mach number  $M_1$  - is continuously increased, Figure 24. (Also other criteria related to some boundary layer integral parameter, such as, for instance,  $H_{32} = 1.545$ , Fig. 6b, may be used.) Incipient separation is generally not felt by the overall flow development as a dramatic effect - hence not easy to detect - and a distinction is frequently made between "true" and "effective" incipient separation, the latter related to the initial growth rate of the shock-induced separation bubble with changing  $M_1$ . Since both conditions will be treated here, it is seen appropriate to first point out

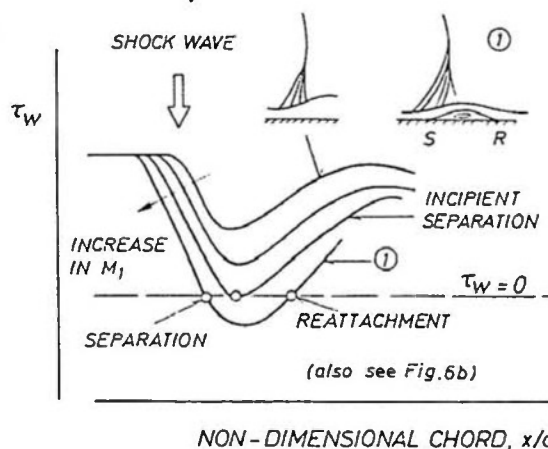


Figure 24: Two-dimensional shock-induced incipient separation, Ref. 2

essential differences between "true" incipient separation and the onset of "effective" or "significant" separation.

As a first example for the definition of "significant" separation, we consider Pearcey's analysis of supercritical airfoil flow [3] already briefly touched when discussing the development of separation in general (Section 4.5.2). For this analysis, various characteristic pressures associated with the flow development in the vicinity of the shock and the trailing edge were defined, Figure 25 (also see Fig. 4):  $p$  is the shock-upstream pressure essentially determining the shock strength,  $p_s$  is the so called "kink" pressure, defined in Fig. 25,  $p_i$  is the pressure at separation, which closely coincides with - and may, therefore, in the absence of separation, also be considered as denoting - the downstream end of the "linear" rise in surface pressure due to the shock (see upstream

influence), and  $p_{TE}$  is the trailing edge pressure. The rapid drop of the latter indicates that separation, here commencing at the foot of the shock, has reached the trailing edge, thus signaling the onset of total separation.

One observes that, as the shock strength is increased, i.e., decreasing  $p_1/p_0$ , a condition will be attained where  $p_2$  is just equal to the sonic pressure  $p^*$  and the "kink" pressure  $p_2$  has a maximum, Fig. 25a. From the experimental results depicted in Fig. 4 one may conclude that this condition coincides with "true" incipient separation since for all data points to the "right" of the maximum separation was observed while the conditions to the "left" of the maximum did not indicate separation. Now, a further increase in the shock strength - and the associated development of the separation bubble - cause  $p_2$  to decrease, at first to the sonic level. This signals, according to Pearcey, the onset of "significant" separation. The reason for this designation is quite obvious: If one raises the

close to the surface converge due to the pressure increase, thus supporting in a "snow-balling" way the growth of the separation bubble, a behavior opposite to the one occurring for subsonic conditions immediately downstream of the shock. It should be noted that this behavior is, of course, closely coupled to Type "A" flow where an independent trailing edge separation is absent.

Another way of determining (and defining) the onset of significant shock-induced separation, based on detailed boundary layer measurements, was proposed by the present author [5]. For this determination, the normalized change in displacement thickness across the shock,  $\Delta\delta^*$ , is plotted versus the shock-upstream Mach number  $M_1$ , Figure 26. Here, one observes, at first, a gradual increase in  $\Delta\delta^*$  with increasing  $M_1$ , followed by a faster rise in this viscous parameter, the latter producing a distinct "kink" in the  $\Delta\delta^*$ -dependence at an approximate shock-upstream Mach number of  $M_1 = 1.320$ . The "kink" condition may safely be taken as the onset of "significant" separation.

Also indicated in Fig. 26 is the "onset" of separation predicted by extrapolating the curve of shock-induced bubble length versus  $M_1$  to zero bubble extent (see Fig. 35). Although not likely to represent the exact "true" incipient separation, since here a constant growth rate of the bubble with  $M_1$ , commencing at the very beginning of separation, is assumed, it gives a good indication of the possible delay between incipient and significant separation occurring on transonic airfoils. Considering Fig. 26, also note the effect of the initial boundary layer condition on the relative  $\delta^*$ -jump across the shock and on the onset of separation.

Marked in Fig. 26 is, in addition to the two stages in the development of shock-induced separation, the onset of total separation, i.e., essentially the shock-upstream Mach number at maximum lift. One notices that these Mach numbers differ widely, at least for the two extreme initial boundary layer conditions investigated, contrary to the local Mach numbers at the onset of true and significant separation, indicating that the bubble growth - shock-induced and/or trailing edge related - is likely to depend stronger than incipient separation on some viscous parameter upstream of the shock boundary layer interaction. It is also noteworthy that in the case of the early - design - airfoil data of Fig. 25, the increase in  $M_1$  between significant and total separation is only  $\Delta M_1 = 0.016$ , while this difference is  $\Delta M_1 \geq 0.035$  for the two transonic airfoils considered here. It is this another indication that airfoil geometry might, next to viscous effects, be crucial to the pace of the separation bubble development.

We shall now turn directly to the sensitivity of incipient or the onset of sig-

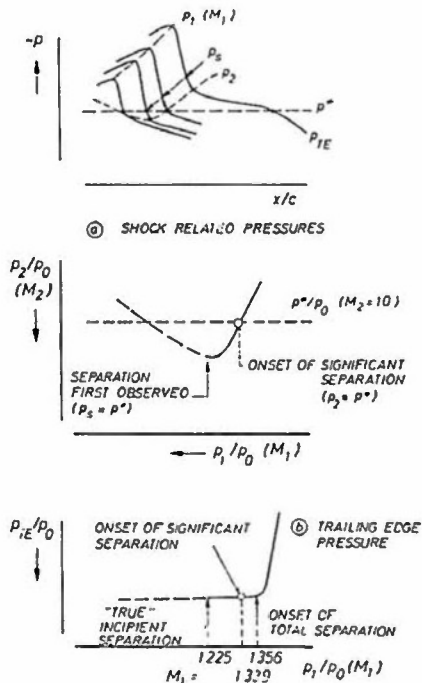
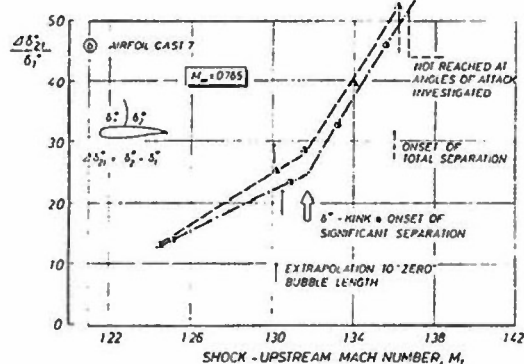
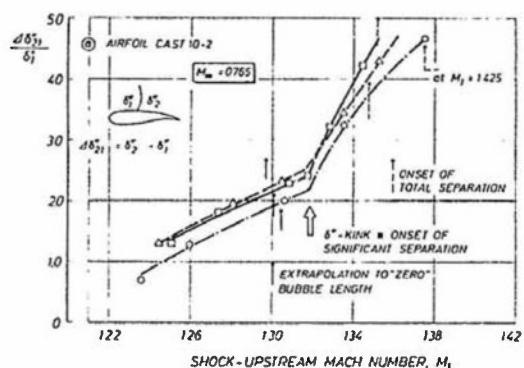


Figure 25: Incipient and significant shock-induced separation, airfoil RAE 102, Ref. 3 (also see Fig. 4)

shock-upstream Mach number further by only  $\Delta M_1 = 0.016$  - as compared to the change of  $\Delta M_1 = 0.10$  between incipient separation and the condition  $p_2 = p^*$  - the onset of total separation, i.e., practically the buffet boundary, is reached. The latter is indicated by the drop in trailing edge pressure shown in Fig. 25b. The reason for the "explosion" of the separation bubble beyond the condition  $p_2 = p^*$  is given in Ref. 3 as follows: For supersonic flow downstream of the shock, the streamlines





AIRFOIL CAST 10-2 (c = 200mm)					AIRFOIL CAST 7 (c = 250mm)				
Re x 10 <sup>-5</sup>	1/4 CHORD	δ <sub>1</sub> <sup>*</sup>	11 <sub>1</sub>		Re x 10 <sup>-5</sup>	TRANS	δ <sub>1</sub> <sup>*</sup>	11 <sub>1</sub>	
195	10%	0.22	1500		29	30%	0.27	1440	
194	7%	0.34	1450		24	7%	0.42	1420	
350	7%	0.35	1440						
			(mm)						

Figure 26: Incipient and significant shock-induced separation on two transonic airfoils, Ref. 5

nificant separation to viscous effects. In that regard, a thorough experimental program was (also) undertaken by ONERA to assess the main parameters affecting shock-induced separation phenomena [2]. In this program, several experimental arrangements were utilized including complete airfoil models, mounted on- and off-center in two-dimensional test sections [33] [34], and channels with interchangeable bumps similar to the one shown in Fig. 11. Incipient separation was determined by inspection of the surface pressure distributions, surface flow visualisation, Stanton probe, and boundary layer measurements by conventional probes and Laser velocimetry.

The analysis of all results revealed that incipient separation is mainly dependent on the shock-upstream Mach number  $M_1$  and the (incompressible) shape factor of the incoming boundary layer,  $H_{11}$ . The incipient separation boundary defined by these parameters is depicted in Figure 27 [2] [5]. It will be noted that the experimental data of ONERA essentially collapse on a single line, very precisely defining the limit between interactions with and without separation. The same holds for the

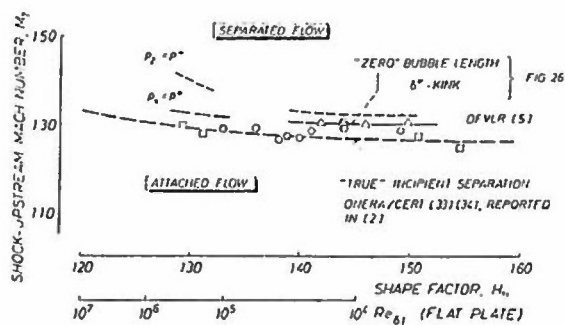


Figure 27: Transonic incipient and significant shock-induced separation boundaries, Ref. 2, 5

DEVLAR data, extracted from Figs. 35 and 26, for the lines representing the "zero" bubble extent and the  $\delta^*$ -kink. As was to be expected after the preceding discussion, the latter exhibit, in essence, a slight positive Mach number shift with respect to "true" incipient separation, however, with the same sensitivity, or insensitivity, to changes in the initial shape factor. Considering the DEVLAR results, it must be mentioned that the data points at  $H_{11} = 1.30$  were obtained from pressure plots similar to Figs. 4 and 25 using the criteria  $p_2 = p^*$  and  $p_1 = p^*$  to determine incipient and the onset of significant separation, respectively. The pressure distributions were measured at a chord Reynolds number of  $Re = 30 \times 10^6$ . The results suggest that the onset of significant separation is slightly more sensitive to viscous changes than "true" incipient separation, which should not be surprising since between the two lies a certain bubble development.

All curves in Fig. 27 exhibit essentially only a very slow increase in separation Mach number with decreasing shape-factor (or increasing  $Re_{01}$ ). The trend of the dependence could, of course, have been expected since lowering the shape factor means a fuller boundary layer profile, hence more resistance to separation. Surprising is, however, the rather minor effect of the initial turbulent boundary layer condition on the onset of separation. The latter can, nevertheless, be easily understood by considering the following mechanism [2]: When increasing the initial shape factor, the supersonic interaction length  $L^*$ , Section 4.5.3, increases rapidly, reducing the severity of the streamwise shock-induced pressure gradient. Since the onset of separation is dependent on  $\delta p/\delta x$ , a spread in the pressure rise due to the shock allows the boundary layer to delay the onset of separation, compensating the less filled profile.

#### Theory

Regarding theory, one may distinguish here between more empirically oriented theo-

ries, making direct use of a number of experimental observations, and more elaborate treatments of the interaction as, for instance, in the multiple deck methods already mentioned [8] [9] [17]. In the former category, Delery [2] developed a simplified theory based on the correlation law for the supersonic interaction length,  $L^*$ , Section 4.5.3. This approach rests on the assumption that (1) incipient separation occurs at the end of the supersonic part of the shock-induced compression, i.e., at the condition  $p_s = p^*$ , Fig. 25, already utilized in the experimental prediction of separation onset and that (2) the development of the dissipative layer through the compression to sonic conditions can be treated by the classical boundary layer equations using an algebraic eddy viscosity model (e.g., Ref. 35) to evaluate the Reynolds shear-stresses. The method, which accounts for changes in the initial boundary layer conditions, provides results in very close agreement with the experimental data discussed above, Figure 28.

Also presented in Fig. 28 are results obtained by Inger and Dean [36] using Inger's non-asymptotic triple deck theory of transonic shock boundary layer interaction [17] employing the definition  $c_f \rightarrow 0$  to determine incipient separation.

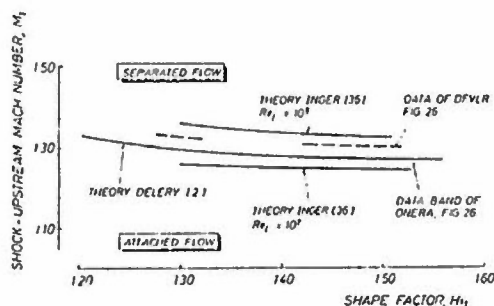


Figure 28: Theoretical predictions of incipient separation

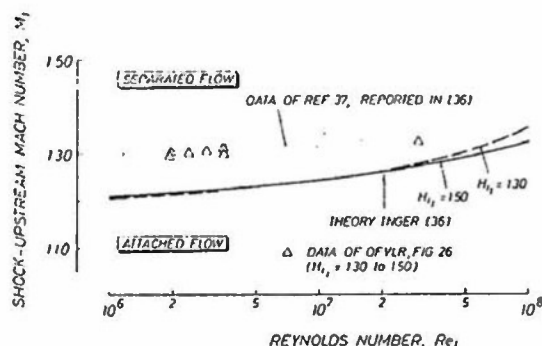


Figure 29: Reynolds number dependence of incipient separation

Main shock-upstream input parameters to the method are, as mentioned earlier, besides the Mach number  $M_1$ , the shape factor  $H_{11}$  and the Reynolds number based on the displacement thickness,  $R\delta_1^*$  (which can be related to an airfoil chord Reynolds number,  $Re_c$ , by an appropriate boundary layer computation), allowing the independent assessment of the influence of these parameters. It is observed that the theory predicts, at a constant Reynolds number, the same low dependence of the critical shock-upstream Mach number on shape factor as shown by the experiments and Delery's method. It predicts, however, also a pronounced influence of the Reynolds number,  $Re_c$ , at constant  $H_{11}$ . The latter effect is more clearly demonstrated in Figure 29 which also shows an experimental data band determined by a careful examination of a large number of transonic interaction tests [37]. Again, there is good qualitative agreement between the theoretical prediction and the experimental results. The consistent discrepancy in the level of the shock-upstream Mach number for incipient separation, also observed in Fig. 28, is, according to Ref. 36, mainly due to the shock-induced pressure rise being assumed to correspond to a normal shock at a given  $M_1$ , rather than to the oblique shock conditions observed in transonic experiments. Correcting for the shock obliquity provides a much better quantitative agreement with experiment [38].

It is stated by Inger in Ref. 39 that no consistent effect of the shape factor (at constant Reynolds number) on incipient separation conditions could be found in the results represented by the data band in Fig. 29, suggesting a possible dominant influence of the Reynolds number,  $Re_c$  (or  $R\delta_1^*$ ). This is somewhat contrary to the tendency depicted in Fig. 27 and the conclusion from it, viz., that incipient separation can be "mapped" in the  $H_{11} - M_1$  - plane and that the effect of the Reynolds number is, at least partly, accounted for by the shape factor. In the

"classical" turbulent boundary layer development, the shape factor is, of course, in non-equilibrium flow (see Section 4.4) not unique at separation and a second "form parameter", i.e., the Reynolds number based on the momentum thickness,  $R\theta$ , must, in addition, be considered [5]. In purely supersonic flow, Hayakawa and Squire [40] found that the overall pressure rise for incipient separation is directly proportional to the square root of the skin friction coefficient of the undisturbed boundary layer, a viscous parameter that can be expressed, for instance, by the form factor and  $R\theta$ .

Concerning the two parameters at separation, another aspect should be considered: It was shown that the upstream influence,  $L^*$ , depends on both the shape factor  $H_{11}$  and the displacement thickness  $\delta_1^*$  of the incoming boundary layer, Section 4.5.3. Since the shock imposed pressure

gradient  $\partial p/\partial x$  is, in turn, dependent on the upstream influence, both viscous parameters are likely to influence incipient separation. Furthermore, Holder et al. [41] have given evidence that the local shock-upstream Mach number required to generate the pressure rise for incipient separation depends on the post-shock expansion which is influenced by surface curvature and possibly by the displacement thickness of the incoming boundary layer, the latter altering, for one, the local effective curvature underneath the interaction [42] [43].

In the context of viscous simulation, the question as to the exact viscous parameter (s) that must be duplicated to achieve the "correct" full-scale incipient separation remains somewhat open. Here, some further research with a well designed transonic experiment is suggested. It seems, nevertheless - following the outline of the preceding paragraph and the results of Delery's theory for incipient separation, which is based on the upstream influence - that

- the correct simulation of the upstream influence by duplicating  $(\delta^*/c)(H_{11}-1)$  will also provide the desired full-scale separation onset. The latter will, in addition, be assured by the low sensitivity of incipient separation to the attendant viscous parameters.

#### Curvature effects

Curvature effects on incipient separation are a further matter of controversy, although of less importance in the present context since the simulation of the full-scale boundary layer development will result in the correct " $K \delta_1$ " (or  $R/\delta_1$ ), where  $K$  and  $R$  are the curvature and radius, respectively, of the surface underneath the interaction (local curvature). According to Inger's theory [36] [44], curvature in the range of interest, i.e.,  $0 \leq K \delta \leq 0.02$ , slightly spreads out the interaction, weakening the adverse pressure gradient along the wall, due, primarily, to the increased shape factor  $H_{11}$ . The resultant effect on incipient separation is indicated in Figure 30(a). It is noticed that, according to this theory, the influence of curvature is rather small, with increasing curvature delaying separation at the lower, but provoking an earlier separation at the higher Reynolds numbers. This is in accordance with the shape factor influence depicted in Fig. 29 indicating that at higher Reynolds numbers the effect of increasing the shape factor (less full boundary layer profiles) seems to prevail while at the lower Reynolds number the corresponding spreading of the interaction, hence reduction in  $\partial p/\partial x$ , seems to be of greater influence.

Calculations on shock boundary layer interaction, accounting for wall curvature, were also carried out by Bohning utilizing the theory of Bohning and Zierep [45], Figure 30(b). Here, the influence

of wall curvature is seen to be very pronounced at small surface radius, but becoming of the order predicted by Inger

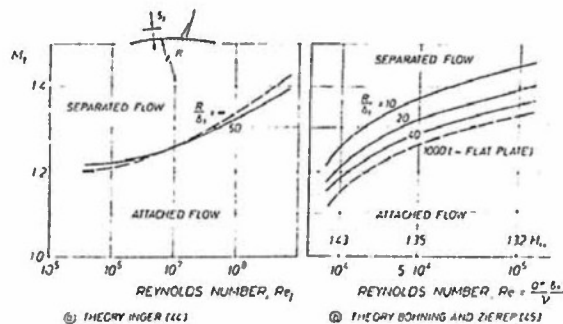


Figure 30: The effect of curvature on incipient separation, Ref. 2

when approaching values of interest here, i.e., curvatures encountered on airfoil or wing upper surfaces. The effect of curvature is here explained by the stronger post-shock expansion developing with increasing curvature which, as mentioned above, raises the shock-upstream Mach number  $M_1$  for a given pressure rise to incipient separation [41], an explanation not quite in accord with Inger's statement of a shape factor effect. Note, that Bohning also predicts a very strong Reynolds number (or shape factor) influence on incipient separation not experimentally observed.

Although, as mentioned, not necessarily required in the present context, new experiments seem in order to clearly establish the effect of wall curvature on shock boundary layer interaction, especially with regard to details of the mechanisms involved.

#### 4.5.4.2 Three-dimensional shock-induced incipient separation

Three-dimensional shock-induced incipient separation may be taken to occur when the skin-friction lines just merge into a single common line essentially parallel to the outer inviscid shock position, Figs. 8 and 31. Inger, employing this definition in his analytical investigation of swept-shock turbulent boundary layer interaction (see Section 4.5.3 [29]), shows that this is equivalent to the vanishing of the total normal wall shear stress component indicating that the process must be quite similar to the one in two-dimensional flow, dominated, at least up to moderate sweep angles, by the same parameters. The relative influence of the sweep angle on incipient separation, as predicted by this theory, is shown in Figure 32 for a straight swept shock and an approach Mach number of  $M_1 = 2.0$ . One notices that the pressure rise to sepa-

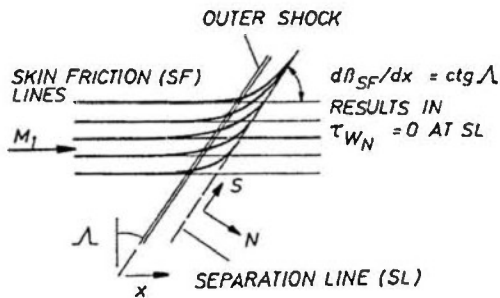


Figure 31: Three-dimensional incipient separation, Ref. 29

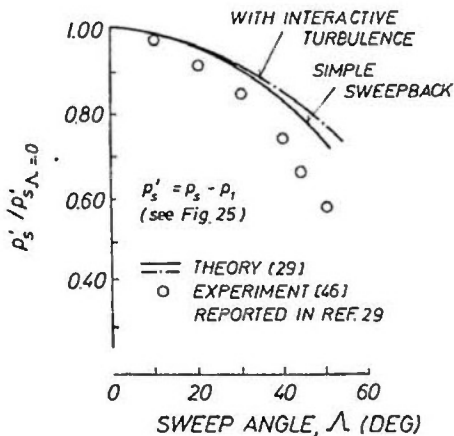


Figure 32: Sweepback effect on incipient separation ( $M_1 = 2.0$ )

ration, i.e.,  $p'_s = p_s - p_1$  (see Fig. 25), gradually decreases with increasing sweepback, in general agreement with the experimental results shown [46]. A similar, but weaker dependence on sweep is predicted for lower shock-upstream Mach numbers. Korkegi [47] also recognizes a reduction in the critical shock-upstream Mach number  $M_1'$  based on a simple correlation whereby the pressure ratio at incipient separation is  $p_s/p_1 = 1.5$  and the component of the Mach number normal to the shock is constant,  $M_{1N}' = 1.2$ , virtually independent of the shock-upstream Mach number  $M_1$  and the Reynolds number. This correlation holds, however, only for large sweep angles, i.e.,  $M_1 \gg 1.0$ .

For the sake of demonstrating the possible magnitude of a reduction in the critical shock-upstream Mach number due to sweep at transonic conditions, it is assumed that (1) the dependence  $p'_s / p'_{s\Lambda=0}$  of Fig. 32 is still valid (approximately) at the lower shock-upstream Mach number of  $M_1 = 1.30$  and that (2) the pressure at separation corresponds, as in the two-dimensional case, to sonic conditions, i.e.,  $p'_s = p^* - p$ . At a sweep angle of  $\Lambda = 30$  degrees, these assumptions lead to a critical "normal" shock-upstream Mach number of  $M_{1N} = 1.280$ , a rather small reduction in the critical Mach number at this relatively large "local" sweepback.

The small effect of sweep on shock-induced incipient separation, certain at moderate sweep angles, indicates that the two-dimensional results, discussed in the preceding section, may directly be transferred to three-dimensional flows. This holds, of course, also for the open questions suggesting that the required two-dimensional experiments be supplemented by appropriate three-dimensional tests with the additional objective of confirming the relation between two- and three-dimensional shock-boundary layer interactions for transonic flows.

#### 4.5.5 Development of Shock-induced Separation and Reattachment

It was indicated in the preceding section that there may exist a certain margin in angle of attack or freestream Mach number between the onset of separation (incipient separation) and the occurrence of total separation, i.e., separation stretching from the foot of the shock to the trailing edge. It is believed that this development of separation is Reynolds number sensitive, hence must be simulated in low Reynolds number wind tunnel tests. The correct full-scale simulation is important since this development determines the margin in freestream conditions between incipient separation and buffet onset and maximum lift.

In transonic flow the local development leading up to shock-induced separation is a purely supersonic process, following the "free interaction" principle [2] [48]. This means that the pressure distribution from just upstream of the shock to the separation pressure  $p_s$  is only dependent on viscous and inviscid parameters of the incoming flow and not affected by the form and extent of the downstream separated region or the agency provoking separation. The simulation of the pressure distribution leading to separation follows, therefore, the same rules as the simulation of the upstream influence treated in Section 4.5.3. The development of the separation bubble with increasing freestream Mach number or incidence is, on the other hand, dependent on the geometric conditions downstream of the shock - consider forward facing steps, compression corners, flat plates or airfoils and wings - so that it is not possible to define a simple and universal scaling law as in the case of the forward influence and incipient separation; however, if one restricts oneself to transonic flow on airfoils and wings, it should at least be possible to determine the essential parameters governing the development of the shock-induced separation bubble and establish, for these closely similar configurations, the proper viscous simulation parameters.



#### 4.5.5.1 The development of separation and possible scaling parameters derived from the airfoil data of Ref. 5

It seems appropriate to consider first in somewhat more detail the development of shock-induced separation as it occurs on a transonic airfoil with increasing angle of incidence for a given freestream Mach number and Reynolds number, Figure 33. Shown in Fig. 33a is the attendant upper surface Mach number distribution as it evolves with increasing incidence. Note-worthy is here the plateau-type pressure distribution, the increasing shock-upstream Mach number in a range between  $M_1 = 1.25$  and  $1.35$ , embracing the onset of shock-induced separation, and the change in the Mach number distribution in the vicinity of the shock and the trailing edge as separation develops. Note, that the distribution for the highest  $M_1$  corresponds to a condition close to maximum lift as shown in the inset to Fig. 33a. Also note the point "R", which indicates the onset of the severe rear adverse pressure gradients [23]. We will refer back to this point below.

The development of separation with increasing  $M_1$  is again demonstrated by employing the chordwise distribution of the shape parameter  $H_{32} = \delta^{**}/\theta$ , Fig. 33b. Characteristic chordwise locations, such as the shock-associated separation point, the bubble reattachment point and the trailing edge separation location, are taken from this figure and plotted together with the shock location as function of the angle of incidence,  $\alpha$ , in Fig. 33c. The following development is indicated, with increasing incidence (or shock-upstream Mach number): At first a rear separation develops - possibly even before a shock wave forms on the upper surface - becoming stagnant just prior to the emergence of a shock-induced separation bubble. The latter forms and spreads downstream with increasing  $\alpha$  without, at first, affecting the location of the rear separation line. As the bubble growth continues, shifting reattachment closer towards this separation line, the boundary layer recovery is no longer sufficient to halt the development of rear separation and the latter spreads rapidly upstream to meet the shock-induced bubble at an angle of attack corresponding closely to the one for maximum lift. Note, that the increase in incidence between the onset of shock-induced separation and total separation amounts to about  $\Delta\alpha = 1^\circ$ . The following characteristics should, in the light of later discussions, be considered now:

1. Fulker and Ashill [23] observed that once the shock associated reattachment line reaches the chordwise position "R", i.e., the beginning of the steep rear pressure rise, the bubble "explodes", leading instantly to total separation, if the shock-upstream Mach number is

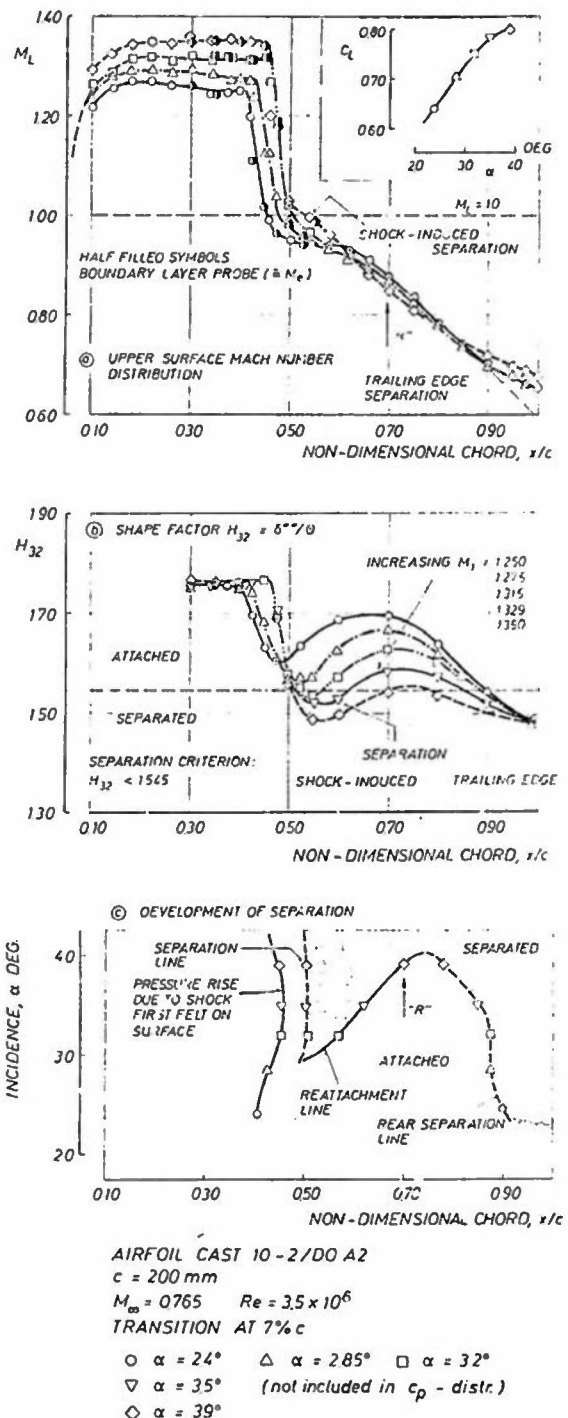


Figure 33: Development of separated regions, Ref. 5

increased by a small amount. Fig. 33c seems to confirm this observation; however, it is not certain whether the final breakdown of the flow is due to the rapid advance in shock-induced separation or rear separation or both. Here, this consideration is, of course, somewhat academic; nevertheless, there might be consequences for the entire viscous simulation process in cases where rear separation

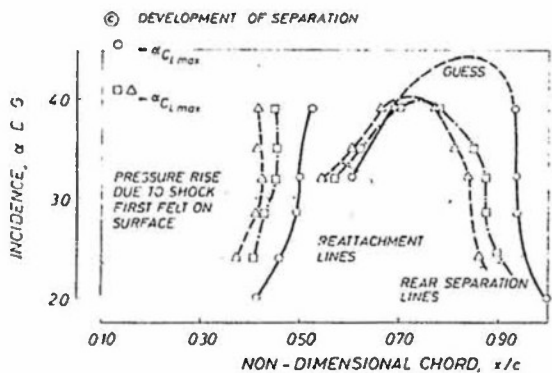
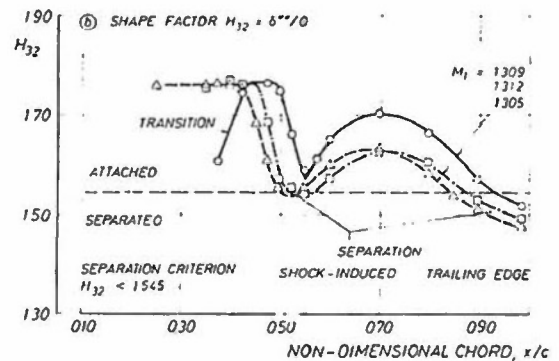
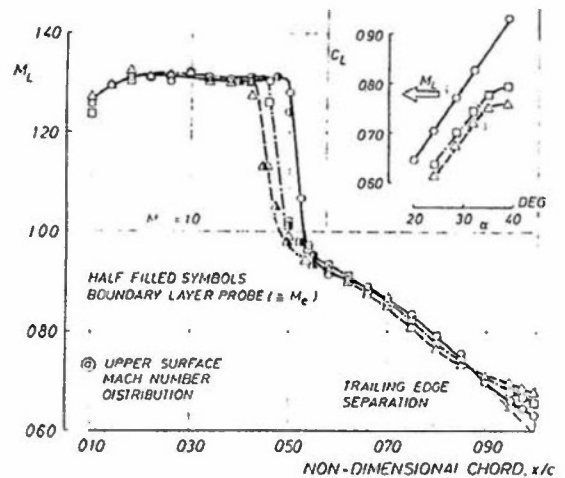
ration rushes over the point (or line) "R" before the separation bubble reaches it. For one, the scaling concept of Ref. 23, which will be addressed later, may no longer be applicable. On the other hand, such a situation may never arise for practical wing designs, at least not at high Reynolds numbers, since shock boundary layer interaction and a certain growth of the associated separation bubble may be needed to trigger the rapid rear separation development.

2. It was already mentioned in Section 4.5.2.1 that the increased turbulence generation associated with shock-induced separation may have a positive influence on the development of rear separation. Further evidence of this phenomenon is given here by the delay in the spread of rear separation as soon as a shock-induced separated region develops (also see Section 4.5.6).

The question to be answered now is how viscous effects will influence the development of both shock-induced and rear separation. To demonstrate this influence, plots similar to the ones of Fig. 33 but for different initial boundary layer conditions, the latter obtained by varying Reynolds number and transition location, are employed. Since it is, for the sake of clarity, not sensible to present all chordwise pressure and shape parameter distributions from which the bubble and rear separation growths were derived, these distributions shall only be considered for one instant in the development of separation, selecting a condition of nearly identical Mach number distributions upstream of the shock, Figures 34a and b. One notices that the flow in the test cases considered is, in accordance with what was said about the dependence of incipient separation on viscous effects, close to separation, with the forward-tripped boundary layer, however, already showing small shock-induced separation bubbles. Regarding the overall state in the boundary layer development, it is indicated that the recovery of the dissipative layer downstream of the shock is much better for the conditions of the aft-tripped thinner boundary layer and that the spread of rear separation is consequently delayed.

To show directly the effect of the initial shock-upstream boundary layer conditions on the growth of the separated regions, characteristic chordwise positions, extracted from plots similar to the ones of Fig. 34b, are again plotted versus the angle of incidence, Fig. 34c. The following general observations can be made:

1. The thinner boundary layer exhibits a noticeably slower growth of the shock-induced separation bubble with increasing angle of incidence. This growth seems to become more rapid as the formerly defined point "R" is exceeded; however, this does not seem to occur in an explosive fashion. Note, that the incidence for maximum lift



AIRFOIL CAST 10-2/DOA2  
 $c = 200 \text{ mm}$   
 $M_\infty = 0.765$

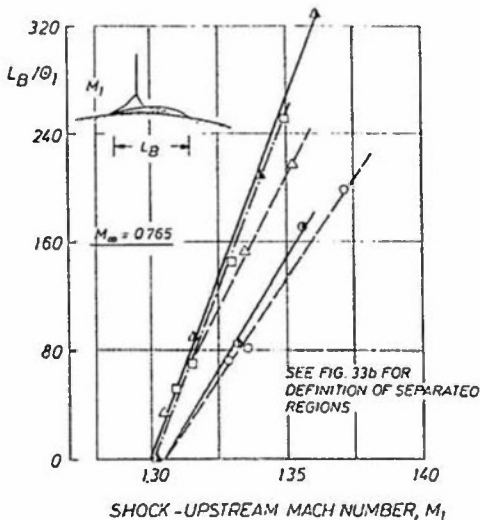
SHOCK-UPSTREAM					
	$Rex \cdot 10^{-6}$	TRANSITION	$\delta_1^*$	$O_1$	$H_{11}$
○	195	30% c	0.220	0.096	150
△	194	7% c	0.340	0.148	146
□	350	7% c	0.350	0.156	144
			mm	mm	

Figure 34: Viscous effects on the development of separation, Ref. 5

is in the case of the thinner initial boundary layer approximately one degree higher than for the forward-tripped thick boundary layer.

2. For the thinner initial boundary layer, a relatively small (5 % c) rear separated region develops initially. This region is stationary up to the highest angle of attack investigated. Whether rear separation spreads upstream as the incidence is further increased remains uncertain; however, it should be noted that in the case of the airfoil CAST 7, which exhibits a smaller rear adverse pressure gradient, rear separation did not occur at all for the aft-tripped initial boundary layer condition (see Fig. 6). In any event, the development of separation is at these conditions directly shock dominated.

The normalized extent of the shock-induced separation bubble, of main concern here, dependent on the shock-upstream Mach number and the initial boundary layer condition is shown in Figure 35 for the airfoils CAST 7 and CAST 10-2 [5]. It is indicated that both airfoils, having similar upper surface contours, at least upstream of the trailing edge region ( $x/c < 0.75$ ), exhibit similar bubble developments, Fig. 35a: The onset of separation occurs for all conditions, as already shown in Section 4.5.4, close to a shock-upstream Mach number of  $M_1 = 1.30$  and an essentially linear bubble development with increasing  $M_1$  ensues which seems to continue to the bubble "blow-up". Also clearly noticeable is the slower progression in the bubble development for the aft-tripped thinner boundary layers.



② EFFECT OF  $M_1$  AND INITIAL BOUNDARY LAYER CONDITIONS ON  $L_B/O_1$

	$Re \times 10^{-6}$	TRANS	$\delta_1^*$	$\theta_1$	$H_{11}$	AIRFOIL
○	195	30% c	0.22	0.096	1.50	CAST 10-2
△	194	7% c	0.34	0.148	1.46	c = 200mm
□	350	7% c	0.35	0.156	1.44	
◐	290	30% c	0.27	0.127	1.44	CAST 7
△	240	7% c	0.42	0.181	1.42	c = 250mm

Note: The boundary layer parameters are averages corresponding to the data points of a specific curve

Figure 35: Extent of the shock-induced separation bubble, Ref. 5

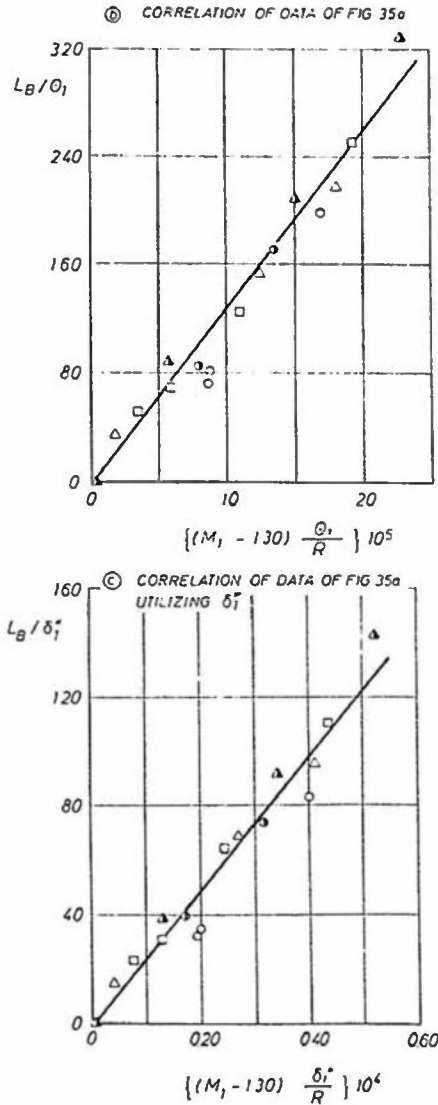


Figure 35: Concluded

In an attempt to correlate the results of the bubble extent and to mark the major influence parameters, a correlation parameter was derived empirically consisting of the shock-upstream Mach number in the form  $(M_1 - 1.30)$  - to account for the dominant influence of this Mach number and the onset of separation - and the initial momentum thickness, non-dimensionalized by the average upper surface contour radius between shock and trailing edge. The non-dimensional bubble extent,  $L_B/O_1$ , is plotted as function of this parameter in Fig. 35b. One observes that this type of correlation provides a rather satisfactory alignment of the experimental results.

It should be noted that, contrary to the simulation parameter for the upstream influence which contains the displacement thickness, the momentum thickness was utilized here since the bubble extent was found to also depend on the reciprocal of



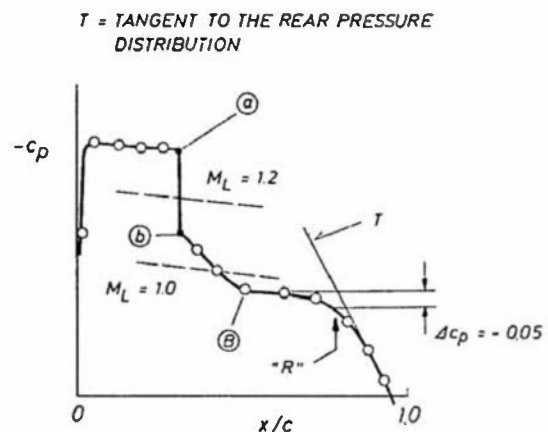
the shape factor (also see Fig. 35c). It must, furthermore, be pointed out that the average contour radius,  $R$ , as defined here, is first of all considered as a measure of the pressure gradient between shock and trailing edge and only secondly as representing the effect of curvature itself. Hence, the correlation is mainly restricted to the configurations and conditions it was derived for and does not warrant the conclusion, although implied by the correlation parameter, that the bubble extent goes to zero when the radius goes to infinity. Concerning the viscous simulation process, the correlation suggests, irrespective of any other conclusion, that

- the duplication of the high Reynolds number momentum thickness  $\theta_1/c$  upstream of the shock will essentially result in a bubble development very similar to the full-scale one. It is believed that the Reynolds number does not enter this correlation directly because the chord-wise distance downstream of the shock over which the effect of the Reynolds number on any boundary layer growth parameter can act is too short (see, for instance, Fig. 20a).

These conclusions are based on one set of data within a rather narrow Reynolds number range, hence further evidence must be obtained to substantiate them. It is, for the same reason, prudent to look at a different approach to the scaling of separated flows over airfoils and wings, here the one of Fulker and Ashill, already variously cited [23]. Their results are compared with the data discussed above. The arguments of these authors are given here in somewhat more detail since they also apply, in part, to the above discussion.

#### 4.5.5.2 The correlation of Fulker and Ashill

Considered is the flow over the outboard region of swept wings where a single shock is present and the flow is quasi-two-dimensional, except possibly in the immediate vicinity of the wing tip. (Needless to say that such considerations are strictly true for airfoil flow.) It is assumed that the flow development is such that the spread of the shock-induced separation bubble is not notably influenced by an interaction with rear separation and that the development of shock-induced separation is as follows: As the incidence is increased, the shock becomes strong enough to cause the development of a bubble. The reattachment point of the bubble 'B' is upstream of the point 'R' already defined, Figure 36. As the shock gains in strength, the bubble grows until 'B' reaches a point at or close to the position 'R' where the bubble bursts, giving rise to the flow break down. For configurations for which this flow model holds, the full-scale separated flow development can, as will be shown later, be simulated



Note: (a) and (b) correspond to the present subscripts 1, upstream of shock, and S, at separation, respectively (also see Figs. 4 and 25)

Figure 36: Characteristic chord locations defined in Ref. 23

by duplicating the bubble extent in the low Reynolds number wind tunnel tests. To do so, it is, of course, first necessary to establish a relation between the dominating viscous and outer flow parameters and the bubble extent.

In deriving such a relation, it is assumed that the bubble length,  $L_B$ , is independent of the streamwise static pressure gradient downstream of the bubble - contrary to the correlation of the previous section - and that, in addition, surface curvature does not affect the flow within the bubble. Thus bubble length may be supposed to depend on the flow conditions at the point 'a', Fig. 36, (or '1', to stay with the present notation) just ahead of the shock. The boundary layer state is, under the condition of only mild pressure gradients ahead of the shock, at this point essentially defined by the momentum thickness  $\theta_1$  and the momentum thickness Reynolds number  $Re_{\theta_1} = u_{\theta_1} \theta_1 / \nu_1$ . The outer inviscid flow is defined by the Mach number  $M_1$ . This leads by "dimensional analysis" [23] to an expression for the bubble length scale of

$$L_B/\theta_1 = f(M_1, Re_{\theta_1}).$$

For swept wing flow of quasi-two-dimensional character,  $M_1$  is interpreted as the Mach number component normal to the shock and  $\theta_1$  is taken to be the momentum thickness of the flow in the direction of the external streamlines by analogy between the latter and a corresponding two-dimensional flow [49] (also see Section 4.5.3, Upstream Influence).

A large number of data, obtained in tests with two wings of moderate sweepback ( $<30^\circ$ ) and of aspect ratio 8 and with a

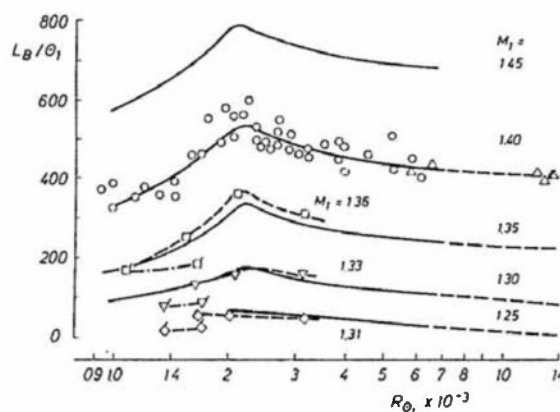
number of airfoils in a Reynolds number range up to  $Re_\infty = 20 \times 10^6$ , was analysed with regard to the bubble development. In these tests, transition was fixed near the upper surface leading edge and, for one wing, at various locations further downstream to study the effect of varying boundary layer thickness at the shock without varying Reynolds number. The bubble length was inferred from the static pressure distributions, as described in Ref. 50.  $\theta_1$  and  $R_{\theta_1}$  determined from these pressure distributions by an infinite yawed-wing version [49] of the lag-entrainment method of Green [51].

The result of the analysis of Fulker and Ashill is depicted in Figure 37 for various shock-upstream Mach numbers  $M_1$ .<sup>1)</sup> Also given in this figure are results corresponding to Figs. 33 through 35 [5]. The data correlation and the comparison of the two sets of data allow the following observations:

1. The data for the airfoils are consistent with those for the swept wings considered, indicating that sweep effects are well represented in the range of shock sweeps investigated ( $0 - 25^\circ$ ) which is in agreement with earlier findings concerning the upstream influence (see Fig. 23). The airfoil data of Ref. 23 extend the correlation up to  $R_{\theta_1} = 14 \times 10^6$ , typical of cruise conditions on the outer wing of a transonic transport aircraft with a mean-chord Reynolds number of  $Re_\infty = 30 \times 10^6$ .

2. The agreement between the results of Ref. 5 and Ref. 23 is quite satisfactory, especially in the qualitative behavior, which shows very little effect of  $R_{\theta_1}$  on the bubble extent at low shock-upstream Mach numbers - indicative of the independence of the onset of separation on viscous conditions - and a pronounced maximum in the bubble length scale at the higher shock-upstream Mach numbers at  $R_{\theta_1} = 2.1 \times 10^6$  independent of  $M_1$ . It is argued by Fulker and Ashill, following Green [52], that the existence of a maximum is related to a change in character with Reynolds number of the velocity profiles of turbulent boundary layers on flat plates. These velocity profiles conform to similarity rules in such a way that they become more resistant to separation as Reynolds number increases. Below a value of about  $R_{\theta_1} = 2 \times 10^3$  to  $5 \times 10^3$ , the similarity rules no longer apply and the profiles become increasingly "full", i.e., resistant to separation, as Reynolds number decreases. Although incipient separation was shown to be fairly independent of viscous effects, at least in the Mach number range considered, the "fullness" of the initial boundary layer profile may,

<sup>1)</sup> The actual measured data points are, for clarity reasons, only shown for  $M_1 = 1.40$ ; the curves represent least square fits through the measured data points.



RESULTS OF REF 23

△ AIRFOIL DATA ○ SWEEP WING DATA — CURVE FITS THROUGH DATA  
NOTE:  $\times 10^6$  OF FIG 36

PRESENT AIRFOIL RESULTS (FIG 35)

□  $M_1 = 1.36$  ▽  $M_1 = 1.33$  ◇  $M_1 = 1.31$

FLAGGED SYMBOLS DENOTE TRANSITION AT 30% CHORD

Figure 37: Correlation of extent of shock-induced separated regions, Ref. 23

nevertheless, be responsible for the rate in the bubble development following incipient separation. One must pursue this matter somewhat further.

3. The data of Ref. 5 obtained with the transition strip located at 30 % chord, denoted by flagged symbols, show at the same  $R_{\theta_1}$  consistently lower values of the normalized bubble extent. The data of Ref. 23 were also partly obtained in tests with different trip locations and the effect of shifting transition at constant Reynolds number may well be hidden in the scatter of the data. One may therefore conclude that the overall evidence is not completely consistent that  $Re$  is a sufficient parameter for the viscous simulation process considered and that further research is warranted.

The comparison between the data of Ref. 5 and Ref. 23 shows some further quantitative disagreement. Firstly, the extent of the bubble is, especially at the lower shock-upstream Mach numbers, less in the case of Ref. 5. Secondly, a separation bubble of certain extent is already indicated by the data of Ref. 23 at a shock-upstream Mach number as low as  $M_1 = 1.25$ , i.e., incipient separation must occur much earlier than indicated either by the results of Ref. 5 or the ONERA data depicted in Fig. 27. The better agreement in bubble extent at the higher shock-upstream Mach numbers suggests that the discrepancy at the lower Mach numbers may be a consequence of the different ways in which incipient separation and the extent of the bubble were determined. Some evidence that also for the results of Fulker and Ashill the boundary for incipient separation may be higher is given by these results themselves; this is outlined below.

Fulker and Ashill have correlated the pressure rise across the shock represented by the Mach number ratio  $M_0/M_b$  ( $\equiv M_1/M_5$ ), where  $M_0$  is the Mach number just upstream of the shock and  $M_b$  is the Mach number at the end of the "linear" surface pressure rise due to the shock, Fig. 36. Figure 38 shows this Mach number ratio as function of the momentum thickness Reynolds number for the results of Ref. 23 and Ref. 5. It can be seen that  $R_{\theta_1}$  represents an excellent correlation parameter for both sets of data; however, the airfoil data of Ref. 5 exhibit consistently lower Mach number ratios. There is, at present, no explanation for this discrepancy except that it is difficult to determine the correct value of  $M$  if only a limited number of pressure orifices is available.

The results of Fig. 38 may be considered as a further correlation of viscous effects on incipient separation: It was pointed out earlier (see Figs. 4 and 25) that incipient separation occurs as soon as the pressure  $p_s$  (here  $p_b$ ) reaches, with increasing shock-upstream Mach number, sonic conditions, i.e.,  $M_b = 1$ . The Mach number ratio is at these conditions equal to the shock-upstream Mach number  $M_1$ . Fig. 38 thus represents the dependence of incipient separation on the viscous parameter  $R_{\theta_1}$ . The results of Fig. 38 confirm the low dependence of the critical shock-upstream Mach number on viscous effects. The relatively high values of  $M_0/M_b$  suggest furthermore that the indication of a separation bubble at  $M_1 = 1.25$  in Fig. 37 may be erroneous.

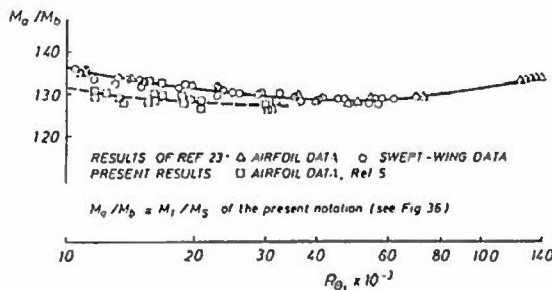


Figure 38: Correlation of pressure rise across the shock, Ref. 23

#### Simulation of full-scale separated flow:

The correlation of the bubble extent in Fig. 37 may, as mentioned above, be used as basis for simulating full-scale separated flow in low Reynolds number wind tunnel tests. Assuming that the shock location and the shock-upstream pressure distribution correspond to full-scale conditions - which they will if the downstream boundary layer development is correct - it is only required to duplicate the full-scale bubble length,  $L_B/c$ , in these wind tunnel tests. The required trip location - assuming that the viscous simulation may be achieved by aft-tripping - can be determined as follows: "Full-scale"

is, for example, for a given freestream condition, taken to correspond to  $Re_\infty = 30 \times 10^6$  with transition occurring at 1% chord. Calculating the full-scale boundary layer development up to the shock, for instance, by the method of Ref. 51, one obtains  $\theta_1$  and  $R_{\theta_1}$  and, via the correlation of Fig. 37,  $L_B/c$ . For the wind tunnel model, the bubble extent  $L_B/c$  can be determined in a similar way as function of the transition location and the Reynolds number range possible in the wind tunnel and presented in form of a carpet-plot  $L_B/c = f(Re_\infty, x/c_{TRANS})$ . The conditions required to duplicate the full-scale  $L_B/c$  can be selected from this plot. The results of such a simulation effort are presented in Figure 39: The separated flow region at the specific freestream conditions of Fig. 39 and a chord Reynolds number of  $Re_\infty = 30 \times 10^6$ , hence most likely also the development of the separation bubble with increasing  $M_1$ , can be simulated either by a transition trip location of  $x/c = 0.15$  and a Reynolds number of  $Re_\infty = 13 \times 10^6$  or, alternatively, by a trip location of  $x/c = 0.30$  and a Reynolds number of  $Re_\infty = 5 \times 10^6$ . The excellent agreement of the pressure distributions for these conditions is taken as evidence of the satisfactory performance of the present simulation procedure.

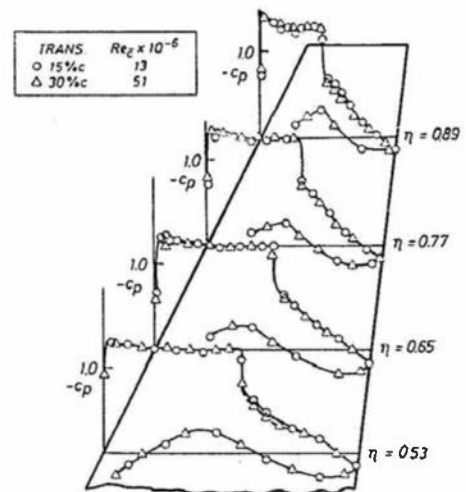


Figure 39: Independent simulation of 'full-scale' pressure distributions at  $M_\infty = 0.780$ ,  $C_L = 0.70$  for a three-dimensional (outer) wing, Ref. 23

#### 4.5.5.3 Change in global boundary layer parameters across the interaction and the simulation of trailing edge flow

For the simulation of the overall flow development, it is important to determine and simulate the conditions in the vicinity of the trailing edge. This, in turn, requires the knowledge of the magnitude of dominant viscous parameters either immediately downstream of the shock - if there is no shock-induced separation - or

at the reattachment point of the separation bubble. In the "belief" that computational methods are not yet able to predict the changes in boundary layer parameters across the shock, at least not in the presence of large separated regions, and also out of curiosity, an attempt was made to correlate the data of Ref. 5 accordingly. The result is depicted in Figure 40 for the ratio of the momentum thickness across the interaction,  $\theta_R/\theta_1$ , where  $\theta_R$  is the momentum thickness either immediately downstream of the shock or at the reattachment point, respectively. The correlation parameter again contains the shock-upstream Mach number in the form ( $M_1 - 1.30$ ), for reasons outlined before, and  $\theta_1$  in the case of attached flow and the normalized extent of the separation bubble,  $L_B/\theta_1$ , for separated flow. One notices, besides the good correlation of the data, that the effect of the shock-upstream Mach number on the momentum thickness ratio is, in the range considered, small in the absence of separation but becomes very pronounced due to the development of separation. Concerning the viscous simulation process, it seems that matching  $\theta_1$  (actually  $\theta_1/c$ ) and bubble length will provide the correct global conditions immediately downstream of the shock boundary layer interaction region. This is likely to hold for other boundary layer thickness parameters as well. The Reynolds number does, for reasons outlined in conjunction with the simulation of the bubble extent, not enter this correlation. The conditions downstream of the interaction may be used as the initial values

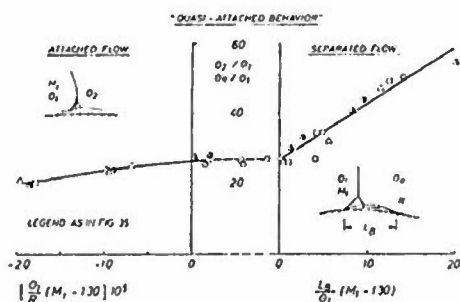


Figure 40: Change in momentum thickness across the shock boundary layer interaction region, Ref. 5

in the treatment of trailing edge flow (see Section 4.6).

Concerning the simulation of trailing edge flow, the following remarks seem in order here since this simulation is, at transonic speeds, so closely related to shock boundary layer interaction:

1. The correct viscous simulation of shock boundary layer interaction in the absence of shock-induced separation by scaling the upstream influence (duplicating  $\delta_1^*$  ( $M_1 - 1$ )) seems to lead to a close approximation of the full-scale trailing

edge flow development, unless the trailing edge flow is, at full-scale conditions, very near separation. This is indicated in Figs. 19 and 20 by the simulation of the high Reynolds number flow on the CAST 10-2 airfoil. Note, that this "successful" simulation occurs in spite of the relatively severe adverse pressure gradients on CAST 10-2. Of course, how close details of the trailing edge flow, e.g., the displacement thickness or the angle of the flow leaving the trailing edge, which depends on the energy balance between the upper and lower surface boundary layers [53], are - or must be - matched, is unknown and should be investigated.

2. The above statements are most likely also valid for the condition of incipient separation

3. The Fulker and Ashill correlation of bubble extent seems, judging from Fig. 39, to lead to the correct simulation of full-scale conditions, including trailing edge flow, in the absence of trailing edge separation. This probably also holds for the condition of flow break-down. However, a somewhat more detailed experiment, including boundary layer measurements and possibly a configuration with more severe rear adverse pressure gradients, should still be carried out to determine the limits of applicability. Regarding the bubble development, one must furthermore investigate, why the aft-tripped thin boundary layer bubble extent in the case of the Ref. 5-data does not follow quantitatively the above correlation, i.e., the uniqueness of  $R_0$  as a correlation parameter must be substantiated in a suitable experiment. In addition, experiments, covering a wider range of viscous conditions, should be performed to qualify the scaling parameter derived from the results of Ref. 5 and to establish its ability to approximate full-scale trailing edge flow, still assuming the latter to be attached.

4. It is not at all established whether the correct simulation of the shock boundary layer interaction process will automatically result in the correct - or sufficiently close - simulation of trailing edge flow in the presence of trailing edge separation at full-scale conditions. Certain is that the former will affect the trailing edge flow "in the right direction". Specific experimental and theoretical studies are, however, required to determine the degree to which this flow can be approximated by simulating the shock boundary layer interaction properly or whether a second (rear)manipulator is required.

There remains one more subject, also very important to the scaling of trailing edge flow, to be covered before summarizing: The generation and possible amplification of turbulence due to the interaction of the boundary layer with a shock whose potential influence on the downstream flow



development was pointed out repeatedly during the preceding discussions.

#### 4.5.6 Turbulence Generation/Amplification due to Shock Boundary Layer Interaction

The shock boundary layer interaction region is, especially in the presence of separation, for one, characterized by large turbulent fluctuations. These may lead, due to an increased turbulent mixing, to "fuller" boundary layer profiles downstream of the interaction as the interaction grows more severe. This phenomenon will possibly not pose a direct problem to the viscous simulation process since the full-scale behavior is likely to be matched if the correct shock-induced bubble development is ensured; still some further analysis of this situation should be carried out. There may, however, arise certain consequences for viscous simulation should the shock boundary layer interaction process act as a strong amplifier to the initial turbulence contained in the boundary layer either due to an increased freestream turbulence or generated by a tripping device. If such amplification is significant in comparison to the self-generation, one must ensure that in the low Reynolds number wind tunnel tests the 'correct' turbulence level (and structure?) prevails.

##### 4.5.6.1 Turbulence generation

Here, we shall consider specific turbulence properties coupled with shock boundary layer interaction to gain some understanding of the turbulence generation - and turbulence persistence downstream - and its importance to the subsequent flow development. For that purpose, the interaction phenomenon is assumed 'steady' in the sense that large scale unsteadiness with large shock motions (e.g., buffet) is absent. Following Ref. 2, we shall employ the kinetic energy  $k = 0.5 (\bar{u}'^2 + \bar{v}'^2 + \bar{w}'^2)$  and the non-dimensional effective Reynolds shear stress  $(-\bar{u}'v')/a_1^2$ , where  $a_1$  is the speed of sound at stagnation conditions, to study the turbulence behavior within and downstream of the interaction region, Figure 41. The turbulence data were obtained from LDA-measurements on a bump model (set-up similar to Fig. 11) at shock-upstream Mach numbers corresponding to incipient separation and separated flow with a relatively large separation bubble. Depicted in Fig. 41 are the maxima of the above parameters in  $y/c$ , i.e., the direction normal to the surface, as function of the normalized streamwise distance.

The plots of Fig. 41 demonstrate that there exists a large production of turbulence in the initial part of the interaction, i.e., in the vicinity of the foot of the shock. This production increases considerably with the advent of separation and streamwise maxima occur in the kinetic energy and shear stress levels which reach

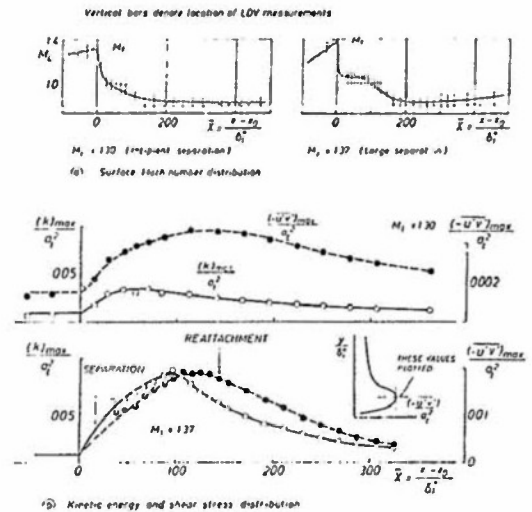


Figure 41: Streamwise development of maximum kinetic energy and shear stress (bump model similar to Fig. 11), Ref. 2

8 to 10 times the levels of the undisturbed boundary layer. One notices, furthermore, that in the presence of separation the maxima are located somewhat upstream of reattachment and that the decreasing turbulence intensity only reaches flat-plate levels after a distance of approximately 150 initial boundary layer displacement thicknesses ( $\delta^*$ ) downstream of reattachment. If one transfers these results to the separated flow conditions on the airfoil CAST 10-2, Fig. 34c, one observes that, with the reattachment point of the shock-induced bubble assumed at  $x/c = 0.60$ , higher turbulence levels would persist down to a chord position of  $x/c = 0.85$  - which corresponds to the location of the "stagnant" rear separation point for the case considered. It is judged that the trailing edge flow must be favorably affected by such a development; however, adequate tests are needed to directly show this type of influence.

##### 4.5.6.2 Turbulence amplification

Anyiwo and Bushnell [54] have identified three primary turbulence amplifier-generator mechanisms and shown, by linear analysis, that these may be responsible for turbulence amplifications across a shock wave in excess of 100 % of the incident turbulence intensity. These mechanisms are

- the direct turbulence amplification, by which turbulence incident upon a shock wave can be amplified by up to 30 % across the shock,
- turbulence generation from acoustic and entropy fluctuation modes incident on a shock, which can generate vorticity fluctuation levels of up to 50 % of the intensity of the incident mode, and

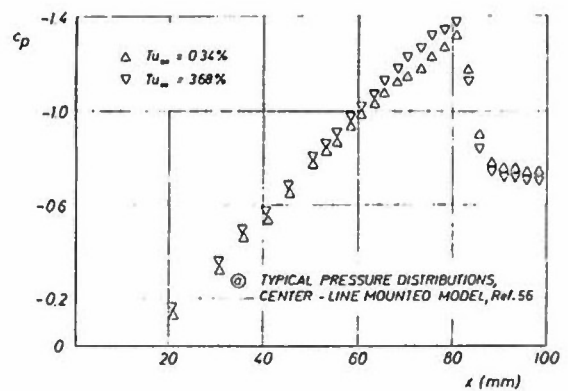
- turbulence 'pumping' by externally driven shock oscillations which may generate, at transonic speeds, turbulence of intensity in excess of 150 % of the shock oscillation intensity.

Considering the turbulence generated in the separated shock boundary layer interaction region of Fig. 41, which is in excess of 400 % of the initial turbulence level, one may certainly neglect the direct turbulence amplification of 30 %. Concerning the turbulence generation from acoustic fluctuations, it is shown in Ref. 55 that pressure fluctuations up to  $\bar{p}/q = 0.015$  have essentially no effect on the maximum turbulence intensity in the separated boundary layer and that the "freestream" turbulence level downstream of the shock is not at all affected by these pressure fluctuations. The influence of self-induced shock oscillations - in the comparison wind tunnel and flight- remains to be studied.

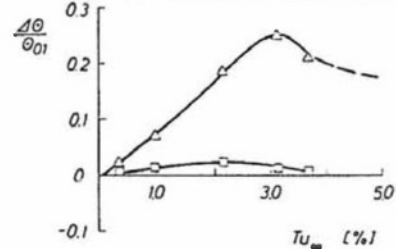
There are, as indicated by the generality of the above statements, no experiments directly aimed at the understanding of the turbulence amplification/generation process in transonic shock boundary layer interactions and its importance to trailing edge flow development. We shall, therefore, consider here, in lieu, briefly one study of wind tunnel environmental effects [56][57] and try to draw some conclusions concerning the possible influence of turbulence amplification. This study was carried out on bi-convex airfoils and "bump" models for free and fixed transition. We will restrict ourselves here to the fixed transition case (also see Section 4.8).

Keeping transition fixed, e.g., by roughness elements, the turbulent boundary layer development upstream of the shock will be dependent on the tunnel turbulence level. This is shown in Figure 42 by the change in shock-upstream momentum thickness for the flow about the bi-convex airfoil and the wall-mounted bump model [56]. It is observed that in the case of the low Reynolds number tests, the effect of the freestream turbulence level is small and, considering the direct influence of  $R_{\theta_1}$  on the extent of the shock-induced separation bubble in Fig. 37, most likely of no consequence to the simulation of shock boundary layer interaction or the downstream flow development. At the higher momentum thickness Reynolds numbers (bump model), a very pronounced influence is, however, evident, although only at turbulence levels far beyond the ones present in contemporary transonic wind tunnels. (For an explanation of the more pronounced effect at the higher Reynolds number, the reader is referred to Ref. 56). Nevertheless, considering these turbulence levels, there are two ways in which the rear flow development may be affected by way of shock boundary layer interaction:

- (1) The extent of the shock-induced separation bubble is changed, altering, in

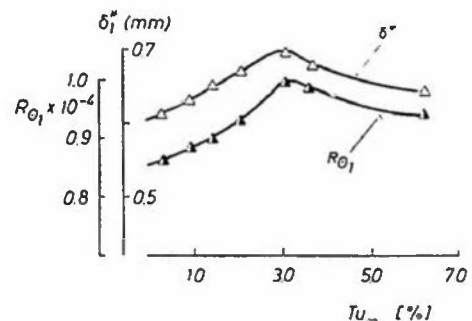


$\Delta\theta = \theta_1 - \theta_{01}$   
("0" refers to zero turbulence level)



- △ 'BUMP' MODEL  $R_{\theta_{01}} = 844 \times 10^3$
- CENTER-LINE MODEL  $R_{\theta_{01}} = 246 \times 10^3$   
(FIXED TRANSITION)

⑥ CHANGE IN MOMENTUM THICKNESS, REF 56



⑦ VARIATION OF INITIAL BOUNDARY LAYER CONDITION (BUMP MODEL), REF 57

Figure 42: Effect of freestream turbulence on the momentum thickness upstream of the shock ( $M_1 = 1.44$ )

turn, the chordwise distance available for the boundary layer recovery. Considering first the change in  $R_{\theta_1}$ , corresponding to the increased momentum thickness upstream of the shock, Fig. 42c [57], and translating this into a change in the bubble extent via Fig. 37, one sees that this influence is negligible, at least at the momentum thicknesses considered. A larger effect occurs, however, due to the direct influence of the freestream turbulence level on the reattachment length [58], which is reflected in a reduced bubble extent, see Fig. 16f of Section 4.8. At a freestream turbulence level of  $Tu_{\infty} = 3.68$

%, the reduction in bubble length of  $\Delta(L_B/\delta^*) = 14$  (for  $\delta^*$  see Fig. 42c) seems, when transferred to the conditions on the CAST 10-2 or CAST 7 airfoils in Fig. 35c no longer negligible. Of course, at turbulence levels of  $Tu_\infty < 1.5\%$  there is no need to worry.

(2) The turbulent mixing within the interaction region is enhanced by the higher initial turbulence levels due to turbulence amplification. Plotted in Figure 43 are velocity profiles and turbulence properties determined upstream of the shock and within the separated region,

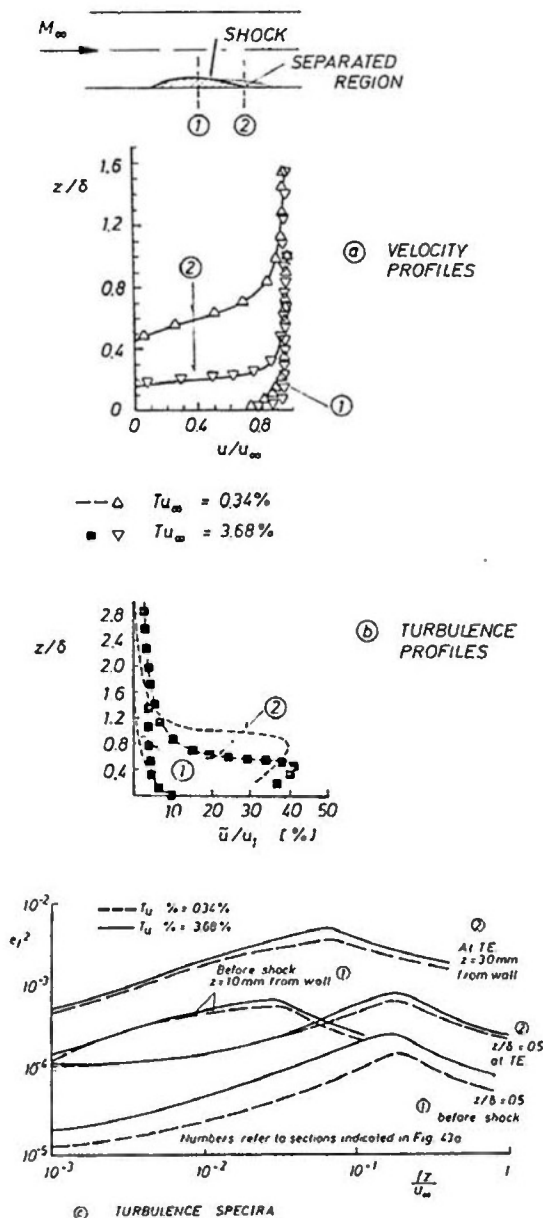


Figure 43: Velocity profiles and turbulence characteristics upstream and within the interaction region, Ref. 59

respectively, for two different freestream turbulence levels [59]. At the higher level ( $Tu_\infty = 3.68\%$ ), the turbulence intensity upstream of the shock is in the outer part of the boundary layer naturally higher, with the difference, however, decreasing as the wall is approached; the velocity profile is 'fuller'. Within the separated region (exactly at the trailing edge of the bump), the maxima in the turbulence intensities are closely the same, despite the difference in the initial levels, and a higher intensity appears only outside the boundary layer. The difference in the location of the maxima as well as the difference in the velocity profiles are due to the somewhat smaller separation bubble present at the higher freestream turbulence level. It is also interesting to note that within the separated region, the turbulence spectra are nearly the same for both turbulence levels in spite of noticeable deviations upstream of the interaction, Fig. 43c. It seems that shock boundary layer interaction, at least in the presence of separation, generates its own turbulence intensity and pattern, which is in accord with observations made by Eaton and Johnston [58] for reattachments downstream of steps, viz., that "initial conditions have been overwhelmed by the time the shear layer reattaches".

The above results suggest that differences in the level and structure of turbulence, contained in the incoming boundary layer due to differences in freestream turbulence, are not amplified by the shock boundary layer interaction in a way that there is a major effect on the flow development downstream of reattachment, at least not at turbulence levels encountered in contemporary wind tunnels ( $Tu_\infty < 1.5\%$ ). This may, of course, be entirely different if larger variations in the initial turbulence properties are introduced, for instance, by tripping devices. Here, well defined experiments on realistic configurations, sensitive to shock-induced and rear separation, are strongly recommended.

#### 4.5.7 Conclusions and Recommended Research

Features and developments associated with transonic shock boundary layer interaction essential within the context of viscous simulation are

(1) the upstream influence which rules the interactive pressure gradient imposed on the boundary layer,

(2) incipient separation whose occurrence signals to the designer that the performance boundaries of an airfoil or wing are (more or less) rapidly being approached as the freestream Mach number and/or angle of incidence are raised,



(3) the development of the shock-induced separation bubble which leads, possibly in conjunction with the development of rear separation, to the total break-down of the flow and

(4) the generation/amplification of turbulence due to the interaction which might have a pronounced influence on the trailing edge flow development.

#### UPSTREAM INFLUENCE

The upstream influence is, in the absence of shock-induced separation, defined as the distance between the chord location where the pressure rise due to the shock is first felt and the location where the pressure has dropped to sonic conditions and, in the presence of separation, as the distance between the former and the location of the separation point. The upstream influence was, for turbulent interactions, found to be only dependent on the viscous parameter  $\delta_1^*$  ( $H_{11} - 1$ ), where  $\delta_1^*$  and  $H_{11}$  are the displacement thickness and the incompressible shape factor, respectively, of the boundary layer immediately upstream of the shock. This means that this parameter, normalized by the model chord, must be duplicated in the low Reynolds number wind tunnel tests in order to simulate the high Reynolds number full-scale upstream influence. This seems to hold for two- and three-dimensional flows ( $\Lambda \leq 30^\circ$ ). It is, furthermore, believed that, if one simulates in the case of attached flow at the shock the upstream influence correctly, one will also obtain the proper simulation of the entire shock boundary layer interaction process, including the subsonic recompression.

Considering the upstream influence in attached flow at the shock, there remain, however, within the present context some open questions indicating the need for further research:

1. How closely must the parameter  $\delta_1^*$  ( $H_{11} - 1$ ) or its components be duplicated to achieve a sufficiently accurate simulation of full-scale shock boundary layer interaction?
2. Do the boundary layer parameters downstream of the interaction (e.g.,  $\delta^*$ ,  $\theta$ ,  $H$ ) correspond to the ones obtained at the (higher) Reynolds number to be simulated?
3. As a consequence of (2), is the simulation of the high Reynolds number trailing edge flow behavior ensured - or what degree of approximation can be attained - if the shock boundary layer interaction is simulated correctly? The former is, of course, required to obtain the full-scale shock location and strength.

Experiments must be carried out at transonic speeds on realistic configurations to answer these questions - and, of

course, to confirm (or reject) the dominance of the above viscous parameter. In the case of a rejection, which is, however, not very likely, the experiments must serve to identify the "true" dominant parameter. The experiments must cover two- and three-dimensional flows with the (preferably independent) variables being characteristic parameters of the incoming boundary layer and the outer inviscid flow, the latter including sweepback and the rear adverse pressure gradient.

#### INCIPIENT SEPARATION

The onset of shock-induced separation (incipient separation) was found to be rather insensitive to viscous effects and there is strong evidence that simulating the upstream influence correctly will also result in a sufficiently accurate simulation of incipient separation. Nevertheless, since it is not entirely sure what parameters of the incoming boundary layer (e.g.,  $H_{11}$  or  $R_{\delta_1^*}$ ) are predominantly responsible for incipient separation and in which way they manifest their influence, a well designed transonic experiment is needed where the variables are the shape parameter  $H_1$ , the boundary layer thickness parameters  $\delta^*$  and  $\theta$ , the Reynolds number based on these parameters, surface curvature (flat plate vs. airfoil or wing) and sweep. The experiments should, of course, be performed in conjunction with the ones related to the upstream influence.

#### DEVELOPMENT OF THE SHOCK-INDUCED SEPARATION BUBBLE

The correlation of Fulker and Ashill [23] of the shock-induced separation bubble extent, viz.,  $L_B/\theta_1 = f(M_1, R_{\theta_1})$ , seems to lead to the correct simulation of full-scale conditions, including the final flow break-down, at least in the absence of an "independently" developing trailing edge separation. An alternative correlation, established by the present author [5], suggests that simply duplicating the momentum thickness upstream of the shock will also lead to the correct full-scale bubble extent and, furthermore, to the right magnitude of this viscous parameter at reattachment; however, the range of viscous conditions covered in this correlation is too narrow for a definite conclusion so that here additional tests are required. Further key questions concerning bubble scaling, indicating needed experimental and theoretical research, are:

1. What is the limit of applicability of the Fulker and Ashill correlation in the presence of an "independent" trailing edge separation development?
2. Why does the bubble extent in the case of the aft-tripped thin boundary layer data of Ref. 5 not follow the correlation of Fulker and Ashill? Is  $R_{\theta_1}$  really unique in scaling the shock-induced bubble extent?

3. How closely correspond the boundary layer parameters at reattachment to the full-scale ones and, as a consequence, can the full-scale trailing edge flow be simulated - or to what degree approximated - by the correct simulation of shock boundary layer interaction?
4. Is, as already indicated above, the duplication of the momentum thickness upstream of the shock sufficient for bubble scaling?

A well designed experiment must be conducted to study, in detail, the structure and pattern of the local development of shock-induced separation - in the range incipient to total separation - dependent on the initial boundary layer condition and on parameters of the outer inviscid flow such as the shock-upstream Mach number  $M_1$  and the rear adverse pressure gradient  $\partial p/\partial x$ . Geometric variables should include sweepback and surface curvature. The experiments can be performed in conjunction with the ones related to the upstream influence and incipient separation.

#### TURBULENCE GENERATION/AMPLIFICATION

Strong evidence was found that the turbulence generated within the shock boundary layer interaction region may have a pronounced influence on the boundary layer development downstream of the interaction, hence on the trailing edge flow behavior. There is, furthermore, evidence, based on results obtained at various wind tunnel turbulence levels, that the magnitude of the shock-upstream turbulence level has no effect on the maximum turbulence intensity within the interaction region, i.e., turbulence generation is much more powerful than amplification. Note, that the overall flow development associated with shock-induced separation is, nevertheless, affected by freestream turbulence, however, only at turbulence levels far in excess of the ones commonly encountered in wind tunnels. Still, an experiment is suggested where the turbulence level and structure of the incoming boundary layer can be varied directly - for instance, by the introduction of different tripping devices - and where its amplification and influence on the rear flow development can be determined. The experiment can also be utilized to study, in detail, the process and influence of turbulence generation.

#### GENERAL CONSIDERATIONS CONCERNING THE EXPERIMENTS

All investigations must be performed for characteristic two- and three-dimensional transonic flow developments on configurations suiting the attendant flow problem. In all instances detailed surface pressure, boundary layer and field measurements

must be carried out using a wide range of appropriate instrumentation including, besides conventional means, hot-wire- and laser-doppler-anemometers, surface hot-film, dynamic pressure and skin friction gages and schlieren and interferometer systems. Needless to say that the experiments must be accompanied and supplemented by a continued literature search and theoretical studies, the latter having the great advantage that parameters can be easily and independently varied. In concluding, it should be noted that at the DFVLR Institute of Experimental Fluid Mechanics three experiments are planned (the models have already been manufactured) to investigate some of the phenomena discussed above; the experiments comprise:

(1) Tests with a 1-meter-chord airfoil, where chord Reynolds numbers of up to  $Re = 20 \times 10^6$  can be attained, and where, for instance, problems related to the dependence of the rear flow development on the shock boundary layer interaction process, including turbulence generation and amplification, can be studied.

(2) Tests with a flat plate model on which a skewed normal shock, generated by a wedge, impinges. The set-up has a large aspect ratio and is designed to study all aspects of "pure" three-dimensional shock boundary layer interactions at transonic (local) conditions.

(3) Tests with a sheared wing, parallel to (2), where the conditions of three-dimensional shock boundary layer interactions can be related to the trailing edge flow development.

#### 4.5.8 References

1. Sobieczky, H., "Verfahren für die Entwurfsaerodynamik moderner Transportflugzeuge", DFVLR Research Report, DFVLR-FB 85-05, 1985.
2. Delery, J., Marvin, J.G., "Turbulent Shock Wave Boundary Layer Interaction", AGARDograph No. 280, 1985.
3. Pearcey, H.H., "Some Effects of Shock-induced Separation of Turbulent Boundary Layers in Transonic Flow past Aerofoils", A.R.C. Technical Report, R. and M. No. 3108, June 1955, reissued 1959.
4. Pearcey, H.H., Osborne, J. and Haines, A.B., "The Interaction between Local Effects at the Shock and Rear Separation - a Source of Significant Scale Effects in Wind Tunnel Tests on Aerofoils and Wings", in AGARD-CP-35, Transonic Testing, Sept. 1968, Paper No. 11.

5. Stanewsky, E., "Interaction between the Outer Inviscid Flow and the Boundary Layer on Transonic Airfoils", Dissertation, TU-Berlin (D 83), 1981 (also Z. Flugwiss. Weltraumforsch. 7 (1983), Heft 4, pp 242-252).
6. Walz, A., "Strömungs- und Temperaturgrenzschichten", Verlag G Braun, Karlsruhe, 1966.
7. East, L.F., "The Application of a Laser Anemometer to the Investigation of Shock-Wave Boundary-Layer Interactions", in AGARD-CP-193, Applications of Non-intrusive Instrumentation in Fluid Flow Research, Sept. 1976, Paper No. 5.
8. Lighthill, M.J., "On Boundary-layer Upstream Influence. II Supersonic Flows without Separation", Proc. Roy. Soc., Ser. A217, 1953, pp 478-509.
9. Stewartson, K., Williams, P.G., "Self-induced Separation", Proc. Roy. Soc., Ser. A312, 1969, pp 181-206.
10. Green, J.E., "Interactions between Shock Waves and Turbulent Boundary Layers", Progress in Aerospace Sciences, Vol. 11, pp. 235-340, Pergamon Press at Oxford, 1970.
11. Peake, D.J., Tobak, M., "Three-dimensional Interactions and Vortical Flows with Emphasis on High Speeds", AGARDograph No. 252, July 1980.
12. Abbiss, J.B., East, L.F., Nash, C.R., Parker, P., Pike, E.R. and Swayer, W.G., "A Study of the Interaction of a Normal Shock Wave and a Turbulent Boundary Layer Using a Laser Anemometer", RAE TR-75141, Feb. 1976.
13. Mathews, D.Ch., "Shock Wave-Boundary Layer Interaction in Two-dimensional and Axially-symmetric Flows Including the Influence of Suction", Ph.D. Thesis, University of Washington, Seattle, 1969.
14. Delery, J., "Interaction onde de choc-couche limite turbulente en transsonique (Recherches en 1978 - 1979)", ONERA RSF-36/7078 AY, July 1980.
15. Sirieix, M., Delery, J., Stanewsky, E., "High Reynolds Number Boundary-Layer Shock-Wave Interactions in Transonic Flow", Lecture Notes in Physics 148, Springer-Verlag, Berlin, 1981, pp. 149-214.
16. Inger, G.R., Lynch, F.T., Fancher, M.F., "Theoretical and Experimental Study of Non-adiabatic Transonic Shock/Boundary-Layer Interactions", AIAA Journal, Vol. 23, No. 10, Oct. 1985, pp. 1476-1482.
17. Inger, G.R., "Application of a Shock-Turbulent Boundary Layer Interaction Theory in Transonic Flow Field Analysis", AIAA Progress in Astronautics and Aeronautics: Transonic Aerodynamics, Vol. 81, AIAA, New York, 1982, pp. 621-636.
18. Rotta, J.-C., "Turbulent Boundary Layer Calculations with the Integral Dissipation Method", Computation of Turbulent Boundary Layers - 1968 AFOSR-IFP Stanford Conference, Vol. I, p. 177.
19. Blackwell, J.A., Jr., "Preliminary Study of Effects of Reynolds Number and Boundary-Layer Transition Location on Shock-induced Separation", NASA TN D-5003, Jan. 1969.
20. Koppenwallner, G., Szodrich, J., (Editors), "Boundary Layer Control by Transition Fixing", DFVLR-Mitteilung 84-17, 1984.
21. Green, J.E., "A Discussion of Viscous-Inviscid Interactions at Transonic Speeds", R.A.E. Technical Report 72050.
22. Spaid, F.W., "Transonic Airfoil and Wing Flow Field Measurements", AIAA 22nd Aerospace Sciences Meeting, Jan 9-12, 1984, Paper No. 84-0100.
23. Fulker, J.L., Ashill, P.R., "A Model of the Flow over Swept Wings with Shock Induced Separation", Paper presented at the IUTAM Symposium on Turbulent Shear Layer/Shock Wave Interactions, Palaiseau, France, Sept 9-12, 1985 (also Springer-Verlag, Berlin, Heidelberg 1986).
24. Montoya, L.C., Banner, R.D., "F-8 Supercritical Wing Flight Pressure, Boundary-Layer, and Wake Measurements and Comparison with Wind Tunnel Data", NASA Technical Memorandum, NASA TM X-3544, June 1977.
25. Freimuth, P., Stanewsky, E., "Pressure Distribution and Boundary Layer Measurements on a 38-degree CAST 7 Sheared-wing Model", unpublished results.
26. Prandtl, L., "On Boundary Layers in Three-dimensional Flow", British Ministry of Aircraft Production Völkner Reports and Transactions, No. 64, 1946.
27. Selby, G.V., "Applicability of the Independence Principle to Subsonic Turbulent Flow over a Swept Rearward-Facing Step", AIAA Journal, Vol. 21, No. 11, Nov. 1983, pp. 1603-1604.
28. Jones, R.T., "Effects of Sweepback on Boundary Layer and Separation", NACA TN-1402, 1947.

29. Inger, G.R., "Analytical Investigation of Swept Shock-Turbulent Boundary Layer Interaction in Supersonic Flow", AIAA 17th Fluid Dynamics, Plasma Dynamics, and Laser Conference, June 25-27, 1984, Paper No. 84-1555 (also see: "Supersonic Viscous-Inviscid Interaction of a Swept Compression Ramp with a Turbulent Boundary Layer", Paper presented at the IUTAM Symposium on Turbulent Shear Layer/Shock Wave Interactions, Palaiseau, France, Sept 9-12, 1985).
30. Dolling, D.S., "Effects of Mach Number on Upstream Influence in Sharp Fin Induced Shock Wave Turbulent Boundary Layer Interaction", AIAA 22nd Aerospace Sciences Meeting, Jan 9-12, 1984, Paper No. 84-0095.
31. Dolling, D.S., "Upstream Influence in Conically Symmetric Flow", AIAA-Journal, Vol. 23, No. 6, June 1985.
32. Peake, D.J., Rainbird, W.J., "The Three-dimensional Separation of a Turbulent Boundary Layer by a Skewed Shock Wave and its Control by the Use of Tangential Air Injection", in AGARD Conference Proceedings No. 168, Flow Separation, 1975, pp. 40/1-40/34.
33. Rodde, A.-M., "Determination des conditions d'apparition du décollement au pied du choc sur le profil LC-100 D a bord de fuite modifié", ONERA RSF-45/1685 AY, June 1980.
34. Gobert, J.L., Seraudie, A., Mignosi, A., "Etude de l'interaction onde de choc-couche limite sur profil LC-100D de 400 mm de corde dans la soufflerie T2", ONERA RT-38/7078 AYD, 1980.
35. Cebeci, T., Smith, A.M.O., Hosinski, G., "Calculation of Compressible Adiabatic Turbulent Boundary Layers", AIAA Journal, Vol. 8, No. 11, Nov. 1970, pp. 1974-1982.
36. Inger, G.R., Deane, A., "Transonic Shock Interaction with a Tangentially-injected Turbulent Boundary Layer", AIAA 22nd Aerospace Sciences Meeting, Paper No. 84-0094, Jan. 1984.
37. Deane, A., Ph.D-Thesis, VPI, (in preparation?)
38. Nandan, N., Stanewsky, E., Inger, G.R., "Airfoil Flow Analysis with a Special Solution for Shock/Boundary-Layer Interaction", AIAA-Journal, Vol. 19, No. 12, Dec. 1981, pp. 1540 - 1546.
39. Inger, G.R., "Some Features of Shock-Turbulent Boundary Layer Interaction Theory in Transonic Flow Fields", in AGARD-CP-291, Computation of Viscous-Inviscid Interactions, Feb. 1981, pp. 18-1 to 18-26.
40. Hayakawa, K., Squire, L.C., "The effect of the upstream boundary-layer state on the shock interaction at a compression corner", J. Fluid Mech. (1982), Vol. 122, pp. 369-394.
41. Holder, D.W., Pearcey, H.H., Gadd, G.E., "The Interaction between Shock Waves and Boundary Layers", A.R.C. Technical Report C.P., No. 180, 1955.
42. Ackeret, J., Feldmann, F., Rott, N., "Untersuchungen an Verdichtungsstößen an Grenzschichten in schnell bewegten Gasen", Mitteilungen aus dem Institut für Aerodynamik der ETH Zürich, No. 10, 1946 (also NASA TM 1113, Jan. 1947).
43. Sobieczky, H., Stanewsky, E., "The Design of Transonic Airfoils under Consideration of Shock Boundary Layer Interaction", 10th ICAS-Congress, Ottawa, Canada, Oct. 3-8, 1976, Paper 75-14.
44. Inger, G.R., "Transonic Shock-Turbulent Boundary-Layer Interaction and Incipient Separation on Curved Surfaces", 14th Fluid and Plasma Dynamics Meeting, AIAA Paper No. 81-1244, June 1981 (also J. Aircraft, Vol. 20, No. 6, June 1983, pp. 571-574).
45. Bohning, R., Zierep, J., "Normal Shock/Turbulent Boundary Layer Interaction at a Curved Surface", AGARD-CP-291, Computation of Viscous-Inviscid Interactions, Feb. 1981, pp. 17-1 to 17-8.
46. Myring, D.F., "The Effect of Sweep on Conditions at Separation in Turbulent Boundary Layer/Shock Wave Interaction", Aero. Quart., March 1977, pp. 111-122.
47. Korkegi, R.H., "A Lower Bound for Three-dimensional Turbulent Separation in Supersonic Flow", AIAA-Journal, Vol. 23, No. 3, March 1985, pp. 475-476.
48. Chapman, D.R., Kuehn, D.M. and Larson, H.K., "Investigation of Separated Flows in Supersonic and Subsonic Streams with Emphasis on the Effect of Transition", NACA TN-3869, March 1957.
49. Smith, P.D., "A Calculation Method for the Turbulent Boundary Layer on an Infinite Yawed Wing in Compressible, Adiabatic Flow", RAE Technical Report 72193, 1972.
50. Fulker, J.L., Ashill, P.R., "A Study of Factors Influencing Shock-induced Separation", RAE Technical Report (to be published)

56. Raghunathan, S., McAdam, R.J.W., "Relative Effects of Reynolds Number and Freestream Turbulence in Transonic Flow", AIAA-Journal, Vol. 23, No. 4, April 1985, pp. 546-550.
57. Raghunathan, S., McAdam, R.J.W., "Freestream Turbulence and Transonic Flow over a 'Bump' Model", AIAA-Journal, Vol. 21, No. 3, March 1983, pp. 467-469.
58. Eaton, J.K., Johnston, J.P., "A Review of Research on Subsonic Turbulent Flow Reattachment", AIAA-Journal, Vol. 19, No. 9, Sept. 1981, pp. 1093-1100.
59. Raghunathan, S., McAdam, R.J.W., "Boundary Layer and Turbulence Intensity Measurements in a Shock Wave/Boundary Layer Interaction", AIAA-Journal, Vol. 21, No. 9, Sept. 1983, pp. 1349-1350.
51. Green, J.E., Weeks, D.J., Brooman, J.W.F., "Prediction of Turbulent Boundary Layers and Wakes in Compressible Flow by a Lag-entrainment Method", ARC R&M 3791, 1973.
52. Green, J.E., "A Discussion of Viscous-Inviscid Interactions at Transonic Speeds", AGARD-CP-35, 1971, Paper No. 2.
53. Hirschel, E.H., Lucchi, C.W., "On the Kutta Condition for Transonic Airfoils", MBB-UFE 122-AERO-MT-651, 1983.
54. Anyiwo, J.C., Bushnell, D.M., "Turbulence Amplification in Shock-Wave Boundary-Layer Interaction", AIAA-Journal, Vol. 20, No. 7, July 1982.
55. Raghunathan, S., Coll, J.B., Mabey, D.G., "Transonic Shock/Boundary-Layer Interaction Subject to Large Pressure Fluctuations", AIAA-Journal, Vol. 17, No. 12, Dec. 1979.

## SECTION 4.6 CLASSICAL SEPARATION, TRAILING-EDGE FLOWS AND BUFFETING

by

J.L. van Ingen  
Department of Aerospace Engineering  
Delft University of Technology  
Kluyverweg 1  
2629 HS Delft, The Netherlands

### Summary

The present chapter gives an overview of those aspects of classical separation, trailing-edge flows and buffeting which are relevant to the simulation process. Viscous flow parameters which should be simulated are defined and some recommendations for further research are given.

### Contents

- List of symbols
- 4.6.1. Introduction
- 4.6.2. Laminar separation
- 4.6.3. Laminar separation followed by turbulent reattachment: the laminar separation bubble
  - 4.6.3.1. Introductory remarks on separation bubbles
  - 4.6.3.2. Some further details on laminar separation bubbles
- 4.6.4. The turbulent flow downstream of a laminar separation bubble
  - 4.6.4.1. Introductory remarks on the turbulent flow downstream of a laminar separation bubble
  - 4.6.4.2. Some further details on the turbulent flow downstream of a laminar separation bubble
  - 4.6.4.3. Some reflections on the turbulence structure downstream of trips and other obstacles
  - 4.6.4.4. On simulation procedures for laminar separation bubbles
- 4.6.5. Trailing-edge flows (not necessarily separated)
- 4.6.6. Turbulent separation
  - 4.6.6.1. Introductory remarks on turbulent separation
  - 4.6.6.2. Simple criteria for turbulent separation
  - 4.6.6.3. Some remarks on shape factor correlations
  - 4.6.6.4. Development of turbulent separation prediction capabilities since 1968 and present state of the art
- 4.6.7. On the possibility of turbulent separation bubbles (e.g. cove separation)
- 4.6.8. On the separation properties of three-dimensional turbulent boundary layers
- 4.6.9. Buffeting
  - 4.6.9.1. Introduction on buffeting
  - 4.6.9.2. Buffet prediction
- 4.6.10. Concluding remarks and recommendations
- 4.6.11. References
- Figures

### List of symbols

Symbols which are used only locally are defined when they occur. Some others are defined below.

$c$	airfoil chord
$c_f$	$= \frac{\tau_o}{\frac{1}{2} \rho U^2}$ , skin friction coefficient
$c_p$	pressure coefficient
$H$	$= \frac{\delta^*}{\theta}$ = shape factor
$h$	$= \frac{H-1}{H}$
$n$	critical amplification factor in the $e^n$ method for transition prediction
$R$	$= \frac{U_\infty c}{\nu}$ chord Reynoldsnumber
$R_\theta$	$= \frac{U_\theta}{\nu}$
$Tu$	effective free-stream turbulence level (%)
$U_\infty$	free-stream speed
$U$	velocity at edge of boundary layer
$x$	coordinate along wall
$\Delta x$	distance along wall downstream of laminar separation
$\gamma$	angle at which the laminar separation streamline leaves the wall
$\gamma$	intermittency
$\delta$	boundary layer thickness
$\delta^*$	displacement thickness
$\theta$	momentum loss thickness
$\lambda$	$= \frac{\delta^*}{\theta}$
$\tau_o, \tau_w$	wall shear stress



$\bar{\tau}_{0,w}$  time-averaged wall shear stress

$$\xi = \frac{\Delta x}{\theta_{\text{sep}} (R_\theta)_{\text{sep}}}$$

#### Subscripts:

sep at separation  
tr at transition  
• free-stream conditions

#### 4.6.1. Introduction

In section 3.2.3, Chan examined the capabilities of computational tools for simulation methodologies; this review is illustrated with typical examples. His last concluding remark in section 3.2.3.6 may be taken as a starting point for the present discussion: "Due to strict requirement of accuracy in aerodynamic tests, applications of computation are limited, at present, to simulations of attached flows. For complex flow simulations, especially with flow separation, further development is needed in better understanding the physical nature of the flow and its modelling".

In section 4.3 Michel describes in some detail the available methods for the prediction of laminar, transitional and turbulent boundary layers.

It is the purpose of the present chapter (4.6) to review flow separation in some more detail and to outline where improvements are needed. This review will not include separation directly induced by shocks; this is the subject of the review by Stanewsky in section 4.5, neither will separation from sharp edges be discussed. Laminar separation (4.6.2), turbulent separation (4.6.6) and the separation bubble, where laminar separation is followed by turbulent reattachment, (4.6.3) and buffeting (4.6.9) are included.

A laminar separation bubble has a significant effect on the development of the downstream turbulent boundary layer. Although at full scale Reynolds numbers large laminar separation bubbles cannot be expected to occur, the subject is discussed at some length in 4.6.3, because these bubbles may occur on windtunnel models. Furthermore this type of flow is discussed to point out the large effects on the downstream turbulent boundary layer development. Similar effects are expected to occur downstream of other "obstacles" to the boundary layer flow (natural transition, trips, non-classical manipulators, shock-boundary layer interaction, etc.).

From these observations it follows that the term "state of the boundary layer", by which in general is meant whether the flow is laminar or turbulent, should be defined much more precise. The whole turbulence structure may be upset by the obstacle, resulting in a non "well-developed" turbulent flow. Even the effects of classical trips should be further analysed; they may have been well researched only in weak pressure gradients. The usual conclusion that the downstream flow rapidly turns into a well-developed turbulent boundary-layer, might not be true in strong pressure gradients.

The development of the upper- and lower surface boundary layers near the trailing-edge of a 2D or 3D wing, and their merging into the wake, has a significant influence on the circulation and through that on pressure distribution and shock location. Therefore the "viscous Kutta-Joukowski condition" has to play an important role in any simulation methodology (4.6.5).

When more than a limited separation region occurs, the resulting unsteady pressures may have an important effect on rigid-body and elastic vibrations of the aircraft structure, impairing comfort and/or the capability to execute the aircraft's mission. We have to distinguish between buffet onset and severe buffet. The first may be related to the occurrence of small separation zones and hence can be expected to be amenable to prediction using methods for the calculation of steady boundary layers. The prediction of severe buffet is much more complicated (4.6.9).

In the discussion of the above mentioned subjects it will be tried to indicate dominant parameters determining these flows, which will have to be duplicated in the windtunnel experiment: for an adequate simulation. It should be remembered, that the present volume is concerned with the windtunnel simulation at low Reynolds numbers of flows around bodies at full scale Reynolds numbers. The required accuracy of any method to predict the various flows, depends on whether we want a full simulation or will be satisfied when the results of the windtunnel experiment become extrapolable to full scale. In the last case the prediction and the resulting manipulation of the flow at model scale is satisfactory when it is assured that the character of the flow in both cases is sufficiently alike. This implies that discontinuous changes of flow character between tunnel and flight Reynolds numbers should be eliminated. Since in the windtunnel the boundary-layers will have to be manipulated to provide the required simulation, predictive methods should be capable of taking into account the effects of classical and future tripping and manipulating devices on the viscous flow.

Before writing the present chapter, the author had to study a large number of references; therefore completeness can not be claimed. Much to his surprise the number of papers containing clear statements about the accuracy of predictive methods of turbulent separation in non-equilibrium flows was rather small. Most of the attention in recent years seems to have been given to equilibrium flows and to the development of strong viscous/inviscid interaction procedures. Much additional research will have to be performed to improve on this situation. Recent progress in the description of non-equilibrium flows has been discussed by Cross in section 4.4 of the present volume. Some recommendations for future research will be given in section 4.6.10.

#### 4.6.2. Laminar separation

The calculation of laminar separation for a prescribed pressure distribution, has for a long time been a controversial subject. The question was whether the boundary layer equations remain valid at separation or that the occurrence of the Goldstein singularity means that the boundary layer concept has to be abandoned at separation. In the last two decades it has become clear that the use of the boundary layer equations can be continued, if only the influence of the boundary layer on the pressure distribution in the separation



zone is taken into account through the procedure of so-called strong viscous-inviscid interaction. In such a procedure the pressure distribution is no longer prescribed and a regular behaviour is obtained by letting the pressure distribution be compatible with the displacement effect of the boundary layer. Provided the pressure distribution upstream of the separation zone is fixed, that means provided the flow downstream of laminar separation up to the trailing-edge is given, which determines the circulation, the prediction of laminar separation has been reduced to a problem of numerical analysis only. This problem can be considered to have been solved and need not further be discussed in this chapter. Care should be taken when calculating a laminar boundary layer for an experimentally determined pressure distribution with separation. Due to the interaction, a pressure gradient relief occurs in the separation zone. A method predicting separation a little bit too late will then predict separation not to occur at all; use of the interaction mode will then be mandatory.

#### 4.6.3. Laminar separation followed by turbulent reattachment: the laminar separation bubble

##### 4.6.3.1. Introductory remarks on separation bubbles

The occurrence of transition downstream of laminar separation is of major concern at low Reynolds numbers such as occur for full scale sailplanes. When transition is followed by reattachment, a so-called short separation bubble is obtained. When the turbulent boundary layer fails to reattach "bursting" is said to occur. These bubbles have been researched extensively only for two-dimensional low speed flows. They may, however, also occur near the leading-edge on windtunnel models for "peaky" type pressure distributions at high subsonic and transonic Mach numbers and in three-dimensional flow. Since for swept wings the spanwise flow component remains attached, it may be expected that the overall characteristics of the bubble will be determined by transition due to the highly unstable reversed flow in chordwise direction which might be derived from 2D results. Bertelrud [27, 28] has even observed a laminar separation bubble near the leading-edge of a fighter at full scale. Therefore simulation of separation bubbles in windtunnel testing may be required for high lift cases. Often it may be necessary to eliminate laminar separation bubbles by tripping.

From the non-dimensionalised laminar boundary layer equations it follows that the position of separation is independent of the Reynoldsnumber, if only the non-dimensional pressure distribution is independent of Reynoldsnumber. Therefore the simulation of this position is guaranteed if the  $\delta^*$  distribution and circulation are simulated correctly. This will depend on the quality of the simulation over the downstream part of the wing, especially in the trailing-edge region. Although the direct effect of a short bubble on lift may be small, it may have a large effect on the downstream development of the turbulent boundary layer and especially on its separation characteristics (section 4.6.4). Therefore in simulating laminar separation bubbles it seems more important to reproduce the downstream effects than the bubble itself (see also section 4.6.4.4.).

In a recent conference on Low Reynolds number Airfoil Aerodynamics at Notre Dame University [29] the subject of laminar separation was discussed extensively. Notably the papers by Gleyzes, Cousteix and Bonnet [30] and Vnn Ingen and Boermans [31] may be consulted. Some additional information may be found in a further paper by Vnn Ingen and Boermans [32]. An important finding in these papers is that transition in bubbles may be predicted with  $e^n$  type methods. A good description of a local inviscid-viscous interaction procedure for separation bubbles may be found in Vatsa and Carter [33]. The subject of 2D and 3D laminar separation bubbles in relation to windtunnel simulations has been discussed by Hall [34].

##### 4.6.3.2. Some further details on laminar separation bubbles

In this section a detailed description is given of the characteristics of laminar separation bubbles at low speed. It is mainly based on research at the Department of Aerospace Engineering of Delft University as it was reported by Vnn Ingen and Boermans [31, 32].

Fig. 1 indicates a schematic of a laminar separation bubble with Separation, Transition and Reattachment. From many different experiments in low speed flow it was found that the separation streamline in the laminar part of the bubble starts straight (fig. 2) and leaves the wall at an angle  $\gamma$  which is related to  $(R_\theta)$  at separation through  $\tan(\gamma) = \frac{B}{(R_\theta)_{\text{sep}}}$  (fig. 3), where B is a universal constant between 15 and 20.

This local correlation seems to be independent of bubble bursting (fig. 4). A universal description of the laminar part of the bubble seems possible by using a non-dimensional coordinate  $\xi$  downstream of separation according to  $\xi = \frac{\Delta x}{\theta_{\text{sep}} R_{\theta \text{ sep}}}$ . Transition in the bubble can be predicted using the  $e^n$  method; n should be

a function of the "effective turbulence level"  $Tu$  (fig. 5). This  $Tu$  should follow from experiments in the respective facilities; at present values are used at Delft according to the following table:

Facility	$Tu(\%)$	n
NACA LTT and similar tunnels	0.10	9.75
Advanced low turbulence tunnels such as at Delft University of Technology	0.06	11.2
Free flight of gliders	0.014	15.0

Reattachment or failure to reattach (bursting) is determined using a reattachment locus obtained from Stratford's limiting pressure distribution for zero wall shear stress. A similar locus has been defined by Hortsm. Fig. 6 gives some typical examples of bubble prediction. A kind of viscous/inviscid interaction procedure prescribing the shape of the separation streamline is used. For bubbles where no appreciable amplification of Tollmien-Schlichting disturbances occurs upstream of separation, a short cut method has been devised to calculate the transition length (straight lines in fig. 7). It is clear that the length of the bubble strongly decreases with increasing Reynoldsnumber. When these bubbles have to be simulated at

lower than full scale Reynolds number, trips will have to be used to simulate the downstream effect of the bubble on the turbulent boundary layer development rather than the length of the bubble (see also section 4.6.4.4). The short cut method reproduces various known criteria for bubble bursting and in addition allows the effect of free stream turbulence level to be accounted for. Through separation bubbles  $\theta$  may strongly increase (fig. 8a); early tripping may thus reduce  $\theta$  at the trailing-edge and hence reduce profile drag (fig. 8b). For this purpose classical trips or air jets are being used extensively in sail-plane practice. The effects of sound on the characteristics of an Eppler 61 airfoil at very low Reynolds numbers is shown in figs. 9 and 10; it follows that sound can be an effective tripping device.

#### 4.6.4. The turbulent flow downstream of a laminar separation bubble

##### 4.6.4.1. Introductory remarks on the turbulent flow downstream of a laminar separation bubble

It has been observed in [30] and [31] that downstream of a laminar separation bubble the momentum loss thickness  $\theta$  may be much larger than for a turbulent boundary layer starting at the laminar separation point. Depending on the pressure distribution downstream of the bubble this effect on  $\theta$  may be amplified. This may have an appreciable effect on turbulent separation. The role of separation bubbles in airfoil leading-edge stalls has been described by Van den Berg [38].

It has been observed [39] that the turbulence intensity in the turbulent boundary layer downstream of reattachment is much higher than would follow from mixing-length models for regular attached turbulent boundary layers. Therefore, when applying boundary layer trips it will not just be sufficient to distinguish between the "laminar and turbulent states" of the boundary layer. The "turbulent state" should be better defined including details about the turbulence structure. Arnal and Juillen [40], see also [30] have shown that the transition process in the separation bubble is markedly different from that on a flat plate in zero pressure gradient. For the flat plate transition occurs through the appearance of turbulent spots; the resulting turbulent boundary layer does not seem to remember the Tollmien-Schlichting effects in its history. For separation followed by transition in larger adverse  $\frac{dp}{dx}$ , the intermittency decreases and the turbulent flow starts to remember its Tollmien-Schlichting history. By analogy it may be expected that the turbulent boundary layer downstream of other "obstacles", such as classical trips, other manipulators and shock wave boundary layer interaction regions, will show similar deviations from the "regular" turbulent boundary layer behaviour. CFD programs used to predict boundary layer flows or used as an aid in simulation procedures only, will have to take these effects into account. This points out the impossibility of a universal turbulence model and the requirement for "zonal modelling" where the model is adapted to the local type of flow.

In order to emphasize this point, section 4.6.4.2 contains a more detailed description of the flow downstream of a separation bubble.

##### 4.6.4.2. Some further details on the turbulent flow downstream of a laminar separation bubble

As a first example of the effect of the laminar separation bubble on the downstream development of the turbulent boundary layer we will discuss some results of a comparison between experiments and calculations for the Eppler E603 airfoil at low subsonic speed. The experiments have been performed by Van Groenewoud [41] in the low speed - low turbulence windtunnel of the Department of Aerospace Engineering at Delft University of Technology. The calculations have been made in Delft by Van Oudheusden [39] using the 1984 version of the NLR program BOLA [42-46]. BOLA uses a model for the mixing length  $\ell$  according to:

$$\ell = \lambda_{0.95} D \tanh \left( \frac{k y}{\lambda_{0.95}} \right)$$

In this equation  $\lambda_{0.95}$  is taken constant at high Reynolds numbers (equal to 0.12); at low Reynolds numbers an appropriate Reynolds number dependent correction is used;  $D$  contains the Van Driest damping,  $k$  is the Von Karman constant. Starting conditions for the calculations have in the present case been introduced by specifying  $c_f$  and  $\theta$ . Experimental pressure distributions at two values of the chord Reynoldsnumber (1.8 and

$3.6 \times 10^6$ ) are shown in fig. 11. At the lower Reynolds number transition occurs downstream of a laminar separation bubble; at the higher Reynolds number no bubble is present.

Calculated skin friction distributions are shown in figs. 12 and 13. It follows that in the low Reynolds number case there is a marked difference between the experimental and calculated results. Even restarting the calculations further downstream with starting conditions equal to the local experimental values does not improve the results. In the high Reynolds number case a good representation of the experimental results is obtained. It should be noted from the figures that the differences observed are not removed by including the customary low Reynolds number correction on  $\ell$ .

It was expected that the increased turbulence intensity downstream of reattachment is causing the deviations at low Reynolds number. Therefore a further experimental investigation using hot wire anemometry in a special boundary layer channel was performed by Van Oudheusden [39]. This channel consists of one flat wall and an adjustable curved opposite wall. The boundary layer is measured on the flat wall. Different pressure distributions can be generated. In the first case investigated, a vanishingly small separation bubble occurred. Figs. 14 through 18 give some results of these experiments. It appears that the expression used in BOLA for the mixing length remains valid. However, even in this case without a large separation bubble, the "constant"  $\lambda_{0.95}$  has to be increased to about 0.19 at reattachment (fig. 17). It takes a considerable length before  $\lambda_{0.95}$  returns to its standard value (fig. 18). A calculation with BOLA using the experimental  $\lambda_{0.95}$  distribution improved the results of the calculation considerably. In the future some cases with larger bubbles will be investigated, a still much larger effect on  $\lambda_{0.95}$  may then be expected.

Some interesting observations on separation bubbles, including the transition process, have been reported by Gleyzes et al [30]. It was also found here that the presence of the bubble has a large effect on the downstream development of  $\theta$ . This paper also gives details of the transition process in long and short bubbles; no difference seems to exist in the transition mechanisms in short or long bubbles. In both cases, laminar instability waves grow and this growth is fairly rapid, because of the strong instability of

boundary layer velocity profiles in an adverse pressure gradient. The difference with the well known transition in zero pressure gradient is that the beginning of transition is not associated with the development of three-dimensional spots, followed by an intermittency region. Here, the amplification of Tollmien-Schlichting waves generates two-dimensional vortices, the desagregation of which leads more or less rapidly to turbulence.

#### 4.6.4.3. Some reflections on the turbulence structure downstream of trips and other obstacles

By analogy to the turbulent flow downstream of a separation bubble, as discussed in section 4.6.4.2, it is the present authors strong belief that similar flow phenomena may occur downstream of tripping devices or the shock-wave boundary layer interaction region. Therefore a warning seems to be in place against often heard remarks, such as:

- "the turbulence structure downstream of a trip should rapidly approach a structure of well-established turbulent flow"
- "the turbulent boundary layer should be as close to a natural transition boundary layer as possible"
- "the trip should have a zero penalty drag".

One could argue of course about the definitions of "well-established" and "natural transition boundary layer". There are already differences between the boundary layers on the model and at full scale due to the difference of Reynolds numbers. What really counts is, that the trip/manipulator should produce the effects required by the simulation methodology and that the related CFD procedures will faithfully reproduce these effects. Even more care should be exercised as soon as non-classical trips such as vortex generators, air jets, heating and cooling or suction are introduced. The need for zonal turbulence modelling becomes clearly apparent here. For the literature survey, which was undertaken before the present contribution was written, not enough time was available to make a detailed study of this subject. It is believed that not enough details on the turbulence structure behind trips, other than in small pressure gradients, would have been found.

A further study will certainly be needed. For further remarks on boundary layer manipulation the reader is referred to chapter 4.9 of the present volume by E.M. Kraft

#### 4.6.4.4. On simulation procedures for laminar separation bubbles

It should be noted that at high (full scale) Reynolds numbers the bubble itself and hence its direct effect on wing characteristics may be expected to be small. What should be simulated is the effect of the bubble on the downstream development of the turbulent boundary layer.

This downstream effect may be expressed by the growth rate of  $\theta$  and hence will depend on the local turbulence structure. How exactly to simulate such a flow is a matter of further research. Simulation methodologies should state the parameters of the boundary layer which has to enter the next streamwise critical region. The CFD method used, then should specify what characteristics the boundary layer should have just downstream of the bubble. This in turn defines the required manipulation of the separation bubble. The CFD method used, should take into account the peculiarities of the turbulence structure downstream of bubbles, trips and other obstacles. There is certainly a need for much detailed experimental research on the subject.

#### 4.6.5. Trailing-edge flows (not necessarily separated)

The viscous flow near the trailing-edge of an airfoil or a 3-D wing has an overriding influence on the circulation and hence on pressure distribution and shock location. Therefore in any simulation/extrapolation methodology the trailing-edge region deserves special attention. The most important aspects for 2D flow are:

1. for lifting cases the boundary layer approaching the trailing-edge along the upper surface tends to be thicker than that at the lower surface; this causes an effective decambering with the associated lift loss;
2. the streamlines in the boundary-layers and the wake near the trailing-edge (also under influence of the trailing-edge angle) are curved which results in a transverse pressure gradient;
3. related to (1) the flow tends to leave the trailing-edge in the direction of the surface which carries the boundary layer with the highest momentum, in general this is the lower surface which contributes to the decambering;
4. additional weakening of the upper surface boundary layer occurs when it is subjected to shock-wave boundary-layer interaction [47].

For a swept wing there is the additional complication that

5. the flow direction for the upper- and lower surface, when viewed in planform may be markedly different (and varying across the boundary layer) when joining up at the trailing-edge.

All of the above influences combined cause an appreciable viscous lift-loss at transonic speeds, which may be strongly dependent upon the Reynolds number. This again emphasises the need for proper simulation methodologies. The boundary-layer approaching the trailing-edge carries with it its whole history (free or tripped transition, shock-wave boundary-layer interaction, adverse pressure gradient between shock and trailing-edge). Any wrong element in the simulation will exert a large influence on the trailing-edge region and hence on the global flow. It appears that parameters to be simulated at the trailing-edge are boundary layer thickness and shape factor. To what extent the turbulence intensity and structure have to be simulated is not clear as yet.

Although a number of methods to calculate 2D airfoil flows (including the trailing-edge region) is available, capable of engineering accuracy (and which may be sufficient for simulation and extrapolation purposes) improvements are needed especially for 3D wings and non-standard airfoils where the boundary-layer (at least on the upper surface) is brought close to or even beyond separation. Well designed experimental investigations will have to be performed to reach this goal.

Extensive and authoritative reviews of the flow phenomena described above may be found in AGARD CP-291 [11] on the Computation of Viscous-Inviscid Interaction (especially paper no. 1 by Le Balleur, no. 2 by Lock and no. 10 by Melnik); an article "Survey of techniques for estimation of viscous effects in external aerodynamics" by Lock and Firmin in [48], the paper [49] by Lock in [25] and a number of papers in [50]. The papers by Lock and Lock and Firmin should be consulted for a description of the idea of calculating a "real viscous flow" by the introduction of an "equivalent inviscid flow". In the 1985 review by Lock [49], recent modifications to the shape factor relations and skin friction formulae, as used in the lag

entrainment method, are described. These modifications are in part based on the ideas of Cross as discussed in section 4.4 of the present volume. This new version of the lag-entrainment method is especially better suited for calculating separated flow. The accuracy is shown to be good for engineering predictions; the reader is referred to Locks paper for a detailed discussion of some examples, a detailed calibration is however difficult because the experimental evidence for fully separated flow is sparse and of unknown accuracy. Further research along these lines should be pursued. For descriptions of recent benchmark experiments the reader is referred to the articles by Thompson and Whitelaw [51] and Nakayama [52]. These (and similar experiments which should be performed) deserve a thorough analysis, aimed at providing the badly needed turbulence modelling for trailing-edge and other separation regions.

#### 4.6.6. Turbulent separation

##### 4.6.6.1. Introductory remarks on turbulent separation

The improved computational capabilities, both due to hardware- and algorithm development, have led to the existence of many important CFD programs for viscous flows. For a review of these the reader is referred to the contributions by Chan (chapter 3.2.3) and Michel (4.3) in the present volume. However, it should not be forgotten that more simple methods, based on empirical correlations, may still be very useful in design and analysis, and certainly in simulation methodologies (see the contribution by Cross in chapter 4.4 in the present volume).

For critical flow phenomena such as shock-wave boundary-layer interactions, we will have to rely much more on empirical correlations, such as have been discussed by Stanewsky in chapter 4.5 of the present volume. In the current chapter we will concentrate on the separation prediction for turbulent flows not directly at the shock. Of course the weakening of a turbulent boundary layer by interaction with a shock, such that further downstream separation is provoked, will be included.

The subject of turbulent separation is in two respects more complicated than in the laminar case. Of course there is in the first place the need for an adequate turbulence model in computational procedures. In the second place it should be observed that, even for a flow which is steady in the mean, turbulent separation is an unsteady process. For a two-dimensional mean flow we can describe the "separation" or "detachment" process by means of a parameter  $\gamma$ , which is the fraction of time the instantaneous flow in the viscous sublayer is forward (Kline et al [53], Simpson [23]). Fig. 19, taken from Simpson [23] illustrates this phenomenon; the related terminology follows from fig. 20. It should be noted that  $\gamma$  is used to define the severity of the backflow which is then expressed in terms such as "incipient detachment", "transitory detachment" ( $\gamma = 50\%$ ), and "detachment" (time mean of wall shear is zero). Note that  $\gamma = 50\%$  and  $\bar{\tau}_w = 0$  are

only found at the same position when the histogram of velocity fluctuations is symmetric. For practical purposes the two positions may be assumed to coincide (Kline et al [53]). Kline and also Simpson use the word "detachment" where previously the word "separation" was used; in their terminology separation represents the flow phenomenon or region that includes detachment, a reverse flow zone and possibly a reattachment zone. In the present work we will be only concerned with the prediction of the mean flow and will stick to the phrase "separation" to denote the occurrence of a mean flow streamline leaving the wall. Observe that the experimental definition of a separation position may depend on the instrumentation or flow visualization procedure which has been used.

Much to the present authors surprise it was found, when studying the relevant literature, that the accuracy of turbulent separation prediction still leaves much to be desired. Many authors seem to stay away from separation (other than at shock wave - boundary layer interaction) and state that their methods "may be applicable to small separations only". Very often they seem satisfied when their methods "give some indication that separation may occur", sometimes due to break-down of the computational procedure.

Much attention has been given in recent years to the development of computational methods for viscous/inviscid interaction. Emphasis seems to have been on the computational procedures, more than on the required turbulence models. Much high quality experimental research will be needed to provide the required benchmarks for turbulence models. These investigations should include the effects of shock wave boundary layer interactions, laminar separation bubbles, trips, etc. on the turbulence structure of the downstream flow.

##### 4.6.6.2. Simple criteria for turbulent separation

In the literature very often the idea of a separation criterion is used to aid in determining when and where separation occurs. There seems to be some confusion in the use of the word "criteria" in relation to the prediction of separation and also of transition. It should be observed that the separation position can be defined precisely: for steady, laminar 2D flow as the position where  $\tau_0 = 0$  or where reversed flow near the wall sets in; for turbulent flow some time-averaged value of  $\tau_0$  should become zero; for 3D flow the topology of the skin-friction lines has to be considered. In all cases a precise definition of separation can be given and the separation position should in principle follow unambiguously from a calculation or experiment. In practice some problems may occur, because it may be difficult to measure wall shear stress or simple calculation methods may not provide  $\tau_0$  directly. Then some other parameter or a combination of parameters, has to be used to check on the occurrence of separation. These parameters should exactly and uniquely be related to  $\tau_0$  and therefore would provide an exact determination of separation. The

word "criterion" then should not be used. Note that the use of  $\frac{\theta}{U} \frac{dU}{dx}$  for non-equilibrium flow does not satisfy our requirements (see also chapter 4.4 by Cross); these parameters can only be used as part of more complicated expressions in which non-equilibrium effects have been taken into account.

Considering the present CFD capabilities we should not be satisfied with any method that does not provide a good prediction of separation. The use of "criteria" to "guessimate" separation should be avoided as far as possible.

With transition criteria the situation is different, because it may not be possible to define uniquely when a flow may be called turbulent. However, once such a definition would be given, the prediction of transition depends only on our ability to compute a transitional flow. Only when available calculation methods cannot distinguish whether the turbulent state has been reached, we are forced to use "transition criteria" which give an approximation only. Examples are Granville's criterion (a certain combination of



pressure gradient data and free stream turbulence level) or the  $e^n$  method which is based on linear stability theory. In these cases the word criterion can and should be used to indicate our inability for an exact prediction.

A number of separation criteria which have been and sometimes are still being used are the following:

- the shape factor  $H$ ; separation values between 2 and 4 have been proposed; it was shown by Cross (chapter 4.4 of this volume and [54]) that  $H = 4$  corresponds to separation of equilibrium flow and that values around 2 may occur in larger adverse pressure gradients as are found near trailing-edges (see also section 4.6.6.3).
- the pressure gradient parameter  $-\frac{\theta}{U} \frac{dU}{dx}$ ; values around 0.004 are often quoted [55].
- rapid growth of  $\delta^*$ .
- Stratford type criteria, where the pressure coefficient at separation, and hence the position of separation, follows from the boundary layer data at the position of minimum pressure and the downstream adverse pressure distribution.
- even the inability to proceed with a calculation procedure has been used as an indication of approaching separation.
- for trailing-edge separation induced by an upstream shock or "flow breakdown" between shock and trailing-edge, correlations between shock-upstream Machnumber, airfoil geometry and shape of the pressure distribution, etc. are being used.
- a well-known correlation for trailing-edge separation due to an upstream shock-wave has been developed by Kahn and Cahill (see discussions of it in the present volume in section 2.2.3.6 by Peterson and in 3.2.3. by Chan).

It should be stressed that criteria and empirical correlations are valid only in circumstances which are comparable to those used to derive them. When, for instance, new airfoil types are introduced, the older correlations may lose their value. One should constantly be aware of this. The more local the correlation is, the more universally it may be valid. With the present state of the art in CFD we should aim at computation of viscous flow in non-critical regions, using the proper shape factor correlations, taking into account the possible departure from equilibrium and, for other methods, using zonal turbulence modelling. It is advised, where possible, not to rely any more on simple correlations and criteria but to make use of the best CFD program which is available within the budget for a certain program. This budget should be at least as high as to allow the use of a boundary layer code with a better than "simple" separation criterion and including (strong) viscous/inviscid interaction. The use of empirical correlations should be reserved for "critical flow phenomena" as defined in chapter 4.2. The discussion on shock wave boundary layer interactions, as given by Stanewsky in chapter 4.5, may be quoted as an example. Furthermore it should be realised that the CFD programs, referred to above, will still rely on empirical information in the form of turbulence models or shape factor correlations.

To illustrate the above discussion on "simple separation criteria" we may refer to an interesting evaluation of such criteria by Hahn [56]. For two-dimensional incompressible flow the following separation criteria have been compared to a number of experimental results.

- Stratford
- Townsend + modified Townsend
- Goldschmied
- Bradshaw - Galea
- Robertson
- Sandborn - Liu
- Boeing boundary layer program based on the Nash-Hicks method.

The Stratford criterion is based upon a division of the boundary layer in a wall region and in an outer region with corresponding simplifying assumptions. This leads to a remarkable simple relation between the pressure coefficient at separation and the (turbulent) boundary layer parameters at the start of the pressure rise.

Roughly speaking all other criteria, except the boundary layer calculation method, are of the Stratford type where separation is predicted using some boundary layer characteristic at the beginning of the pressure rise region and the pressure distribution downstream; for further details see [56]. All criteria have been applied to measured pressure distributions which all show pressure gradient relief near separation. All calculations have been made for extrapolated pressure distributions, however, without taking into account the viscous/inviscid interaction. Fig. 21 shows, as an example, the results for experimental data due to Schubauer and Klebanoff. This shows clearly that some methods give early separation, some would not have shown separation at all if the real measured pressure distribution would have been used without interaction. Note that Townsend predicts  $C_p$  at separation very close, it should be observed however that his criterion was developed using these same experimental data.

An impression of the (lack of) accuracy can be obtained from figs. 22 through 27. A general conclusion is that a full boundary layer calculation gives better results than the simple Stratford type criteria. However the boundary layer calculations should be improved by using a strong interaction procedure. It should be noted that [56] dates from 1973. Our CFD capabilities have since then increased to such an extent that there is not much need to stick to the simple criteria.

Hahn's discussion of separation criteria for compressible flow is mainly restricted to transonic flow and especially in the shock region; trailing-edge separation is not discussed. Since the date of Hahn's review our knowledge on shock-wave boundary layer interaction has much improved; this has been discussed by Stanewsky in chapter 4.5 of the present volume, to which the reader is referred.

#### 4.6.6.3. Some results on shape factor correlations

Interesting shape factor correlations, in relation to "separation" and "detachment" have been discussed by Kline et al [53, 57] and by Simpson in his review paper: "Two-dimensional turbulent separated flow" [23].

The discussion by Kline relates to fig. 28 where a correlation plane of  $h$  vs  $\lambda$  is given, where  $h = \frac{H-1}{H}$  and  $\lambda = \delta^*/\delta$ . The wall-wake correlation according to Coles (curve W-W in fig. 28) is not most only weakly dependent on Reynolds number, and, in a zone of either "detachment" or reattachment  $h = h(\lambda)$  is linear and independent of  $Re$ . Separation for equilibrium flow according to Coles occurs for  $\lambda = 0.5$  and  $H = 4$ . Included in fig. 28 is the Sandborn-Kline correlation for "incipient detachment" (curve I-D). Kline mentions that all known points for detachment recorded in the literature are shown in the figure.

With the exception of flows far from equilibrium, all data center on the intersection of curve W-W and curve I-D, but considerable scatter exists. Simpson's version of the h-A diagram is reproduced here as fig. 29. Its description by Simpson in [23] is as follows:

"Sandborn and Kline observed that a family of power-law profiles seemed to fit data near where appreciable intermittent backflow was observed. This family of profiles yielded the relation

$$h = \frac{H-1}{H} = (2 - \frac{\delta^*}{\delta_{0.995}}) - 1$$

which is shown on fig. 29. The mean wall shearing stress is greater than zero at this condition. Another family of power-law mean velocity profiles that had zero shearing stress at the wall were used to describe conditions at detachment (eqn. 6 of Sandborn and Kline). Fig. 29 shows this h vs.  $\delta^*/\delta$  relation at turbulent detachment, which also correlates laminar detachment data. The shaded regions on this figure show the data used by Sandborn and Kline and Kline et al. (1983) that support these relationships.

Fig. 29 also shows h vs.  $\delta^*/\delta$  paths taken by several backward facing step reattaching and adverse-pressure-gradient-induced detaching flows. Using a modified Coles law-of-the-wall and law-of-the-wake mean velocity profile model, Kline et al. showed that the h vs.  $\delta^*/\delta$  path is only weakly Reynolds number dependent even for low  $\delta^*/\delta$  and is nearly the same for flows on flat or low curvature surfaces. The Perry and Schofield correlation produces a path among these data, as do the experiments of Chu and Young (1975). This path can be approximated by

$$h = 1.5(\delta^*/\delta)$$

for high Reynolds numbers. Note that it crosses the h vs.  $\delta^*/\delta$  relationships for intermittent backflow and detachment in the shaded regions. For near-equilibrium flows satisfying the Coles velocity profile model, intermittent transitory detachment occurs at  $\delta^*/\delta = 0.42$ , and  $H = 2.70$  (end of quote).

Although the description in the h-A plane, as quoted above, has been very useful in clarifying the "separation"/detachment characteristics of turbulent boundary layers, it draws too heavily on equilibrium flows and its related "wall-wake" velocity profile description. In order to make further progress the departure from equilibrium should be accounted for. A worthwhile start with this has been made by Cross in chapter 4.4 of the present volume. This line of attack has to be further pursued to arrive at a computational procedure which is sufficiently advanced to describe two- (and three-) dimensional turbulent separation to such an accuracy that it can be used for simulation purposes. In the opinion of the present writer we have not yet reached this state completely. In the next chapter we will briefly review the development of turbulent separation prediction in the last two decades, define the present state of the art and indicate where further research is needed.

#### 4.6.6.4 Development of turbulent separation prediction capabilities since 1968 and present state of the art

An important milestone to start any review of turbulent boundary layer prediction is the first Stanford conference in 1968 [58]. In this conference 33 incompressible two-dimensional boundary layer flows have been documented and 28 different methods have been used to compute these flows. Possible inaccuracies in the data were indicated using a "momentum balance" method obtained by integrating the momentum integral equation (without Reynolds normal stresses) w.r.t. x. Putting the skin-friction term in the righthand side of the equation and all remaining terms in the left-hand side, both sides were listed for all flows for various streamwise stations. As soon as an unbalance shows up, this may be due to inaccurate data, flow convergence or divergence or the existence of an important contribution of the normal Reynolds stresses. Especially near separation the two last mentioned effects may occur.

Although some of the 33 flows considered, showed separation in the experimental results, no precise conclusions on the suitability of the various methods for the prediction of separation could be drawn, either because the experiments were not extended far enough in the separated region or due to uncertainties about the momentum balance. Also the occurrence of pressure gradient relief near separation in the experimental results, without the use of viscous-inviscid interaction procedures in most of the computations, may have caused problems. Furthermore the uncertainty about the effect of the normal Reynolds stresses or a pressure gradient normal to the wall near separation may have been important. It is of course very difficult to distinguish between the various effects mentioned.

The outcome of this important conference was rather disappointing with regard to the quality of separation prediction at that time (1968).

From the conclusions of the evaluation committee we quote [58, pages 470 and 471].

"We have drawn no conclusion relative to the prediction of separation since none of the methods currently in use is really legitimate there, and the available data are likewise suspect. New carefully-cross-checked data thru separation are critically important. Some of the present methods which appear to show separation need to be critically examined to be sure the predictions are predictions of real physics and not just mathematical peculiarities of the formulation".

The above quotations clearly point out the deficiencies in separation prediction for incompressible turbulent flow as of 1968. They should not be taken to mean that a reasonable engineering accuracy, which might be sufficient for simulation/extra-polation methodologies, might not be obtained through small improvements.

The entrainment method, as first developed by Head [59], was one of the methods showing good results at the Stanford I meeting. Later it was improved by Green [60] through inclusion of a lag effect. The method is often used and seems to have been accepted for engineering calculations. As later developments also point to a preference to use the (lag)entrainment concept (see Chan, section 3.2.3 and Cross, chapter 4.4, both in the present volume) it seems useful to review the entrainment concept with special emphasis on its separation prediction qualities. In Green's version it is easy to take into account extraneous influences on

the turbulence structure by suitable adjustments to the dissipation length scale  $L/\delta$  (free-stream turbulence, longitudinal curvature, flow convergence or divergence).

Although the underlying mechanisms are not yet well established and probably quite different from case to case, the method may be useful for engineering purposes. Figs. 30a through 30e give some comparisons of Green's method with experimental data for the RAE 2814 airfoil at  $M = 0.725$ . It should be observed that some nominally 2D flows can suffer from flow convergence or divergence (detected through failure of the momentum balance). Differences between theory and experiment can also be due to growth of Reynolds normal stresses near separation. In making the comparisons Green has in some cases forced the calculated  $\theta$  to fit the experimental data by assuming that the whole difference was due to convergence or divergence; the calculated values of  $H$  and  $C_f$  are then in general improved. From these results it may be concluded that for

engineering purposes the two-dimensional version of the method can be accepted; some improvement near separation would be welcome however.

The prediction of the development of two-dimensional separated turbulent boundary layers by the lag-entrainment method has been discussed by East et al in [61]. An inverse mode has been added in which  $\delta^*$  is prescribed. It follows that the standard form (applied to low speed flows and transonic shock-induced separated flows) underestimates the shape parameter and overestimates the adverse pressure gradient in the separated region. The authors suggest that primarily this is due to the use of the shape parameter relationship which has a substantial influence on the predictions in separated flow but is based only on attached flow data. A modified relationship gives much improvement. Questions remain with regard to the quality of the experimental data (convergence/divergence) and the "equilibrium locus" used in the method which is based on attached flow data. More experimental data are needed.

Recently Lock described some modifications to the lag-entrainment method to improve upon its accuracy for separated flow (see section 4.6.5). Cross (see chapter 4.4) combined the entrainment concept with his modification of the Coles wall-wake description of turbulent boundary layers. Although all these results are promising, much more work than can be done in the present review, has to be performed to arrive at a definite procedure which is sufficiently accurate for simulation purposes. This is certainly the case for 3D boundary layers to which the lag-entrainment method has been extended by Smith [62, 63], see also section 4.6.8.

When reviewing the development and present status of turbulent boundary layer separation prediction, there is an impressive list of AGARD Conference Proceedings and Lecture Series to be consulted ([1] through [15]). In the present section we will briefly review this material as far as it is concerned with separation prediction.

In AGARD CP-83 (1971) Green reviews the (in 1971) current understanding of viscous-inviscid interactions, with particular reference to the characteristics of interactions on transonic swept wings and their dependence on Reynolds number. It is stated that "Away from shock waves, boundary layer separation depends on the upstream history of the flow in such a way that there is little point in attempting to isolate the separation process from the boundary layer development which precedes it. Boundary-layer development must be regarded as a whole and, if predictions have to be made, the only course open is to use a well-proven boundary-layer calculation method".

AGARD CP-102 (1972) contains a now classical paper by A.M.O. Smith on "Aerodynamics of high-lift airfoil systems". It gives an evaluation of the accuracy of some existing methods for the prediction of turbulent separation, namely Goldschmied, Stratford, Head and the Cebeci-Smith boundary-layer method. The last three mentioned "proved satisfactory for purposes of general engineering analysis". Some typical results for incompressible flow are shown in figs. 31, 32 and 33. Fig. 34 gives some further results obtained by the Cebeci-Smith method. It is concluded that "for rear separation (no laminar bubble-reattachment situation) existing boundary layer methods are sufficiently accurate" to justify their further engineering use. It is also claimed that the Cebeci-Smith method "can account for high Reynolds number and Mach number effects accurately".

In AGARD CP-168 (1975) the paper by Sirieix on "Decollement turbulent en écoulement bidimensionnel" (turbulent separation in 2D flow) quotes an analysis, extended to subsonic compressible flow that has been performed by Gerhart et al [64]. Eight different methods have been tested against experimental results by Alber et al [65] in one experimental set-up (fig. 35). Much more scatter is obtained than in the Cebeci-Smith exercise of fig. 34. Sirieix then concludes that even if separation in most "classical" cases is predicted well by the most elaborate boundary layer calculation methods (Bradshaw and Ferris), there remain certainly "rebellion cases".

In AGARD CP-174 (1975) Wu et al study transonic high Reynolds number flow separation with a severe upstream disturbance; a shock-generated local separation interacting with the downstream trailing-edge separation is a good example of such a phenomenon. "The boundary layer after suffering a disturbance, will deviate from the normal equilibrium status. Obviously, this disturbed flow will not react in the same manner to the downstream adverse pressure gradient as would the normal boundary layer flow". The test model used was a long and shallow cavity configuration. A controlled upstream disturbance is then provided by the rearward facing step of the cavity (height approximately equal to the boundary layer thickness). This provides a significant local separation and "enables the flow to go through the process of expansion, mixing, reattachment, recompression and relaxation. These are the significant ingredients encountered in most upstream disturbances". The downstream reattachment mechanism is provided by the forward facing step which gives a positive pressure gradient sufficiently strong to separate the flow locally. In the present reviewers opinion this is the type of experiment which should be used as benchmark for turbulence modelling.

AGARD LS-73 (1975) gives a good review of the status of computational procedures in 1975. A general conclusion is that the increased computational capabilities have resulted in many machine codes that can generate solutions but that there is an urgent need for more well-designed experiments to develop and test turbulence models. It is also realised that zonal modelling may be the way to go.

In AGARD CP-204 (1976) a good review of problems and possibilities of local prediction for engineering applications is given. As long as separated regions have a modest extension, accuracy was considered by some speakers to be sufficient for the purpose stated. Others noted a lack of understanding and computing capability especially for more extended separations.

Even in AGARD CP-271 (1979), especially devoted to "Turbulent Boundary Layers. Experiments, Theory and Modelling" not much new information on turbulent separation was provided; emphasis was on large-scale coherent structures and more advanced numerical viscous codes. The need for better turbulence models was clearly stated. It also was observed that turbulent normal stresses in streamwise direction have to be taken into account in the neighbourhood of separation. Progress was thought to be held up by the lack of good



experimental data on separating turbulent flow. To quote a remark made by Klebanoff in the final Round Table Discussion: "I have been observing and listening to the accounts of what has been accomplished and, in view of the difficulties that have been revealed relative to the handling of the very strong pressure gradients, and the difficulties in calculating separation, I believe I am permitted the observation that not much substantive progress has been made in the last 30 years". Of course it should be reiterated that the required accuracy for prediction or extrapolation purposes may be different and that good engineering methods might be based on current capabilities.

In AGARD CP-291 (1980) excellent reviews are given of the 1980 state of the art in the computation of viscous-inviscid interactions. Much attention is given to the coupling procedures as such; the viscous part has - in general - been restricted to the use of relatively simple integral methods. In this way the main viscous effects are represented reasonably well. It is not easy to grasp the accuracy of the various computations. Especially systematical research to establish the level of accuracy of the methods to predict separation is absent. Further study is needed to determine whether available methods and their further developments are suitable for "predictions", "simulations" or "extrapolations". Many of the methods presented stay away from separated flows. Nevertheless some methods may give good engineering results.

The 1980/1981 Stanford II conference on "Complex Turbulent Flows" [66] certainly deserves to be reviewed in the present chapter, if alone to show that even in the early eighties the prediction of turbulent separation is still a problem. For the present purpose the following flow cases, from the many discussed at the conference, are of interest:

- a. the NACA 4412 stalled airfoil at low speed
- b. Some transonic airfoils
- c. Internal flows

In the cases mentioned under (b) attention was restricted to fully attached boundary layers, as it was felt that separated cases involved complicating features that would best be addressed in the conference section dealing exclusively with separated flow. Some reservation was expressed in using these datasets because of uncertainties due to wind tunnel wall- and pitot tube interference.

A very important example of an internal flow is the stalled diffuser studied by Simpson et al. This case will be discussed separately below. Case (a) is concerned with "massive separation", the prediction of which may not be very sensitive to details of turbulence modelling. This is probably the reason that good predictability was reported. However prediction of the separation position itself does depend on the quality of the turbulence model. Not much progress in this respect was reported. It was stated that "the search for a universal model of turbulence, which can provide answers of an engineering accuracy for a wide range of turbulent homogeneous and shear flows is premature and may remain 'illusory'. As a consequence the idea of 'zonal modelling' was strongly advocated by Kline. This means that not a universal turbulence model is sought but that in different zones, where different types of flow occur, a different turbulence model is used. In the present context of turbulent flow calculations related to the simulation problem, this means that it may be necessary to develop different turbulence models for attached or separated flows, the flow downstream of various trips, separation bubbles, natural transition or shock-wave boundary layer interaction, or in the trailing-edge regions.

Some further conclusions from this meeting deserve to be quoted:

- "Integral methods have emerged as providing powerful, yet economical, approaches providing their limitations are recognized and respected. It is a level at which one is modelling turbulent flows rather than turbulence ....."
- "At the differential level the Conference results have underlined that mixing-length models should not be used in compressible flows, for the length to reattachment seems to be consistently overpredicted ....."
- "The general accuracy of results involving separated flows was significantly worse than for corresponding attached flows. For a flow involving separation, the Reynolds stress methods did no better than the less sophisticated approaches, and, in a restricted sense, the integral methods gave the best accuracy".
- "It is clear that there are great difficulties involved in truly three-dimensional computations".

From the previous review it has to be concluded that, although much progress has been made on viscous flow computation, a clear picture on the prediction of turbulent separation has not yet been obtained. We can do no better than conclude this review by referring to a recent authoritative discussion on two-dimensional turbulent separation by R.L. Simpson [23] (47 pages text, about 400 references and 93 figs!). An important contribution to the subject has been given by Simpson himself and his group [67, 68].

Present reviewer considers this to be the most complete recent review of the subject. It is not easily digested in sufficient detail; therefore we will restrict ourselves to some main conclusions.

In [23] both airfoil and diffuser flows are discussed. Many of the results shown have been obtained by Simpson and co-workers in the channel shown in fig. 36a and 36b. Results on shape factor correlations have been discussed already in section 4.6.6.3 in relation to the work of Kline.

Some important statements made by Simpson which are relevant to the present discussion are very briefly summarized below.

- Normal Reynolds stress terms play an important part in both the momentum and the turbulence energy equations for flows approaching separation.
- Eddy viscosity and mixing-length values decrease as detachment is approached.
- The turbulent energy production through the normal stresses is important in separating flows. Fig. 37 shows this for flows approaching detachment.
- Streamwise surface curvature influences the behaviour of a turbulent boundary layer.
- Turbulent shear stress near reattachment is very much higher than at detachment for the same mean velocity profile shape factor. Some distance downstream of reattachment these stresses decay to levels as found for attached boundary layers (fig. 38). Note that results, as shown in fig. 38 can only be used in computational procedures if these can be brought in the form of a universal correlation.
- Shock-induced detachment produces a flow structure similar to that for detached incompressible flows. Mean velocity profiles and the turbulence structure downstream of reattachment look qualitatively like that for incompressible reattaching flows.
- Clearly, more experiments are needed to firmly establish the nature and structure of separating and reattaching flows (including effects of wall curvature and compressibility).
- Calculation methods need substantial improvement before they can be used confidently to compute flows for which we do not already know the answers from experiments.

As a main conclusion of the present review emerges the following:

- the accurate prediction of 2D turbulent separation leaves much to be desired, although slight improvements on the entrainment type methods might be sufficient for simulation purposes

- much more attention should be given to zonal turbulence modelling with particular attention to separation/detachment and reattachment zones.

#### 4.6.7. On the possibility of turbulent separation bubbles (e.g. "cove separation")

It might be possible that in turbulent flows, developing under an adverse pressure gradient followed by a strong favourable pressure gradient, a "turbulent separation bubble" will form. This might be the case for instance on the lower surface of a rear loaded airfoil ("cove separation"). During the literature review which was undertaken before writing the present paper, no direct information on this type of flow was encountered. It can be expected however that turbulent separation rapidly followed by turbulent reattachment, will show a peculiar turbulence structure. Indeed a good candidate flow for zonal turbulence modelling!

#### 4.6.8. On the separation properties of three-dimensional turbulent boundary layers

A good review of the 1984-knowledge of the three dimensional turbulent boundary layer, including its separation characteristics, can be found in the report on an FDP-Round table discussion [24]; some updating has been given in [26].

In addition to the problems already encountered in the 2D-case (such as the lack of adequate turbulence models, the need to use strong interaction procedures) there arise some new problems. Prominent is the question of the direction of the shear stress vector in relation to that of the velocity gradient vector: the two need not coincide. It appears that the cross-wise eddy viscosity is smaller than that in the streamwise direction. In general it may be concluded that current turbulence models are inadequate for 3D-separation prediction but that this will not show up in cases where pressure forces dominate over the shear stresses. In the contribution of Young to [24] reference is made to work by Cross (see also chapter 4.4 in the present volume) in which integral methods are developed using velocity profiles in 2D and 3D which combine the 2D law of the wall with a 3D wake-law. With reference to some promising results obtained in 2D it is hoped that extensions to 3D may give an improvement over existing methods for flows involving limited regions of separation. In total the conclusion about 3D turbulent boundary layer separation must be that our knowledge is inadequate and that well-planned and carefully executed experiments are needed to provide a data base that will challenge the development of computational methods and provide basic insight into important viscous phenomena.

#### 4.6.9. Buffeting

##### 4.6.9.1. Introduction on buffeting (contributed by J.B. Peterson)

Aircraft buffet is the aeroelastic response of the aircraft structure to the randomly fluctuating aerodynamic forces developed by separated flows, primarily on the wings. Models of new aircraft designs are usually tested in wind tunnels to determine where buffet might be encountered. For transport aircraft the concern is primarily for the boundaries of buffet onset since buffet brings about unpleasant vibrations and degradation of performance. Fighter aircraft, on the other hand, regularly maneuver in the buffet area and their concerns are (1) the effects of buffet vibrations on aircraft instrumentation such as navigation and fire control equipment, (2) degradation of performance because of increased drag and decreased lateral stability which detracts from tracking capability and (3) excessive structural loads on the aircraft tail surfaces.

Many different methods are used to conduct buffet tests in wind tunnels. The two most widely used methods are (1) measure the response of a dynamically scaled aeroelastic model at buffet conditions and (2) measure the pressure fluctuations on a rigid wind-tunnel model and calculate the dynamic response when these pressures act on the flexible airplane structure. Each of these methods has its advantages and disadvantages, and there is still considerable room for improvement in the accuracy and the simplicity of these procedures. The dynamically scaled aeroelastic model method has been shown to give reasonably accurate results [69], but the construction of the model is very complicated and expensive. The model in [69] was constructed with steel spars in the wings and fuselage connecting segmented sections made of balsa and fiberglass, ballasted to the required mass. Research on methods of constructing dynamically scaled aeroelastic models of simpler construction such as composite construction materials may improve the practicality of buffet tests considerably. The method of measuring pressures and then calculating the structural response requires that the pressures be measured over almost the entire surface of the wing (and tails, for cases where the tails might be involved in the buffet response of the airplane). In cases where the buffet pressure can cause deformation of the wing structure, enough to effect the pressures, this method cannot be used. In cases where the structure is not deformed significantly, this method requires a considerable amount of pressure instrumentation. The development of a less complicated method of measuring the fluctuating pressures over an entire wing may well be an area for future research in this field. Whether there is a Reynolds number effect on buffet and; if so, how much of an effect there is, is still a subject for research. Configurations that have sharp leading edges and little camber such as the sharp-leading-edge delta wing in [70] show little Reynolds number effect on the angle of attack for buffet onset, presumably because separation is forced to occur on the sharp leading edge. However, a sharp-leading-edge delta wing with camber, especially configurations with highly deflected leading-edge flaps will probably have Reynolds number effects. The blunt-leading-edge rectangular wing tested by Boyden [70] showed large Reynolds number effects on the angle of attack for buffet onset, but transition was not fixed during this test (see figure 4 of section 2.2.2, High Aspect Ratio Wings).

Other tests with blunt leading edges and transition fixed [71, 72, 73] correlated well with full scale indicating that the Reynolds number effects are small (see figures 5, 6 and 7 of section 2.2.2, High Aspect Ratio Wings). Probably, Reynolds number effects are very configuration dependent and categorizing the types of configurations that have Reynolds number effects is a field for future research. The state of the boundary layer at separation is probably very important to the subsequent development of the separated flow at buffet. If the boundary layer is laminar at the separation point at full-scale Reynolds numbers, then the boundary layer should be laminar at low Reynolds numbers, too. In order to duplicate the relative thickness of the laminar boundary layer at separation in low Reynolds number flow, it might be possible to use suction through porous surfaces to reduce the relative boundary layer thickness to match the relative thickness of the full-scale Reynolds number flow. On those configurations that have a turbulent boundary

layer at the separation location, fixing transition would seem to hold promise of simulating higher Reynolds number results in a wind tunnel. Of course, the relative thickness of the turbulent boundary layer ought to be duplicated too, perhaps with surface suction to reduce the thickness to the relative thickness of the full-scale Reynolds number flow. Determination of the important boundary layer parameters ( $\theta$ ,  $\delta^*$  and  $H$ ) for simulating full-scale Reynolds number flow in buffet is an area for research. Various locations and means of fixing transition should be investigated to determine if full scale Reynolds number flow could be duplicated by controlling the position of transition. It may be that boundary-layer trips that would act as tiny vortex generators might be effective in simulating high Reynolds numbers in low Reynolds number flows. The use of computational fluid dynamics to extrapolate wind-tunnel-buffet results to full-scale Reynolds numbers is an area that requires much development. At present, CFD is not able to calculate complicated three-dimensional buffet flows reliably. Perhaps development of better turbulence models for use in buffet calculations would enable better buffet calculations to be made. Future aircraft may have active control devices to suppress or eliminate buffet. Simulation of higher Reynolds numbers on these devices may require development of new procedures. Also, future aircraft may have extensive amounts of laminar flow on the wings which may or may not make simulation of higher Reynolds numbers more difficult.

It may then be concluded that research on simulation of higher Reynolds numbers in buffet tests is complicated by the fact that buffet is a very configuration dependent phenomenon. Further research into the Reynolds number sensitivity of various configurations such as sharp leading-edge configurations with camber of deflected leading-edge flaps is certainly warranted. Previous results on round leading-edge wings have shown that fixing transition with boundary layer trips has been successful at simulating higher Reynolds number results in the wind tunnel in some cases [71, 72, 73].

#### 4.6.9.2. Buffet prediction

As has been stated in section 4.6.9.1, a valid windtunnel investigation on buffeting would require a dynamically scaled aeroelastic model in addition to the requirement of duplicating full scale Mach and Reynolds numbers. Using a rigid model instead, measuring the pressure fluctuations on this model and calculating the dynamic response when these fluctuating pressures would act on the real aircraft structure, assumes that these pressure fluctuations would not be influenced by the actual flexible response. Whether this is sufficiently true could be a matter of debate. Once the idea of using a rigid model at the correct Mach number has been accepted, we only have left the scale effect due to Reynolds number. It might be that the simulation procedure for buffet research would then be very similar to those for steady forces and moments. It should not be ruled out however that other boundary layer parameters have to be reproduced than for steady force measurements. Further research into this matter may be required.

Recently an experimental study of buffeting has been started in the transonic windtunnel T2 at ONERA/CERT [74] using a 180 mm chord RA16 airfoil at  $M = 0.7$  and  $R = 4 \times 10^6$ . From unsteady pressure measurements it follows that buffeting is related to an oscillation in the location of the upsideside shock wave, coupled with boundary layer separation downstream of the shock. Frequencies of the order of 100 Hz are found which do not correspond to any mechanical vibration of the airfoil. In some recent studies of airfoil related buffet by Basler at DFVLR [75] it was shown that: (These results were communicated to the present author by dr. E. Stancwsky).

- buffet onset (here the beginning of strong shock oscillations) occurred as soon as total separation occurred on the airfoil upper surface. "True" buffet onset is hence related to the development of separation and therefore governed, in the present context, by the viscous parameters dominating separation.
- the buffet process may be closely related to the growth rate of the separation bubble with increasing shock-upstream Mach number. This growth rate depends on some boundary layer thickness parameter upstream of the shock (see 4.5) and hence on Reynolds number. Basler found accordingly that the buffet frequency for a turbulent boundary layer interaction decreased with Reynolds number.

Simple prediction methods have been developed by e.g. Thomas in which the extent of the separated zone is taken as a measure for the occurrence and severity of buffeting. For two-dimensional airfoils it is claimed that buffet onset is reached when the turbulent separation point has moved upstream from the trailing-edge up till 90% chord [76, 77].

For three-dimensional wings the chord-wise extent of the separated zone is weighed with the distance to the root chord. In this way some measure for the unsteady wingroot bending moment is said to be obtained [78].

Before the above mentioned, simplified, methods of buffet prediction can be used with confidence, an extensive research program has to be carried out in which the results of various methods are compared with each other and with the full scale results.

#### 4.6.10. Concluding remarks and recommendations

As a general conclusion of the present chapter 4.6 on "classical separation, trailing-edge flows and buffeting" it has to be stated that our present capabilities for turbulent separation prediction are at a disappointingly low level. It is therefore not surprising that the usual recommendation that "much more research is needed" is also given here. Furthermore, even if separation could be predicted accurately, there remains the question about the proper simulation methodology. A few important points seem to be:

- turbulent separation should occur at the right position, with the correct boundary layer thickness and with proper downstream effects on circulation for instance
- for laminar separation the proper downstream development of the reattaching turbulent boundary layer is the most important.

Some specific recommendations are:

1. Laminar separation bubbles may have a large effect on turbulence structure at and downstream of reattachment. Adequate turbulence models in a sufficiently general form still have to be developed for this type of flow. It seems less important to simulate the bubble itself than its downstream effects.
2. Similar remarks as under 1, may apply to the turbulence structure downstream of trips and shock wave boundary layer interaction regions.
3. Turbulent separation prediction in 2D flows requires better (turbulence) modelling including Reynolds

normal stresses, normal pressure gradients and strong interaction procedures.

4. Although no fully satisfactory methods for turbulent separation prediction in simulation methodologies are readily available, it is expected that for 2D flows workable methods can be obtained by not too extensive modifications to the present state of the art (exemplified by the lag-entrainment method).
5. Reliable prediction of 3D turbulent separation requires much more experimental research to derive adequate shape factor correlations and turbulence models.
6. Separation near a trailing-edge should be such that the correct circulation is obtained. (More general, even without separation, the flows approaching the trailing-edge along the upper- and lower surface respectively, should be such that the correct circulation is obtained). Important parameters may be momentum loss, displacement thickness, shape factor, turbulence structure.
7. Research on simulation of higher Reynolds numbers in buffet tests is complicated by the fact that buffet is a very configuration dependent phenomenon. Further research into the Reynolds number sensitivity of various configurations such as sharp leading-edge configurations with camber of deflected leading-edge flaps is certainly warranted.
8. Before simplified methods of buffet prediction, as discussed in 4.6.9.2, can be used with confidence, an extensive research program has to be carried out in which the results of various methods are compared with each other and with the full scale results.

#### 4.6.11. References

##### AGARD Conference Proceedings

1. CP-35 Transonic aerodynamics, 1968.
2. CP-83 Facilities and techniques for aerodynamic testing at transonic speeds and high Reynolds number, 1971.
3. CP-93 Turbulent shear flows, 1971.
4. CP-102 Fluid dynamics of aircraft stalling, 1972.
5. CP-168 Flow separation, 1975.
6. CP-174 Windtunnel design and testing techniques, 1975.
7. CP-204 Prediction of aerodynamic loading, 1976.
8. CP-210 Numerical methods and windtunnel testing, 1976.
9. CP-226 Unsteady airloads in separated and transonic flow, 1977.
10. CP-271 Turbulent boundary layers - experiments, theory and modelling, 1979.
11. CP-291 Computation of viscous-inviscid interactions, 1980.
12. CP-296 Boundary layer effects on unsteady airloads, 1980.
13. CP-348 Windtunnels and testing techniques, 1983.
14. CP-365 Improvements of aerodynamic performance through boundary layer control and high lift systems, 1984.
15. CP-374 Transonic unsteady aerodynamics and its aeroelastic applications, 1984.

##### AGARD Lecture Series

16. LS-73 Computational methods for inviscid and viscous two- and three-dimensional fields, 1975.
17. LS-74 Aircraft stalling and buffeting, 1975.
18. LS-94 Three-dimensional and unsteady separation at high Reynolds numbers, 1978.

##### AGARDographs

19. AG-223 Fernholz, H.H. and Finley, P.J.: A critical compilation of compressible turbulent boundary layer data. AGARDograph no. 223, 1977.
20. AG-253 Fernholz, H.H. and Finley, P.J.: A critical commentary on mean flow data for two-dimensional compressible turbulent boundary layers. AGARDograph no. 253, 1980.
21. AG-263 Fernholz, H.H. and Finley, P.J.: A further compilation of compressible boundary layer data with a survey of turbulence data. AGARDograph no. 263, 1981.
22. AG-266 Spee, B.M. and Yoshihara, M. (eds): Applied Computational Transonic aerodynamics, 1982.
23. AG-287 Simpson, R.L.: Two-dimensional turbulent separated flow, Vol. 1, 1985.

##### AGARD Reports

24. R-719 Three-dimensional boundary layers. Presentations at an AGARD FDP Round Table Discussion on 3D Boundary Layers. Brussels, 24 May 1984  
Contains:



H. Yoshihara: Introductory Remarks.  
 Michel, R.: Three-dimensional boundary layers and shear flows activities at ONERA/CERT.  
 Hornung, H.: Three-dimensional boundary layers. A report on work in Germany.  
 Van den Berg, B.: Three-dimensional boundary layer research at NLR.

Young, A.D.: Brief review of current work in the U.K. on three dimensional boundary layers.  
 Cebeci, T.: Problems and opportunities with three dimensional boundary layers.  
 Whitehead, R.E.: Summary Remarks.

- 25. R-723 Aircraft drag prediction and reduction, 1985.
- 26. R-741 Computation of three-dimensional boundary layers including separation. AGARD-FDP-VKI Special course, April 14-18, 1986. (Speakers: Cousteix, Bradshaw, Van den Berg, Arnal, Hirschel, Cebeci, Le Balleur, MacDonald Govindam).

Further references quoted in the text

- 27. Bertelrud, A.: An experimental and computational investigation of a swept wing flow at subsonic speeds. AIAA Paper 78-1200.
- 28. Bertelrud, A.: Local skin friction and static pressure on a swept wing in flight. AIAA Paper 80-0423CP.
- 29. Muller, TH.J. (editor): Proceedings of the conference on low Reynolds number airfoil aerodynamics. The University of Notre Dame, UNDAS-CP-77 B123, June 1985.
- 30. Gleyzes, C., Cousteix, J. and Bonnet, J.L.: Theoretical and experimental study of low Reynolds number transitional separation bubbles. [29], p. 137-152).
- 31. Ingen, J.L. van and Boermans, L.M.M.: Research on laminar separation bubbles at Delft University of Technology in relation to low Reynolds number airfoil aerodynamics ([29], p 89-124).
- 32. Ingen, J.L. van and Boermans, L.M.M.: "Aerodynamics at low Reynolds numbers: a review of theoretical and experimental research at Delft University of Technology". Paper nr. 1 in "Aerodynamics at low Reynolds numbers,  $10^4 < Re < 10^6$ , International Conference Organised by the Royal Aeron. Soc., London, 15-18 October 1986.
- 33. Vatsa, V.N. and Carter, J.E.: Analysis of airfoil leading-edge separation bubbles. AIAA Journal, Vol. 22, no. 12, December 1984, p 1697-1704.
- 34. Hall, M.G.: Scale effects in flows over swept wings. Paper no. 1 in [2].
- 35. Dobbinga, E., Ingen, J.L. van, Kooi, J.W.: Some research on two-dimensional laminar separation bubbles. AGARD CP-102, paper nr. 2. Lisbon, 1972.
- 36. Ingen, J.L. van: On the calculation of laminar separation bubbles in two-dimensional incompressible flow. In AGARD CP-168: Flow Separation, Göttingen, 1975.
- 37. Ingen, J.L. van: Transition, pressure gradient, suction, separation and stability theory. In AGARD CP-224: Laminar-Turbulent Transition, Copenhagen, 1977.
- 38. Berg, B. van den: Role of laminar separation bubbles in airfoil leading-edge stalls. AIAA Journal, Vol. 19, No. 5, May 1981, p 553-556.
- 39. Oudheusden, B. van: Experimental investigation of transition and the development of turbulence in boundary layer flow in an adverse pressure gradient. Engineering Thesis, Delft, 1985 (limited distribution).
- 40. Arnal, D. and Juillen, J.C.: Resultats experimentaux relatifs a l'influence des processus de transition sur la structure initiale d'une couche limite turbulente. Paper 22 in [10].
- 41. Groenewoud, G.J.H. van: An experimental and theoretical investigation of boundary layer transition on the Eppler 603 airfoil section in the windtunnel and in free flight. Unpublished Thesis, Delft 1982 (limited distribution).
- 42. Lindhout, J.P.F., Moek, G., Boer, E. de and Berg, B. van den: A Method for the Calculation of 3D Boundary Layers on Practical Wing Configurations. NLR MP 79003U. Also: Journal of Fluids Eng., Vol. 103, pp 104-110.
- 43. Boer, de and Lindhout: User's guide of BOLA, the NLR calculation system for 3D-boundary layers of non-developable surfaces, Version I, NLR Memorandum IN-83-016U.
- 44. Bruin, de and Boer, de: User's guide of BOLA-2D, the NLR-method for the calculation of (quasi) two-dimensional boundary layers, NLR Memorandum AI-82-014-U.
- 45. Bruin, de: Scrutinization of the constants used in the turbulence model of the boundary layer calculation method BOLA, NLR Memorandum AI-83-017U.
- 46. NLR Memorandum AI-84-019.
- 47. Hirschel, E.H. and Lucchi, C.W.: On the Kutta condition for transonic airfoils. MBB-UFE 122-AERO-MT-651, 1983.

48. Roe, P.L. (ed.): Numerical methods in aeronautical fluid dynamics; Proceedings Conf. Univ. of Reading, 1981. And especially a contribution by Lock and Firmin: "Survey of techniques for estimating viscous effects in external aerodynamics", p 337-430.
49. Lock, R.C.: Prediction of the drag of wings at subsonic speeds by viscous/inviscid interaction techniques. Paper no. 10 in [25].
50. Cebeci, T. (ed.): Numerical and physical aspects of aerodynamic flows 11, 1983.
51. Thompson, B.E. and Whitelaw, J.H.: Characteristics of a trailing-edge flow with turbulent boundary-layer separation. J. Fluid Mech., 1985, Vol. 157, p 305-326.
52. Nakayama, A.: Characteristics of the flow around conventional and supercritical airfoils. J. Fluid Mech., 1985, Vol. 160, p 155-179.
53. Kline, S.J., Bardina, J.G. and Strawn, R.C.: Correlation of the Detachment of Two-dimensional Turbulent Boundary layers. AIAA Journal, Vol. 21, no. 1, January 1983, p 68-73.
54. Cross, A.G.T.: Parameters affecting shock boundary layer interaction and "classical" separation. Note YAD5110, British Aerospace Brough, February 1986. (See also section 4.4 of present volume and ICAS 1986).
55. Nash, J.F. van MacDonald, A.G.J.: The calculation of momentum thickness in a turbulent boundary layer at Mach number up to unity. ARC-CP 963, 1967.
56. Hahn, M.: Evaluation of separation criteria and their application to separated flow analysis. AFFDL-TR-72-145, 1973.
57. Kline, S.J.: Contribution to round table discussion in [11].
58. Coles, D.E. and Hirst, E.A.: Proceedings Computation of Turbulent Boundary Layers - 1968-AFOSR-IFP-Stanford Conference. Vol. I: Methods, Predictions, Evaluation and Flow Structure. Vol. II: Compiled Data.
59. Head, M.R.: Entrainment in the turbulent boundary layer, R&M 3152, 1958.
60. Green, J.E., Weeks, D.J. and Brooman, J.W.F.: Prediction of turbulent boundary layers and wakes in compressible flow by a lag-entrainment method. R&M 3791, 1973.
61. East, L.F., Smith, P.D. and Merryman, P.J.: Prediction of the development of separated turbulent boundary layers by the lag-entrainment method. RAE-TR-77046, 1977.
62. Smith, P.D.: Calculation methods for three-dimensional turbulent boundary layers. R&M 3523, 1966.
63. Smith, P.D.: An integral prediction method for three-dimensional compressible turbulent boundary layers. R&M 3739.
64. Gerhart, P.M. and Bober, L.J.: Comparison of several methods for predicting separation in a compressible turbulent boundary layer. NASA TM X-3102, 1974.
65. Alber, I.E. et al: An experimental investigation of turbulent transonic viscous-inviscid interactions. AIAA Journal, Vol. 11, May 1973.
66. The 1980-1981 AFOSR-HTTM-Stanford Conference on: Complex turbulent flows. Comparison of computation and experiment. September 14-18, 1981. Stanford (data 1980).
67. Collins, M.A. and Simpson, R.L.: Flowfield prediction for separating turbulent boundary layers. Rept. WT-4. South. Meth. Univ. Dept. Civil and Mech. Eng., Feb. 1976.
68. Simpson, R.L., Chew, Y.T. and Shivaprasad, B.G.: The structure of a separating turbulent boundary layer. Part 1: Mean flow and Reynolds stresses, Part 2: Higher order turbulence results. Dec. 1981. Shilok, K., Shivaprasad, B.G. and Simpson, R.L.: Transverse velocity measurements. J.F.M., Vol. 113, Dec. 1981.
69. Hanson, P.W.: Evaluation of an Aeroelastic Model Technique for Predicting Airplane Buffet Loads. NASA TN D-7066, February 1973.
70. Boyden, R.P. and Johnson, W.G.: Results of Buffet Tests in a Cryogenic Wind Tunnel. NASA TM 84520, September 1982.
71. Reed, W.H., III: Comparisons of Flight Measurements with Predictions from Aeroelastic Models in the NASA Langley Transonic Dynamics Tunnel. AGARD Conference Proceedings No. 187. Flight/Ground Testing Facilities Correlation. April 1976.
72. Hopps, R.H. and Danforth, E.C.B.: Correlation of Wind Tunnel and Flight-Test Data for the Lockheed L-1011 Tristar Airplane. AGARD Conference Proceedings no. 242. Performance Prediction Methods, May 1978.
73. Elsenaar, A.: Experiences with Transition Fixation in the High-Speed Regime at NLR. Grenzschichtsteuerung durch Transitionsfixierung (Boundary Layer Control by Transition Fixing), DFVLR Mitteilung 84-17.
74. Michel, R.: Private communication.

75. Basler, D.: Paper presented at the AIAA Aerospace Sciences Meeting, Reno, Nev. Jan. 1987.
76. Thomas, F.: Ermittlung der Buffeting-Grenzen von Tragflügeln. Dornier Bericht 65/6, 1965.
77. Thomas, F. and Redeker, G.: A method for calculating the transonic buffet boundary including the influence of Reynolds number. Paper no. 3 in [2].
78. Redeker, G. and Proksch, H.J.: The prediction of buffet onset and light buffet by means of computational methods. Paper 22 in [7].



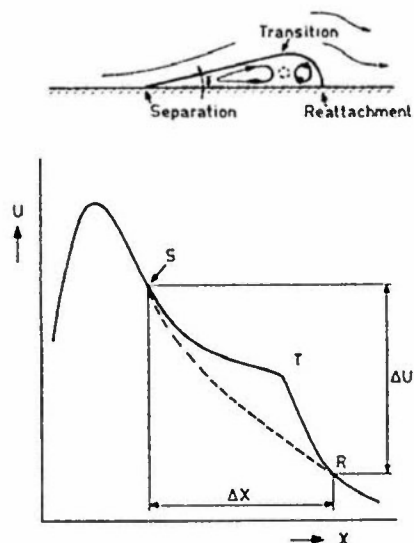


Fig. 1: Schematic diagram of flow field and pressure distribution in a laminar separation bubble (S = separation, T = transition, R = reattachment).

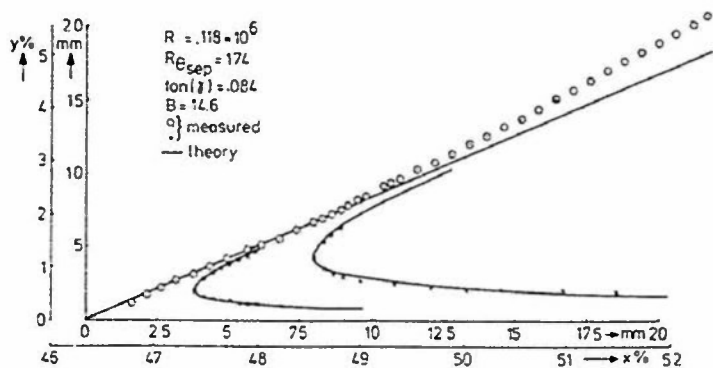


Fig. 2: Streamlines in a laminar separation bubble obtained from flow visualization with smoke (taken from [35]).

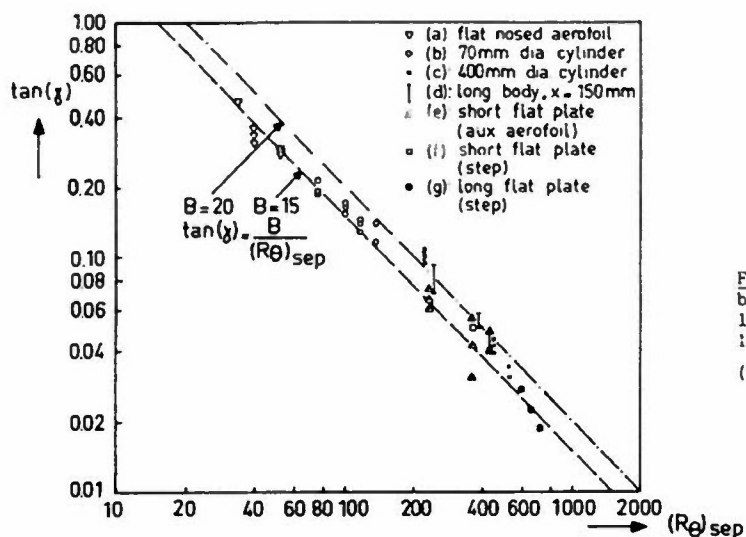


Fig. 3: An empirical correlation between the angle  $\gamma$  at which the laminar separation streamline leaves the wall and  $(Re)_{sep}$  (taken from [35]).

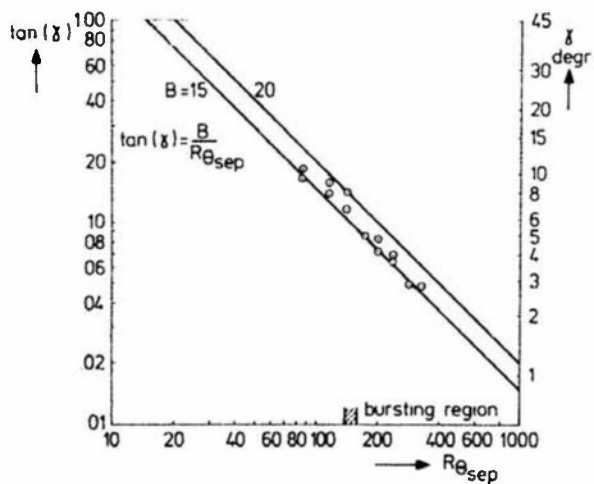


Fig. 4: Separation angles  $\gamma$  measured on a Wortmann FX66-S-196V1 airfoil with and without bursting (taken from [36]).

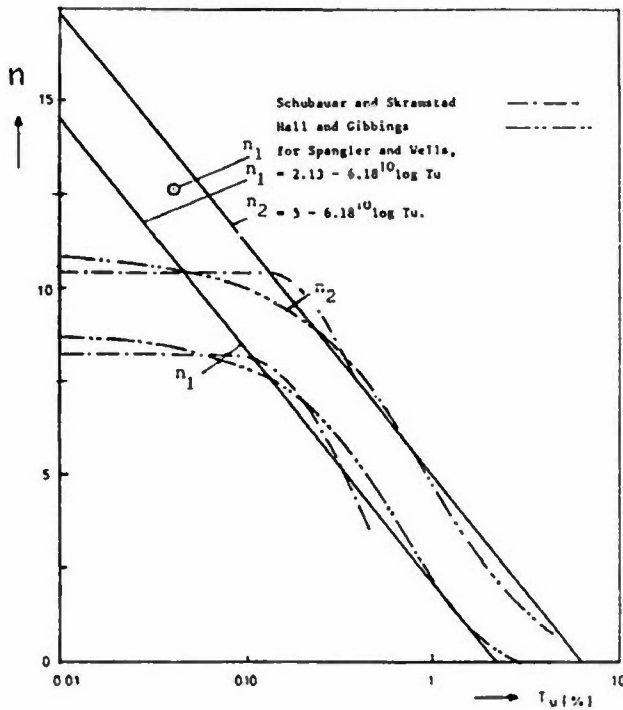
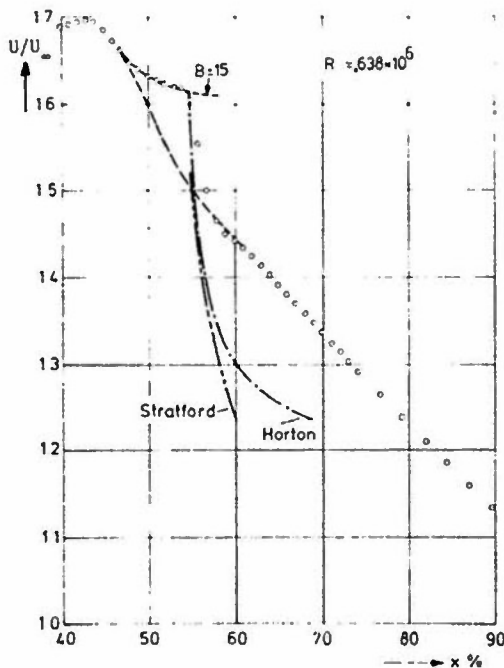
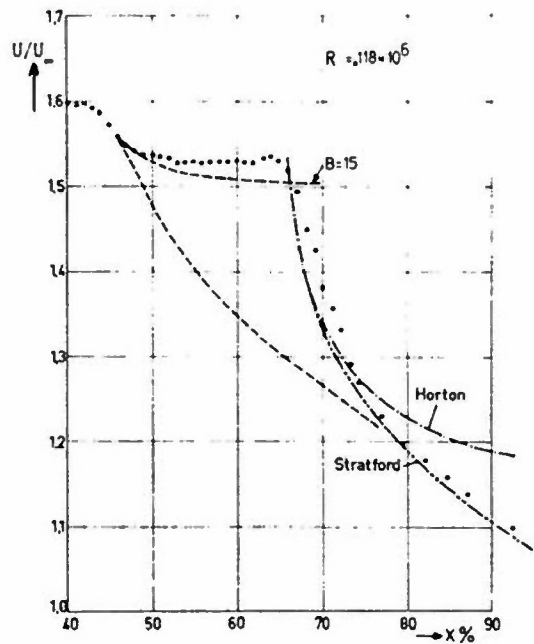


Fig. 5: The critical amplification factor  $n$  in the  $e^n$  method for transition prediction as a function of the "effective turbulence level"  $Tu$  (%). (Taken from [37]).  
 $n_1$  = beginning of transition region  
 $n_2$  = end of transition region.



(a)  $R = .638 \cdot 10^6$



(b)  $R = .118 \cdot 10^6$

Fig. 6: Some typical examples of the prediction of the pressure distribution, transition and reattachment/bursting of laminar separation bubbles on a Wortmann FX66-S-196V1 airfoil (taken from [36]).

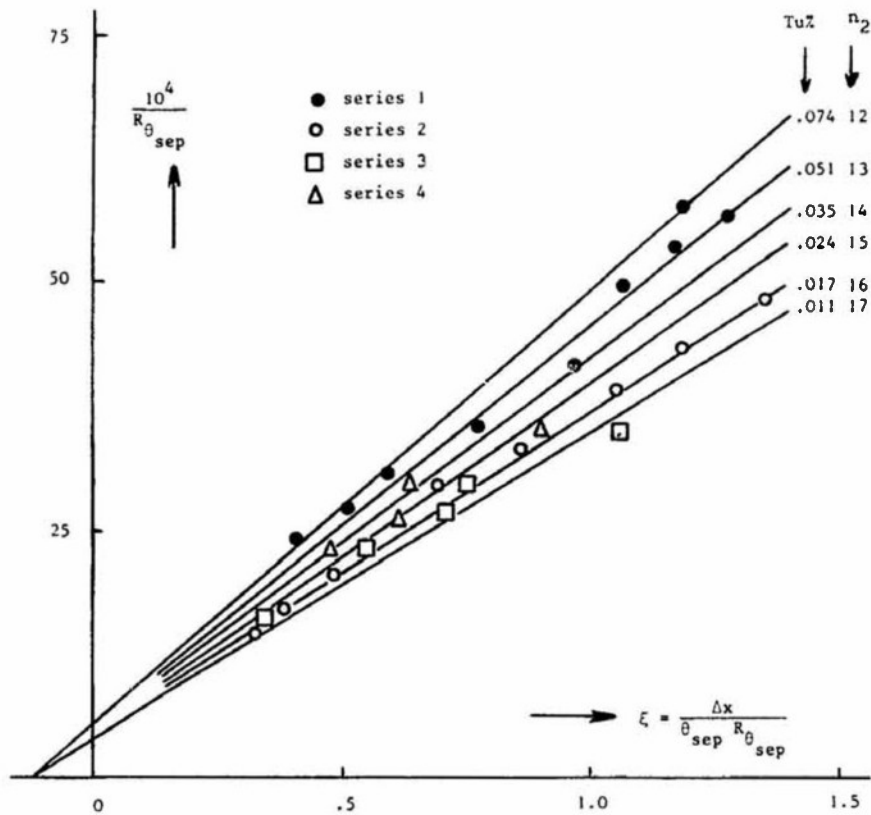
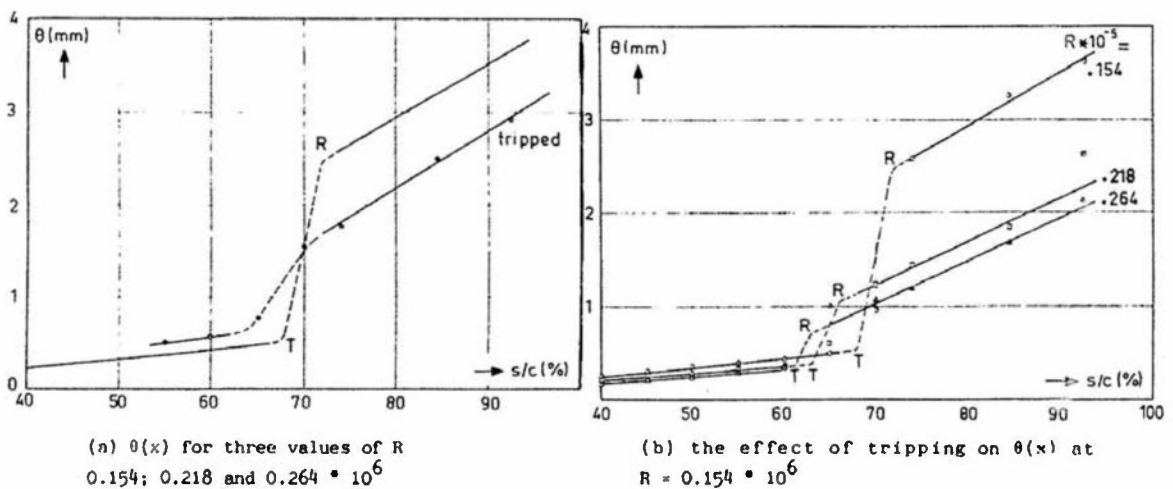


Fig. 7: Results of van Ingen's short-cut method for the prediction of the end of transition ( $n_2$ ) in the laminar separation bubble (taken from [37]).

Series 1: Wortmann airfoil FX66-S-196V1,  $\alpha = 1^\circ$  in a small noisy tunnel; series 2: the same airfoil in a large low turbulence tunnel; series 3: circular cylinder with tail in a large low turbulence tunnel; series 4: the same as series 3 but noise from the small tunnel recorded on tape and reproduced in the test section of the large low turbulence tunnel.



(a)  $\theta(x)$  for three values of  $R$   
0.154; 0.218 and 0.264  $\cdot 10^6$

(b) the effect of tripping on  $\theta(x)$  at  
 $R = 0.154 \cdot 10^6$

Fig. 8: Growth of momentum loss thickness  $\theta$  through a laminar separation bubble on a Wortmann FX66-S-196V1 airfoil including the effect of early tripping (taken from [31, 32]).

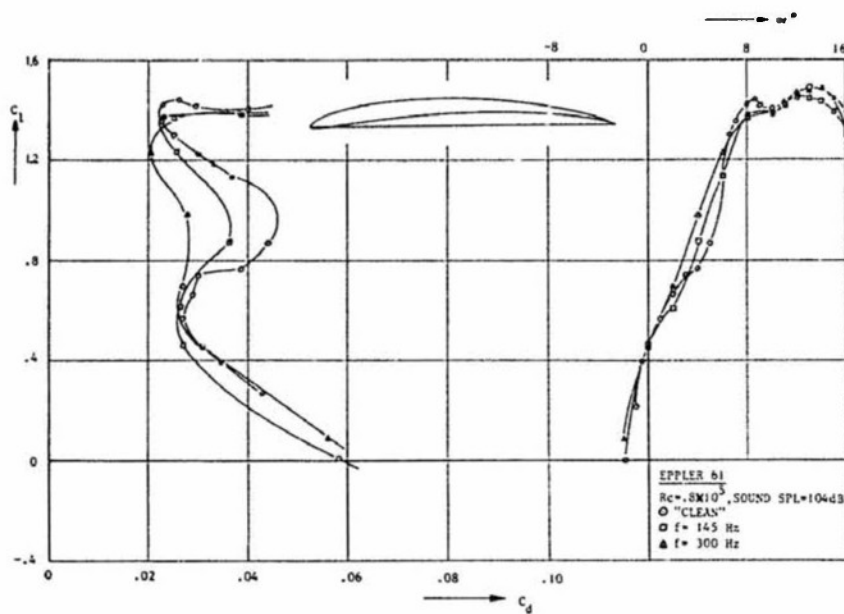


Fig. 9: Measured characteristics of the Eppler E61 airfoil at low Reynolds numbers including the effect of single frequency sound disturbances (measurements at the Department of Aerospace Eng. Delft, see [31]).

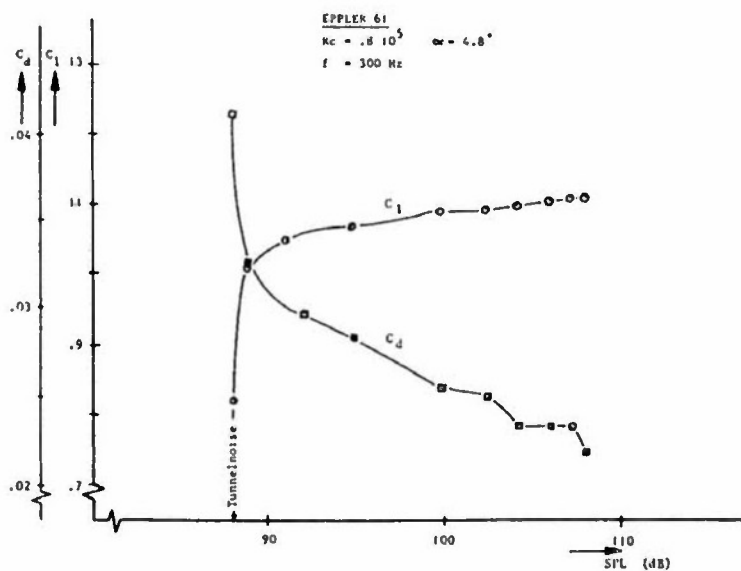


Fig. 10: The effect of sound pressure level at 300 Hz on lift and drag of the E61 airfoil (measurements Dept. Aerospace Eng., Delft, see [31]).

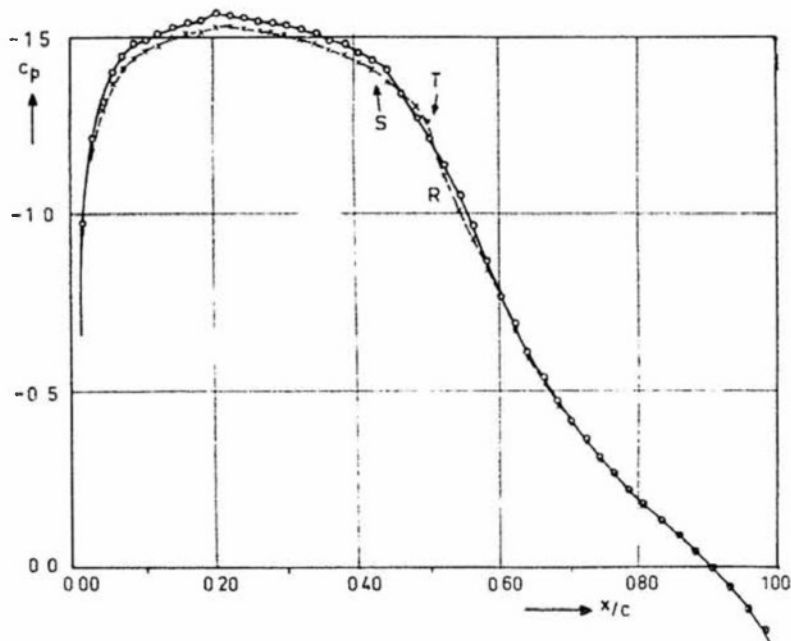


Fig. 11: Measured pressure distributions on the upper surface of the Eppler 603 airfoil.  $\alpha = 5^\circ$ , ---  $R = 3.62 \cdot 10^6$ ; -x-  $R = 1.82 \cdot 10^6$ . S = separation, T = transition, R = reattachment (taken from [41]).

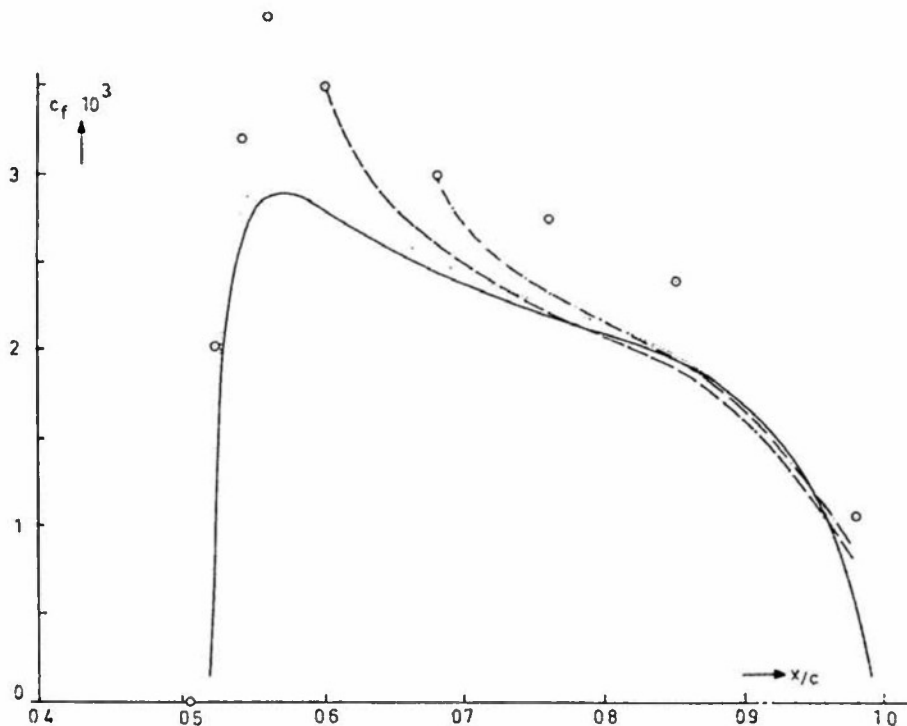
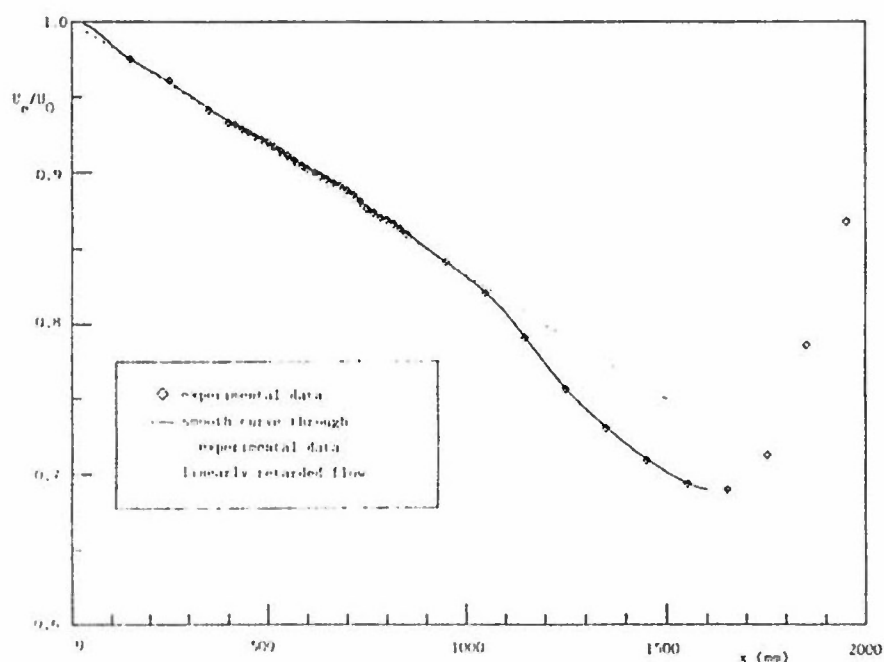
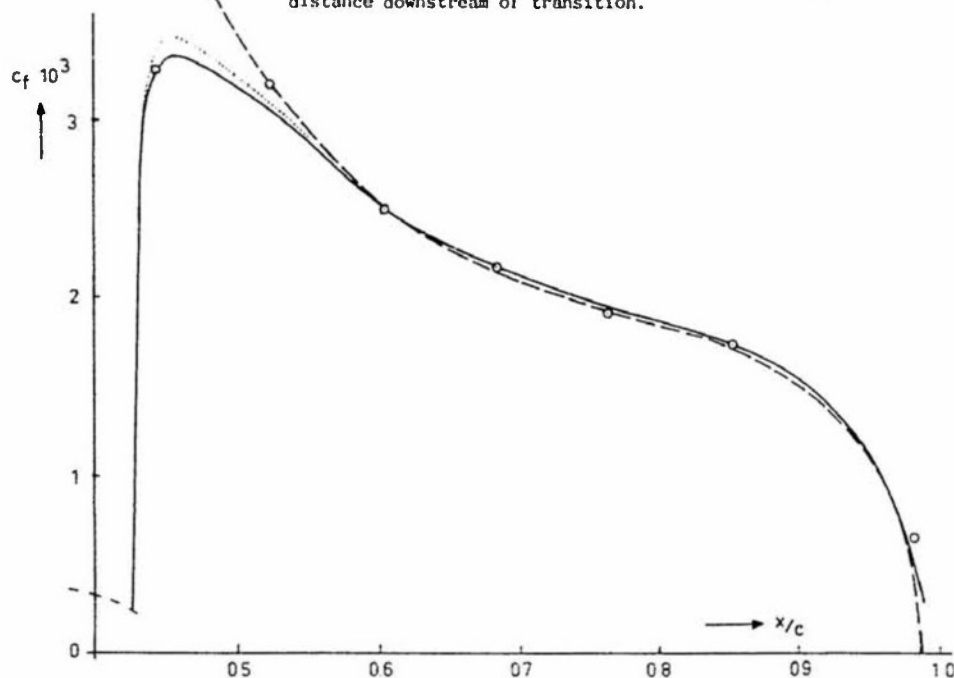


Fig. 12: Comparison between experimental and computed skin friction for the upper surface of the Eppler 603 airfoil,  $\alpha = 5^\circ$ ,  $R = 1.82 \cdot 10^6$ . Note that in this case transition is preceded by laminar separation. Experimental values (O) taken from [41]. Calculations using BOLA-2D taken from [39]. — standard calculation started at measured transition position; .... low Reynolds number correction included, -.-.-.- starting from experimental values some distance downstream of transition.

**Fig. 13:** Comparison between experimental and computed skin friction for the upper surface of the Eppler 603 airfoil,  $\alpha = 5^\circ$ ,  $R = 3.62 \cdot 10^6$ . No laminar separation bubble present. Experimental values (o) taken from [41]). Calculations using BOLA-2D taken from [39].

— standard calculation started at measured transition position, ..... low Reynolds number correction included, ----- starting from experimental values some distance downstream of transition.



**Fig. 14:** Boundary layer-edge velocity  $U$  obtained from the experimental pressure distribution in a boundary layer channel used by van Oudheusden at Delft [39] to investigate the mixing length of turbulent boundary layers downstream of transition.  $U_0$  = reference velocity at entrance of channel. For comparison the distribution for the Howarth linearly retarded flow has been included in the figure.

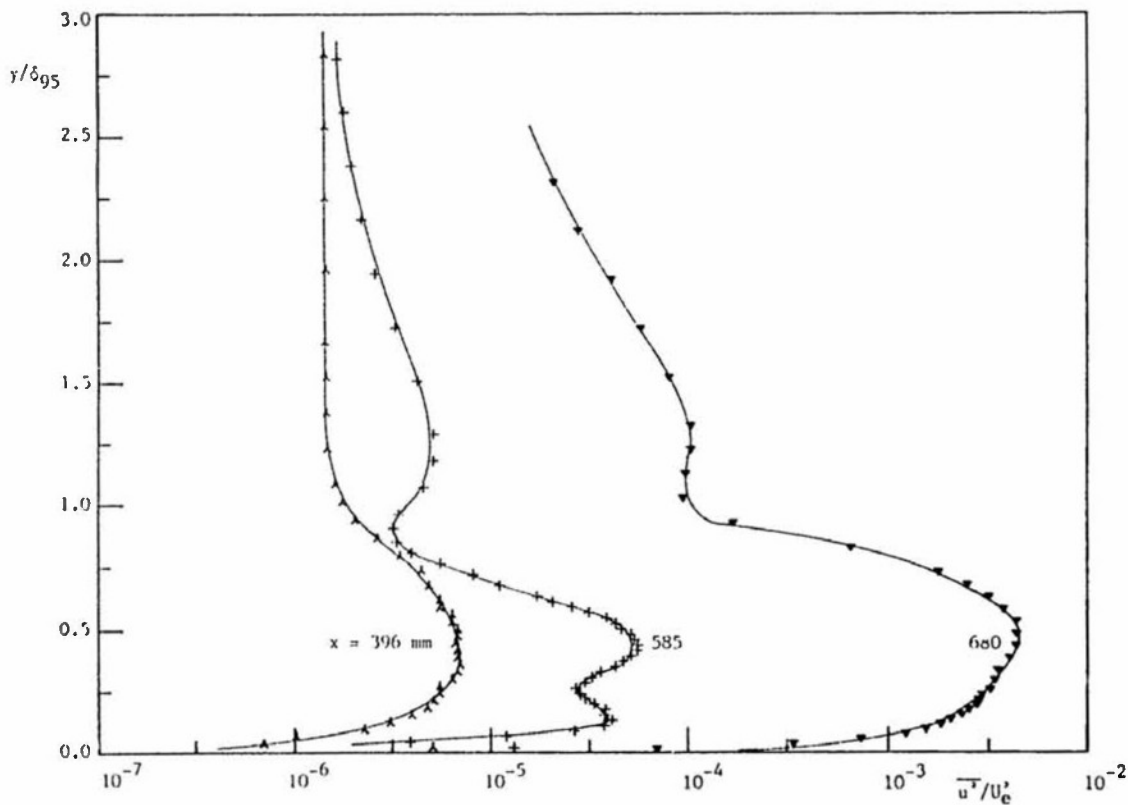
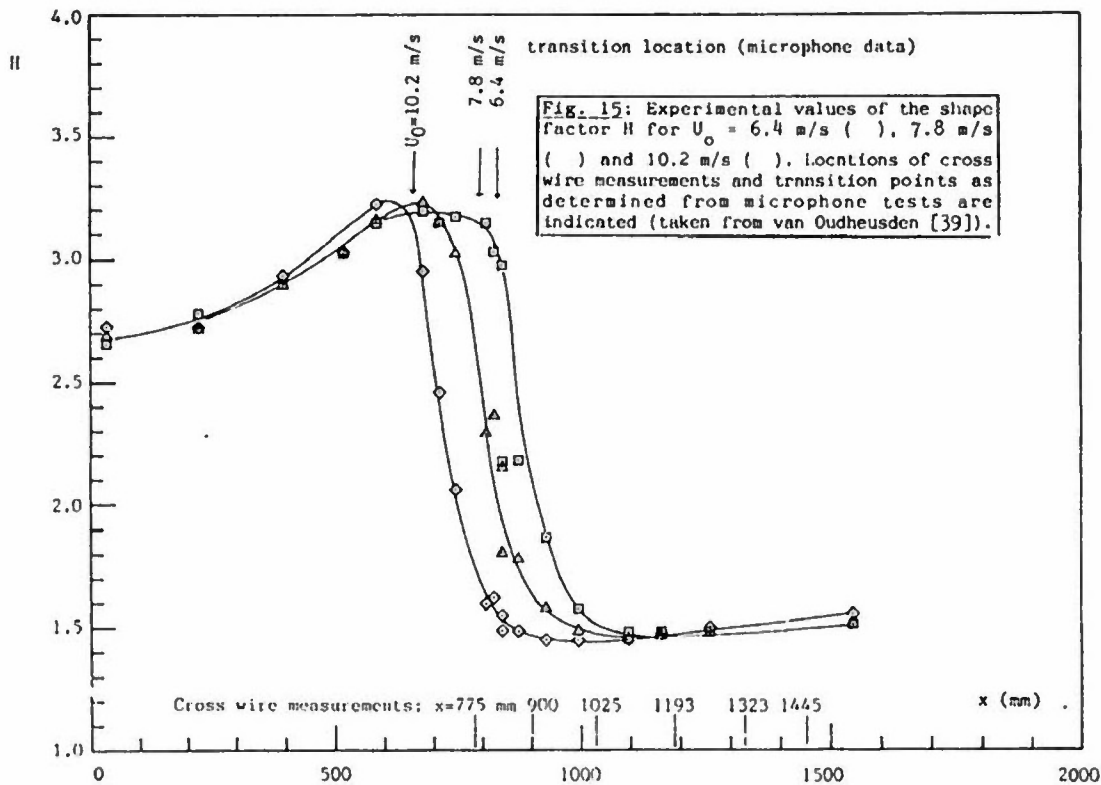


Fig. 16a: Distribution of the streamwise fluctuation component for the boundary layer according to figs 14 and 15 for  $U_0 = 10.2$  m/s, (taken from van Oudheusden [39]).

(a) the laminar region; note the log scale.



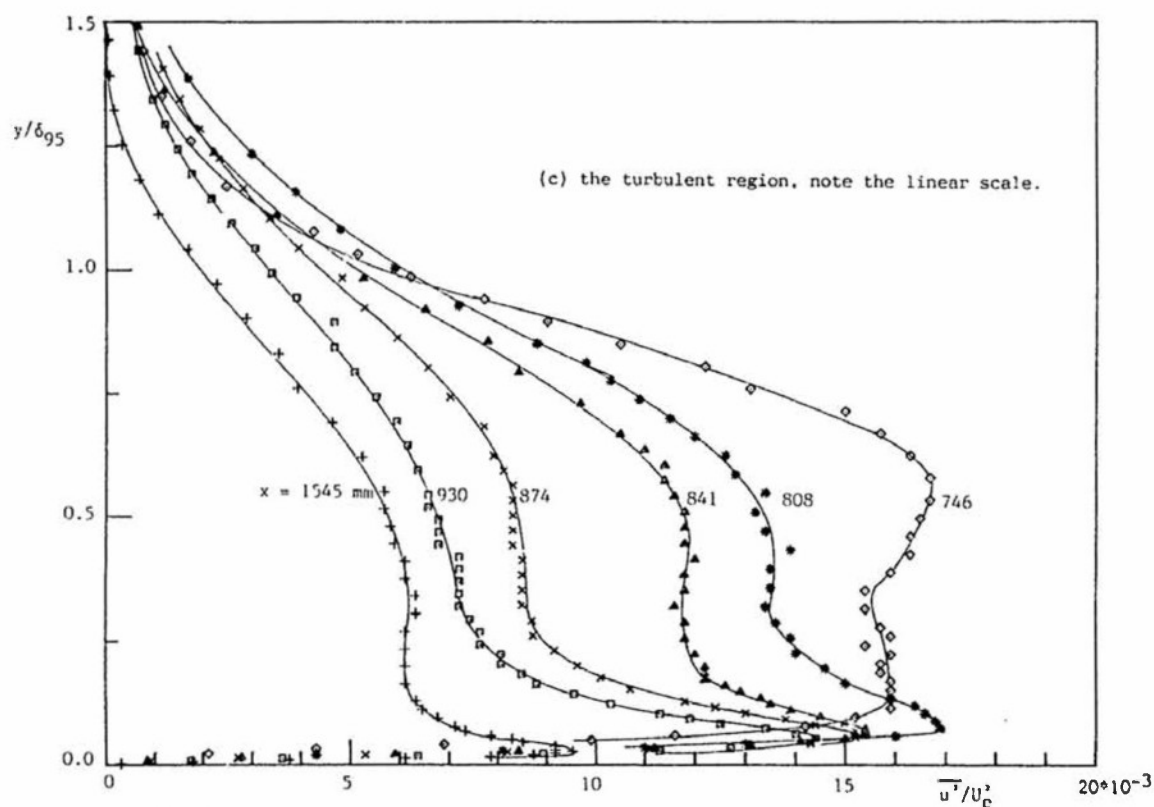
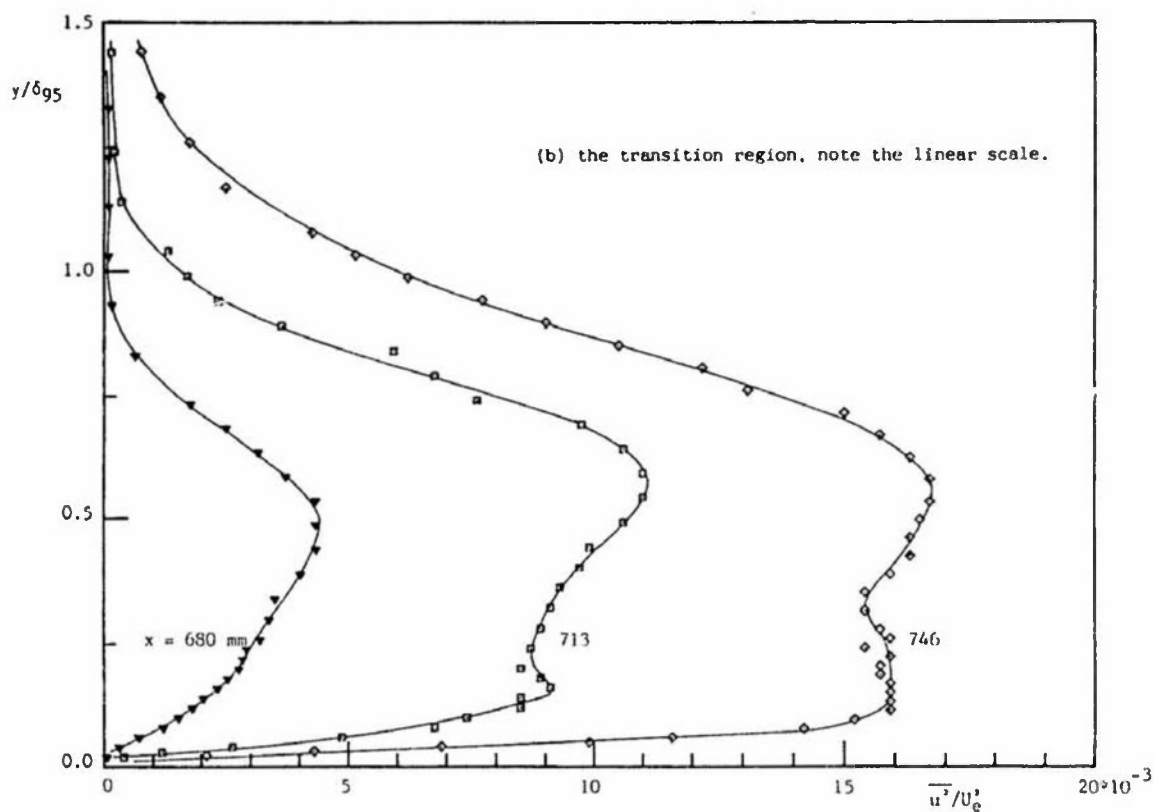


Fig. 16 b/c: Distribution of the streamwise fluctuation component for the boundary layer according to figs 14 and 15 for  $U_0 = 10.2 \text{ m/s}$ , (taken from van Oudheusden [39]).

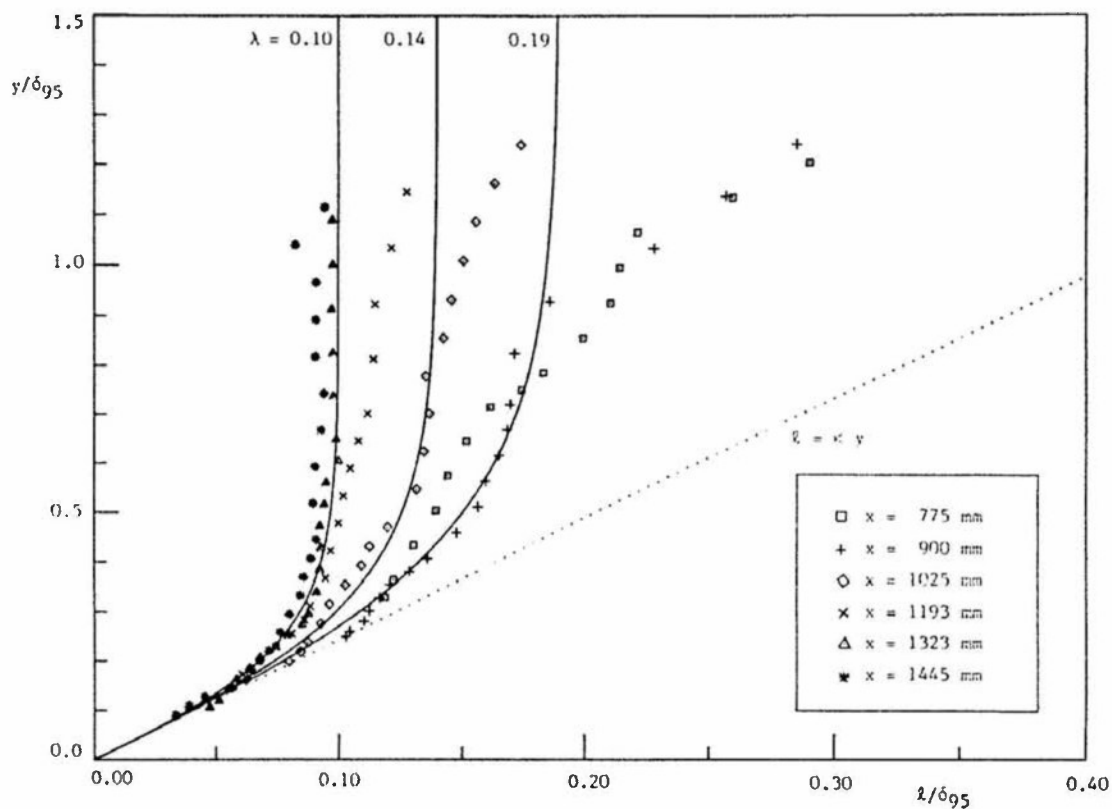


Fig. 17: Mixing length profiles in the turbulent region of van Oudheusden's boundary layer at  $U_0 = 10.2$  m/s. Comparison with  $\ell = \lambda_\infty \delta_{95} D \tanh(ky/\lambda_\infty \delta_{95})$  (taken from [39]).

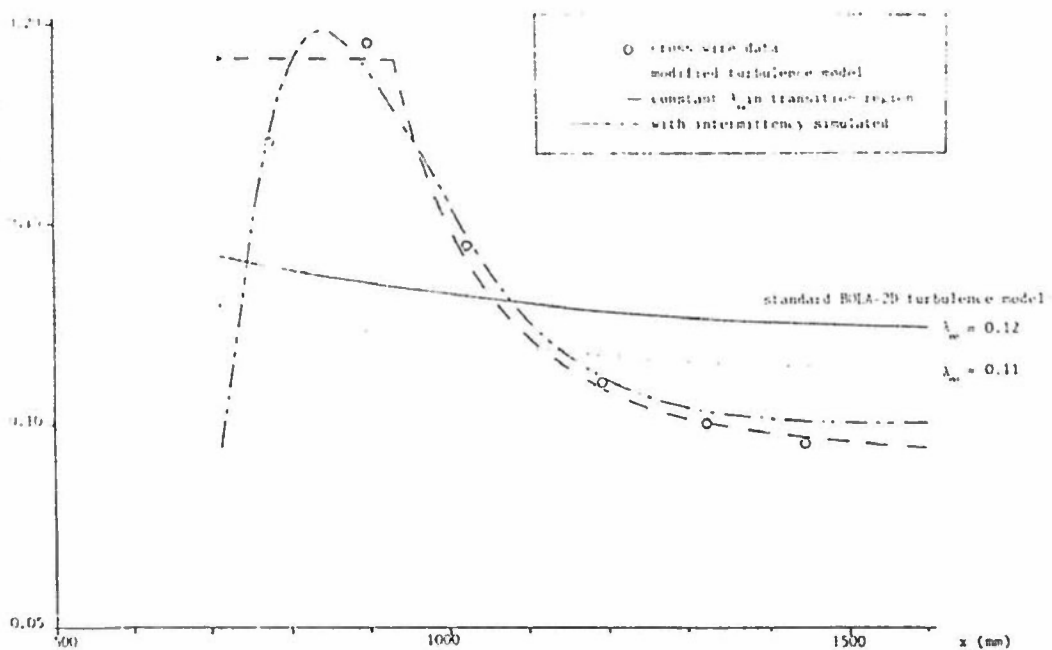


Fig. 18: Various developments of mixing length parameter  $\lambda_w$  with streamwise distance  $x$  used by van Oudheusden [39] in BOLA-2D calculations.

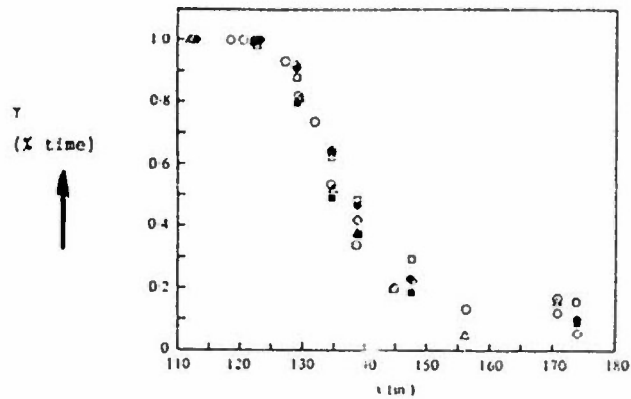


Fig. 19: Streamwise distribution of the fraction of time that the flow moves downstream near the wall for a typical mean two-dimensional separating turbulent boundary layer. Data due to Simpson et.al. (for further details consult Simpson [23], page 2 and fig. 1).

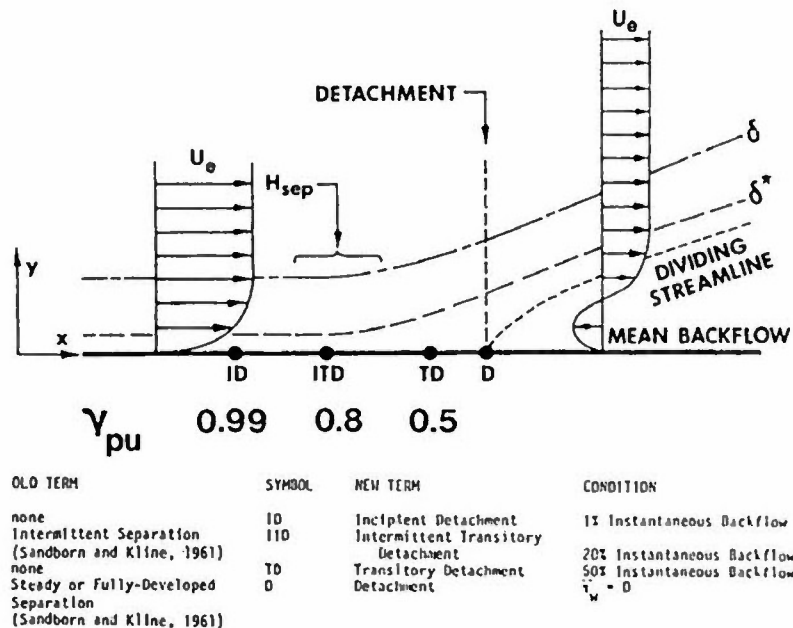


Fig. 20: Definitions of two-dimensional turbulent detachment states. Distances not to scale. "Percent Instantaneous Backflow" means along a spanwise line at a given time, or percent of time at a point (taken from Simpson, [23], fig. 2).

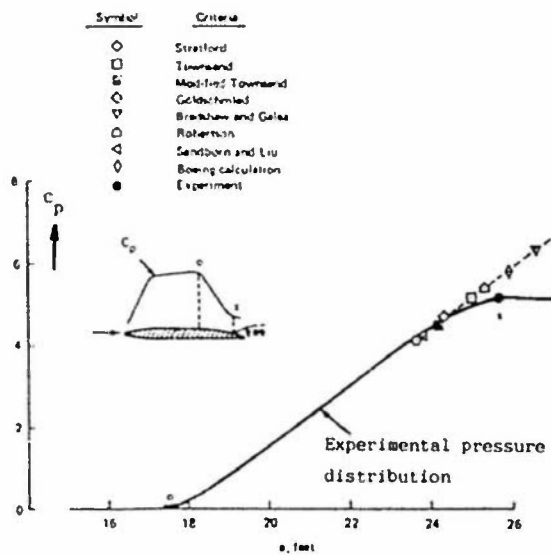


Fig. 21: Evaluation of some separation criteria for the Schubauer and Klebanoff experimental data (Hahn [56]).

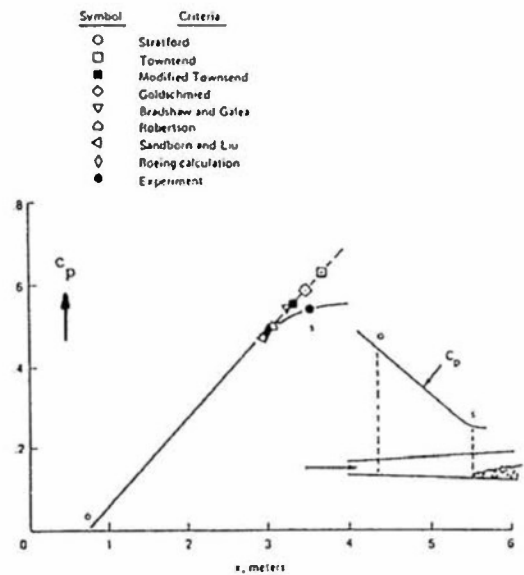


Fig. 22: Evaluation of some separation criteria for the Ludwig and Tillman experimental data (Hahn [56]).

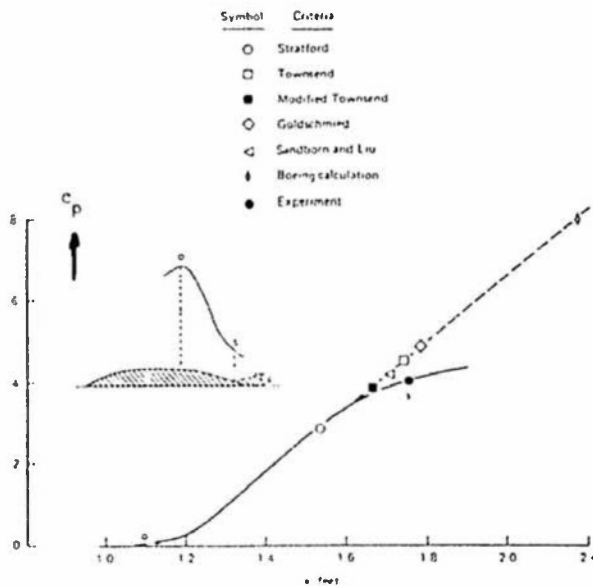


Fig. 23: Evaluation of some separation criteria for one of Boeing's experimental data (Hahn [56]).

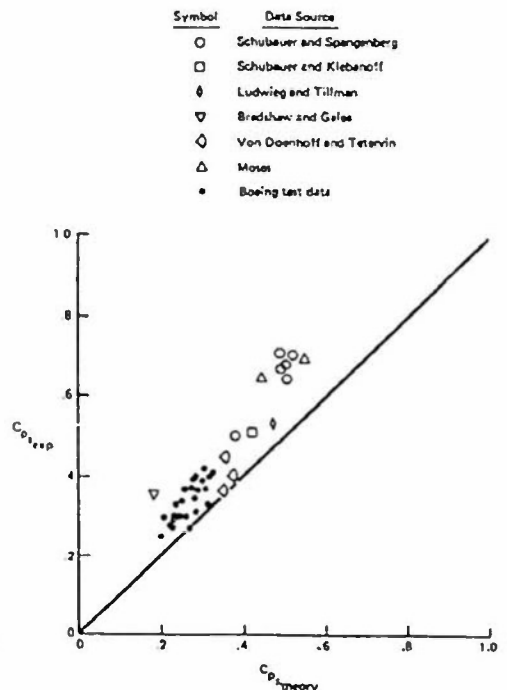


Fig. 24: Evaluation of Stratford's separation criterion with experimental data (Hahn [56]).

Symbol	Data Source
○	Schubauer and Spangenberg
□	Schubauer and Klebanoff
◇	Ludwig and Tillman
▽	Bradshaw and Gales
◊	Van Doenhoff and Tetervin
△	Moses
•	Boeing test data

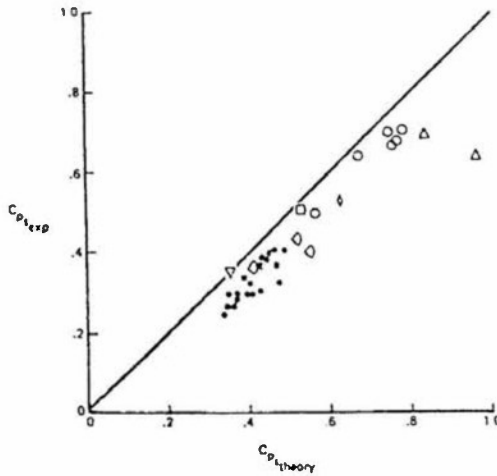


Fig. 25: Evaluation of Townsend's separation criterion with experimental data (Hahn [56]).

Symbol	Data Source
○	Schubauer and Spangenberg
□	Schubauer and Klebanoff
◇	Ludwig and Tillman
▽	Bradshaw and Gales
◊	Van Doenhoff and Tetervin
△	Moses
•	Boeing test data

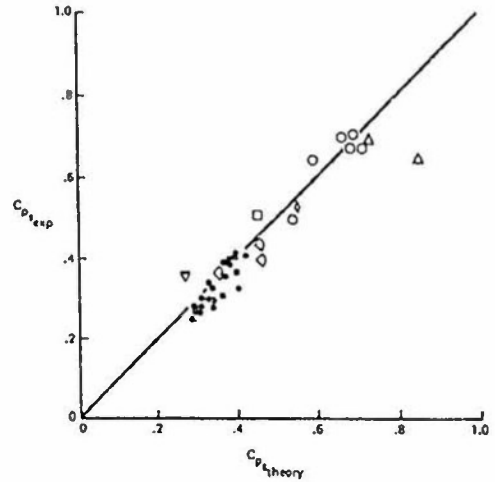


Fig. 26: Evaluation of the "modified" Townsend separation criterion with experimental data (Hahn [56]).

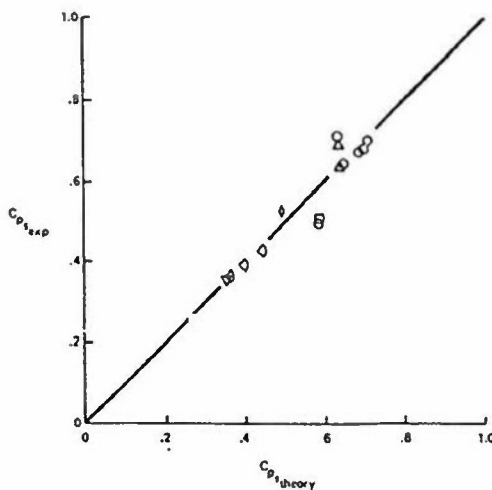


Fig. 27: Evaluation of Boeing Boundary Layer Computer Program with experimental data (Hahn [56]).

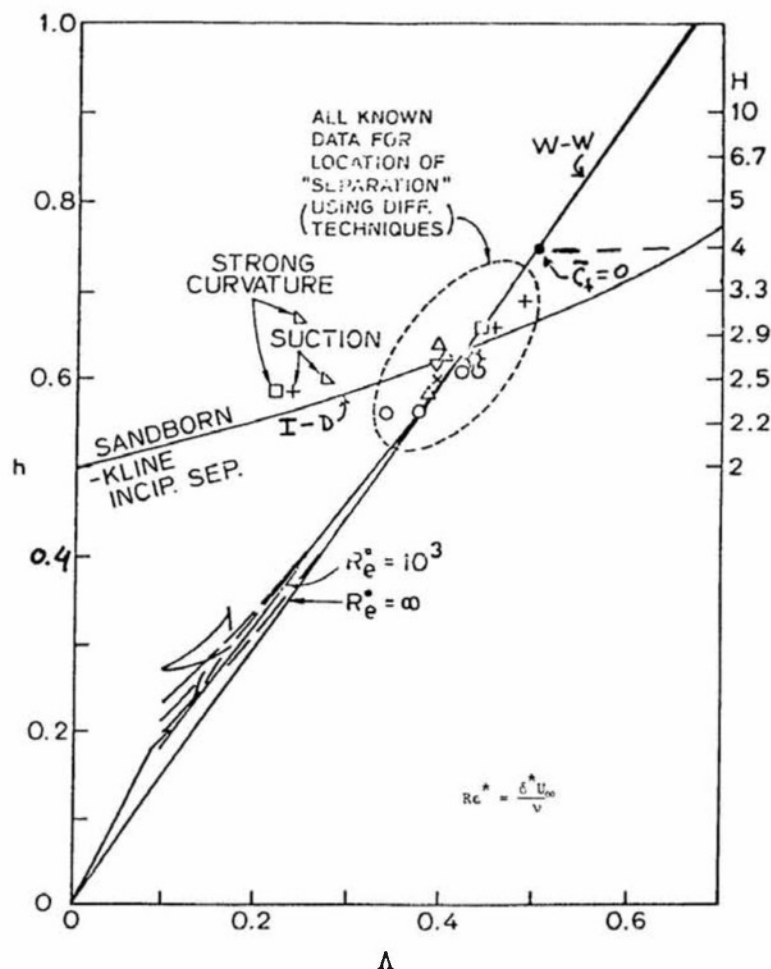


Fig. 28: Shape factor correlation for flow detachment according to Kline [57].  
 $h = (H-1)/H$ ,  $H = \delta^*/\delta$ ,  $\Lambda = \delta^*/\delta$ .

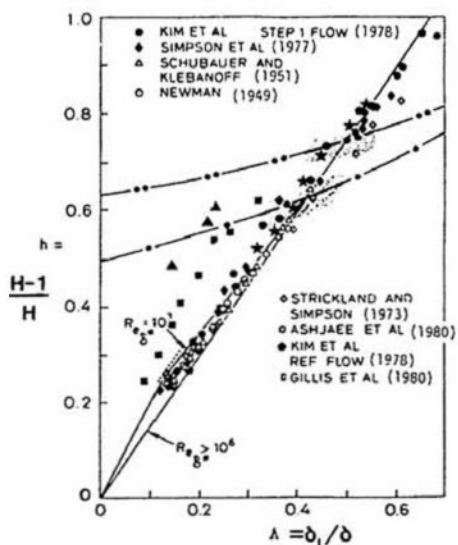


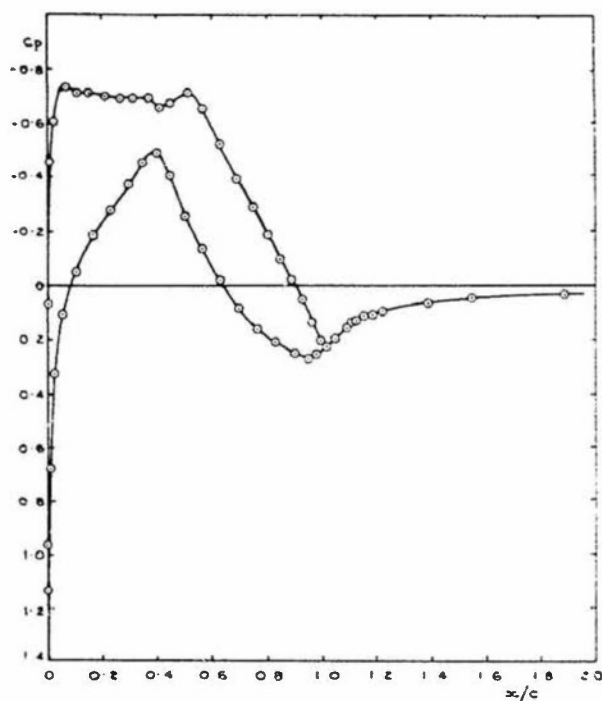
Fig. 29: Simpson's version [23] of Kline's shape factor correlation given in Fig. 28. The following is the caption to Fig. 26 of [23]:

$h$  vs.  $\delta^*/\delta$  plot of data for detaching and reattaching flows. Shaded regions - data reviewed by Sandborn and Kline (1961). ---, equation (6) and (7) of Kline et al. (1983); -.-, equation (IV.13); . . ., data of Chou and Sandborn (1973); . . ., data of Sandborn and Liu (1968); . . ., data of Wadcock (1979); . . ., data of So and Mellor (1972).

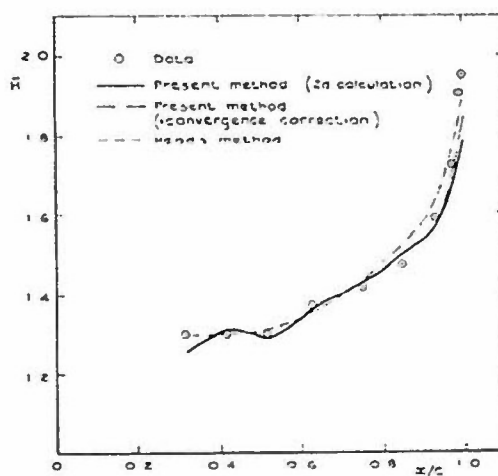
References mentioned above are those of [23]; this report (page 15) should be consulted for a detailed description of the correlation. Eq. IV.13 which is referenced above reads:

$$h = \frac{H-1}{H} = \left[ 2 - \frac{\delta^*}{\delta_{0.995}} \right]^{-1}$$

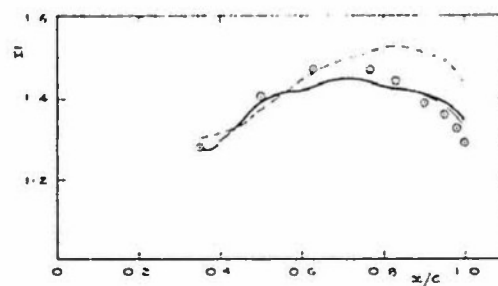
For --- the mean value of wall shear stress is zero; for -.- the mean value is positive.



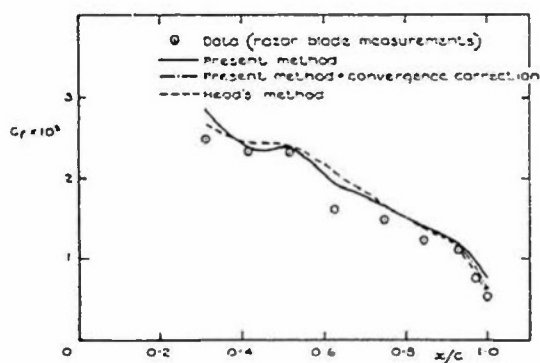
a. Measured pressure distribution



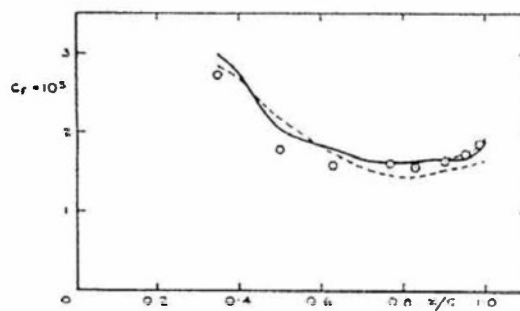
b. Shape parameter on upper surface



c. Shape parameter on lower surface



d. Skin friction on upper surface



e. Skin friction on lower surface

Fig. 30: Comparisons between experimental data and calculations using Head's entrainment method and Green's lag-entrainment method (= "present method" in the figures); for the two-dimensional aerofoil section RAE 2814 at  $M = 0.725$  and  $R = 15 \times 10^6$  (taken from Green [60]).



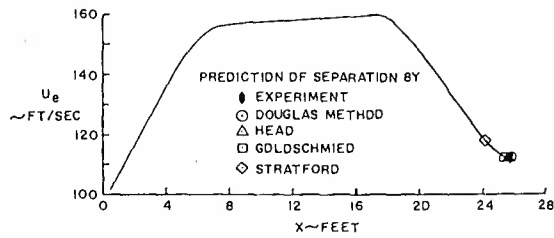


Fig. 31: Comparison of predicted separation points with experiment for the airfoil like body of Schubauer and Klebanoff (taken from A.M.O. Smith [4]).

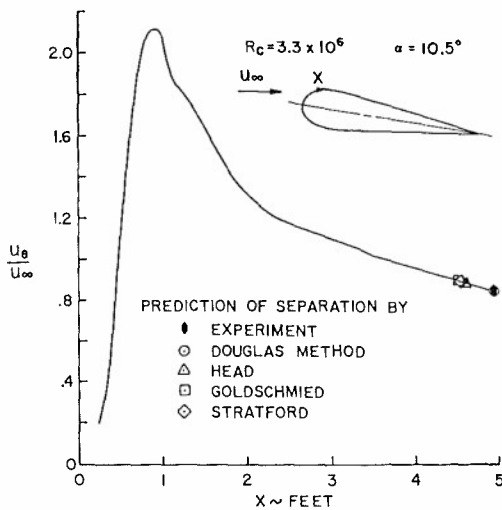


Fig. 32: Comparison of predicted separation points with experiments for Newman's airfoil (taken from A.M.O. Smith [4]).

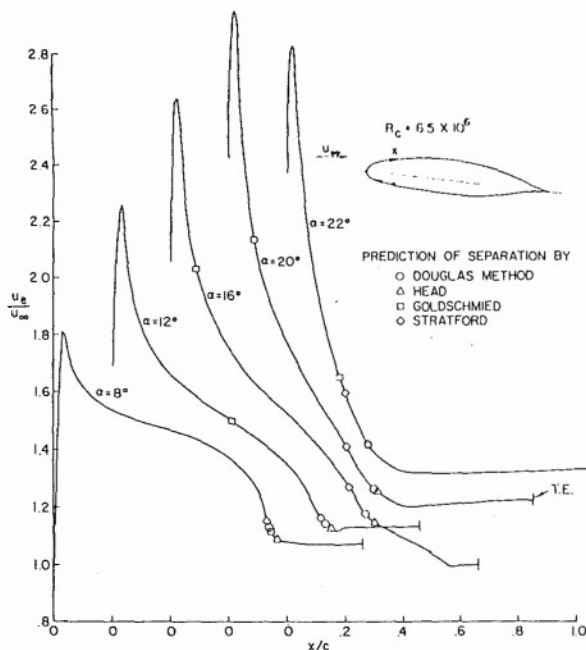


Fig. 33: Predicted separation points for the experimental pressure distribution on the NACA 66,2-420 airfoil (taken from A.M.O. Smith [4]).

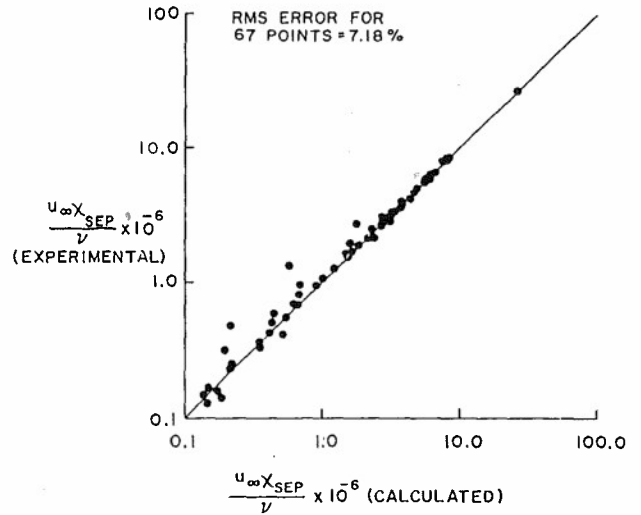


Fig. 34: Accuracy of predicting turbulent separation points by the Cebeci-Smith method (taken from A.M.O. Smith [4]).

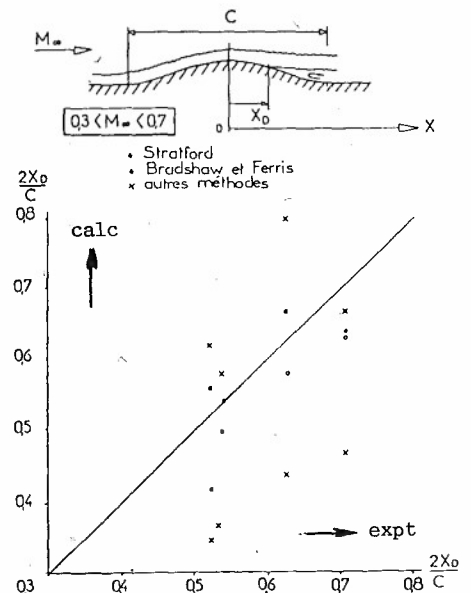


Fig. 35: Prediction of turbulent separation in a subsonic compressible flow (taken from the review paper by Sirieix in [5]).

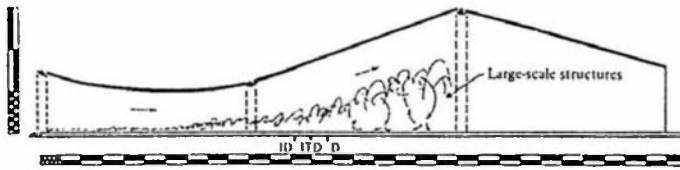


Fig. 36a

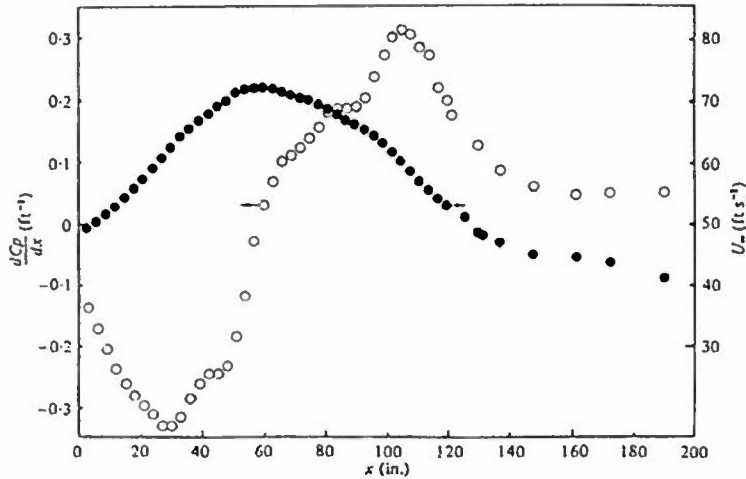


Fig. 36: Experimental set-up and pressure distribution used by Simpson et.al. for their studies on turbulent separation; major divisions on the scales are 10 inches (taken from Simpson [23]).

Fig. 36b

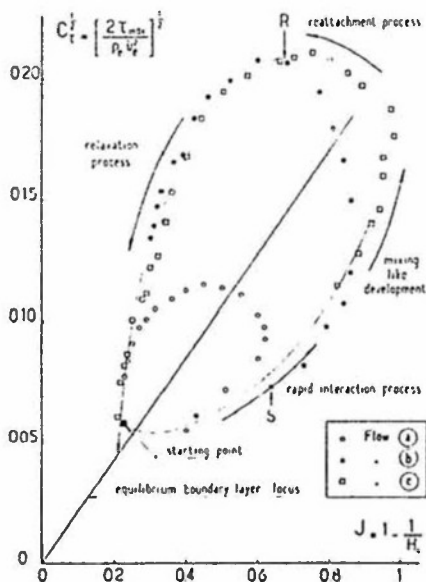


Fig. 38: Variation of maximum shear stress and hysteresis near detachment and reattachment according to Delery (AIAA Journal, 21, pp 180-185, 1983). Figure taken from Simpson [23].

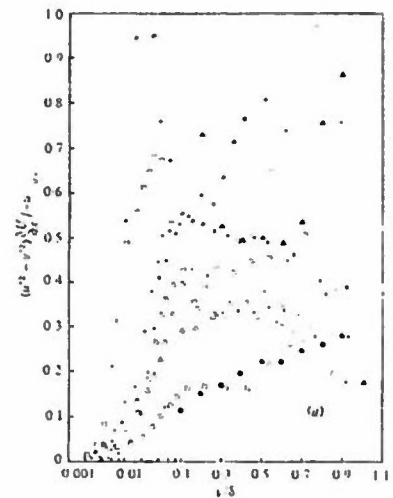


Fig. 37: The contribution of normal stresses to turbulence energy production upstream of detachment, expressed as the ratio of normal stresses production to shear-stress production. This figure is taken from Simpson [23]; for a detailed explanation of this figure the reader should consult [23], page 17.

## SECTION 4.7

## VORTEX FLOWS

Edward M. Kraft  
 Calspan Corporation/AEDC Division  
 Arnold Air Force Base, Tennessee

## 4.7.1 Introduction

For today's high performance aircraft, separation and vortical flow is a fact of life. The design challenge is to control vortex separation and make it work to improve the aircraft performance. Vortical flows are generally complex and correspondingly difficult to model analytically. Consequently subscale simulation remains the primary developmental tool for vehicle optimization, particularly in a high speed maneuver. Therefore, it is essential to understand the physical aspects of vortical flows that effect subscale simulation.

Peake and Tobak (Ref.1) have outlined some fundamental issues concerning the current knowledge of vortical flows. A brief summary of some of their key questions and current assessment is given below:

1. Do we have an unambiguous definition of separation in three dimensions? - We have an unambiguous definition if the separation line is considered always to emanate from a saddle point. Complications arise, however, because flow configurations exist where the conditions for 3-D separation appear to be present; skin friction lines on the body surface converge onto a particular line and, in cross flow planes, streamlines corresponding to trajectories of the velocity components in these crossflow planes roll up around what appear to be vortex cores. But within the limits of numerical or experimental resolution, the particular skin friction lines on which others converge do not appear to emanate from a saddle point. Frequently, they appear to emerge from the region of the attachment node (i.e., stagnation point) on the nose of the body.
2. Do we understand the structure and mechanisms of separation and the ensuing coiled up vortical motions? - We have a good understanding in mean flow terms in that we know how to draw topological structures of separated flows and we can envision how the structure changes with variations of the governing parameters (e.g., angle of attack). We do not have a firm grasp of the relation between structural features and physical quantities such as surface pressures, turbulence quantities, etc.
3. Is it possible to formulate a principle that will distinguish between the scale of vital and unimportant organized vortical structure? There is experimental evidence of small scale streamwise vortices immersed in the boundary layer. An example is illustrated in Ref. 2. Studies on boundary layer transition and the associated longitudinal vortices developing from amplifying instabilities in the laminar zone imply that these vortices may be exerting an important influence on the development of the leeward flow. In Ref. 3, the existence and behavior of longitudinal vortices with respect to Reynolds number was investigated. According to these studies the vortex distribution in the boundary layer can be sketched as seen in Fig. 1. Pressure measurements in the boundary layer across the wing span have been carried out by Ginoux (Ref.4). An example is given in Fig. 2, where the effects of free-stream Reynolds number on the development of longitudinal vortices is shown. The longitudinal vortices have been found within the region about the plane of symmetry (i.e. the attached flow regime). However, in Ref. 5 it is reported that there is evidence of longitudinal vortices in the attached inboard flow downstream of the leading edge when shock induced separation occurs. All these studies lead to the conclusion that longitudinal vortices develop within the laminar boundary on delta wings with sufficiently large leading-

edge sweep angles. They are triggered by very small irregularities of the leading edge. The intensity of the vortices depends on free-stream Reynolds number, velocity of the transverse flow, and under certain conditions, also on the thickness and nose of the leading edge (Ref. 4). It is unclear, however, whether small scale vortices of this type are the precursors to 3-D separation, whether they are modifiers, whether their effect is relatively minor, or whether all or some of these conditions apply.

4. Do we understand the flow mechanisms leading to vortex breakdown? - We have conceptual notions only. No theory currently yields the flow detail in the breakdown zone, nor an accurate location of breakdown to compare with experimental results.
5. Do we understand the instability mechanisms leading to leeside wake asymmetries at high angles of attack? - Currently we have conceptual notions only. The prevalent theoretical models are the use of impulsive flow analogy and the stability of the flow past a 2-D cylinder. Resolution of the flow in the tip of a forebody is a major obstacle to further understanding.
6. Can modeling the vortical flows by essentially inviscid approaches provide us with satisfactory insight into the flow physics? For configurations where the location of separation is well defined, for example the salient edge of a sharp leading edge wing, the flow is virtually independent of the oncoming boundary layer properties at high Reynolds numbers. The viscosity causes the separation, the location is determined by the edge geometry, after which the flow may be modeled as an inviscid flow. However, the details of the flow field are not represented correctly (i.e., the pressure distribution for shock-induced separation and leading edge separation look very much alike).

Many of these physical phenomena are also important issues in determining the proper techniques for subscale simulation.

The primary types of vortical flows of interest to us in terms of proper subscale simulation at transonic speeds are forebody vortices, wing leading edge vortex flows, vortex breakdown and vortex/shock interactions. This section will explore the fundamental aspects of these types of flow and suggest areas where further research is required.

#### 4.7.2 Physical Aspect of the Subscale Simulation of Vortex Flow

For each of the vortical flows of interest we will examine, in turn, the physical parameters that influence the subscale simulation of such flows.

##### 4.7.2.1 Forebody Vortex Flows

It has long been recognized that long slender missile bodies are sensitive to forebody vortex formation. The trend in fighter aircraft forebodies has been to longer nose configurations for improved performance and to package avionics. Correspondingly more emphasis is now being given to the design of aircraft forebodies to properly control separation and vortex formation.

For proper subscale simulation of forebody vortex flows, it is essential to produce separation at the proper location, to produce the proper boundary layer type flow (laminar, transitional, or turbulent) at separation, to generate the correct leeside vortex pattern (symmetric or antisymmetric), and to produce the correct trajectory of the shed vortices.

As discussed in Ref. 6, and summarized in Section 2.2.1 of this report, the side force and normal force coefficient are highly dependent on the nature of the boundary layer (see Fig. 2.2.1-5 for

example). Clearly, for a subscale simulation, the Reynolds number may be low enough that the flow is inadvertently laminar or transitional when it should be turbulent. Even though the total side force and normal force coefficients on the ogive-cylinder reported in Ref. 6 were comparable when the boundary layer was laminar or turbulent, investigation of the pressure distribution on the body clearly indicated that the details of the separation and vortex formation are entirely different depending upon the nature of the boundary layer. This can be illustrated by relating the flow over an axisymmetric body at high angle of attack to flow over a two-dimensional cylinder. The pressure distribution on a two-dimensional cylinder at different Reynolds numbers is shown in Fig. 3, taken from Ref. 7. For low Reynolds number when the boundary layer is laminar, flow separation occurs early at approximately 80 deg and discrete well defined vortices are formed. As the Reynolds number increases to  $0.7 \times 10^6$  the flow becomes transitional. This is the range of Reynolds number in which the minimum drag coefficient occurs on a two-dimensional cylinder and in which no coherent vortex shedding can be detected. Finally, as Reynolds number increases further the boundary layer becomes fully turbulent. With a turbulent boundary layer the flow at the surface is sufficiently energized that separation does not occur until an azimuthal angle of approximately 110 deg is reached. Comparing Fig. 3 with Fig. 2.2.1-6 clearly illustrates that the same fundamental response of the boundary layer to variation in Reynolds number occurs in the three-dimensional flow of an axisymmetric body at angle of attack. The result is that if the Reynolds number for a subscale simulation is not sufficiently high to generate a turbulent boundary layer (if that is the full scale condition), the location of the separation line and the pressure recovery on the leeward side of the body can be distinctly different than in flight. The resulting vortex formation and vortex trajectory can have an entirely different interaction with other parts of the vehicle such as fins or the vertical tail of an aircraft.

The traditional method for ensuring the boundary layer is turbulent in a subscale simulation is to trip the boundary layer. Section 2.2.1 summarizes the inconsistencies that can arise from different tripping techniques. Clearly further research is required in order to ensure that the correct vortex generation is simulated on a slender forebody at angle of attack.

Perhaps an even more difficult flow to correctly simulate in a subscale experiment is the formation and shedding of asymmetric vortices from a slender body at high angles of attack. Asymmetric vortex shedding can also occur at flight conditions and produce significant side forces at high angles of attack as illustrated in Fig. 4, taken from Ref. 8. Advanced fighter aircraft are expected to provide a stable weapons platform even at such large incidence angles. Hence it is imperative that such asymmetries be properly simulated in the wind tunnel if they indeed occur in flight. The control system designer would not appreciate the surprise from such a change in the lateral stability coefficients if they were not predicted in subscale developmental tests. Conversely, the designer would not appreciate a subscale data base that indicates strong side forces because of asymmetric vortex formation if that condition did not truly exist in flight. To avoid such difficulties, many aircraft designers use chines or strakes to fix the separation location. For these types of vehicles, subscale simulation is not as difficult.

One of the stronger influences on axisymmetric vortex production has nothing to do with scale effects, but with minute asymmetries introduced by slight irregularities in the model forebody geometry, the flow uniformity of the wind tunnel, or alignment of the model support mechanism. As discussed in Ref. 6, considerable care must be exercised in assuring that any asymmetric vortices formed on a slender body are not created by these slight irregularities. This requires that an axisymmetric body be systematically rotated about its axis through the angle of attack range.

As a model of asymmetric vortex formation we will follow the model of Peake and Tobak (Ref. 1) and assume an asymmetric disturbance to originate at the nose, of the same rotation, say, at the port side primary vortex. If this disturbance amplifies in the vicinity of the enclosing saddle point as a consequence of instability of the inflexional velocity profiles, there will be an effective increase

in the vorticity of the port-side primary vortex. This vortex will enlarge slightly and move away from the surface as shown in Fig. 5(a). As the relative incidence increases, the feeding shear layer continues to stretch, as shown in Fig. 5(b). A further increase

in relative incidence, in conjunction with the appearance of gross unsteadiness of the secondary vortices, causes the elongated shear layer itself to pass through a shedding stage, as shown in Fig. 5(c), until there is definite evidence of a third spiral vortex motion as shown in Fig. 5(d). In order that the two vortices of the same rotational direction be able to coexist in tandem on the left hand side, the rules of topology require a new saddle point to be inserted between them, as shown in Fig. 5(c). As the relative incidence increases still further, the starboard side primary vortex begins to grow, as shown in Figs. 5(d) and (e), resulting eventually in the repetition of the shedding process for the opposite side: these incidences at which shedding occurs correspond with the maximum induced side loads. Note that the one crossflow streamline emanating from the enclosing saddle point to the body at A1 as shown, for example, in Fig. 5(e), always partitions to the left and right-hand sides of the wake. Except during the shedding process, each flow field is composed of well organized spiral vortex motions.

Factors influencing the angle of attack for the onset of vortex asymmetry for bodies of revolution include nose bluntness, strakes, nose half angle, Mach number, Reynolds number, etc. For pointed nose bodies, the onset of asymmetry occurs at an angle of attack approximately equal to twice the semi-apex of the nose. Cylindrical afterbodies behind the nose tend to reduce the angle of attack for asymmetric vortex shedding. For complete aircraft models asymmetry tends to occur at greater angles of attack, possibly as a result of favorable noncircular fuselage effects.

Only some semi-empirical data for restricted  $Re - M$  ranges on cone cylinder configurations exists for predicting the vortex starting positions, spacings, and strengths for asymmetric vortex formation (see for example Thomson and Menisori, Ref. 9). At the present time no purely theoretical means for predicting the onset of asymmetric vortex shedding exists.

#### 4.7.2.2 Wing Leading Edge Vortex Flows

Wing leading edge vortex flows for delta wings is very nicely summarized in Section 2.2.3. The fundamental physical aspects of subscale simulation can best be discussed by considering sharp and blunt leading edge wings separately.

##### Sharp Leading Edge Wings

The presence of a salient edge to fix vortex formation significantly reduces the sensitivity of the flow to scale effects as long as the separation remains at the salient edge (e.g. regions 1,2,3, and 6 in Fig. 2.2.3-5). The primary influence of Reynolds number is to reduce the pressure in the vortex, move the secondary separation line, and spread the vortex core as illustrated in Fig 2.2.3-8. When the boundary layer at separation is turbulent the core is tighter and the characteristics of the vortex are purely kinematical. This is why inviscid rotational flow computations (i.e. Euler codes) can reasonably model vortex flows over sharp leading edges at high Reynolds numbers. In fact, the inviscid computational methods may be useful in estimating the scale effects for sharp leading edge wings. In any event, even though there are localized effects of Reynolds number, the overall integrated effects are only a weak function of scale and, in general, vortex flows that emanate from a salient edge are considered to be largely independent of Reynolds number effects.

In regions 4 and 5 of Fig. 2.2.3-5 the vortex does not separate from the sharp leading edge of the wing, but instead is induced by a shock wave. In this case, one would expect the Reynolds number to influence primarily the nature of the boundary layer/shock wave interaction. Hence, it is anticipated that these classes of flows will be more Reynolds number sensitive. To date no systematic evaluation of Reynolds number effects on shock generated vortex flows has been made.

### Round Leading Edge Wings

For a round leading edge, the vortex separation position is not fixed by geometric features and intuitively one would expect that Reynolds number would have a larger influence on the primary vortex formation than for a sharp leading edge. That this is indeed the case is illustrated in Fig. 6, taken from Manie, Neron, and Schmitt (Ref. 10). In Fig. 6, the angle of attack at which vortical flow is initiated is strongly dependent on the Reynolds number for this round leading edge wing. Beyond a "critical" Reynolds number the formation of the primary leading edge vortex is delayed to rather high angles of attack. This behavior has been related by Brocard and Monte (Ref. 11) to the type of laminar separation bubble that occurs at very low angles of attack. At low Reynolds number the bubble is long and is directly at the origin of the vortical flow generation, whereas such an influence cannot be noted at high Reynolds number, when the bubble is short or nonexistent.

Poll (Ref. 12) has systematically examined the effects of sweep angle, leading edge bluntness, and Reynolds number on leading edge vortex flow of a swept back wing (note not a delta wing). His investigation revealed that for sweep angles in excess of 15-deg there are at least three different ways in which a spiral vortex can be generated over a swept wing. These are:

- 1) A full span vortex can be formed by a rolling up of a shear layer which leaves the wing surface at the primary separation line. This type of vortex flow is very similar in appearance to the flows generated on sharp-edged thin delta wings at incidence.
- 2) A part-span vortex can be formed when conditions are such that the shear layer from the primary separation reattaches to form a short bubble on the inboard portion of the wing but fails to reattach on the more heavily loaded outboard sections. That part of the shear layer which does not reattach rolls up to form the vortex.
- 3) A part span vortex can be formed when the boundary layer flow downstream of a short separation bubble leaves the surface close to the bubble along a line of secondary separation. This secondary separation line forms first in the vicinity of the tip where loading is highest and the resulting free shear layer rolls up to form the vortex.

In the results presented in Ref. 12, type 1) was observed for all the wing sections tested when the unit Reynolds number was  $1 \times 10^6/\text{m}$ . When the unit Reynolds was increased to  $2 \times 10^6/\text{m}$ , the section with the sharp leading edge continued to generate type 1) while the two rounded sections tested produced type 2) at 30-deg sweep and type 3) at 56-deg wing sweep. In general, it was found that the incidence necessary for the onset of spiral vortex flow depended strongly upon the leading edge radius and that dependence upon Reynolds number increases with increasing leading edge radius. This is illustrated in Fig. 7. In Ref. 12, it is also stated that Reynolds number, sweep, and incidence are insufficient in themselves to determine the type of flow which will occur on a given airfoil section. The authors recommend that future experimental work should include measurements of the wind tunnel disturbance environment.

### Compressibility Effects

A common vortex flow test technique is to perform flow visualization studies on models in water tunnels. Although this can be useful for qualitative evaluation of vortex trajectories over complicated geometries, caution must be exercised in trying to extrapolate quantitative information from low speed tests to high speed performance. Compressibility effects can have a pronounced effect on vortex behavior. Brown (Ref. 13) found from a theoretical study that as Mach number increases, the ratio of the axial velocity at the core to the external velocity decreases as shown in Fig. 8. It



was also found that the compressibility drastically changes the behavior of the circumferential velocity. At  $M = 0$  the circumferential velocity increases toward the vortex axis whereas at higher Mach numbers this velocity component decreases toward the axis (also shown in Fig. 8).

Voropoulos and Wendt (Ref. 14) performed laser doppler velocimeter measurements of compressibility effects on the lee-side vortical flow field of a delta wing at incidence. It was found that the axial velocity excess in the vortex core observed at low Mach numbers became an axial velocity deficit at Mach numbers above 0.6. This is shown in Fig. 9. At  $M = 0.80$  the results suggest the appearance of a conical shock below the primary vortex. A similar occurrence of a shock wave pattern for  $M_N < 1$  was also observed by Szodrach (Ref. 5). Obviously, as the free-stream velocity increases, the additional velocities induced by the primary vortex can cause the local velocity to go supersonic resulting in a local shock wave. This phenomena cannot be simulated in a water tunnel. So far, no evidence of a Reynolds number dependency exists for this phenomenon.

#### • 4.7.2.3 Vortex Breakdown

Another important design consideration in relation to the control of vortical flows is the breakdown of vortices. If the vortex breaks down before the trailing edge considerable loss of performance can result. If vortex breakdown occurs differently on each wing, then the lateral stability of the vehicle can be significantly affected. As illustrated in Ref. 15, there are two fundamental types of vortex breakdown - spiral and axisymmetric. Spiral vortex breakdown is the more prevalent form of vortex breakdown in most wing flows. The spatial regimes of vortex breakdown are:

Approach Flow: Characterized by a concentrated vortex core embedded in a flow that may be approximated as irrotational.

Breakdown Region: Characterized by rapid changes in axial direction. Has three subintervals of approximately equal length

- approach flow is decelerated and a stagnation point is formed on the vortex axis
- flow reversal occurs near the axis
- original direction of axial flow is restored and a large increase of turbulent intensity occurs

Downstream Vortex Structure: A new vortex structure with an expanded core is established.

Vortex breakdown has been observed only in highly swirling flows. The maximum values of the swirl angle,  $\tan^{-1}(v/w)$ , is invariably greater than about  $40^\circ$ , where  $v$  and  $w$  are the azimuthal and axial velocities, respectively. An apparently necessary condition for breakdown is a positive or adverse pressure gradient. A third condition invariably found with breakdown, and related to adverse pressure gradients, is a divergence of the stream tubes in the vortex core immediately upstream of the breakdown. A more detailed description of vortex breakdown is given in Refs. 16 and 17.

The primary parameters that may influence vortex breakdown are wing incidence, wing sweepback, Reynolds number, and pressure gradient. The influence of incidence and sweepback on the location of vortex bursting over a delta wing was explored by Lambourne and Breyer (Ref. 15) and typical results are shown in Figs 10 and 11. In Fig. 11, the distance from the apex to the position of vortex breakdown is conveniently correlated with the parameter  $\gamma = \cos^{-1}(\cos \alpha \sin \Lambda)$ , the angle between the leading edge and the free stream direction. It may be noted that  $\gamma$  is closely related to the angle between the vortex axis and the free stream. In practice vortex bursting may fix an upper limit to the range of incidence and a lower limit to the range of sweepback over which flow with leading edge vortices can be used.

As summarized in Fig. 2.2.3-16, the onset of vortex breakdown at the trailing edge is independent of Reynolds number. This conclusion is reinforced in Fig. 12, also taken from Ref. 15. In addition, the comparison in Ref. 18 of wind tunnel and flight data indicate a good correlation of trailing edge vortex breakdown even though the wind tunnel Reynolds number was 1/20th of the flight condition. This

independence with Reynolds number is the reason that reasonable qualitative understanding of vortex breakdown and vortex interaction with other aerodynamic surfaces can be obtained in low Reynolds number water tunnel experiments.

The dependence of vortex breakdown on external stream pressure gradient has been explored in detail by Delery, Horowitz, Leuchter, and Solignac (Ref. 19). The flow field along the core of a vortex in a series of adverse pressure gradients was probed in detail with a laser velocimeter. The influence of the external pressure gradient on the pressure gradient in the vortex core is shown in Fig. 13. The comparison clearly brings out the very large amplification of the pressure gradients along the axis, compared with those in the outer flow. This is attributable to a phenomenon characteristic of vortex flows, related to the high rotation rates. In Fig. 13,  $K_p = (p - p_0)/q_0$  is the pressure coefficient referenced to stilling chamber conditions. The limit of vortex breakdown can be defined by the intensity of the pressure gradient and the vortex strength.

In summary, vortex breakdown is dominated by the geometric conditions of the wing and the external pressure gradient. Reynolds number has very little influence on the location of vortex breakdown. Consequently, subscale simulation of vortex breakdown can be easily accomplished if the wing geometry is correctly modeled and the appropriate pressure gradient over the model is simulated. The implication is that factors that influence the free stream distribution such as wall interference and flow quality will have a more pronounced influence on vortex breakdown than viscous simulation.

#### 4.7.2.4 Vortex/Shock Wave Interaction

The interaction of a vortex with a shock wave is a special case of the influence of the external pressure gradient on vortex breakdown. A detailed laser velocimeter and pressure probe study of vortex/shock interaction is presented in Ref. 20. The shock/vortex interaction is schematically represented in Fig. 14. The phenomenon is characterized by the Mach number which defines the shock intensity and the swirl rate  $\tau$  which is the ratio between the maximum tangential velocity and the local external velocity. Actually, the vortex behavior, in particular as breakdown is concerned, depends on the local shape of the longitudinal and tangential velocity distribution. The parameter  $\tau$  is only a very rough characterization of this.

The passage of the vortex through the shock increases the helix angle,  $\gamma = \tan^{-1}(V_t/V_x)$  everywhere and particularly in the central part of the vortex where the axial component is slowed down the most. We thus conceive that a state may be reached at a certain shock intensity where  $\gamma$  is close to the critical value of  $50^\circ$ , locally, which will burst the structure at the slightest disturbance. The effect of the shock on the rate of swirl is shown in Fig. 15. The quasi-invariance of the tangential velocity  $V_t$  combined with the decrease in the axial external velocity increases the rate of swirl  $\tau$ , thus increasing the 'fragility' of the vortex making it more vulnerable to a possible breakdown. A vortex breakdown limit curve in terms of  $\tau$  and the pressure drop across the shock is shown in Fig. 16.

Although a systematic study of the influence of Reynolds number vortex/shock interactions has not been performed to date, up to the point of vortex breakdown it can be argued that the laminar and turbulent viscous forces are negligible compared with the pressure and acceleration terms. The viscosity is important only insofar as it creates vorticity when the vortex is formed. Based on this argument, an inviscid numerical model of the vortex/shock interaction using the Euler equations has been developed in Ref. 20. The results of the calculation are presented in Fig. 16 as the inviscid flow calculation. The good agreement with the experiment justifies the inviscid approximation.

#### 4.7.3 Recommended Future Research

Based on the review of vortex flow phenomena presented in Section 4.7.2 future research requirements on vortex flow simulation will be discussed. Although there is much worthwhile research

to be performed on all basic vortex phenomena, these recommendations will concern only subscale simulation. In all experimental research it is strongly urged that body surface pressures, surface skin friction lines, surface streamline visualization, vortex trajectory visualization, and vortex core velocities be obtained. As suggested in Ref. 21, these multiple pieces of information are necessary to understand the detailed behavior of the flow. Isolated measurements, such as pressure distributions, can often be inconclusive. It is also recommended that computational fluid dynamics be used to gain further understanding of vortical flow features. For simple representative geometries, the Navier Stokes equations can be solved to provide detailed flow features. First attempts at such calculations are presented in Refs. 22 and 23. When the computations are calibrated with measured flow features they can be invaluable for either interpolating quantities throughout the flow domain or determining the flow parameters not measured (for example, the skin friction lines).

In the large, research has not been performed to address the issues of subscale simulation of vortical flows. Consequently, the future research recommended below is directly aimed at alleviating this deficiency. The recommended research is:

- 1) A systematic scaling law analysis needs to be performed on the vortical flows of interest. Appropriate length scales and physical phenomena need to be defined as a guide to proper subscale simulation of vortical flows. The scaling laws determined need to be evaluated against full-scale phenomena.
- 2) Systematic studies of boundary layer tripping influence on vortex separation needs to be performed. Specific objectives are to determine the influence of trips and tripping techniques on
  - a. symmetrical vortex shedding on forebodies,
  - b. asymmetrical vortex separation on forebodies
  - c. reattachment and secondary vortex formation on sharp leading-edgewings,
  - d. shock induced vortices on sharp edged wings with supersonic leading edges, and,
  - e. primary vortex separation on round leading edge wings.
- 3) Systematic studies need to be performed to determine the causes of asymmetrical vortex formation on forebodies. Only if we can recognize under which set of conditions we should expect asymmetric vortex formation can we hope to confidently simulate such flows. Care must be taken in such research to assure true scaling phenomena are isolated, and the asymmetries are not artifacts of flow quality or model precision.
- 4) The role of streamwise vortices in the formation of vortical flows needs to be ascertained.
- 5) One last conclusive experiment needs to be performed to determine the independence of vortex breakdown on the Reynolds number.

#### REFERENCES

1. Peake, O.J. and Tobak, M. "On the Issues Concerning Flow Separation and Vortical Flows in Three Dimensions," in AGARD-CP-342, April 1983, Paper No.1.
2. Grad-el-Hak, M. and Blackwelder, R. F. "The Discrete Vortices from a Delta Wing," AIAA Journal, Vol.23, No. 8, June 1985, pp. 961-962.
3. Ginoux, J.J. "Recent Developments in Boundary Layer Research," AGARDograph 97, 1965.
4. Ginoux, J. J. "Instabilité de la Couche Limite sur Ailes en Fleche," Zeitschr. f. Flugwissenschaften, 15.Jahrg., Heft 8Jg, 1967, pp 302-305.
5. Szodrach, J. "Experimental Study of Supersonic Viscous Laminar Flow Over a Slender Delta Wing," NASA TM 81 248, 1980.

6. Lamont, R. P. "Pressures Around an Inclined Ogive Cylinder with Laminar, Transitional, or Turbulent Separation," AIAA Journal, Vol. 20, No. 11, Nov. 1982, pp. 1492-1499.
7. Roshko, A. "Experiments on the Flow Past a Circular Cylinder at Very High Reynolds Number," Journal of Fluid Mechanics, Vol. 10, Part 3, 1961, pp. 345-356.
8. Headley, J. W. "Analysis of Wind Tunnel Data Pertaining to High Angle-of-Attack Aerodynamics, Vol. 1, FFDL-TR-78-94, July 1978.
9. Thomson, K. D. and Morrison, D. P. "The Spacing, Position, and Strength of Vortices in the Wake of Slender Cylindrical Bodies at Large Incidence," Journal of Fluid Mechanics, Vol. 50, Part 4, 1971, pp. 751-783.
10. Manie, F., Neron, M., and Schmitt, V. "Experimental and Computational Investigation of the Vortex Flow Over a Swept Wing," ONERA T.P. No. 1984-93, September 1984.
11. Brocard, Y. and Manie, F. "Etudes des caracteristiques de l'ecoulement tourbillonnaire sur une aile en flèche," L'Aeronautique et l'Astronautique No. 82, 1980.
12. Poll, D.I.A. "On the Generation and Subsequent Development of Spiral Vortex Flow Over a Swept-Back Wing," in AGARD-CP-342, April 1983.
13. Brown, S. N. "The Compressible Inviscid Leading Edge Vortex," Journal of Fluid Mechanics, Vol. 22, Part 1, 1965, pp. 17-32.
14. Vorropoulos, G. and Wendt, J. F. "Laser Velocimeter Study of Compressibility Effects on the Flow Field of a Delta Wing," in AGARD-CP-342, April 1983.
15. Lambourne, N. C. and Bryer, D. W. "The Bursting of Leading-Edge Vortices - Some Observations and Discussion of the Phenomena," ARC R&M No. 3282, 1962.
16. Hall, M. G. "Vortex Breakdown," Annual Review of Fluid Mechanics, Vol. 4, 1972, pp. 195-218.
17. Leibovich, Sidney. "The Structure of Vortex Breakdown," Annual Review of Fluid Mechanics, Vol. 10, 1978, pp. 221-246.
18. Wentz, W. H., Jr. and Kohlman, D. L. "Vortex Breakdown on Slender Sharp-Edged Wings," Journal of Aircraft, Vol. 8, No. 3, March 1971, pp. 156-161.
19. Delery, J., Horowitz, E., Leuchter, O., and Solignac, J. L. "Fundamental Studies on Vortex Flows," Recherche Aérospatiale 1984-2, pp. 1-24.
20. Miller, David S. and Wood, Richard M. "Leeside Flows over Delta Wings at Supersonic Speeds," Journal of Aircraft, Vol. 21, No. 9, September 1984, pp. 680-686.

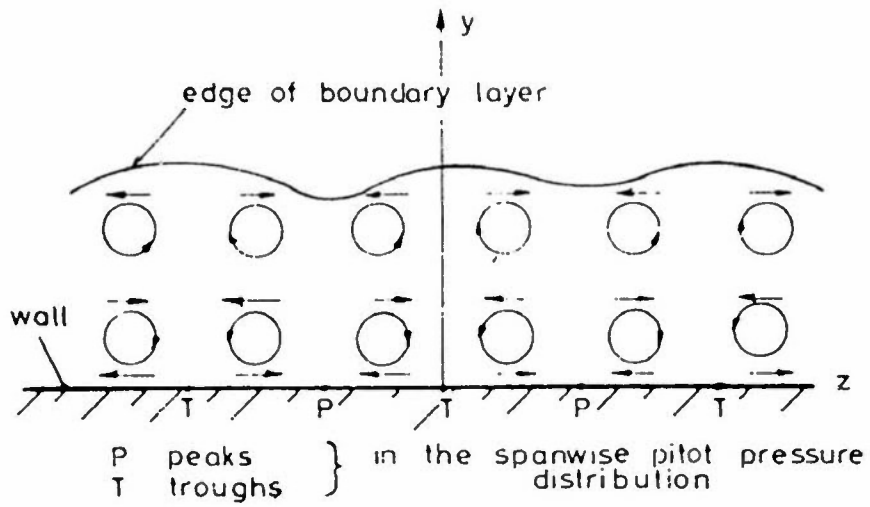


Figure 1. Vortex distribution in the boundary layer (from Ginoux).

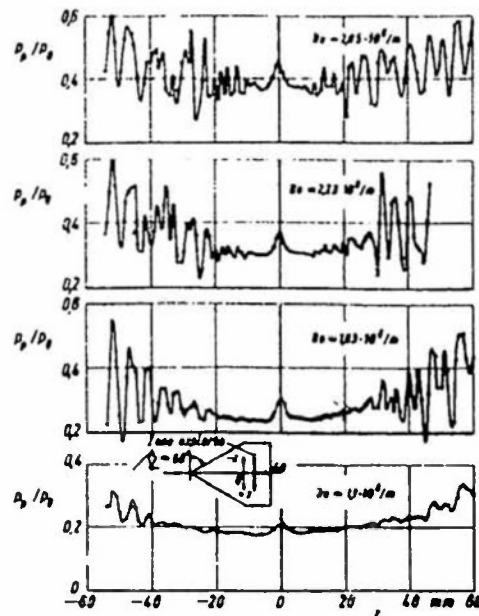


Figure 2. Effect of Reynolds number on longitudinal vortex development (from Ginoux).

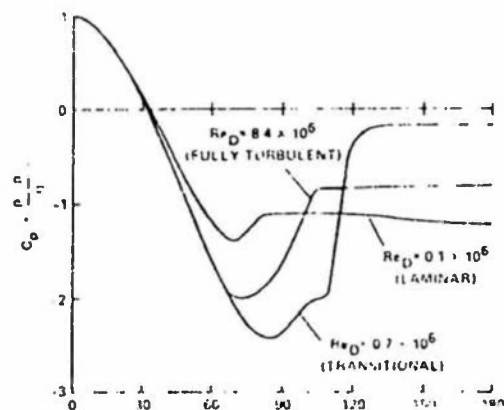


Figure 3. Two-dimensional cylinder pressure distribution at different Reynolds number (from Roshko).

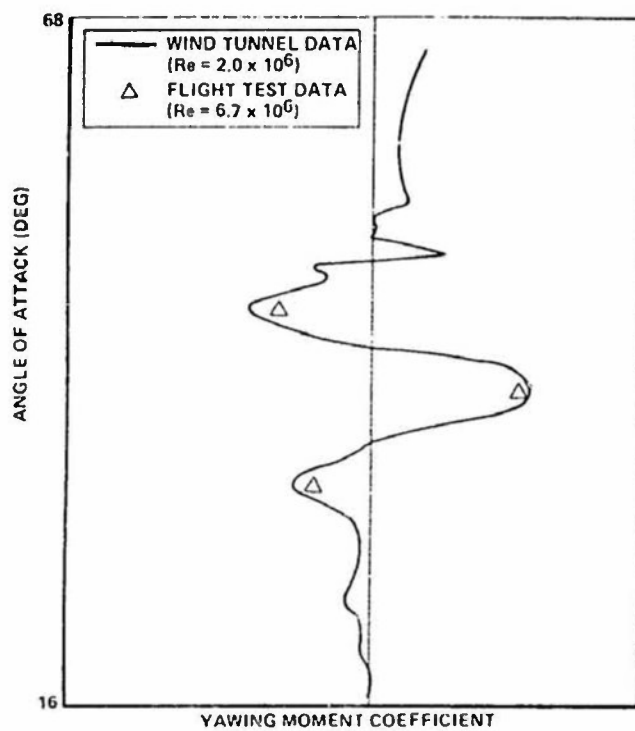


Figure 4. Yawing moment on a fighter aircraft at zero sideslip (from Headley).

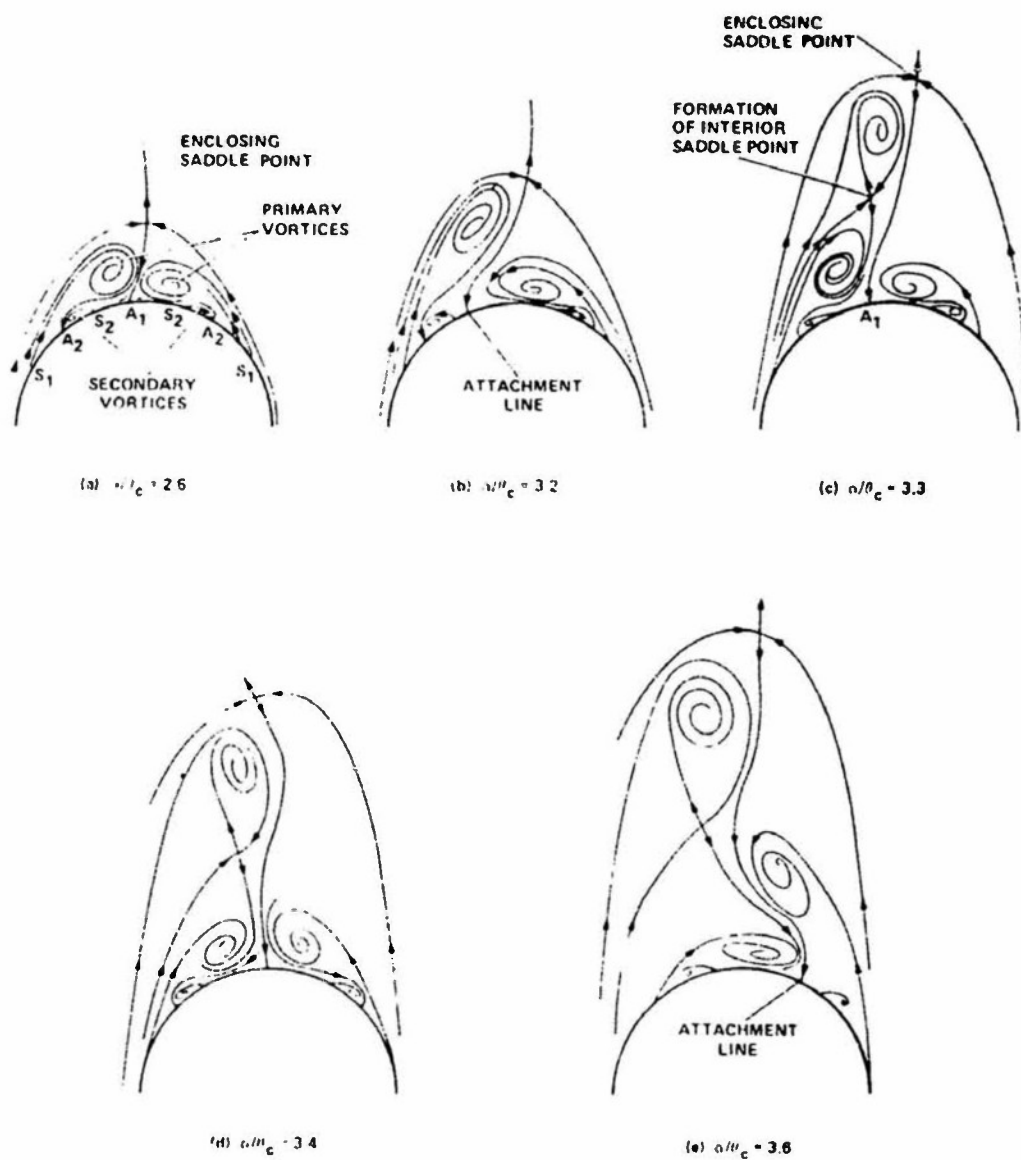


Figure 5. Conceptual development of asymmetric leeside vortex wake structure (from Peake and Tabak).



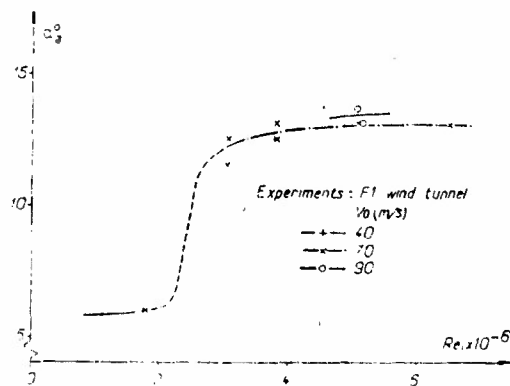
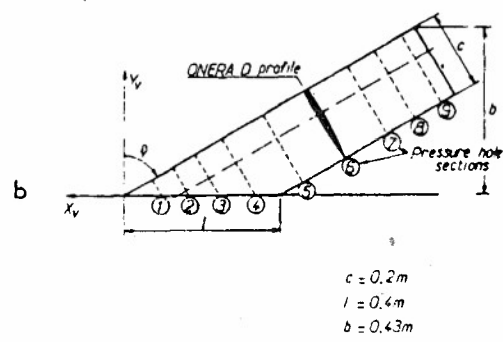
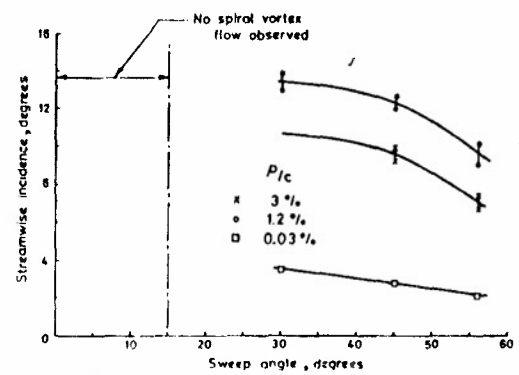
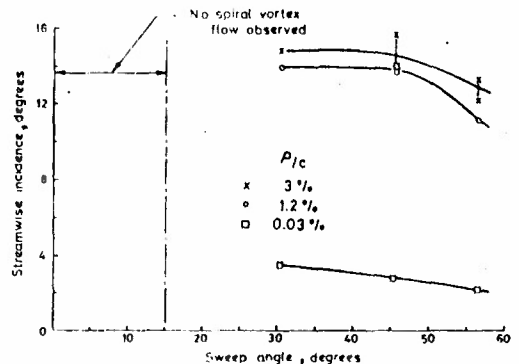


Figure 6. Appearance of leading edge vortex flow on a wing (from Manie, Neron, and Schmitt).



a. Approximate location of the boundary between attached flow and spiral vortex flow at a unit Reynolds No. of  $1.0 \times 10^6/\text{m}$ .



b. Approximate location of the boundary between attached flow and spiral vortex flow at a unit Reynolds No. of  $2.0 \times 10^6/\text{m}$ .

Figure 7. Influence of sweep, thickness, and Reynolds number on the formation of a spiral vortex (from Poll).

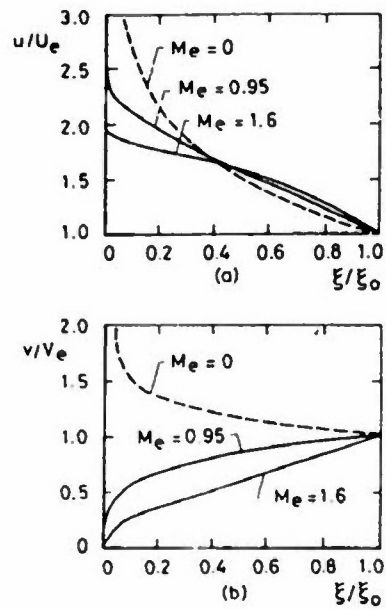


Figure 8. Axial ( $u$ ) and Tangential ( $v$ ) velocity distributions in a compressible vortex for various Mach numbers (from Brown).

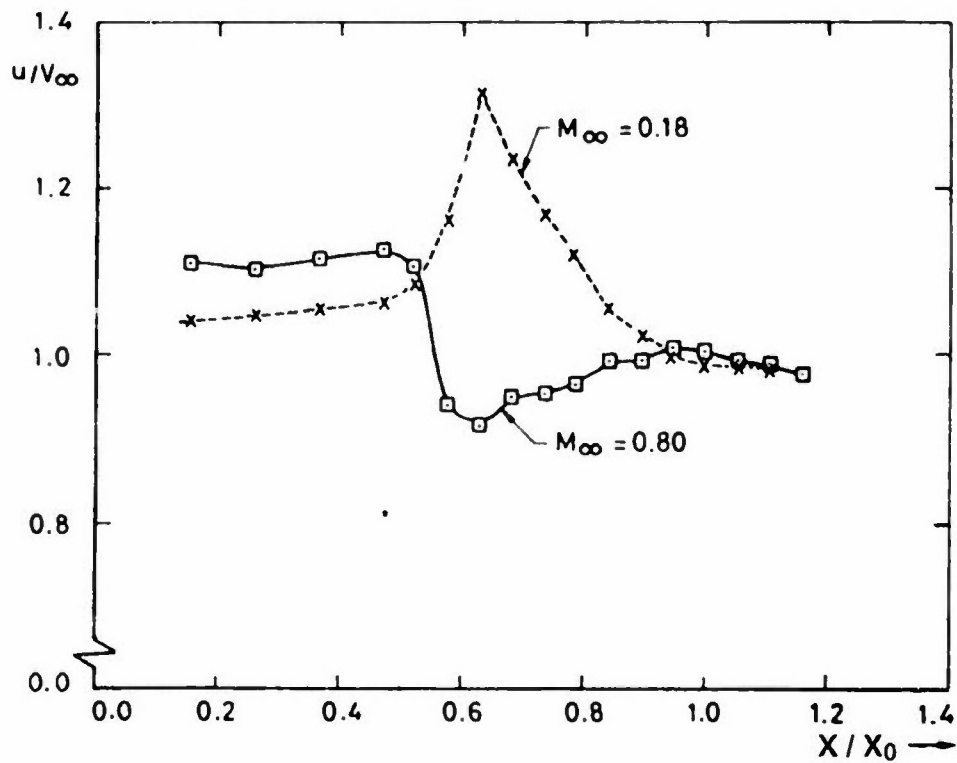


Figure 9. Axial velocity distributions for  $M_\infty = 0.18$  and  $0.80$  at the 50 % chord station (from Vorropoulos and Wendt).

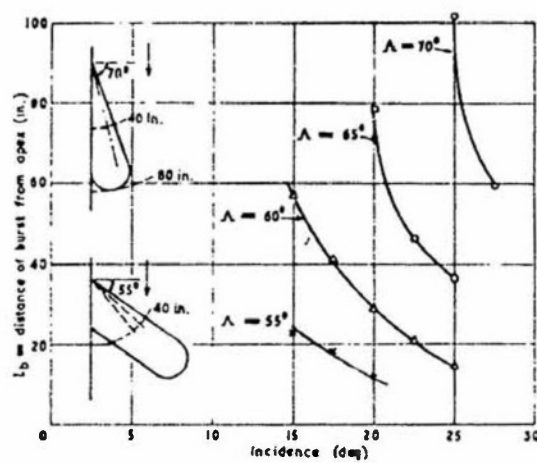


Figure 10. Variation of burst position with incidence and sweepback (from Lambourne and Breyer).

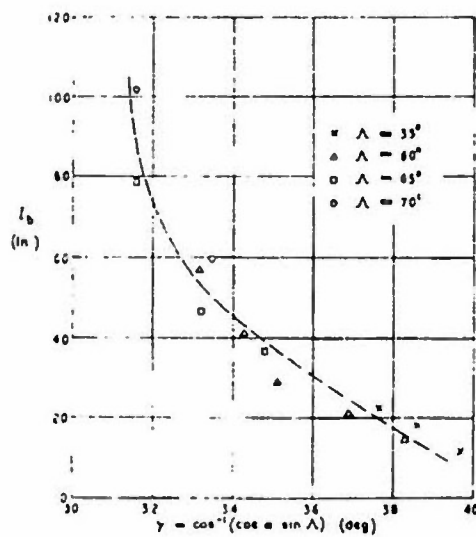


Figure 11. Burst position plotted against  $\gamma$ , the angle between the leading edge and free stream (from Lambourne and Breyer).

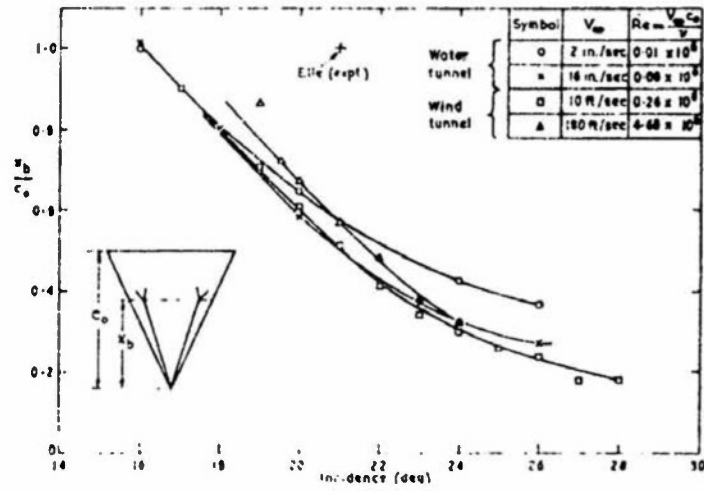


Figure 12. Burst position versus incidence for various Reynolds numbers, delta wing,  $\lambda = 65$  deg (from Lambourne and Breyer).

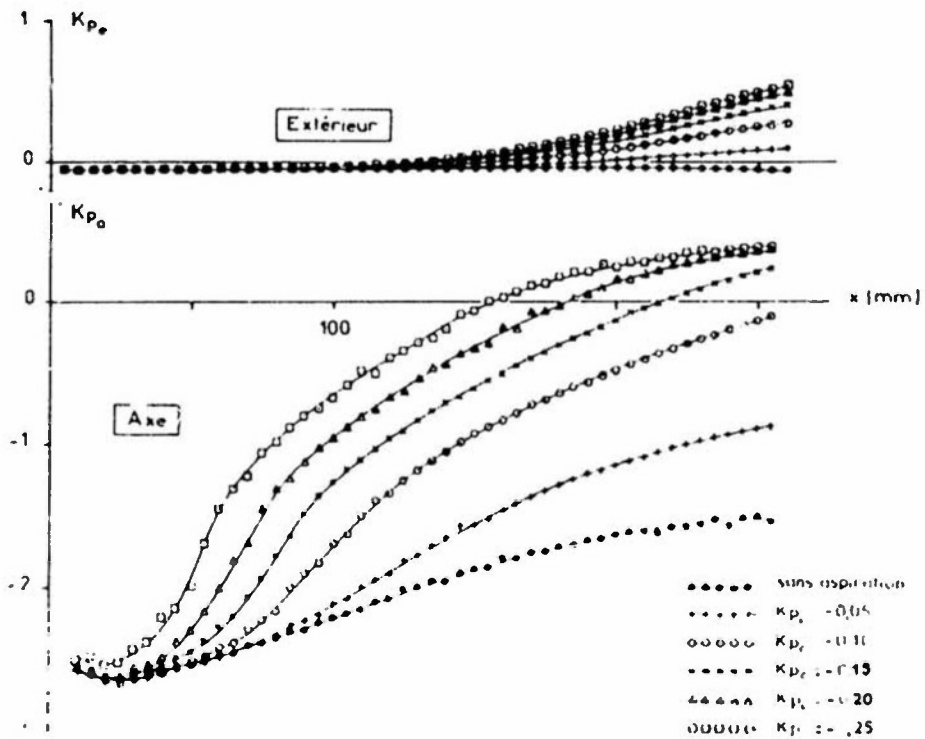


Figure 13. Pressure distribution along the axis of a vortex with variations in the external pressure gradient (from Delery, Horowitz, Leuchter, and Solignari).

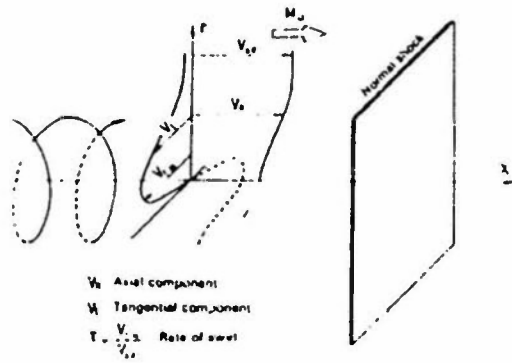


Figure 14. Schematic representation of a shock-vortex interaction (from Miller and Wood).

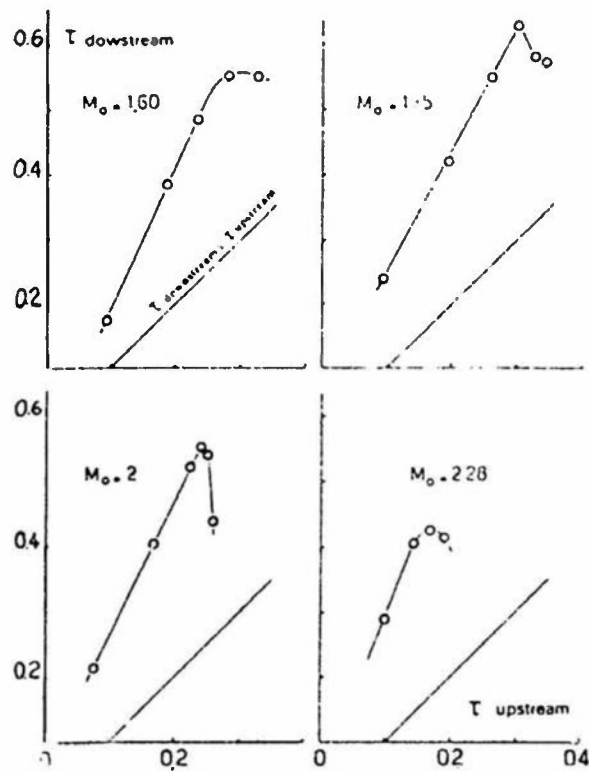


Figure 15. Effect of the shock on the rate of swirl (from Miller and Wood).

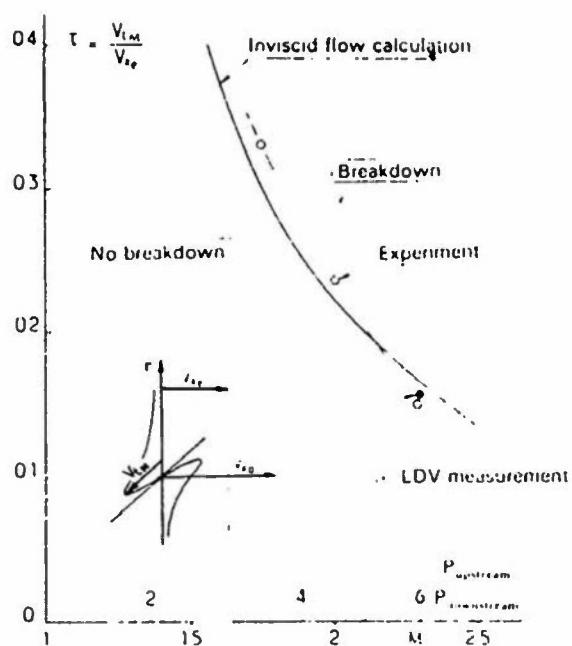


Figure 16. Breakdown limit curve with uniform axial distribution (from Miller and Wood).

# SECTION 4.8 ENVIRONMENTAL EFFECTS ON TRANSITION AND BOUNDARY LAYER CHARACTERISTICS

by

C. Ciray  
Aeronautical Engineering Dept.  
Middle East Technical University  
Inönü Bulvarı, Ankara, Turkey

## Nomenclature

$C$	Chord length or wind tunnel working section perimeter, (L)
$C_1$	Wind tunnel perimeter of 1 ft x 1 ft working section = 1.20 m, (L)
$C_D$	Drag coefficient, (1)
$C_F$	Friction coefficient, (1)
$C_L$	Lift coefficient, (1)
$C_p$	Pressure coefficient, (1)
$H$	Shape parameter, $\delta^*/\theta$ , (1)
$H_1$	Shape parameter before the shock, (1)
$H_2$	Shape parameter after the shock, (1)
$G_0$	Clauser shape parameter, $\int (u_e - U/U_e)^2 dy / \int (U_e - U/U_e) dy$ , (1)
$G$	Turbulence intensity corrected $F$ , $G_0(1 - \alpha T)$ , (1)
$k$	Trip size (L)
$M$	Mesh size of turbulence generating grid, (L)
$M_{pk}$	Peak Mach number at the shock, (1)
$M_\infty$ $M_0$	Mach number of the external flow, (1)
$p$ or $p_s$	Static pressure
$p_T$	Total pressure
$p'$ or $p'_s$	r.m.s. of static pressure fluctuations
$p'_T$	r.m.s. of total pressure fluctuations
$Re_x$	Reynolds number based on distance in $x$ direction, (1)
$Re_v$	Vorticity Reynolds number $\cdot y^2/\nu \cdot dU/dy$ , (1)
$Re_{ii}$	Momentum Reynolds number at the point of instability, (1)
$Re_{itr}$	Momentum Reynolds number at transition point, (1)
$Re_t$ or $Re_T$	Transition Reynolds number based on distance, (1)
$I$ or $I_u$	Turbulence intensity, $U'_1/U_e$ , (1)
$I_{\tau}$	Taylor's parameter, $T(X/M)^{1/5}$ , (1)
$T_{AW}$	Adiabatic wall temperature, (T)
$T_w$	Wall temperature, (T)
$U'_1$	r.m.s. of velocity fluctuations in 1 direction, (LT <sup>-1</sup> )
$U_e$	Mean external velocity, (LT <sup>-1</sup> )
$U$	Instantaneous velocity, (LT <sup>-1</sup> )
$\bar{U}$	Mean velocity, (LT <sup>-1</sup> )
$U_\tau$	Shear stress velocity, $U_\tau = \tau_w/\rho = U_e C_f/2$ , (LT <sup>-1</sup> )
$x$	Distance from leading edge, (L)
$x_s$	Shock position at a given turbulence intensity, (1)
$x_{s0}$	Shock position at quiescent flow, $T = 0$ , (1)
$x_k$	Trip position (L)
$x_{t0}$	Untripped transition position, (L)
$x_t$	Transition position, (L)
$x_i$	Position of point of instability, (L)
$y$	Normal distance from wall, (L)
$\alpha$	Angle of attack, or a constant, (1)
$\delta$	Boundary layer thickness, (L)
$\delta_1$	Boundary layer thickness before the shock, (L)



$\delta_2$	Boundary layer thickness after the shock, (L)
$\delta_{BS}$	Boundary layer thickness before the shock, (L)
$\delta^*$	Displacement thickness, (L)
$\lambda$	Pohlhausen parameter $= \delta^2 \cdot dUe/dx/v$ , (1)
$\lambda_{ij}$	Pohlhausen parameter based on $\theta = \theta^2 \cdot dUe/dx/v$ , (1)
$\lambda_{ij}$	Mean Pohlhausen parameter used by Granville, (1)
$\rho$	Density, (FL-3)
$\nu$	Kinetic viscosity, (L <sup>2</sup> T <sup>-1</sup> )
$\theta$	Momentum thickness, (L)
$\tau_w$	Wall shear stress, (FL-2)

#### 4.8 ENVIRONMENTAL EFFECTS ON TRANSITION AND BOUNDARY LAYER CHARACTERISTICS

##### 4.8.1 INTRODUCTION AND NATURE OF ENVIRONMENTAL EFFECTS

A boundary layer develops under the influence of internal interactions or mechanisms controlled by the field equations and by inputs through the boundaries of the control volume surrounding the portion of the boundary layer in question. The inputs are coming through material and non-material boundaries as shown in Fig. 1.

The environmental effect is understood to be the component of the boundary conditions that are random functions of time and/or spatial coordinates. Hence momentum, pressure, entropy, and surface irregularity are quantities which give rise to environmental effects. These quantities are only random functions of time at a non-material boundary whereas they can as well be random functions of spatial coordinates at a material boundary when they act as an environmental effect. A boundary layer developing on a rough surface is an example of the latter case. Therefore a perfectly motionless, non-vibrating but rough boundary may be considered as an environmental effect with respect to the non-slip condition and also to temperature and/or heat flux conditions if these latter two exist all along the rough boundary.

It can be inferred that, for the boundary layer developing on a wing of an airplane flying in a perfectly calm weather without any atmospheric disturbance, the environmental effect may be produced only by the material boundaries. Yet, if the model of the same wing is tested in a wind tunnel, momentum, entropy, and pressure (noise) fluctuations generated in the wind tunnel will constitute the environmental effects through the non-material boundaries as well. Therefore estimation of boundary layer characteristics (hence transition) from wind tunnel data requires not only Reynolds number extrapolation but also distinction of the influence of the individual environmental factors (elements) and their extrapolation to full scale flight conditions.

Suppose that  $C_D$  is measured for a given configuration in a wind tunnel for a range of Reynolds number represented by the full line portion of the upper curve M in Fig. 2 for a known wind tunnel (W.T.) environmental condition (say turbulence intensity). Suppose also that, the correction necessary to bring  $C_D$  to zero environmental effect is shown by  $\Delta C_D[W.T. Env]$ , that is the curve m in the same figure. By subtracting m from curve M, a point 1 on M will be brought to 2 on the new curve N. Curve N is representing zero environmental effect curve and the point 2 corresponds to  $C_D$  for zero environmental effect at W.T. Reynolds number. Reynolds number extrapolation to flight Reynolds number at zero environmental effect will bring  $C_D$  to point 3 on curve N. If  $\Delta C_D$  at the flight environmental condition (say for a different turbulence intensity) is represented by the curve n, the  $C_D$  at flight Reynolds number and environmental conditions will be shown by point 4.

1. If the environmental effect was not considered then the Reynolds number effect alone would bring 1 to 4 in.

2. If the environmental effect was Reynolds number independent, then at flight Reynolds number,  $C_D$  for zero flight environmental effect would be represented by the point 4' so that the distance 1-2 which is equal to  $4''-4'$  would also be equal to the distance  $4''-3$ . The actual  $C_D$  for flight conditions has to be represented by the point 4 where the distance 4-3 is equal to  $\Delta C_D$  on curve n at  $Re_{FL}$ . It becomes clear that an environmental effect is not a Reynolds number effect, but a Reynolds number effect may exist in the extrapolation of environmental effects to full scale flight conditions, at least in principle.

The effect of the turbulence level of the wind tunnel environment has long been recognized to be influential in hastening transition and has also been led to formulations that relate transition point to turbulence level for subsonic flows. Similarly, acoustical disturbances in subsonic flows at very low wind tunnel turbulence levels has been recognized to influence the transition.

But the importance of environmental effects on boundary layer simulation, transition and development has been emphasized more with the advent of more stringent requirements imposed on wind tunnel results [47]. Figures 2b [48] and 2c [49] demonstrate that these requirements such as tolerable errors below a few drag counts from different wind tunnel data can be expected only if the role of the environmental effects influencing the boundary layer characteristics are quantitatively accounted for.

The environmental effects are classified for the purpose of this chapter as the wind tunnel flow disturbances, wind tunnel acoustical disturbances, and model effects for each flow regime. Wind tunnel flow disturbance effects mean more specifically velocity (momentum), pressure and temperature (entropy) fluctuations of the wind tunnel flow having an impact on the boundary layer flow characteristics, development and transition. The main effect meant by wind tunnel acoustical disturbances is the effect of the noise on the boundary layer. By model effects, the effects of surface irregularities, non-adiabatic wall temperature changes, changes in attitude, and vibration of the model are understood.

The chapter is organized in five sections. Section 4.8.2 is devoted to the subsonic regime, with sub sections on wind tunnel flow disturbances, wind tunnel acoustical disturbances, and effects of disturbances of the model. Section 4.8.3 is for transonic-supersonic flows and is organized with the same subsections as 4.8.2. Section 4.8.4 is devoted to theoretical means for the prediction of the environmental effect.. Finally, Section 4.8.5 resumes with some concluding remarks. Each subsection is organized in an order reflecting the chronological development of the effect studied.

It should be noted that this chapter is essentially devoted to the environmental effects on transition and boundary layer characteristics. The actual transition phenomenon or boundary layer characteristics are treated in specialized sections such as that of R. Michel's. Therefore, the reader must consult these sections if he wants a general account of transition and boundary layer characteristics. Also some of the studies reported here are reviewed in subsections 2.3.1.5 to 2.3.1.8 of this report under the title of Flow Quality, Temperature Nonequilibrium, Surface Roughness, and Model Deformation.

## 4.8.2 Subsonic flow

### 4.8.2.1 Wind Tunnel Flow Disturbances

#### Transition

Flow disturbances simply mean the influence of external turbulence on a laminar boundary layer, therefore affecting the transition. The functional relation of turbulence quantities to transition is generally represented on', through the turbulence intensity:

$$T = \frac{U_1}{U_e} \text{ where } U_1 = (\overline{U_1^2})^{1/2}.$$

Goldstein [1], following G. I. Taylor [2], reminds us that transition is not only a function of  $T$  "but depends also on the scale of the turbulence producing mechanism". G. I. Taylor adopts the view that transition is enhanced by the pressure gradient fluctuations caused by the turbulence of the flow field. With further assumptions drawn largely from isotropic turbulence studies behind a grid of bars (mesh size  $M$ ), the critical  $Re_\delta$  or  $Re_x$  for transition is related to:

$$T_a = T \left( \frac{X}{M} \right)^{1/5}$$

which is called Taylor's turbulence parameter by Hall and Gibbings [2]. It appears that Taylor's parameter  $T_a$  is a constant at transition for all  $X$ ,  $T$ , and  $M$  combinations. If the transition distance  $X$  is replaced by  $R_x$ , Fig. 3 can be used to find the combined effect of turbulence intensity  $T$  and turbulence scale represented by the mesh size  $M$ . The experimental points in Fig. 3 are reported [3] to belong to Hislop [4]. Hislop [4] reports that his measurements could not be correlated on the basis of  $T_a$  where the mesh sizes he used were  $M = 1''/2$ ,  $1''$  and  $2''$ , Fig. 3. However, Schubauer's data [5] obtained with higher turbulence intensities and larger mesh sizes, such as  $M = 1''$ ,  $3 1''/2$ , and  $5''$ , seem to correlate on the basis of  $T_a$ . In their review section, Hall and Gibbings [3] conclude that  $T_a$  is a good correlation parameter for high turbulence intensities and larger turbulence scales. It should be noted that the above information and deliberations are for zero pressure gradient. Dryden, et al. [6], also found that the effect of external turbulence cannot be satisfactorily correlated only with the turbulence intensity but that the scale of turbulence had to be introduced. They used correlations of fluctuations between neighboring points in order to study the critical Reynolds number of spheres and found that the length scale as well as the intensity had to be introduced into the correlation.

On the other hand, in order to consider the influence of turbulence intensity and pressure gradient, Van Driest and Blumer [7] start with the assertion that transition occurs "when the ratio of inertial stress to viscous stress is a maximum". The ratio is named vorticity Reynolds number,  $Re_v$ , and defined as:

$$Re_v = \frac{y^2}{\nu} \cdot \frac{dU}{dy}.$$

The maximum vorticity Reynolds number occurs for the Blasius profile, at a relative height of 0.57 of the boundary layer thickness,  $\delta$ , and this figure is almost equal to 0.6, which is the relative height of the point where high frequency bursts occur. They show that:

$$\frac{Re_v}{Re_\delta} = A + B \lambda$$

where  $\lambda$  is the Pohlhausen parameter and  $A$  and  $B$  two constants to be specified experimentally. For fluctuating flows

$$\lambda = - \frac{\delta^2}{\mu U_e} \cdot \frac{dP}{dx} = \frac{\delta}{\nu} \cdot \frac{d\overline{U}e}{dx}$$

is perturbed as:

$$\lambda = \overline{\lambda} + \lambda' \text{ and } \frac{dP'}{dx} \text{ is taken proportional to } \rho \frac{U_1^2}{Y}.$$

With further assumption that the maximum size  $\lambda$  of disturbing eddies should be proportional to  $\delta$ , then the basic relation:

$$\frac{Re_v}{Re_\delta} = A + B \overline{\lambda} + C Re_\delta \cdot T^2$$

is obtained.  $Re_v$ , A, B, and C are constants to be obtained experimentally. The relation contains the pressure gradient and turbulence intensity effects simultaneously in the same equation.

The experimental constants are supplied in Ref. [7], for various classes of boundary layers such as for Falkner-Skan profiles with or without mean pressure gradient. With respect to the assumptions involved and the number of experimentally determined constants, I. Tani [8] remarks: "In view of the questionable assumptions concerning mixing length and free stream turbulence effects, however the relation may be looked upon simply as an empirical correlation formula." This type of formula has been used by Wells [9] for the case of zero pressure gradient and found to fit the experimental points for the range of

$$Re_x < 2.5 \times 10^6$$

corresponding to  $T > 0.002$  which is the threshold of the influence of acoustical disturbances as reported below. It would be worthwhile to test the complete Van Driest-Blumer type of equation with non-zero pressure gradient against experimental data and to find its range of validity. Also it would be interesting and beneficial to find out the threshold for the acoustical (or noise) effects when pressure gradient is present.

Junkhan-Serovy [10] reports the dependence of transition Reynolds number  $Re_t$  on turbulence intensity in the form of:

$$4 \times 10^4 < Re_t < 4 \times 10^5 \text{ when } 0.4\% < T < 8.3\%$$

for a flat plate with zero pressure gradient and states that for favorable pressure gradient:

- transition region increases in size and
- $Re_t$  decreases with increasing T.

Wells [9] gives basically the two figures, namely Figs. 4 and 5, for the variation of  $Re_t$  with T. Figure 4 contains results obtained in two different wind tunnels (the LTV and National Bureau of Standards) for low T range ( $T < 0.003$ ) and Fig. 5 for higher range of T. The Fig. 5 contains the correlation

$$\frac{2200}{Re_t^{1/2}} = 1 + 38 \cdot 2 \cdot T^2 Re_t^{1/2}$$

as a full line and it is of the type given by Van Driest-Blumer analysis [7].

Wells experimented at the L.T.V. Research Center, Dallas, in an open circuit wind tunnel with a long circular test section that he calls a boundary layer channel with 12 different settling chambers and different screens. He obtained higher  $Re_t$  as shown in Figs. 4 and 5 when compared to the results of Schubauer and Skramstadt, Dryden, Hall and Hislop in the N.B.S. tunnel for the same turbulence intensities T, when  $T < 0.003$ . More information about the experimental setup and experiments can be found in Refs. [11] and [12]. The large differences in  $Re_t$  between the two different facilities for the same T as observed in Fig. 4, is ascribed to a noise effect. This has been later the subject of another study by Spangler and Wells [13] where the main result is shown in Fig. 6 and will be discussed further in sub-section 4.8.2.2.

Hall-Gibbings [3] review the works of Van Driest-Blumer, Grabtree, Granville, Smith and Gamberoni, Van Ingen, Joffe-Chamuse and Smith, and that of Michel. They conclude in summary as follows:

- The minimum variables required for a reliable prediction of transition are:

$$T, \lambda_\theta = \frac{\theta^2}{\nu} \cdot \frac{dU}{dx}, \text{ and } R_\theta,$$

in spite of the fact that turbulence scale, frequency spectrum and the previous history of the flow such as the locus of  $T$ ,  $\lambda_\theta$ ,  $R_\theta$  are influencing the transition.

- Acoustic disturbances influence transition when  $T < 0.2\%$ .
- For  $dp/dx = 0$ , Fig. 7, the start of transition is given by:

$$\ln(R_\theta - 190) = -103T + 6.88,$$

and the end of transition is given by:

$$\ln(R_\theta - 320) = -44.7T + 7.70$$

The equation for the start of transition as a function of  $T$  is based on data points of a number of experimentators reported in Ref. [3] and has a reasonable reliability. Yet as pointed out in the same work the end of transition equation has a weakness in the sense that it is based on only three experimental points. For

$$\lambda_\theta = \frac{\theta^2}{\nu} \frac{dU}{dx} \neq 0,$$

Fig. 8 gives the dependence of  $R_\theta$  at transition as a function of  $\lambda_\theta$  and  $T$  in graphical form [3].

Granville [14] expressed the  $R_{\theta tr} - R_{\theta i}$  as a function of  $\lambda_\theta$ , Fig. 9, stressing the influence of the history of the B/L after the point of instability.  $R_{\theta tr}$  and  $R_{\theta i}$  are the Reynolds numbers based on momentum thicknesses at the points of transition and instability whereas  $\bar{\lambda}_\theta$  is defined as:

$$\bar{\lambda}_\theta = \frac{\theta^2}{\nu} \cdot \frac{d\bar{U}_e}{dx} = \int_{X_i}^{X_{tr}} \frac{\theta^2}{\nu} \cdot \frac{d\bar{U}_e}{dx} \cdot dx / (X_{tr} - X_i).$$

A transition criterion similar to that of Granville but including the effect of external turbulence intensity is given and described in Section 4.3.3.1.2 of this report, (see Fig. 7 of the appropriate section).

It is observed that most of the experimental work related to the influence of external turbulence on transition in the incompressible range were made before the early 70's and go back as early as the 30's. The use of modern sensing elements such as laser doppler anemometers and powerful data acquisition systems will help to increase the accuracies and reduce the scatter common to all experimental work of this kind. A better picture of transition development along the chord, the span, and in the direction perpendicular to the wall can undoubtedly be obtained.

The external turbulence is usually represented by the turbulence intensity,  $T$ . Yet the influence of the scale of turbulence which has been shown to be influential has not received much attention. It is generally accepted that external turbulence cannot be represented by a single parameter. It is of course desirable to have a minimum number of parameters. Yet it can be argued that external turbulence has at least to be described through its power spectrum, the peaks in the spectrum, and the associated wave numbers in addition to the intensity. Taylor's hypothesis of frozen turbulence may not be adequate for the determination of meaningful wave numbers in this respect [15] if the experimentator operates with the hot wire.

Studies to obtain the influence of external turbulence on transition using some closure model are not numerous. Arnal and Michel [16] have an attempt in this direction. They try to predict the transition with a modified K- $\epsilon$  model, using the Jones and Launder model for taking account of the effect of viscosity on turbulence by "viscous functions". Figure 10 shows the displacement thickness Reynolds number at transition as function of the turbulence intensity as obtained from K -  $\epsilon$  model and

experiments, (flat plate boundary layer). The agreement is not bad. Unfortunately, important weaknesses of the model appeared in other applications, essentially attributable to the fact that it does not take account in any way of the stability properties of the laminar boundary layer. It does not seem, finally, that a transport equations model should be recommended for transition problems [17].

The final observation about turbulence effects on laminar boundary layer transition is that most of the experimental work was performed for a flat plate with or without pressure gradient, or on airfoils, but three-dimensional configurations have not been treated at all or reported in readily available literature. It is felt that the observations outlined above suggest the need and direction of some research work for the future.

J. E. Green [18] reviews the experimental works of Charnay, Compte-Bellot, Mathieu [19] and that of Huffman, Zimmerman, Bennett [20] about the effect of free stream turbulence on flat plate (zero pressure gradient) turbulent boundary layer characteristics. The influence of turbulence is studied with respect to turbulence intensity,  $T$ , while the length scale of turbulence (at least the integral longitudinal scale) has been the same or almost the same for all intensities. The main qualitative conclusions are that

- a thicker boundary layer
- a fuller velocity profile (smaller  $H$ ) and
- higher shear stresses

are obtained with increasing  $T$ .

Another important result is that the law of the wall representation is almost not influenced, whereas the velocity defect region is critically influenced. Charnay, Compte-Bellot and Mathieu propose [19] for the velocity defect region the expression:

$$\frac{U_e - U}{U_\tau - \alpha U_1'} = f\left(\frac{y}{\delta}\right) \text{ instead of } \frac{U_e - U}{U_\tau} = f\left(\frac{y}{\delta}\right)$$

where  $\alpha = 0.29$  in [19] and it is taken as  $1/3$  in [19]. Green [18], gives for the Clauser shape parameter, the relation

$$G = G_0 \left(1 - \alpha \frac{U_1'}{U_\tau}\right) = \frac{H-1}{H} \sqrt{\frac{2}{C_f}}$$

to take into account the influence of turbulence intensity on  $G$ .  $G_0$  is the shape parameter at quiescent external flow conditions which is taken as 6.4 or 6.5 (Clauser value is 6.1).

Green deduces a number of relations to calculate the fractional increase in  $C_f$  and the fractional decrease in  $H$  in terms of  $T$  when  $R_0$  is held constant. He obtains:

$$\frac{\Delta C_f}{C_f} = 4.8 T$$

$$\frac{\Delta H}{H} = -(2.4 - 0.25 H) T$$

Also the fractional decrease in  $R_0$  when  $H$  is maintained constant is calculated as:

$$\frac{\Delta R_0}{R_0} = -\left(\frac{0.27}{C_f} - 0.97 \sqrt{\frac{2}{C_f}}\right) T$$

With the definition of the effective Reynolds number of a turbulent boundary layer in the presence of a turbulent external flow as "the Reynolds number at which the same  $H$  would be obtained if the external flow was quiescent", it is shown that a turbulence intensity of  $T = 1\%$  corresponds to almost 60% fractional decrease in  $R_0$  and this effect increases with decreasing  $C_f$ , hence increasing  $R_0$ .

Green [18] also gives a series of results, Fig. 11, obtained through calculations to show the influence of pressure gradient (high lift airfoils) and the change in mean mixing length of the outer boundary layer on some boundary layer characteristics. Figures 11b and 11c show that the influence of changing the mixing length of the outer boundary layer in the ratios of 1/0.9 and 1/0.8 are hardly noticeable on the development of momentum and displacement thicknesses for the nominal Reynolds number of  $7 \times 10^6$ . The change in nominal Reynolds number from  $7 \times 10^6$  to  $12 \times 10^6$  and to  $21 \times 10^6$  alter critically  $\theta$  and  $\delta^*$ . Yet Fig. 11d reveals that the effect of varying the outer boundary layer mixing length on the shape parameter  $H$  is by no means small. Indeed it is observed from the same figure that, changing mixing length in the ratio of 1/0.9 gives the same variation in  $H$  as the change of the nominal Reynolds number from  $7 \times 10^6$  to  $12 \times 10^6$ , that is an increase in  $Re$  of  $12/7 = 1.7$  times.  $Re$  increases by a factor of 3 for a change of mixing length of 1/0.8.

Meier and Kreplin [21] tried to see the influence of turbulence intensity, boundary layer history, turbulence scale, and power spectrum of turbulence on boundary layer characteristics. The measurements were made in an open wind tunnel with a convergent nozzle upstream of the working section whose wall was used as a flat plate. The nominal turbulence level in the wind tunnel was 0.06% and turbulence intensity was changed by means of different grids placed at various places in the settling chamber and the nozzle. The transition was fixed at 50 mm from the leading edge and boundary layer characteristics were measured at a fixed point, namely 850 mm from the leading edge. Some of their results are summarized below:

1. Figure 12a shows the velocity profile  $U/U_t$  at the fixed measuring section for various turbulence intensities at the leading edge. The authors specify that the external turbulence intensities at the measuring station are almost the same for different intensities at the leading edge. It is observed that the curve is unique for the inner wall region whereas the outer region is heavily influenced by the turbulence intensities. Furthermore, the higher the turbulence level  $T$ , the smaller is the deviation of the velocity defect region from logarithmic distribution. That means the law of wake is less influential as reflected by the shape factor  $n_1$ . The two different curves for the same intensity (i.e. 0.06%) clearly indicates the influence of history (note the shift in the zero of Fig. 12a).
2. Figure 12b shows the  $C_f$  as a function of turbulence intensities corresponding to the measurements mentioned above. The calculations of Green are also shown. According to Meier and Kreplin's experimental results the theoretical values of Green overestimate the friction coefficients significantly.
3. Figures 12c and 12d show how various grids located at different positions create quite different spectra of velocity fluctuations  $U'$  and integral length scale  $L_x$  at a given point (1420 mm from leading edge) for the same  $T = 0.2\%$  measured at this point.
4. Figure 12e shows the correlation attempted by the two authors for the relative change in  $C_f$  versus the length scale nondimensionalized with respect to the boundary layer thickness which indicates a decrease in  $C_f$  with increasing  $L_x$ .
5. High turbulence levels at the leading edge generate nonuniformities which cause changes in boundary layer structure, such as for example the increase in displacement thickness due to momentum loss because of tripping wire.

Hancock and Bradshaw, in a more recent work [22], have covered a wider spectrum in the matrix of  $T$  and scale of external turbulence again for  $dP/dx = 0$  on a flat plate, compared to all of the already available information from previous workers, Fig. 13a. Length scale is defined in the form of dissipation length  $L_\epsilon U$ ,  $u$  meaning longitudinal component of velocity fluctuation has been used in the definition



$$U_e \frac{\overline{d(U_1)_e^2}}{dX_g} = - \frac{\overline{(U_1)_e^2}^{3/2}}{L_e^u}$$

where  $X_g$  is measured from the turbulence generating grid. Figure 13a indicates that the region covered in  $T$  and  $L_e^u$  is:

$$0.018 < T < 0.06 \text{ and } 0.67 < \frac{L_e^u}{\delta_{995}} < 5.$$

1. The authors use an empirical parameter in the form of

$$Tx100 \left( \frac{L_e^u}{\delta_{995}} + 2 \right)$$

obtained by trial and error in order to correlate  $\Delta C_f/C_{f_0}$  and obtain a good fit for their own data, Fig. 13b (top). But for  $\Delta C_f/C_{f_0} > 0.05$  or for larger  $T$  (or their special parameter), the extent of the scatter area is of the same order as  $\Delta C_f/C_{f_0}$  when data of other workers are plotted, Fig. 13b (lower). Whether this special parameter is adequate or not, it combines Green's [18] inference that  $\Delta C_f/C_{f_0}$  is proportional to  $T$  and confirms Meier and Kreplin's [21] finding that  $\Delta C_f/C_{f_0}$  is inversely proportional to length scale more convincingly, (see also Fig. 12e). The paper by Hancock and Bradshaw [22] gives the correlation between relative increments in  $C_{f_0}$  and  $H_0$  as:

$$\frac{\Delta H}{H_0} = 0.47 \frac{\Delta C_f}{C_{f_0}}$$

and plotted in Fig. 13c (top). This is very close to the relation given by Green [18]. Indeed the latter formulation is given as:

$$\frac{\Delta H}{H_0} = -(2.4 - 0.25 H_0)T.$$

This becomes with  $\Delta C_f/C_{f_0} = 4.8 T$

$$\frac{\Delta H}{H_0} = -(0.05 - 0.052 H_0)T$$

or taking  $H_0 \sim 1.3$

$$\frac{\Delta H}{H_0} = -0.44 T.$$

2. The paper [22] explains the decrease in  $\Delta C_f/C_{f_0}$  with increasing length scale by the wall effect which reduces the normal component of turbulent fluctuations affecting the boundary layer below the free stream. If this supposition is true, it would perhaps be more realistic to define the length scale as  $L_e^v$  rather than  $L_e^u$ , i.e.:

$$U_e \frac{\overline{d(U_2)_e^2}}{dX_g} = - \frac{\overline{(U_2)_e^2}^{3/2}}{L_e^v}$$

Figure 13c (lower) shows the relative incremental increase in  $\delta_{995}/\theta$  in terms of  $\Delta C_f/C_{f_0}$ . It would be instructive to be able to control the data in the figure, with respect to Green's formulation:

$$\frac{\Delta R_\theta}{R_\theta} = - \left( \frac{0.27}{C_{f_0}} - 0.97 \frac{2}{C_f} \right) T.$$

3. Finally, the influence of external turbulence on mean velocity distribution is shown in Fig. 13d, also taken from the same reference [22]. The top two curves belong to low turbulence level and small scale, whereas the lower six curves are for high turbulence intensity ( $0.0362 < T < 0.0468$ ) and large length scale

$$\left(1.69 < \frac{L_e^u}{\delta_{995}} < 2.72\right)$$

and measured at different  $x$  positions along the plate. These curves confirm once more that logarithmic law (inner wall region) is not influenced by the external turbulence and further it is extended with increasing turbulence intensity and scale. The full lines are given by the usual

$$\frac{U_1}{U_\tau} = \frac{1}{\kappa} \ln \frac{yU_\tau}{\nu} + C + \frac{1}{\kappa} g\left(\frac{y}{\delta}\right)$$

with

$$g\left(\frac{y}{\delta}\right) = (1 + 6 \frac{y}{\delta})\left(\frac{y}{\delta}\right)^2 - (1 - 4 \frac{y}{\delta})\left(\frac{y}{\delta}\right)^3$$

on the grounds that it is more correct and realistic [23, 24]. The paper does not offer any physical explanation for the penetration of the law of the wall region into the wake region and  $\pi$  values that give the solid lines are not given. The simplest explanation that can be offered is that larger scales, larger or equal to  $\delta$ , are bringing and spreading the wall region behavior to the whole thickness of the boundary layer. Therefore  $\pi$  may be found to be strongly related to the scale than to the intensity.

The above studies show that turbulent velocity fluctuations as an environmental parameter affect the boundary layer characteristics through its intensity, spectrum, scale and also through the history of these parameters. For the time being, extensive experimental work seems to be necessary to lead to, to supplement, or to confirm any theoretical work with the aim to predict the environmental effects. It has to be pointed out that while it is extremely worthwhile to design experimental work to isolate the role of individual parameters of the environment, it is equally important to find out the weight of the role of each parameter when more than one of them are concurrently present while affecting the boundary layer. Perhaps the historical evolution of the external flow turbulence intensity, spectrum and scale should be measured and documented for a given wind tunnel and experimental setup, in conjunction with the boundary layer measurements to help to define a special "signature" for a given wind tunnel. It is recommended that wall shear stresses be measured by direct techniques to the extent possible.

#### 4.8.2.2 Wind Tunnel Acoustical Disturbances

##### Transition:

The dependence of transition position on turbulence intensity is shown in Fig. 4, taken from Wells [9], for different wind tunnels when  $T > 0.3\%$ . For smaller turbulence intensities, different wind tunnels have different transition Reynolds numbers at the same  $T$  values. Spangler and Wells [13] in a follow-up paper, discuss the acoustical effect which was stated as the cause of this discrepancy referred to in the previous paper by Wells. A rotating vane provided the acoustical disturbance without producing momentum fluctuations. It is illustrated in Fig. 6 that  $R_t$  is sensitive to the frequency of the disturbing noise. It is further explained that the spectrum of the noise is also an important factor. For example, the insensitivity of transition at 82 c/s to noise whereas there is a dependence at 76 c/s, is attributed to the fact that the spectrum for 76 c/s contains the critical peak at 20 c/s which excites the occurrence of transition in accordance with stability theory, whereas for 82 c/s such a peak does not exist in the spectrum. It is further emphasized that some frequencies were effective and the location of the transition could be varied simply by changing its intensity. But slight change in the fundamental frequency causes a complete loss of control.

Murthy-Steinle [25] referring to [26] and [27] state that there is some evidence to show that free stream pressure fluctuations do not have any measurable influence on turbulent boundary layers. They go further to suggest that pressure fluctuations do not affect the transition as they deduce from measurements made on the 10° AEDC cone in Mach number range of 0.4 to 1.2. This point will be discussed at the proper place in subsection 4.8.3. But it has to be reminded that Murthy-Steinle deductions are based on data in high subsonic range for the AEDC cone [28] and also the data show a scatter of  $\pm 20\%$  in transition location even when  $M < 0.8$  or  $0.9$ . With that kind of scatter, it seems necessary to be able to separate the weight of the role of other parameters in order to see whether the pressure fluctuations alone are or are not influential at all.

It is worthwhile to remind once more about the scarcity of studies related to the role of external pressure fluctuations on transition and on the boundary layer characteristics.

#### 4.8.2.3 Disturbance on the Model

Disturbances on the model, understood in the manner of the definition of the environmental effect appear in three different ways:

- The influence of roughness distributed continuously on the material boundary or the rough boundary problem,
- The influence of individual or a row of roughnesses, and
- The vibration of the model.

The first problem, i.e. the influence of distributed (uniform) roughness on boundary layer characteristics such as the velocity distribution and  $C_f$  has long been studied and will not be considered here. The reader is referred to the classical work of Young [29], Schlichting [30], and references in these books.

#### Transition:

How distributed roughness affects the transition has not received the same attention. The dependence of transition Reynolds number both on roughness Reynolds number and the pressure gradient as reported by Feindt [31] is shown in Fig. 14.

The second problem, i.e., the influence of individual or a row of roughnesses is studied within the context of inducing transition i.e. boundary layer tripping, and is considered in Section 4.9 of this report (not under environmental effects). The deformation of the boundary or deformation of the boundary with time (vibration, third question) is discussed in the following.

The work by Gougat and Martin [32] aims to study both static (i.e. not moving) and dynamic (i.e. vibrating) phenomena on a limited portion of a flat plate to determine the effect on transition seemingly at zero nominal pressure gradient. The location of transition is defined as the location  $X$  (from leading edge) where the maximum of  $T$  across the thickness of the boundary layer is observed. This is seen in Fig. 15a for flat plate and for bumps (with heights  $\pm a$ ) 100 mm long. The location of the maximum of velocity fluctuations power spectrum is seen to be at  $0.35$  of  $y/\delta$  and this corresponds to  $0.40$  of  $U/U_e$ .

In Fig. 15b, it is seen that a bump of  $\pm 1$  mm moves the transition in the upstream direction by 37%. Yet whether the bump is plus or minus makes a difference of only 3% in the upstream migration of the transition. Reference [32] only suggests that the transition position advances if the bump is set into vibration. It is appropriate to call attention to the need to study transition in the presence of vibrating portions of a solid boundary which is likely to affect the transition as suggested above.

#### 4.8.3 Transonic-Supersonic Flows

It appears that the interest in transition studies with respect to environmental effects are more numerous for supersonic flows than for transonic flows. This may be because of the knowledge that the effect of compressibility is small on the performance of a boundary layer. Yet, today a few drag counts are required in wind tunnel practice. Therefore, research directed towards the estimate of the influence of turbulence intensity, scale and power spectra, acoustical disturbances, orientation spectra, etc. on transition in transonic Mach number range is necessary.

##### 4.8.3.1 Wind Tunnel Flow Disturbances

###### Transition:

Laufer [33] gives the following results for the effect of turbulence intensity  $T$  for supersonic flows with regard to transition, for a series of experiments conducted in a Mach number range of  $1.7 < M < 4$  and a turbulence intensity range of  $0.6\% < T < 7\%$ . It is stated that: for  $M < 2.5$ ,  $T$  is effective on transition whereas for  $M > 2.5$ ,  $T$  is not anymore influential.

###### Shock B/L Interaction for a Turbulent Boundary Layer:

Transonic flow over a bump was studied [34] for varying free stream turbulence intensities  $T$ , and the measurement results for shock position  $x_s$ ,  $Re_\theta$  (Reynolds number based on momentum thickness) are given as a function of  $T$ . The boundary layer is turbulent starting from the monoplane grids controlling the turbulence level in the wind tunnel. From Fig. 16a (left), it is seen that the shock position moves  $n$  in the downstream direction with  $T$  for a constant  $M_\infty$ . The  $\delta^*$  and  $\theta$  first increase with increasing  $T$  up to a maximum, then both decrease when  $T$  continues to increase. The increase in  $\theta$  cannot account for the continuous downstream movement of the shock location. Therefore, the authors conclude that the turbulence intensity of the environment has a direct effect on shock interactions, hence on shock location. An explanation in physical terms of "direct effect on shock interaction hence on shock location" is not given. But the following explanation may be considered. From Fig. 16d (obtained from the follow up study by the same authors to be reported below) it is noted that the magnitude of the turbulence level for the boundary layer before and after the shock is the same for  $T_\infty = 3.68\%$  and  $0.34\%$ . Hence at higher turbulence level the contribution to momentum flux term in the momentum equation is higher on the supersonic face of the shock, therefore pushing the shock in the downstream direction to reach a higher pressure for balance. Figure 16a (right) shows the dependence of Mach number before the shock i.e.  $M_{pk}$  as a function of turbulence level  $T$ . The authors observe that  $M_{pk}$  is more sharply influenced by  $T$  for  $M_{pk} > 1.3$  and conclude that turbulence plays a rather important role when large separation zones are present as is demonstrated in the follow up study [35]. The latter study by the same authors and for the same bump and experimental conditions concentrates on details of the flow at two different stations before and after the shock for different turbulence intensities, i.e.  $0.3\% < T < 6\%$ . Figures 16b,c,d,e,f show the results obtained for  $M_{pk} = 1.44$  which corresponds to a separated zone behind the bump with reattachment to the wind tunnel floor at the trailing edge. In Fig. 16b the velocity profiles measured before and after the shock indicate that the separated zone thickness decreases with increasing  $T$  and one has fuller profiles at both stations for higher  $T$ .

Figure 16c shows that  $H_2/H_1$  and  $\delta^*_{2/\delta^*_1}$  are especially sensitive to  $T$  when  $T < 2\%$  but  $\theta_2/\theta_1$  is not as sensitive. The role of  $T$  on longitudinal intensity distribution of turbulence is indicated in Fig. 16d and it is observed that the maximum turbulence intensity is almost unchanged in the separated zone whereas its location has approached the bump surface. For the same  $y/\delta_{BS}$  the role of increasing environmental turbulence level seems to appear as a reduction in longitudinal turbulence intensity down to  $y/\delta_{BS} = 0.6$ . The reduction may be attributable to the fact that increased external turbulence suppress the thickness of the separation bubble as observed from Fig. 16b. Figure 16e shows that the turbulence spectra are altered before the shock with a change in  $T$ , whereas it is not changed after the shock. The decrease in separation length with increasing  $T$  is seen in Fig. 16f.

It may be recalled from studies related to the parameters of the external turbulence affecting the boundary layer characteristics in compressible flow that the role of the turbulence scale was important. There is no reason why it is not so in shock boundary layer interaction. Also, how the shock influences the turbulence and scale of the external flow is worthwhile to study in a deeper way. It is, for example, very interesting to note that the relative intensity  $T$  is the same before and after the shock according to Fig. 16d.

#### Temperature Fluctuations and Heat Transfer

The other parameter that has been given some attention within flow disturbances is temperature fluctuation. The study by Dekeyser and Burnage [36] is theoretical and also not directly related to transition. It may as well be included in Subsection 7.4 where theoretical prediction is considered. The study is concerned with the development of entropy fluctuations represented by  $s'$ , in 2D boundary layer flow. Entropy fluctuations result from the interaction of an entropy gradient and irrotational velocity fluctuations where for the latter ones pressure fluctuations are responsible. The development of

$$(\overline{s'^2})^{1/2}$$

is schematically shown in Fig. 17 for a 2D flow with a mean velocity  $V_\infty$ . It is assumed that the sound sources are moving with a velocity  $V_s$ , the entropy gradient is  $\partial s / \partial x_3$ ; then the symbols in Fig. 17 are as follows:

$$M_* = \frac{V}{a_o}, V_* = V_\infty - V_s, s' = \frac{1}{c_p} \frac{\partial s}{\partial x_3}, 2\pi\xi = \frac{M_* a_o \cdot x_1}{V_\infty}$$

where  $a_o$  is the speed of sound and  $\Lambda$  corresponds to some sort of macroscale of pressure fluctuations in terms of  $\xi$ .

Morkovin [37] states that at  $M = 1.76$  in a well designed supersonic tunnel no influence on transition of entropy fluctuations is observed. Lynch, et al. [38] report a number of significant changes on boundary layer characteristics and transition caused by heat transfer at the model wall. Their experiments have been conducted on a 14% thick 4-in. chord aft loaded modern airfoil in a 1-foot cryogenic wind tunnel. They have studied various conditions such as:

1. Subcritical attached flow conditions with no transition fixation at  $Re = 7 \times 10^6$  and  $M = 0.72$ . From Fig. 18a it is seen that wall temperatures higher than the adiabatic one decreases the  $C_L$  whereas  $C_D$  increases by one drag count per 1% increase of  $T_w/T_{aw}$ . The reverse is true for cooling.
2. Typical cruise conditions at  $Re 7.5 \times 10^6$ ,  $M = 0.74$ , with a moderate strength shock (no shock induced separation) are illustrated in Fig. 18b. The same trend is observed for different angles of attack tested within the study. Detailed pressure measurements performed within the shock boundary layer interaction region are shown in Fig. 18c which also includes theoretical predictions after Inger's triple deck theory. It is observed that an increase in wall temperature relative to the adiabatic wall moves the shock in the upstream direction mainly because of the influence of the heating on the development of the boundary layer before the shock (see also Section 4.5).
3. Separation (buffet) onset conditions were tested and Fig. 18d shows various results. It is seen that cooling has little effect on  $C_L$  whereas heating decreases  $C_L$  appreciably. The separation is hastened by heating and near trailing edge pressure coefficients decrease appreciably with heating. Correspondingly shock wave moves upstream with heating. The authors conclude that a deviation in  $T_w/T_{aw}$  of more than 1% is unacceptable for the definition of the buffet onset conditions.

4. Separation progression at angles of attack beyond buffet onset is more pronounced with heat transfer, Fig. 18e. The interesting thing here is that  $C_L$  is much influenced by heating and cooling than the buffet onset and that  $C_p$  near the trailing edge is more influenced by cooling than by heating which is just the opposite of the behavior at buffet onset conditions.

It is not very clear if the temperature distribution, though different than adiabatic temperature and changing with time, is "uniform" on the model wall or if there was any randomness with respect to time and position. But it is seen that even 1% deviation of the wall temperature for this small airfoil causes significant deviations in aerodynamic characteristics and flow conditions. With larger exposed areas and on three-dimensional configurations, flow behavior and therefore aerodynamic characteristics may even be altered more severely.

Dougherty and Fisher [28] report experimental results of the non-adiabatic wall effect on transition of the 10° AEDC cone performed in flight. These results are reproduced in Fig. 19. The solid line is given by the expression

$$\frac{Re_T}{Re_{TAW}} = \left( \frac{T_w}{T_{AW}} \right)^{-7}$$

which clearly indicates the strong dependence of transition on wall temperature. The flight test envelope covered a range of Mach numbers as  $0.4 < M < 2$  and unit Reynolds number (per m) of  $3.20 \times 10^6 < Ue/v_c < 16.40 \times 10^6$ .

#### Transition

Pate and Schueler [39] attempt to rationalize the supersonic wind tunnel noise effect on transition. They correlate the transition Reynolds number (based on distance) with the noise parameters of the tunnel, namely:

$C_f$  Boundary layer skin friction coefficient of wind tunnel wall

$\delta^*$  Boundary layer displacement thickness of wind tunnel wall

$C$  Wind tunnel wall perimeter

and have shown that the correlation holds for each tunnel, as in Fig. 20.

The correlation is further extended to include the relative size of tunnels, Fig. 21. This correlation is given as:

$$Re = 0.0141 (C_p)^{-2.55} [0.56 + 0.44 (C_1/C) / (\delta^*/C)^{1/2}]$$

and is valid for all the supersonic wind tunnels, Mach numbers, and Reynolds numbers within the tested cases.  $C_1$  in the above expression is the perimeter of a 1-ft tunnel i.e.  $C_1 = 4$  ft. The range of Mach numbers covered is  $3 < M < 8$  and the unit Reynolds number varies as:

$$0.1 \times 10^6 < Re/in. < 1.1 \times 10^6.$$

The wind tunnel sizes range from 1 ft to 16 ft. Figures 22, 23, and 24 also taken from the same reference [39], show how the correlation given above represents the available data for various tunnels as a function of unit Reynolds number, size, and Mach number. Later Pate [40] reported on transition for a 10° cone under supersonic conditions. The noise parameters ( $C_f$ ,  $C$ ,  $\delta^*$ ) are shown to be good indicators of  $Re_t$  for cones too, Fig. 26. The Mach number range is  $3 < M < 4$  and the wind tunnel size varies from 12-in. to 40-in. (AEDC VKF Tunnels D and A). The tests were performed with a clean

surface and with spherical roughness. It is seen, Fig. 25, that  $Re_t$  is tunnel size dependent and increases with increasing size. Here  $(Re_t/in.)_\infty$  and  $(Re_t/in.)_\delta$  represent the unit Reynolds number based on velocities of the external flow and at the edge of boundary layer thickness. Figure 26 contains the transition point correlation for special nondimensional parameters (shown on the figure) for a wide range of Mach numbers and supersonic wind tunnels and both for planar and cone models.

Bergstrom and Raghunathan [41] comment on the possible representation of  $Re_t$  vs. the r.m.s. of the pressure fluctuations [more precisely  $P'/P$ ] to discern the true dependence of  $Re_t$  on local effects, particularly of Mach number which would be obscured if  $\delta^*$ ,  $C_f$  type parameters are used. Dougherty, Jr. [42] reports microphone measurements of pressure fluctuations on a  $10^\circ$  cone in the AEDC PWT 16S at 58-ft downstream of the throat. He shows that, Fig. 27, his  $Re_t$  measurements correlate with Pate-Schueler formula for a Mach number down to 2. Furthermore, the r.m.s. values of pressure fluctuations  $P'$  are shown to be a function of the tunnel wall boundary layer parameters  $\delta^*$ ,  $C_f$ , and  $C$ , Fig. 28, where:

$$\Delta C_p = \frac{P'}{q_\infty}$$

The empirical fit is:

$$\Delta C_p = 0.1613 \{C_f |\delta^*/C|^{1/2} \times 10^5 - 5\}$$

The relation of  $\Delta C_p$  to  $Re_t$  for the wind tunnel and the limits of his experiments are, Fig. 29:

$$Re_t = 1.695 \times 10^6 (\Delta C_p)^{-0.627}$$

This expression is indicating that  $Re_t$  and  $\Delta C_p$  are strongly related in spite of the fact that the relation is not universal. The study also reveals that the Pate-Schueler relation, Figs. 21 and 26, can be used down to a Mach number of 2.

In the transonic range Credle and Carleton [43] experimented with a  $10^\circ$  angle cone in two different wind tunnels. The overall r.m.s. levels measured on the cone were functions of the wind tunnel wall and free stream noise and the influence on transition is as seen in Fig. 30 [18] i.e. higher noise level reducing transition Reynolds number.

Dougherty and Fisher [28] report the results obtained on the  $10^\circ$  AEDC cone. Experiments were performed in various wind tunnels in U.S.A., England and France also in flight with the same cone. The range covered in Mach and unit Reynolds number in these tests were:

$$0.20 < M < 5.50 \text{ and } 0.80 \times 10^6 < \frac{Ue}{v} < 41.5 \times 10^6$$

Transition detection was made with surface pitot tube and typical detection data is reproduced in Fig. 31a. Some of the important results are summarized below.

1. From the comparison of the Figs. 31b, 31c, and 31d that flight data yield almost the same  $Re_T$  (end of transition Reynolds number) under the same  $M$  and  $Ue/v$  for low noise level wind tunnels (i.e.  $P'_s/q_\infty < 0.01$ ) when  $M < 1$ . When  $M > 1$  (or so), transition develops much earlier than in flight conditions even for low noise tunnels. For higher noise level tunnels ( $P'_s/q_\infty > 0.01$ ) the disagreement between flight and wind tunnel data is more severe, Fig. 31d. The authors explain that the noise levels can be reduced by taping the slots and thus bringing  $Re_T$  obtained in the wind tunnel closer to that of the flight. More information on this aspect is given in [44]. Finally, the authors [28] offer the correlation of  $Re_T$  to  $P'_s/q_\infty$  within  $\pm 20\%$  as in Fig. 31e with the expression:

$$Re_{ET} \propto \left( \frac{P'_s}{q_\infty} \right)^{-1/4}$$



2. The data for  $Me > 3$  in low noise wind tunnels agree with Pate's correlation, Fig. 27.
3. The authors relate the distinguishing features for disturbance spectra signature to the geometry of the wind tunnels, i.e. to the slots or to the perforations of the test sections. As said before, by taping the slots it has been possible to reduce the noise level.

In a recent paper, Murthy and Steinle [25] have used exactly the same data of the previous paper [28] for low noise level wind tunnels and plotted what they call the equivalent Reynolds number of transition vs  $C_{p,rms} = p's/q_\infty$ , Figs. 32a and 32b. The equivalent  $Re_t$  (or  $T$ ) is obtained by reducing the transition Reynolds number measured at a given Mach number to a reference Mach number equal to 0.8. The reduction procedure is made according to

$$Re_{t(or T),eq.} = Re_{t(or T)} - (M - 0.8) \times 3 \times 10^6$$

The authors thus remove the compressibility effect from the data. In this way they obtain Figs. 32a and 32b which show that the transition Reynolds number is independent of  $C_{p,rms}$ , at least in the Mach number range of  $M < 0.8$  or  $0.9$ .

Murthy and Fisher [25] show further that momentum fluctuation i.e.  $(\rho u)'$  is influential even on the equivalent Reynolds number of transition (beginning and end) as shown in Figs. 32c and 32d. They suggest

$$Re_{t(or T),eq} \sim (\rho u)^{-n} r.m.s. \%$$

where  $n = 1/4$  for beginning and  $n = 1/6$  for end of transition and

$$|Re_{t,eq}/Re_{T,eq}| \sim (\rho u)^{-1/12} r.m.s. \%$$

In view of the large scatter of the data used in the two studies reported above, namely Refs. [28] and [25], the first thing that is normal to think is to question the accuracies involved in such measurement. The thorough study of the reference [28] shows that utmost care is taken in data acquisition. But whether this utmost care is enough for the study of environmental effects or not needs further studies.

In spite of the fact that the accuracies in the data acquisition may be considered to be satisfactory, the data reduction and presentation to lead to correlations or physical explanations present a more severe problem. The choice of the independent parameters, to maintain one set of parameters constant while seeking a correlation between the dependent and one of the independent parameters, or to sort out the individual weight of each parameter when more than one of them are contributing to the dependent parameter require further studies in the future.

#### Transition and Tripping

Transition controlled by tripping is also considered in the paper of Pate [40] together with the heat transfer effect. The effective or knee point, upstream of which all  $x_t$  are trip dominated is seen in Fig. 33a, within the Mach number range  $3 < M < 5$ . The knee point can also be viewed as a transition point obtained for a specified trip roughness size, trip location, and a specific unit Reynolds number for which the transition location remains fixed no matter how much the unit Reynolds number is increased.

Figure 33a shows results for trip roughnesses made of spheres of diameter 0.01-in. and located at  $X_k = 4.9$ -in. and the untripped conditions. The effective point is obtained at approximately 8-in. for a unit Reynolds number of  $0.3 \times 10^6$  and this point remains fixed (almost) for unit Reynolds number larger than  $0.3 \times 10^6$ . The transition point changes drastically for smaller unit Reynolds number

(Region II) and strongly before that (Region I) as in the case of untripped conditions. The Potter-Whitfield correlation is also applied to date of the study [40] and is shown in Fig. 33b. The correlation considers the heat transfer effect and is applicable to both planar and cone models. It further provides the trip size required to locate transition anywhere between undisturbed smooth surface transition location and trip position. This correlation is effective for 2D surface wires and single row of spheres. The knee point cannot be obtained from the Potter-Whitfield correlation.  $X_{to}$  which appears in the correlation is the nontripped transition distance and can be obtained from Fig. 26, if experimental information does not exist.

#### 4.8.3.3 Disturbances on the Model

The role of distributed roughness on boundary layer characteristics was not touched in the Subsection 4.8.2.3 for subsonic flows. The case of supersonic or transonic flow seems not to call a widespread attention. The only source available to the author was made through the courtesy of J. B. Peterson, Jr. from NASA, Langley and is dating from 1959 [45]. Therefore, main conclusions of this paper are reported below in order to call the attention on the subject since no related work appears to have been done recently. The experimental work by Goddard was made on the surface of cylindrical body under supersonic conditions in the range of  $1.98 < M < 5$  and  $3 \times 10^6 < Re < 8 \times 10^6$ . Skin friction measurements were made on the basis of measuring the average skin drag of the cylinder rather than the local skin drag. Velocity profiles have been obtained by pitot tubes. The paper gives detailed data of measured average skin friction with respect to Mach number, Reynolds number based on cylinder corrected length and relative roughness size (relative to cylinder length). It appears that  $C_f$ , the average skin drag coefficient, decreases with  $M$  and also the role of compressibility is entirely via the change in wall density, Fig. 34a, where  $C_{fi}$  represents the incompressible skin drag coefficient.  $C_f/C_{f0}$ , where  $C_{f0}$  corresponds to the drag coefficient for smooth surfaces, is only a function of  $k U_\infty/\nu$  in which  $k$  is the average thickness of the roughness, Fig. 34b, as in the case of incompressible flows. Another interesting result is that the critical roughness below which the surface is hydraulically smooth is obtained with roughness Reynolds number  $k U_\infty/\nu = 10$  almost as in the incompressible case. The velocity profiles follow the inner wall region logarithmic distribution and the shift in the velocity profile  $\Delta(U/U_\infty)$  for supersonic case is only a function of roughness Reynolds number and follows the same law as that for the incompressible case, Fig. 34c.

#### 4.8.4 Theoretical Development for Prediction

Almost all of the results explained in the previous subsections are based on experimental studies whereas the parameters used in these correlations are determined with engineering judgement and some dimensional analysis.

- Arnal-Michel's semi-empirical study [16] relates external turbulence intensity to transition prediction through turbulence modeling and boundary layer equations.
- The Dekeyser-Burnage [36] gives information about the development and formation of entropy fluctuations starting from a mean entropy gradient and pressure or velocity fluctuations.

The way environmental disturbances enter the boundary layer and lead to instabilities and finally to transition, is studied at least for the part of excitation of the normal modes, by "receptivity".

#### Receptivity

This subject has been reviewed in the AGARD R.709, Special Course on Stability and Transition of Laminar Flow by Reshotko [46]. The receptivity is described as "the means by which a particular forced disturbance enters the boundary layer and the nature of its signature in the disturbance flow". Therefore, physically the signature of a disturbance is aimed to be obtained within the boundary layer with reference to a given disturbance. Three different receptivity problems namely, external

turbulence, acoustic disturbance and propagating sound waves for which "some" information exists is reviewed. The reader is referred to this course note [46].

But the concluding remark will be repeated here, since it guides future work in this field: "Although much progress has been made in identifying and understanding receptivity issues in the last ten years or so, much remains to be done. The detailed character of free stream turbulence as observed in wind tunnels has yet to be measured and the finer points of its signature in the boundary layer leading to excitation of Tollmien-Schlichting waves clarified. The receptivity to acoustic disturbances is in better shape. Initial value analysis are an additional tool for providing guidance toward the resolution of receptivity issues."

#### 4.8.5 Conclusion and Recommendations

The following is a summary conclusion containing some recommendations concerning the environmental effect on transition and some boundary layer characteristics.

1. In the subsonic range the way that external turbulence influences the turbulent boundary layer characteristics has been studied for zero pressure gradient by Charnay, et al. [19] and Green [18]. But those with non-zero pressure gradient require still more attention. Green's [18] deductions based on some calculations show that boundary layer characteristics may largely be influenced by the mixing length of the external turbulence. But now that length is related to pressure gradient, still requires experimental verification and more information on flow details is needed.
2. Transition in subsonic 2-D flow has been the center of attention and a number of correlations for the estimation of the influence of the external turbulence intensity [9,7,3] is supplied, either with or without zero pressure gradient.

The only information existing on the influence of wind tunnel acoustical disturbances on the transition is the not well defined cut-off turbulence intensity level of 0.3%. Yet the noise spectrum characteristics are critical for transition location when external turbulence intensity  $T < 0.004$  or so. Basic work is needed, to relate wind tunnel characteristics at least to estimate the noise spectrum at the test location of the wind tunnel which can then be used as a boundary condition or a disturbance source for the kind of boundary layer to be met in an actual wind tunnel test.

Model vibration and the way it influences the boundary layer characteristics and the transition has almost received no attention. There is some evidence that a local vibration on the model [32] will provoke an earlier transition. Research in this area appears to be necessary since this will also be used in the estimations related to actual flight conditions.

3. External turbulence intensity affects transition position for supersonic flows if  $M > 2.5$  [33]. Yet how the external turbulence is affecting flow properties is a matter for investigation. The effects of external turbulence on flow properties and separation associated with shock boundary layer interaction and on the shock position studies have found scarce interest. Only external turbulence intensity influence on these characteristics has been investigated for a given bump shape [34,35]. It is noted that turbulence intensity variation influences the separated zone behind the shock quite significantly. Similar studies for various realistic shock boundary layer interaction for different configurations are necessary.

4. Non-adiabatic wall temperatures even of the order of one percent are shown to be affecting the overall aerodynamic characteristics significantly [38] in the transonic regime for a modern airfoil. It is stated that even 1% deviation from adiabatic conditions is unacceptable to define buffet onset. Since in the experiments of this investigation [38] the temperature distribution on the model was uniform, it would be important to investigate the consequences when there are local departures from adiabatic wall temperature of higher percentages. This may be more important actual in flight performance predictions.
5. With the exception of the influence of acoustical disturbance on transition location under supersonic conditions for which the correlations exist for 2-D boundary layer and boundary layers on conical shape, almost all of the environmental effects studied so far are for 2-D boundary layers. There exists a big gap for similar investigations for 3-D cases.
6. External turbulence has been represented by turbulence intensity  $I$  as a usual practice. Turbulence scale and/or its spectrum is very seldom quoted or taken into consideration. The studies [21] and [22] emphasize the role of scale in characterization of the external turbulence.
7. Almost all of the investigations are empirical in nature and restricted to specific cases. Intense and widely spread studies of receptivity is necessary for the assessment of the signature of various disturbances on the transition and boundary layer characteristics.
8. Environmental effects on turbulent boundary layer characteristics of supersonic flows is especially worthwhile to be studied since such a flow forms upstream as the input to a shock/boundary layer interaction region.

In short, environmental effects seem to be a section of fluid dynamics that has been neglected or that has not been studied systematically and in an organized manner. Yet with the need of increased accuracies required from recent wind tunnel measurements and the need for reduced discrepancies of the experimental data obtained from different wind tunnels, the wind tunnel environmental effects have to be accurately assessed. Looking at the breadth and delicacy both from experimental and theoretical point of view, the subject of environmental effect on transition and boundary layer characteristics appears challenging and rewarding for fluid dynamicists.

## ENVIRONMENTAL EFFECTS INFLUENCING BOUNDARY LAYER CHARACTERISTICS AND TRANSITION

1. S. Goldstein (ed). Modern Developments in Fluid Dynamics. 1957, Vol. 1, p. 327.
2. G. I. Taylor. Proc. Roy. Soc. A. 156 (1936), pp. 307-310.
3. Hall, D. J. and Gibbings, J. C. Influence of stream turbulence and pressure gradient upon boundary layer transition. Journal Mechanical Engineering Science, Vol. 14, No. 2, 1972, pp. 134-146, 11 a 13.
4. Hislop, G. S. "The Transition of a Laminar Boundary Layer in a Wind Tunnel. Ph.D. Thesis, Cambridge, 1940.
5. Schubauer, G. B. "The Effect of Turbulence on Transition on the Boundary Layer of an Elliptic Cylinder. Proc. 5th Int. Congress, Applied Mech., 1938. John Wiley and Sons, Chichester.
6. Dryden, H. L., Schubauer, G. B., Mook, W. C., Jr., and Skramstad, H. K. Measurements of Intensity and Scale of Wind Tunnel Turbulence and their Relation to the Critical Reynolds Numbers of Spheres. NACA Tech Report 581, 1937.
7. Van Driest, E. R. and Blumer, C. B. "Boundary Layer Transition; Free-Stream Turbulence and Pressure Gradient Effects. AIAA Journal, 1, 1963, pp. 1303-1306, 11 a 87.
8. I. Tani. Boundary Layer Transition. Annual Review of Fluid Mechanics, Vol. 1, 1969, pp. 169-196.
9. Wells, C. S. Effects of Free-Stream Turbulence on Boundary Layer Transition. AIAA Journal, Vol. 5, No. 1, January 1967, pp. 172-174, 11 a 11.
10. Junkhan, G. H. and Serovy, G. K. "Effects of Free-Stream Turbulence and Pressure Gradient on Flat Plate Boundary Layer Velocity Profiles and on Heat Transfer. ASME Journal of Heat Transfer, May 1967, p. 169, 11 a 15.
11. Wells, C. S. and Spangler, J. G. A Facility for Basic Boundary Layer Experiments. LTV Research Center Report O-71000/2R-32, 1962.
12. Wells, C. S. Experimental Investigation of the Effects of Free Stream Turbulence on Boundary Layer Transition. LTV Research Center Report O-71000/5R-6, 1965.
13. Spangler, J. G. and Wells, C. S. Effects of Free Stream Disturbances on Boundary Layer Transition. AIAA Journal, Vol. 6, No. 3, 1968, p. 543. 11 a 10; 11 4 a 10.
14. Granville, P. S. The Calculation of Viscous Drag of Bodies of Revolution. David Taylor Model Basin Report 849, 1953.
15. Ciray, C. On the Definition of Wave Number in Turbulence. M.E.T.U. Journal of Pulse and Applied Sciences.
16. Arnal, D. and Michel, R. Effects of Free-Stream Turbulence on Turbulent Boundary Layers and on Boundary Layer Transition. Euromech 72 (Boundary Layers and Turbulence in Internal Flows) 1976. 11 a 14.
17. Private communication with R. Michel.
18. Green, J. E. On the Influence of Free-Stream Turbulence on a turbulent Boundary Layer as it Relates to Wind Tunnel Testing at Subsonic Speeds. AGARD-R-602.
19. Charnay, G., Compte-Bellot, G., and Mathieu, J. Development of a Turbulent Boundary Layer on a Flat Plate in an External turbulent Flow. Paper in AGARD CP 93.1971.
20. Huffman, G. D., Zimmerman, D. R., and Bennett, W. A. The Effect of Free Stream Turbulence on Turbulent Boundary Layer Behavior. AGARD Specialist' Meeting "Boundary Layer Effects in Turbomachines." Paris, April 1972.
21. Meier, H. E. and Kreplin, H-P. Influence of Free-Stream Turbulence on Boundary Layer Development. AIAA Journal, Vol. 18, No. 1, January 1980.
22. Hancock, P. E. and Bradshaw, P. The Effect of Free-Stream Turbulence on Boundary Layers. Fluid Engineering Division, Trans. ASME, Vol. 105, September 1983, pp. 284-289.
23. Finley, P. J., Phone, K. C., and Poh, C. J. Velocity Measurements in a Thin Turbulent Water Layer Houille Blanche. Vol. 21, 1966, p. 713.
24. Dean, R. B.
25. Murthy, S. V. and Steinle, F. W. Effects of Compressibility and Free Stream Turbulence on Boundary Layer Transition in High Subsonic and Transonic Flows. AIAA Paper B6-0764, 1986.

26. Ragunathan, S., Coll, J. B., and Mabey, D. G. Flat Plate Turbulent Boundary Layers Subject to Large Pressure Fluctuations. AIAA Journal, Vol. 17, No. 1, January 1979, pp. 105-106.
27. Weeks, D. J. and Hodges, J. An Experimental Investigation of the Influence of Acoustic Disturbances on the Development of a Turbulent Boundary Layer. A.R.C. R.M. 3825, 1978.
28. Dougherty, N. S., Jr. and Fisher, D. F. Boundary Layer Transition on a 10-deg Cone-Wind Tunnel/Flight Data Correlation. AIAA Paper No. 80-0154, Presented at AIAA 18th Aerospace Sciences Meeting, Pasadena, California, January 14-16, 1980.
29. Young, A. O. J. of Royal Aero. Soc. p. 534, 1950.
30. Schlichting, H. boundary Layer Theory. McGraw-Hill.
31. Feindt, E. G. Investigations on the Dependence of Laminar-Turbulent Transition on Surface Roughness and Pressure Gradient. Jb. Schiffbautech. Ges. 1957, No. 50, p. 180.
32. Gougat, P. and Martin, F. Influence d'un deformation periodique de pario sur le developement des instabilites naturelles conduisant a la transition. AGARD-CP 224, p. 18.9, 1977, III 6 a 86.
33. Laufer, J. Factors Affecting Transition Reynolds Numbers on Models in Supersonic Wind Tunnels. Journal of the Aeronautical Sciences, Vol. 21, No. 7, July 1954, I 1 b 21:II 4 b 21.
34. Raghunathan, S. and McAdam, R.J.W. Free-Stream Turbulence and Transonic Flow over a Bump Model. AIAA Journal, Vol. 21, No. 3, March 1983, pp. 467-469. I 1 b 78.
35. Raghunathan, S. and McAdam, R.J.W. Boundary-Layer and Turbulence Intensity Measurements in a Shock Wave/Boundary-Layer Interaction. AIAA Journal, Vol. 21, No. 9, September 1983, pp. 1349-1350, I 1 b 8 77.
36. Dekeyser, I. and Burnage, H. Production de fluctuations d'entropie par interection d'une couche a gradient d'entropie et d'un champ acoustique. C.R. Ac.Sc. Paris, t. 280, Serie A, pp. 1393-1396, Mai 1975, 12 ? 7:1 3 ? 7.
37. Morkovin, M. V. On Transition Experiments at Moderate Supersonic Speeds. J. of Aero. Sciences, Vol. 24, No. 7, 1957, pp. 480-486.
38. Lynch, F. T., Fancher, M. F., Patel, D. R., and Inger, G. R. Nonadiabatic Model Wall Effects on Transonic Airfoil Performance in Cryogenic Wind Tunnel. "Wind Tunnels and Testing Techniques," AGARD CP 348, Cesme, September 1983.
39. Pate, S. R. and Schueler, C. J. Radiated Aerodynamic Noise Effects on Boundary Layer Transition in Supersonic and Hypersonic Wind Tunnels. AIAA Journal, Vol. 7, No. 3, 1969, pp. 450-457.
40. Pate, S. R. Supersonic Boundary-Layer Transition: Effects of Roughness and Free-Stream Disturbances. AIAA Journal, Vol. 9, No. 5, May 1971, pp. 797-802, (Also AIAA Paper No. 70-586, Induced Boundary-Layer Transition at Supersonic Speeds: Combined Effects of Roughness and Free-Stream Disturbances, Presented at the AIAA 5th Aerodynamics Testing Conference, Tullahoma, Tennessee, May 1970), II 4 b 31.
41. Bergstrom, E. R. and Raghunathan, S. Aerodynamic Noise and Boundary Layer Transition Measurements in Supersonic Test Facilities. AIAA Journal, Vol. 10, No. 11, November 1972, pp. 1531-1532. II 4 b 45.
42. Dougherty, N. S., Jr. Correlation of Transition Reynolds Number with Aerodynamic Noise Levels in a Wind Tunnel at Mach Numbers 2.0-3.0. AIAA Journal, Vol. 13, No. 12, December 1975, pp. 1670-1671. II 4 b 49.
43. Credle, O. P. and Carleton, W. E. Determination of Transition Reynolds Nubmer in the Transonic Mach Number Range. AEDC-TR-70-218, 1970.
44. Oougherty, N. S., Jr. and Steinle, F. W., Jr. Transition on Reynolds Number Comparisons in Several Major Transonic Tunnels. AIAA Paper No. 74-627, AIAA 8th Aerodynamic Testing Conference, Bethesda, MD, July 8-10, 1974.
45. Goddard, F. E., Jr. Effect of Uniformly Distributed Roughness on Turbulent Skin Friction Drag Supersonic Speeds. Journal of the Aero/Space Sciences, Vol. 26, No. 1, January 1959.
46. Reshotko, E. Environment and REceptivity. AGARD-R-709.
47. Steinle, F. and Stanewsky, E. Wind Tunnel Flow Quality and Data Accuracy Requirements. AGARD Report 184, Edited by R. O. Dietz, 1983.
48. Oven, F. K., Stainback, P. C., and Harvey, W. D. An Evaluation of Factors Affecting the Flow Quality in Wind Tunnels. AGARD Conference Proceedings CP 348, Paper No. 12, 1983.
49. McCroskey, W. J. Wall Interference in Wind Tunnels. F.O.P. Specialist Meeting, London, May 1982.

## BIBLIOGRAPHY

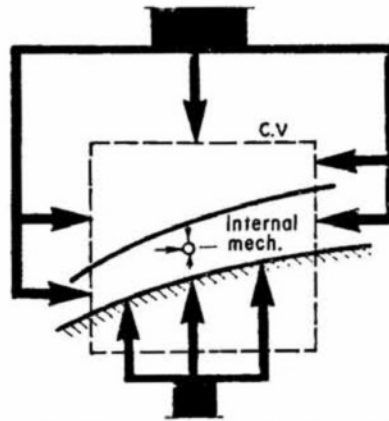
1. Mack, L. "On the Effect of Freestream Turbulence on Boundary-Layer Transition, Low-Speed Boundary-Layer Transition Workshop II," Rand Corporation, Santa Monica, CA, 1976. I 1 a 1
2. Mitchner, M. "Propagation of Turbulence from an Instantaneous Point Disturbances," J. Aero. Sci.
3. Klebanoff, P. S., and Tidstrom, K. D. "Mechanism by Which a Two-Dimensional Roughness Element Induces Boundary-Layer Transition," Physics Fluids 15 (1972), pp. 1173-1188. III 6 ? 4.
4. Kovasznay, L.S.G. "Turbulence in Supersonic Flow," J. Aero. Sci., Vol. 20, No. 10, 1953.
5. Martinot-Lagarde, A. "Introduction au spectre de la turbulence," N.T. G.R.A. 55, Paris, 1946.
6. Green, J. E. "On the Influence of Free-Stream Turbulence on a Turbulent Boundary Layer, as it Related to Wind-Tunnel Testing at Subsonic Speeds," RAE Report TR 72201. I 1 a 16.
7. Potter, J. Leith and Whitfield, Jack O. "Effect of Unit Reynolds Number, Nose Bluntness, and Roughness on Boundary Layer Transition," Presented at AGARD Meeting on "Boundary Layer Research, London, England, April 25-29, 1960 (AGARD Paper No. R-256).
8. Carver, D. B. "Heat-Transfer Tests on the Rockwell International Space Shuttle Orbiter with Boundary-Layer Trips (DH-54)," AEDC-TR-76-28 (AD-AD24553), Arnold Engineering Development Center, May 1976.
9. Pate, S. R. and Schueler, C. J. "The Influence of Radiated Aerodynamic Noise on Model Boundary-Layer Transition in Supersonic and Hypersonic Wind Tunnels," Presented at the Boundary-Layer Transition Specialists Study Group Meeting, San Bernardino, CA, July 1967. II 4 b 27:II 4 c 27.
10. Pate, S. R. and Schueler, C. J. "Effects of Radiated Aerodynamic Noise on Model Boundary-Layer Transition in Supersonics and Hypersonic Wind Tunnels," AEDC-TR-67-236 (AD-666644), Arnold Engineering Development Center, March 1968. II 4 b 28:II 4 c 28.
11. Pate, S. R. and Schueler, C. J. "An Investigation of Radiated Aerodynamic Noise Effects on Boundary Layer Transition in Supersonic and Hypersonic Wind Tunnels," Presented at the AIAA 3rd Aerodynamic Testing Conference, San Francisco, CA (AIAA Paper No. 68-375), April 1968. II 4 b 29:II 4 c 29.
12. Pate, S. R. and Eaves, R. H. "Sensitivity of Boundary-Layer Transition to Surface Irregularities for Space Shuttle Applications," Journal of Spacecraft and Rockets, December 1973. III 6 b 32:III 6 c 32.
13. Potter, J. Leith and Whitfield, Jack D. "Preliminary Study of the Effect of Unit Reynolds Number on Transition Sensitive Data," AEDC-TN-57-37 (ADI 35 338), Arnold Engineering Development Center, September 1957.
14. Potter, J. Leith and Whitfield, Jack D. "Boundary-Layer Transition Under Hypersonic Conditions," AEDC-TR-65-99 (AD-462716), Arnold Engineering Development Center, May 1965, presented at AGARD Specialists Meeting on Recent Developments in Boundary Layer Research, Naples, Italy, AGARDograph 97, Part III, May 1965.
15. Potter, J. Leith. "Observations on the Influence of Ambient Pressure on Boundary-Layer Transition," AIAA Journal, Vol. 6, No. 10, October 1968, pp. 1907-1911. I 2 ? 35.
16. Whitfield, Jack D. and Potter, J. Leith. "The Relation Between Wall Temperature and the Effect of Roughness on Boundary-Layer Transition," Journal of Aerospace Sciences, Vol. 28, No. 8, August 1961, pp. 663-664. II ? 36:III 8 ? 36
17. Laufer, J. "Aerodynamic Noise in Supersonic Wind Tunnels," Journal of the Aerospace Sciences, Vol. 28, No. 9, 1961, pp. 685-692. II 4 b 38
18. Maddalon, D. V. "Effect of Varying Wall Temperature and Total Temperature on Transition Reynolds Number at Mach 6.8," AIAA Journal, Vol. 7, No. 12, 1969, pp. 2355-2357.
19. Sheets, N. W. "Free-Flight Boundary Layer Transition Investigation at Hypersonic Speeds," AIAA Paper No. 65-127, 1965.
20. Benek, J. A. and High, M. O. "A Method for the Prediction of the Effects of Free-Stream Disturbances on Boundary-Layer Transition," AEDC-TR-73-15B, October 1973. I 1 ? 46



21. Oougherty, N. S., Jr. and Steinle, Frank W. "Transition Reynolds Number Comparisons in Several Major Transonic Tunnels," AIAA Paper No. 74-627, Presented at AIAA 8th Aerodynamic Testing Conference, Bethesda, MD, July 8-10, 1974. ?? b 47
22. Pate, S. R. "Comparison of NASA Helium Tunnel Transition Data with Noise-Transition Correlation," AIAA Journal, Vol. 12, No. 11, November 1974, p. 1615. II 4 ? 48
23. Gortler, H. "On the Three-Dimensional Instability of Laminar Boundary Layers on Concave Walls," NACA Tech. Memo 1375, 1954.
24. Ragab, S. A. and Nayfeh, A. H. "On Gortler Instability," Virginia Polytechnic Institute and State University, Blacksburg, VA 24061, 1979.
25. Liepmann, H. W. "Investigations on Laminar Boundary Layer Stability and Transition on Curved Boundaries," NACA Wartime Report W-107, 1943.
26. Liepmann, H. W. "Investigation of Boundary Layer Transition on Concave Walls," NACA Wartime Report W-87, 1945.
27. Jackson, Francis J. and Heckl, Manfred A. "Effect of Localized Acoustic Excitation on the Stability of a Laminar Boundary Layer," ARL 62-362, June 1962. II 4 a 50
28. Beckwith, I. E. "Development of a High Reynolds Number Quiet Tunnel for Transition Research," AIAA Journal, Vol. 13, No. 3, March 1975, pp. 300-306.
29. Beckwith, Ivan E. and Bertram, Mitchell H. "A Survey of NASA Langley Studies on High-Speed Transition," NASA TM X-2566, July 1972.
30. Reshotko, Eli. Boundary-Layer Stability and Transition," Annual Review of Fluid Mechanics, Vol. 8, 1976, pp. 311-349.
31. Kendall, J. M. "Study of the Effect of Free-Stream Turbulence Upon Disturbance in the Pre-Transitional Laminar Boundary Layer," AFWAL-TR-82-3002, Part I, 1982. I 1 ? 58
28. Kendall, J. M. "Experiments on the Generation of Tollmien-Schlichting Waves in a Flat Plate Boundary Layer by Weak Free-Stream Turbulence," AIAA Paper 84-0011, 1984. I 1 a 59
29. Leventhal, L. and Reshotko, E. "Preliminary Experimental Study of Disturbances in a Laminar Boundary-Layer Due to Distributed Surface Roughness," AIAA Paper 81-1224, 1981. III 6 ? 60
30. Thomas, A.S.W. and Lekondis, S. G. "Sound and Tollmien-Schlichting Waves in a Blasius Boundary-Layer," Phys. Fluids, Vol. 21, No. 11, 1978, pp. 2112-2113. I 1 a 64
31. Tsuge, S. and Rogler, H. L. "The Two-Dimensional Viscous Boundary Value Problem for Fluctuations in Boundary Layers," AIAA Paper 83-0044, 1983. I 1 a 65
32. Herbert, T. "Subharmonic Three-Dimensional Disturbances in Unstable Plane Shear Flows," AIAA Paper No. 83-1759, 1983. I 1 a 66
33. Rogler, H. L. "The Coupling Between Free-Stream Disturbances, Driver Oscillations, Forced Oscillations and Stability Waves in a Spatial Analysis of a Boundary Layer," AGARO-CP-224, 1977.
34. Murdock, J. M. "The Generation of a Tollmien-Schlichting Wave by a Sound Wave," IUTAM Symposium on Laminar-Turbulent Transition, Stuttgart 1979, Springer Verlag, 1980.
35. Shapiro, P. "The Influence of Sound Upon Laminar Boundary Layer Instability," Report No. 83458-83560-1, Massachusetts Institute of Technology, Cambridge, Massachusetts, 1977. II 4 ? 69
36. Leehey, P. "Leading Edge Effect in Laminar Boundary Layer Excitation by Sound," Shapiro P. IUTAM Symposium on Laminar-Turbulent Transition, Stuttgart 1979, Springer Verlag 1980. II 4 ? 70
37. Tam, C.K.W. "The Excitation of Tollmien-Schlichting Waves in Low Subsonic Boundary," J. Fluid Mech., Vol. 109, 1981, pp. 483-501. II 4 ? 72
38. Stuart, J. T. "On the Non-Linear Mechanics of Wave Disturbances in Stable and Unstable Parallel Flows," Part 1, J. Fluid Mechanics, Vol. 2, 1960, pp. 353-370. II 4 ? 73
39. Kachanov, Yu. S. and Levchenko, V. Ya. "Resonant Interactions of Disturbances in Transition to Turbulence in a Boundary Layer," (in Russian), Preprint No. 10-82, I.T.A.M., USSR Academy of Sciences, Novosibirsk, 1982.
40. Braslow, A. L. and Knox, E. C. "Simplified Method for Determination of Critical Height of Distributed Roughness Particles for Boundary Layer Transition at Mach Numbers from 0 to 5," NACA TN 4363, 1958. III 6 c 75
41. Carmichael, B. H. "Surface Waviness Criteria for Swept and Unswept Laminar Suction Wings," Norair Report NOR-59-438 (BLC-123), 1959. III 6 ? 76

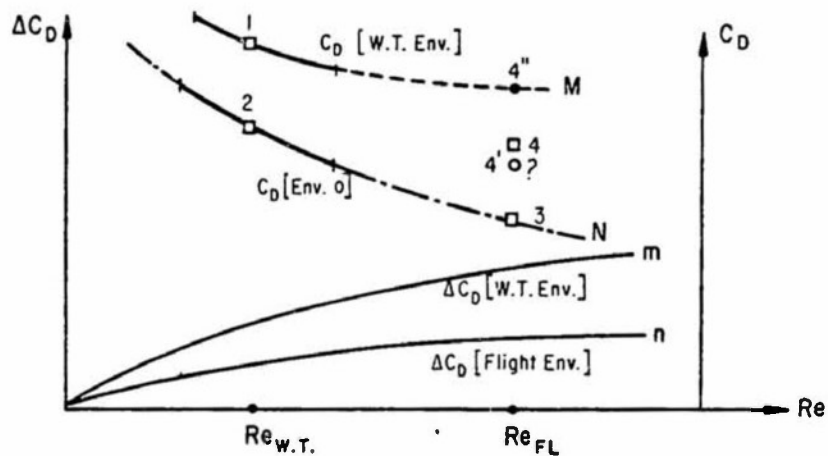
42. Harvey, W. D. and Robbitt, P. J. "Some Anomalies Between Wind Tunnel and Flight Transition Results," AIAA Paper No. 18-1225, Presented at AIAA 14th Fluid and Plasma Dynamic Conference, Palo Alto, CA, June 23-25, 1981.
43. Setles, Perkins-Bogdonoff. "Upstream Influence Scaling of 2D and 3D Shock/Turbulent Boundary Layer Interaction at Compression Corners," AIAA Paper 81-0334, 1981.
44. Lighthill, M. J. "On Boundary Layer Upstream Influence II Supersonic Flows without Separation," Proc. Roy. Soc. Series A, Vol. 217, 1953, p. 478 .
45. Kiyotaka, H. and Squire, L. C. "The Effect of Upstream Boundary Layer State on the Shock Interaction at a Compression Corner," J.F.M., Vol. 122, 1982, p. 369.
46. Delery. "Investigation of Strong Shock/Turbulent Boundary Layer Interaction in 2D Transonic Flows with Emphasis on Turbulence Phenomenon," AIAA Paper 81-1245, June 1981. Also AIAA Journal, Vol. 21, No. 2, February 1983, pp. 180-185.
47. Pfenniger, W. and Bacon, J. W., Jr. "Influence of Acoustical Disturbances on the Behavior of Swept Laminar Suction Wing," Report NOR 62-124 (8LC-141), October 1942, Northrop Company, Hawthorne, CA. II 4 a 88
48. Taylor, G. I. "Some Recent Developments in the Study of Turbulence," Proc. 5th Int. Congress of Applied Mechanics, 1938, John Wiley & Sons, Chichester. I I a 89
49. Braslow, A. L. "Review of the Effect of Distributed Surface roughness on Boundary Layer Transition," Report 254, AGARD, NATO, 1960. III 6 ? 90
50. Ragunathan, S. and McAdam, R.J.W. "Free-Stream Turbulence and Attached Subsonic Turbulent Boundary Layer," AIAA Paper 82-0029, January 1982. I I a 91
51. Dods, J. B., Jr. and Hanley, R. D. "Evaluation of Transonic and Supersonic Wind Tunnel Background Noise and Effects of Surface Pressure Fluctuations Measurements," AIAA Paper 72-1004, Palo Alto, CA, 1972. II 4 b 92
52. Pate, S. R. and Schueler, C. S. "Radiated Aerodynamic Noise Effects on Boundary Layer Transition in Supersonic and Hypersonic Wind Tunnels," AIAA Journal, Vol. 7, No. 3, March 1969, pp. 450-457.
53. Cha, B. T. and Kovasznay, L.S.G. J.F.M. 3 Part 5, February 1958.
54. Michel, R. Aeron. Rep. 58, Office Nationale d'Etude Recherche, 1952.
55. Smith, A.M.O. and Geronzi, N., Douglas Aircraft Company Report ES-26388, 1956.
56. Ingen, J. L. Von, Aeron. Eng. Dept., Oef. Rep. VTH-74, 1956.
57. Michel, R. "Effects of Flow Turbulence and Noise on Aerodynamic Phenomena and Wind Tunnel Results," AGARD-R-615, 1974.
58. Timme, A. "Effects of Turbulence and Noise on Wind-Tunnel Measurements at Transonic Speeds," Fluid Motion Problems in Wind Tunnel Design, AGARD-R-602, April 1973.
59. Huffman, G. D., Zimmerman, O. R., and Bennett, W. A. "The Effect of Boundary layer Effects in Turbomachines," AGARDograph 164, 91, 1972.

## INPUT THROUGH NON MATERIAL BOUNDARY



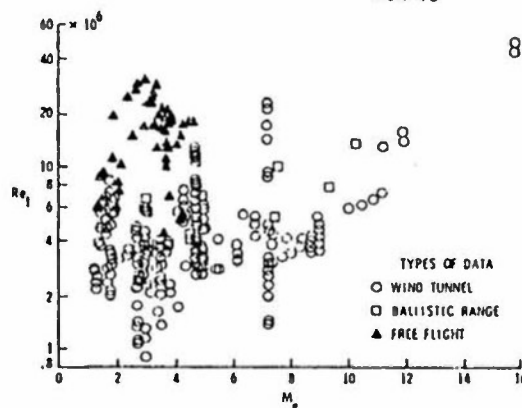
## INPUT THROUGH MATERIAL BOUNDARY

Figure 1. Description of environmental inputs.



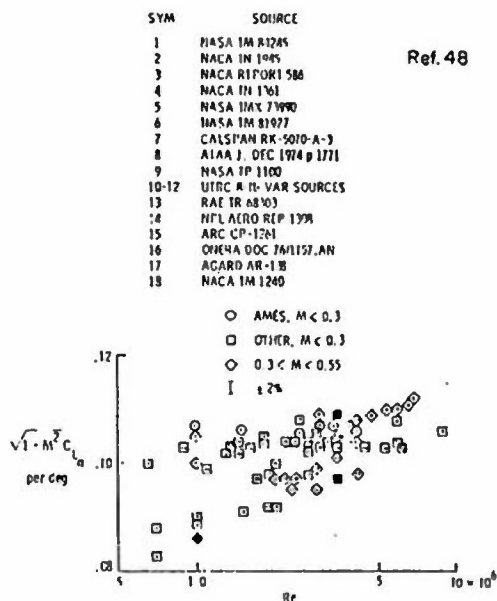
a. Model of environmental effects on wind tunnel data extrapolation.

Ref. 48



b. Variation of transition Reynolds number with Mach number.

Figure 2. Wind tunnel environmental influences.



2c. Reynolds number effects on NACA 0012 model lift curve slope measured in several facilities.

Figure 2. Concluded.

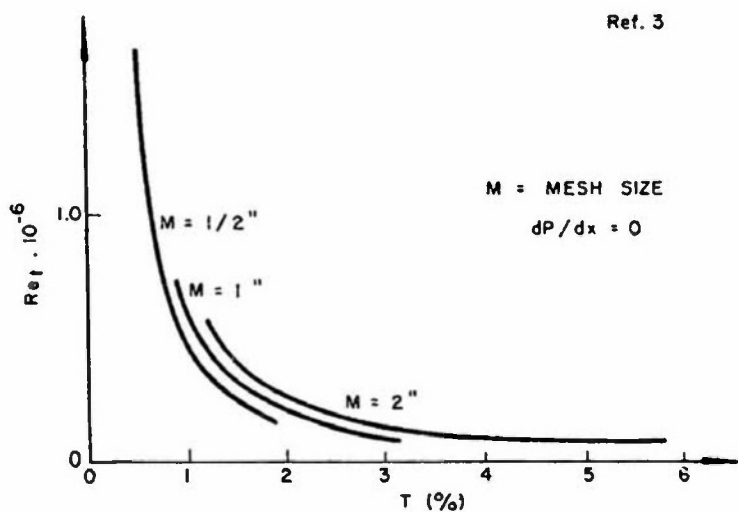


Figure 3. Turbulence intensity and scale effects on transition.

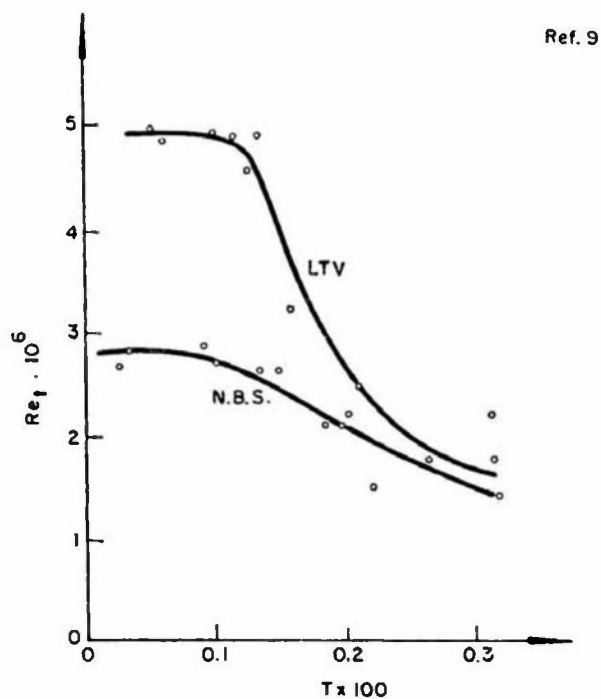


Figure 4. Turbulence effect on transition Reynolds number in two wind tunnels.

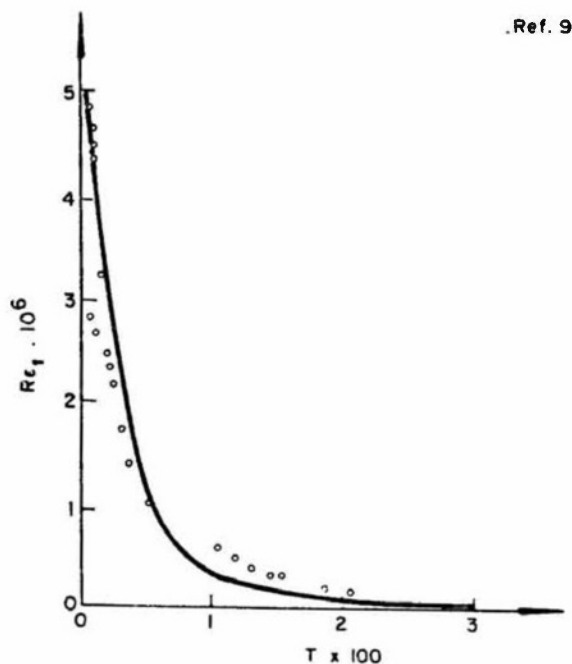


Figure 5. Turbulence effects on transition Reynolds number.

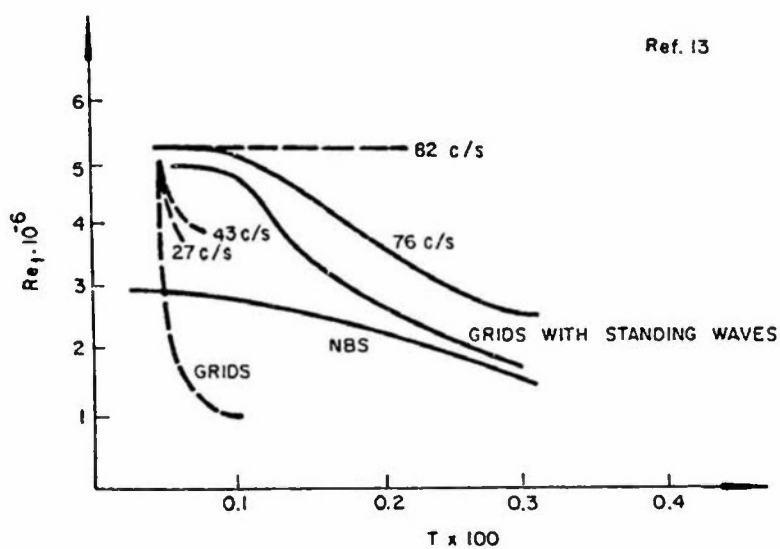


Figure 6. The influence of noise and turbulence on transition Reynolds number.

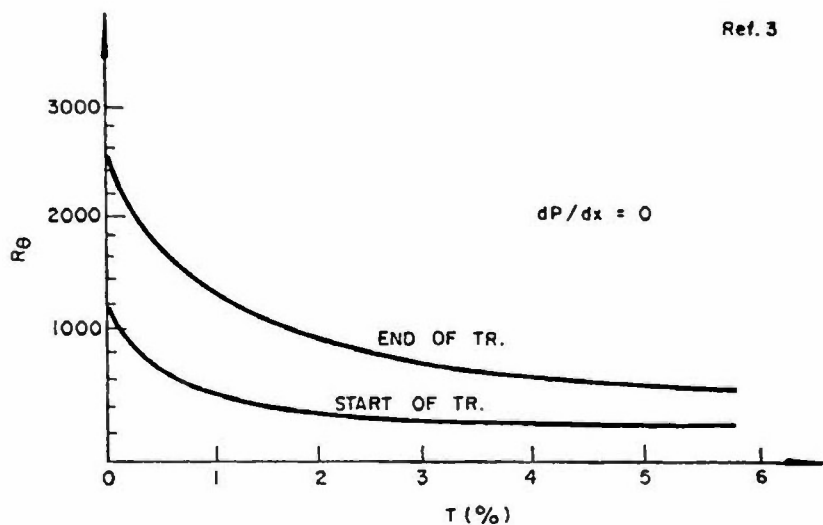


Figure 7. The influence of turbulence on start and end of transition on a flat plate.

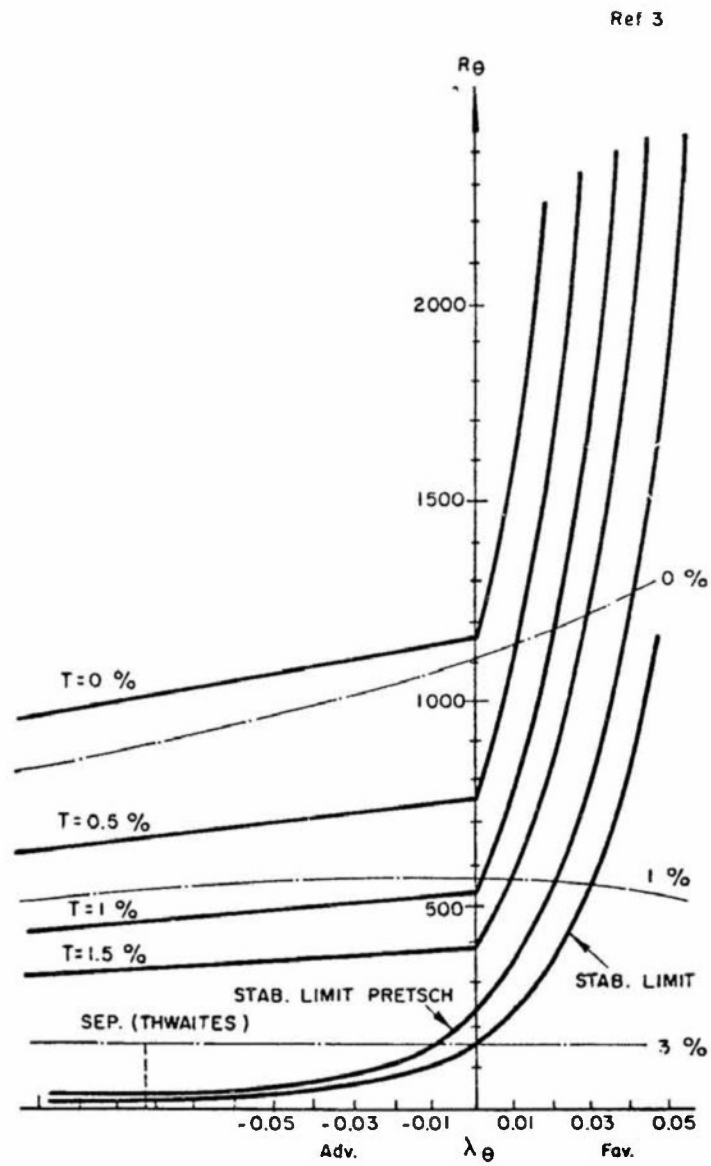


Figure 8. The influence of pressure gradient and turbulence on transition.



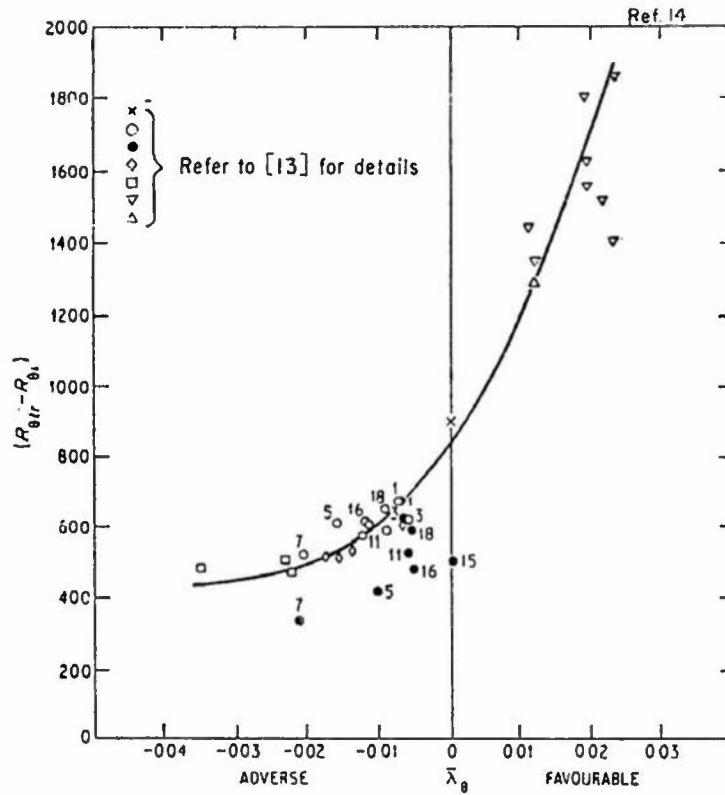


Figure 9. Results for the effect of pressure gradient upon the beginning of transition accounting for the development of the boundary layer.

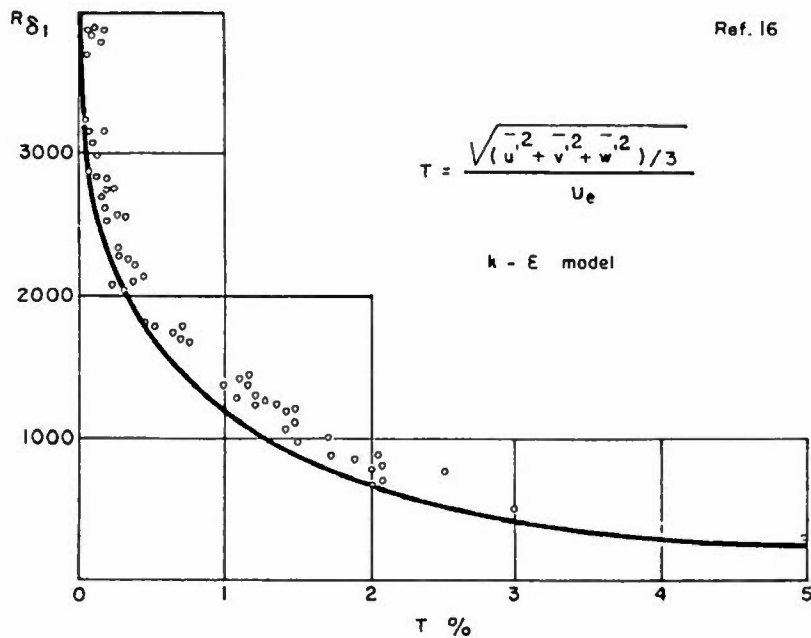
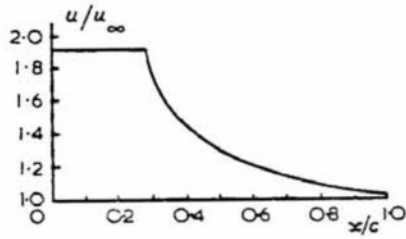
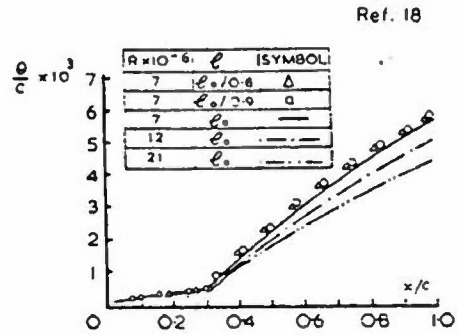


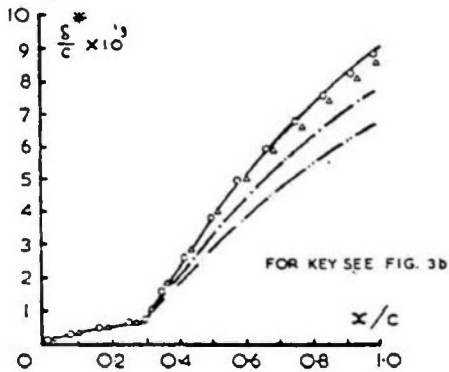
Figure 10. Comparison of theory and experiment for turbulence effect on  $R_{\delta_1}$  at transition.



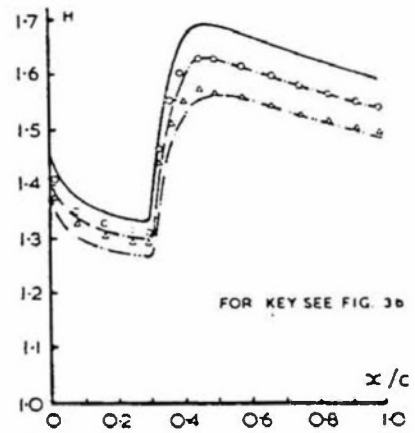
a. Streamwise velocity distribution.



b. Momentum thickness distribution.

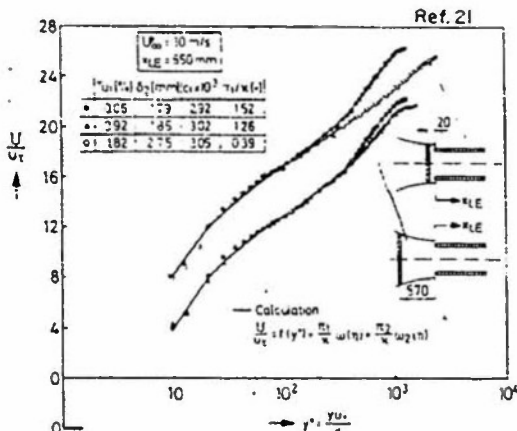


c. Displacement thickness distribution.

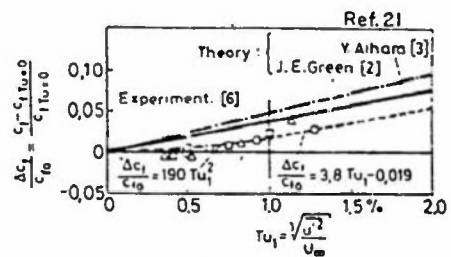


d. Shape parameter distribution.

Figure 11. Calculated influence of mixing length and Reynolds number on boundary-layer development on an aerofoil upper surface.

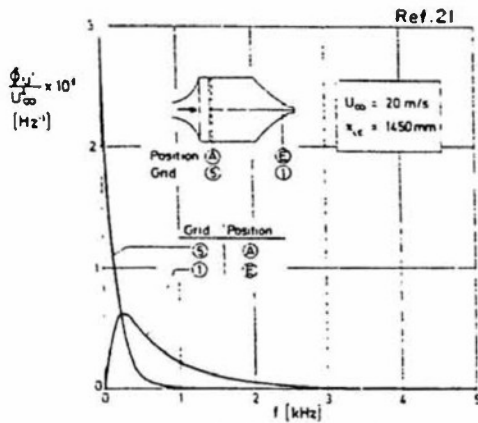


a. Velocity profiles at different intensities  $Tu_1$  and nonuniformities in the freestream.

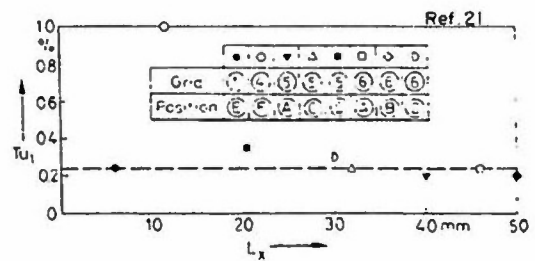


b. Changes of the local skin friction with the freestream turbulence intensity; comparison between theory and experiment.

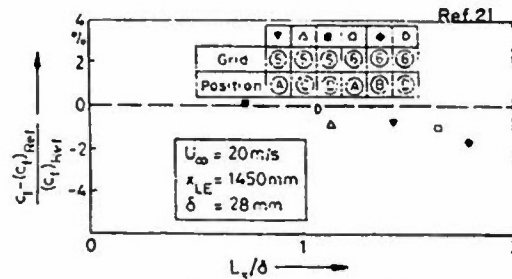
Figure 12. The influence of turbulence on boundary layer characteristics.



c. Spectra of  $u'$  for two different grids and positions at  $Tu_1 \approx 0.2\%$ .

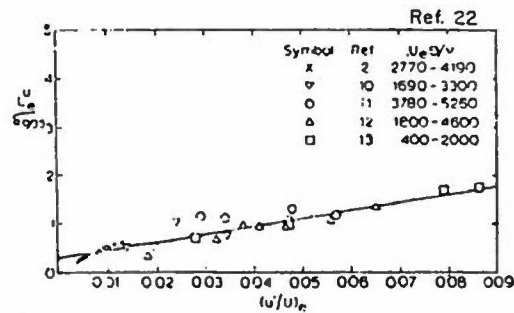


d. Turbulence intensities  $Tu_1$  and integral length scales  $L_x$  for different grids and positions.

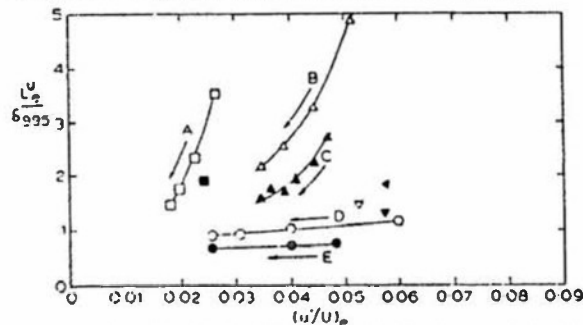


e. Measured skin friction coefficients for different integral length scales  $Tu_1 \approx 0.2\%$   $[(C_f)_{ref} = C_f \text{ at } L_x = \delta]$ .

FIGURE 12. Concluded.

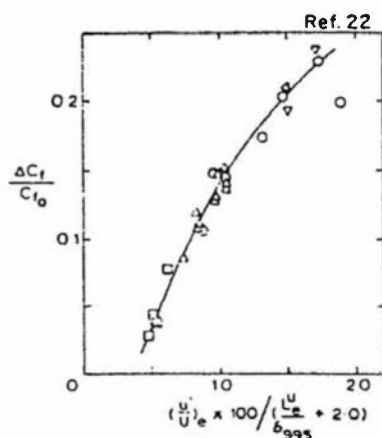


Previous workers parameters: range of momentum thickness Reynolds number,  $U_e \theta / \nu$ , shown.

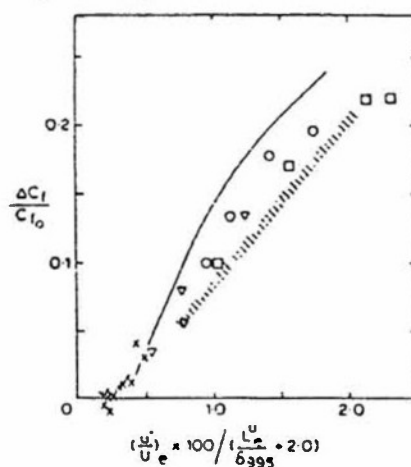


Present measurements:  $U_e \theta / \nu > 2000$ . A, B, C, D, and E identify profile sets: points in each set correspond to different length measuring stations along plate.

13 a. Free-stream turbulence intensities and length-scale ratios used in experiments.  
Figure 13. The influence of turbulence on boundary layer characteristics of a flat plate.

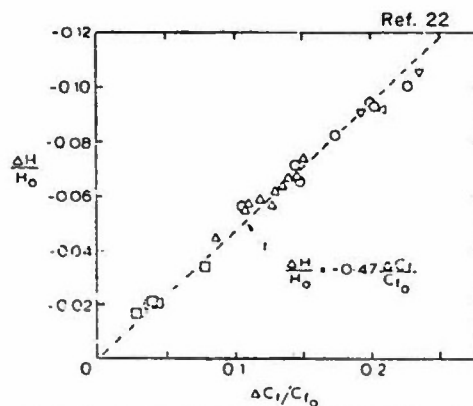


Present measurements: parameter range and symbols as in

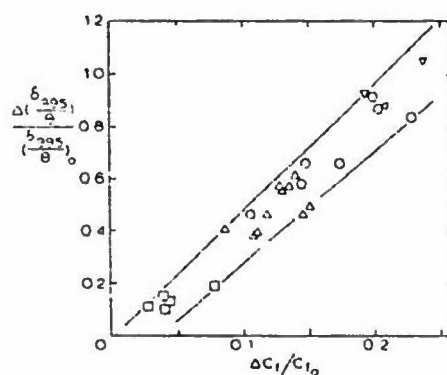


Present and previous measurements: fit to data of Figure 2 (a), symbols for other workers' data as in Figure 1 (a). Hatching as on dry present analysis of Chamay /12/. For data of Blair see (8).

- 13 b. Correlation of fractional change in skin-friction coefficient as a function of free-stream intensity and length scale:  $C_{f_0}$  is value in low-turbulence stream at same  $U_e$   $\theta/v$ .

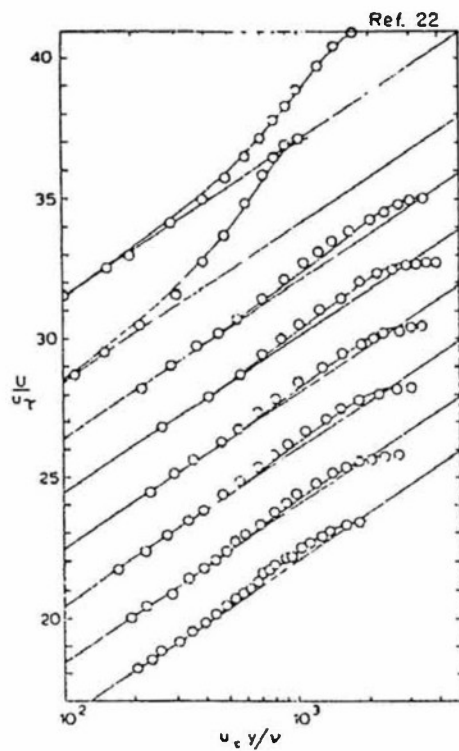


Correlation between fractional increase in shape parameter  $\delta^*/\theta$  and  $C_f$ : present data; symbols as in Figure 1(b).



Correlation between fractional increase in shape parameter  $\delta_{995}/\theta$  and  $C_f$ : symbols as in Figure 1(b).

- 13 c. Correlation between fractional increase in shape parameter with  $\Delta H/H_0$  and  $\delta_{995}/\theta$ .



13 d. Mean velocity profiles on "logarithmic law" plot. Top two profiles, low-turbulence stream; bottom six profiles 152 mm grid, plate leading edge 2.06 m from grid, profile set C in Figure 1(b),  $x$  increases upwards. Solid lines, equations (4) and (5). Ordinate scale refers to lowest profile.

Figure 13. Concluded

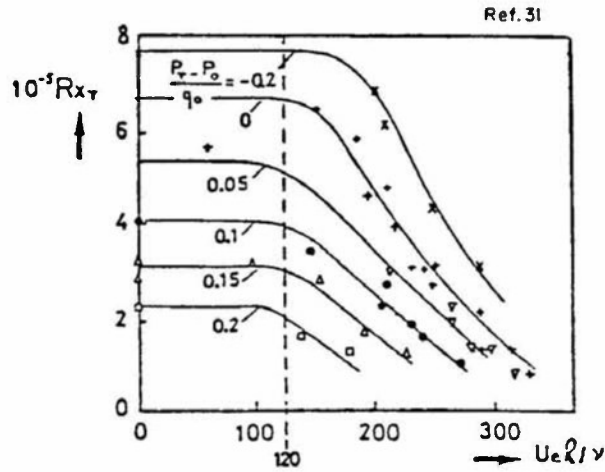
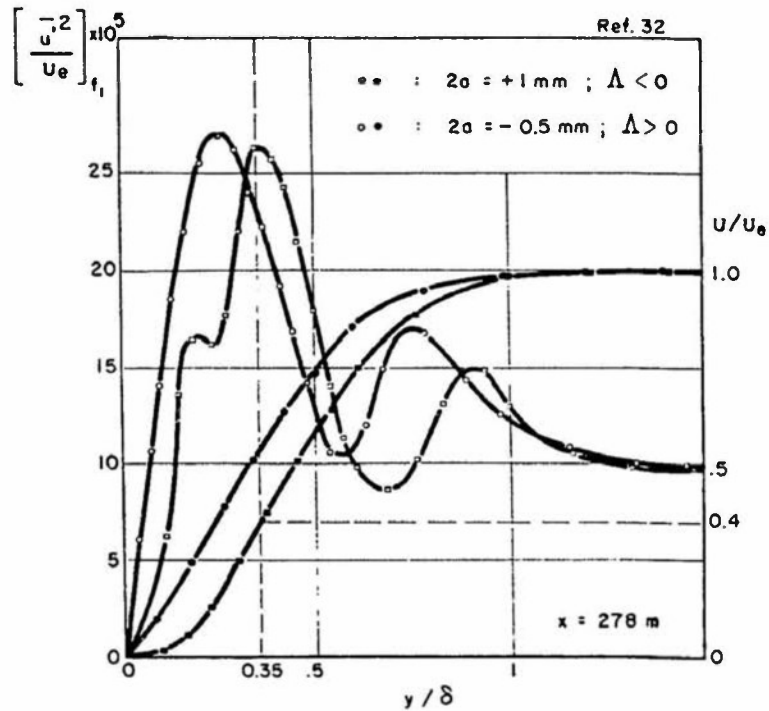


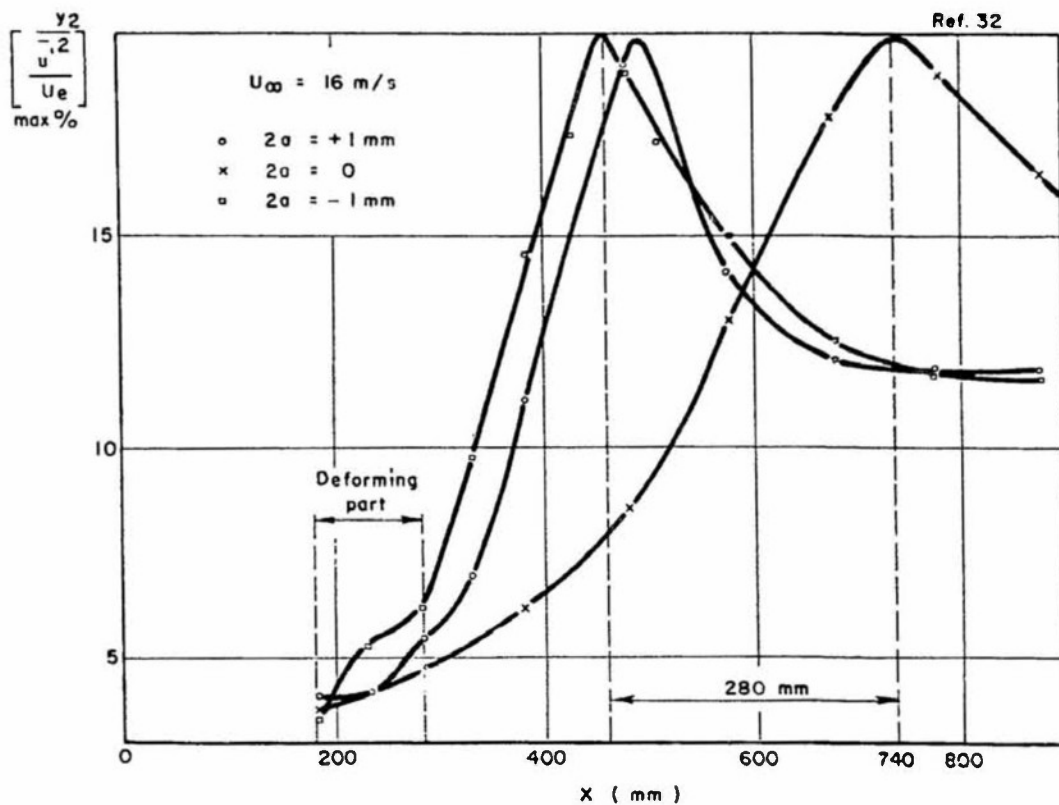
Figure 14. Influence of pressure gradient and distributed roughness on transition Reynolds number.  $U_e$ ,  $P_0$  and  $q_0$  denote velocity, static pressure and dynamic pressure at the test section entrance.



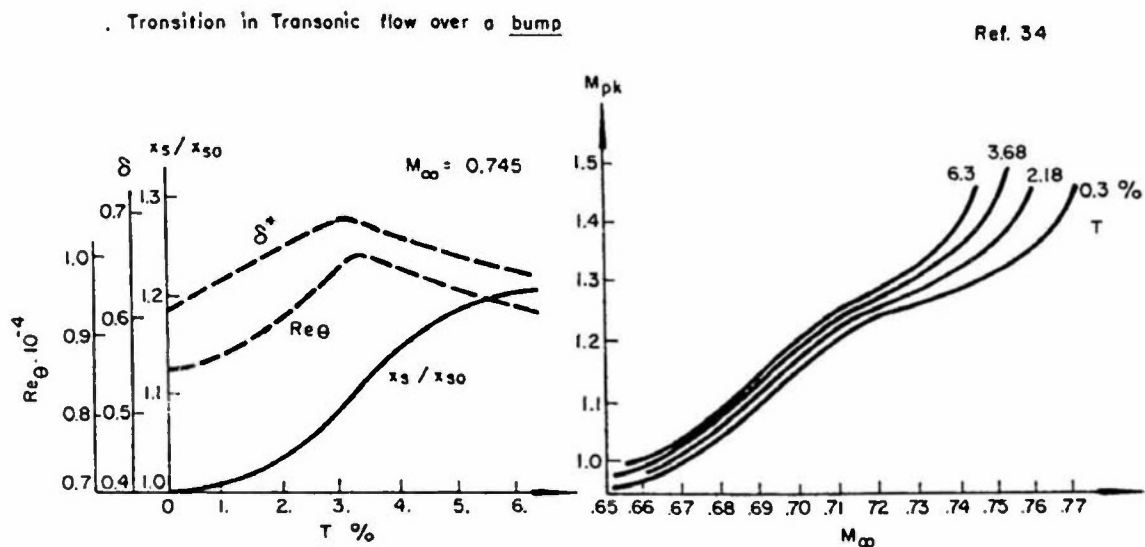
a. Turbulence across the boundary layer.

Figure 15. Distribution of turbulence in a flat plate boundary layer.





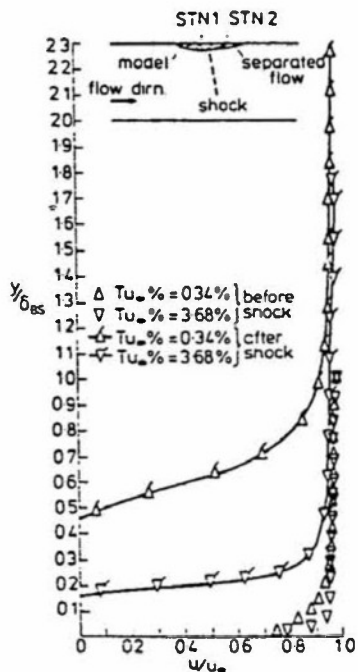
b. Maximum turbulence along the plate.  
Figure 15. Concluded



a. Boundary layer properties.

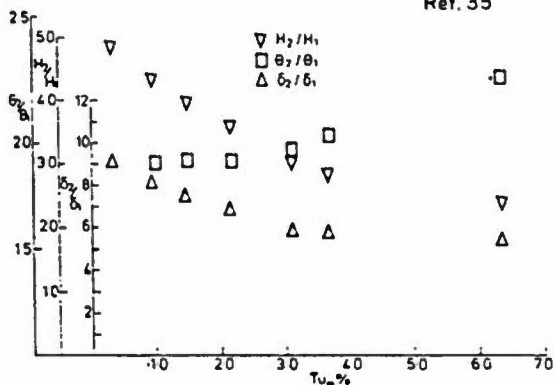
Figure 16. Transition studies for transonic flow over a bump.

Ref. 35

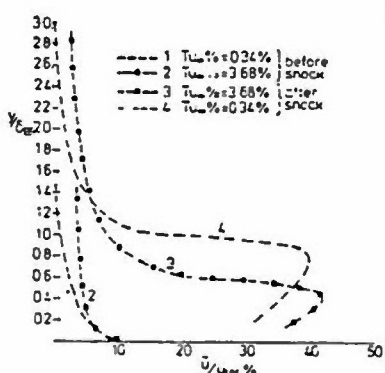


b. Velocity profiles.

Ref. 35

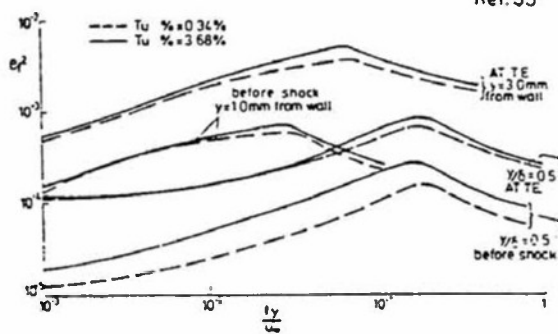


c. Variation of compressible shape parameter ratios, momentum thickness ratio, and boundary-layer thickness ratio, across the shock, with freestream turbulence level.



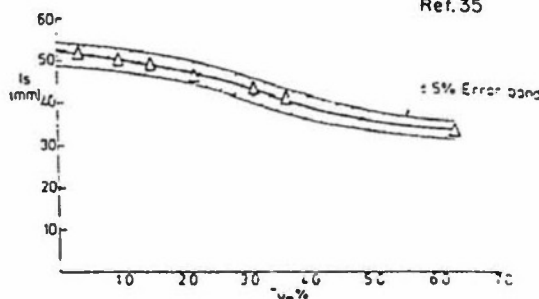
d. Turbulence profiles.

Ref. 35



e. Turbulence spectra.

Ref. 35



f. Effect of freestream turbulence on separated flow length

Figure 16. Concluded.

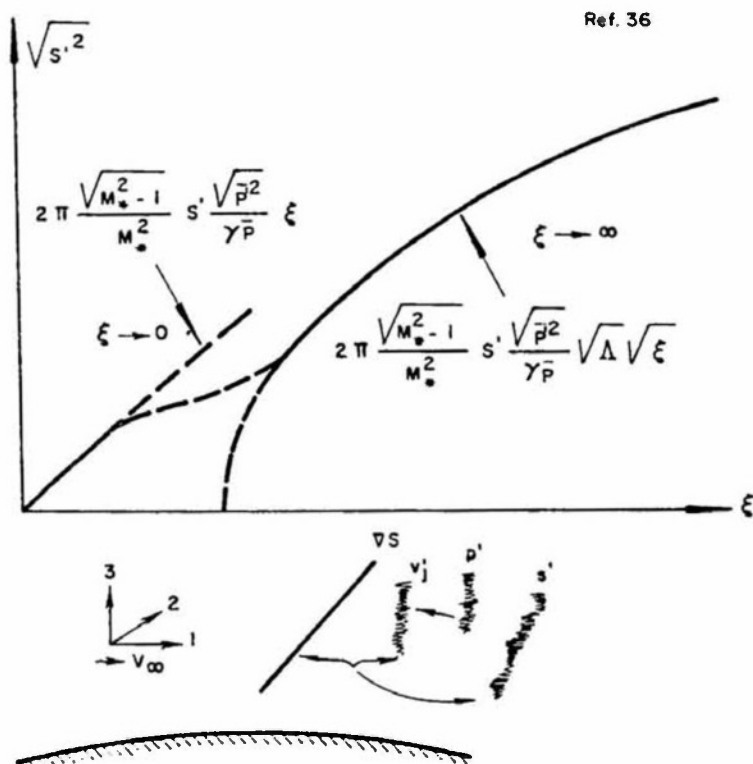


Figure 17. The influence of entropy fluctuations.

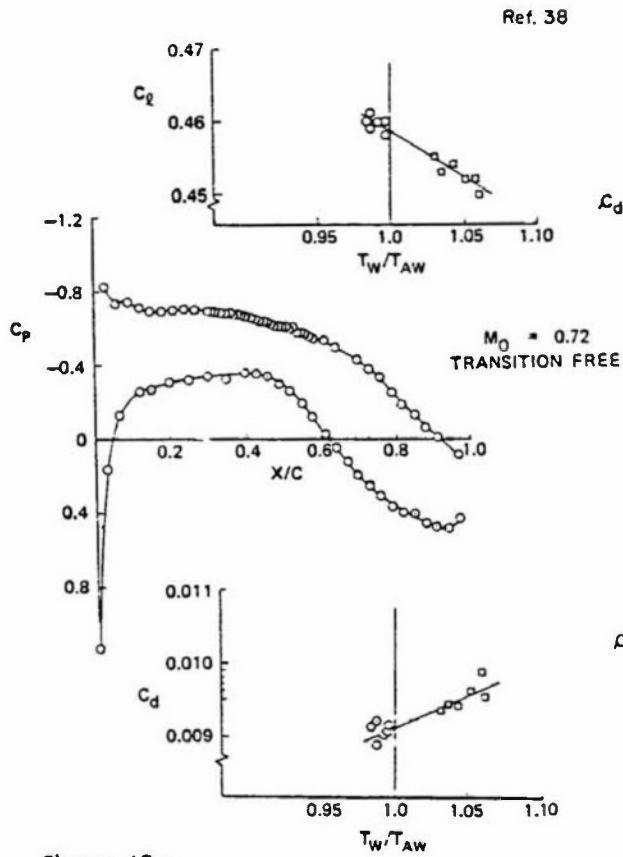


Figure 18 a.  
Wind-tunnel measured effect of  
Nonadiabatic wall on airfoil drag.

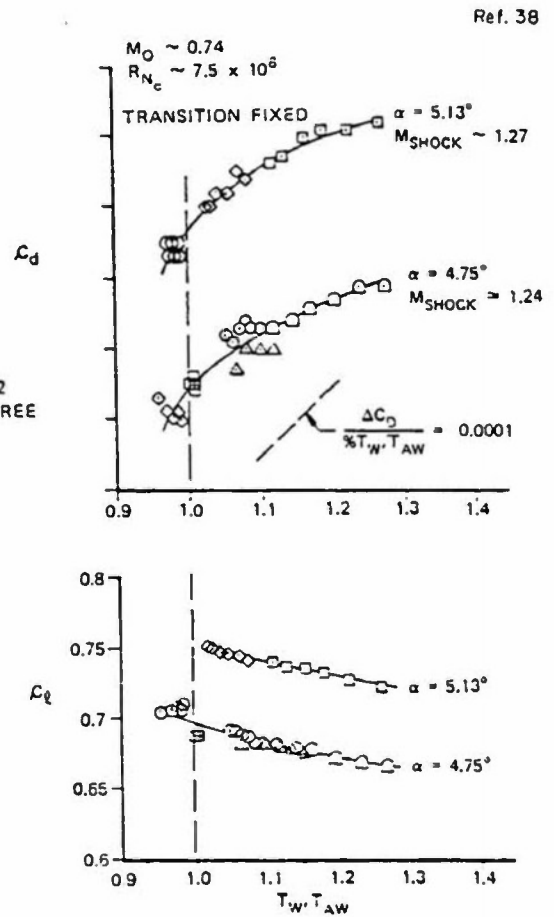


Figure 18 b.  
Wind-tunnel measured effect of  
Nonadiabatic wall on airfoil cruise  
drag and lift characteristics.

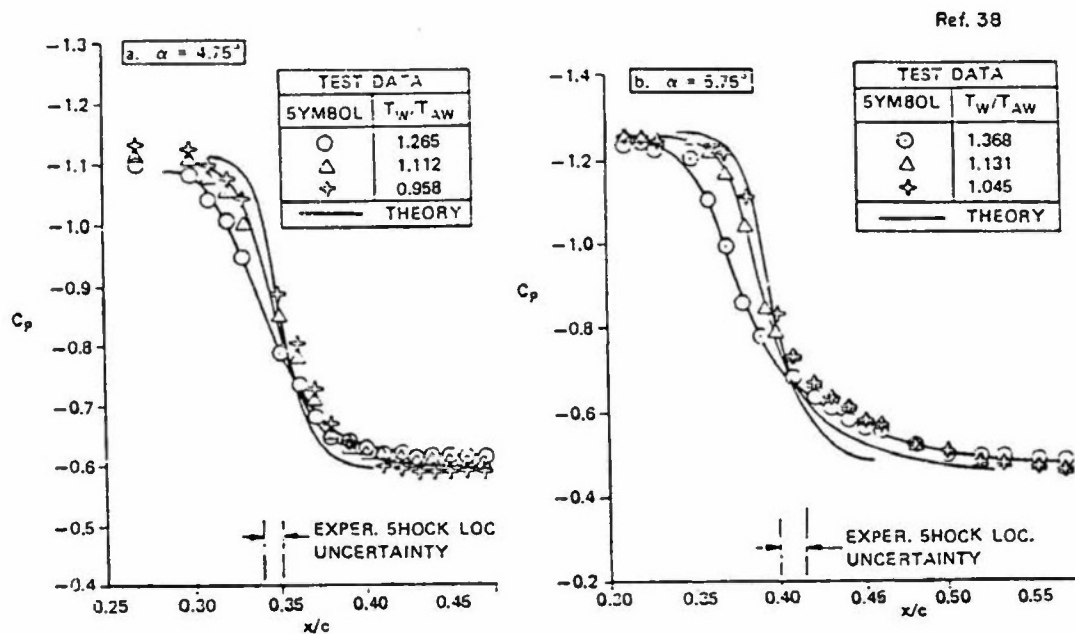


Figure 18 c.

Typical experimental and theoretical wall pressure distribution across the SBLI zone for various Nonadiabatic surface temperatures ( $M_\infty = .74$ ,  $Re_c = 7.5 \times 10^6$ ).

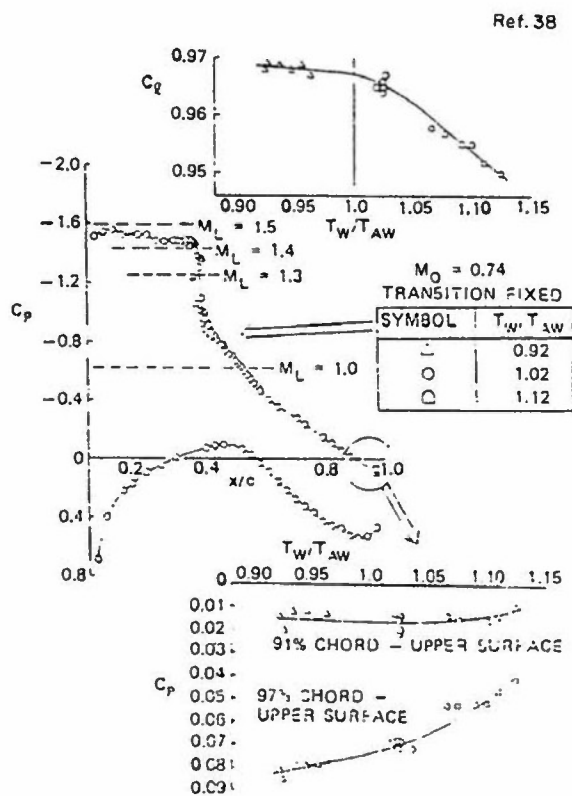


Figure 18 d.

Wind-tunnel measured effect of Nonadiabatic wall on airfoil buffet onset.

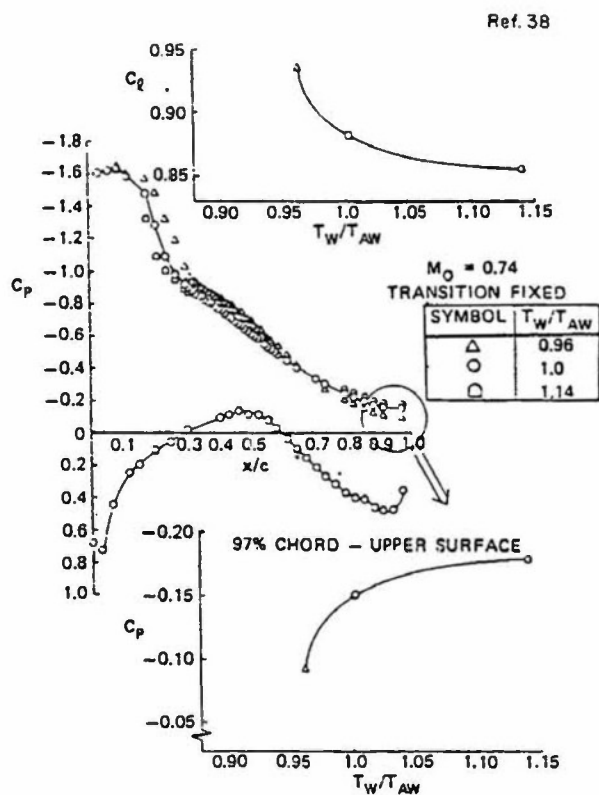
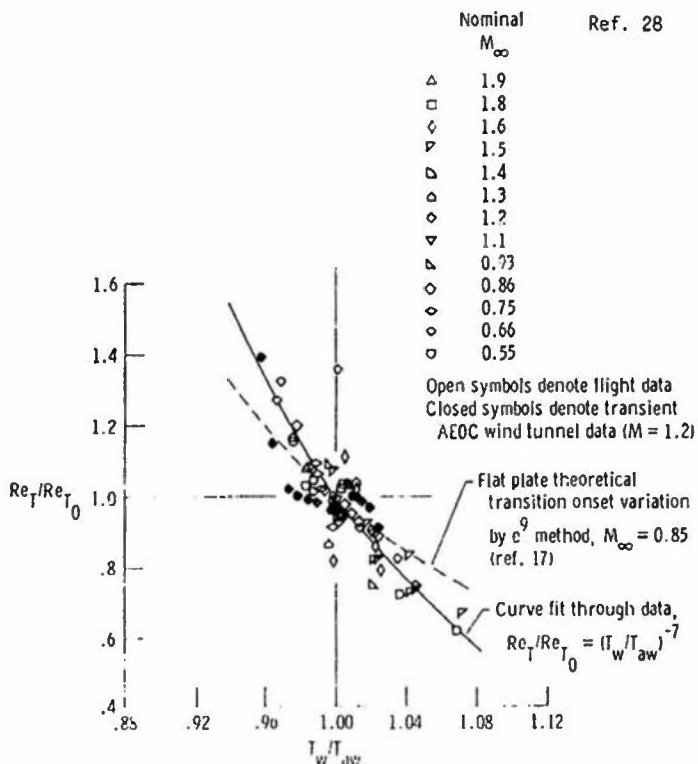


Figure 18e.

Wind-tunnel measured effect of Nonadiabatic wall on airfoil characteristics near maximum lift.

Figure 18. Concluded.

Figure 19. Influence of  $T_W/T_{AW}$  on cone transition.

Ref. 39

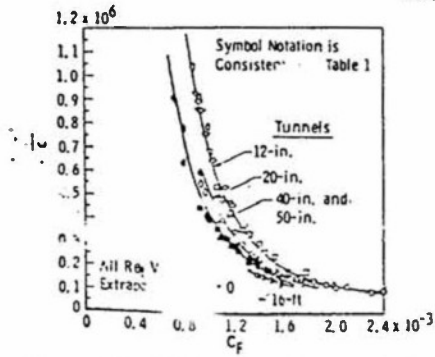


Figure 20. Influence of tunnel size on the transition correlation.

Ref. 39

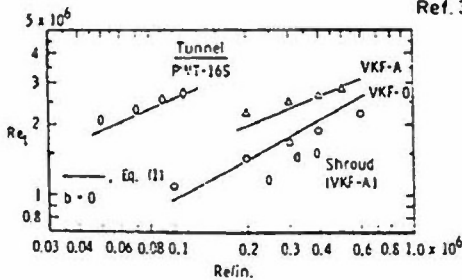


Figure 22. Comparison of measured and estimated transition Reynolds numbers from several tunnels at  $M_\infty = 3.0$ .

Ref. 39

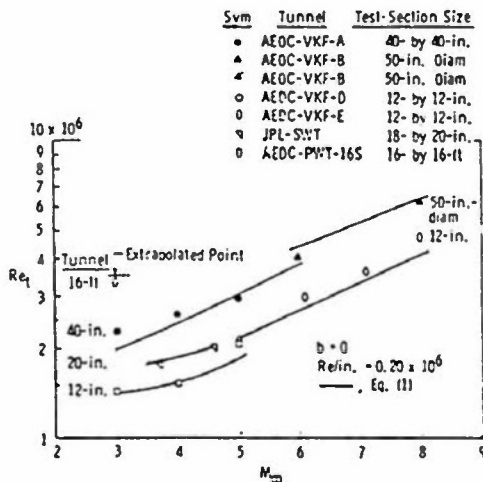


Figure 24. Variation of transition Reynolds number with increasing tunnel Mach number.

Ref. 39

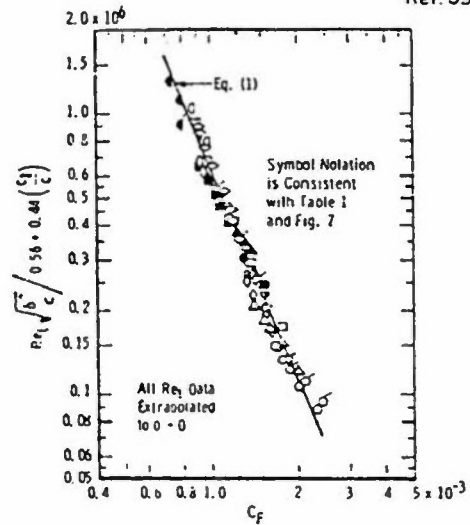


Figure 21. Correlation of transition Reynolds number.

Ref. 39

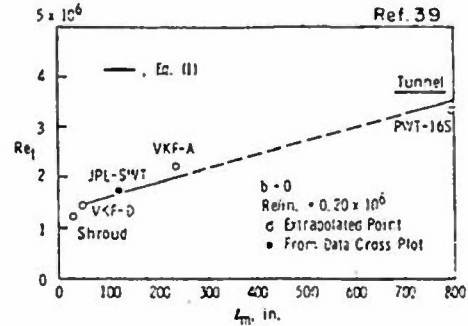
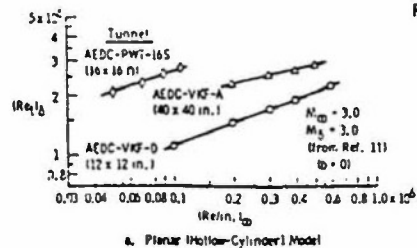


Figure 23. Effect of the tunnel size on transition Reynolds number at  $M_\infty = 3.0$ .

Ref. 40



a. Planar Hollow-Cylinder Model

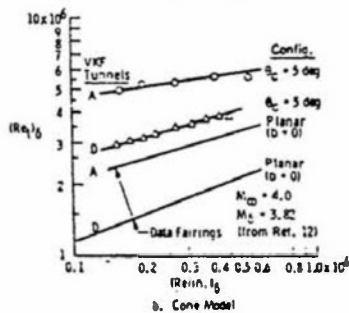


Figure 25. Variation of adiabatic smooth wall transition Reynolds number with tunnel size.



Ref. 40

Cone Correlation  $\Delta$  From Ref. 12. Based on Data from Ten Different Wind Tunnel Facilities Varying in Size from 12 in. to 54 in., Mach Number Range from 3 to 14, and  $(Re)_{\infty}$  Range from  $0.1 \times 10^6$  to  $1.2 \times 10^6$ .

Planar Correlation  $\circ$  From Ref. 11. Based on Data from Nine Different Wind Tunnel Facilities Varying in Size from 1 to 16 ft, Mach Number Range from 3 to 8, and  $(Re)_{\infty}$  Range from  $0.05 \times 10^6$  to  $1.1 \times 10^6$  (Adiabatic Wall).

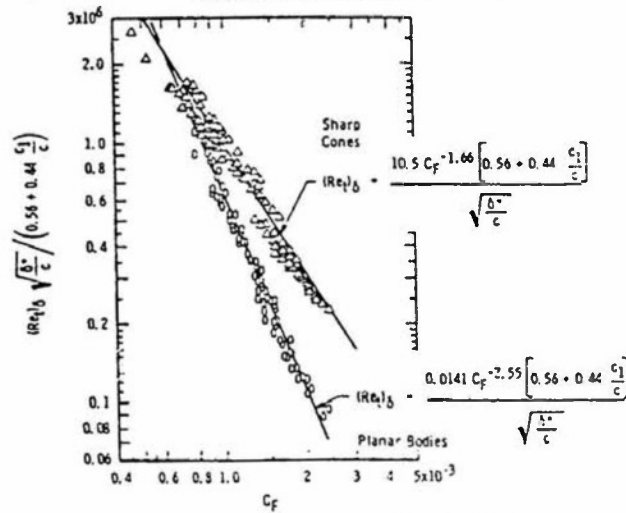


Figure 26. Correlation of transition Reynolds numbers.

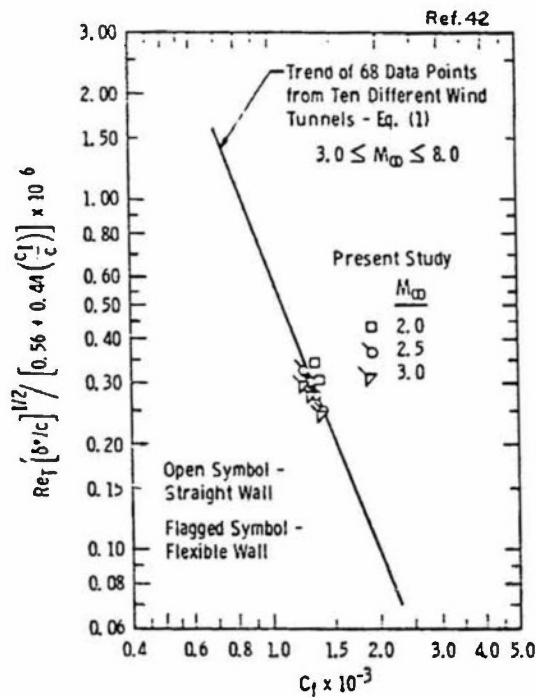


Figure 27. Hollow cylinder transition data correlation in tunnel 165 (Pate and Schueler).

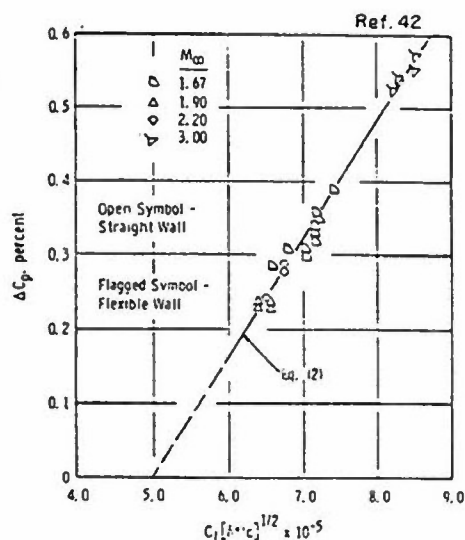


Figure 28. Correlation of noise levels measured on cone with tunnel wall boundary-layer properties.

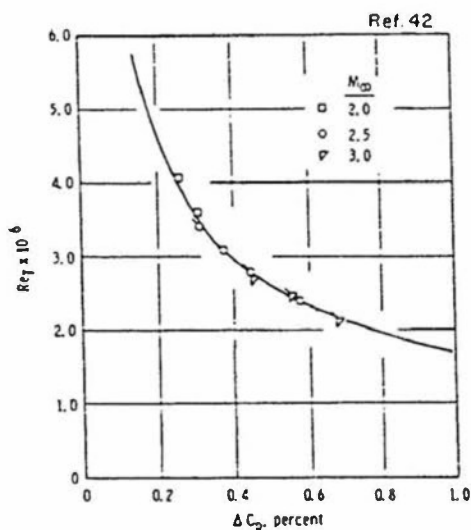


Figure 29. Correlation of hollow cylinder transition data with noise levels measured on cone.

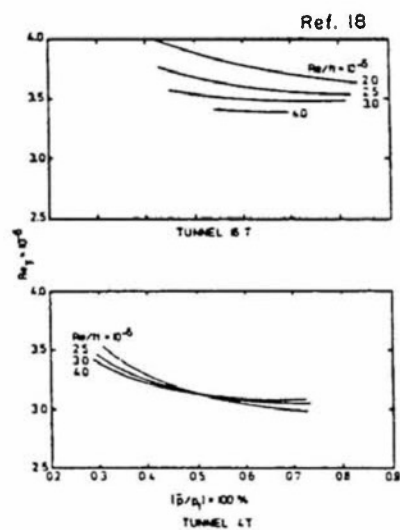


Figure 30. Correlation of transition Reynolds number and test section noise levels in tunnels 16T and 4T,  $0.60 < M < 1.00$ .

Ref. 28

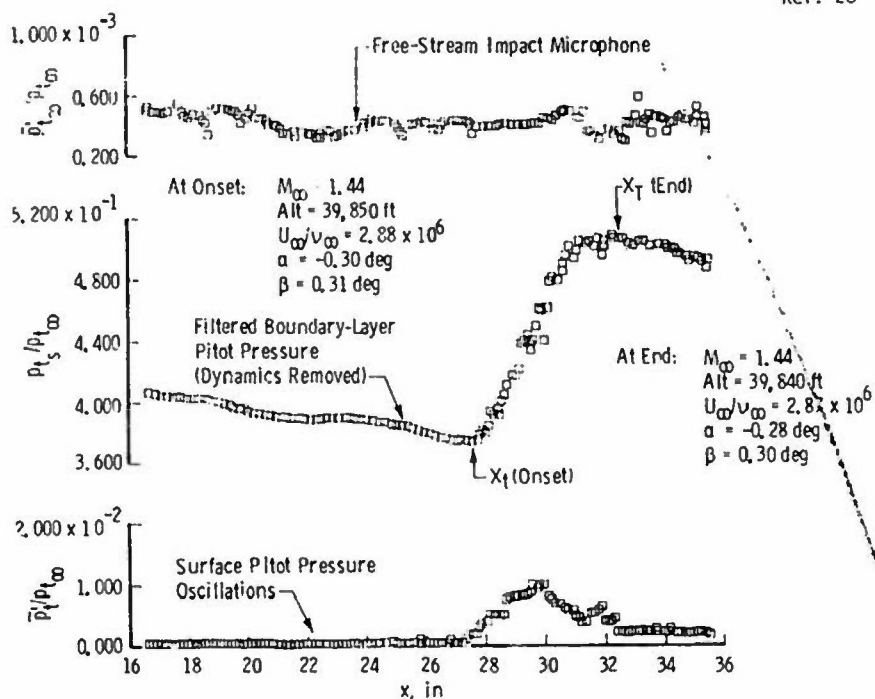
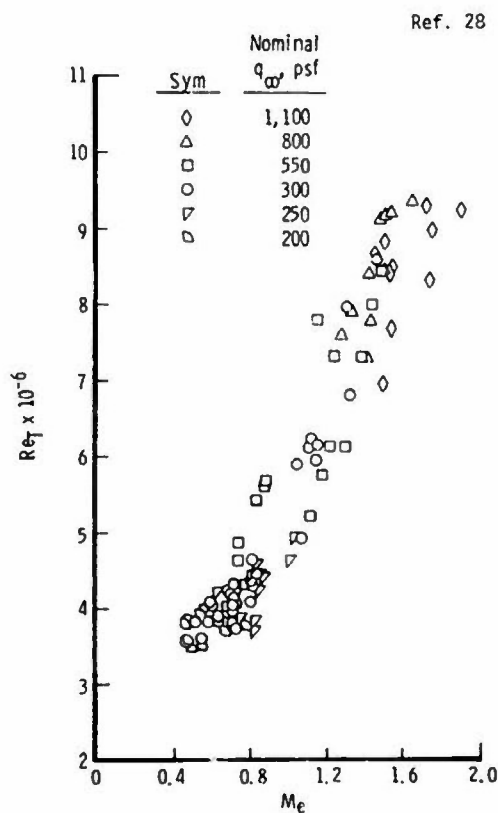


Figure 31 a. Typical pitot pressure profile in-flight.

Figure 31 b. In-flight transition Reynolds numbers as a function of  $M_e$ .

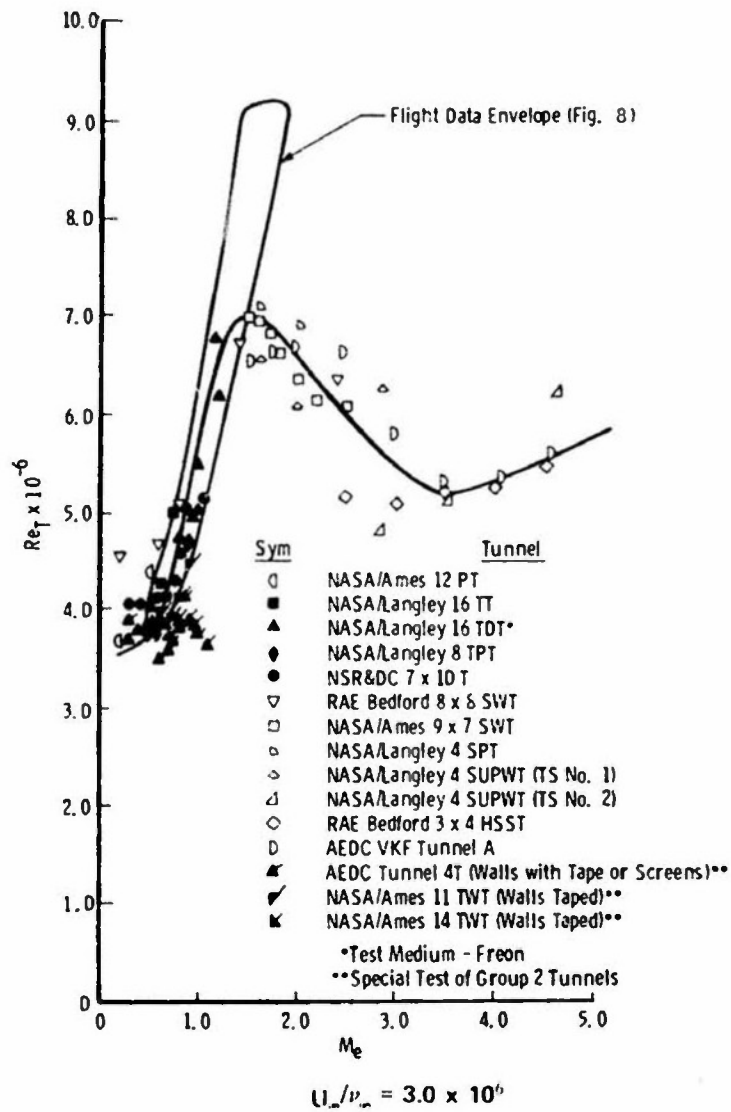


Figure 31 c. Transition Reynolds numbers in lower-disturbance-level wind tunnels.

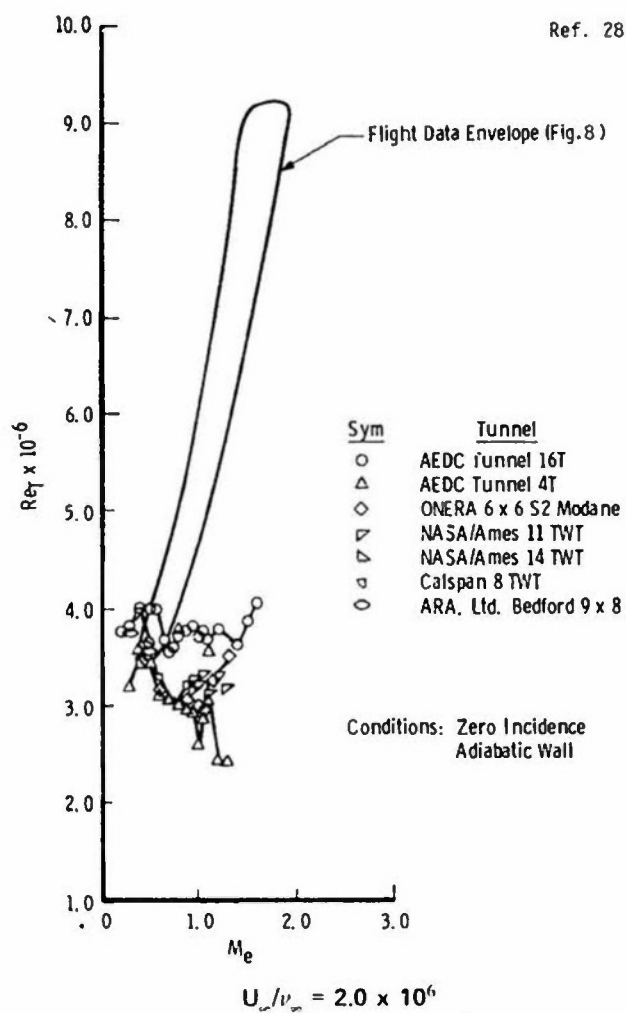


Figure 31 d. Transition Reynolds numbers in disturbance-level wind tunnels.

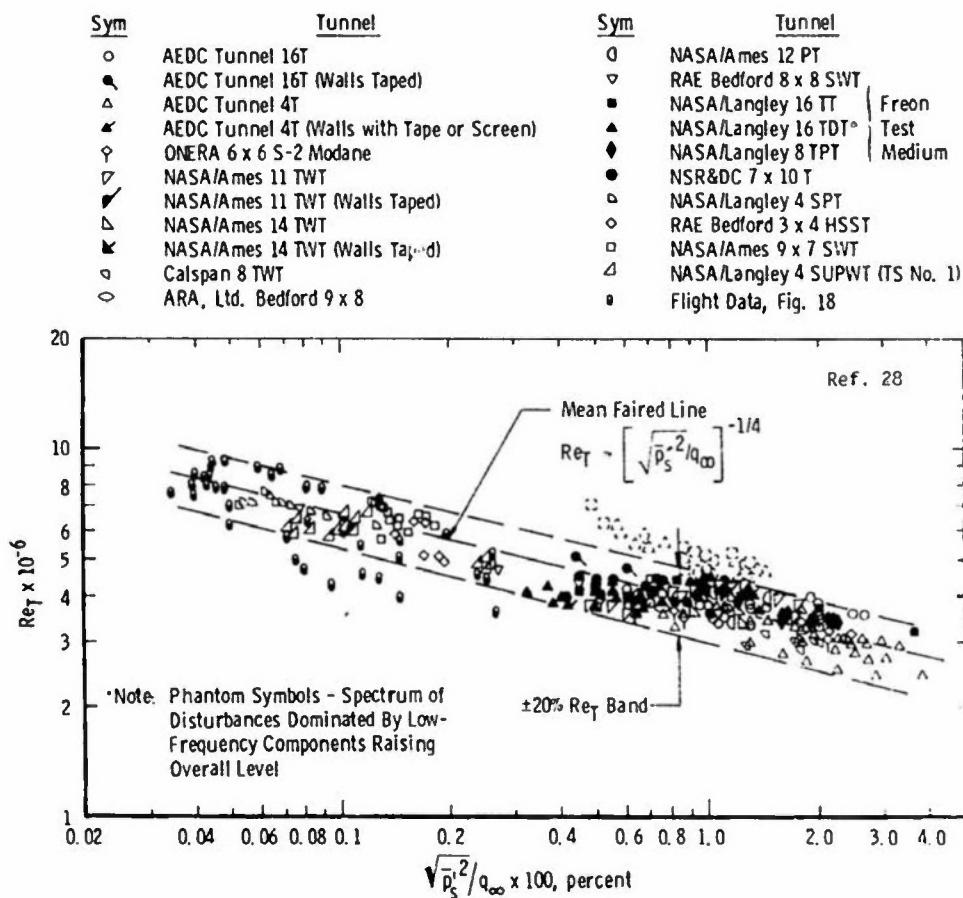
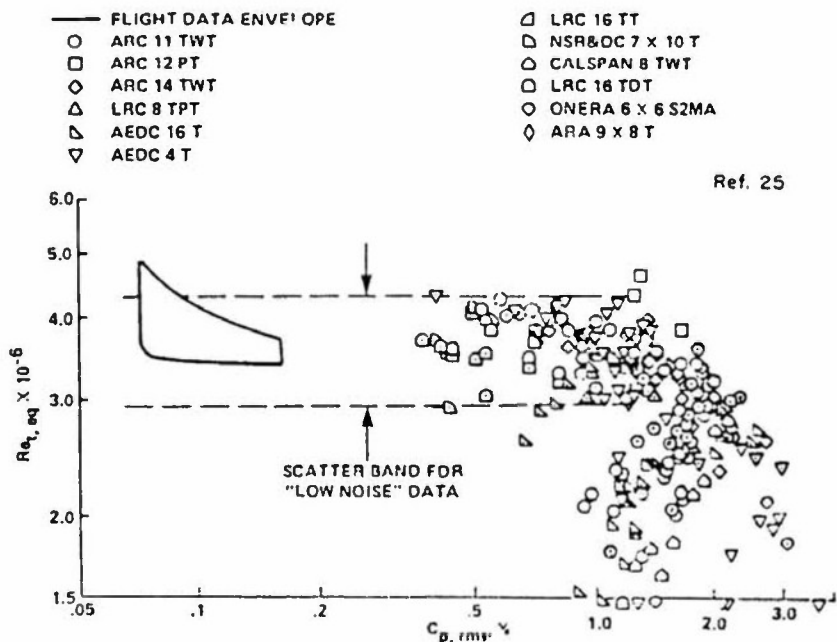


Figure 31 e. Overall correlation of data.

Figure 32 a. Equivalent beginning-of-transition Reynolds number as a function of pressure fluctuation level for ten degree cone flow,  $M = 0.4$  to  $1.2$ .

Ref. 25

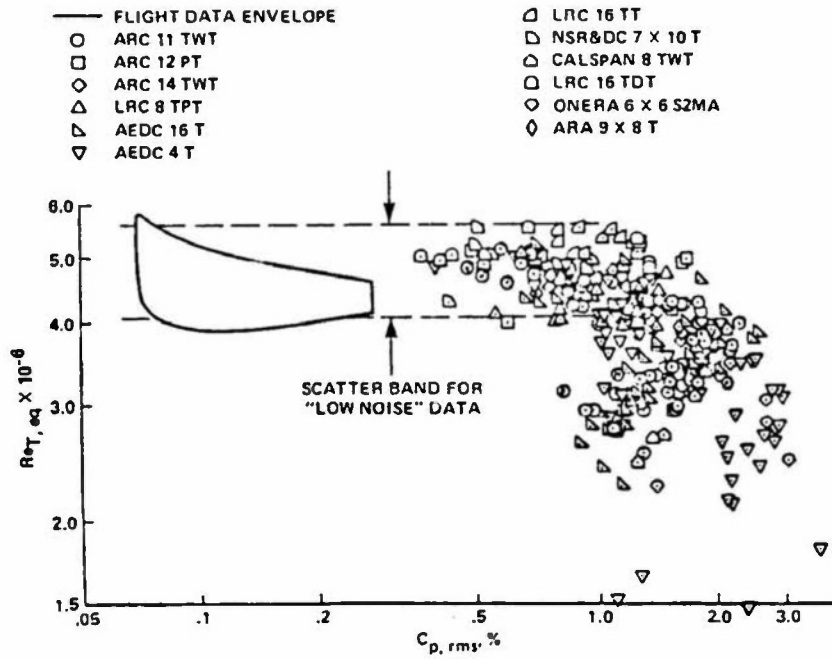


Figure 32 b. Equivalent end-of-transition Reynolds number as a function of pressure fluctuation level for ten degree cone flow,  $M = 0.4$  to  $1.2$ .

Ref. 25

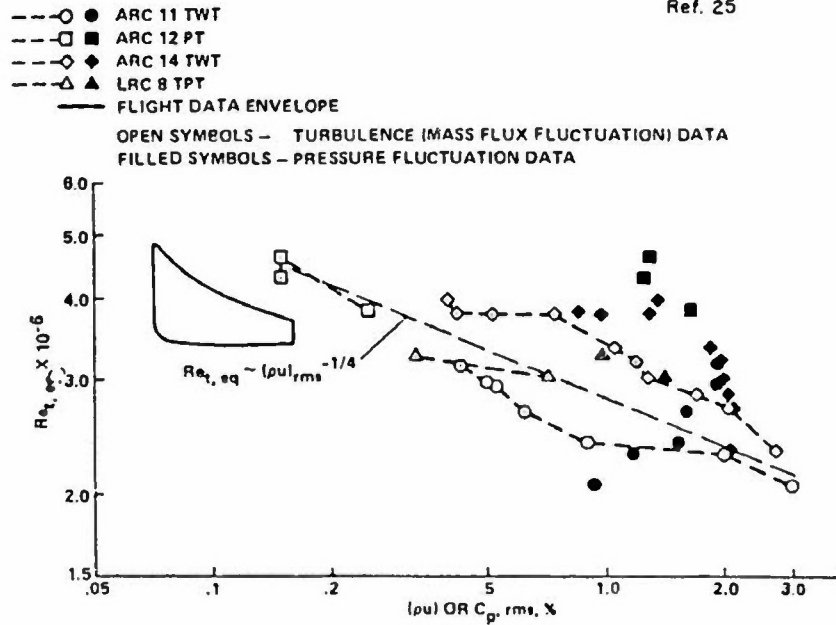


Figure 32 c. Comparative plot showing relative influences of free stream turbulence level and pressure fluctuation level on equivalent beginning-of-transition Reynolds number for ten degree cone flow,  $M = 0.4$  to  $1.2$ .



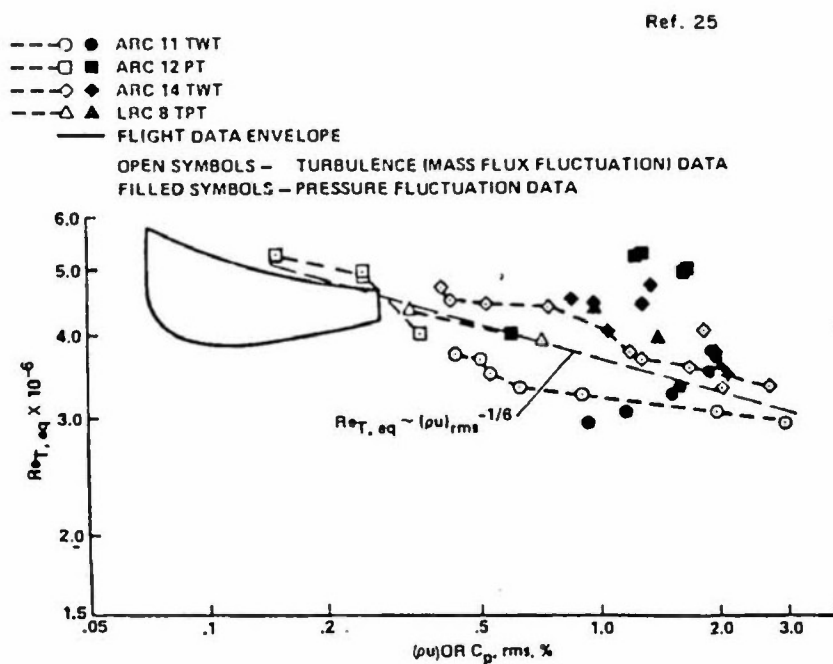


Figure 32 d. Comparative plot showing relative influences of free stream turbulence level and pressure fluctuation level on equivalent end-of-transition Reynolds number for ten degree cone flow,  $M = 0.4$  to  $1.2$ .

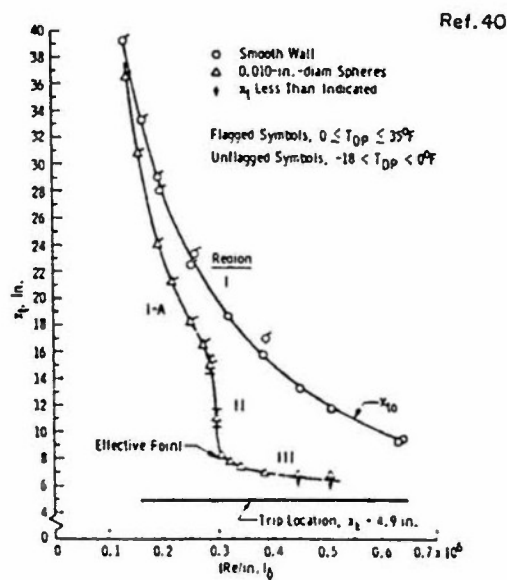


Figure 33 a. Effect of spherical roughness on transition location,  $M_0 = 2.89$ , VKF-Tunnel A.

Ref. 40

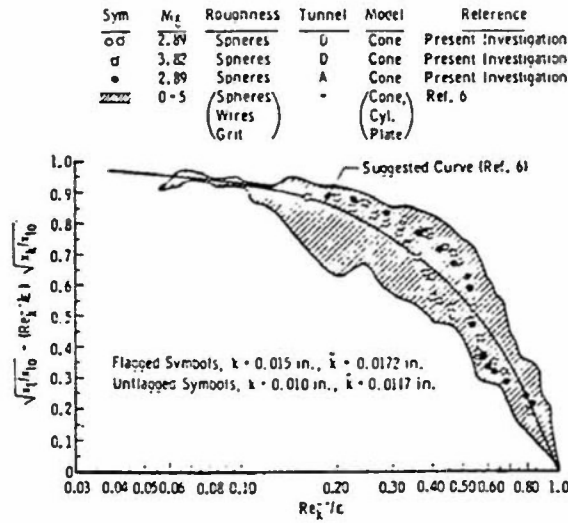


Figure 33 b. Correlation of tripped results using the method of Potter-Whitfield.

Ref. 45

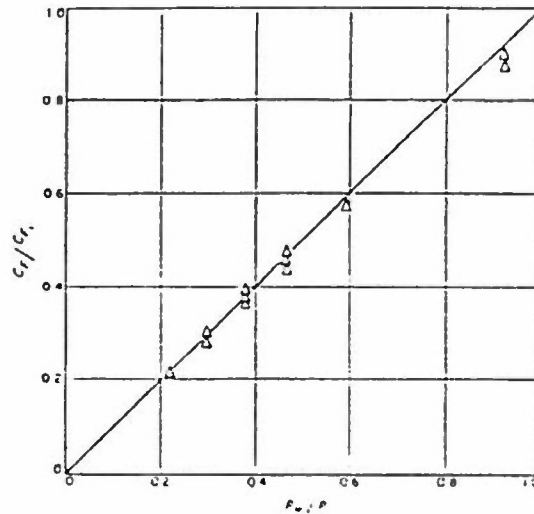


Figure 34 a. Ratio of compressible to incompressible skin-friction-drag coefficients for a rough surface vs. ratio of wall density to free-stream density.

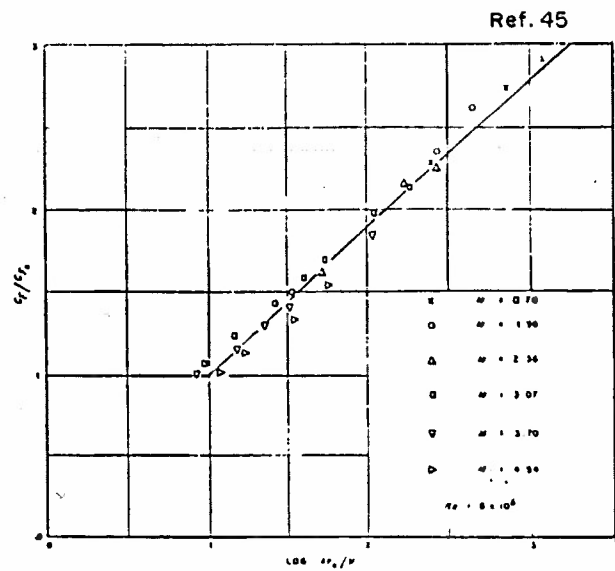


Figure 34 b. Ratio of skin-friction-drag coefficients for a rough surface to that for a smooth surface vs  $\log kv_* / \nu$ .

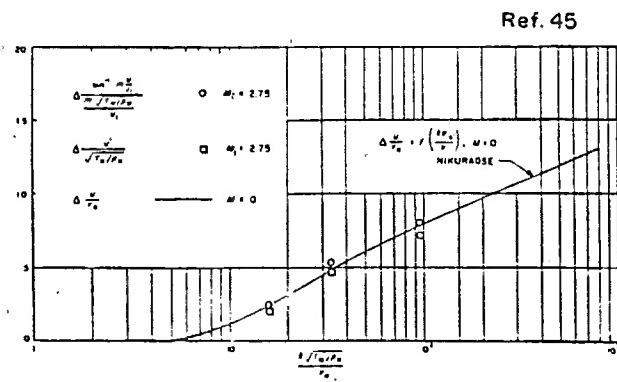


Figure 34 c. Effect of roughness on velocity profiles.

## SECTION 4.9

### BOUNDARY LAYER MANIPULATION

Edward M. Kraft

Calspan Corporation/AEDC Division

Arnold Air Force Base, Tennessee

#### 4.9.1 Introduction

It is clear that, left to its own development, the boundary layer on a model used in a subscale simulation may have little resemblance, in general, to the boundary layer on the full-scale vehicle. Consequently, it is inevitable that some sort of manipulation of the viscous dominated regions on the model will have to be performed in order that the wind tunnel results can be extrapolated to flight. The elements necessary for a successful viscous simulation are:

1. An understanding of what parameters need to be controlled in the subscale experiment to provide a surprise-free extrapolation to flight.
2. Means for manipulating and controlling the required viscous parameters.
3. Methods for determining that the viscous parameters were properly controlled in the wind tunnel.
4. An understanding of how the wind tunnel data need to be extrapolated to flight from whatever conditions were established in the wind tunnel.

One must also keep in mind that different boundary layer manipulation techniques will be applied for different test requirements. The viscous simulation criteria for determining cruise drag performance will generally be different than the criteria for the determination of buffet onset or post-stall performance of an aircraft. In addition, different requirements may exist for various components of a vehicle; for example, the wing, the forebody, or the nozzle/afterbody region. In this section an overview of the elements required for boundary layer manipulation will be presented and some suggested areas for future research will be discussed.

#### 4.9.2 Viscous Simulation Parameters

It is currently impossible to simultaneously reproduce all the scaled viscous parameters in a subscale wind tunnel experiment. Nor does it appear practical in the future, even with further research, to attempt to completely simulate all the viscous parameters. Hence the thrust of the discussion on boundary layer manipulation presented here will be based on the premise that it is impossible to simulate all the parameters simultaneously and that progress will be made when the most important parameters are identified and robust methods for controlling these parameters are developed such that extrapolation to flight will exhibit the correct physical phenomenon. Therefore the first order of business is to identify the viscous parameters that are the most important and that can be confidently manipulated in the wind tunnel. The primary emphasis in this section will be for the parameters that influence the flow on the wing.

Unequivocally, the highest priority for a proper simulation in a transonic wind tunnel test is that the model-scale test must reproduce the full-scale location of the shock wave. Unless the shock is in the correct position with the correct shock strength, the wing loading distribution, wave drag, and influence of the shock on the viscous parameters, particularly separation, cannot be easily extrapolated to the flight condition. Unfortunately, because of the sensitivity of shock systems in the transonic regime, the location of the shock wave on the wing can be easily influenced by numerous non-viscous phenomena such as wall interference, support interference, flow nonuniformity, humidity, and aeroelastic effects. It is presumed in the present discussion that these other phenomena have been accounted for and do not influence the shock. However, a word of caution is necessary here because these other phenomena can also be functions of apparent viscous parameters such as the unit

Reynolds number in the wind tunnel (see Section 2.3.1 or Section 4.8). In addition, any experimental investigation into scaled viscous effects must recognize and account for these non-viscous phenomena.

The basic principals of dynamic simulation require scaling the mass, momentum, and energy relations. Although future research may unlock more primitive descriptions of the basic criteria for scaling viscous effects, current practice is concerned with the scaling of integrated or global properties such as  $\delta$ ,  $\delta^*$ ,  $H$ , and  $c_f$ . In addition, other parameters such as transition location,  $x_t$ , trailing edge pressure,  $C_{pTE}$ , and the turbulence structure,  $T_u$ , appear to be important indicators of the boundary layer behavior. Hence the task for deciding how to manipulate the boundary layer is to determine which of these parameters must be properly scaled at critical points on the vehicle.

The ideal boundary layer manipulation technique would match the flight transition location, simulate the proper parameters at the shock location, introduce the correct turbulence structure downstream of the shock, and recover the flight trailing edge conditions. This invokes images of an almost continuous array of trips, blowing or suction, or surface heating or cooling devices. Before judging the impracticality of such an approach one must ascertain the gains to be made by an improved simulation of Reynolds number dependent phenomena. However, for a practical boundary layer manipulation one must develop a priority list of criteria. In developing the priority list one must keep in mind the ability to confidently control the parameter of interest and the utility of that parameter in performing an extrapolation to flight.

As a minimum requirement, transition location must be manipulated to at least provide the correct boundary layer behavior (laminar or turbulent) at the shock location. Aside from this, the actual transition location is only important in how it influences the development of the other parameters. It is essential, however, to know the actual transition location in the wind tunnel test in order to perform a correct extrapolation of skin friction to the full scale conditions.

Based on the discussion of Section 4.5, for a proper interaction between the shock wave and the boundary layer the most important parameter to be simulated is the combined parameter  $\delta^* (H_i - 1)/c$ . It is also pointed out that the exact high Reynolds number value of the displacement thickness and the shape factor, which would automatically lead to the correct  $\delta^* (H_i - 1)/c$ , cannot be attained simultaneously, at least not by such simple means as manipulating the transition location. If, however, a manipulation technique is developed to duplicate the  $\delta^* (H_i - 1)/c$ , it appears that extrapolation to flight conditions would be easily attainable. If a boundary layer manipulation technique cannot be developed it may be necessary to further decide which of the parameters,  $\delta^*/c$  or  $H_i$ , is the more important. Of these two parameters, one probably has least control of  $H_i$ , but serendipitously the shape factor frequently approaches the full scale value at the shock location when one uses simple techniques such as tripping. Hence, the boundary layer displacement thickness is probably the parameter that will require attention in the subscale simulation.

As an illustration of the interplay between  $\delta^*$  and  $H_i$ , Prof. Michel has performed a simple analysis of controlling the boundary layer parameters on a flat plate by varying the trip location. The results are presented in Fig. 1. In Fig. 1 a fictitious shock location is selected at  $x/c = 0.6$ . The objective of the calculation, using incompressible boundary layer theory, is to determine how the parameter  $\delta^* (H_i - 1)/c$  varies at the fictitious shock location between full- and subscale conditions and with different wind tunnel transition locations. A full scale Reynolds number of  $50 \times 10^6$  produces transition at  $x/c = 0.1$  and a value of 0.00021 for the shock interaction parameter. Assuming a "wind tunnel" Reynolds number of  $6 \times 10^6$ , transition locations were selected to either match the shock interaction parameter or the displacement thickness at the fictitious shock location. To match  $\delta^* (H_i - 1)/c$  between flight and wind tunnel at the shock requires transition to occur at  $x/c = 0.465$ . To match  $\delta^*$  at the shock, on the other hand, requires transition to occur at  $x/c = 0.35$ . It should be noted in Fig. 1, that when  $\delta^* (H_i - 1)/c$  is matched at the shock,  $\delta^*/c$  in the wind tunnel is only 72% of the full scale condition. It is an interesting coincidence that matching  $\delta^* (H_i - 1)/c$  at the shock

requires an aft trip location (approximately 15% of chord ahead of the shock). This may, in part, suggest why aft tripping is successful in improving the shock boundary layer interaction.

Shock induced incipient-separation appears to be insensitive to simulation of any of the viscous parameters, but is largely controlled by the shock Mach number. This underscores the necessity of duplicating the correct shock position which in turn will generally duplicate the correct shock Mach number and hence the shock induced separation characteristics.

Of more difficulty is the simulation of the trailing edge characteristics, particularly for a Type B trailing edge separation. The trailing edge separation can have a very strong influence on the shock location. To date, no single criteria has been identified for which parameter to simulate for correct trailing edge behavior. At best, one may resort to the technique of Khan and Cahill (Ref. 1) to determine the sensitivity of trailing edge separation to changes in Reynolds number as summarized in Section 2.2.3.6. The parameter used in Ref. 1 for the correlation is

$$K = \frac{(M_e^2 - 1)}{(\gamma + 1)cM_e^2}$$

where  $\epsilon = (c_f/2)^{1/2}$ , and  $M_e$  is the local Mach number. Both  $M_e$  and  $c_f$  are the values immediately upstream of the terminal shock. This correlation suggests that  $c_f$  at the terminal shock may be the viscous parameter to be controlled.

The review of flow separation in Section 4.6 suggests that separation criteria should relate directly to  $c_f$ . In lieu of the difficulty of discerning  $c_f$ , however, the correlations for separation have been based on more easily measurable or calculable quantities and are of the form

$$h = \frac{H-1}{H} = \Lambda(\delta^*/\delta)$$

as illustrated in Fig. 4.6.30. These correlations seem to be a very weak function of Reynolds number. It is also noted in Section 4.6.5.4.1 that separation, when it occurs, happens very rapidly and the prediction of separation is not very sensitive to the particular choice of the critical value of  $H$ . The cause of separation is the adverse pressure gradient. The viscous parameters just determine the strength of the pressure gradient required to separate the boundary layer. What is not clear in determining the viscous parameters that must be simulated for flow separation is whether particular values of  $c_f$ ,  $h$ , or  $\delta^*/\delta$  (or their combinations) are causes of the separation (and hence a means for controlling separation) or just measurements that determine separation has occurred.

For trailing edge flows, whether separated or not, the viscous parameters that should be simulated are shape factor and boundary layer thickness (see Section 4.6.8). The consistency of the trailing edge parameters with parameters established elsewhere on the body, e.g., shock location, has not been established. Since the trailing edge flow is a result of the history of the boundary layer upstream, it may be impossible to control the trailing edge independent of other viscous similitude criteria.

In summary of the discussion of viscous parameters required for simulation, *the current understanding of the most important viscous parameters for various test requirements and their response to manipulation is incomplete.* A systematic experimental/numerical investigation of the variation of all pertinent boundary layer parameters with different manipulation strategies should be performed. For example, considering boundary layer tripping alone, basic numerical simulations at subscale conditions for two-dimensional flow over an airfoil can be performed applying tripping strategies to match (1) flight transition location, (2) selected parameters, say  $\delta^*$ , at the shock location, (3) viscous parameters at separation, or (4) some trailing edge condition such as  $\delta^*$  at the trailing edge. In this way the interaction of each of the viscous parameters with different manipulation strategies can be explored leading to an understanding of the pertinent parameters that should and can be duplicated

in the wind tunnel. The basis for extrapolating the results to full scale conditions must also be considered in evaluating the various simulation strategies. The investigation needs to be extended to include other manipulation techniques such as suction/blowing or heating/cooling. Furthermore, these types of studies should also be extended to other important viscous flows such as forebody vortex flows, nozzle afterbody flows, etc.

#### 4.9.3 Boundary Layer Manipulation Techniques

As mentioned before, the ideal boundary layer manipulation technique will match the flight transition location, simulate the proper parameters at the shock location, introduce the correct amount of turbulence downstream of the shock, and recover the flight trailing edge conditions. In addition, one would like the manipulations devices to be easily applied to any wind tunnel model and to be adaptable to the changing conditions in the test program (angle of attack and Mach number). At first thought this approach would appear to be prohibitively expensive in model fabrication and testing time, and perhaps not worthy of further consideration. However, the advantages to correctly predicting full-scale conditions will decide how much one is willing to invest in the wind tunnel program. If these techniques can be used to avoid surprises in the flight vehicle that require redesign and retooling or if an optimized vehicle instead of a conservatively designed vehicle gives the manufacturer a competitive advantage, the expense of sophisticated testing techniques will be justified. The expense of having to modify an aircraft design late in the development cycle to overcome some deficiency not identified in the wind tunnel program will easily pay for advanced techniques. The legendary costs of operating a fleet of C-5 transport aircraft if the drag is one count too high also suggests the payoff for more advanced testing techniques.

Boundary layer manipulation devices can be categorized as those that promote transition in a desired fashion or those that control the growth of the boundary layer parameters. The first category, boundary layer tripping, is the most widely applied and perhaps easiest boundary layer manipulation technique. The second category, control of the boundary layer parameters is less developed. Current understanding of the techniques used for either tripping or control are given below.

##### 4.9.3.1 Boundary Layer Tripping Methods

The basic state of the art of tripping techniques is summarized in Section 2.3.2. Our current knowledge of the properties of boundary layer tripping techniques, at least in terms of distributed roughness, is reasonably complete. If we can define a desired transition location, then generally a trip can be sized to assure transition at that location. In addition, it has been clearly established that for the more popular trips such as carborundum grit, ballontini balls, distributed disks, etc., the boundary layer profiles downstream of the tripping device recover to a basic law of the wall turbulent profile. It should be recognized, however, that our working knowledge for sizing such trips is based on data bases for zero pressure gradient flows (e.g., Ref. 2). The primary research that should be performed on basic distributed roughness boundary layer trips is to determine if the pressure gradient is an important parameter in determining trip size and to accurately determine trip drag.

Even though our knowledge of the mechanical properties of distributed roughness boundary layer tripping is reasonably complete, our basis for locating and sizing trips needs to be improved. The existing correlation techniques for placing trips at the flight transition location, such as the Braslow-Knox criteria (Ref. 2) or the Potter-Whitfield correlation (Ref. 3), were developed two decades ago and do not reflect current understanding about facility environmental effects such as turbulence or the influence of unit Reynolds number on tunnel calibration and were developed with very little variation of the boundary layer conditions such as pressure gradient or nonequilibrium effects. Consequently it would be useful to revisit some of these basic experiments and finalize the working relationships required to confidently locate and size trips.

On the other hand, if the simulation of the boundary layer requires placement of the trip at a location different than full-scale transition location, very little information is available on how to size or locate the trips. For example, if it is desired to duplicate the displacement thickness at the shock location then there exists no systematic correlation to suggest where to locate the trip or what size trip should be used. Hence, in conjunction with the determination of the critical viscous parameters, a whole new range of experimental information on trip effects on viscous parameters at other critical locations on the model needs to be explored.

Another consideration that has not been introduced into the existing methodology of transition fixing is the primary natural cause for transition. For example, the entire approach to transition fixing is premised on consideration of two-dimensional Tollmien-Schlichting transition models to either force transition at the full scale location or to provide a minimum thickness boundary layer at the shock location (i.e., aft tripping). In nature, transition on three-dimensional wings is more frequently caused by cross-flow instabilities or leading edge contamination. These modes of transition are not reflected in current tripping practices. If one considers, for example, the standard criteria for leading edge contamination to cause transition, namely,

$$R_0 = 0.404 \left( \frac{U_\infty r}{\nu} \frac{\tan \Lambda \sin \Lambda}{2} \right)^{1/2} < 100$$

where  $r$  is the leading edge radius and  $\Lambda$  is the leading edge sweep, then if the geometry is faithfully scaled by a factor, say S.F., the value of  $R_0$  will be lower by a factor of  $(S.F.)^{1/2}$  in the wind tunnel. It is obvious, therefore, that for many scaled wind tunnel experiments, leading edge contamination will not occur although it may be the primary mechanism for transition at full scale. The importance of simulating leading edge contamination in a wind tunnel experiment has been completely overlooked.

Are the boundary layer properties downstream of transition caused by cross-flow instability or leading edge contamination different than boundary layer properties downstream of a tripped boundary layer, and if so, are the differences important in subscale simulation? When cross-flow instability causes transition, periodic streaks have been observed in the direction transverse to the flow direction (e.g., Ref. 5). According to Poll (Ref. 6), the behavior of the flow when leading edge contamination causes transition to turbulence is different if the leading edge contamination is caused by wires at the leading edge or by massive contamination caused by a turbulent boundary layer at the wing-sidewall (or fuselage) intersection. At a minimum, it would seem that leading edge contamination contributes to the transition locus on the wing surface. Are the details of the transition flow features important to subscale simulation? Or, is it only necessary to know where transition should occur because of cross-flow instability or leading edge contamination and position a trip there? *There is no current knowledge base of the nature of these flow structures to decide this issue.*

As a starting point to these and other issues, it is important to understand the fundamental physical characteristics of tripping mechanisms to determine the influence a trip may have on the other viscous parameters. The current knowledge of the physical behavior of various tripping techniques is given below.

#### Two-Dimensional Roughness Elements

For a given two-dimensional roughness element the change in transition location is a gradual one with increasing velocity. The basic mechanism by which a two-dimensional roughness element induces earlier transition to turbulence is by the destabilizing influence of the flow in the immediate downstream vicinity of the element. Fundamental experiments to determine the mechanism by which 2-D roughness elements induce boundary layer transition have been performed by Klebanoff and Tidstrom (Ref. 6). Some of the important results from the experiments are summarized here.



The experimental setup consisted of a two-dimensional roughness element in the form of a cylindrical rod attached two feet from the leading edge of a 12 ft long, 4½ ft wide, flat plate in the National Bureau of Standards wind tunnel. The actual roughness height,  $k$ , of the 1J16 in rod was 0.066 in. Constant current hot-wire anemometry was used to probe the recovery zone downstream of the roughness element. The recovery zone is defined as the region in the downstream vicinity of the roughness where the mean flow has been distorted by the presence of the roughness.

The basic disturbance created by the two-dimensional roughness element is in the form of waves of varying frequencies and a change in the inflection properties of the basic Blasius velocity profile. These combine to promote transition to turbulence in the same physical manner as on a smooth flat plate. There is no indication of the existence of discrete vortices in the transition process. This is illustrated in Fig. 2, where the spectra of measured fluctuations of the streamwise velocity in the region downstream of the roughness element as a function of frequency are shown. At the lower Reynolds number, close to the roughness element, the fluctuations are composed of relatively high frequencies and in the downstream direction there is a continuous change to lower and lower frequencies. If discrete vortices were present, one would expect to observe the same frequency at a downstream position. The two vertical lines at the top of Fig. 2 are the frequencies corresponding to the upper and lower branches of the Tollmien-Schlichting stability diagram. It is illustrated in Fig. 2a that in the downstream direction the higher frequencies are damped and the dominant frequencies which emerge lie within the Tollmien-Schlichting zone of instability. In Fig. 2a the end of the recovery zone is  $x-x_k = 4.5$  in.

At the higher unit Reynolds number, shown in Fig. 2b, a similar damping of the frequencies generated by the roughness occurs up to 3-in. from the trip but at 4.5-in. the behavior has reversed itself with an increase in amplitude of the higher frequencies. The increase in amplitude of the higher frequencies continues to increase further downstream. At the end of the recovery zone, in contrast to the lower Reynolds number case where a dominant frequency emerged within the T-S zone of instability, there is a range of frequencies present. This behavior is governed by the initial disturbance spectrum and the manner in which the various frequencies are amplified. Thus, it is evident that basically one is dealing with an instability problem within the recovery zone, and that this region is considerably more unstable than the basic Blasius flow over the flat plate.

The measurements of the mean velocity profiles in the recovery zone are shown in Fig. 3. It is obvious from Fig. 3 that the velocity profiles change from a separated profile with an inflection to the Blasius profile as one progresses downstream. Increasing unit Reynolds number also increases the magnitude of the inflection. Based on linear stability theory, Klebanoff and Tidstrom concluded that the inflectional velocity profiles encountered in the recovery zone cause a rapid amplification of the instability waves. The disturbances are larger than they would be without roughness and lead to a premature transition. The trip does not introduce new disturbances into the boundary layer, but strongly amplifies the existing perturbations.

When increasing the roughness height or the velocity, the transition location moves gradually upstream. A correlation of the influence of trip size on transition is given in Fig. 4 from Ref. 7. The ratio  $R_{XT}/(R_{XT})_0$  is shown as a function of  $k/\delta_k^*$ , where  $(R_{XT})_0$  is the transition Reynolds number untripped and  $\delta_k^*$  is the displacement thickness at the location of the trip if the trip were not present. An additional parameter correlated in Fig. 4 is the turbulence,  $T$ . It can be seen that appreciable effects occur for roughness elements of height equal to 0.2 to  $0.4\delta_k^*$ , but that the forward movement of the transition process is very gradual.

The fundamental behavior of the mean boundary layer parameters,  $\delta^*$ ,  $\theta$ , and  $H$ , downstream of a 0.066-in. diameter roughness element located at 2 ft from the leading edge of the flat plate used by Klebanoff and Tidstrom is illustrated in Fig. 5. The shape factor,  $H$ , changes from a relatively high value associated with the separated laminar layer to the Blasius value of 2.6 at the recovery

position. It is interesting to note the independence with unit Reynolds number of  $H$  at the end of the recovery zone. At approximately 4.5 in. or 70-diameters downstream from the roughness element the boundary layer has a velocity profile and growth which are characteristic of a boundary layer without roughness. The kink in the curves of  $\theta$  reflect the downstream extent of the actual flow separation within the recovery zone with the kink apparently indicating the end of the separated region. The extent of the separated region varies within the range of 30 to 40 roughness diameters and exhibits some dependency on the unit Reynolds number; however, the change is small, and the range of parameters is too small to accurately assess the behavior.

The data of Fig. 5 illustrates the influence of both Reynolds number and  $k/\delta_k^*$  since the experiment incorporated a change in both parameters. To determine just the influence of Reynolds number on  $H$ , additional experiments were performed by Klebanoff and Tidstrom varying trip size and location to maintain a constant  $k/\delta_k^*$ . These results are shown in Fig. 6. Using  $H$  as a measure of the velocity profile then comparison of Figs 5 and 6 show that the stability of the flow depends on both  $k/\delta_k^*$  and the roughness Reynolds number. However, the dependence of the shape of the velocity profile on the latter appears to be a relatively weak one.

The influence of the two-dimensional trip on the velocity fluctuations downstream of the trip location are illustrated in Fig. 7. The variation of  $u'/U$ , at the end of the recovery zone, is shown for a range of unit Reynolds numbers, and compared with the intensity that would exist at the same position without the roughness. It is seen that for the critical Reynolds number, the turbulence level downstream of the recovery zone approaches the same structure as for a naturally transitioned turbulent boundary layer.

### Three-Dimensional Roughness Elements

In contrast to two-dimensional roughness, transition moves rapidly forward toward a three-dimensional roughness element with a relatively small increase in velocity after a critical velocity has been reached. The essential flow features of a three-dimensional roughness element have been defined by flow visualization (e.g., Refs 8 and 9). At subcritical Reynolds numbers, two sets of vortices have been delineated as the predominant flow features. One set of vortices is a closely spaced pair of spiral filaments which form on the near wake, spiral upward at the rear of the roughness, and at the height of the roughness turn and trail downstream. The other set is a horseshoe vortex, close to the surface, which wraps around the front of the roughness element forming a pair of streamwise vortices which extend downstream. The vortical structures are illustrated in Fig. 8 for a flow around a cylindrical roughness element. The flow visualization studies have also yielded the observation that as the free-stream velocity is increased, a waviness appears on the vortex filaments, and this waviness increases with increasing velocity until the filaments roll up into hairpin vortices.

The basic manner in which transition to turbulence is triggered for the three-dimensional element is open to conjecture. For example, Ref. 10 suggests that these vortices generate a three-dimensional laminar boundary layer with a cross flow velocity component. Then the possibility exists that transition occurs via a cross-flow instability, much in the same manner as it would for a rotating disk or swept wing.

To try to understand the tripping process, fundamental experiments on an isolated hemispherical or cylindrical tripping element on a flat plate have been performed recently by Klebanoff, Cleveland, and Tidstrom (Ref. 11). The hemispherical roughness elements had nominal diameters,  $d$ , of 3.18 and 6.36 mm and were placed at various  $x$ -locations from the leading edge of the plate. For comparison a

cylindrical element with  $d = 3.18$  mm,  $k/d = 1.0$ , and positioned at  $x_k = 91.4$  cm was also tested with its axis in the  $y$ -direction. Detailed measurements were made downstream of the roughness element using standard constant temperature hot wire anemometry.

To determine the phenomena responsible for the transition to turbulence, the flow downstream of the roughness element was probed with two hot wires separated in the  $y$ -direction ( $y$  is normal to the plate). A major feature observed in the oscillograms of the output signals from the hot wires was a phase reversal once the critical Reynolds number was exceeded at the  $x$  station of the measurement. In addition, the phase reversal occurred only within a lateral extent comparable to the diameter of the roughness. It is unlikely that a three-dimensional wave motion could provide the appropriate phase reversals. Instead it appears that there is a rapid change from an initial wave motion of relatively short wave length to a vortex. The change from wave to vortex was determined to occur within a distance of 7.5 times the trip height.

The frequency content of the eddy shedding process for the single element suggested the Strouhal number should be defined with the characteristic velocity  $U_k$  and characteristic length  $\delta^*$  as

$$S = f\delta^*/U_k$$

where  $U_k$  is the velocity that exists in the boundary layer at the height of the roughness element without the roughness element present and  $\delta^*$  is the displacement thickness at the trip location. Traditionally, Strouhal number is characterized by the effective trip height,  $k$ . The appropriateness of  $\delta^*$  as the characteristic length is clearly illustrated in Fig. 9. In Fig. 9a, the Strouhal number referenced to  $k$  is shown to be a strong function of Reynolds number whereas in Fig. 9b it is clearly seen to be only weakly dependent on Reynolds number. Also in Fig. 9b, a comparison is made of the shedding frequencies of the hemispherical and cylindrical elements. The Strouhal number for the cylindrical element is lower than for the hemispherical element and exhibits a greater dependence on  $Re_k$  at the lower Reynolds numbers, i.e.,  $Re_k < 800$ . It is suggested by the results shown in Fig. 9b that the details of the eddy shedding process are dependent on the geometric characteristics of the tripping element.

To further determine the role of the eddy shedding in the transition process, the behavior of the eddies were observed with the free-stream velocity oscillated sinusoidally at low frequencies (1 and 2 Hz). It was observed in the experiments that the intensity of the eddies is highly modulated which provides an explanation for the random occurrence of turbulent spots downstream of the roughness element. Although there is a continuous generation of eddies by the roughness element, since the eddy shedding process is highly modulated, eddies of relatively weak intensity may damp, and not all eddies participate in the evolution of the turbulent spot. The high degree of correlation of the duration of turbulent spots with the duration of eddy shedding, coupled to the fact that when the eddy shedding is periodic with the frequency of the free-stream oscillation the turbulent spots also become periodic, leads to the conclusion that not only is the eddy shedding essential to the transition process but the eddies, although modified in form, are intrinsic to the vortical structure of the turbulence.

The spanwise distributions of the mean,  $U$ , and fluctuating,  $u'$ , velocities measured 14.9 roughness heights downstream of the roughness element are shown in Figs. 10 and 11, respectively. At the subcritical Reynolds number the spanwise distribution of  $U$  clearly shows the presence of the two pairs of streamwise vortices observed in previous flow visualization studies. The pair of vortex filaments rotate in such a direction as to transfer momentum away from the plate at  $z = 0.0$  cm, and the horseshoe vortex rotates so as to transfer momentum towards the plate at  $z = \pm 0.5d$ . The spanwise distribution of  $u'$  at the subcritical Reynolds number reflects a low level of unsteadiness in the two sets of stationary vortices. At the higher Reynolds number, the peak in the spanwise distribution of  $u'$  indicates the presence of the hairpin vortices. With increasing Reynolds number the peak increases in intensity and extends further from the surface. It can also be inferred that the spanwise extent of the eddy is on the order of  $z/d > \pm 0.5$ , centered about  $z = 0.0$  cm, and that the disturbed boundary

layer can be separated into two regions; and outer region,  $y/k \geq 1.0$ , where the hairpin eddy is dominant, and an inner region  $y/k \leq 1.0$ , where the two sets of vortices alluded to at the subcritical Reynolds number still play a role.

The hairpin eddies downstream of the roughness have a marked resemblance to the eddies generated in connection with the secondary inflectional instability which occurs in the later stages of natural transition (see Ref. 12). However, the eddy shedding frequency associated with the roughness varies with  $U^2$  rather than  $U^{3/2}$  as in the natural transition case.

Measurements were also made at various x-stations downstream of the roughness element at various unit Reynolds numbers. The mean velocity profiles in the immediate vicinity of the roughness,  $x-x_k = 1.27 \text{ cm } (7.5k)$ , are compared in Fig. 12 with the Hartree profile for a two-dimensional separated layer. The upper value of unit Reynolds number,  $4.82 \times 10^5/\text{m}$ , is slightly above critical. It is seen in Fig. 12 that the measured profiles are even more inflectional than the Hartree profile suggesting that the profiles are sufficiently inflectional to sustain an incipient wave type of instability which can develop into a rolled-up vortex, and eddy generation at and above the critical Reynolds number. Also there is an indication in Fig. 12 that the inflection increases with increasing Reynolds number. This may contribute to a very rapid increase in amplification.

The consideration of the inflectional instability provides a simple model for the behavior of a three-dimensional roughness element. The critical roughness Reynolds number reflects the separation into linear and nonlinear instabilities. In the linear range, at subcritical Reynolds number, the disturbance, although it may be initially amplified, cannot sustain itself. It can dissipate laterally, and damps as it travels downstream into more stable regions where the mean flow profiles become less and less inflectional. At some Reynolds number the instability becomes nonlinear. In this range the disturbance can no longer be characterized by linear theory. A frequency which may be stable according to linear theory may well be unstable when it is nonlinear. The amplification in the nonlinear range of Reynolds number is extremely rapid, and the instability results in a rolled-up vortex. The vortex is intrinsic to the transition process. The final onset of turbulence results from vortical instability, and the complex vortex-vortex interaction of the shedding vortices with the pre-existing stationary vortices.

Finally, consideration is given to the state of the boundary layer downstream of the roughness element. In Fig. 13 the mean velocity distributions at various  $x-x_k$  distances from the element for the subcritical and barely critical Reynolds number are compared with the mean velocity profile measured without the roughness. For subcritical Reynolds number the Blasius profile is recovered. At the unit Reynolds number just above critical the mean velocity distribution is indicative of transitional flow consisting of intermittent turbulent spots. Measurements of the mean velocity profile for Reynolds number above the critical value are compared in Fig. 14 with a turbulent boundary layer profile measured by Purtell (Ref. 13). It is seen in Fig. 14 that at the higher Reynolds numbers, the boundary layer transitions to a fully developed turbulent profile. Correspondingly, the velocity fluctuations for the fully transitioned profiles are shown in Fig. 15. In comparison with the measurements of Purtell, the turbulence level of the fully transitioned boundary layer is similar to the turbulence level of a naturally transitioned turbulent boundary layer. Hence, for a Reynolds number above critical for a single three dimensional roughness element in the absence of a pressure gradient, the behavior of the boundary layer downstream of the element is identical to that for a naturally transitioned turbulent boundary layer.

Experiments to determine the characteristics of distributed three dimensional roughness elements have been performed by Sinclair and Strike (Ref. 14) at the Arnold Engineering Development Center (AEDC). Boundary layer trip performance data were obtained on a 7-deg half angle sharp nose cone at subsonic and transonic speeds in the AEDC Tunnels A and 4T. The performance of a single and triple row of disks, #60 carborundum grit in a random and prescribed pattern, and two-dimensional wire loops were evaluated. The trips were located 16 inches from the tip of the cone where the undisturbed

laminar boundary layer thickness was about 0.050 inches. The primary device for detecting the onset and end of transition were surface mounted constant temperature hot film anemometers. In addition, boundary layer pitot pressure surveys, model surface pressure and temperature distributions, flush mounted acoustic gage, and free-stream pitot acoustic and constant hot wire anemometer data were obtained to support the analysis.

The critical roughness Reynolds number for which the trip effectively moved transition to the trip location ( $x_k$ ) was determined by plotting the experimentally defined transition location ( $x_t$ ) on the model as a function of the free-stream Reynolds number as shown in Fig.16. Once the locus of transition locations was determined, a straight line was drawn through the points to the model station coinciding with the trip location. Typical results for various disk and grit samples are illustrated in Fig.17. The carborundum grit was applied in a random dense pattern and in a carefully spaced pattern. The randomly spaced grit produced a slightly lower critical Reynolds number than the carefully spaced grit. However, it was noted following the removal of the trip from the model that some of the tripping elements were missing from the carefully spaced grit trip. Therefore, the apparent decrease in trip effectiveness may have been the result of the lack of a sufficient number of tripping elements. The durability of carborundum trips during testing highlights one of the difficulties of carborundum grit trips, in addition to the difficulty of defining the effective trip height. The disks trips produced as low a critical Reynolds number as the grit trips. The advantage of using the disks is that their geometry (trip height and spacing of the elements) is well defined and durable. At subsonic and transonic speeds a single row of disks was as effective as multiple rows of disks.

The results of the trip studies were correlated with the local Mach number that would exist in an undisturbed laminar layer at the top of the tripping element,  $M_k$ , as shown in Fig.18. For comparison, the traditional Braslow-Knox criteria (Ref. 2) defines the critical roughness Reynolds number as

$$Re_k = \rho_k u_k k / \mu_k$$

and it is assumed to vary with the local Mach number at the edge of the boundary-layer,  $M_E$ . The Potter-Whitfield (Ref. 3) correlation defines the critical trip Reynolds number as

$$Re_k' = Re_k (T_k / T_w)^{0.5} + 0.5$$

Both correlations can be redefined in terms of the free stream Reynolds number and edge Mach number as

$$Re_k' = Re_\infty (M_k / M_E) (T_k / T_w)^{0.5} + 0.5, \text{ Braslow-Knox}$$

$$Re_k' = Re_\infty (M_k / M_E) (T_k / T_w)^{0.5} + 0.5, \text{ Potter-Whitfield}$$

The critical trip Reynolds number for the distributed grit was estimated to be 600 from the Braslow-Knox criteria and 800 for the Potter-Whitfield criteria for Mach numbers less than 2. As seen from the correlation shown in Fig. 18 these values are very conservative for subsonic and transonic conditions; that is the recommended trips are too large. Additional data obtained from a few other sources is also included in Fig. 18. It is seen in Fig. 18 that multiple rows of tripping elements are no more effective than a single row in transonic flows, but do become important in supersonic flows.

The mean velocity distribution in the boundary layer downstream of the tripping elements was compared with the classical law of the wall and logarithmic velocity profiles for a turbulent boundary layer. A typical result is shown in Fig. 19 for a disk trip. It is seen that immediately behind the trip ( $x_s = 17.5$  in) the velocity profile is representative of a transitional profile whereas further downstream the mean velocity distribution transitions into a fully developed turbulent profile. Correspondingly, the Reynolds shear stress distribution in the fully transitioned boundary layer downstream of the trips reflects the same behavior as a naturally transitioned turbulent boundary layer as demonstrated in Fig. 20. Consequently, similar to the isolated roughness element,



distributed three-dimensional tripping elements in the absence of a pressure gradient produce the same type of turbulent boundary layer as natural transition.

The effect of the three-dimensional tripping elements on the boundary layer properties downstream of the trips is summarized in Fig. 21. It is seen that for those tripping elements that were effective in causing early transition of the boundary layer, the displacement thickness,  $\delta^*$ , and momentum thickness,  $\theta$ , exhibit the typical overthickening caused by a tripping element. Also there is no noticeable difference in the boundary layer properties because of the difference in the tripping elements. It is interesting to note that the shape factor,  $H = \delta^*/\theta$ , reverts to the natural transition value, although in a shorter distance. As mentioned in Section 4.9.2 the shape factor is the least controllable of the boundary layer parameters, but fortuitously may be the easiest parameter to duplicate full scale values.

### Suction/Blowing Heat Transfer, and Compliant Surfaces

It is well known that mass or heat transfer at a surface can have a strong effect on the stability of a laminar boundary layer. Consequently, these are potential mechanisms for controlling transition location in a subscale experiment. To date, the majority of research performed in the areas of mass and heat transfer at a surface has had the objective of delaying transition for laminar flow control. Hence, little information is available in the use of these techniques as a boundary layer tripping device. However, if one maintains the broader perspective of boundary layer manipulation to also include the possibility that it may be required to delay transition in a scale test, then there may even be more utility in the mass and heat transfer techniques.

Following Liepmann Brown, and Nosenchuck (Ref.15) the relative effects of various parameters within the boundary layer can be seen from the boundary layer momentum equation written in the form

$$\rho u u_x + \rho v u_y + p_x - \mu_T u_{yy} = \mu u_{yy}$$

The effect of surface heating in a gas for which  $\mu_T > 0$  is such that at the wall  $u_{yy} > 0$ , and hence must lead to an inflection point in  $u(y)$ , and therefore increased instability. Cooling has the opposite effect, and in liquids, for which usually  $\mu_T > 0$ , heating stabilizes and cooling destabilizes the boundary layer. The equivalence of the term  $\mu_T \gamma_{uy}$  and of an effective  $p_x$  has been used to demonstrate the relation between surface heating and stability (Liepmann and Fila, Ref. 16). For example, heating the surface in a gas has roughly the same effect as an adverse pressure gradient.

Similarly, the term can be locally interpreted as a nonvanishing  $\rho v u_y$  at the surface. Consequently, in a gas, cooling and heating of the surface is roughly equivalent to suction and blowing or negative and positive surface displacements of a compliant surface, respectively, with

$$v_n = - \frac{1}{\rho} \frac{dp}{dT} \frac{dT}{dy}$$

For water, the role of cooling and heating are reversed.

The influence on stability for these various techniques is manifested through a change of the inflection point of the boundary layer profile. For example, for a gas, cooling the surface, suction, or negative surface displacement will move the inflection point of the boundary layer closer to the surface making the boundary layer less responsive to the Tollmien-Schlichting waves and hence more stable.

Experiments representative of these effects have been performed by Saarić and Reed (Ref.17) for the effect of weak mass injection on boundary layer transition. They used porous titanium and Dynapore panels inserted in a flat plate and introduced disturbances to the boundary layer with a vibrating ribbon. The mean and disturbance-flow velocities were measured with a hot wire anemometer.

The integrated disturbance amplitude for two different porosity arrangements are shown in Figs. 22a and b. For the results shown in Fig. 21a, a dimensionless disturbance frequency of  $F = 20$  was introduced into the boundary layer with one porous strip open on the panel. The average suction velocity over the strip was  $5.5 \times 10^{-3} U_\infty$  where  $U_\infty = 14$  m/s. In Fig. 22b, seven strips were open on an upstream porous panel and two more porous strips were open on a downstream panel. The total mass flow rate is the same as for the single porous strip. The experimental results agree well with the linearized triple-deck stability analysis of Reed and Nayfeh (Ref. 18) which also provides a suction optimization scheme. The optimization scheme supported by these experiments suggest the suction should be concentrated near the  $R_1$  branch of the neutral stability curve for efficiency.

The influence of the porous strips on transition Reynolds number is shown in Fig. 23. Both the one-strip and seven-strip cases are included to show the effect of local blowing velocity on the stability characteristics; i.e., average mass flow rate is constant, but the one-strip case has seven times the local blowing velocity of the seven-strip case. For the no-blowing case, a disturbance frequency  $F=20$  was introduced and transition was forced at  $x = 280$  mm with  $Re = 2.4 \times 10^6$ . As clearly seen, suction delays transition and increased suction rates do not appear to induce large local hole effects. Conversely, small blowing does not introduce any catastrophic behavior either - just an orderly forward shift in transition location. Unfortunately, measurements of the downstream boundary layer properties after transition are not presented, hence the quality of the transitioned boundary layers cannot be examined.

A word of caution is necessary here. For flow over a swept three-dimensional wing flow with crossflow, the use of slot or porous plate suction may disrupt the crossflow in the boundary layer hence deleteriously effecting the simulation. This may be most apparent if crossflow-instability or leading edge contamination are the primary mechanisms for transition in the boundary layer.

#### Wave Superposition Principles

A new technique that may be used to control transition is the principle of wave superposition. These techniques were pioneered by Llepmann, Brown, and Hosenchuck (Refs. 15 and 19). Additional experiments have been performed by Thomas (Ref. 20). The wave superposition principle is premised on the introduction of Tollmien-Schlichting waves with controlled amplitude and phase to interact with other disturbances that may grow and lead to transition. By phasing the generated disturbances with existing disturbances, the instabilities can be enhanced leading to early transition. Similarly, by generating equal amplitude waves antiphased to the existing disturbances it is possible to disrupt the growth of the instabilities and delay transition. It is this latter approach that has been explored because of the potential for laminar flow control.

The experiments of Refs. 15 and 19 used flush mounted heater strips to excite instability waves in a laminar boundary layer on a flat plate in a water tunnel. Similar heating strips were located downstream in order to excite the control disturbances. It was demonstrated that using a feedback loop activated by measured wall shear stress it was possible to reduce the amplitude of naturally occurring instability waves. A significant increase in the transition Reynolds number was achieved. One important feature of this technique is that the velocity profiles are not affected, just the instability waves. Using surface strip heaters is very effective in water because of the very good thermal coupling that can be achieved with water and the strong temperature dependency of the viscosity.

Thomas (Ref. 20) performed similar experiments except he used vibrating ribbons to excite the flow of air in a wind tunnel. The spectra of the fluctuations corresponding to a normalized wave frequency of  $F = 110$  are shown in Fig. 24 at a location corresponding to  $R_{x1}$ . When only the first ribbon is used it can be seen that the spectrum of the velocity fluctuations has a broadband character with a readily

identifiable peak at 80 Hz. A broadband peak centered around 40 Hz can also be identified along with a similar peak at 120 Hz. Evidently, for this particular case, transition is taking place by a subharmonic wave interaction. The spectral levels are dramatically reduced when the second ribbon is in operation, and the spectrum is very similar to that which is obtained if no excitation is present on either ribbon. An exception can be seen around 80 Hz where some energy still remains that would otherwise not be present. These data therefore show that delays of transition have been achieved, but that it is not possible to return the flow completely to its base state with the superposition scheme.

The wave superposition principle has been demonstrated to influence transition on a flat plate, but to date most of the experiments have been aimed at transition delay, not early transition as typically required for viscous simulation. Also no experimental information on the boundary layer parameters downstream of transition have been presented. An open question about practical applications is the effectiveness of this concept when the initial disturbances enter the boundary layer over a region or some receptance area around and near a leading edge and not at a discrete point as in the experiments to date. In addition, the applications in three-dimensions have not been explored at all.

#### 4.9.3.2 Viscous Parameter Control Techniques

It is evident from the discussions of Sections 4.3 and 4.5 that boundary layer tripping alone will not create a proper viscous simulation. Consequently, consideration must also be given to boundary layer manipulation techniques that control the development of the boundary layer parameters of the model surface. The most obvious techniques for such control are distributed blowing or suction and distributed heating or cooling of the surface. Of these, blowing and suction at the surface probably has the best means for direct control of the viscous parameters. It is obvious that the boundary layer thickness and displacement thickness in a scaled boundary layer are always too thick and the removal of mass in the boundary layer can be effective in reducing these thicknesses. Green (Ref. 21) and Bore (Ref. 22) illustrated through simple numerical simulations that distributed suction could effectively control the development of the displacement thickness and shape factor to essentially duplicate full scale conditions. Examples from Green's calculations for localized and distributed suction are shown in Figs. 25 and 26. Although localized suction could be used to control the shape factor over the aft part of the airfoil, distributed suction was required to simultaneously control the shape factor and displacement thickness. Consequently distributed suction appears to be a viable boundary layer manipulation technique that can be used to simulate various viscous parameters. Although adding provisions for boundary layer suction appears to add a significant complication to the testing process, significant advances have been made in the practical applications of these techniques in the development of laminar flow control (e.g., Ref. 23) and shock/boundary layer interaction control (Ref. 24). What has to be done is to perform experiments using similar mechanical devices to try to control the important viscous parameters.

#### 4.9.4 Viscous Parameter Measurement Techniques

The primary viscous parameter to be routinely measured in a wind tunnel test is the transition location. The basic techniques for transition detection can be divided into three general categories:

1. surface sensor techniques such as heat transfer measurements,
2. visualization techniques such as sublimation observations, and
3. optical techniques such as shadowgraph images and laser interferometry.

These categories are usually distinct, although the second and third divisions are nominally similar.

Measuring techniques used to detect transition differ in sensitivity to each of the various aspects involved in the physical mechanisms of the transition process. Generally, two detection techniques applied to the same boundary layer will yield slightly different indications of transition, because each is dependent upon, or at least emphasizes, a different flow parameter. For example, the



optical method based upon shadowgraphs and the sensor method based upon the variation in the measured heat transfer distribution may yield somewhat different indications of transition location. This follows from the fact that the shadowgraph is sensitive to changes in density gradients as the flow becomes turbulent and is a record of the boundary layer at an instant in time; whereas, the heat transfer measurement tends to be a time averaged value sensitive to the average change in heat flux level transmitted to the model surface by the laminar and turbulent flows. In addition, each of these two sets of results is somewhat subject to individual interpretation.

The surface sensor techniques include thermocouples and/or heat transfer gages, surface mounted heat film gages, dynamic pressure transducers, acoustic monitors, laser heated slugs, pitot pressure probes, and anemometer probes. Each of these techniques has been shown to be useful in determining transition and the basic principles underlying their application are well understood. Consequently there is no need for a major research program to improve on these techniques. Care in the application and interpretation of any one technique will provide useful information on transition.

The gages, transducers, and slugs are limited as to the area of a model surface that they can monitor because of restrictions imposed by the sensor size and model geometries. This may be overcome, in part, by causing transition to move along the model, usually by changing the wind tunnel unit Reynolds number by altering tunnel stagnation pressure. Probes, on the other hand, may be moved along the model surface while tunnel conditions are maintained at a nominally constant level. However, probes may under certain conditions alter the flow field under investigation by their presence. In either case, considerable attention must be paid to model and test installation design before the experiments are performed and the application of these techniques is generally a unique installation for each model tested.

The visualization techniques include sublimation, evaporation, thermographic phosphors, and infrared scanning. These methods are used to observe flow patterns on a surface area at a single test condition and require documentation by photographs or video recording after allowing the selected medium sufficient time to conform to the flow pattern details. The sublimation and evaporation techniques are frequently used but unfortunately require recoating for each test condition and hence only a few selected conditions are ever evaluated in a test program. The thermographic phosphors and infrared scanning techniques are based on the differences in heat transfer between a laminar boundary layer and a turbulent boundary layer. In supersonic flow the temperature gradients through transition are sufficiently large that these techniques are effective. However, in transonic flow the temperature gradient between laminar and turbulent flow is very small and hard to detect. Also provisions must be made to insulate the model surface to avoid model temperature transients as the tunnel environment and model heat up. There has been, however, sufficient promise shown for the thermographic phosphors and infrared scanning techniques in the transonic regime that further research is warranted.

For high Reynolds number wind tunnels, additional problems arise. Because of model surface finish requirements at high Reynolds numbers it is essentially mandatory for non-intrusive optical techniques to be used to determine transition. One such approach is infrared thermography, but fundamental and practical limitations appear to prevent its use for transition detection in a high Reynolds number facility such as the National Transonic Facility (NTF) or the Köln Kryo-Kanal (KKK). The calculated range of temperature change across the transition region on a model transport wing at transonic Mach numbers is illustrated in Fig. 27 from Ref. 25. It is seen that the temperature changes associated with transition in conventional wind tunnels, in which only marginal results have been obtained, are far larger than those at conditions of interest in a high Reynolds number facility. An innovative alternative is needed, perhaps based on properties of coherent light reflected from model surfaces or transmitted through the model boundary layer from sources in the model surface.

The optical techniques offer the great advantage of being non-intrusive and not requiring modification of the model. Schlieren and shadowgraph imagery have been applied many times and are

based on (1) observed turbulence in the boundary layer or the fading of the clearly defined attached laminar boundary layer on a model in a schlieren picture or (2) the change in growth rate in the observed boundary layer thickness. There is, therefore, a chance for large uncertainties associated with interpretation and these techniques can only be applied to simple bodies since the view must be tangent to the body surface.

A scanning laser interferometer offers the promise of being the ideal transition detection device in that it is noninterfering, does not require modification of the model, and interpretation is perhaps more straight forward. The technique is based on the observation that turbulence in a boundary layer produces high frequency shifts in the interferometric fringes created by the integrated density fluctuations along the path of a beam of coherent light passing through the boundary layer. Two approaches are presently available for studies to prove the principle underlying this technique: (1) a single point probe which can be mounted on a traversing mechanism to survey along a model surface and (2) a probe that optically scans along a model surface. The instrumentation for the scanning model provides a real time display of the boundary layer status along a length of model surface, or discrete locations along the surface can be selected for frequency measurements. This approach can be used viewing the surface either tangentially or vertically. Clearly, further research should be devoted to the development and verification of these laser interferometric techniques.

Viscous parameter measurement implies, in addition to the traditional transition detection, the need for monitoring the essential viscous parameters at critical locations. The trailing edge pressure coefficient and even the trailing edge boundary layer distribution can be routinely measured in a test program. However, much more difficult is the determination of the viscous parameters at the shock location, at incipient separation, or the location and extent of separated regions. Most conventional probing techniques have a high probability of interfering with the sensitive nature of the flow field. Laser velocimetry offers an opportunity for nonintrusive measurements in the boundary layer but are not easily applied for routine testing. Perhaps the only practical techniques for future application will be the inference of the viscous parameters through computations based on limited measurements such as the transition location and trailing edge pressure. Based on the determination of the most important viscous parameters to be simulated, this computational approach opens up an entire new area for research to develop valid correlation techniques.

#### 4.9.5 Recommended Research

As a result of the review of boundary layer manipulation techniques the following research activities are suggested:

1. The single most important research to be done is to identify which of the viscous parameters so far identified in Chapter 4 that must be controlled at critical locations on the model in a subscale experiment to allow correct extrapolation to full scale conditions. These parameters must be defined for each type of fundamental test requirement, e.g., cruise drag, buffet boundary, vortex shedding, post stall performance, etc.
2. Based on the criteria developed in 1) boundary layer manipulation techniques must be developed that will produce the desired control of the relevant parameters. The primary candidates for further development are boundary layer tripping and boundary layer suction. The research should explore the effectiveness of boundary layer manipulation devices for families of favorable and adverse pressure gradients. Correlations should be developed to define the boundary layer parameters such as  $H$ ,  $\delta^*$ , or  $\theta$  that will occur downstream of the boundary layer manipulation device. These correlations will be the basis for selecting a boundary layer manipulation device to produce the desired effect defined in 1).
3. Research needs to be performed to determine the flow structures in a transitioned boundary layer downstream of a cross-flow instability or leading edge contamination induced

transition. These flow features need to be compared with the flow features downstream of the boundary layer manipulation devices examined in 2) to evaluate the adequacy of conventional tripping in simulating other than streamwise instability induced transition.

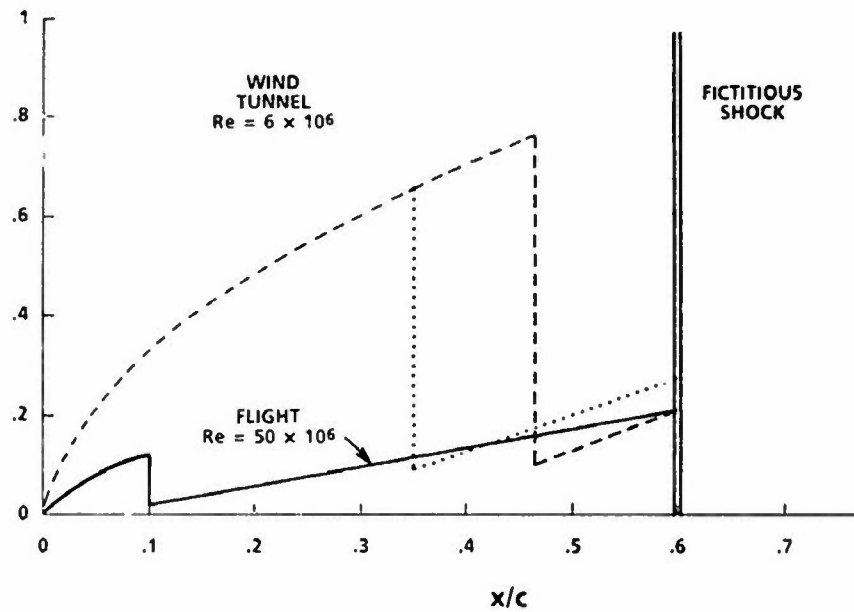
4. The use of CFD in extrapolating the Reynolds number sensitive parameters from the subscale to the full scale conditions must be explored in conjunction with the boundary layer state that will be determined in the wind tunnel as a result of applications of 2).
5. Nonintrusive boundary layer measurement techniques must be developed to the point of practical application. The use of laser interferometry to determine transition location should be further developed. In addition, the use of CFD to infer viscous parameters that cannot be easily measured should be explored.

#### REFERENCES

1. Khan, Mohammad M. S., and Cahill, Jones F. "New Considerations on Scale Extrapolation of Wing Pressure Distributions Affected by Transonic Shock Induced Separation," Lockheed Georgia Company LG 83ER0055, March 1983.
2. Eraslow, Albert L. and Knox, Eugene C. "Simplified Method for Determination of Critical Height of Distributed Roughness Particles for Boundary-Layer Transition at Mach Numbers from 0 to 5," NACA TN 4363, Langley Aeronautical Laboratory, September 1958.
3. Potter, L. Leith and Whitfield, Jack D. "Effects of Unit Reynolds Number, Nose Bluntness, and Roughness on Boundary Layer Transition," AEDC-TR-605, March 1960.
4. Poll D.L.A. "Transition in the Infinite Swept Attachment Line Boundary Layer," the Aeronautical Quarterly, Vol. XXX, November 1979, pp. 607-629.
5. Arnal, D., Coustols, E., and Juillen, J. C. "Etude experimentale et theorique de la transition sure une aile en fleche infinie," La Recherche Aerospatiale, No. 4, 1984, pp. 275-290.
6. Klebanoff, P. S. and Tidstrom, K. D. "Mechanism by Which a Two-Dimensional Roughness Element Induces Boundary-Layer Transition," The Physics of Fluids, Vol. 15, No. 7, July 1972, pp. 1173-1188.
7. Dryden, H. L. "Transition from Laminar to Turbulent Flow," Turbulent Flows and Heat Transfer, High Speed Aerodynamics and Jet Propulsion, C.C. Lin, editor, Princeton University Press, 1959.
8. Gregory, N. and Walker, W. S. "The Effect on Transition of Isolated Surface Excrescences in the Boundary Layer," ARC R&M No. 2779, 1956.
9. Tani, I., Komoda, A., Komatsu, Y., and Luchi, M. "Boundary Layer Transition by Isolated Roughness," Aero Research Institute, Tokyo University, Rept. No. 375, November 1962.
10. Arnal, D. "Description and Prediction of Transition in Two-Dimensional, Incompressible Flow," in AGARD Report No. 709.
11. Klebanoff, P. S., Cleveland, W. G., and Tidstrom, K. D. "On the Interaction of a Three-Dimensional Roughness Element with a Laminar Boundary Layer," AEDC-TR-87-7, March 1987.
12. Klebanoff, P. S., Tidstrom, K. D., and Sargent, L. M. "The Three Dimensional Nature of Boundary Layer Instability," Journal of Fluid Mechanics, Vol. 12, Part 1, January 1962.
13. Pirtlell, L. F., Klebanoff, P. S., and Buckley, F. T. "Turbulent Boundary Layer at Low Reynolds Number," Physics of Fluids, Vol. 24, May 1981, p. 802.
14. Sinclair, D. W. and Strike, W. T., Jr. "Boundary Layer Transition-Trip Study at Subsonic and Transonic Speeds in AEDC Tunnels A and 4T," unpublished internal AEDC report, 1986.
15. Liepmann, H. W., Brown, G. L., and Nosenchuck, D. M. "Control of Laminar-Instability Waves Using a New Technique," Journal of Fluid Mechanics, Vol. 118, 1982, pp. 187-200.
16. Liepmann, H. W. and Fila, G. H. "Investigation of Effects of Surface Temperature and Single Roughness Elements on Boundary Layer Transition," NACA Report No. 890, 1947.
17. Saric, W. S. and Reed, H. L. "Effects of Suction and Weak Mass Injection on Boundary-Layer Transition," AIAA Journal, Vol. 24, No. 3, March 1986, pp. 383-389.
18. Reed, H. L. and Nayfeh, A. H. "Numerical-Perturbation Technique for Stability of Flat Plate Boundary Layers with Suction," AIAA Journal, Vol. 24, No. 2, February 1986, pp. 208-214.

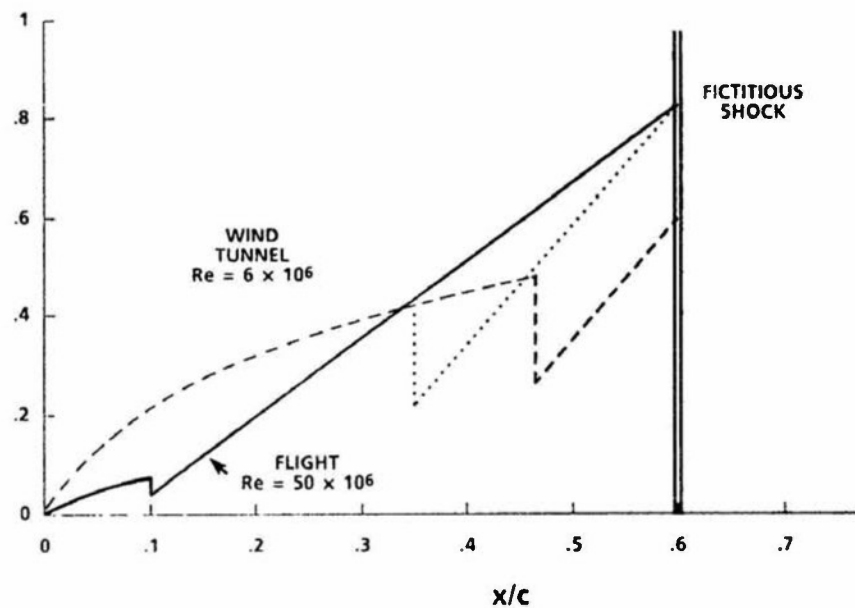
19. Liepmann, H. W. and Nosenchuck, D. M. "Active Control of Laminar-Turbulent Transition," Journal of Fluid Mechanics, Vol. 118, 1982, pp. 201-204.
20. Thomas, A.S.W. "The Control of Boundary-Layer Transition Using a Wave-Superposition Principle," Journal of Fluid Mechanics, Vol. 137, 1983, pp. 232-250.
21. Green, J. E. "Some Aspects of Viscous-Inviscid Interactions at Transonic Speeds and Their Dependence on Reynolds Number," in AGARD-CP-83, 1971, Paper No. 2.
22. Bore, C. L. "On the Possibility of Deducing High Reynolds Number Characteristics Using Boundary Layer Suction," in AGARD-CP-83, 1971, Paper No. 23.
23. Braslow, Albert L. and Fischer, Michael C. "Design Considerations for Application of Laminar Flow Control Systems to Transport Aircraft," in AGARD-R-723, 1985, Paper No. 4.
24. Krogmann, P. Stanewsky, E., and Thiede, P. "Effects of Suction on Shock/Boundary Layer Control and Shock-Induced Separation," Journal of Aircraft, Vol. 22, No. 1, 1985, pp. 37-42.
25. Fancher, M. F. "The Need for an Optical Transition Detection System in NTF," in NASA Conference Publication 2243, March 1962.

$$\delta^*(H_i - 1)/c \times 10^{-4}$$



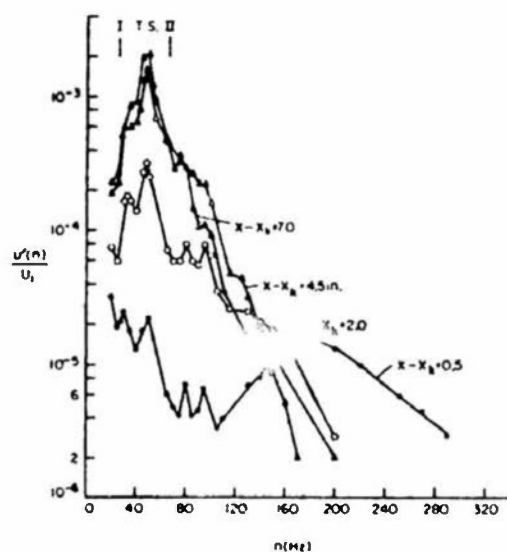
a. Shock / boundary layer interaction parameter.

$$\delta^*/c \times 10^{-4}$$

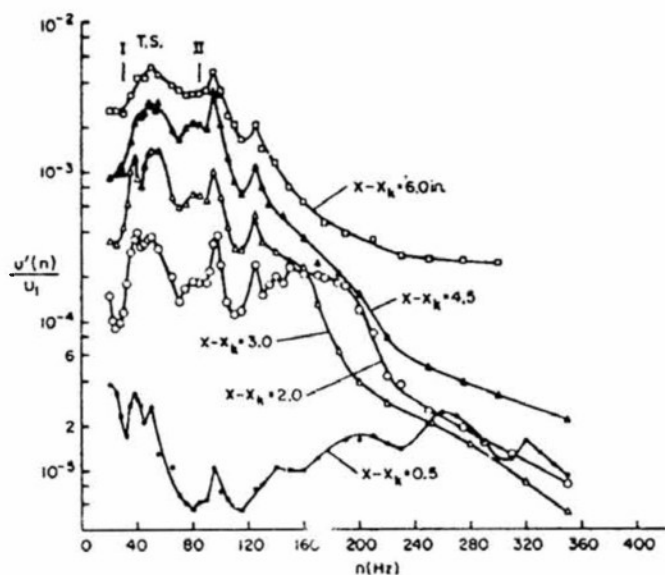


b. Displacement thickness.

Figure 1. Study of the interaction between shape factor and displacement thickness.



a.  $U_0/\nu = 1.16 \times 10^5 / \text{ft}$



b.  $U_0/\nu = 1.42 \times 10^5 / \text{ft}$

Figure 2. Spectra of velocity fluctuations downstream of a 0.066-in diameter roughness element at  $x_k = 2.0$  ft,  $y = 0.06$  in. (Ref. 6).

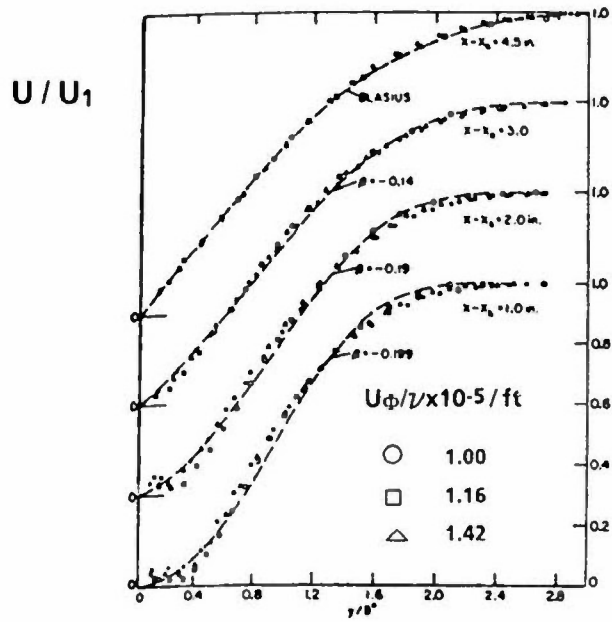


Figure 3. Mean velocity measurements downstream of a 0.066-in diameter roughness element compared with Hartree profiles. (Ref. 6).

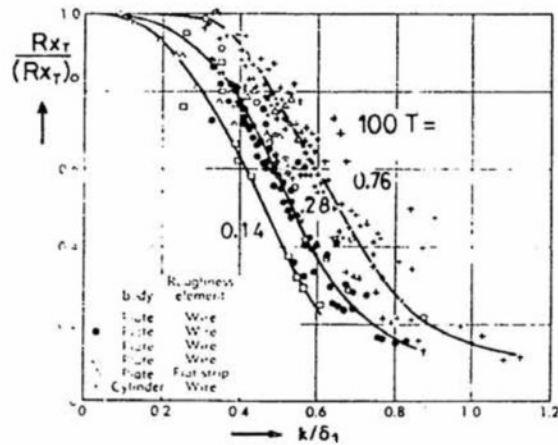


Figure 4. Correlation of transition Reynolds number with roughness elements for smooth plates. (Ref. 7).



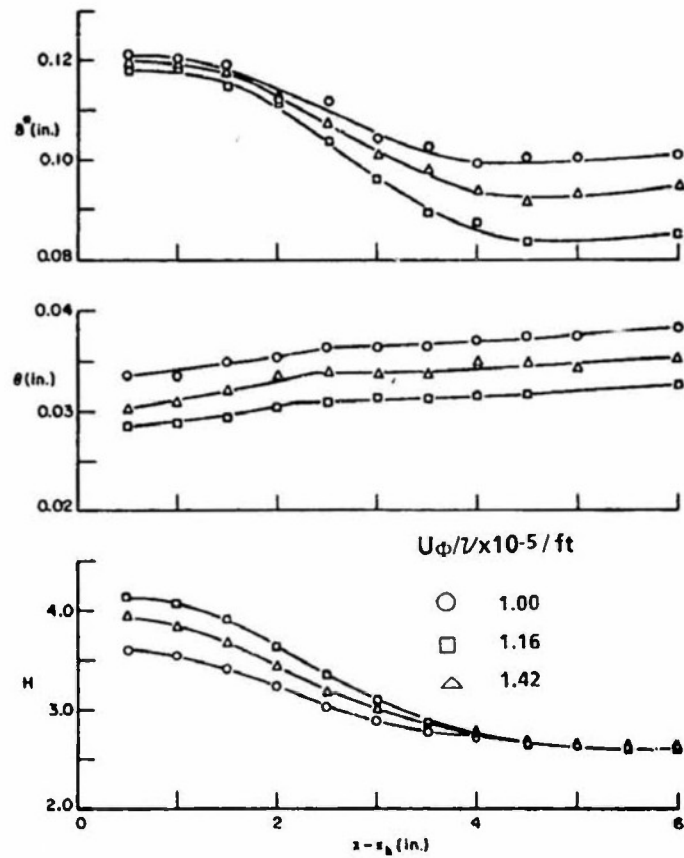


Figure 5. Distribution of boundary layer parameters downstream of a 0.066-in diameter roughness element. (Ref. 6).

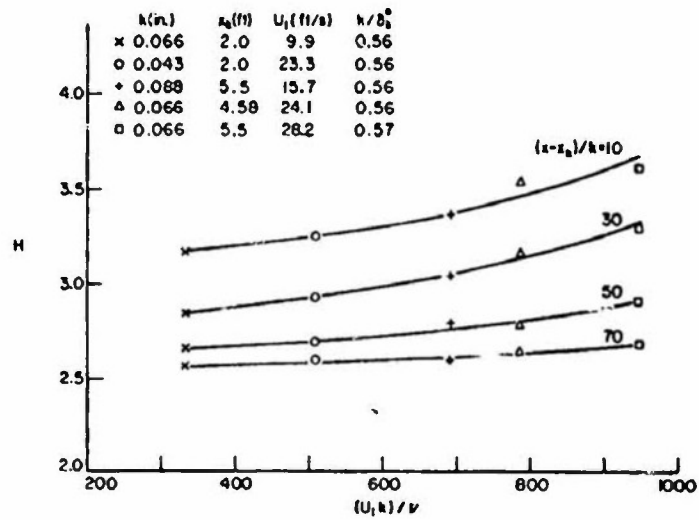
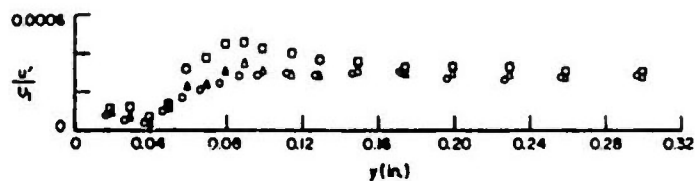
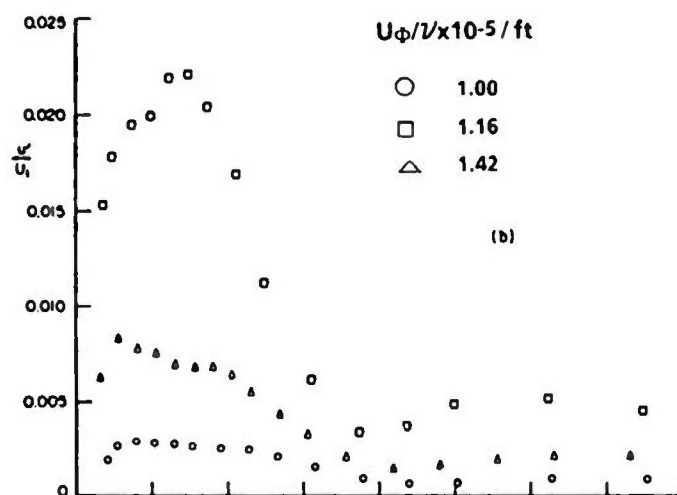


Figure 6. Variation of the shape parameter with roughness Reynolds number with  $k/\delta^*$  fixed. (Ref. 6).



a.  $x - x_k = 0.5$  in



b.  $x - x_k = 4.5$  in

Figure 7. Velocity fluctuation downstream of a 0.066-in diameter roughness element illustrating increase in amplification within the recovery zone. (Ref. 6).

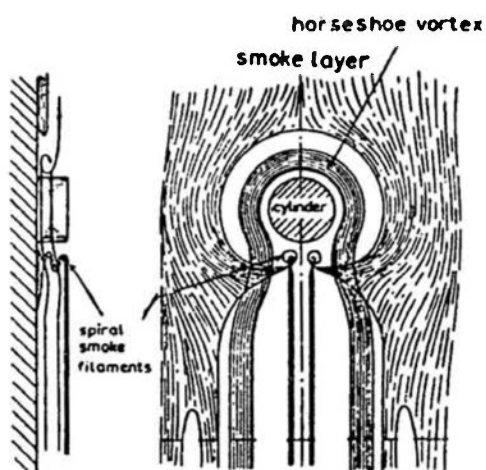


Figure 8. Representation of flow past a cylindrical roughness on a flat plate. (Ref. 8).

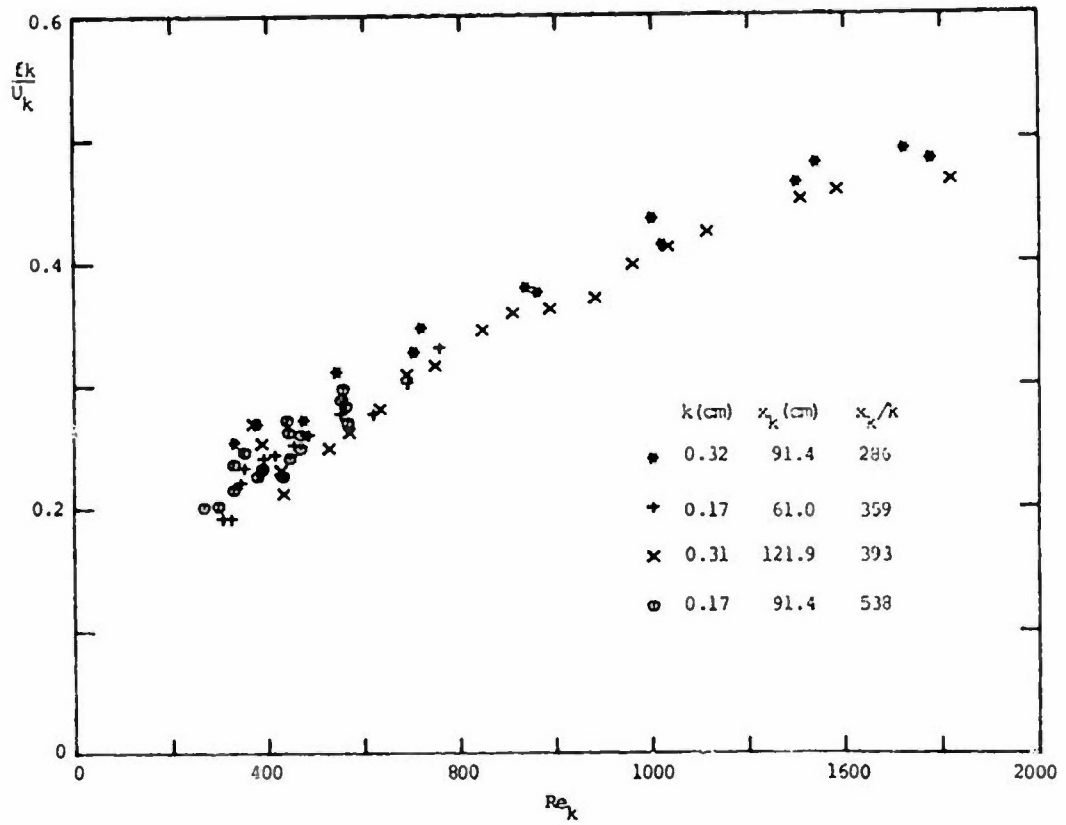
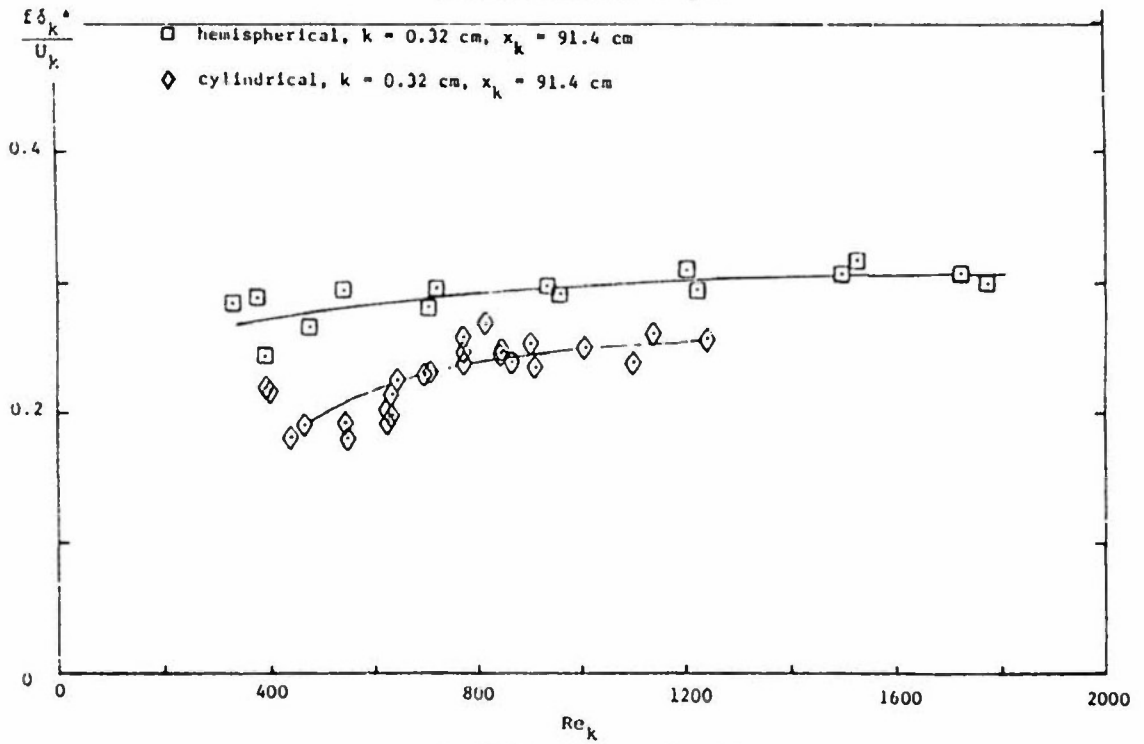
a.  $k$  as reference lengthb.  $\delta^*$  as reference length

Figure 9. Influence of tripping elements on Strouhal number. (Ref. 11).

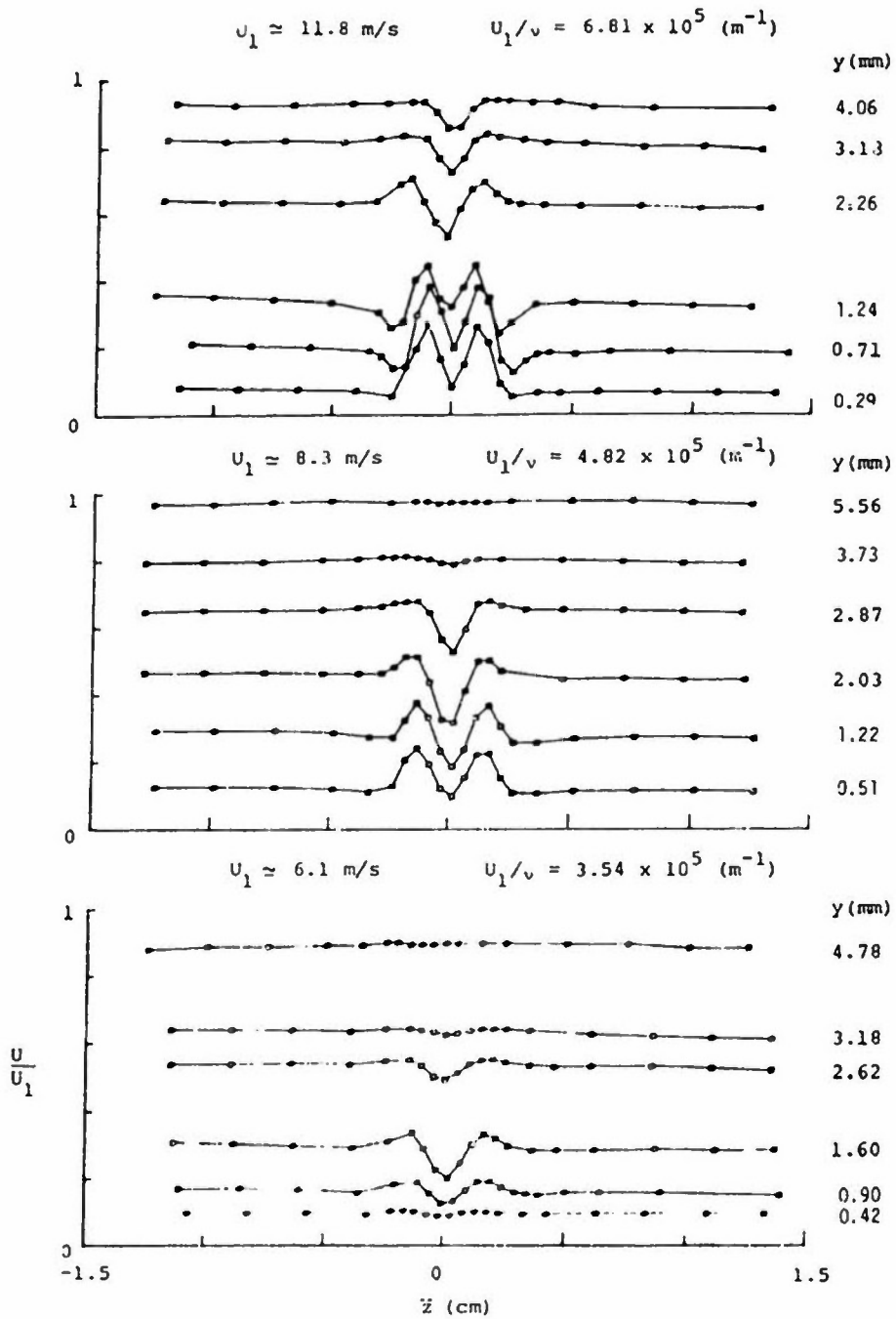


Figure 10. Spanwise distributions of mean velocity at various positions from the surface for varying unit Reynolds number;  $k = 1.7 \text{ mm}$ ,  $x_k = 91.4 \text{ cm}$ ,  $x = 2.54 \text{ cm}$ . (Ref. 11).

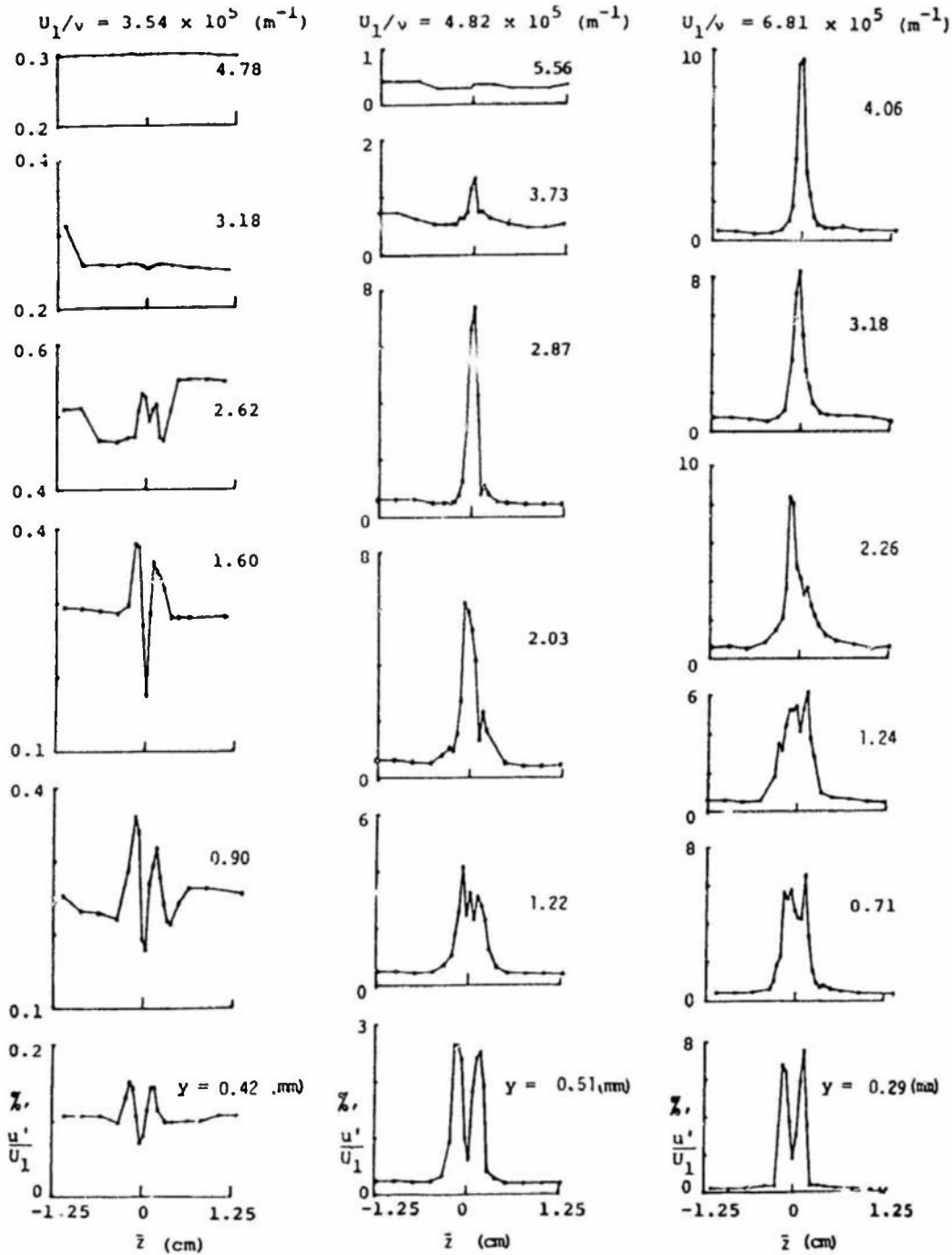


Figure 11. Spanwise distributions of the intensity of  $u$ -fluctuation at various positions from the surface for varying unit Reynolds number;  $k = 1.7 \text{ mm}$ ,  $x_k = 91.4 \text{ cm}$ ,  $x = 2.54 \text{ cm}$ . (Ref. 11).

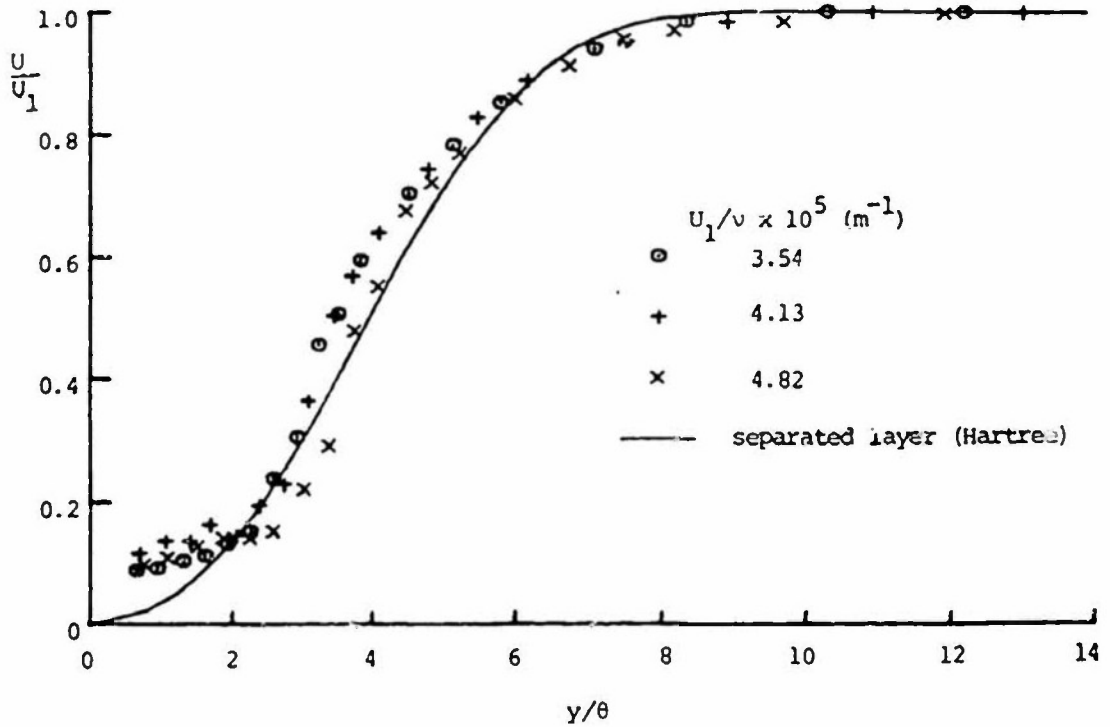


Figure 12. Comparison of mean-velocity profiles 1.27 cm downstream of a hemispherical roughness element with the separated Hartree profile,  $k = 1.7$  mm,  $x_k = 91.4$  cm, (Ref. 11).

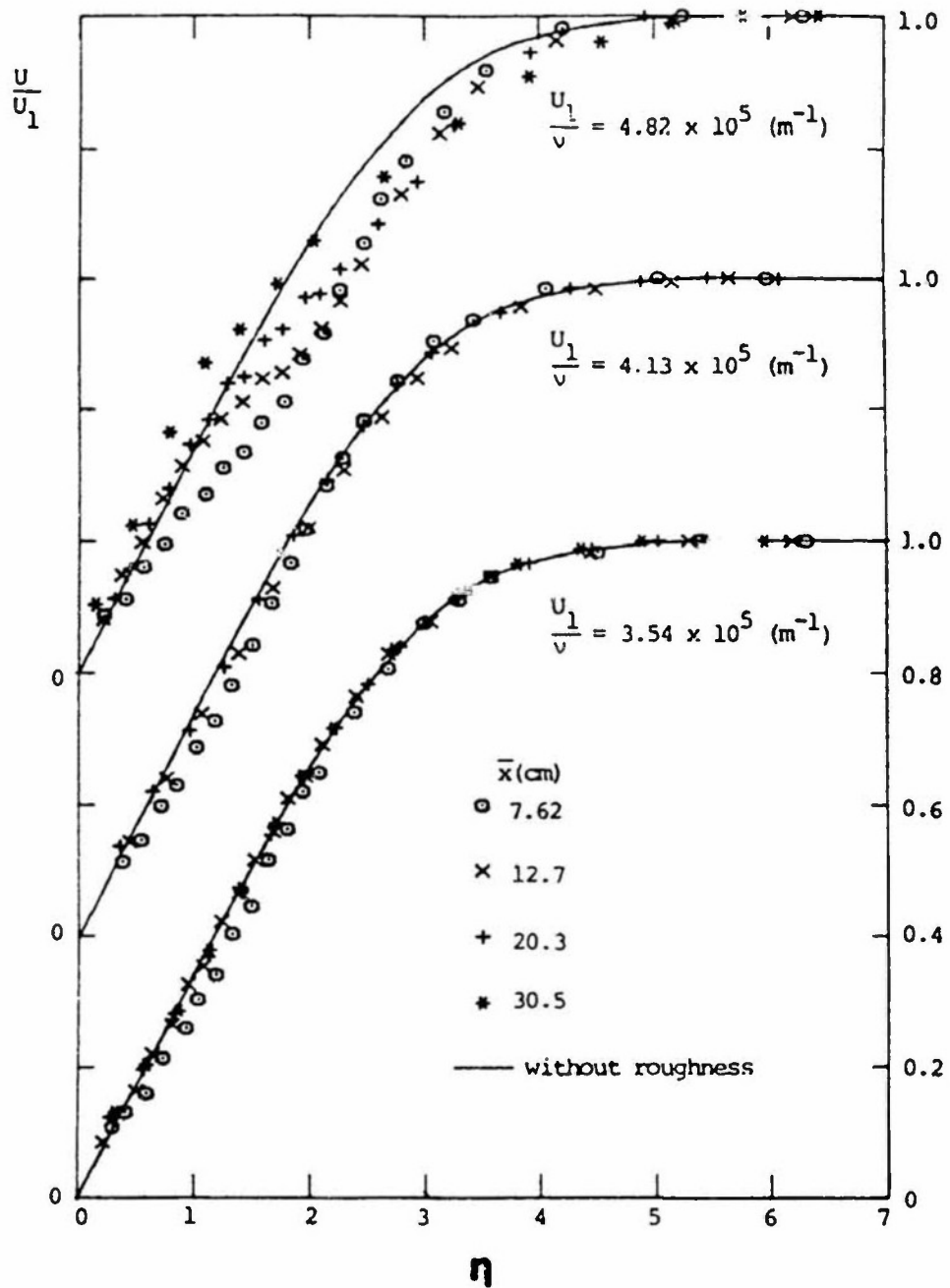


Figure 13. Comparison of mean-velocity profiles downstream of a hemispherical roughness element with the mean-velocity profile without roughness,  $k = 1.7$  mm,  $x_k = 91.4$  cm, (Ref. 11).



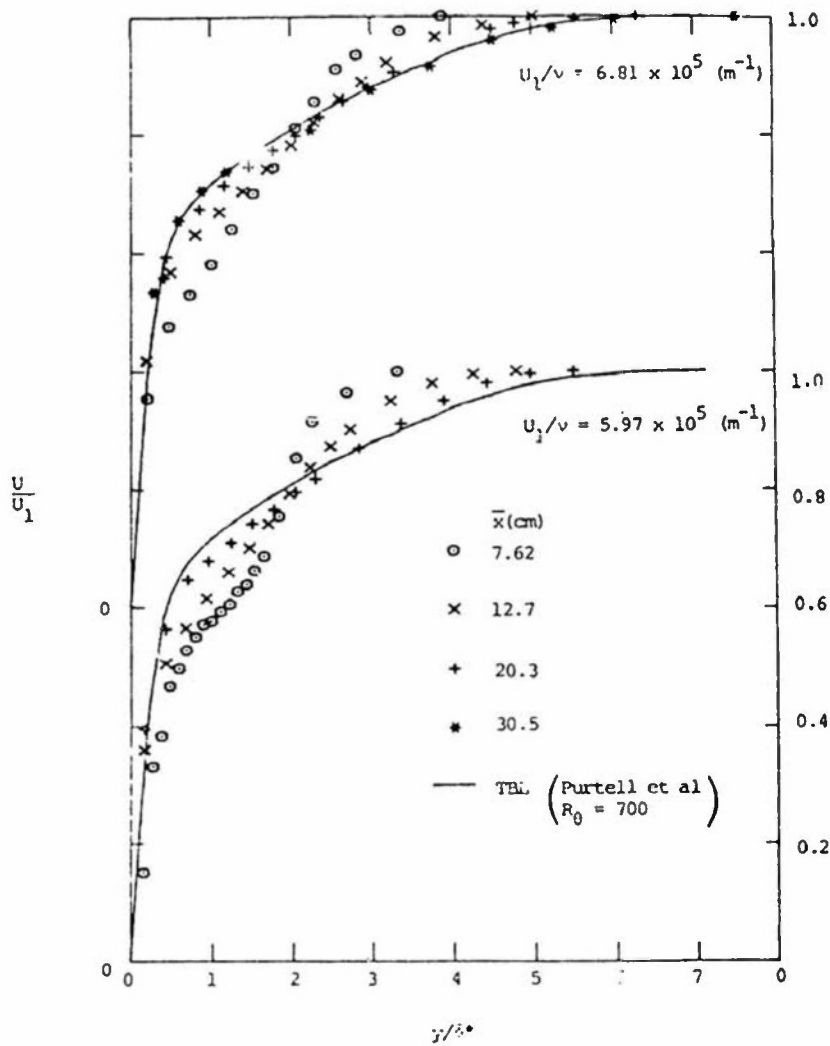


Figure 14. Comparison of mean-velocity profiles downstream of a hemispherical roughness element with the mean-velocity profile for fully developed turbulent boundary layer,  $k = 1.7 \text{ mm}$ ,  $x_k = 91.4 \text{ cm}$ , (Ref. 11).



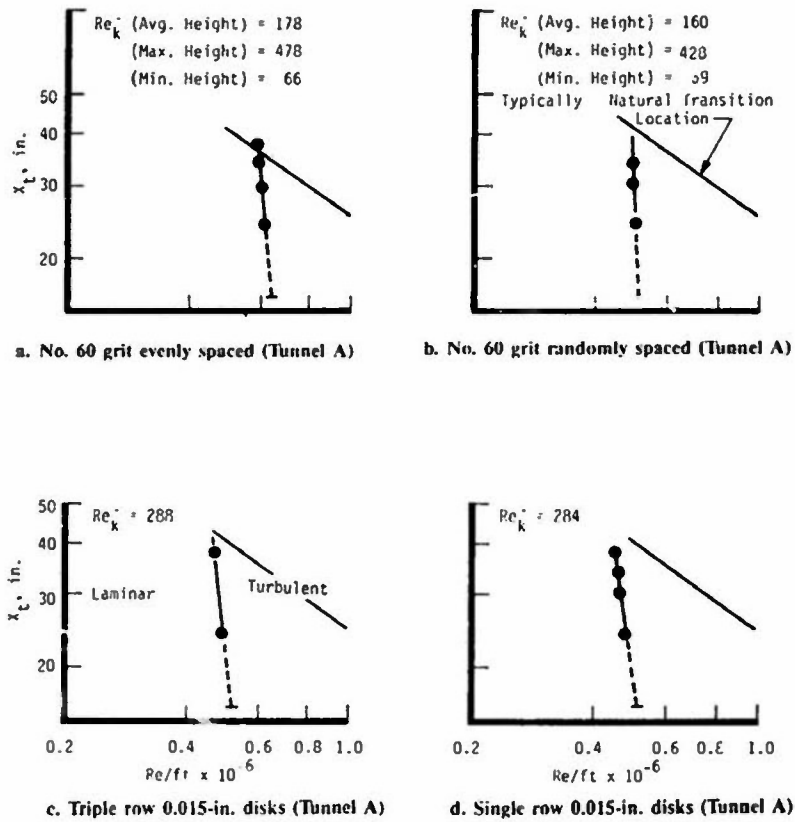


Figure 17. Transition locations of a tripped boundary layer on the cone. (Ref. 14).

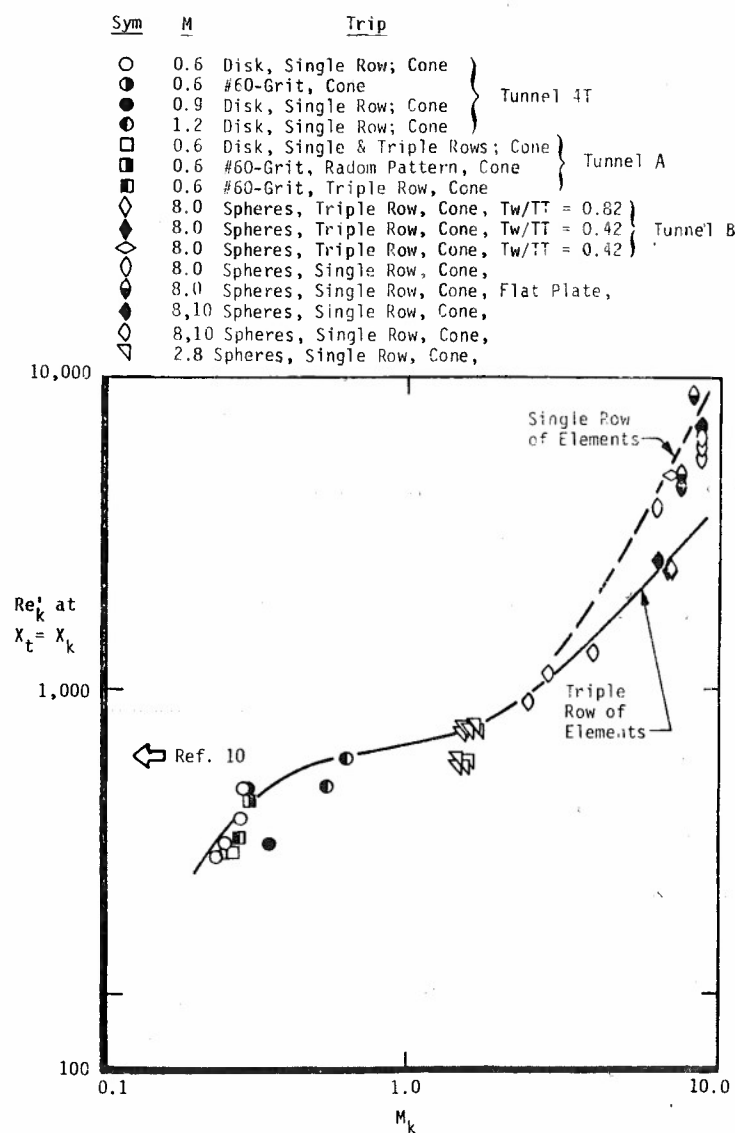


Figure 18. A correlation of the critical trip Reynolds number as a function of the local trip Mach number. (Ref. 14).

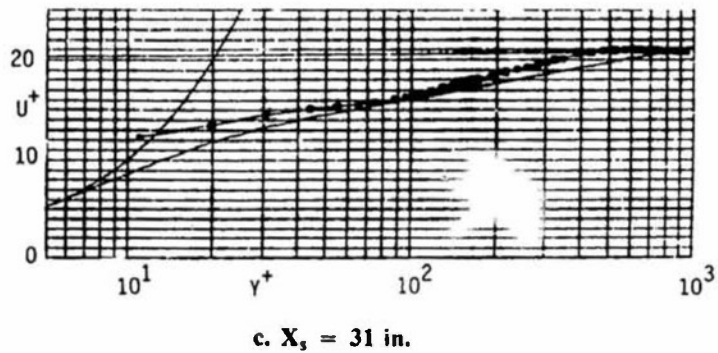
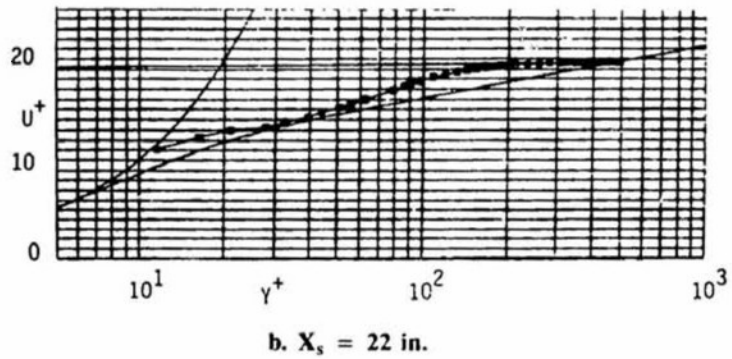
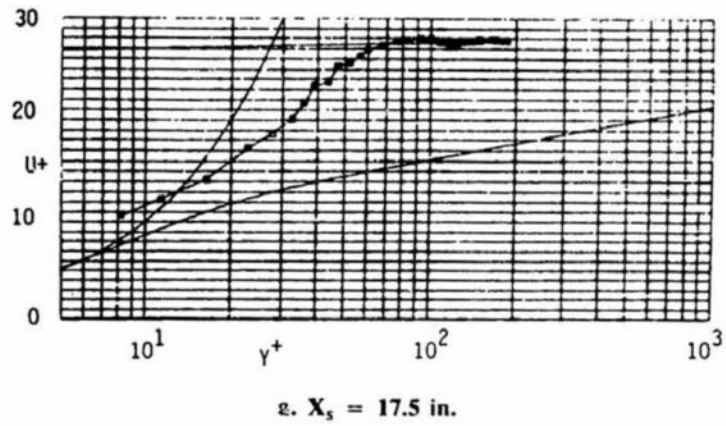
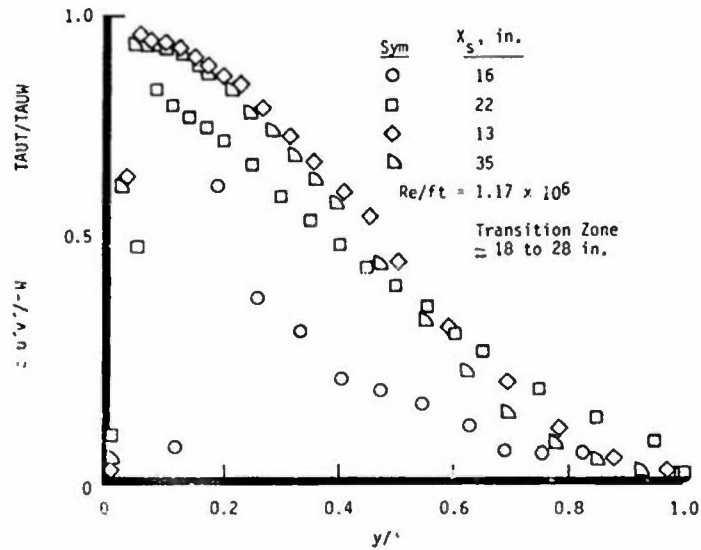


Figure 19. Velocity profiles downstream of a 0.015-in disk trip,  $M_\infty = 0.6$ ,  $Re/ft = 0.63 \times 10^6$ . (Ref. 14).



a. Natural transition

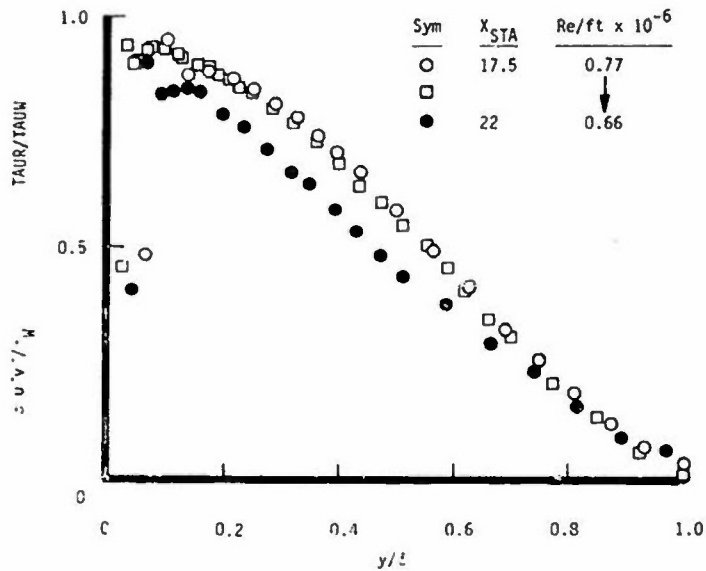
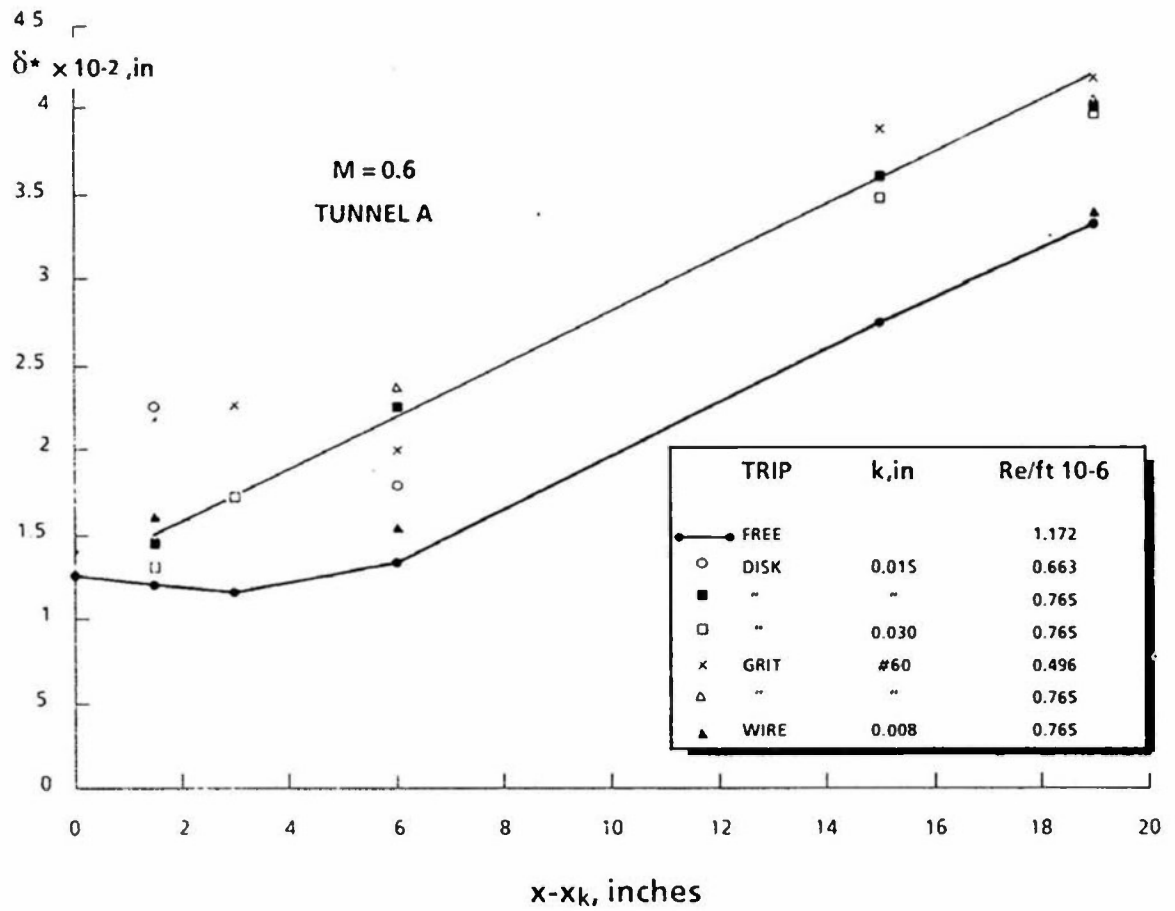
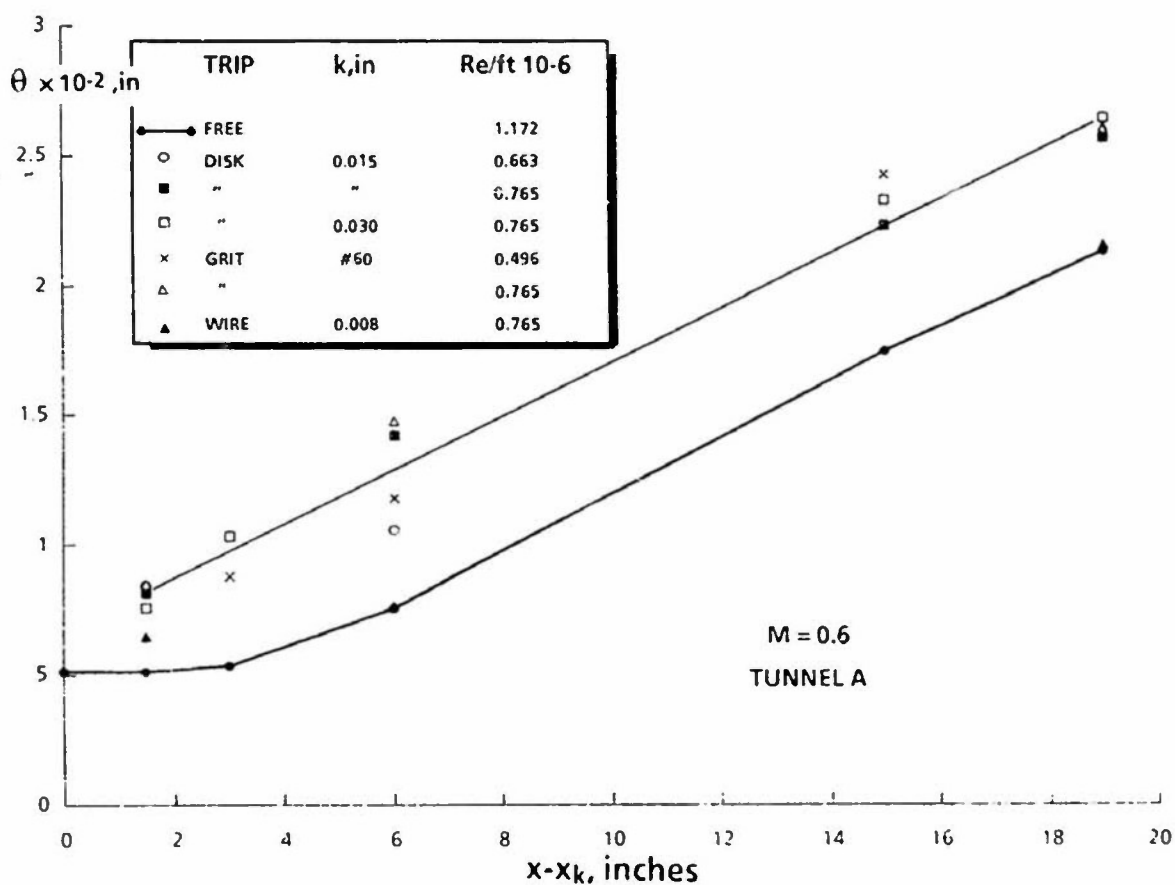
b. Single row of disks ( $k = 0.015$ ).

Figure 20. Shear stress distribution through the boundary layer downstream of a 0.015-in. disk trip at  $M = 0.60$ . (Ref. 14).

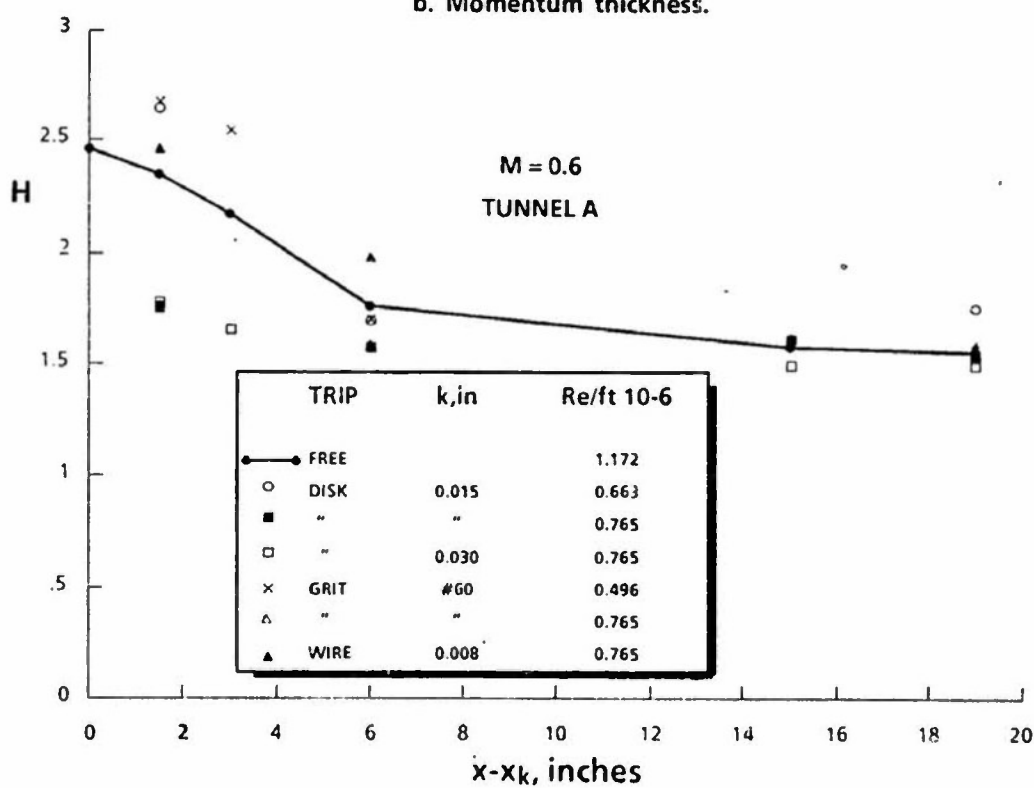


a. Displacement thickness.

Figure 21. Distribution of boundary layer properties downstream of tripping elements on a 7-deg cone at  $M = 0.60$ . (Ref. 14).



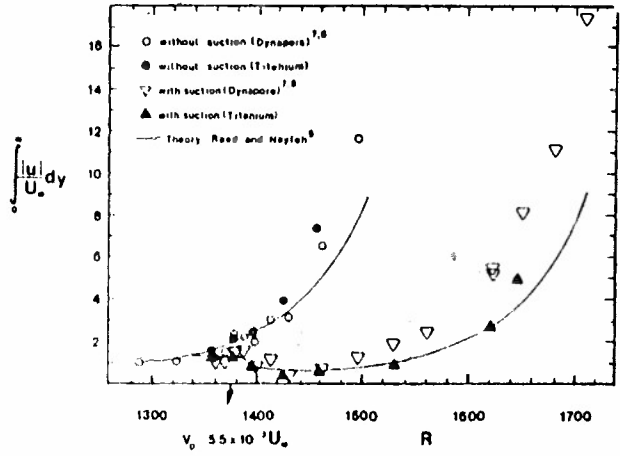
b. Momentum thickness.



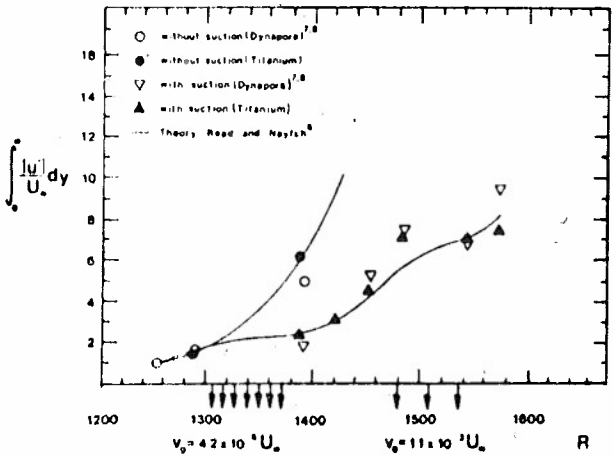
c. Shape factor.

Figure 21. Concluded.





a. Single strip,  $Re = 9.74 \times 10^5$ ,  $U_{\infty} = 14$  m/s,  $F = 20$ .



b. Multiple strips,  $Re = 9.24 \times 10^5$ ,  $U_{\infty} = 14$  m/s,  $F = 25$ .

Figure 22. Integrated disturbance amplitude for boundary layer suction. Strip locations and suction rates are indicated on the horizontal scales. (Ref. 17).

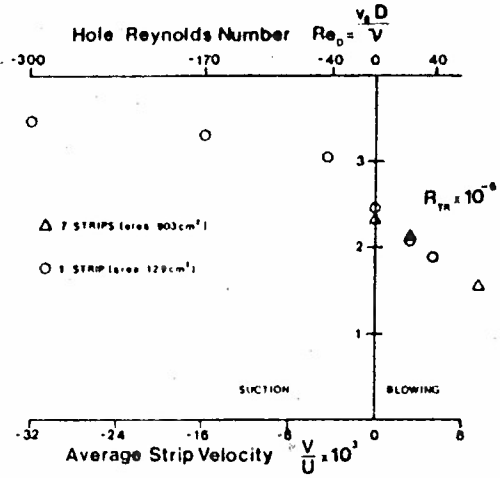


Figure 23. Effect of suction on transition Reynolds number. (Ref. 17).

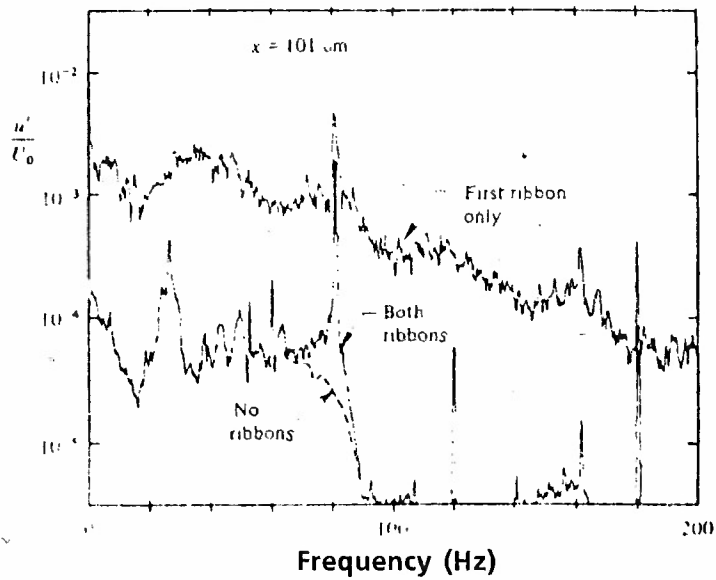


Figure 24. The spectrum of velocity fluctuations in the boundary layer for a wave frequency of  $F = 110$  arising from the first ribbon. (Ref. 20).

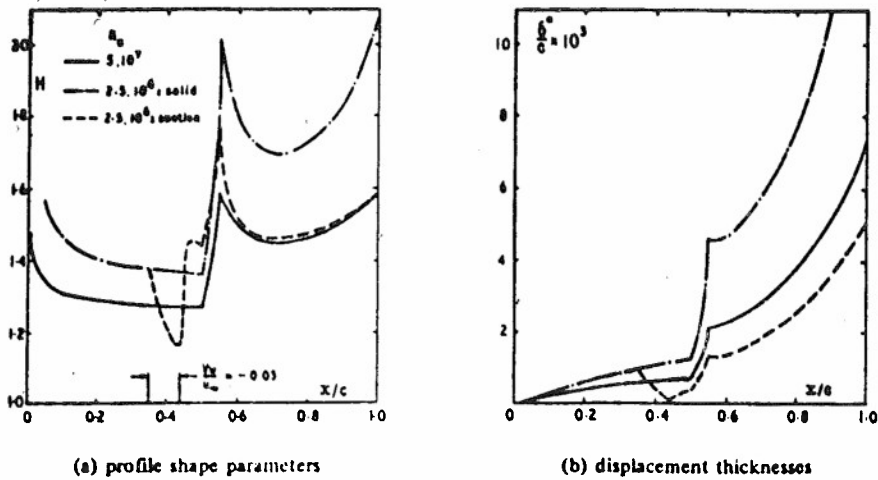
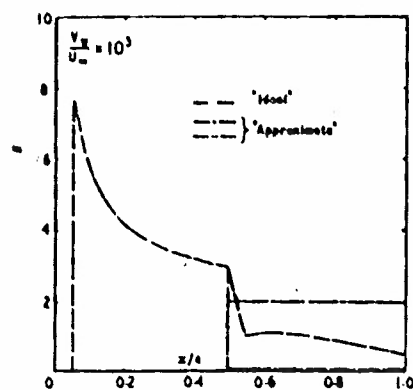
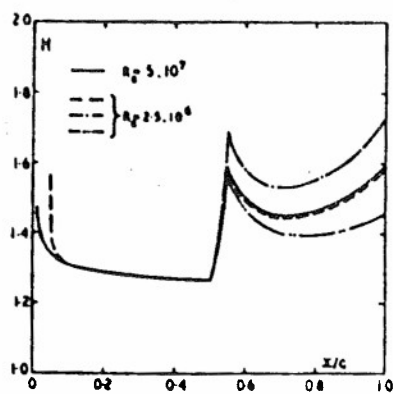


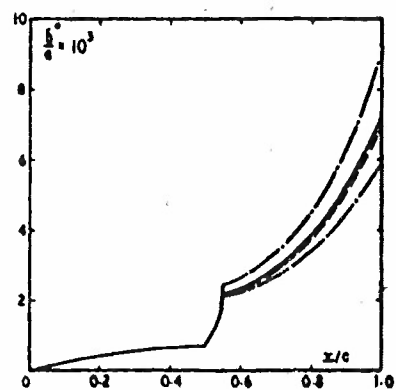
Figure 25. Partial simulation of high Reynolds number using localized suction. (Ref. 21).



(a) suction velocity



(b) profile shape parameters



(c) displacement thicknesses

Figure 26. Simulation of high Reynolds number using distributed suction. (Ref. 21).

## SECTION 4.10 SUMMARY OF FUTURE RESEARCH AND CONCLUSION

by E. Stanewsky  
 Institut für Experimentelle Strömungsmechanik  
 Deutsche Forschungs- und Versuchsanstalt  
 für Luft- und Raumfahrt e.V.  
 Bunsenstrasse 10, D-3400 Göttingen, FRG

The improvement of full-scale transonic performance prediction, especially under off-design conditions, requires boundary layer simulation and control in low Reynolds number wind tunnel tests. The physics of the flow associated with such a viscous simulation were reviewed and research needed to verify the results of the present study and to fill the gaps in our knowledge were outlined.

In a first step, the Research Committee defined flow phenomena critical in the present context, distinguishing between phenomena involving the direct interaction between the outer inviscid flow and the boundary layer - thus being potential contributors to major scale effects - and phenomena primarily affecting the boundary layer development without having a direct influence on the outer flow. The former include shock boundary layer interaction, trailing edge flow, classical (low speed) separation and vortex flows, the latter comprising the formation of body and wing vortices, vortex breakdown and asymmetrical vortex shedding. It was attempted to establish for these phenomena dominant viscous and outer inviscid flow parameters, i.e., parameters that must be duplicated in a low Reynolds number simulation process. The implementation of such a process requires, in addition, the understanding and predictability of the boundary layer development as it occurs naturally on a given aerodynamic surface or as it evolves under the influence of the wind tunnel environment or by boundary layer manipulation. Accordingly, relevant aspects of the laminar and turbulent boundary layer development, including non-equilibrium boundary layers and free and forced transition, environmental effects and boundary layer manipulation techniques were reviewed.

In concluding Section 4, the primary results of the present study with emphasis on research still needed shall briefly be recapitulated, following in essence the sequence given by the table of contents (see Figure 1 of Section 4.2 and for a

tabular summary Table 1 of the present section).

### Boundary layer development and transition:

In any viscous simulation scenario, it is generally required to compute the boundary layer development, commencing in the stagnation region of a given aerodynamic configuration, at least up to the encounter with a critical phenomenon, e.g., up to a shock wave, under full-scale as well as wind tunnel conditions. Concerning the laminar boundary layer development, it is stated in Section 4.3 that its theoretical treatment for weak interactions with the outer flow field is, for all relevant configurations, "well in hand". Considering "classical" equilibrium turbulent boundary layers, it is reasonable to assume that the numerical codes available today are able to predict the boundary layer development, at least for incompressible flow, up to its separation by direct or inverse mode calculations. For compressible equilibrium boundary layers, turbulence modelling is, for certain conditions, still insufficient: More systematic experimental and theoretical studies must be conducted in order to obtain fundamental data on the structure of turbulence, especially at non-adiabatic wall conditions and in the presence of streamwise wall curvature. The former relates to the - in practice - important question of the influence of wall temperature on turbulent skin friction. Here, valuable information may be obtained from tests in cryogenic wind tunnels which, in addition, provide the tool for much needed fundamental research on turbulent boundary layers at high Reynolds numbers. In three-dimensional flow some uncertainty evolves from the question of the direction of the shear stress vector in relation to that of the velocity gradient vector which need, as was observed in some experiments, not coincide. It appears that this is due to the cross-wise eddy viscosity being smaller than that in the streamwise direction. Since boundary layer calculations are generally based on the classical hypoth-

esis of the coincidence of the shear stress and velocity vectors, an improvement of three-dimensional turbulence models seems to be required.

Boundary layer transition still carries a great number of open questions and research is needed in the experimental as well as the theoretical domain. Needs for experimental studies are particularly pressing in three-dimensional flows:

- Transition criteria have been established based on but a few experimental data. These criteria must be verified in experiments where the main influence parameters are systematically varied.
- Knowledge concerning the influence of noise, freestream turbulence and surface roughness on three-dimensional transition is totally insufficient.

Most data on transition are for flat plates and cones and there is, generally, a lack of systematic results for realistic transonic configurations such as airfoils and wings where pressure gradients play an essential role. Here, research is particularly needed on the effect of wall temperature on transition in the presence of non-zero pressure gradients since the influence of wall temperature is highly dependent on such gradients. Due to the environmental effects, present in wind tunnel tests, it is highly desirable to supplement such tests by in-flight investigations. Concerning (stability) theory, it is stated in Section 4.3 that the amplification method ( $e^n$ ) is the most promising approach to transition prediction in the present domain of interest, provided all effective parameters - such as freestream turbulence - are properly accounted for.

Turbulent non-equilibrium boundary layers: For turbulent flow, an important consideration is its departure from equilibrium since here the similarity solutions so frequently used in boundary layer calculations no longer apply. Including non-equilibrium effects in the velocity profile is particularly revealing in the analysis of the state of the boundary layer, and it is essential for determining important scale parameters and establishing separation criteria. It is outlined in Section 4.4 how the description of the velocity profile by a revised version of the law of the wall and wake can be utilized for a detailed examination of the effect of a departure of the boundary layer development from equilibrium. Applying the law of the wall and wake to the development leading to separation, it is shown, for instance, that the shape parameter at separation - and this is especially important in the present context - is highly dependent on the relative pressure gradient parameter, i.e., departure from equilibrium. This explains the apparent inconsistency between established separation criteria, generally based on equilibrium flows ( $H = 4$ ), and

experimental observations, say, on airfoils with trailing edge separation, where shape parameters of  $H = 2$  at separation were observed. The revised law of the wall and wake can also be applied to three-dimensional flow.

A general conclusion of Section 4.4 is: Theoretical methods are increasingly becoming available which, though initially developed largely from the consideration of simpler flows, aim to treat very complex flows involving separation, large normal pressure gradients and shock waves. This requires a full description of the incoming boundary layer away from the traditional description based on boundary layer momentum and displacement thickness. Future experiments must similarly aim to provide all relevant flow parameters and boundary conditions, such as skin friction, velocity profile, pressure gradient parameter, skin friction lines in three-dimensional flow, and so on.

Classical separation, trailing edge flow and buffeting: If one considers classical separation within the present context, two critical locations where such separations may occur can be identified: the leading edge region where the initial natural state of the boundary layer is in most instances laminar and the trailing edge region where, for all practical situations, a turbulent boundary layer prevails. Laminar separation bubbles, likely - but not exclusively - to be present in low Reynolds number wind tunnel tests for peaky-type pressure distributions, may have a large effect on the turbulence structure at and downstream of reattachment, hence on the subsequent turbulent boundary layer development. It is indicated in Section 4.6 that adequate turbulence models in a sufficiently general form still have to be developed for this type of flow; suitable experiments must be conducted to achieve this goal. For the simulation of such laminar separation bubbles in low Reynolds number wind tunnel tests, it is suggested that the bubble be manipulated in a way that results in the "correct" magnitude of the dominant viscous parameter upstream of the next streamwise critical region.

Considering turbulent boundary layer separation, it is advocated in Section 4.6 that one should predict the boundary layer development leading to separation (by CFD) for given initial conditions, provided, e.g., downstream of the shock boundary layer interaction region, and dependent on the attendant pressure gradients. One should then use "criteria" that will identify the location of separation. This means, in essence, that improved computational procedures must be provided, accounting for the departure of the boundary layer from equilibrium, and that, similarly, reliable separation "criteria" for two- and three-dimensional flows must be established. A promising step in this direction has been undertaken by Cross who combined the entrainment

concept with his revised version of Coles' wall-wake description of turbulent boundary layers (see Section 4.4). It is judged in Section 4.6 that by not too extensive modifications to the present state-of-the-art, as exemplified by Cross' work, sufficiently reliable methods can be obtained for the prediction of separation for simulation purposes, at least for two-dimensional flows. It is, furthermore, stated in Section 4.6 that

- the reliable prediction of three-dimensional separation requires much more experimental research in order to derive adequate shape factor/pressure gradient parameter correlations and turbulence models (The latter also applies to the flow downstream of trips and shock boundary layer interaction in two-dimensional flows.),
- the trailing edge flow development - attached or separated - on the upper and lower surfaces of an airfoil or wing should be such that the correct circulation is obtained. Important parameters to be considered here are the momentum loss, the displacement thickness, the shape factor and the turbulence structure. How closely these parameters must be duplicated to simulate full-scale flow - or whether it is sufficient to just avoid separation, should it not occur at full-scale conditions - is not known and requires additional experimental and theoretical studies (also see the section on shock boundary layer interaction).

Buffet onset is strongly related to the development of separation on an airfoil or wing. This implies that if one simulates the flow development leading to total separation correctly, buffet onset should also be adequately represented. The subsequent buffeting process has been found in transonic flow to be closely coupled to the growth rate of the shock-induced separation bubble which was shown to depend, in turn, primarily on the boundary layer momentum thickness upstream of the shock (see section on shock boundary layer interaction). Whether the "correct" simulation of the bubble extent under steady conditions will, however, also result in an adequate representation of the full-scale unsteady buffeting process (e.g., the duplication of relative frequency and amplitude of the shock oscillations) remains open and a subject for future research. It is, furthermore, suggested in Section 4.6 that in order to establish and/or verify (needed) simplified methods for buffet prediction, a suitable research program should be carried out where various methods can be compared with each other and especially with corresponding flight test results.

**Shock boundary layer interaction:** Shock boundary layer interaction seems to be the most important phenomenon in transonic flow, at least for large aspect ratio wings, since the interaction not only

severely affects the local flow structure but, due to the impact of the shock on the boundary layer, also the entire flow development up to and beyond the trailing edge, hence the total flow field. Shock boundary layer interaction comprises three main elements whose full-scale simulation should be ensured in the low Reynolds number wind tunnel tests: the upstream influence, which rules the interactive pressure gradient imposed on the boundary layer, the onset of shock-induced (incipient) separation and the development of the shock-induced separation bubble. The upstream influence was, for turbulent interactions, found to be only dependent on the viscous parameter  $\delta_1^+$  ( $H_{11}-1$ ), where  $\delta_1^+$  and  $H_{11}$  are the displacement thickness and the incompressible shape factor, respectively, immediately upstream of the shock. It is believed that duplicating this parameter, normalized by the proper chord length, in the low Reynolds number wind tunnel tests will result in an adequate simulation of the entire shock boundary layer interaction process in the absence of shock-induced separation. This seems to hold for two- and three-dimensional interactions up to local sweep angles of the shock of  $\Lambda = 30^\circ$ .

Incipient separation in two- as well as three-dimensional flows was found to be rather insensitive to viscous effects and there exists strong evidence that simulating the upstream influence correctly will also result in a sufficiently accurate representation of full-scale incipient separation. Beyond that stage in the interaction, it seems that the dominant viscous parameter for the development of the shock-induced separation bubble with increasing shock upstream Mach number (shock strength) is the momentum thickness upstream of the shock. This result is supported by two independent correlations of the bubble extent on airfoils and wings, one based on the shock-upstream momentum thickness and the local Reynolds number based on momentum thickness, the other based on just the momentum thickness and the average radius of curvature of the surface between shock and trailing edge, the latter mainly representing the sustained adverse pressure gradients prevailing in that region. With the duplication of the normalized momentum thickness upstream of the shock it seems thus possible to simulate the full-scale shock-induced bubble development including the final breakdown of the flow (buffet onset), at least in the absence of an "independently" spreading trailing edge separation.

There remain, however, within the present context, several unresolved issues which require further experimental and theoretical research effort:

- The results, summarized above, are partly based on a rather limited number of experiments so that in some instances, especially in three-dimensional flow, well designed experiments



must be carried out at transonic speeds on realistic configurations to confirm (or reject and re-define) the dominance of the viscous parameters identified above.

- Although there is some positive evidence, it must be conclusively determined how closely the boundary layer parameters at the downstream face of the shock boundary layer interaction region (e.g.,  $\delta^*$ ,  $\theta$ ,  $H$ ) correspond to the ones at the (higher) Reynolds number to be simulated.
- Partly as a consequence thereof, one must investigate whether the simulation of the high Reynolds number trailing edge flow behavior is ensured - or what degree of approximation can be achieved - if the shock boundary layer interaction is simulated correctly. Proper simulation of the trailing edge flow conditions is, of course, required to obtain the full-scale shock location and strength.
- What are the limits of applicability of the shock-induced bubble simulation in the presence of an "independently" developing trailing edge separation?

A further aspect of shock boundary layer interaction that was addressed in Section 4.5 is the generation and amplification of turbulence due to the interaction. Here, strong evidence was found that the turbulence generation, especially in the presence of separation, may have a pronounced influence on the boundary layer development downstream of the interaction, hence on the trailing edge flow behavior. There is, furthermore, evidence that the magnitude of the shock-upstream turbulence has no effect on the maximum turbulence intensity within the interaction region, i.e., turbulence generation seems much more powerful than turbulence amplification. Nevertheless, the overall flow development associated with shock-induced separation is affected by freestream turbulence; however, only at turbulence levels far in excess of the ones commonly found in wind tunnels.

The open questions related to the viscous simulation of transonic shock boundary layer interaction may be answered by some thorough bench-mark experiments predominantly involving realistic configurations such as airfoils, sheared wings and complete three-dimensional wings of sufficient size. Variables of such experiments must be characteristic parameters of the incoming boundary layer ( $\delta^*$ ,  $\theta$ ,  $H$ , local Reynolds number, turbulence intensity and structure) and the outer inviscid flow (shock strength ( $M_1$ ), pressure gradient parameters upstream of the shock and in the trailing edge region) and geometric parameters including sweep angle and curvature. In all experiments detailed surface pressure, boundary layer, wake and field measurements must be carried out using a wide range of appropriate instrumentation. The experiments must, of course, be supplemented by extensive theoretical studies (which have the added

advantage that parameters can be easily and independently varied).

**Vortex flows:** Vortical flows are generally complex and correspondingly difficult to model analytically so that subscale wind tunnel testing frequently remains the primary developmental tool for vehicle optimization, especially with regard to high speed maneuvers. The types of vortical flows of interest in the present context, considered in Section 4.7, comprise forebody vortices, wing leading edge vortex flows, vortex breakdown and vortex/shock interaction. For the correct simulation of the vortical flow development, it seems, first of all, important to duplicate the full-scale primary separation line. Here, some guidance concerning critical viscous parameters may be obtained from the discussion of shock boundary layer interaction (Section 4.5) and classical separation (Section 4.6). The proper type of boundary layer at separation, i.e., laminar, transitional or turbulent, must, of course be ensured. One must, furthermore, generate the correct leeside vortex pattern and produce the correct vortex trajectory in the subscale wind tunnel tests.

Considering the different types of vortical flows enumerated above, one can clearly distinguish, within the present context, between phenomena sensitive and insensitive to viscous changes. The former include, for instance, (fore)body vortices, with the formation and shedding of asymmetric vortices from a slender body at high angle of attack being a particularly challenging task for viscous simulation, and wing leading edge vortex flow in the presence of round leading edges. The second category of phenomena includes the vortex development off sharp leading edge wings, where viscous effects are largely restricted to the secondary separation, vortex breakdown, whose occurrence is dominated by geometric conditions and the attendant external pressure gradient, and, similarly, shock/vortex interaction, where viscosity is important only insofar as it creates vorticity when the vortex is formed.

It is concluded in Section 4.7 that, in the large, research has not been performed to address the issues of subscale simulation of vortical flows. To alleviate this deficiency the following research is recommended:

- A systematic scaling law analysis needs to be performed on vortical flows of interest. Appropriate length scales and physical phenomena must be identified as a guide to proper subscale simulation. The scaling laws determined must be evaluated against full-scale flow development.
- Systematic studies of the influence of boundary layer tripping on vortex separation are needed. Specific objectives are to determine the influence of the state and condition

of the incoming boundary layer, as altered by tripping and tripping techniques, on symmetrical and asymmetrical vortex shedding on forebodies, reattachment and secondary vortex formation on sharp leading edge wings, shock-induced vortices on sharp edged wings with supersonic leading edges, and primary vortex separation on round leading edge wings.

- Further systematic studies must be carried out to determine the cause of asymmetric vortex formation on forebodies. Here, care must be taken to assure that true scaling phenomena are isolated and the asymmetries are not artifacts of flow quality (wind tunnel environment) or model precision.
- Vortex breakdown was found to be dominated mainly by geometric conditions on the wing and the external pressure gradient. Here, one last conclusive experiment needs to be performed to determine (confirm) the independence of vortex breakdown on Reynolds number.

It is strongly urged that in all experimental research body surface pressures, surface skin friction lines, surface streamline visualization, vortex trajectory visualization and vortex core velocities be obtained. These multiple pieces of information are necessary to understand the detailed behavior of the flow. It is also recommended that CFD be used to gain further understanding of vortical flow features.

Environmental effects on transition and boundary layer characteristics: In Section 4.8 it is distinguished between environmental effects entering the flow about the wind tunnel model through disturbances to the freestream, i.e., velocity, pressure and temperature fluctuations, and effects directly related to the wind tunnel model such as, for instance, surface roughness, non-adiabatic wall temperature conditions and model vibration. The model flow is mainly influenced by changes to boundary layer transition and the (turbulent) boundary layer characteristics.

It is stated in Section 4.8 that, although a wide body of information is available in certain areas, environmental effects have not been studied in a systematic and well organized manner. Yet the need for increased accuracy in contemporary wind tunnel testing make such studies and the detailed assessment of the wind tunnel environment a necessity. In the following, some major deficiencies concerning the present subject are pointed out:

- The effect of external turbulence on the characteristics of the turbulent boundary layer has mainly been studied for zero-pressure gradient flows; flows with non-zero pressure gradients still require more detailed experimental and theoretical attention, especially with regard to the relation

between pressure gradient and the mixing length of the external flow and its influence on the characteristics of the turbulent boundary layer. Also needed are more detailed studies of the effect of the turbulence scale.

- The information on the influence of wind tunnel acoustical disturbances on transition is not well defined beyond the cut-off turbulence intensity of 0.3 %. Yet the noise spectrum characteristics are critical for the transition location. Concerning the process of viscous simulation, it is required to determine these characteristics at the model location of a given wind tunnel so that they can be used as boundary condition for the necessary prediction of the boundary layer development on the wind tunnel model.
- The effect of external turbulence on certain flow phenomena, such as, for instance, shock boundary layer interaction and trailing edge separation, has not been sufficiently investigated. Such investigations should be carried out for configurations of various degrees of sensitivity to viscous changes (keeping, however, in mind that fairly high turbulence levels seem to be needed before any effect is felt). Similarly the accumulative effect of non-adiabatic wall conditions on such flow phenomena should be further studied.
- There is a considerable gap in our knowledge about the influence of environmental effects on three-dimensional flows.

In order to better understand the way certain environmental disturbances act on the boundary layer characteristics, improved theoretical methods must be devised.

Boundary layer manipulation: It is obvious that, left to its own development, the boundary layer on a model in subscale simulation may have little resemblance, in general, to the boundary layer on the full-scale vehicle. Consequently, it is inevitable that some sort of manipulation in viscosity dominated regions on the model will have to be performed for an improved prediction of full-scale conditions. It is also obvious, to quote Section 4.9, that the ideal boundary layer manipulation technique in any viscous simulation process would match the flight transition location, simulate the proper parameters at the shock location, introduce the correct turbulence structure downstream of the shock and recover the flight trailing edge condition, totally without otherwise disturbing the flow. Meeting all of these conditions is, of course, impracticable and also, judging from the present studies, not necessary.

Boundary layer manipulation devices can be categorized as those that promote (or delay) transition in a desired fashion or those that control the growth of the



(dominant) boundary layer parameters. In the first category, boundary layer tripping is the most widely applied and perhaps easiest boundary layer manipulation technique, although strongly limited in its application by the attendant model pressure distribution. More freedom is here provided by relying, for instance, on the effect of suction/blowing, heat transfer or compliant surfaces. The latter techniques also provide the tools for the control of the development of the (turbulent) boundary layer. Note, that an integral part of boundary layer manipulation is the identification of the transition location and the determination of the magnitude of dominant viscous parameters, which are being duplicated in the low Reynolds number wind tunnel tests, by measurement and/or computation.

As a result of the review of boundary layer manipulation in Section 4.9, the following research activities are suggested:

- It is most important to identify, as far as this has not been accomplished by the present committee effort (see Sections 4.5 and 4.6), the viscous parameters that must be controlled at critical locations on the model to allow the correct simulation of or extrapolation to full-scale conditions. These parameters must be defined for each fundamental test requirement, e.g., cruise drag, buffet boundary, vortex shedding and so on.
- Based on these criteria, boundary layer manipulation techniques must be developed that will produce the desired control of the relevant parameters. (Primary candidates are here boundary layer tripping, boundary layer suction and surface cooling.) Research should explore the effectiveness of the boundary layer manipulation devices for families of favorable and adverse pressure gradients. Correlations should be developed to define the boundary layer parameters, such as  $H$ ,  $\delta^*/c$ ,  $\theta/c$ , that will occur downstream of the manipulation device.
- Research needs to be performed to determine the flow structure in a transitioned boundary layer downstream of a cross-flow instability or leading edge contamination induced transition. These flow features must be compared to those downstream of the manipulation devices developed in order to evaluate the adequacy of conventional tripping in simulating other than streamwise instability transition.

Finally, non-intrusive boundary layer measurement techniques, such as, for instance, laser interferometry to determine transition location, must be improved and developed to the point of practical application. In addition, the use of CFD to infer viscous parameters that cannot be easily measured should be explored.

To conclude Section 4.10, relevant results and research requirements related to boundary layer simulation and control in low Reynolds number wind tunnel tests are summarized below in tabular form.

FLOW PHENOMENON	DOMINANT PARAMETERS	NEEDED FUTURE RESEARCH
<b>SBLI<sup>+</sup></b> - Upstream influence - Incipient separation - Separation bubble	$[\delta_1^*/c][H_{i1}-1]$ $H_{i1}, M_1$ $\theta_1, M_1$	- Verification of dominant parameters especially in 3-D flows - Boundary layer parameters downstream of SBLI region in relation to full-scale flow - Is additional manipulation of trailing edge flow required? - Importance of turbulence generation/amplification to trailing edge flow - Improve theory
<b>CLASSICAL SEPARATION/TRAILING EDGE FLOW</b> (also see non-equilibrium boundary layers)	$H_i, \pi_r$ $\delta^*, \theta$	- Improvement of theoretical methods to account for non-equilibrium effects in 2-D/3-D flows. Establish shape factor/pressure gradient parameter correlation for 3-D flows - Improve turbulence modelling for flows with transition occurring in laminar separation bubbles - Improve turbulence modelling for strong viscous/inviscid interactions
<b>VORTEX FLOW</b>	For primary separation line see SBLI and CLASSICAL SEPARATION	- Conduct scaling law analysis for vortical flows. Identify appropriate length scales - Determine the effect of tripping (state and condition of incoming boundary layer) on vortical flows of interest
<b>BOUNDARY LAYER DEVELOPMENT</b> - Equilibrium turbulent boundary layer - Transition (also see environment) - Non-equilibrium boundary layers (also see classical separation)		- Turbulence modelling in the presence of $T_w/T_{wAD} \neq 1$ and curvature - Fundamental research at high Reynolds numbers - Verify transition criteria - Influence of noise, turbulence and surface roughness on 3-D transition - Establish transition criteria for realistic transonic configurations. Effect of $T_w/T_{wAD}$ for $dp/dx \neq 0$ - Provide experiments with a complete description of the incoming boundary layer (velocity profiles, wall shear stress, etc.)
<b>ENVIRONMENT</b> (also see transition)		- Influence of external turbulence on turbulent boundary layer for $dp/dx \neq 0$ - Effect of turbulence scale on turbulent boundary layer development - Effect of turbulence on certain flow phenomena (SBLI, classical separation) - Influence of noise on transition at $Tu > 0.3$ - Improve develop/theory
<b>MANIPULATION</b>		- Effectiveness of boundary layer manipulation devices for $dp/dx \neq 0$ . Define boundary layer parameters ( $H_i, \delta^*, \theta$ , turbulence structure) downstream of specific manipulation devices - Boundary layer structure downstream of cross-flow instability transition in comparison to tripped boundary layer - Improve non-intrusive boundary layer measurement techniques - General: Find an inexpensive device that is easy to install, remotely controllable, does not disturb the flow and also measures the boundary layer condition upstream of "critical" flow phenomena

<sup>+</sup>SBLI = Shock boundary layer interaction.

$\delta^*, \theta, H_i$  = Displacement thickness, momentum thickness, incompressible shape factor.

$\pi_r$  = Relative pressure gradient parameter

$T_w$  = Wall temperature.

Subscripts: 1 = upstream of shock      AD = Adiabatic wall conditions

Table 1: Summary of results and major research requirements.

REPORT DOCUMENTATION PAGE			
1. Recipient's Reference	2. Originator's Reference	3. Further Reference	4. Security Classification of Document
	AGARD-AR-224	ISBN 92-835-0457-7	UNCLASSIFIED
5. Originator	Advisory Group for Aerospace Research and Development North Atlantic Treaty Organization 7 rue Ancelle, 92200 Neuilly sur Seine, France		
6. Title	BOUNDARY LAYER SIMULATION AND CONTROL IN WIND TUNNELS		
7. Presented at			
8. Author(s)/Editor(s)	Various		9. Date
			April 1988
10. Author's/Editor's Address	Various		11. Pages
			460
12. Distribution Statement	This document is distributed in accordance with AGARD policies and regulations, which are outlined on the Outside Back Covers of all AGARD publications.		
13. Keywords/Descriptors	<div style="display: flex; justify-content: space-between;"> <div> Transonic wind tunnels Boundary layer flow </div> <div> Simulation Fluid dynamics </div> </div>		
14. Abstract	<p>This report contains the results of a study performed by AGARD Working Group 09 on boundary layer simulation in wind tunnels with emphasis on the transonic speed regime. The working group was active under the auspices of the AGARD Fluid Dynamics Panel. The participants in the study represented Canada, France, Germany, Italy, Netherlands, United Kingdom, United States, and Turkey.</p> <p>This report is intended to display the current state-of-the-art in boundary layer simulation where Reynolds number is or cannot be simulated and give attention to wind tunnel effects as well as to document the physical aspects of boundary layer simulation and the research needed. Finally, a simulation methodology is proposed which can serve wind tunnel user and operator as an ordered thinking process for the design of wind tunnel tests where viscous effects are important.</p> <p>This Advisory Report was prepared at the request of the Fluid Dynamics Panel of AGARD.</p>		

**END**